Charles University
Faculty of Science

Study programme: Inorganic chemistry (P1401)
Branch of study: 4XANOR (1401V000)

Mgr. Ondřej Bárta

Ferrocene phosphinoguanidine donors

Ferrocenové fosfinoguanidinové donory

Doctoral thesis

Supervisor: prof. RNDr. Petr Štěpnička, Ph.D., DSc.

Prague, 2020

Prohlášení:

Prohlašuji, že jsem závěrečnou práci zpracoval samostatně a že jsem uvedl všechny použité informační zdroje a literaturu. Tato práce ani její podstatná část nebyla předložena k získání jiného nebo stejného akademického titulu.

V Praze, 24. září 2020

Podpis

The research project presented in this Thesis was financially supported by the Charles University Grant Agency (project no. 130317), by the Czech Science Foundation (project no. 17-02495S), and by the Charles University Research Centre program (project no. UNCE/SCI/014).

Acknowledgement

Nine years ago, at the beginning of my chemistry studies, prof. Petr Štěpnička, Ph.D. took me under his wing and since then, he has always been kind, caring and patient supervisor and provided me with plethora of useful advices. For that, I would like to express my immense gratitude to him. I would also like to acknowledge all the co-workers who contributed with their expertise to the work presented in this Thesis. Among them, special thank goes to dr. Ivana Císařová, our wonderful crystallographer. Moreover, I thank my colleagues and friends in the "organometallic lab 316" for fruitful discussions, suggestions and pleasant work environment.

Last but not least, I would like to thank my parents, sister; family and my beloved soulmate who all has been supportive and encouraging for the whole time of my studies and always cheered me up.

Table of Contents

Abstract

The „Ferrocene phosphinoguanidine donors" project presented in this Thesis targeted on the synthesis, coordination chemistry and catalytic applications of a rather uncommon class of compounds combining phosphine and guanidine functional groups in their molecules. Two series of such compounds based on ferrocene backbone (henceforth fc = ferrocen-1,1′-diyl) were studied.

Firstly, a reliable synthetic route towards polar phosphinoguanidinium chlorides $[R_2PfcCH_2NHC(NH_2)_2]Cl$, where R = *iso*-propyl, cyclohexyl, phenyl and 2-furyl, was developed and these ligands were tested as supporting ligands in palladium-catalysed Suzuki-Miyaura-type reactions in biphasic aqueous mixtures and in rhodium-catalysed hydroformylation of 1-hexene. Deduced from the results, the hydrophilic guanidinium tag had a beneficial effect on the catalytic activity and, particularly, the electron-rich phosphines from this series could serve as a useful alternative to commonly used ligands for catalytic applications in polar or aqueous reaction media.

Phosphinonitriles R_2PfcCN obtained as intermediates during the synthesis of the abovementioned ligands were additionally used for the preparation of the dimeric complexes $[Au_2(\mu\text{-}R_2PfcCN)_2][SbF_6]_2$, in which the gold(I) centre was stabilised by nitrile coordination. These complexes proved to be highly active precatalysts in gold(I)-mediated cyclisation of *N*-propargyl amides to 2-substituted 5-methyleneoxazolines. The reaction rates correlated with the donor properties of the phosphine moieties with the complex bearing the least donating phosphine showing the best catalytic results.

A second compound series included phosphinoguanidines $Ph_2PfcNC(NHR')_2$ (R′ = *iso*-propyl, cyclohexyl and 2,6-xylyl), representing the first examples of *N*,*N*′,*N*′′-trisubstituted phosphinoguanidines isolated to date. The coordination behaviour of these ligands towards palladium(II) was studied extensively. During these studies, complexes covering various possible coordination modes of these ligands were prepared and characterised, including unique complexes containing the Fe→Pd dative bond and unprecedented mononuclear palladium(II) guanidinate complexes. These results initiated further studies into the reactivity and possible catalytic application of this so far neglected highly-functionalised ligands.

Keywords: Phosphine ligands; Ferrocene ligands; Guanidines; Coordination compounds; Catalysis.

Shrnutí

Předkládaná disertační práce „Ferrocenové fosfinoguanidinové donory“ cílila na rozšíření dosud málo početné skupiny sloučenin, v jejichž strukturách se kombinují fosfinové a guanidinové funkční skupiny. Byly studovány zejména dvě série takových látek se strukturou založenou na ferrocenovém skeletu (dále fc = ferrocen-1,1′-diyl).

První skupinou látek byly polární chloridy fosfinoguanidinia $[R_2PfcCH_2NHC(NH_2)_2]Cl$, kde R = *iso*-propyl, cyklohexyl, fenyl a 2-furyl. Tyto hydrofilní fosfiny byly testovány jako podpůrné ligandy v palladiem katalyzovaných spojovacích reakcích Suzukiho-Miyaurova typu ve vodném bifázovém prostředí a v rhodiem katalyzované hydroformylaci 1-hexenu. Z výsledků vyplynulo, že guanidiniový substituent měl pozitivní vliv na katalytickou aktivitu a zejména elektronově bohaté fosfiny z této série tak mohou být užitečnou alternativou pro některé katalytické reakce prováděné v polárních či vodných rozpouštědlech.

Meziprodukty při syntéze výše zmíněných ligandů, fosfinonitrily R_2PfcCN, byly dále využity pro přípravu nitrilovou skupinou stabilizovaných dimerních komplexů $[Au_2(\mu\text{-}R_2PfcCN)_2][SbF_6]_2$. Jejich katalytická aktivita byla porovnána ve zlatem katalyzované cyklizaci propargylamidů za vzniku 5-methylen-4,5-dihydrooxazolů. Bylo zjištěno, že se jedná o vysoce aktivní katalyzátory, přičemž rychlost reakce korespondovala se sigma-donorovými vlastnostmi fosfinů s tím, že reakce probíhala nejrychleji v přítomnosti elektronově nejchudšího fosfinu.

Druhou připravenou skupinou látek byly fosfinoguanidiny typu $Ph_2PfcNC(NHR')_2$, kde R′ = *iso*-propyl, cyklohexyl a 2,6-xylyl. V tomto případě se jedná o vůbec první izolované *N*,*N*′,*N*′′-trisubstituované fosfinoguanidiny. U těchto sloučenin bylo následně studováno především koordinační chování vůči palladnatému centru. Na strukturách získaných komplexů byla demonstrována široká paleta dostupných koordinačních módů zmíněných ligandů. Byly připraveny a charakterizovány jak komplexy obvyklé, tak v některých případech vzácné (koordinace za účasti dativní vazby Fe→Pd), až unikátní (první popsaný fosfinoguanidinátový palladnatý komplex). Získané výsledky otevírají cestu k dalšímu studiu reaktivity a případné katalytické aktivity této dosud opomíjené skupiny vysoce funkcionalizovaných ligandů.

Klíčová slova: Fosfinové ligandy; Ferrocenové ligandy; Guanidiny; Koordinační sloučeniny; Katalýza.

1. Introduction

1.1 Phosphines – properties and catalytic applications

Catalytic applications of phosphine ligands or, more accurately, phosphine-transition metal complexes began to emerge in the late 1940s. At that time Reppe reported that phosphine-coordinated nickel complexes were more efficient catalysts for cyclotrimerisation of olefinic and acetylenic substrates than other nickel salts.[1] Since then, homogeneous transition metal catalysis became one of the most important fields of research in chemistry and, currently, hundreds of new phosphine ligands and their transition metal complexes are developed every year.[2]

Extensive research in this area obviously demonstrated positive effect that auxiliary phosphine ligands exerted on metal-catalysed reactions. Expectedly, phosphines do not interact with the reactants directly, since all the relevant transformations take place on a transition metal centre (**Scheme 1.1**). However, they play the key role in controlling reactivity of the metal centre and stabilise it during the catalytic cycle.

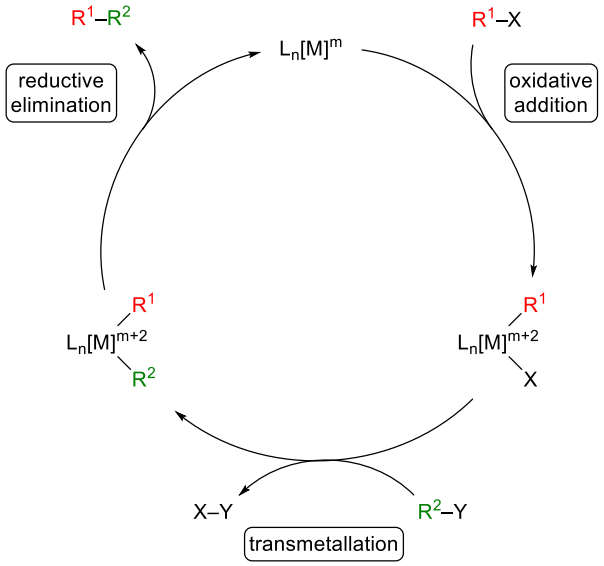

Scheme 1.1. General representation of typical transition metal-mediated catalytic cycle.

According to the HSAB theory,[3] phosphines are soft bases capable of σ-donation and π-back donation. Substitution pattern at the phosphorus atom has a substantial effect on these two contributions to donor characteristics of a phosphine ligand. Generally, electron-donating substituents increase electron density at the phosphorus atom, making it stronger σ-donor and weaker π-acceptor and vice versa. As a consequence, strongly σ-donating, electron-rich phosphine increases after coordination the electron density at a catalytically active metal centre and thus enhances the rate of oxidative addition. Conversely, electron-poor phosphine supports

the reductive elimination step. It is, however, far from easy to describe the donor properties of phosphines by simple, experimentally accessible parameters. Brønsted basicity[4] can be used as it, to some extent, correlates with the donor strength. One of the most popular methods is based on recording the carbonyl stretching frequencies $\nu_{CO}(A_1)$ of $[Ni(CO)_3(phosphine)]$,[5] $[RhCl(CO)(phosphine)_2]$[6] or other metal carbonyl complexes. The values then describe the π-acceptor strength. Recently, the $^1J_{PSe}$ coupling constant of corresponding phosphine selenides $R_3P{=}Se$ was introduced as a convenient parameter for probing the basicity of phosphines.[7] The interaction constant reflects the s-character of the lone pair and, consequently, it is not entirely an electronic parameter, but is also affected by the geometry at the phosphorus atom. This contribution is more pronounced for phosphines with sterically demanding substituents.

The size of the phosphine ligand is a second property, which could be changed directly by substituent variation. In principle, phosphines with bulky substituents create large steric hindrance around the metal centre. Therefore, products of the catalytic cycle are released from the coordination sphere more easily. Based on this assumption, sterically demanding phosphines (which are also often strong σ-donors) received considerable attention and showed supreme results in various catalytic applications.[8] Several parameters are commonly used when describing the size of a phosphine. The cone angle, introduced in 1970 by Tolman, is defined as the "apex angle of a cone centred on the metal, just large enough to enclose the van der Waals radii of the outermost atoms of the ligand".[9] This approach, despite its simplicity, describes the steric demands of a phosphine very well and is still popular. However, several other methods, such as solid angle,[10] ligand repulsive energy,[11] or ligand buried volume,[12] were developed to assess the phosphine size more precisely. For bidentate chelating diphosphines, another steric parameter, namely the P-M-P angle (*i. e.*, the ligand bite angle), was proposed.[13] Its value can be determined from crystal structures. However, in that case, the value is a compromise between ligand and metal ion preferred angles. The *natural* bite angle, on the other hand, is defined as "the preferred chelation angle determined only by ligand backbone straints and not by metal valence angles" and it can be obtained from computational molecular modelling.[14]

Another way how to modify catalytic performance of phosphine ligands is to incorporate additional functional groups to their structures. These additional functionalities can serve for various purposes depending on their nature.

One of the properties that could be altered by adjacent functional groups is solubility, since an efficient catalyst should be soluble in the solvent used for the reaction. The green chemistry principles[15] emphasise the use of non-toxic solvents, preferably water. Unfortunately, conventional phosphine complexes, despite they are excellent catalyst components, are usually insoluble in water. To overcome this problem, hydrophilic functional

groups are attached to solubilise the phosphine in aqueous media. Sulphonate is the group of choice for this purpose, but other acidic groups, amines or polyethers are used as well.[16] Catalysts based on water-soluble phosphines can be advantageously used for reactions in aqueous biphasic mixtures. In this setup, the catalyst is dissolved in aqueous phase with the possibility of its recycling, whereas the starting materials and the products, remaining in a non-miscible organic phase, can be simply separated by extraction and decantation. This approach was successfully implemented in industry.[17, 16a]

Phosphines equipped with additional donor groups are important class of so-called *hybrid ligands* which are, by definition, "bi- or polydentate ligands that contain at least two different types of chemical functionality capable of binding to metal centres".[18] *Hemilabile ligands* are a special type of hybrid ligands.[19] In their case, a strongly donating group (such as phosphine for the soft metal ions) is combined with a weaker donor, which can reversibly de-coordinate in the presence of another ligand or solvent. This behaviour could be useful for catalytic applications assuming that de-coordination leads to an activation of the catalyst while coordination, on the other hand, results in stabilisation of its resting state (**Scheme 1.2a**). Some of the hybrid phosphines can directly participate in substrate activation by metal-ligand cooperation (**Scheme 1.2b**). Such ligands are classified as *cooperating ligands* and typically contain acid-base or redox-active groups in their structures.[20]

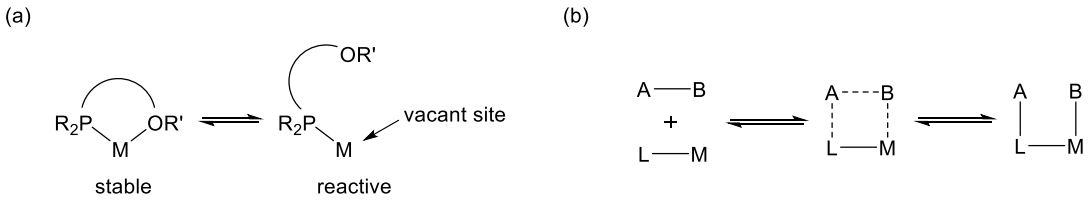

Scheme 1.2. (a) Principle of hemilabile coordination of hybrid ligands; (b) activation of substrate by ligand-metal cooperation.

Obviously, all the aforementioned principles can be combined to design highly active, custom-tailored ligands for specific catalytic applications (**Scheme 1.3**). In this context, it is worth to mention ligands from the cataCXium family excelling in C-C cross-coupling reactions,[21] Buchwald-type biaryl-substituted phosphines designed for palladium catalysed reactions,[22] or complexes of PNP-pincer ligands active in (de)hydrogenation reactions.[23] Notably, all these very successful ligands comprise a chemically stable backbone. Therefore, when thinking about the cornerstone of a new ligand, ferrocene scaffold could be an option.

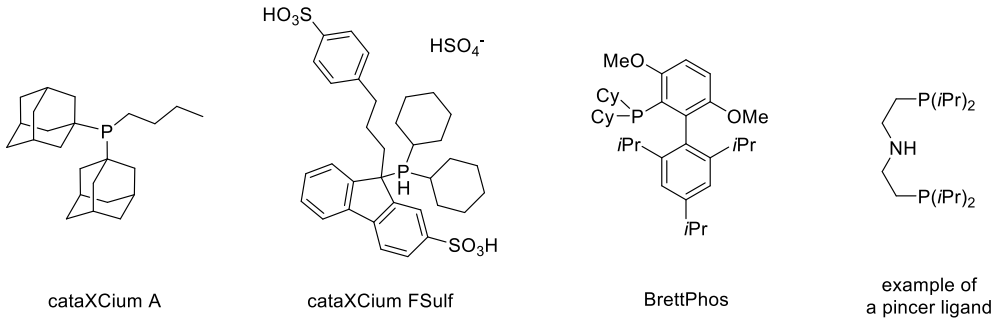

Scheme 1.3. Selected examples of highly functionalised ligands.

1.2 Ferrocene-based phosphines

Ferrocene was discovered unintentionally in the early 1950s by two research groups as an unusually stable inorganic compound of elemental composition $C_{10}H_{10}Fe$.[24, 25] It was some sort of a riddle for chemists, who were quite uncertain about its structure until it was finally revealed by X-ray diffraction analysis.[26, 27] And it was the recognition of ferrocene structure, comprising of two cyclopentadienyl rings coplanarly coordinated to an iron(II) ion *via* their delocalised π-systems, that initiated rapid development of metallocene and organometallic chemistry. For pioneering work in this field, the Nobel Prize was awarded to G. Wilkinson and E. O. Fischer in 1973.

Chemical stability of ferrocene arises from obeying the "18-electron rule" and also from its aromaticity given by complete delocalisation of the cyclopentadienyl ring electrons. Although highly chemically stable, the molecule is not inert. It can undergo reversible one-electron oxidation to form ferrocenium cation, which process is so distinctive and reproducible that ferrocene/ferrocenium pair serves as one of commonly used internal standards in electrochemistry.[28] The redox potential varies with substitution at the cyclopentadienyl rings and correlates well with Hammett constants of the substituents.[29] This means that electron-donating substituents shift the redox potential to more negative values, *i. e.*, the derivative is easily oxidised, and vice versa.

As for chemical reactivity, ferrocene can be functionalised by reaction protocols typical for aromatic compounds. For example, various acylferrocenes can be prepared by Friedel-Crafts acylation or Vilsmeier formylation.[30] Another reaction of great importance in ferrocene chemistry is lithiation. By choice of appropriate reaction conditions, lithiation can be driven to specific positions on ferrocene scaffold and, after subsequent reaction with electrophiles, a wide range of derivatives can be synthesised.[31]

Among all the ferrocene-based compounds,[32, 33] ferrocenylphosphines are possibly the most studied ones and further research into their properties is motivated by successful commercial applications of several compound types in catalysis (**Scheme 1.4**). The foundation

of the field was laid by Sollott who studied the reaction of ferrocene with phosphorus trichloride under Friedel-Crafts conditions. In addition to the expected ferrocenyl mono- and disubstituted phosphine chlorides, he also obtained symmetrical trisubstituted triferrocenylphosphine, which compound was, curiously, the first ferrocenylphosphine bearing solely carbon-bonded substituents at phosphorus.[34] Later on, ferrocenyldiphenylphosphine was prepared by the same approach[35] as a typical representative of monophosphinylated ferrocenes. The considerable advantage of ferrocene monophosphines is their stability and the fact that they are, unlike many conventional organic phosphines, easy to handle, well-defined crystalline materials. Some of them exhibit favourable catalytic activities. For example, sterically hindered ligand Q-Phos (**I**) excelled in palladium-catalysed cross-coupling reactions of unactivated substrates.[36] However, the advances in ferrocene monophosphine chemistry were overshadowed by performance of ferrocene-based diphosphines in homogeneous transition metal catalysis.

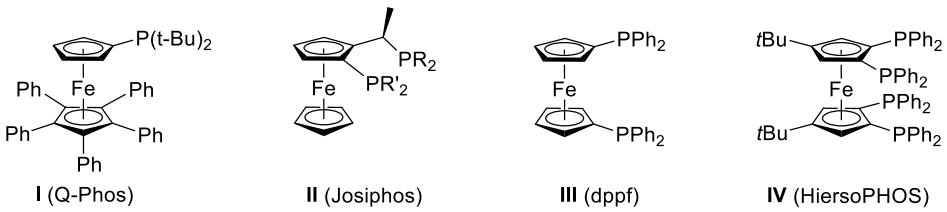

I (Q-Phos) **II** (Josiphos) **III** (dppf) **IV** (HiersoPHOS)

Scheme 1.4. Ferrocene-based phosphines widely used in catalysis.

Josiphos ligand family (**II**)[37] belongs to the so-called "privileged" ligands for asymmetric catalysis. In the structure of these ligands, planar chirality, a significant property of 1,2-disubstituted ferrocenes with non-matching substituents, is combined with central chirality at one of the substituents. The coordination of these diphosphines to metal ions is described by relatively wide bite angles (approximately 93° on average) which, together with steric hindrance caused by bulky substituents on the phosphorus atoms, enforces *cis*-coordination of these ligands and keeps the chirality elements in proximity of a catalytically active centre. This unique steric arrangement is responsible for a high activity and enantioselectivity of Josiphos ligands in various synthetic transformations, such as catalytic hydrogenations of multiple bonds, hydrofunctionalisations, or C-C bond forming reactions.[38]

In spite of numerous successful applications of chiral ferrocene phosphines, the rather simple diphosphine, 1,1'-bis(diphenylphosphino)ferrocene (dppf, **III**) still remains the most frequently studied and utilised ferrocene ligand. Its convenient synthesis was reported in 1971[31b] and, soon after, the first reports on promising catalytic activity of dppf-transition metal complexes in cross-coupling reactions were published.[39] Since then, complex [$PdCl_2$(dppf)] was titled by a nickname "magic catalyst" and dppf ligand itself became a standard part of "ligand kits" used for the development of new transition metal catalysed processes. The wide palette of

applications of dppf in cross-coupling reactions was thoroughly reviewed in several book chapters and review articles.[40] The high catalytic activity of dppf can be explained by its large bite angle (natural bite angle value is 99°),[41] which supports the reductive elimination step, and by its conformational flexibility. The latter factor was investigated in numerous coordination studies, which revealed that dppf can act either as monodentate donor or as bidentate ligand in chelating or bridging mode (**Scheme 1.5**).

In addition to the aforementioned "traditional" coordination modes, dppf can also enter into a rather peculiar κ^3*P*,*Fe*,*P*'-coordination interactions with dative bond between the electron-rich iron atom and the ligated metal ion. This coordination mode was firstly described for 1,1'-ferrocenylditiolate palladium(II) complex[42] in 1983 and, based on growing number of examples,[43] it seems that it is a common feature of 1,1'-disubstituted ferrocene ligands with donor atoms directly attached to the ferrocene scaffold. However, the requirements for this coordination mode to emerge are still scarcely explored, although the nature of the known examples suggests a delicate interplay between electronic and steric properties of the donor moieties. Finally, it should be noted that only examples with donor-symmetric ligands have been reported thus far.

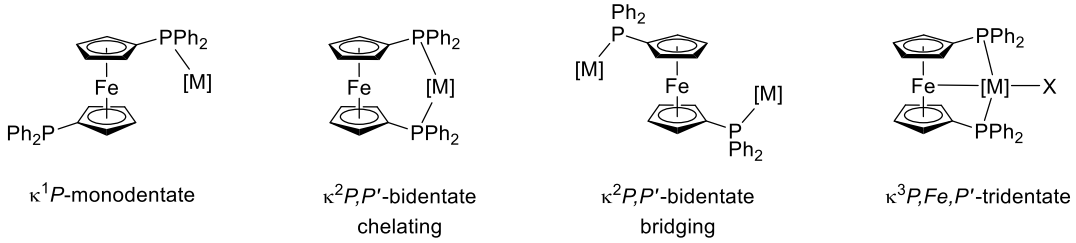

Scheme 1.5. Coordination modes of dppf.

The success of dppf in homogeneous catalysis initiated further research into its analogues and derivatives. One way how to modify the dppf molecule is to exchange phenyl groups for other substituents. Some of these P-alkyl derivatives showed even higher catalytic activities than dppf itself. In particular, bulky and electron-rich 1,1'-bis(di-*tert*-butyl-phosphino)ferrocene (dtbpf) was found to be remarkably active in Suzuki-Miyaura coupling[44] and in Pd-catalysed amination[45] of unactivated substrates.

Another option is to functionalise one or more of the remaining positions of the cyclopentadienyl rings. Highly functionalised ferrocene polyphosphines synthesised by Hierso and co-workers (**IV**)[46] could serve as an example of such derivatives. These ligands were tested in palladium-catalysed C-H activations of heterocycles.[47]

Another approach towards dppf derivatisation, essential for this work, is a replacement of one diphenylphosphino group for a different functionality with a specified function. Such

functionality can be an additional donor group, in which case a hybrid ligand is obtained, or a hydrophilic moiety providing access to water-soluble ferrocene phosphines. In some cases, both principles are efficiently combined.[48]

The synthetic pathways towards 1'-functionalised ferrocenylphosphines are usually based on lithiation/functionalisation reactions. Two of the most convenient routes start from easily accessible 1,1'-dibromoferrocene (**Scheme 1.6**).[49] When reacted with organolithium reagents, the bromine substituents are selectively and stoichiometrically replaced by lithium to provide lithium salts.[50] Following *Route A*, 1,1'-dibromoferrocene is initially reacted with one equivalent of butyllithium to obtain monolithiated intermediate, which is in turn reacted either with a suitable electrophile or with chlorophosphine (depending on what is more favourable) to produce 1'-functionalised bromoferrocene. The latter is subsequently reacted with another equivalent of butyllithium and the remaining functional group is installed. *Route B* starts by reaction of 1,1'-dibromoferrocene with two equivalents of butyllithium giving dilithiated ferrocene, which further reacts with dichlorophosphine to form ferrocenophane phosphine. Strained ferrocenophane ring is subsequently opened in a reaction with organolithium reagent to produce lithium salt of phosphinoferrocene which, in the final step, reacts with an electrophile to form the product. Although *Route B* requires more equivalents of organolithium reagent, it can be beneficial for synthesis of ferrocenylphosphines unsymmetrically substituted at the phosphorus atom.

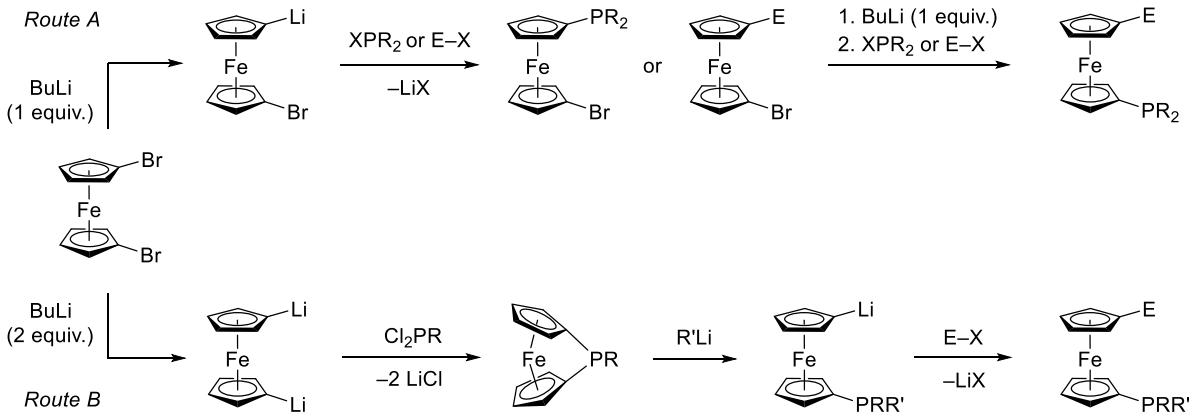

Scheme 1.6. Most common synthetic routes to 1'-functionalised ferrocenylphosphines.

From the plethora of 1'-functionalised ferrocenylphosphines, only examples relevant for this work, *i. e.*, phosphines partially soluble in water (**Scheme 1.7**) and P,N-donors (**Scheme 1.8** and **Scheme 1.9**), are selected and discussed below.

An archetypal representative of ferrocenylphosphines equipped with acidic group is the carboxylated derivative, 1-(diphenylphosphino)-1'-ferrocenecarboxylic acid (Hdpf, **V**), firstly reported in 1996.[51] Subsequently, it was shown that this hybrid ligand can coordinate various

metal ions in P-monodentate,[52] or P,O-chelating[53] fashion. Later on, polymetallic complexes in which the dpf⁻ anion coordinates as an P,O-bridge between hard and soft metal centres were described.[54] Furthermore, rhodium(I) complexes of Hdpf proved to be active and recyclable catalysts for hydroformylation of 1-hexene.[55]

Hdpf was also used as a starting material in the synthesis of a wide range of compounds in which phosphinoferrocene moiety was connected with a flexible functional pendant by amide bond (compounds **VI**-**X**). The amide substituents often served as a hemilabile donor and the pendants were equipped with additional functionalities such as amino-acid fragments, amines, ureas, guanidines, phosphines or sulphonates. Substantial conformational flexibility and a rich palette of coordination modes were manifested *via* coordination reactions, mostly with platinum-group metals. Catalytic activity of many of these ligands and complexes was evaluated in cross-coupling reactions performed in aqueous reaction mixtures or under biphasic setup with promising results. The achievements in chemistry of these derivatives was concisely reviewed.[56]

Lately, the influence of phosphine substitution on donor and catalytic properties was probed when selected carboxamides (namely **VI** and **X**) with varied substituents at the phosphorus atom were compared in Pd-catalysed cyanation and in Suzuki-Miyaura reactions. It was concluded, that phosphines with bulky electron-rich substituents were more active in Suzuki-Miyaura coupling than the phenyl-substituted ones.[57] The opposite trend was noted for the cyanation reactions.[58]

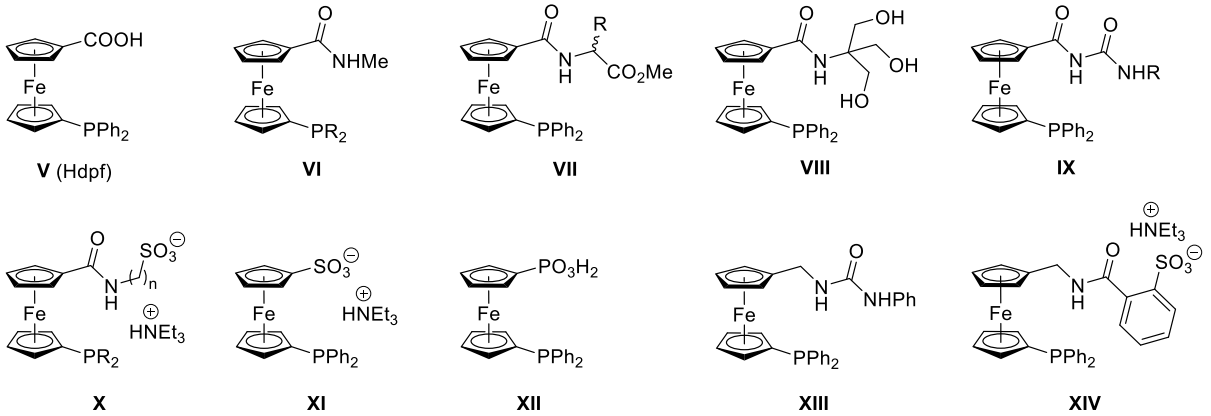

Scheme 1.7. Selected representatives of polar, 1'-functionalised ferrocenylphosphines.

Very recently, sulphonate analogue of Hdpf, *viz* Ph_2PfcSO_3H, was prepared and isolated in the form of its triethylammonium salt (**XI**). Coordination preferences of this compound were evaluated through reactions with palladium(II) and rhodium(I) precursors.[59,60] Selected palladium(II) complexes were tested as catalysts for Suzuki-Miyaura-type coupling of aroylchlorides with boronic acids providing benzophenones,[59] and for oligomerisation of

ethylene.[61] Catalytic activity of rhodium(I) complexes was, on the other hand, examined in hydroformylation reactions.[60] A related phosphonate analogue $Ph_2PfcPO_3H_2$ (**XII**) was also synthesised. However, it was found to be rather unstable and, therefore, not suitable for catalytic applications.[62]

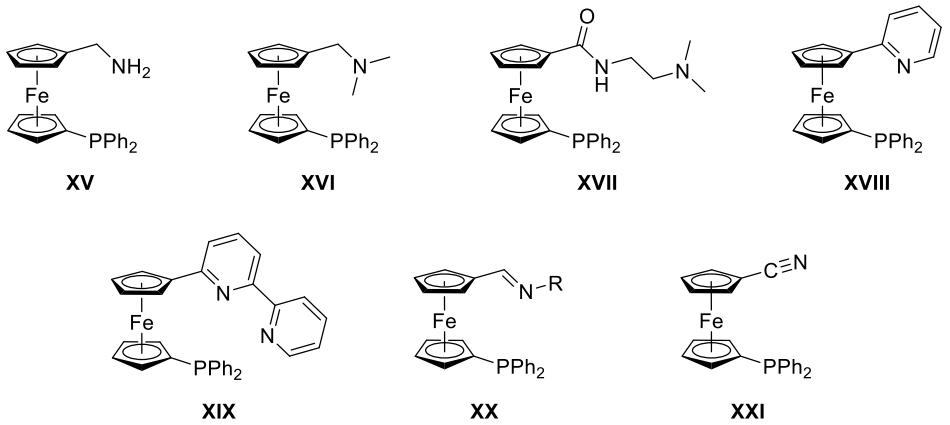

Scheme 1.8. Selected ferrocene-based P,N-donors.

Among 1'-functionalised ferrocenylphosphines, hybrid P,N-donors are of particular importance. Amine or imine groups are the typical secondary donor moieties present in these compounds (**Scheme 1.8**). 1'-(Aminomethyl)-1-(diphenylphosphino)ferrocene (**XV**), was originally prepared as a useful synthon for the preparation of other functional ligands (compounds **XIII** and **XIV** in **Scheme 1.7**).[63] In addition, its coordination chemistry towards Cu(I) was investigated lately, giving rise to a P,N-chelated complex and an obscure multinuclear mixed-valent copper(I/II) complex.[64]

The effect of pendant arm properties on the coordination flexibility of a ligand can be demonstrated by comparing the coordination behaviour of two compounds bearing the NMe_2 donor groups in their structures, namely $Ph_2PfcCH_2NMe_2$ (**XVI**) and $Ph_2PfcC(O)NHCH_2CH_2NMe_2$ (**XVII**). The first one, linked by a methylene spacer, reacts with $PdCl_2$ precursor to form a P,N-bridged dimer.[65] The latter one, with a longer, carboxamide-based linker, coordinates as a *trans*-chelating ligand.[66]

Similar trends were observed in coordination chemistry of ferrocenylphosphines containing pyridine-type substituents. Thus, pyridyl-substituted derivative Ph_2PfcPy (**XVII**) coordinates to $PdCl_2$ in *cis*-chelating fashion,[67] while in the case of its bipyridyl analogue $Ph_2PfcBipy$ (**XIX**), coordination of the terminal pyridine ring leads selectively to *trans*-chelated isomer.[68] Interesting behaviour induced by ligand geometry was observed in complex *cis*-[Rh(cod)(Ph_2PfcPy-κ^2*P,N*)][PF_6], in which weak interaction between rhodium(I) centre and neighbouring hydrogen atom of cyclopentadienyl ring was identified. In the iridium analogue,

the hydrogen atom entered the coordination sphere *via* oxidative addition of one CH group in the cyclopentadienyl ring to the iridium centre.[69]

Ferrocenyl iminophosphine ligands $Ph_2PfcCH{=}NR$ (**XX**) formed chelate complexes with Pd(0) and Ni(0), which were used in Suzuki-Miyaura cross-coupling[70] and in ethylene oligomerisation, respectively.[71] Conversely, phosphinonitrile Ph_2PfcCN (**XXI**) is one of the simplest hemilabile ferrocene P,N-donors. Its coordination chemistry, especially with coinage-metals, however, is incredibly rich in motives and variations.[72] Most of the structures of its complexes is based on combinations of P-monodentate and P,N-bridging coordination modes. Moreover, dimeric complexes $[Au_2(\mu\text{-}Ph_2PfcCN\text{-}\kappa^2P,N)_2]X_2$ (X = $[SbF_6]^-$, NTf_2^-, OTf^-) are highly active catalysts in gold(I)-catalysed reactions.[72b, 73]

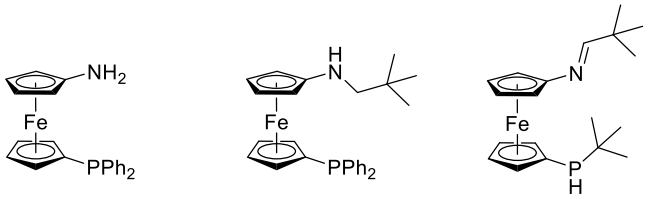

XXII **XXIII** **XXIV**

Scheme 1.9. Hybrid, 1,1'-substituted ferrocene-based P,N-donors with the nitrogen atom directly attached to the ferrocene backbone.

Donor-symmetric 1,1'-disubstituted ferrocene ligands with nitrogen donor atoms directly attached to the ferrocene backbone are quite common and widely used for stabilisation of lanthanide and actinide ions,[74] platinum-metals,[75] and even main group elements.[76] In a striking contrast, analogous donor-unsymmetric 1'-nitrogen-substituted ferrocenylphosphines have been studied very scarcely thus far (**Scheme 1.9**). The crucial synthon for the preparation of such ligands, *i. e.*, 1-(diphenyphosphino)-1'-aminoferrocene (**XXII**), was firstly reported in 1998,[77] but the convenient and reliable synthetic procedure was reported only recently.[78] In the original paper, the preparation of complex $[PdCl_2(Ph_2PfcNH_2)]$ was additionally described; however, no additional structural information was provided for this compound. Ph_2PfcNH_2 with protected phosphine group reacts with aldehydes to form imine which, after reduction and deprotection, provides N-substituted amine as it was demonstrated by the synthesis of $Ph_2PfcNHCH_2tBu$ (**XXIII**).[79] Unfortunately, no reports on coordination chemistry of this lidand have been published yet. Finally, phosphine imines *t*BuHPfcN=CR (**XXIV**) were unintentionally prepared during attempted synthesis of azaphospha[2]ferrocenophanes.[80]

To the best of my knowledge, the three compounds listed above (and the corresponding reaction intermediates leading to them) are the only examples of donor-unsymmetric 1'-nitrogen-substituted ferrocenylphosphines. Nevertheless, Ph_2PfcNH_2 can be certainly utilised

as a starting material for the synthesis of a plethora of amine-derived compounds, and it is just a matter of time, when new ligands of this type emerge. One class of compounds easily accessible from amines are guanidines.

1.3 Guanidines – properties, synthesis and applications in ligand design

Guanidines are nitrogen-rich organic compounds derived from the eponymous parent congener of the formula $(NH_2)_2C{=}NH$. Due to their unique properties, namely high basicity, hydrogen bonding ability and biocompatibility, they found wide applications in various fields including organocatalysis, supramolecular chemistry or bioinorganic chemistry.[81]

The most striking property of guanidines is their basicity. Guanidine itself is considered one of the strongest organic bases comparable in strength to alkaline hydroxides. The high basicity of guanidine origins from a gain of resonance energy upon formation of a guanidinium cation, in which six electrons are delocalised over three equivalent Y-shaped resonance forms. This is sometimes refered to as Y-aromaticity.[82] The symmetry is diminished for N-substituted guanidines which are, therefore, generally less basic as it was shown for a series of methylated guanidines.[83] Beside of this effect, basicities correspond well with Hammett inductive constants σ_I of the substituents.[84]

A significant property of substituted guanidines closely related to basicity is the tautomerism between imino and amino forms (**Scheme 1.10**). The tautomerisation equilibrium can be studied using ^{15}N NMR spectroscopy, as it was done for arginine[85] and N-arylguanidines.[86] In the case of amino acid arginine, in which guanidine moiety is substituted with an electron-donating alkyl chain, the imino-form was more populated. On the other hand, amino-form was preferred for guanidines with electron-withdrawing aryl substituents. Therefore, it can be concluded that for the most stable tautomer, imine nitrogen will be preferentially connected to the most electon-withdrawing substituent.

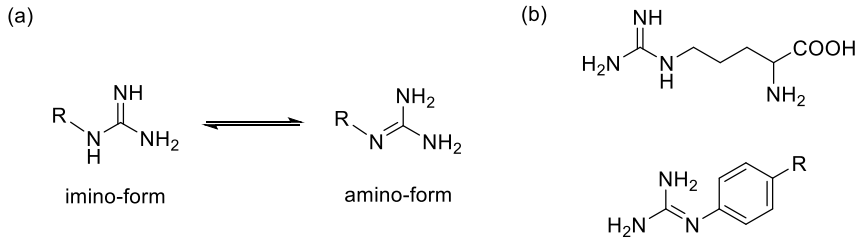

Scheme 1.10. (a) Tautomeric forms of *N*-substituted guanidines; (b) predominant tautomers of arginine (top) and arylguanidines (bottom).

Another distinctive feature of guanidines is their ability to support structures via intra- and intermolecular hydrogen bonds. In the case of guanidinium salts, it is indeed the key structure-building factor of the crystals.[87] By means of hydrogen bonding, guanidines can interact with and change conformation structures of substances,[88] or even redirect reactions by navigating the substrates into specific positions.[89]

Guanidines are usually synthesised by guanylation of the corresponding amines. A variety of guanylation reagents can be applied depending on the substrate (**Scheme 1.11**).[81, 90] Many of the most versatile reagents are based on activated ureas or thioureas. Methylation of thiourea with methyl iodide leads to isolable *S*-methylisothiouronium salt, which proved to be a generally applicable guanylation agent. It reacts with primary amines at room temperature, however, elevated temperatures are required for the reactions of secondary amines.[91] Even more active reagent is aminoiminomethanesulfonic acid, which can be obtained by thiourea oxidation. This reagent converts most of the amines into guanidines at room temperature and, since only mild conditions are required, it is also suitable for guanylation of amino acids.[92] These reagents can be utilised in the synthesis of both monosubstituted and polysubstituted guanidines.[83] Furthermore, pyrazole derivatives, namely 3,5-dimethyl-1-pyrazolylformaminidium nitrate[93] and 1*H*-pyrazole-1-carboxamidine hydrochloride,[94] give excellent yields of *N*-monosubstituted guanidines. On the other hand, *N,N',N''*-trisubstituted and *N,N,N',N''*-tetrasubstituted guanidines can be prepared by the reaction of amines with carbodiimides.[95] The reaction proceeds more readily when a catalytic amount of organometallic reagent such as diethylzinc or butyllithium is added.[96] Compared to hydroamination methods listed above, direct alkylations of guanidine moiety are of limited use.

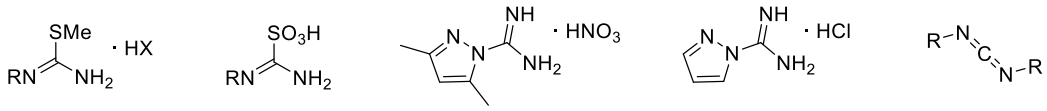

Scheme 1.11. Commonly used guanylation reagents.

Guanidines are widely applied as ligands in coordination chemistry. However, their mode of coordination strongly depends on the acid-base form of the guanidine (**Scheme 1.12**). Obviously, guanidinium cations cannot coordinate to metal centres since no donor atom is available for a dative bond formation. In contrast, neutral guanidines can coordinate by imine-type nitrogen to a vast variety of metal ions spanning from lithium, through late transition metals to main group elements.[97] However, in the most complexes, guanidine moiety is present in its deprotonated form, *i. e.*, as a guanidinate anion. Guanidinates are considered hard donors with a preference to coordinate hard metal centres. Numerous guanidinate complexes of main group and early transition metals have been described, in which guanidinate binds as

a monodentate, chelating or bridging ligand.[98] Conversely, guanidinate complexes with late transition metals are still uncommon.[99]

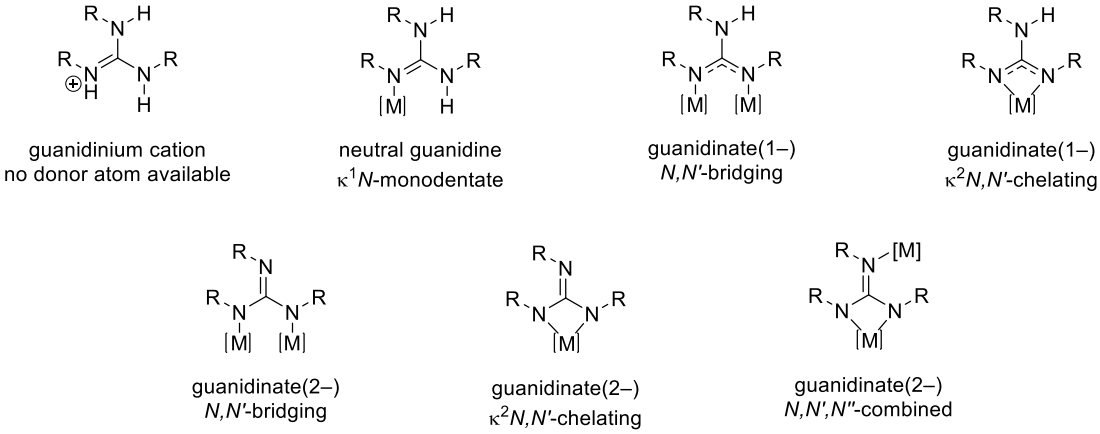

Scheme 1.12. Possible coordination modes of different guanidine forms.

Various hybrid donors can be designed by combining guanidine moiety with additional donor groups. Guanidines with adjacent nitrogen-containing donor groups are possibly the most investigated class of guanidine-based hybrid ligands. Compounds equipped with pyridine substituents, aliphatic amines or cyano group were prepared and studied as ligands in transition metal complexes.[100] Guanidine-substituted thiolates were reported to form polynuclear complexes with copper(II).[101] Specifically, arylguanidines can act as N,C-chelating donors as it was demonstrated in cyclometallated palladium(II) and platinum(II) complexes.[102]

In the case of guanidine-substituted phosphines, two series of ligands should be distinguished. First one comprises phosphines bearing a cationic guanidinium tag that have been extensively studied as hydrophilic ligands in catalysis in polar media (**Scheme 1.13**). The chemistry of these derivatives started to develop in the 1990s, when [(3-guanidinium)propyl]phenylphosphines (**XXV**) were prepared and studied as catalysts for the Heck reaction in water.[103] Especially high activities, exceeding that of TPPTS, exhibited these ligands in Castro-Stephens coupling in aqueous acetonitrile.[104] Later, guanylated triphenylphosphines (**XXVI** and **XXVII**) were prepared and their catalytic activity was examined in Castro-Stephens coupling,[104] in Sonogashira coupling in water,[105] and in Suzuki-Miyaura cross-coupling performed in aqueous ethyleneglycol.[106] Chiral phosphinoguanidinium salts derived from BINAP (**XXVIII**) were evaluated in asymmetric hydrogenation reactions,[107] while diphosphine guanidinium salts based on xanthene backbone (**XXIX**) showed good activities and high regioselectivities in hydroformylation of oct-1-ene performed in ionic liquids. The catalyst immobilised in ionic liquid could be recycled and used for several subsequent runs.[108] Recently, two types of ferrocene-based guanidinium phosphines, in which the guanidinium tag was

connected to ferrocene scaffold by amide (**XXX** and **XXXI**) or by methylene linker (**XXXII**), and their palladium(II) complexes were prepared. Their catalytic activity was probed in Suzuki-Miyaura-type cross-coupling in aqueous reaction mixtures.[109]

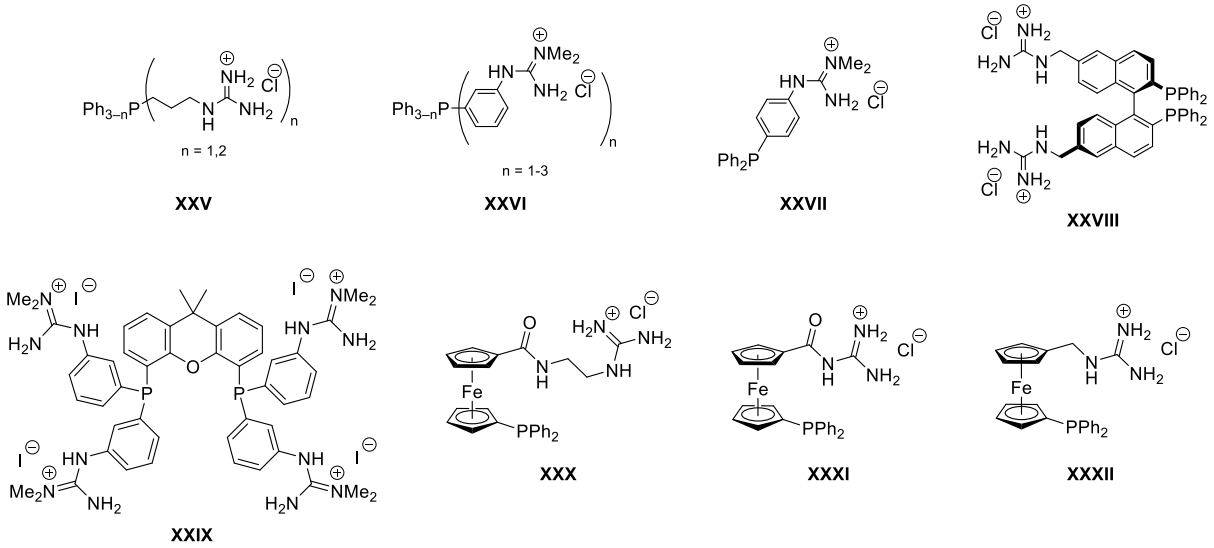

Scheme 1.13. Guanidinium-substituted phosphines.

Second group of ligands consists of phosphines bearing *neutral* guanidine substituents (**Scheme 1.14**). First examples of these ligands were diorganophosphinous-*N*-(*N*',*N*',*N*'',*N*''-tetramethyl)guanidines and organophosphonous-bis-*N*-(*N*',*N*',*N*'',*N*''-tetramethyl)guanidines (**XXXIII** and **XXXIV**), in which guanidine moiety is directly bonded to the phosphorus atom. Coordination chemistry of these compounds with transition metal carbonyls was studied. In most cases, these compounds acted as P-monodentate ligands with the exception of a tricarbonylmolybdenum(0) complexes wherein they coordinated as P,N-chelating and P,N,N-bis-chelating ligands.[110] Stelzer described triphenylphosphine derivative equipped with a guanidine fragment in *meta*- and *para*-position of the phenyl ring. However, he only used these phosphines as intermediates in the synthesis of the corresponding guanidinium salts mentioned above.[106] On the other hand, triphenylphosphine functionalised with guanidine in *ortho*-position (**XXXV**) was used to study rhenium(I)-formyl bond formation. In this particular case, the guanidine tag served as a base assisting the heterolytic hydrogen cleavage.[111] Only recently, guanidine attached by an ethylene spacer to PPh_2 group (**XXXVI**) was formed *in situ* and immediately coordinated to (pentamethylcyclopentadienyl)rhodium(III) fragment. Subsequent chloride abstraction and deprotonation provided P,N,N-bis-chelate complex. It was also demonstrated that this complex is able to cleave hydrogen and reversibly deprotonate water.[112]

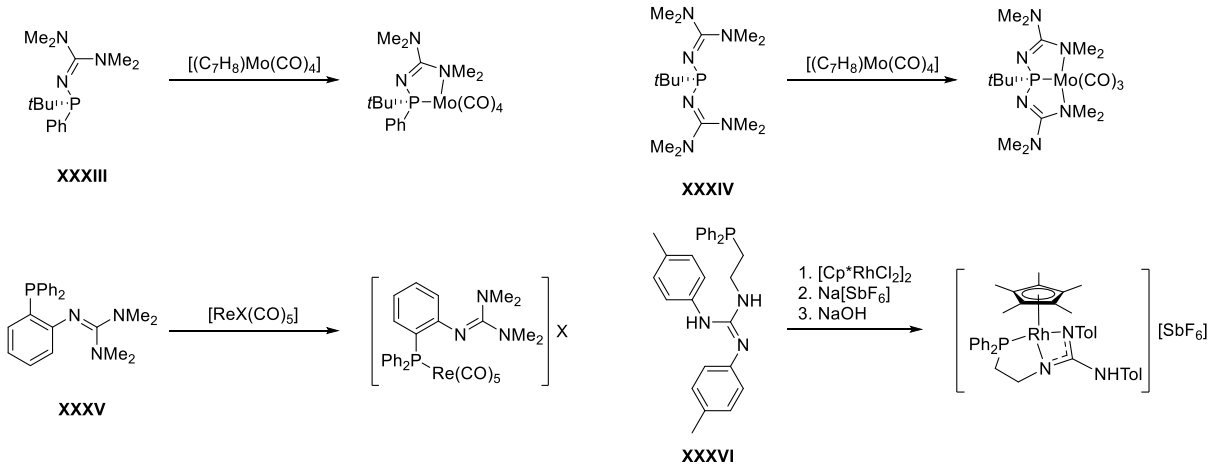

Scheme 1.14. Neutral phosphinoguanidines and their complexes.

It is apparent, that guanidine phosphines have been studied only scarcely thus far, although, as it can be deduced from the reported examples, they possess a great potential for application in catalysis either as highly polar or cooperating ligands. Preparation of new ligands of this type (and their complexes) leading to a better understanding of these compounds is necessary for this potential to be explored and adequately exploited.

2. Aims of the Thesis

The research presented in this Thesis targets on the synthesis and characterisation of novel ferrocene-based phosphines equipped with additional guanidine functional substituents. It is motivated by the lack of examples and information about this type of ligands – not only in ferrocene chemistry, but in general. Literature search revealed that the reported examples of these compounds can be generally divided into two categories, *i. e.*, phosphines with cationic guanidinium pendants and neutral phosphinoguanidines, as illustrated in the Introduction. Following this categorisation, two series of new ferrocene derivatives were designed (**Scheme 2.1**).

Ligands of *Series A* are ferrocene phosphines bearing flexible guanidinium pendants and were proposed as a continuation of my previous work, during which phenyl-substituted derivative (compound **XXXII** in **Scheme 1.13**) was prepared and characterised.[109b] This ligand provided promising results in preliminary catalytic tests. Therefore, I decided to build upon this topic and to prepare a series of ligands differing by their phosphine substituents with the aim to find a general and reliable synthetic route to these donors. The next goal was to evaluate these ligands in common metal-catalysed reactions such as Suzuki-Miyaura-type cross-couplings or hydroformylation with emphasis on the effect of the guanidinium tag and phosphine substituents on catalytic performance of these compounds.

Ligands of *Series B* were designed in view of the so far insufficient research on neutral phosphinoguanidines and, additionally, on 1,1'-substituted ferrocene-based P,N-donors with nitrogen atom directly attached to the ferrocene backbone. It was inspired by their donor-symmetric analogues, namely by dppf (compound **III** in **Scheme 1.4**) and ferrocene bis(guanidines).[75b] The ligands of this series were proposed as new donor-unsymmetric P,N-hybrid ligands, the first of their kind. The main goal was to develop a convenient synthetic pathway to these ligands and, subsequently, to study their coordination behaviour towards palladium(II) precursors with a focus on the possible coordination modes of these potentially polydentate ligands.

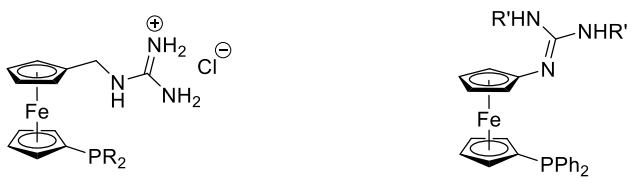

Series A *Series B*

Scheme 2.1. Ligands discussed in this Thesis.

3. Summary of the results

3.1 Phosphinonitriles R_2PfcCN as intermediates on the way to ligands of Series A and as ligands for gold(I)-catalysis

Phosphinoamines of the formula $R_2PfcCH_2NH_2$ (**1**, fc = ferrocene-1,1'-diyl) are crucial intermediates in the synthesis of phosphinoguanidines of *Series A*. The original phenyl-substituted derivative **1c** was prepared by a multi-step procedure (**Scheme 3.1**).[63a] In the first step, diphenylphosphino group was introduced by lithiation and phosphinylation of 1,1′-dibromoferrocene. In the following step, the second cyclopentadienyl ring was formylated to produce an aldehyde, which was subsequently converted into an oxime. The reduction of the oxime ultimately provided **1c**, which was isolated as a hydrochloride. However, this procedure, despite it proved reliable for the synthesis of **1c**, could bring several drawbacks when considering the synthesis of compounds with varied phosphine substituents. The most striking issue is that the most sensitive group, *i. e.*, the phosphine moiety, is installed already during the first step, which could require additional protecting and deprotecting steps, especially in the case of alkyl-phosphines which are prone towards oxidation.

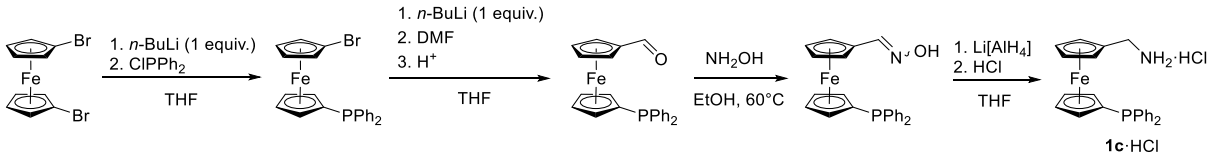

Scheme 3.1. The original synthesis of phosphinoamine **1c**.

Therefore, an alternative and more general procedure was proposed and applied, which was based on phosphinonitriles **5** as precursors of phosphinoamines **1** (**Scheme 3.2**). Lithiation of 1,1'-dibromoferrocene (**2**) with 1 equivalent of *n*-butyllitihium followed by cyanation with *p*-tosyl cyanide provided, after column chromatography and crystallisation, stable bromonitrile **3**[113,72d] in 75% yield. This reaction sequence could be performed on a multigram scale and **3** is, therefore, easily accessible starting material for further syntheses. Additionally, a compound of intense purple colour, which is rather uncommon for ferrocene derivatives, was isolated as a minor side-product of the aforementioned reaction. This compound was identified by X-ray diffraction analysis as *N*-[bis(1'-bromoferrocenyl)methylene]cyanamide (**4**). Its formation could be explained by the reaction of lithiated bromoferrocene with **3** present in the reaction mixture followed by the reaction of the resulting imine salt with *p*-tosyl cyanide. This side-reaction is affected by the concentration of the reaction mixture and is suppressed in diluted solutions.

The bromonitrile **3** was converted by the standard lithiation/phosphinylation sequence into a series of phosphinonitriles **5** with varied substituents at the phosphorus atom. This series

included a pair of phosphines with electronically and sterically similar electron-donating alkyl groups, namely *iso*-propyl (**5a**) and cyclohexyl (**5b**), and a pair of compounds with flat, conjugated, electron-withdrawing aryl groups, specifically phenyl (**5c**)[72a] and 2-furyl (**5d**), as the phosphine substituents. All of these compounds were isolated as air-stable crystalline solids in good to excellent yields after column chromatography and crystallisation. Subsequently, they were employed in the synthesis of phosphinoamines **1** (see section 3.2).

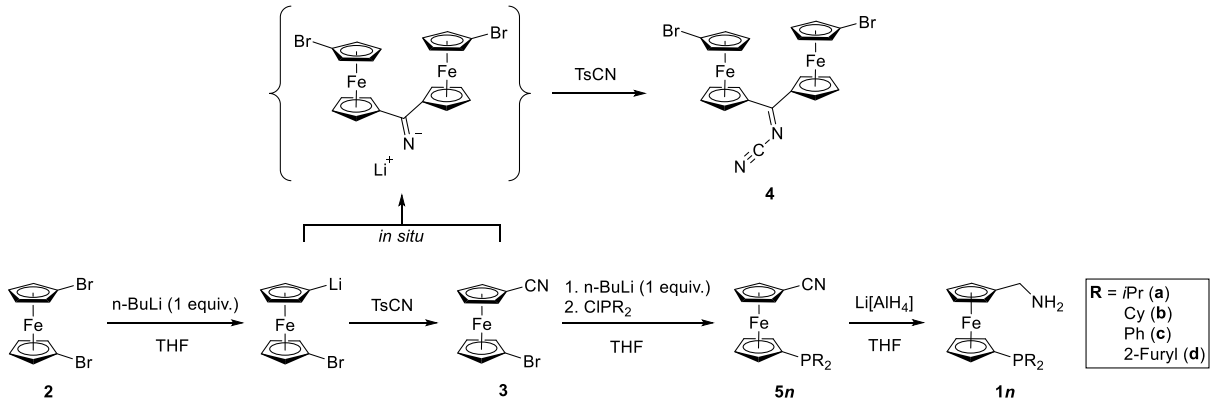

Scheme 3.2. The synthesis of phosphinoamines **1** employing phosphinonitriles **5** as the key intermediates.

Moreover, with the electronically distinct phosphines **5** in hands and inspired by successful applications of the phenyl-substituted congener **5c** in gold(I)-mediated catalysis,[72b,73] the influence of phosphine substituents on the catalytic properties of these ligands was assessed. For this purpose, dimeric, self-stabilised gold(I) complexes **7** were prepared as precatalysts by a two-step procedure (**Scheme 3.3**). The phosphinonitriles **5** were reacted with chloro(tetrahydrothiophene)gold(I) to almost quantitatively produce complexes **6**. Subsequent chloride removal with silver(I) hexafluoroantimonate resulted in the formation of dimeric complexes **7** as bench-stable gold(I) precatalysts stabilised by nitrile coordination. Additionally, the reaction of phosphinonitriles **5** with potassium selenocyanate[114] provided the corresponding phosphinoselenides **8**.

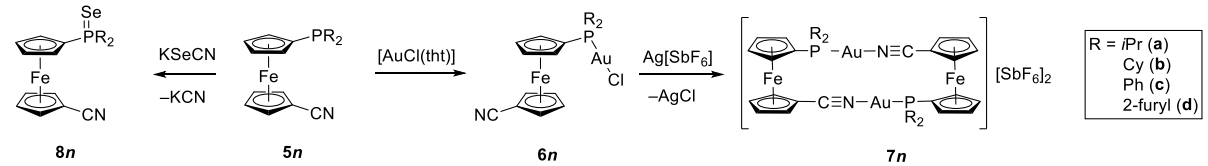

Scheme 3.3. Preparation of precatalysts **7** and phosphinoselenides **8**.

All newly prepared compounds were characterised by standard spectroscopic methods. Additionally, molecular structures of compounds **5d**, **6d**, **7d** (structures of this furyl-substituted compounds are depicted in **Figure 3.1**), **6a**, **6b** and **7b** were determined by single-crystal X-ray diffraction analysis. For details and structural parameters see *Appendix A*.

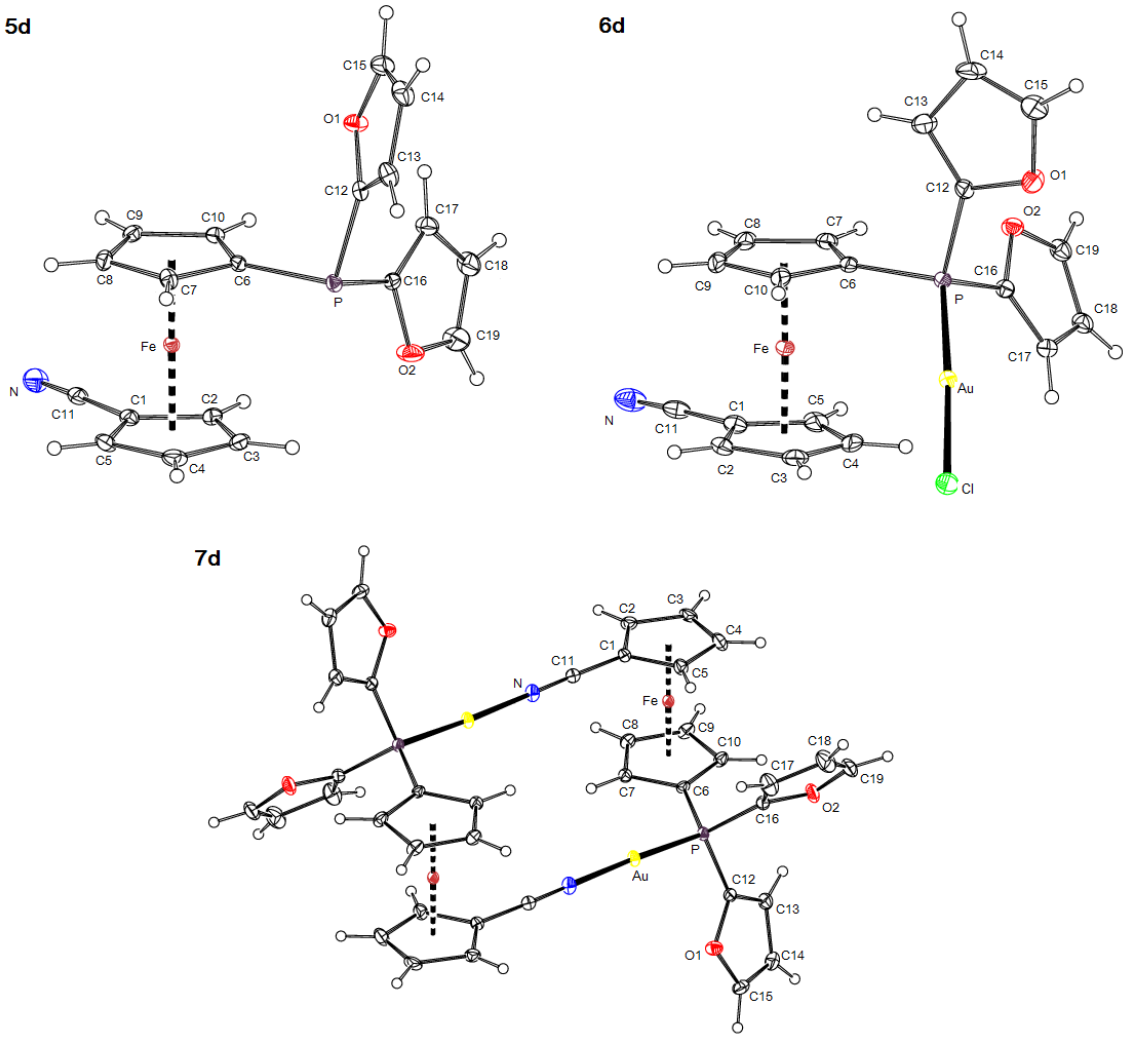

Figure 3.1. ORTEP drawings of the molecular structures of compounds **5d**, **6d** and of the cation of **7d**. Displacement ellipsoids enclose the 30% probability level.

The electronic properties of phosphines **5** were assessed through several parameters (**Table 3.1**). The interaction constants $^{1}J_{PSe}$ of selenides **8** indicated that, due to the presence of electron-withdrawing nitrile group, phosphines **5** were poorer σ-donors than their respective unsubstituted analogues $FcPR_2$ (Fc = ferrocenyl), and that furyl-substituted phosphine **5d** was the least donating derivative in the series, whereas cyclohexyl-substituted phosphine **5b** was the best σ-donor. This conclusion was further supported by ν_{CN} stretching frequencies for complexes **7**. The highest value for complex **7d** suggested that the shift of electron density from weakly anti-bonding molecular orbital to σ-donating lone pair of the nitrile group coordinated to gold(I)

cation was the most significant in this complex, compensating the influence of the π-accepting phosphine group. This was in agreement with a loss of the stabilisation energy for dimer dissociation E_{dis} obtained by DFT calculations.

Table 3.1. Selected parameters illustrating properties of compounds **5**, **7** and **8**.

Parameter	Ligand				
	5a	**5b**	**5c**	**5d**	PPh_3
k [10^{-3} min^{-1}] [a]	20.8(2)	20.2(2)	32.5(7)	32.9(10)	25.7(7)
ν_{CN} for **5** [cm^{-1}] [b]	2224	2225	2225	2228	–
ν_{CN} for **7** [cm^{-1}] [b]	2263	2256	2273	2274	–
E_{dis} for **7** [kcal mol^{-1}] [c]	27.4	26.8	29.4	32.9	–
$^1J_{PSe}$ for **8** [Hz] [d]	715	708	741	777	735 [e]
$^1J_{PSe}$ for $FcPR_2(Se)$ [Hz] [f]	700	n. a.	733	769	–

[a] Rate constants of the gold(I)-catalysed cyclisation of propargyl amides **9** determined from fitting the kinetic profile in the range of 10-60 min. [b] IR spectra recorded in Nujol mulls. [c] Dissociation energies of isolated dimeric cations calculated by DFT. [d] NMR spectra recorded in $CDCl_3$. [e] Data adopted from ref. [115]. [f] Data adopted from ref. [116].

Gold(I)-mediated cyclisation of *N*-propargyl amides (**9**) into 2-substituted 5-methyleneoxazolines (**10**)[117] was selected as a model reaction for catalytic studies with complexes **7** (**Scheme 3.4**). Using 1 mol.% of the Au(I) precatalyst, the cyclisation of the prototypical phenyl-substituted substrate **9a** was completed at room temperature within 3 hours for all precatalysts **7**. However, the phosphine substitution had a substantial impact on the reaction kinetics (**Figure 3.2**). The reaction rate qualitatively correlated with the donor properties of the phosphines. The precatalysts with the less donating phosphines (**7d** and **7c**) reacted significantly faster than their electron-rich analogues (**7a** and **7b**). Interestingly, when the archetypal complex $[Au(MeCN)(PPh_3)][SbF_6]$[118] was used as the precatalyst, the reaction rate was just in between the values obtained for the aforementioned two groups of complexes **7**, as could be predicted by comparing the interaction constants $^1J_{PSe}$.

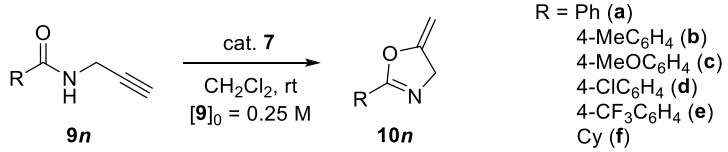

Scheme 3.4. Gold(I)-mediated cyclisation of *N*-propargyl amides (**9**) into 2-substituted 5-methyleneoxazolines (**10**).

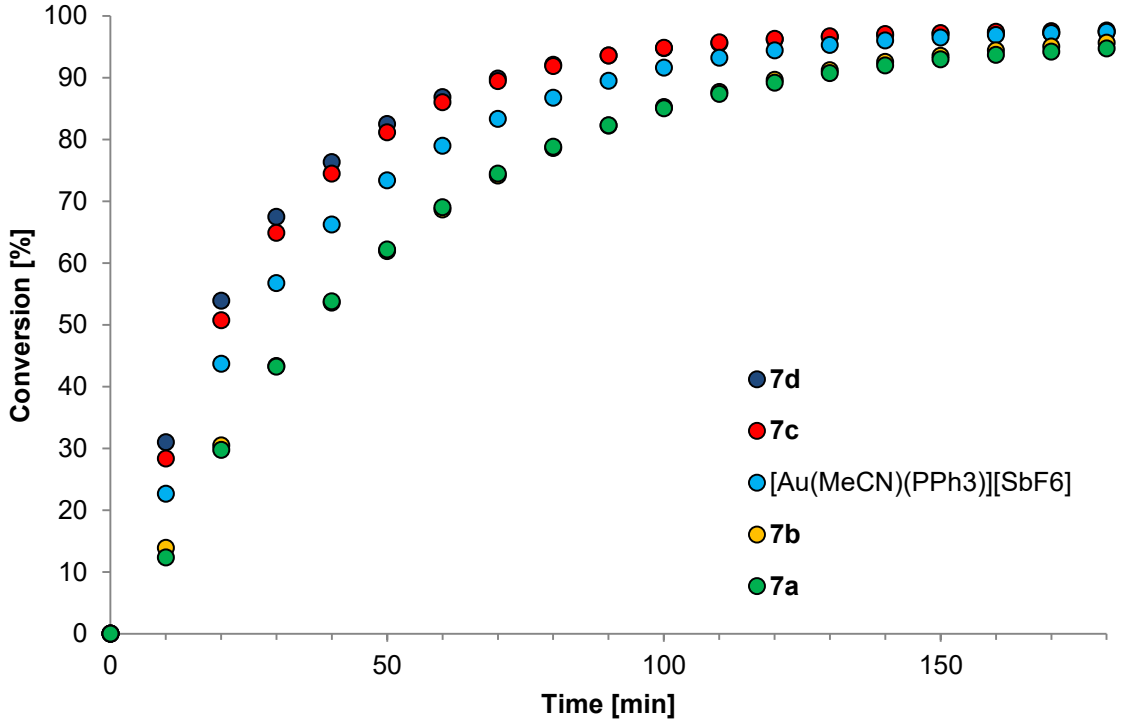

Figure 3.2. Kinetic profiles of the cyclisation of **9a** to **10a** catalysed by different Au(I) catalysts. Conditions: $[\mathbf{9a}]_0$ = 0.25 M in CD_2Cl_2, 25 °C, [Au] = 1 mol. %.

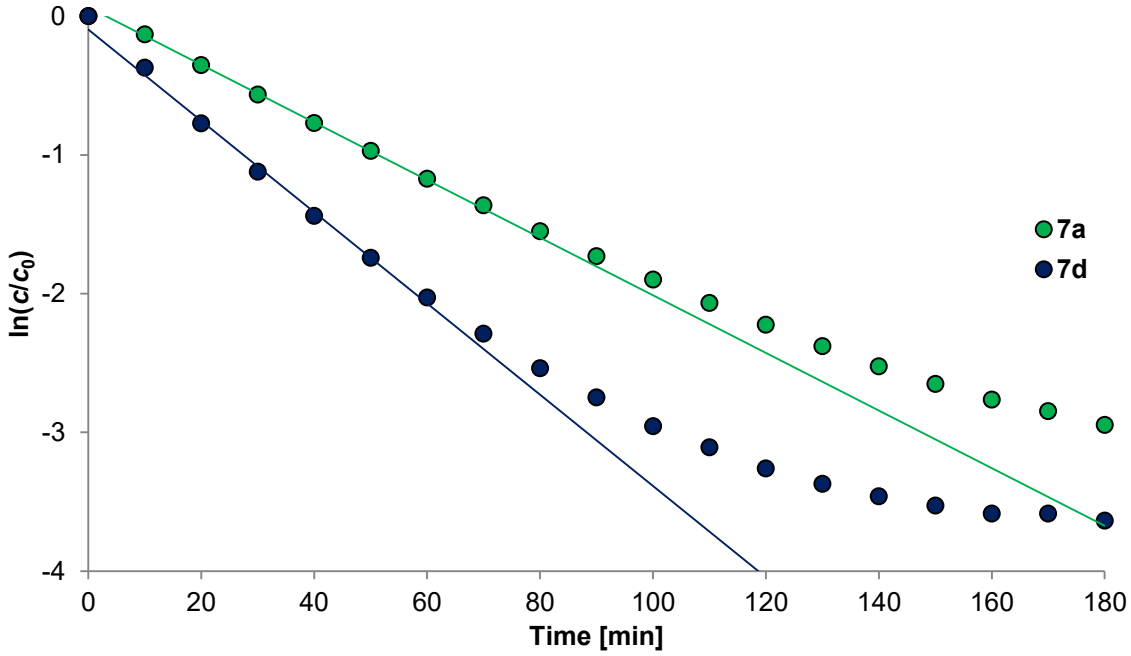

Figure 3.3. Kinetic plots ($\ln(c/c_0)$ vs. time) for cyclisation of **9a** with precatalysts **7a** and **7d** demonstrating the departure from the ideal first-order profile at extended reaction times.

The kinetic profiles indicated that the cyclisation was a first-order reaction with respect to the amide substrate. However, a departure from an ideal profile was observed at higher conversions suggesting a partial decomposition of the catalyst, especially for the electron-poor phosphines (**Figure 3.3**). This assumption was confirmed by another experiment, in which an additional equivalent of substrate **9a** was added to the reaction mixture with **7d** as the catalyst after 1 hour (at that time, nearly 90% conversion of the initial equivalent of **9a** was achieved). The cyclisation of the second equivalent of **9a** proceeded at a slower rate (approximately a half of the original value).

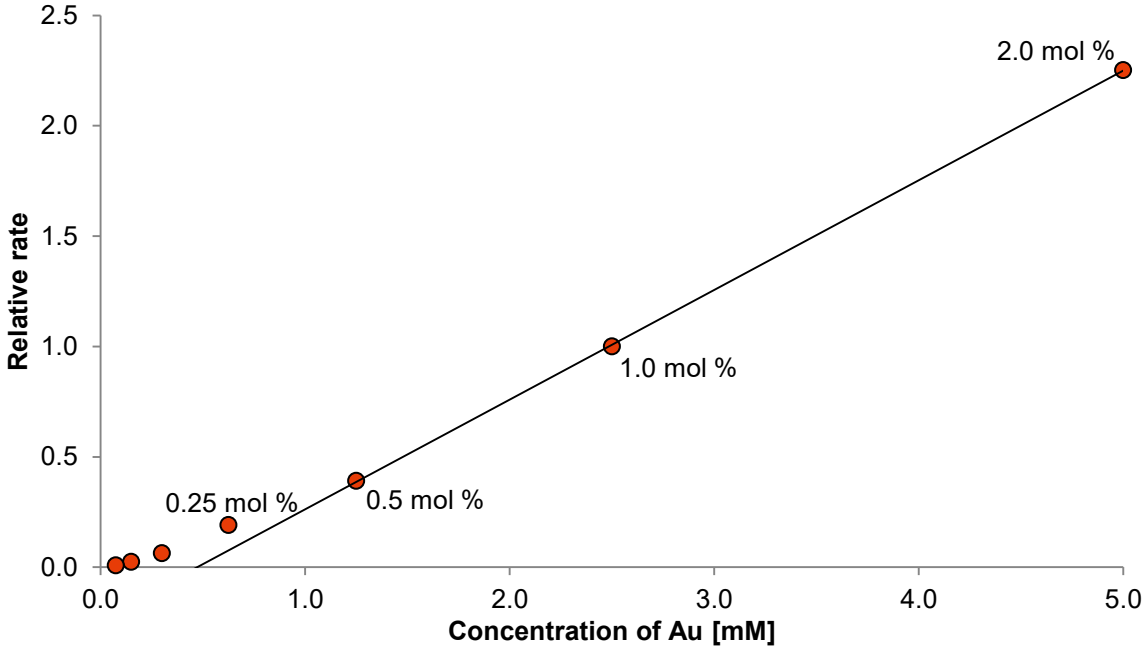

Figure 3.4. The dependency of the reaction rate for cyclisation of **9a** on gold concentration.

Expectedly, lowering of the catalyst loading slowed down the reaction but, interestingly, no threshold concentration, under which the reaction would stop, was found. The cyclisation of **9a** was initiated with as little as 0.03% of Au(I) when using **7d** as precatalyst (**Figure 3.4**). Conversely, the reaction did not proceed in the presence of strongly coordinating chloride anions, presumably due to regeneration of catalytically inactive complexes **6**.

In summary, complexes **7** proved to be unique self-stabilised and highly active precatalysts for gold(I)-catalysed reactions, whose catalytic properties could be fine-tuned through phosphine substitution.

3.2 The phosphinoguanidinium ligands of Series A – synthesis and catalytic properties

The reduction of phosphinonitriles **5** with lithium aluminium hydride provided phosphinoamines **1** in nearly quantitative yields. However, these compounds were poorly

defined hygroscopic materials prone towards oxidation and, therefore, were immediately used for the reaction with 1*H*-pyrazole-1-carboxamidine hydrochloride in the presence of triethylamine to produce phosphinoguanidinium chlorides **11** in good yields (around 70% over two steps) after purification by column chromatography and crystallisation (**Scheme 3.5**). Phosphines **11** were isolated as well-defined crystalline solids and no oxidation was observed upon storing for several months. The compounds were characterised by common spectroscopic techniques and the molecular structures of the *iso*-propyl- and of the furyl-substituted derivatives (**11a** and **11d**) were determined by single-crystal X-ray diffraction (**Figure 3.5**).

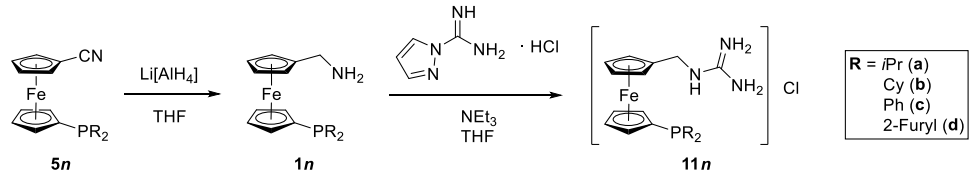

Scheme 3.5. The preparation of phosphinoguanidinium chlorides **11**.

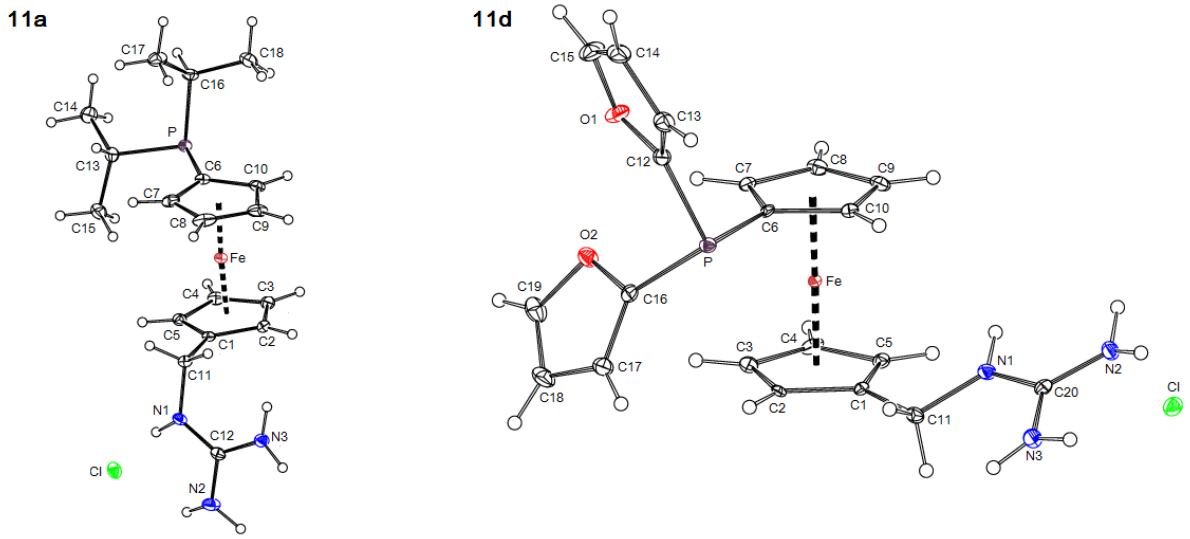

Figure 3.5. ORTEP diagrams of the molecular structures of ligands **11a** and **11d**. Displacement ellipsoids are scaled to the 30% probability.

Phosphines **11** were further reacted with di-μ-chloro-tetracarbonyldirhodium(I) to produce rhodium(I) complexes **12** which were isolated in essentially quantitative yields as slightly hygroscopic, poorly soluble solids (**Scheme 3.6**). The carbonyl stretching frequencies ν_{CO} of complexes **12** served as a measure of donor properties of phosphines **11** and the values 1946 (**12b**) ≈ 1947 (**12a**) < 1970 (**12c**) < 1982 (**12d**) cm^{-1} indicated a decrease in the donor ability with increasing electron-withdrawing nature of the phosphine substituent.

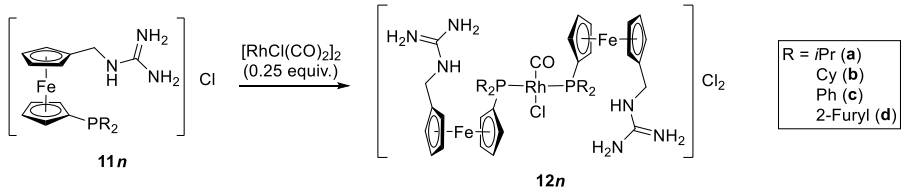

Scheme 3.6. The preparation of rhodium(I) complexes **12**.

Phosphinoguanidinium chlorides **11** were employed as supporting ligands in palladium-catalysed Suzuki-Miyaura-type reactions. The catalytic properties of **11** were initially probed in a reaction between aromatic acyl chlorides and boronic acids producing substituted benzophenones.[119] In a model reaction, *p*-toluoyl chloride was reacted with 4-(trifluoromethyl)phenyl boronic acid in the presence of sodium carbonate as a base and 0.1 mol.% of a catalyst generated *in situ* from palladium(II) acetate and the selected phosphine in a vigorously stirred C_6D_6/water mixture at 50°C for 1 hour. The conversion was then evaluated by quantitative ^{19}F NMR using (trifluoromethyl)benzene as an internal standard. In the absence of a phosphine ligand, the reaction proceeded rather poorly. The yield increased rapidly, when a phosphine was introduced, however, the performance of ligands **11** was only comparable with that of simple phosphines such as triphenylphosphine (**Table 3.2**).

Table 3.2. NMR yields for the model reaction of *p*-toluoyl chloride with 4-(trifluoromethyl)phenyl boronic acid using various *in situ* generated catalysts (the yields reported are an average of two independent runs).

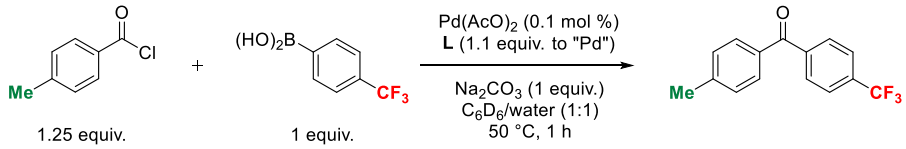

Catalytic system	NMR yield	Catalytic system	NMR yield
$Pd(AcO)_2$	30%	$Pd(AcO)_2$/**11a**	80%
$Pd(AcO)_2/PPh_3$	83%	$Pd(AcO)_2$/**11b**	84%
$Pd(AcO)_2/PCy_3$	85%	$Pd(AcO)_2$/**11c**	93%
$Pd(AcO)_2/FcPPh_2$	86%	$Pd(AcO)_2$/**11d**	**95%**

The conversions obtained within the series of ligands **11** indicated the correlation with donor properties of the phosphine since the reaction proceeded best in the presence of the least donating phosphine and *vice versa*. Unfortunately, no clear trend was confirmed in the subsequent study with different substrates (**Table 3.3**). Actually, the observed conversions

suggested that in each case the reaction outcome resulted from a complicated interplay between electronic properties of the substrates and electronic and steric properties of the ligands. Nevertheless, in all cases conversions of 65% or higher were achieved. Among the ligands **11**, the catalytic system based on phenyl-substituted phosphine **11c** provided the most uniform results. As for the substrates, the reactions proceeded generally better with electron-poor 4-(trifluoromethyl)phenyl boronic acid. Conversely, lower conversions were typically achieved in the reactions of trifluoromethyl-substituted benzoyl chlorides.

Table 3.3. The evaluation of the influence of the phosphine ligands **11** on the cross-coupling of various aroyl chlorides with boronic acid (the yields reported are an average of two independent runs).

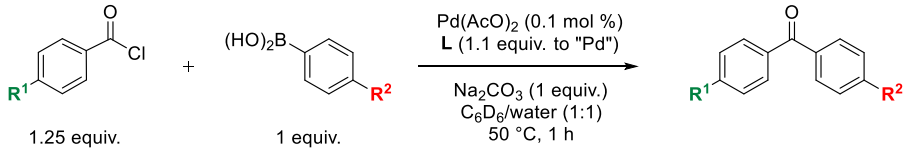

R¹	R²	Ligand/NMR Yield			
		11a	**11b**	**11c**	**11d**
Me	CF_3	80%	84%	93%	**95%**
CF_3	Me	**82%**	71%	81%	70%
H	CF_3	**89%**	82%	88%	81%
CF_3	H	69%	72%	**74%**	66%
CF_3	CF_3	89%	85%	87%	**91%**

Surprisingly, the results obtained for the "classical" Suzuki-Miyaura cross-coupling between boronic acids and aryl bromides producing substituted biphenyls performed under the same reaction conditions were quite different (**Table 3.4**). Negligible conversions were obtained when the reaction was catalysed with unsupported palladium(II) acetate and the yields remained low even when electron poor aryl-substituted phosphines were added. On the other hand, in the presence of electron-rich alkyl-substituted phosphines, the yields increased significantly. The best results were obtained with the cyclohexyl-substituted ligand **11b**, which can be attributed to a combined effect of the strongly donating bulky phosphine group and the hydrophilic guanidinium tag (the conversions achieved with tricyclohexylphosphine were notably lower).

Table 3.4. Suzuki-Miyaura cross-coupling catalysed by various *in situ* generated catalysts (the yields reported are an average of two independent runs).

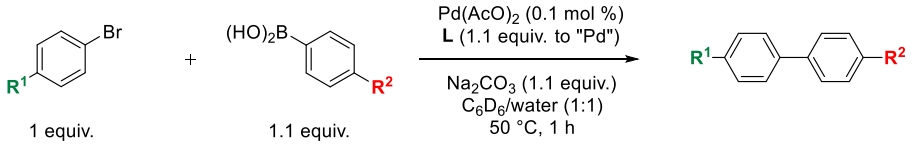

Catalytic system	Substrates/NMR Yield	
	R¹ = Me, **R²** = CF_3	**R¹** = CF_3, **R²** = Me
$Pd(AcO)_2$	<1%	5%
$Pd(AcO)_2/PPh_3$	6%	25%
$Pd(AcO)_2/PCy_3$	38%	29%
$Pd(AcO)_2/FcPPh_2$	8%	56%
$Pd(AcO)_2$/**11a**	**52%**	75%
$Pd(AcO)_2$/**11b**	47%	**91%**
$Pd(AcO)_2$/**11c**	14%	34%
$Pd(AcO)_2$/**11d**	9%	7%

In addition to the aforementioned palladium(II)-catalysed reactions, phosphines **11** were also tested in rhodium(I)-catalysed hydroformylation of 1-hexene employing defined complexes **12** as precatalysts. The reactions were performed at a hexene-to-rhodium ratio of 400 without *any* additional co-catalyst under 10 bar of synthesis gas at 80 °C for 5 hours. Disappointingly, the conversions were negligible (below 10%) for the reactions performed in neat 1-hexene, toluene or water. Substantially better results were obtained when dimethylsulfoxide was used as a solvent, presumably due to increased solubility of precatalysts **12**. In DMSO, almost quantitative conversions were achieved for the most of the catalyst with the exception of the furyl-substituted compound **12d**, for which dissociation of weakly coordinating phosphine group presumably led to catalyst deactivation (**Table 3.5**). In all cases, heptanals were produced with a high selectivity; the fraction of the isomerised product, *i. e.*, 2-hexene, was below 4%. The selectivities towards the linear aldehydes were rather moderate and were affected by donor ability of the phosphine ligands. Electron-poor phosphines in **12c** and **12d** favoured the formation of linear products, whereas precatalysts **12a** and **12b** featuring electron-rich phosphine moieties led to formation of almost equal amounts of linear and branched products. Expectedly, increasing a hexene-to-rhodium ratio led to the decrease of achieved conversions, albeit without the loss of selectivity.

Table 3.5. The results of the hydroformylation experiments. Conditions: 0.75 mL 1-hexene (6 mmol), dimethyl sulfoxide (0.75 mL), 10 bar of syngas (H_2/CO = 1:1), 80 °C, reaction time 5 h.

Catalyst	1-Hexene:Rh	Conv. [%]	2-Hexene [%]	Aldehydes [%]	*n*/*iso*
12a	400	95	1	94	1.1
12a	800	92	2	92	1.1
12a	1600	8.4	0.1	8.3	1.4
12b	400	99	1	98	1.1
12b	800	85	1	84	1.1
12b	1600	51	1	50	1.2
12c	400	99	4	95	2.2
12c	800	93	4	89	2.3
12c	1600	47	1	46	2.6
12d	400	59	2	57	2.6
12d	800	53	1.3	52	2.7
12d	1600	43	1	42	2.8

3.3 The phosphinoguanidine ligands of Series B – synthesis and coordination chemistry

Inspired by the previously published *N,N',N''*-trisubstituted ferrocenyl guanidines,[120] phosphinylated analogues of these compounds, ligands **13**, were proposed as new donor-unsymmetric, hybrid P,N-ligands. Initially, phosphinoguanidines **13** were synthesised following the procedure employed for their non-phosphinylated analogues.[121,120] Thus, phosphinoamine **14** was reacted with the corresponding carbodiimide in the presence of a catalytic amount of diethylzinc in toluene at 50 °C. However, compared to the original report, higher amounts of the catalyst and longer reaction times were required, especially in the reactions with carbodiimides bearing bulky substituents. Therefore, complementary procedure was applied, in which amine **14** was firstly deprotonated with *n*-butyllithium to form an amide salt, which was in turn reacted with the carbodiimide to cleanly and rapidly produce the target compounds (**Scheme 3.5**). Both procedures afforded phosphinoguanidines **13** in good yields as air-stable crystalline materials – *iso*-propyl-substituted **13a** and 2,6-xylyl-substituted **13c** – or as an amorphous solid – cyclohexyl-substituted **13b**. The compounds were characterised by the common spectroscopic techniques and the molecular structures of **13a** and **13c** were determined (**Figure 3.6**).

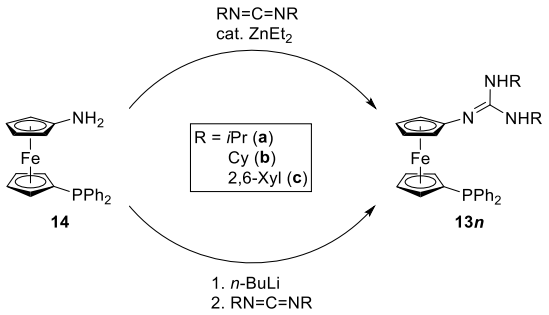

Scheme 3.5. The synthesis of phosphinoguanidines **13**.

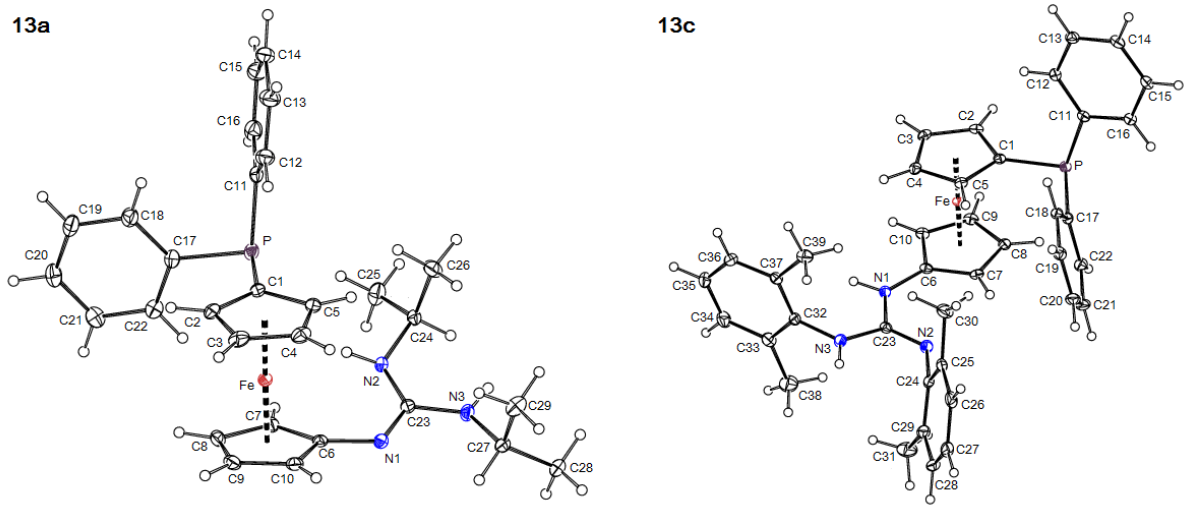

Figure 3.6. Molecular structures (ORTEP) of ligands **13a** and **13c** with the 30% probability displacement ellipsoids.

In the case of the xylyl-substituted compound **13c**, the imino-form **13c'** was the more stable tautomer in the solid state, as confirmed by the X-ray structural analysis. In solution, however, an equilibrium between the tautomeric forms was observed at room temperature (**Scheme 3.6**). VT NMR experiments showed that at low temperatures (0 °C or below), the imino-form **13c'** was the only tautomer present in the mixture. Upon increasing temperature, however, a dynamic equilibrium with the amino-form **13c** was established, which resulted in an averaging of the NMR signals. Notably, only the amino-form was observed for the compounds **13a** and **13b**. This could be rationalised assuming that the alkyl-substituted nitrogen atoms in **13a** and **13b** are more basic than the ferrocenyl-substituted one, favouring the amino-form. On the other hand, in **13c** all guanidine substituents are aromatic and, consequently, the nitrogen atoms are of roughly similar basicity, which gives rise to a more dynamic system.

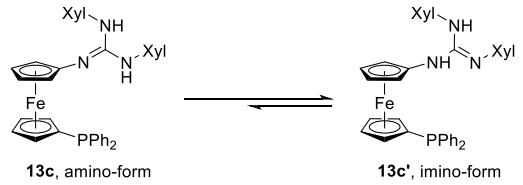

Scheme 3.6. Tautomeric forms of the xylyl-substituted phosphinoguanidine **13c**.

The coordination preferences of ligands **13** were probed *via* reactions with palladium(II) precursors. In the reaction with 1 equivalent of $[PdCl_2(MeCN)_2]$, phosphinoguanidines **13a** and **13b** provided selectively the *cis*-chelated complexes **15a** and **15b** (**Scheme 3.7**). These complexes were isolated as crystalline solids and their structures were confirmed by single-crystal X-ray diffraction (**Figure 3.7**). The same reaction employing ligand **13c** provided a mixture of three major species, possibly due to the increased steric bulkiness of the ligand. The products were identified as the expected *cis*-chelate product **15c**, the chloride-bridged dimer $[PdCl(\mu\text{-}Cl)(\mathbf{13c}\text{-}\kappa P)]_2$, and the cationic complex $[PdCl(\mathbf{13c}\text{-}\kappa^3 P,N,Fe)]Cl$. Unfortunatelly, none of these complexes could be isolated in a pure form.

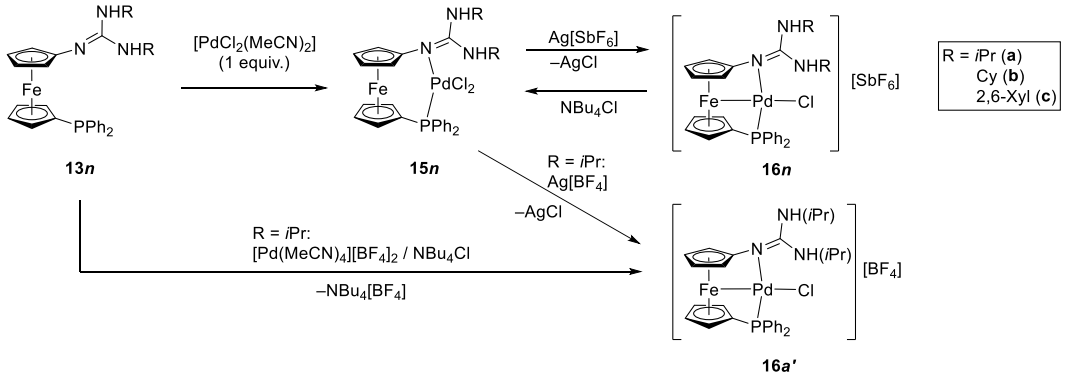

Scheme 3.7. The preparation of the palladium(II) complexes **15** and **16**.

The reactions of complexes **15a** and **15b** with silver(I) salts resulted in the formation of cationic complexes **16a**, **16a'** and **16b**, in which the loss of one of the chloride ligands is compensated by Fe→Pd dative interaction (**Scheme 3.7**). Complex **16a'** was alternatively prepared by the reaction of **13a** with $[Pd(MeCN)_4][BF_4]_2$ in the presence of NBu_4Cl as the chloride source. Analogous complex **16c** was prepared by adding $Ag[SbF_6]$ to the mixture of **13c** and $[PdCl_2(MeCN)_2]$ (note that the intermediate complex **15c** could not be isolated). The reactions of complexes **16** with 1 equivalent of NBu_4Cl regenerated complexes **15** with the exception of complex **16c**, for which the same mixture of species as described above was obtained. Complexes **16** were isolated as crystalline solids in good yields (typically around 70%).

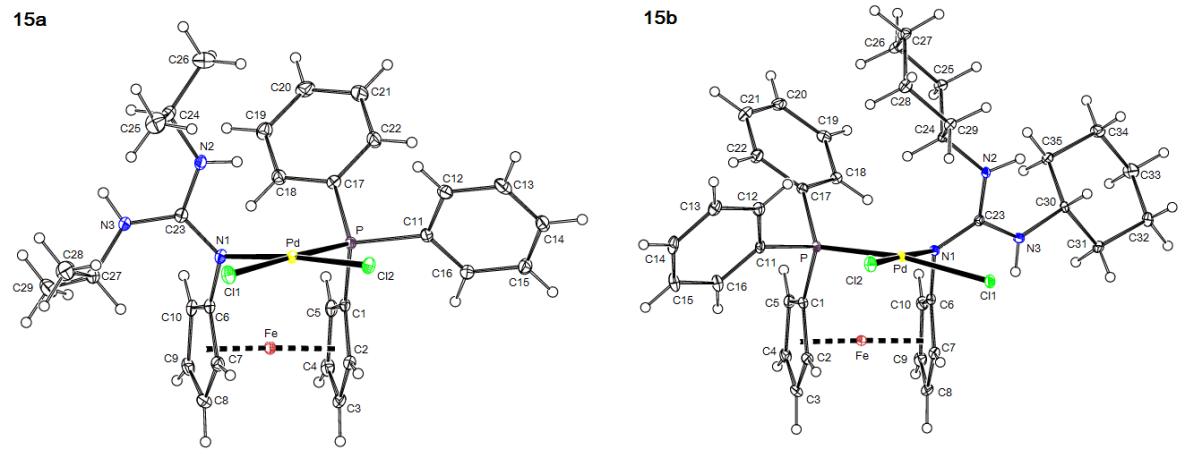

Figure 3.7. Views of structures of complexes **15a** and **15b** with displacement ellipsoids set to the 30% probability level.

The molecular structures of complexes **16a**, **16b** and **16c**·1/4CH_2Cl_2, *i. e.*, the complexes with $[SbF_6]^-$ as a counter-anion, were determined by X-ray diffraction analysis (**Figure 3.8**). The Fe-Pd distances found in these structures (**16a**: 2.7590(5) Å; **16b**: 2.7956(5) Å; **16c**: 2.7821(5) Å) are slightly longer than the sum of the covalent radii (2.71 Å).[122] Interestingly, the values were roughly halfway between those determined for similar complexes of symmetrical bis-phosphines (2.877(2) Å in [Pd(dppf-κ^3*P,P′,Fe*)(PPh_3)])[123] and of bis-guanidines (2.714(1) Å in [PdCl{Fe(η^5-$C_5H_4NC(NMe_2)_2)_2$}-κ^3*N,N′,Fe*)][$PdCl_4$])[75b]. The nature of the bonding interactions in complexes **16** was extensively studied by physicochemical techniques (NMR spectroscopy, UV-Vis spectroscopy, Mössbauer spectroscopy and cyclic voltammetry) in combination with DFT calculations. For detailed discussion of the results see *Appendix C*.

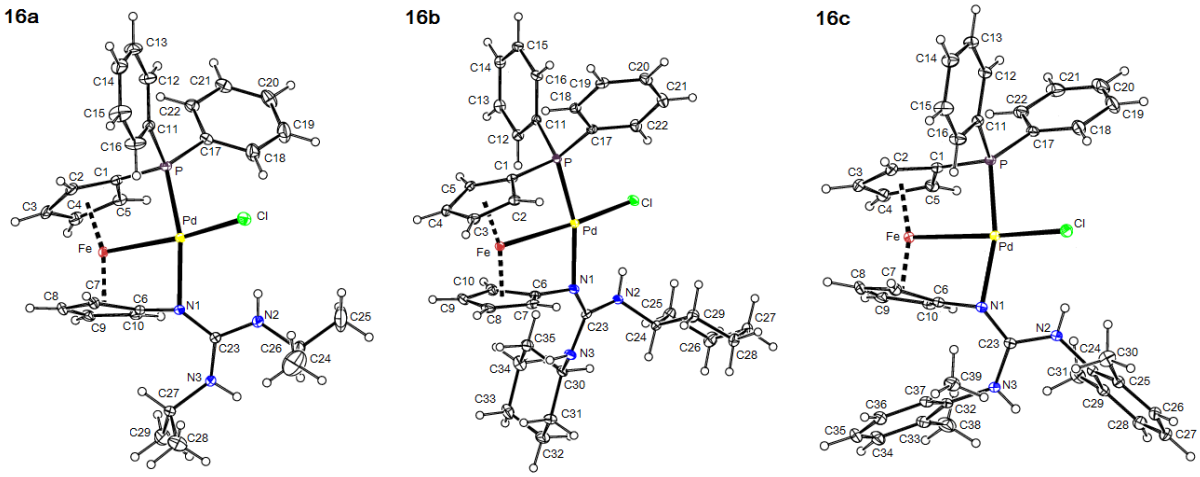

Figure 3.8. Structures of cations in complexes **16a**, **16b** and **16c**·1/4CH_2Cl_2 with displacement ellipsoids at the 30% probability level. Anions and solvent molecules are omitted for clarity.

During subsequent reactivity studies described below, only the prototypical *iso*-propyl-substituted guanidine **13a** was used as a model ligand (see *Appendix D* for the description of the experiments). Thus, in the reaction of **13a** with platinum(II) precursor [$PtCl_2(DMSO)_2$], the *cis*-chelated complex **17** was selectively produced, which was isostructural with the palladium(II) complex **15a**. The subsequent chloride removal using sodium tetrakis[3,5-bis(trifluoromethyl)phenyl]borate (Na[BArF]) resulted in the formation of chloride-bridged dimeric cationic complex **18** (**Scheme 3.8**). Interestingly, no signs of a complex that would be a platinum(II) analogue of **16a** were found in the spectra of the crude reaction mixture containing **18** as the sole product. This resembled the reactivity of ferrocene bisphosphines, among which only the most sterically demanding ones coordinated to platinum(II) in κ^3*P,P′,Fe* fashion, whereas the less bulky ligands formed halogen-bridged dimers.[124] Notably, attempts to perform the analogous reaction sequence, *i.e*, coordination of **13a** followed by halogen abstraction, with nickel(II) ion were unsuccessful, typically leading to oxidised ligand and unidentified nickel species.

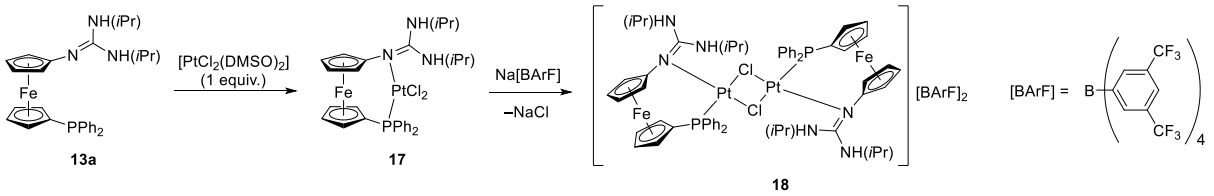

Scheme 3.8. Preparation of the platinum(II) complexes **17** and **18**.

The ^{1}H NMR spectra of complexes **17** and **18** indicated chelation-induced, fixed conformations of the ferrocene ligands, which make the ferrocene protons diastereotopic. Therefore, eight resonances in the range of 3.9-5.5 ppm were observed in the spectra of **17**. In the spectra of **18**, multiple signals were found in the region of 4.0-5.6 ppm due to presence of all four possible stereoisomers of **18** in the solution (each represented by eight ferrocene proton signals). The ratio of the isomers was not constant. The two major and two minor isomers observed immediately after dissolving the crystalline material equilibrated over time (*ca*. 24 h) to the approximately 1:1:1:1 mixture. The coordination of the ligand was further confirmed by the ^{31}P NMR spectra displaying one singlet with ^{195}Pt satellites (δ_P = 2.2 ppm, $^1J_{PPt}$ = 4125 Hz) in the case of **17**, and four singlets with ^{195}Pt satellites (δ_P = 2.3, 3.0, 5.0, 5.4 ppm; the $^1J_{PPt}$ interaction constants were not resolved) in the case of **18**. The shift of the ν(CN) stretching bands towards lower wavelengths compared to the free ligand (ν(CN) ≈ 1580 cm^{-1} in **17** and **18** *vs*. 1594 cm^{-1} in **13a**) in the IR spectra of complexes **17** and **18** additionally confirmed the coordination of the imine-type nitrogen of the guanidine group.[125]

The molecular structures of complexes **17** and **18**·2$CHCl_3$ were determined by X-ray diffraction analysis (**Figure 3.9** and **Table 3.6**). In both cases, the coordination substantially affected the geometry of the ligand donor groups. In comparison with the free ligand **13a**, the shift of electron density from donor atoms to platinum(II) centre resulted in a shortening of the P-C bonds of the phosphine group and in an elongation of the C6-N1 and N1-C23 bonds of the guanidine unit. The induced partial positive charge at the C23 atom was then compensated by electron density shift from the *iso*-propyl-substituted nitrogen atoms, which was manifested through a shortening of the C23-N2 and C23-N3 bonds. Nevertheless, the C23-N1 bond remained the shortest in the CN_3 unit, partially retaining its imine-like nature. The cyclopentadienyl rings of ferrocene scaffold in both structures were forced into the 1,1′-conformation;[126] however, the tilt angles of the rings remained small (below 5°). The geometry at the platinum(II) centre in complex **17** was roughly similar to that of its palladium(II) analogue **15a** (see *Appendix C*). Finally, although structures **17** and **18**·2$CHCl_3$ formally shared the same set of donor atoms around platinum(II) centre and the general trends such as the effect of the *trans*-influence[127] were preserved, small but significant differences could be observed between those two geometries. Compared to those in **17**, the Pt-P and Pt-N1 distances were shorter and, conversely, the Pt-Cl distances were longer in **18**·2$CHCl_3$ due to dimeric nature of this complex. Also, the Cl-Pt-Cl angle (≈ 84°) in **18**·2$CHCl_3$ departed more significantly from the ideal value for the square-planar geometry (90°). The dihedral angle between {P, Pt, N1} and {Cl, Pt, Cl(a), Pt(a)} planes 6.01(8)° described the chloride-bridged dimeric unit in **18**·2$CHCl_3$ as essentially planar.

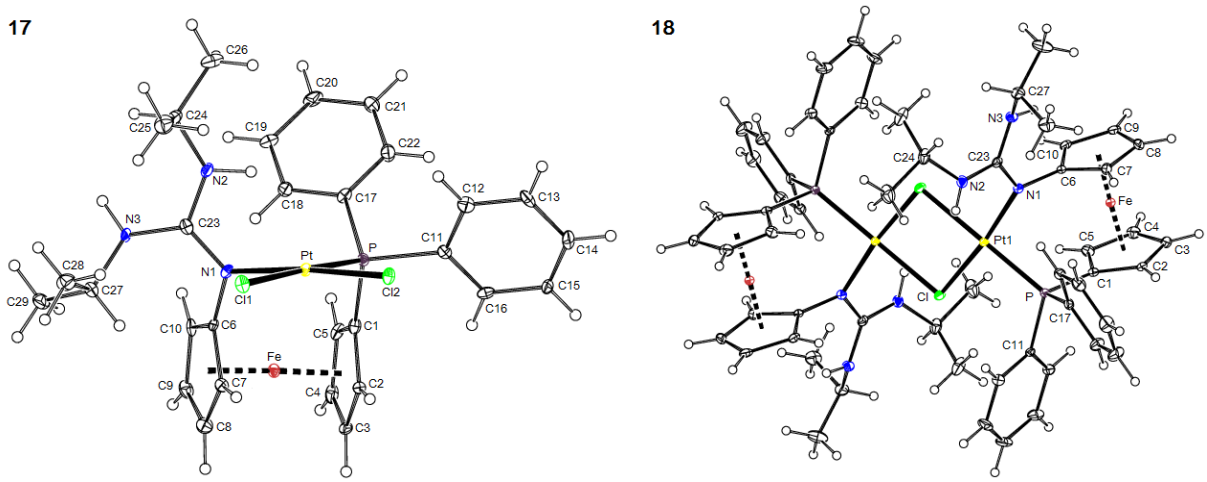

Figure 3.9. Structural diagrams of complex **17** and the cation in compound **18**·2$CHCl_3$ (the anion and solvent molecules are omitted for clarity). The displacement ellipsoids enclose the 30% probability level.

Table 3.6. Selected distances and angles for platinum(II) complexes **17** and **18**·2$CHCl_3$ (in Å and deg).

Parameter[a]	**17**	**18**·2$CHCl_3$
Pt-P	2.243(2)	2.2370(8)
Pt-N1	2.042(5)	2.029(3)
Pt-Cl(*trans*)[b]	2.372(1)	2.4047(8)
Pt-Cl(*cis*)[b]	2.296(2)	2.3221(8)
P-Pt-N1	92.4(2)	93.73(8)
Cl(*trans*)-Pt-Cl(*cis*)[b]	88.66(5)	83.78(3)
P-Pt-Cl(*cis*)[b]	93.06(5)	93.07(3)
N1-Pt-Cl(*trans*)[b]	85.7(2)	89.12(8)
Fe-Cg1/Fe-Cg2	1.647(2)/1.645(3)	1.633(1)/1.639(2)
∠Cp1,Cp2	4.9(3)	1.5(2)
τ	–2.2(5)	–12.0(2)
P-C1	1.787(7)	1.791(3)
P-C11/P-C17	1.821(5)/1.841(6)	1.816(3)/1.816(3)
C6-N1	1.419(8)	1.429(4)
C23-N1	1.330(8)	1.342(4)
C23-N2	1.340(8)	1.343(4)
C23-N3	1.352(8)	1.349(4)
N1-C23-N2/N3	118.1(5)/123.3(6)	119.2(3)/119.6(3)
N2-C23-N3	118.6(6)	121.3(3)
N2-C24/N3-C27	1.464(8)/1.471(8)	1.485(4)/1.482(4)

[a] Definitions: Cp1 and Cp2 are the cyclopentadienyl rings C(1-5) and C(6-10), respectively; Cg1/Cg2 are their centroids. τ torsion angle C1-Cg1-Cg2-C6. [b] Cl(*trans*)/Cl(*cis*) represent the Cl atoms in positions *trans*/*cis* with respect to the P atom.

Guanidines **13** reacted with acids to form corresponding guanidinium salts, as it was demonstrated by the reaction of **13a** with hydrogen chloride (**Scheme 3.9**). The reaction proceeded instantaneously and, after evaporation of solvents and crystallisation, guanidinium chloride **19** was obtained in a good yield as a stable crystalline solid. It is worth mentioning that reaction times longer than 5 minutes resulted in a gradual oxidation of **19**, as the phosphine group was more prone to oxidation in the acidic environment. The chloride **19** could be advantageously used as a starting material for the synthesis of diverse guanidinium salts varying in the counteranion by salt metathesis reactions. In this regard, guanidinium hexafluoroantimonate(V) **20** was prepared by metathesis of **19** with potassium hexafluoroantimonate(V) (**Scheme 3.9**). Crystallisation of the crude product from

dichloromethane/hexane mixture resulted in isolation of dichloromethane solvate **20**·CH_2Cl_2. Upon storage, the clathrated solvent was slowly released over the period of several weeks, resulting in disintegration of the original crystalline material into powder.

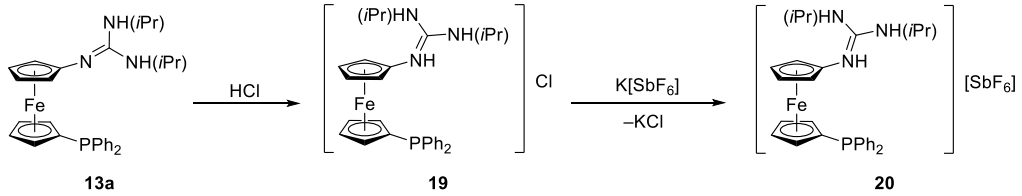

13a **19** **20**

Scheme 3.9. Preparation of guanidinium phosphines **19** and **20**.

The NMR spectra of guanidinium salts **19** and **20** did not differ substantially from those of neutral guanidine **13a**. In the ^{1}H NMR spectra, the observed signals shifted only slightly while remaining in the expected regions. The most significant change in the ^{13}C NMR spectra was a shift of the C^{ipso} atom of the ferrocene scaffold directly bonded to the guanidinium unit to lower frequencies ($\Delta\delta_C \approx 20$ ppm), which is consistent with a decrease in electron density at the nitrogen atom after protonation. Conversely, the signal of the C^{ipso} atom of the guanidinium moiety shifted only negligibly ($\Delta\delta_C \approx 3$ ppm). In the ^{31}P NMR spectra, the phosphine group was expectedly manifested as a slightly broadened singlet at $\delta_P \approx -20$ ppm. In the IR spectra of compounds **19** and **20**, the signals attributable to N-H stretching (3000-3500 cm^{-1}) were significantly broadened, presumably due to intermolecular hydrogen bonding. Furthermore, the C-N stretching modes of guanidinium group were shifted to higher wavelengths (approximately 1635 cm^{-1} and 1610 cm^{-1}) compared to the parent **13a**.

The molecular structures of guanidinium salts **19** and **20**·CH_2Cl_2 were authenticated by X-ray diffraction analysis (**Figure 3.10** and **Table 3.7**). The most significant differences in the structures of these molecules in comparison to neutral phosphinoguanidine **13a** could be expectedly found in the geometry of the guanidinium unit. The protonation occurring at the N1 nitrogen atom was accompanied by the loss of its imine-like character, which led to elongation of the N1-C23 and N1-C6 bonds. Conversely, delocalisation of the positive charge over the guanidinium unit resulted in a shortening of the C23-N2 and C23-N3 bonds. Overall, the delocalised CN_3 unit was almost planar with the N-C-N angles close to the ideal value 120°. The C-N bond lengths were in the range of 1.32-1.35 Å (which are values in-between those typical for single and double C-N bonds), the longest being the N1-C23 bond. Dihedral angles between the least-square planes {C23, N1, N2, N3} of the guanidinium moiety and {C(6-10)} of cyclopentadienyl ring were 44.38(8)° in **19**, and 75.5(2)° in **20**·CH_2Cl_2. Otherwise, the (diphenylphosphino)ferrocene units in both molecules showed regular geometries comparable with other structurally related compounds. The cyclopentadienyl rings adopted an approximate

1,3′-conformation in **19** (τ ≈ 135°) and, rather surprisingly, a more sterically strained 1,1′-conformation in **20**·CH_2Cl_2 (τ ≈ –19°).[126]

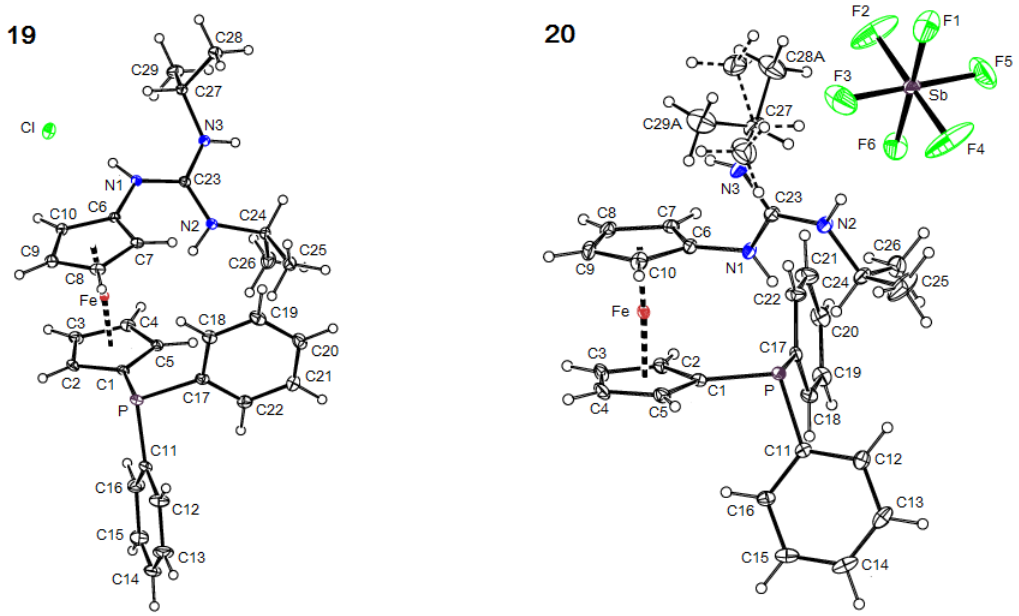

Figure 3.10. ORTEP drawings of guanidinium phosphines **19** and **20**·CH_2Cl_2 (the solvent molecules are omitted for clarity) with the displacement ellipsoids set to the 30% probability level.

Table 3.7. Selected distances and angles for guanidinium salts **19** and **20**·CH_2Cl_2 (in Å and deg).

Parameter[a]	**19**	**20**·CH_2Cl_2
Fe-Cg1/Fe-Cg2	1.6487(7)/1.6586(7)	1.649(1)/1.654(1)
∠Cp1,Cp2	6.02(8)	3.6(2)
τ	135.22(9)	–18.8(2)
P-C1	1.818(1)	1.814(3)
P-C11/P-C17	1.835(1)/1.838(1)	1.829(3)/1.832(3)
C6-N1	1.413(2)	1.420(4)
C23-N1	1.351(2)	1.347(3)
C23-N2	1.333(2)	1.326(4)
C23-N3	1.331(2)	1.325(4)
N1-C23-N2/N3	118.5(1)/119.8(1)	119.8(3)/118.9(3)
N2-C23-N3	121.7(1)	121.4(3)
N2-C24/N3-C27	1.470(2)/1.477(2)	1.474(4)/1.471(4)

[a] Definitions: Cp1 and Cp2 are the cyclopentadienyl rings C(1-5) and C(6-10), respectively; Cg1/Cg2 are their centroids. τ torsion angle C1-Cg1-Cg2-C6.

The coordination preferences of both aforementioned guanidinium phosphines, *i. e.*, compounds **19** and **20**, were again studied in reactions with $[PdCl_2(MeCN)_2]$ (**Scheme 3.10**). In these reactions, compound **19** resembled the structurally related compounds, namely guanidinium chloride **11c**[109b] and ammonium chloride $(Ph_2PfcCH_2NHMe_2)Cl$ (**XVI**·HCl).[65] Specifically, the reaction of $[PdCl_2(MeCN)_2]$ with 1 equivalent of **19** produced zwitterionic complex **21** as the major product (^{31}P NMR: $\delta_P \approx 23$ ppm). When 2 equivalents of ligand **19** were reacted with the same precursor, cationic complex **22** was identified as the dominant product ($\delta_P \approx 18$ ppm). However, these compounds were accompanied by traces of other coordination species, namely **15a** ($\delta_P \approx 26$ ppm), **16a** ($\delta_P \approx -5$ ppm) and another compound, which was not yet identified ($\delta_P \approx 33$ ppm). Such reactivity could be attributed partly to the acid-base activity of the guanidinium group, but mainly to the coordination non-innocence of the chloride anion. Unfortunately, these compounds were inseparable from each other by precipitation or crystallisation, which prevented the isolation of the major products in pure form. Nevertheless, it was found that complex **21** could be selectively prepared by the reaction of complex **15a** with 1 equivalent of hydrogen chloride. Subsequent crystallisation of the crude product from saturated chloroform solution provided complex **21** as a well-defined, chloroform-solvated crystalline material.

The coordination chemistry of ligand **20** containing a non-coordinating hexafluoroantimonate(V) anion was more straightforward. Thus, the reaction of **20** with $[PdCl_2(MeCN)_2]$ at 1:1 ligand-to-metal ratio produced selectively the dimeric, chloride-bridged complex **23**, which was isolated in pure form by crystallisation. The reaction at 2:1 ligand-to-metal ratio led to the poorly-soluble cationic complex **24**, which spontaneously separated from the reaction mixture as a precipitate.

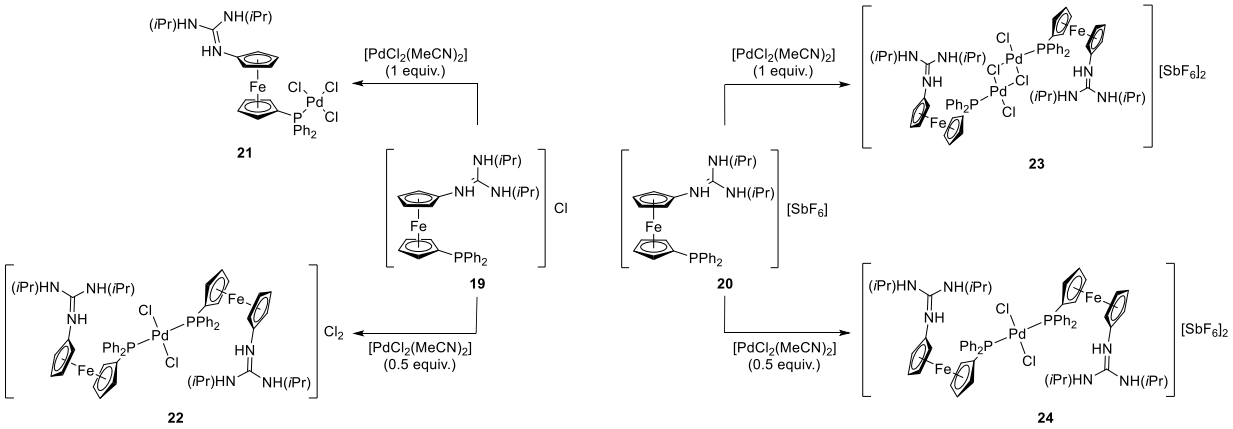

Scheme 3.10. Coordination chemistry of guanidinium phosphines **19** and **20** towards palladium(II).

The ^{1}H NMR spectra of complexes **21**, **23** and **24** were unexceptional with all signals located in the expected regions. The signals due to the protons of the ferrocene scaffold (in each case presented as four separated multiplets of equal intensity) were observed in the range of δ_H 4.3-5.3 ppm. The chemical shifts in the ^{13}C NMR spectra were comparable to those of free ligands. However, signals due to the C^{ipso} carbon atoms directly bonded to the phosphorus atom were split into doublets with much higher interaction constants ($^{1}J_{CP} \approx 60$ Hz) than in the case of free ligands ($^{1}J_{CP} \approx 4$ Hz). Moreover, in the spectra of **24**, the interaction between carbon and two phosphorus nuclei resulted in appearance of characteristic virtual triplets.[128] In the ^{31}P NMR spectra, signals with chemical shifts typical for the given complex type were observed: δ_P = 23.9 ppm for **21**, 31.2 ppm for **23** and 16.9 ppm for **24**. The IR spectra of complexes **21**, **23** and **24** were roughly similar to those of free ligands with broad N-H stretching bands at 3000-3400 cm^{-1} and sharp C-N stretching bands at 1600-1650 cm^{-1}.

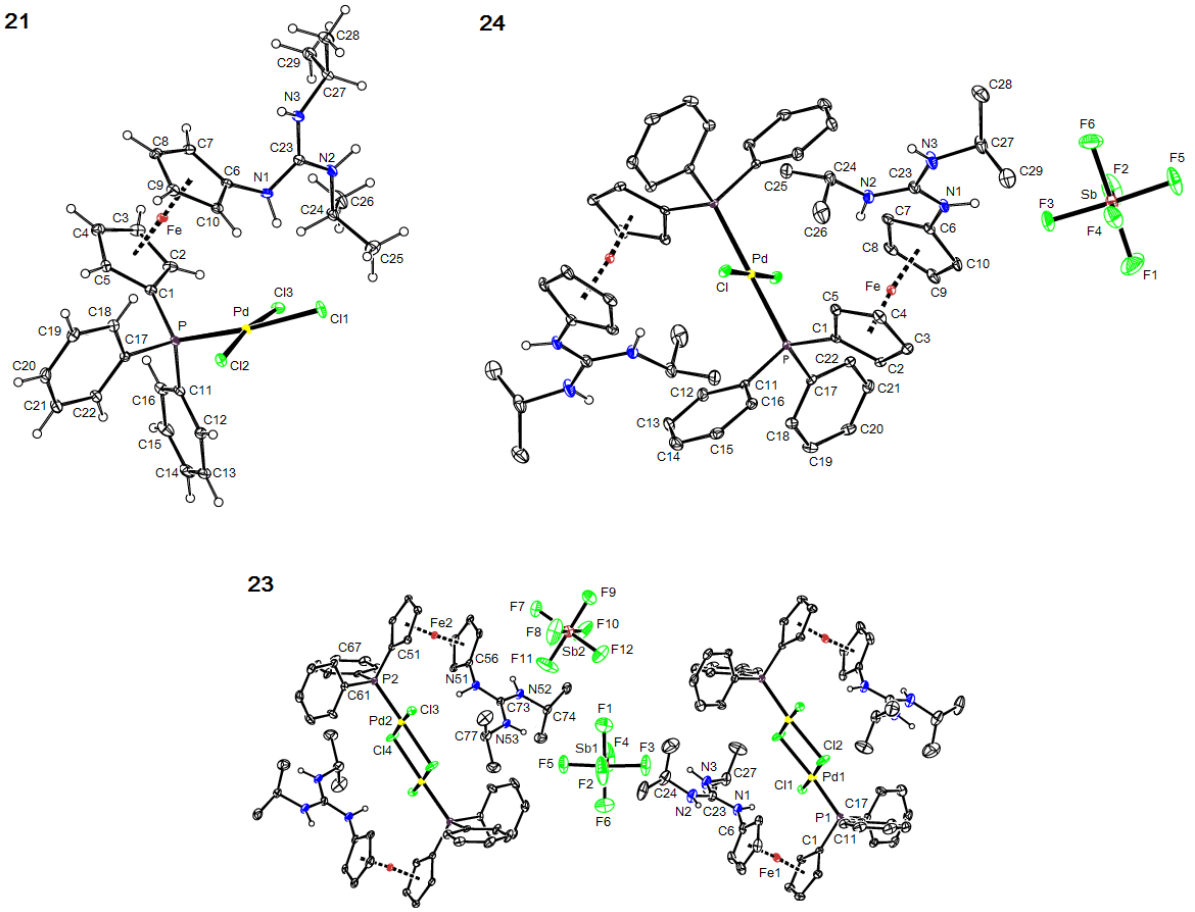

Figure 3.11. Molecular structures of complexes **21**·2.5$CHCl_3$, **23**·2CH_2Cl_2 and **24** with the displacement ellipsoids scaled to the 30% probability level. The hydrogen atoms, except those of guanidinium units, are omitted from structures of **23**·2CH_2Cl_2 and **24** for clarity. For the same reasons, solvent molecules are not included.

Table 3.8. Selected distances and angles for palladium(II) complexes **21**·2.5$CHCl_3$, **23**·2CH_2Cl_2 and **24** (in Å and deg).

Parameter[a]	**21**·2.5$CHCl_3$	**23**·2CH_2Cl_2[c]		**24**
		Fe1	Fe2	
Pd-P	2.2369(6)	2.221(2)	2.232(2)	2.3249(9)
Pd-Cl(*trans*)[b]	2.3719(6)	2.419(2)	2.426(2)	-
Pd-Cl(*cis*) [b]	2.2944(6)	2.288(1)	2.283(1)	2.296(1)
	2.3237(6)	2.322(2)	2.319(2)	
P-Pd-Cl(*cis*)[b]	92.90(2)	87.41(5)	87.45(5)	85.93(3)
	88.74(2)	96.49(6)	96.20(5)	94.07(3)
Cl(*trans*)-Pd-Cl(*cis*)[b]	88.52(2)	91.14(6)	90.95(5)	-
	90.52(2)	85.21(6)	85.32(6)	
Fe-Cg1	1.654(1)	1.653(3)	1.648(3)	1.654(2)
Fe-Cg2	1.653(1)	1.652(3)	1.649(3)	1.656(2)
∠Cp1,Cp2	4.4(1)	4.5(4)	3.0(3)	7.0(2)
τ	81.8(2)	68.2(4)	–67.0(4)	141.3(3)
P-C1	1.807(3)	1.785(6)	1.789(5)	1.798(3)
P-C11	1.814(2)	1.802(6)	1.803(6)	1.816(4)
P-C17	1.817(2)	1.804(6)	1.810(6)	1.815(4)
C6-N1	1.424(3)	1.421(8)	1.423(7)	1.415(4)
C23-N1	1.347(3)	1.320(9)	1.344(7)	1.348(5)
C23-N2	1.329(3)	1.339(8)	1.331(7)	1.321(5)
C23-N3	1.335(3)	1.334(9)	1.329(7)	1.326(5)
N1-C23-N2	120.1(2)	119.5(6)	118.7(5)	119.1(3)
N1-C23-N3	119.2(2)	120.8(6)	120.3(5)	119.8(4)
N2-C23-N3	120.7(2)	119.7(6)	121.0(5)	121.2(4)
N2-C24	1.471(3)	1.48(1)	1.472(8)	1.475(6)
N3-C27	1.475(3)	1.472(9)	1.464(8)	1.469(5)

[a] Definitions: Cp1 and Cp2 are the cyclopentadienyl rings C(1-5) and C(6-10), respectively; Cg1/Cg2 are their centroids. τ torsion angle C1-Cg1-Cg2-C6. [b] Cl(*trans*)/Cl(*cis*) represent the Cl atoms in positions *trans*/*cis* with respect to the P atom. [c] The asymmetric unit of **23**·2CH_2Cl_2 comprises of two independent molecules, in which the corresponding atoms are labelled as follows: Fe1…Fe2; Cl1…Cl3; Cl2…Cl4; Cl2a…Cl4b; P1…P2; Np…N(p+50) and Cq…C(q+50).

The molecular structures of complexes **21**·2.5$CHCl_3$, **23**·2CH_2Cl_2 and **24** were determined by X-ray diffraction analysis (**Figure 3.11** and **Table 3.8**). Generally, the geometry of the guanidinium units in all three complexes was comparable with that of the free ligands (see above). On the other hand, the P-C distances were shorter as the coordination induced a shift of the electron density from the substituents to the phosphorus atom. As for the geometry around

the palladium(II) centre, bond lengths and angles in **21**·2.5$CHCl_3$ were very close to those found in the structurally related complexes [$PdCl_3${$Ph_2PfcCH_2NHC(NH_2)_2$}]·Me_2CO[65] and [$PdCl_3${$Ph_2PfcCH_2NHMe_2$}]·1.5$CHCl_3$.[109b] In all these complexes, the Pd-P distances were approximately 2.24 Å, the Pd-Cl distances pertaining to chlorine atoms oriented in positions *cis* with respect to the phosphorus atom were in the range of 2.29-2.33 Å, whereas the bond from palladium to chlorine atom, which is *trans* to the phosphorus atom, was elongated due to *trans*-influence (*ca*. 2.38 Å). The angles around palladium(II) differed from the ideal value of 90° only marginally. Similar geometry around palladium(II) centres was found in both crystallographically independent molecules present in the structure of **23**·2CH_2Cl_2. However, the Pd-Cl distances were longer, especially for the bridging chlorine atoms. The interligand angles were still close to 90°, but the values were not so uniform; the smallest angle was enclosed by the bridging chlorine atoms (*ca*. 85°). The chloride-bridged dimeric fragments were nearly planar with dihedral angles between the {P, Pd, Cl(terminal)} and {Pd, 2×Cl(bridging), Pd} planes below 6°. The geometry around the palladium(II) centre in **24** strongly resembled that of the structurally related complex [$PdCl_2${$Ph_2PfcCH_2NHC(NH_2)_2$}$_2$]·2MeOH·2H_2O.[109b] The coordination environment was almost ideally square-planar. However, the P-Pd-Cl angles (85.93(3)°and 94.07(3)°) slightly differed from the ideal value due to steric hindrance.

In search for further accessible coordination modes of the phosphinoguanidine ligands, complexes containing deprotonated ligand **13a** coordinated in a P,N,N′-tridentate, doubly-chelating fashion were prepared (**Scheme 3.11**). For this purpose, complex **15a** was selected as a starting material producing, after deprotonation with 1 equivalent of potassium bis(trimethylsilyl)amide, complex **25**, which was subsequently isolated by crystallisation from saturated diethyl ether solution in the form of its diethyl ether solvate **25**·Et_2O as a dark red crystalline solid. In the solid state, complex **25**·Et_2O was stable toward air and moisture, but labile in an acidic environment. In the reaction with 1 equivalent of HCl, it was converted back into the starting complex **15a**.

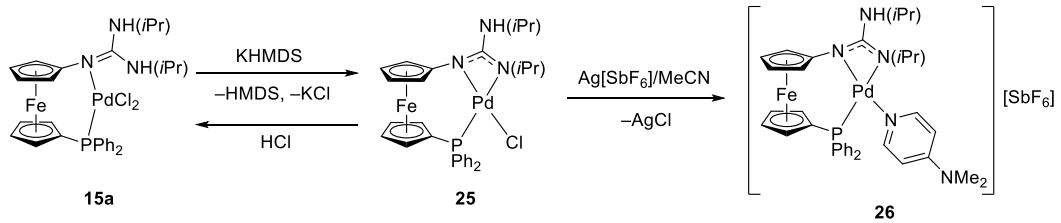

Scheme 3.11. Preparation of the guanidinate complexes **25** and **26**.

Complex **25**·Et_2O is one of the rare examples of mononuclear palladium(II)-guanidinate complexes[99] and, to my best knowledge, the sole example wherein the guanidinate ligand is combined with a phosphine moiety. Moreover, it opened an access to complexes with varied ligands by chloride abstraction/ligand introduction reaction sequence. This approach was demonstrated by treating **25**·Et_2O with silver hexafluoroantimonate(V) in acetonitrile solution followed by reaction of the acetonitrile-stabilised intermediate with 4-(dimethylamino)pyridine to produce cationic complex **26**, which was purified by crystallisation. It should be noted, that cationic complexes of this type could be potentially interesting for catalysis since they possess an easily accessible site for substrate coordination in the proximity of strongly basic guanidinate group, which in turn could activate the substrate for further reactions by deprotonation. However, more research in this direction is required.

In the ^{1}H NMR spectra of complexes **25**·Et_2O and **26**, the presence of two chemically non-equivalent *iso*-propyl substituents was clearly manifested as the CH_3 groups gave rise to two well-separated doublets at high field. The signal of the CH fragment of the *iso*-propyl group attached to the deprotonated guanidine nitrogen could be observed as a simple septet in the case of **26**, or as a doublet of septets in the case of **25**·Et_2O. The additional splitting was caused by the interaction with ^{31}P nucleus of the phosphine group (J_{HP} = 14.9 Hz) and was confirmed by recording decoupled $^{1}H\{^{31}P\}$ NMR spectra. The CH fragment of the other *iso*-propyl group was in both cases manifested as a doublet of septets due to the interaction with the adjacent NH proton (its signal was conversely observed as a doublet). The proton signals of ferrocene scaffold were observed as four multiplets in the range of 3.4-5.0 ppm. The signals in the $^{13}C\{^{1}H\}$ NMR were found in the expected regions. However, compared to the neutral uncoordinated ligand **13a**, they were generally shifted to a lower field. The difference was expectedly the highest for the signals attributable to the nuclei directly connected to the guanidinate group, *i. e.*, for C^{ipso}-N of ferrocene scaffold ($\Delta\delta_C \approx 10$ ppm) and for C^{ipso} of guanidinate ($\Delta\delta_C \approx 20$ ppm). In the $^{31}P\{^{1}H\}$ NMR spectra, the signal of the coordinated phosphine group was found at $\delta_P \approx 35$ ppm. The IR spectra showed the C-N stretching mode of guanidinate close to 1600 cm^{-1}.

The molecular structures of complexes **25**·Et_2O and **26** were established by X-ray diffraction analysis (**Figure 3.12** and **Table 3.9**). In both structures, the ferrocene scaffold adopted its regular geometry. The coordination environment enforced an approximate 1,1′-conformation of the cyclopentadienyl rings (τ = 10.6(1)° and 13.9(1)°, respectively),[126] but did not result in tilting, which remained low (below 2°). The geometry around the coordinated phosphorus atom was comparable to that in the parent complex **15a**; however, the Pd-P distances were slightly shorter, which can be explained by the differences in *trans*-influence of the chloride and guanidinate ligands. Significant changes were observed in the geometry of the guanidinate unit. Compared to complex **15a**, the deprotonation associated with the chelate

coordination of the guanidinate donor group led to differentiation of the C23-N bonds. The bond from the central carbon atom C23 to the formally deprotonated nitrogen atom N2 was significantly shortened (compare 1.344(3) Å in **15a** and 1.310(2) Å in **25**·Et_2O or 1.316(2) Å in **26**) and gained a partial double bond character. Conversely, bond C23-N1 was substantially elongated (1.337(3) Å in **15a** and 1.389(2) Å in **25**·Et_2O or 1.391(2) Å in **26**). Bonds C23-N3 and C6-N1 were elongated only slightly, while the bonds to *iso*-propyl substituents remained virtually unchanged. In addition, N-C-N angles diverted from the ideal value (120°). The chelate coordination resulted in narrowing of the N1-C23-N2 angle (in both structures *ca*. 111°), and the angle enclosed by *iso*-propyl substituted nitrogen atoms was the most open (*ca*. 127°), possibly due to increased steric demands of the *iso*-propyl substituents. The angles were similar to those found for chelating *N,N′,N′′*-triphenylguanidinate (Tpg^-) ligand in [{Pd(μ-Tpg^-)(Tpg^-)}$_2$].[129] The CN_3 moiety, however, remained nearly planar and with the adjacent cyclopentadienyl ring it subtended a dihedral angle of approximately 70°. The coordination environment was severely distorted from the ideal square-planar geometry, the calculated τ_4 index values[130] were 0.21 and 0.19 for **25**·Et_2O and **26**, respectively. The smallest interligand angle was associated with the guanidinate chelate ring (N1-Pd-N2 ≈ 65°). The Pd-N bonds in both complexes were of similar lengths (≈ 2.06 Å), comparable with the parameters of [{Pd(μ-Tpg^-)(Tpg^-)}$_2$].[129]

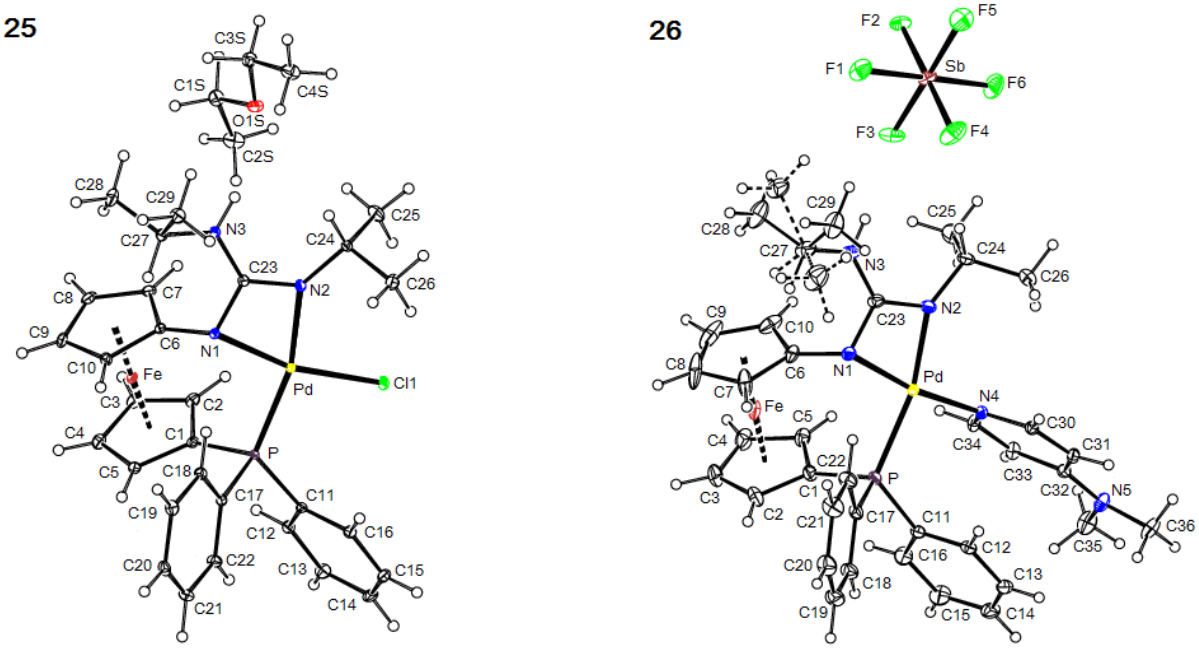

Figure 3.12. Views of molecular structures of complexes **25**·Et_2O and **26**. The displacement ellipsoids enclose the 30% probability level.

Table 3.9. Selected distances and angles for palladium(II) complexes **25**·Et_2O and **26** (in Å and deg).

Parameter[a]	**25**·Et_2O	**26**
Pd-P	2.2442(5)	2.2601(6)
Pd-N1	2.061(1)	2.046(1)
Pd-N2	2.061(1)	2.064(2)
Pd-*A*[b]	2.3147(5)	2.062(1)
P-Pd-N1	98.51(4)	97.43(4)
N1-Pd-N2	65.15(5)	65.51(6)
N2-Pd-*A*[b]	102.36(4)	105.83(6)
P-Pd-*A*[b]	94.07(2)	91.41(4)
Fe-Cg1/Fe-Cg2	1.6451(7)/1.6501(7)	1.640(1)/1.645(1)
∠Cp1,Cp2	1.55(8)	1.5(1)
τ	10.6(1)	13.9(1)
P-C1	1.796(1)	1.788(2)
P-C11/P-C17	1.820(1)/1.827(1)	1.812(2)/1.820(2)
C6-N1	1.422(2)	1.426(2)
C23-N1	1.389(2)	1.391(2)
C23-N2	1.310(2)	1.316(2)
C23-N3	1.353(2)	1.348(2)
N1-C23-N2/N3	110.6(1)/122.6(1)	110.5(1)/122.5(2)
N2-C23-N3	126.8(1)	127.1(2)
N2-C24/N3-C27	1.458(2)/1.470(2)	1.463(2)/1.477(3)

[a] Definitions: Cp1 and Cp2 are the cyclopentadienyl rings C(1-5) and C(6-10), respectively; Cg1/Cg2 are their centroids. τ torsion angle C1-Cg1-Cg2-C6. [b] *A* = Cl1 for **25**·Et_2O, *A* = N4 for **26**.

4. Conclusion

In accordance with the postulated aims of the Thesis, a series of phosphinoguanidinium chlorides [$R_2PfcCH_2NHC(NH_2)_2$]Cl (**11**, R = *iso*-propyl (**a**), cyclohexyl (**b**), phenyl (**c**) and 2-furyl (**d**)) with varied phosphine substituents was synthesised *via* an originally developed multi-step procedure from the easily accessible 1-bromo-1′-cyanoferrocene (**3**). Lithiation of **3** followed by phosphinylation led to phosphinonitriles R_2PfcCN (**5**), which after reduction to amines and subsequent guanylation provided **11** in good yields.

Catalytic properties of catalysts generated *in situ* from palladium(II) acetate and phosphines **11** were evaluated in palladium-catalysed Suzuki-Miyaura-type cross-coupling reactions in aqueous solvent mixtures. In the reaction between aroylchlorides and boronic acids producing benzophenones, the differences in catalytic activity of phoshines were negligible and ligands **11** were only comparable with simple phosphines such as triphenylphosphine. On the other hand, in the "classical" reaction between aryl bromides and boronic acids producing biaryls, the influence of phosphine on catalytic performance was substantial. Whereas in the presence of electron-poor phosphines the conversions were under given conditions negligible, almost full conversions were achieved when phosphines **11a** or **11b** were used, which could be attributed to combined positive effects of polar guanidinium tag and the electron-rich phosphine groups. Furthermore, defined complexes [RhCl(CO)(**11**-κ*P*)$_2$] (**12**), prepared in the reaction of ligands **11** with [Rh(μ-Cl)$(CO)_2]_2$, were tested as catalysts in rhodium-catalysed hydroformylation of 1-hexene. All complexes exhibited high selectivity towards aldehyde formation but with only modest stereoselectivity.

Phosphinonitriles **5**, which emerged as intermediates during the synthesis of ligands **11**, were additionally used to prepare dimeric gold(I) complexes [Au_2(μ-**5**-κ*P,N*)$_2$][SbF_6]$_2$ (**7**). These bench-stable complexes were employed as precatalysts in gold(I)-mediated cyclisation of *N*-propargyl amides to 2-substituted 5-methyleneoxazolines. It was demonstrated that the reaction rate of the cyclisation correlated with the electronic properties of the phosphine and the complex **7d** with the least donating phosphine in the series was identified as the most active catalyst. Although the catalyst suffered from partial decomposition during the reaction, the self-stabilising nature of the precatalyst given by coordination of the nitrile group enabled to use relatively low catalyst loadings. Furthermore, no threshold concentration of the precatalyst, under which the cyclisation would not be initiated, was found which is not typical for gold(I) catalysed reactions.

Neutral phosphinoguanidine ligands $Ph_2PfcNC(NHR')_2$ (**13**, R′ = *iso*-propyl (**a**), cyclohexyl (**b**) and 2,6-xylyl (**c**)), were successfully prepared by two complementary synthetic pathways. The first method was based on a reaction of phosphinoamine **14** with corresponding

carbodiimide in the presence of a catalytic amount of diethyl zinc. In the second and more reliable procedure, the carbodiimide was reacted with amide salt generated from **14** by deprotonation with stoichiometric amount of *n*-butyllithium. Phosphines **13** represent the first examples of *N,N′,N′′*-trisubstituted phosphinoguanidines isolated and characterised to date. Subsequently, they were used as ligands for the preparation of palladium(II) complexes *cis*-[$PdCl_2$(**13**-κ^2*P,N*)] (**15**) and [PdCl(**13**-κ^3*P,N,Fe*)][SbF_6] (**16**). The nature of the Fe-Pd interaction in the latter ones was rigorously described by spectroscopic measurements and by quantum-chemistry calculations. Additionally, platinum(II) complexes *cis*-[$PtCl_2$(**13a**-κ^2*P,N*)] (**17**) and [Pt(μ-Cl)(**13a**-κ^2*P,N*)]$_2$(BArF)$_2$ (**18**) were prepared and used to compare coordination preferences of **13** depending on the metal centre. Attempts to prepare analogous nickel(II) complexes were unfortunately unsuccessful.

Protonation of **13a** provided guanidinium salts [**13a**H]X (X = Cl (**19**), [SbF_6] (**20**)). Their reactions with [$PdCl_2$(MeCN)$_2$] resulted in an isolation of complexes [$PdCl_3$(**13a**H-κ*P*)] (**21**), [PdCl(μ-Cl)(**13a**H-κ*P*)]$_2$[SbF_6]$_2$ (**23**) and *trans*-[$PdCl_2$(**13a**H-κ*P*)$_2$][SbF_6]$_2$ (**24**), which can be considered as typical for monodentate phosphine ligands.

The palette of possible coordination modes of ligand **13a** was extended by preparation of complexes [PdCl(**13a**$^-$-κ^3*P,N,N′*)] (**25**) and [Pd(**13a**$^-$-κ^3*P,N,N′*)(dmap)][SbF_6] (**26**), in which the ligand is coordinated in its singly deprotonated, guanidinate form. Since the majority of palladium(II) complexes with guanidinate ligands are of polynuclear nature, complexes **25** and **26** are rare examples of mononuclear palladium(II) guanidinate complexes and, to my best knowledge, the only examples wherein the guanidinate ligand is combined with phosphine moiety. Further studies into reactivity and potential applications of this unprecedented type of complexes are currently in progress.

5. References

1. W. Reppe, W. J. Schweckendiek, *Liebigs Ann.* **1948**, *560*, 104-116.
2. (a) *Homogeneous Catalysis with Metal Phosphine Complexes*, ed. L. H. Pignolet, Plenum, New York, 1983; (b) *Phosphorus(III) Ligands in Homogeneous Catalysis: Design and Synthesis*, eds. P. C. J. Kamer and P. W. N. M. van Leeuwen, Wiley, Chichester, 2012.
3. R. G. Pearson, *J. Am. Chem. Soc.* **1963**, *85*, 3533-3539.
4. W. A. Henderson, C. A. Streuli, *J. Am. Chem. Soc.* **1960**, *82*, 5791-5794.
5. C. A. Tolman, *J. Am. Chem. Soc.* **1970**, *92*, 2953-2956.
6. A. Roodt, S. Otto, G. Steyl, *Coord. Chem. Rev.* **2003**, *245*, 121-137.
7. U. Beckmann, D. Süslüyan, P. C. Kunz, *Phosphorus Sulfur Silicon Relat. Elem.* **2011**, *186*, 2061-2070.
8. C. A. Fleckenstein, H. Plenio, *Chem. Soc. Rev.* **2010**, *39*, 694–711.
9. (a) C. A. Tolman, *J. Am. Chem. Soc.* **1970**, *92*, 2956-2965; (b) C. A. Tolman, *Chem. Rev.* **1977**, *77*, 313-348.
10. D. White, B. C. Taverner, P. G. L. Leach, N. J. Coville, *J. Comput. Chem.* **1993**, *14*, 1042-1049.
11. T. L. Brown, *Inorg. Chem.* **1992**, *31*, 1286-1294.
12. A. Poater, B. Cosenza, A. Correa, S. Giudice, F. Ragone, V. Scarano, L. Cavallo, *Eur. J. Inorg. Chem.* **2009**, 1759–1766.
13. (a) P. Dierkes, P. W. N. M. van Leeuwen, *J. Chem. Soc., Dalton Trans.* **1999**, 1519-1529; (b) P. W. N. M. van Leeuwen, P. C. J. Kamer, J. N. H. Reek, Peter Dierkes, *Chem. Rev.* **2000**, *100*, 2741-2769.
14. C. P. Casey, G. T. Whiteker, *Isr. J. Chem.* **1990**, *30*, 299-304.
15. P. Anastas, N. Eghbali, *Chem. Soc. Rev.* **2010**, *39*, 301-312.
16. (a) *Aqueous-Phase Organometallic Catalysis: Concepts and Applications*, eds. B. Cornils and W. A. Herrmann, Wiley-VCH, Weinheim, 2004; (b) K. H. Shaughnessy, *Chem. Rev.* **2009**, *109*, 643-710.
17. (a) Y. Dror, J. Manassen, *J. Mol. Catal.* **1977**, *2*, 219-222; (b) B. Cornils, E. G. Kuntz, *J. Organomet. Chem.* **1995**, *502*, 177-186.
18. W.-H. Zhang, S. W. Chien, T. S. A. Hor, *Coord. Chem. Rev.* **2011**, *255*, 1991– 2024.
19. (a) C. S. Slone, D. A. Weinberger, C. A. Mirkin, *Prog. Inorg. Chem.* **1999**, *48*, 233-350; (b) P. Braunstein, F. Naud, *Angew. Chem. Int. Ed.* **2001**, *40*, 680-699.
20. (a) M. Trincado, H. Grützmacher, *Cooperating Ligands in Catalysis* in *Cooperative Catalysis: Designing Efficient Catalysts for Synthesis*, ed. R. Peters, Wiley-VCH, Weinheim, 2015, ch. 3, pp. 67-109; (b) J. R. Khusnutdinova, D. Milstein, *Angew. Chem. Int. Ed.* **2015**, *54*, 12236-12273.

21. (a) A. Zapf, A. Ehrentraut, M. Beller, *Angew. Chem., Int. Ed.* **2000**, *39*, 4153–4155. (b) C. A. Fleckenstein, H. Plenio, *Chem. Eur. J.* **2008**, *14*, 4267-4279.
22. (a) R. Martin, S. L. Buchwald, *Acc. Chem. Res.* **2008**, *41*, 1461-1473; (b) D. S. Surry, S. L. Buchwald, *Chem. Sci.* **2011**, *2*, 27-50.
23. L. Alig, M. Fritz, S. Schneider, *Chem. Rev.* **2019**, *119*, 2681-2751.
24. T. J. Kealy, P. L. Pauson, *Nature* **1951**, *168*, 1039-1040.
25. S. A. Miller, J. A. Tebboth, J. F. Tremaine, *J. Chem. Soc.* **1952**, 632-635.
26. G. Wilkinson, M. Rosenblum, M. C. Whiting, R. B. Woodward, *J. Am. Chem. Soc*. **1952**, *74*, 2125-2126.
27. E. O. Fischer, W. Pfab, *Z. Naturforsch.*, **1952**, *7b*, 377-379.
28. R. R. Gagne, C. A. Koval, G. C. Lisensky, *Inorg. Chem.* **1980**, *19*, 2854-2855.
29. G. L. K. Hoh, W. E. McEwen, J. Kleinberg, *J. Am. Chem. Soc.* **1961**, *83*, 3949-3953.
30. P. J. Graham, R. V. Lindsey, G. W. Parshall, M. L. Peterson, G. M. Whitman, *J. Am. Chem. Soc.* **1957**, *79*, 3416-3420.
31. (a) F. Rebiere, O. Samuel, H. B. Kagan, *Tetrahedron Lett.* **1990**, *31*, 3121-3124; (b) J. J. Bishop, A. Davison, M. L. Katcher, D. W. Lichtenberg, R. E. Merrill, J. C. Smart, *J. Organomet. Chem.* **1971**, *27*, 241-249.
32. *Ferrocenes: Homogeneous Catalysis, Organic Synthesis, Material Science*, eds. A. Togni and T. Hayashi, Wiley-VCH, Weinheim, 1995.
33. *Ferrocenes: Ligands, Materials and Biomolecules*, ed. P. Štěpnička, Wiley, Chichester, 2008.
34. G. P. Sollott, E. Howard, *J. Org. Chem.* **1962**, *27*, 4034-4040.
35. G. P. Sollott, H. E. Mertwoy, S. Portnoy, J. L. Snead, *J. Org. Chem.* **1963**, *28*, 1090–1092.
36. N. Kataoka, Q. Shelby, J. P. Stambuli, J. F. Hartwig, *J. Org. Chem.* **2002**, *67*, 5553-5566.
37. A. Togni, C. Breutel, A. Schnyder, F. Spindler, H. Landert, A. Tijani, *J. Am. Chem. Soc.* **1994**, *116*, 4062-4066.
38. H.-U. Blaser, B. Pugin, F. Spindler, E. Mejía, A. Togni, *Josiphos Ligands: From Discovery to Technical Applications* in *Privileged Chiral Ligands and Catalysts*, ed. Q.-L. Zhou, Wiley-VCH, Weinheim, 2011, ch. 3, pp. 93-136.
39. T. Hayashi, M. Konishi, M. Kumada, *Tetrahedron Lett.* **1979**, *20*, 1871-1874.
40. (a) K.-S. Gan, T. S. A. Hor, *1,1'-Bis(diphenylphosphino)ferrocene. Coordination Chemistry, Organic Syntheses, and Catalysis* in *Ferrocenes: Homogeneous Catalysis, Organic Synthesis Materials Science*, eds. A. Togni and T. Hayashi, Wiley-VCH, Weinheim, 1995, ch. 1, pp. 3-104; (b) S. W. Chien and T. S. A. Hor, *The Coordination and Homogeneous Catalytic Chemistry of 1,1'-Bis(diphenylphosphino)ferrocene and its Chalcogenide Derivatives* in *Ferrocenes: Ligands, Materials and Biomolecules*, ed. P. Štěpnička, Wiley, Chichester, 2008, ch. 2, pp. 33-116; (c) T. J. Colacot, *Platinum Met. Rev.* **2001**, *45*, 22-30.

41. M.-N. Birkholz, Z. Freixa, P. W. N. M. van Leeuwen, *Chem. Soc. Rev.* **2009**, *38*, 1099–1118.
42. D. Seyferth, B. W. Hames, T. G. Rucker, M. Cowie, R. S. Dickson, *Organometallics* **1983**, *2*, 472-474.
43. M. R. Ringenberg, *Chem. Eur. J.* **2019**, *25*, 2396-2406 and references cited herein.
44. T. J. Colacot, H. A. Shea, *Org. Lett.* **2004**, *6*, 3731-3734.
45. B. C. Hamann, J. F. Hartwig, *J. Am. Chem. Soc.* **1998**, *120*, 7369-7370.
46. E. Lerayer, L. Radal, T. A. Nguyen, N. Dwadnia, H. Cattey, R. Amardeil, N. Pirio, J. Roger, J.-C. Hierso, *Eur. J. Inorg. Chem.* **2020**, 419-445.
47. R. V. Smaliy, M. Beaupérin, H. Cattey, P. Meunier, J.-C. Hierso, J. Roger, H. Doucet, Y. Coppel, *Organometallics* **2009**, *28*, 3152-3160.
48. P. Štěpnička, *1'-Functionalised Ferrocene Phosphines: Synthesis, Coordination Chemistry and Catalytic Applications* in *Ferrocenes: Ligands, Materials and Biomolecules*, ed. P. Štěpnička, Wiley, Chichester, 2008, ch. 5, pp. 177-204.
49. M. S. Inkpen, S. Du, M. Driver, T. Albrecht, N. J. Long, *Dalton Trans.* **2013**, *42*, 2813-2816.
50. L.-L. Lai, T.-Y. Dong, *J. Chem. Soc., Chem. Commun.* **1994**, 2347-2348.
51. J. Podlaha, P. Štěpnička, J. Ludvík, I. Císařová, *Organometallics* **1996**, *15*, 543-550.
52. P. Štěpnička, J. Podlaha, R. Gyepes, M. Polášek, *J. Organomet. Chem.* **1998**, *552*, 293-301.
53. P. Štěpnička, I. Císařová, *J. Chem. Soc.*, *Dalton Trans*. **1998**, 2807-2811.
54. J. Kühnert, P. Ecorchard, H. Lang, *Eur. J. Inorg. Chem.* **2008**, 5125-5137.
55. A. M. Trzeciak, P. Štěpnička, E. Mieczyńska, J. J. Ziółkowski, *J. Organomet. Chem.* **2005**, *690*, 3260-3267.
56. P. Štěpnička, *Coord. Chem. Rev.* **2017**, *353*, 223-246.
57. J. Schulz, P. Vosáhlo, F. Uhlík, I. Císařová, P. Štěpnička, *Organometallics* **2017**, *36*, 1828-1841.
58. J. Schulz, F. Horký, I. Císařová, P. Štěpnička, *Catalysts* **2017**, *7*, 167.
59. M. Zábranský, I. Císařová, P. Štěpnička, *Organometallics* **2018**, *37*, 1615-1626.
60. M. Zábranský, I. Císařová, A. M. Trzeciak, W. Alsalahi, P. Štěpnička, *Organometallics* **2019**, *38*, 479-488.
61. M. Zábranský, W. Oberhauser, G. Manca, I. Císařová, P. Štěpnička, *Organometallics* **2019**, *38*, 1534-1543.
62. F. Horký, I. Císařová, J. Schulz, P. Štěpnička, *J. Organomet. Chem.* **2019**, *891*, 44-53.
63. (a) K. Škoch, I. Císařová, P. Štěpnička, *Organometallics* **2015**, *34*, 1942-1956; (b) K. Škoch, I. Císařová, P. Štěpnička, *Organometallics* **2016**, *35*, 3378-3387.
64. K. Škoch, I. Císařová, P. Štěpnička, *J. Organomet. Chem.* **2016**, *819*, 248-254.
65. P. Štěpnička, M. Zábranský, I. Císařová, *ChemistryOpen* **2012**, *1*, 71-79.
66. P. Štěpnička, B. Schneiderová, J. Schulz, I. Císařová, *Organometallics* **2013**, *32*, 5754-5765.

67. P. Štěpnička, J. Schulz, T. Klemann, U. Siemeling, I. Císařová, *Organometallics* **2010**, *29*, 3187-3200.
68. I. R. Butler, M. Kalaji, L. Nehrlich, M. Hursthouse, A. I. Karaulov, K. M. A. Malik, *J. Chem. Soc., Chem. Commun.* **1995**, 459-460.
69. T. Yoshida, K. Tani, T. Yamagata, Y. Tatsuno, T. Saito, *J. Chem. Soc., Chem. Commun.* **1990**, 292-294.
70. S. Teo, Z. Weng, T. S. A. Hor, *J. Organomet. Chem.* **2011**, *696*, 2928-2934.
71. Z. Weng, S. Teo, T. S. A. Hor, *Organometallics* **2006**, *25*, 4878-4882.
72. (a) K. Škoch, I. Císařová, P. Štěpnička, *Inorg. Chem.* **2014**, *53*, 568-577; (b) K. Škoch, I. Císařová, P. Štěpnička, *Chem. Eur. J.* **2015**, *21*, 15998-16004; (c) K. Škoch, F. Uhlík, I. Císařová, P. Štěpnička, *Dalton Trans.* **2016**, *45*, 10655-10671; (d) K. Škoch, I. Císařová, F. Uhlík, P. Štěpnička, *Dalton Trans.* **2018**, *47*, 16082-16101.
73. B. Michelet, D. Leboeuf, C. Bour, K. Škoch, F. Horký, P. Štěpnička, V. Gandon, *ChemPlusChem* **2017**, *82*, 442-448.
74. P. L. Diaconescu, *Acc. Chem. Res.* **2010**, *43*, 1352-1363.
75. (a) C. Metallinos, D. Tremblay, F. B. Barrett, N. J. Taylor, *J. Organomet. Chem.* **2006**, *691*, 2044-2047; (b) L. R. R. Klapp, C. Bruhn, M. Leibold, U. Siemeling, *Organometallics* **2013**, *32*, 5862-5872.
76. J. Oetzel, N. Weyer, C. Bruhn, M. Leibold, B. Gerke, R. Pöttgen, M. Maier, R. F. Winter, M. C. Holthausen, U. Siemeling, *Chem. Eur. J.* **2017**, *23*, 1187-1199.
77. I. R. Butler, S. C. Quayle, *J. Organomet. Chem.* **1998**, *552*, 63-68.
78. K. Škoch, I. Císařová, J. Schulz, U. Siemeling, P. Štěpnička, *Dalton Trans.* **2017**, *46*, 10339-10354.
79. M. Ritte, C. Bruhn, U. Siemeling, *Z. Naturforsch. B* **2014**, *69b*, 906-912.
80. S. Dey, W. Sun, J. Müller, *Inorg. Chem.* **2016**, *55*, 3630-3639.
81. (a) *Guanidines as Reagents and Catalysts I*, ed. P. Selig, Springer International Publishing, Cham, 2017; (b) *Guanidines as Reagents and Catalysts II*, ed. P. Selig, Springer International Publishing, Cham, 2017.
82. (a) P. Gund, *J. Chem. Educ.* **1972**, *49*, 100-103; (b) A. Gobbi, G. Frenking, *J. Am. Chem. Soc.* **1993**, 115, 2362-2372.
83. S. J. Angyal, W. K. Warburton, *J. Chem. Soc.* **1951**, 2492-2494.
84. P. J. Taylor, A. R. Wait, *J. Chem. Soc., Perkin Trans. 2* **1986**, 1765-1770.
85. K. Kanamori, J. D. Roberts, *J. Am. Chem. Soc.* **1983**, *105*, 4698-4701.
86. R. E. Botto, J. H. Schwartz, J. D. Roberts, *Proc. Natl. Acad. Sci. USA* **1980**, *77*, 23-25.
87. J. M. Adams, R. W. H. Small, *Acta Cryst.* **1974**, *B30*, 2191-2193.
88. J. N. Scott, N. V. Nucci, J. M. Vanderkooi, *J. Phys. Chem. A* **2008**, *112*, 10939–10948.

89. T. Šmejkal, B. Breit, *Angew. Chem. Int. Ed.* **2008**, *47*, 311-315.
90. C. Alonso-Moreno, A. Antiñolo, F. Carrillo-Hermosilla, A. Otero, *Chem. Soc. Rev.* **2014**, *43*, 3406-3425.
91. J. H. Short, U. Biermacher, D. A. Dunnigan, T. D. Leth, *J. Med. Chem.* **1963**, *6*, 275-283.
92. A. E. Miller, J. J. Bischoff, *Synthesis* **1986**, 777-779.
93. F. L. Scott, D. G. O'Donovan, J. Reilly, *J. Am. Chem. Soc.* **1953**, *75*, 4053-4054.
94. M. S. Bernatowicz, Y. Wu, G. R. Matsueda, *J. Org. Chem.* **1992**, *57*, 2497-2502.
95. E. W. Thomas, E. E. Nishizawa, D. C. Zimmermann, D. J. Williams, *J. Med. Chem.* **1989**, *32*, 228-236.
96. C. Alonso-Moreno, F. Carrillo-Hermosilla, A. Garcés, A. Otero, Isabel López-Solera, Ana M. Rodríguez, A. Antiñolo, *Organometallics* **2010**, *29*, 2789-2795.
97. (a) P. J. Bailey, S. Pace, *Coord. Chem. Rev.* **2001**, *214*, 91-141; (b) M. P. Coles, *Dalton Trans.* **2006**, 985-1001.
98. (a) F. T. Edelmann, *Adv. Organomet. Chem.* **2008**, *57*, 183-352; (b) F. T. Edelmann, *Adv. Organomet. Chem.* **2013**, *61*, 55-374; (c) F. T. Edelmann, *Chem. Soc. Rev.* **2009**, *38*, 2253-2268; (d) C. Jones, *Coord. Chem. Rev.* **2010**, *254*, 1273-1289.
99. J. Francos, V. Cadierno, *Dalton Trans.* **2019**, *48*, 9021-9036.
100. (a) A. Hoffmann, J. Börner, U. Flörke, S. Herres-Pawlis, *Inorg. Chim. Acta* **2009**, *362*, 1185-1193; (b) S. Herres-Pawlis, P. Verma, R. Haase, P. Kang, C. T. Lyons, E. C. Wasinger, U. Flörke, G. Henkel, T. D. P. Stack, *J. Am. Chem. Soc.* **2009**, *131*, 1154-1169; (c) M. J. Begley, P. Hubberstey, P. H. Walton, *J. Chem. Soc., Dalton Trans.* **1995**, 957-962.
101. A. Neuba, U. Flörke, W. Meyer-Klaucke, M. Salomone-Stagni, E. Bill, E. Bothe, P. Höfer, G. Henkel, *Angew. Chem. Int. Ed.* **2011**, *50*, 4503-4507.
102. (a) P. Agarwal, N. Thirupathi, M. Nethaji, *Organometallics* **2016**, *35*, 3112-3123; (b) P. Saxena, J. M. Thomas, C. Sivasankar, N. Thirupathi, *New J. Chem.* **2019**, *43*, 2307-2327; (c) P. Elumalai, N. Thirupathi, M. Nethaji, *Inorg. Chem.* **2013**, *52*, 1883-1894.
103. H. Dibowski, F. P. Schmidtchen, *Tetrahedron* **1995**, *51*, 2325-2330.
104. A. Hessler, O. Stelzer, H. Dibowski, K. Worm, F. P. Schmidtchen, *J. Org. Chem.* **1997**, *62*, 2362-2369.
105. H. Dibowski, F. P. Schmidtchen, *Tetrahedron Lett.* **1998**, *39*, 525-528.
106. P. Machnitzki, M. Tepper, K. Wenz, O. Stelzer, E. Herdtweck, *J. Organomet. Chem.* **2000**, *602*, 158-169.
107. P. Guerreiro, V. Ratovelomanana-Vidal, J.-P. Genêt, P. Dellis, *Tetrahedron Lett.* **2001**, *42*, 3423-3426.
108. P. Wasserscheid, H. Waffenschmidt, P. Machnitzki, K. W. Kottsieper, O. Stelzer, *Chem. Commun.* **2001**, 451-452.

109. (a) H. Charvátová, I. Císařová, P. Štěpnička, *Eur. J. Inorg. Chem.* **2017**, 288-296; (b) O. Bárta, I. Císařová, P. Štěpnička, *Eur. J. Inorg. Chem.* **2017**, 489-495.
110. J. Münchenberg, A. K. Fischer, H. Thönnessen, P. G. Jones, R. Schmutzler, *J. Organomet. Chem.* **1997**, *529*, 361-374.
111. T. S. Teets, J. A. Labinger, J. E. Bercaw, *Organometallics* **2013**, *32*, 5530-5545.
112. M. Carmona, J. Ferrer, R. Rodríguez, V. Passarelli, F. J. Lahoz, P. García-Orduña, L. Cañadillas-Delgado, D. Carmona, *Chem. Eur. J.* **2019**, *25*, 13665-13670.
113. A. Chesney, M. R. Bryce, R. W. J. Chubb, A. S. Batsanov, J. A. K. Howard, *Synthesis* **1998**, 413-416.
114. P. Nicpon, D. W. Meek, *Inorg. Chem.* **1966**, *5*, 1297-1298.
115. R. P. Pinnell, C. A. Megerle, S. L. Manatt, P. A. Kroon, *J. Am. Chem. Soc.* **1973**, *95*, 977-978.
116. B. Milde, M. Lohan, C. Schreiner, T. Rüffer, H. Lang, *Eur. J. Inorg. Chem.* **2011**, 5437-5449.
117. A. S. K. Hashmi, J. P. Weyrauch, W. Frey, J. W. Bats, *Org. Lett.* **2004**, *6*, 4391-4394.
118. E. Herrero-Gómez, C. Nieto-Oberhuber, S. López, J. Benet-Buchholz, A. M. Echavarren, *Angew. Chem., Int. Ed.* **2006**, *45*, 5455-5459.
119. M. Blangetti, H. Rosso, C. Prandi, A. Deagostino, P. Venturello, *Molecules* **2013**, *18*, 1188-1213.
120. D. Nieto, S. Bruña, A. González-Vadillo, J. Perles, F. Carrillo-Hermosilla, A. Antiñolo, J. M. Padrón, G. B. Plata, I. Cuadrado, *Organometallics* **2015**, *34*, 5407-5417.
121. C. Alonso-Moreno, F. Carrillo-Hermosilla, A. Garcés, A. Otero, I. López-Solera, A. M. Rodríguez, A. Antiñolo, *Organometallics* **2010**, *29*, 2789-2795.
122. B. Cordero, V. Gómez, A. E. Platero-Prats, M. Revés, J. Echeverría, E. Cremades, F. Barragán, S. Alvarez, *Dalton Trans.* **2008**, 2832-2838.
123. M. Sato, H. Shigeta, M. Sekino, S. Akabori, *J. Organomet. Chem.* **1993**, *458*, 199-204.
124. K. M. Gramigna, J. V. Oria, C. L. Mandell, M. A. Tiedemann, W. G. Dougherty, N. A. Piro, W. S. Kassel, B. C. Chan, P. L. Diaconescu, C. Nataro, *Organometallics* **2013**, *32*, 5966-5979.
125. I. Georgieva, N. Mintcheva, N. Trendafilova, M. Mitewac, *Vib. Spectrosc.* **2001**, *27*, 153-164.
126. S. I. Kirin, H.-B. Kraatz, N. Metzler-Nolte, *Chem. Soc. Rev.* **2006**, *35*, 348-354.
127. T. G. Appleton, H. C. Clark, L. E. Manzer, *Coord. Chem. Rev.* **1973**, *10*, 335-422.
128. W. H. Hersh, *J. Chem. Educ.* **1997**, *74*, 1485-1488.
129. K. T. Holman, S. D. Robinson, A. Sahajpal, J. W. Steed, *J. Chem. Soc., Dalton Trans.* **1999**, 15-18.
130. L. Yang, D. R. Powell, R. P. Houser, *Dalton Trans.* **2007**, 955-964.

6. List of Abbreviations

BArF	tetrakis[3,5-bis(trifluoromethyl)phenyl]borate
BINAP	2,2′-Bis(diphenylphosphino)-1,1′-binaphthyl
Bipy	2,2′-bipyridyl
Bu	butyl
cod	1,5-cyclooctadiene
dmap	4-(dimethylamino)pyridine
dppf	1,1′-bis(difenylfosfino)ferrocene
Hdpf	1-(diphenylphosphino)-1'-ferrocenecarboxylic acid
*i*Pr	*iso*-propyl
Et	ethyl
Fc	ferrocenyl
fc	ferrocene-1,1′-diyl
Me	methyl
Ph	phenyl
Py	2-pydidyl
*t*Bu	*tert*-butyl
tht	tetrahydrothiophene
Tpg	*N,N′,N′′*-triphenylguanidine
TPPTS	triphenylphosphine-3,3′,3′′-trisulfonic acid trisodium salt

7. Statement of Contribution

The candidate (Ondřej Bárta) designed and optimised all synthetic procedures and prepared all new ligands and complexes described in this Thesis and in *Appendices A-D*. He also recorded (IR, UV-Vis, NMR spectra) and interpreted (NMR, MS, IR, UV-Vis) the characterisation data for these compounds. Furthermore, the candidate performed all the catalytic experiments described in *Appendix A* and interpreted the collected kinetic data. Additionally, he conducted and evaluated the Pd-catalysed cross-coupling experiments presented in *Appendix B*. Finally, he partly participated on writing of the publications presented in *Apendices A-C*.

The contributions by other authors are as follows. Petr Štěpnička collected the NMR data for some compounds, and also recorded and interpreted the electrochemical data presented in *Appendix C*. He also refined the X-ray structural data. Finally, he concluded the research projects and wrote the publications presented in *Apendices A-C*. Ivana Císařová collected the X-ray structural data for all the compounds. Jiří Schulz performed the quantum-chemistry calculations described in *Appendix A*. Ewa Mieczyńska and Anna M. Trzeciak conducted and evaluated the hydroformylation experiments described in *Appendix B*. Robert Gyepes performed and interpreted the quantum-chemistry calculations described in *Appendix C*. Adam Alemayehu collected the Mössbauer spectroscopy data presented in *Appendix C*.

8. List of Appendices

Appendix A

O. Bárta, I. Císařová, J. Schulz, P. Štěpnička, Assessing the influence of phosphine substituents on the catalytic properties of self-stabilised digold(I) complexes with supporting ferrocene phosphinonitrile ligands. *New J. Chem.* **2019**, *43*, 11258-11262.

Appendix B

O. Bárta, I. Císařová, E. Mieczyńska, A. M. Trzeciak, P. Štěpnička, Synthesis and Catalytic Evaluation of Phosphanylferrocene Ligands with Cationic Guanidinium Pendants and Varied Phosphane Substituents. *Eur. J. Inorg. Chem.* **2019**, 4846-4854.

Appendix C

O. Bárta, R. Gyepes, I. Císařová, A. Alemayehu, P. Štěpnička, Synthesis and study of Fe→Pd interactions in unsymmetric Pd(II) complexes with phosphinoferrocene guanidine ligands. *Dalton Trans.* **2020**, *49*, 4225-4229.

Appendix D

Synthetic procedures, characterisation data and selected crystallographic parameters for compounds **17**-**26**. *Unpublished results*.

Appendix A

O. Bárta, I. Císařová, J. Schulz, P. Štěpnička, Assessing the influence of phosphine substituents on the catalytic properties of self-stabilised digold(I) complexes with supporting ferrocene phosphinonitrile ligands. *New J. Chem.* **2019**, *43*, 11258-11262.

NJC

PAPER

View Article Online
View Journal | View Issue

Cite this: *New J. Chem.*, 2019, 43, 11258

Assessing the influence of phosphine substituents on the catalytic properties of self-stabilised digold(I) complexes with supporting ferrocene phosphinonitrile ligands†

Ondřej Bárta, Ivana Císařová, Jiří Schulz and Petr Štěpnička *

Received 17th May 2019,
Accepted 21st June 2019

DOI: 10.1039/c9nj02555c

rsc.li/njc

Gold(I) phosphine complexes are often used in catalysis, but the role of their auxiliary ligands still remains poorly understood. Thus, building on our previous research, we prepared a series of Au(I) complexes $[Au_2(\mu\text{-}R_2PfcCN)_2][SbF_6]_2$ (fc = ferrocene-1,1′-diyl) to assess the effect of phosphine groups PR_2 on the catalytic properties of these highly catalytically active, dimeric compounds. Catalytic testing in Au-mediated cyclisation of *N*-propargyl amides to 2-substituted 5-methyleneoxazolines showed that weaker donating phosphines gave rise to more active, albeit partly destabilised, catalysts. Nevertheless, thanks to their self-stabilisation by reversible nitrile coordination, $[Au_2(\mu\text{-}R_2PfcCN)_2]^+$ cations readily converted into catalytically active species (by dissociation) and, in addition, remained catalytically active even at very low metal loadings. The experimental results were supported by the trends in $^1J_{PSe}$ coupling constants for $R_2P(Se)fcCN$ as a measure of ligand basicity, and by DFT calculations.

Introduction

Research interest in homogeneous gold-catalysed reactions has increased tremendously in recent decades, leading to useful synthetic methods that efficiently exploit the ability of gold(I) species to activate unsaturated bonds *via* coordination.[1] However, the influence of the auxiliary ligands (L) on the performance of the presumed active species LAu^+ has been mostly overlooked.[2]

Recently, we have prepared dimeric complexes $[Au_2(\mu(P,N)\text{-}L)_2]X_2$, where L is 1′-(diphenylphosphino)-1-cyanoferrocene (**1c**)[3] or 2-(diphenylphosphino)benzonitrile and X is a weakly coordinating anion. These compounds are bench-stable and silver-free[4,5] instant precursors of highly active Au(I) catalysts,[6,7] which resemble the commonly used pre-catalysts $[(R_3P)Au(MeCN)]X$,[2d,4] although their phosphinonitrile ligands provide both a strongly coordinating donor moiety and a labile donor group. With previous work,[8] we have shown that the nitrile group plays a key role in determining the catalytic activity of $[Au_2(\mu\text{-}L)_2]X_2$ complexes. In this study, we focus on the influence of phosphine substituents on the catalytic properties of complexes $[Au_2(\mu(P,N)\text{-}R_2PfcCN)_2][SbF_6]_2$ (fc = ferrocene-1,1′-diyl) using Au-mediated cyclisation of *N*-propargylamides to 5-methyleneoxazolines[9] as a test reaction and phosphine selenides to probe the ligand properties.[10]

Results and discussion

To achieve the goals of this study, additional phosphinonitrile ligands $R_2PfcC{\equiv}N$ (**1**) bearing electronically distinct phosphino substituents [R = iso-propyl (**a**), cyclohexyl (Cy, **b**), and 2-furyl (Fur; **d**)] were prepared to complement the archetypal representative **1c**.[3,6] These compounds were obtained by successive lithiation/functionalisation[11] of 1,1′-dibromoferrocene (**2**), as shown in Scheme 1.[12] Ligands **1** were subsequently converted into chloridogold(I) complexes **5** and then into the target digold(I) complexes $[Au_2(\mu(P,N)\text{-}R_2PfcCN)_2][SbF_6]_2$ (**6**). To gain further insight into the donor properties of ligands **1**, selenides **7** were prepared from free phosphines *via* reactions with KSeCN[13] (Scheme 1).

In addition, syntheses performed on a relatively large scale, especially during the first steps, enabled us to isolate and ultimately characterise an intensely purple minor side-product detected[12] during the transformation of **2** into **3** as the cyanamide $(Brfc)_2C{=}NC{\equiv}N$ (**4**). This compound arises by addition of the intermediate BrfcLi to the cyanide group in the already formed **3**, followed by reaction of the resulting imine salt with TsCN (see the ESI†).

All compounds have been characterised by spectroscopic methods and by elemental analysis. In their NMR spectra,

Department of Inorganic Chemistry, Faculty of Science, Charles University, Hlavova 2030, 128 40 Prague, Czech Republic. E-mail: petr.stepnicka@natur.cuni.cz

† Electronic supplementary information (ESI) available: Experimental details including structure determination, additional structural diagrams and kinetic plots, details on DFT calculations, copies of the NMR spectra and coordinates of DFT computed structures. CCDC 1909789–1909795. For ESI and crystallographic data in CIF or other electronic format see DOI: 10.1039/c9nj02555c

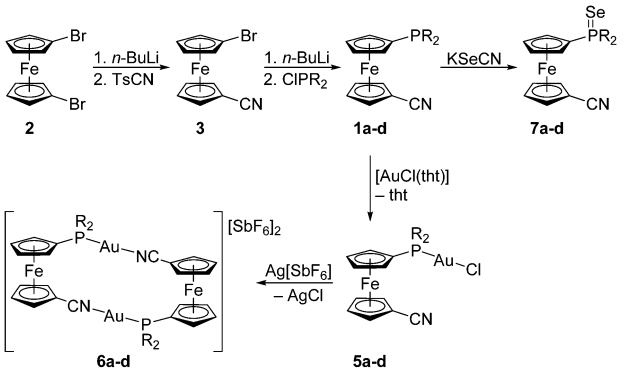

Scheme 1 Synthesis of complexes **6** and phosphine selenides **7** [R = isopropyl (**a**), cyclohexyl (**b**), phenyl (**c**), and 2-furyl (**d**); Ts = 4-toluenesulfonyl, tht = tetrahydrothiophene]. Note: only compounds **1c**, **5c** and **6c** have been previously reported.

phosphines **1** showed characteristic signals due to the ferrocene unit and to the phosphine substituents; the ^{31}P NMR signals were observed at δ_P 0.1 (**1a**), −8.0 (**1b**), −17.7 (**1c**)[3] and −66.1 (**1d**) ppm. The ^{13}C NMR signals of the CN groups occurred at $\delta_C \approx 120$, while the IR bands attributable to the $\nu_{C\equiv N}$ modes were observed in the narrow range of 2224–2228 cm^{-1}. Coordination of **1**, yielding chloridogold(I) complexes **5**, resulted in a shift of the ^{31}P NMR signals to a lower field, while the signature of the CN substituents changed only marginally. Upon converting **5** into dimers **6**, the ^{31}P resonances shifted to slightly higher fields, while the $\nu_{C\equiv N}$ bands moved to higher energies.[14]

The molecular structures of **1d**, **5d** and **6d** are depicted in Fig. 1; those of the chloridogold(I) complexes **5a**, **5b** and **5d** and of dimer **6b** are presented in the ESI,† along with additional data and structural diagrams. The gold(I) ions in complexes **5** are linearly coordinated (Cl–Au–P = 175–177°), showing shorter

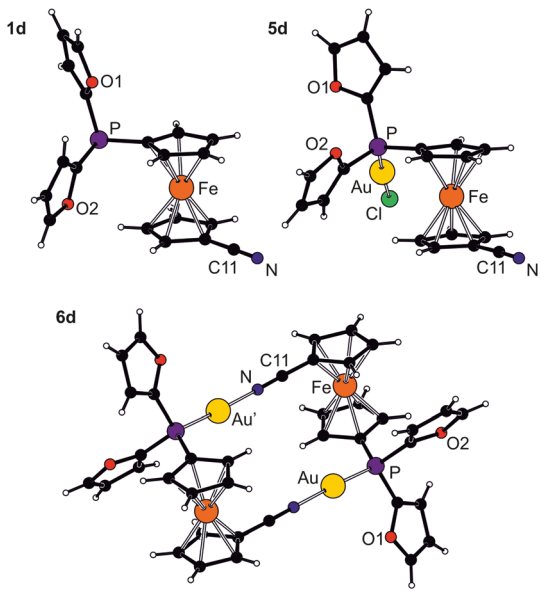

Fig. 1 View of the molecular structures of **1d**, **5d** and of the complex cation in the structure of **6d**. Additional plots and further structural data are available in the ESI.†

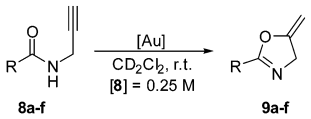

Scheme 2 Au-catalysed cyclisation of propargyl amides **8** to oxazolines **9** [R = Ph (**a**), 4-MeC$_6$H$_4$ (**b**), 4-MeOC$_6$H$_4$ (**c**), 4-ClC$_6$H$_4$ (**d**), 4-CF$_3$C$_6$H$_4$ (**e**), and Cy (**f**)].

Au–P bonds in compounds with weaker donating phosphines due to increased π-back donation (Au–P: 2.2361(6), 2.2319(7), 2.2287(6),[6] and 2.2191(6) Å for **1a–d**, respectively). Although X-ray diffraction analysis confirmed the dimeric nature of **6** in all cases, the structure of **6a** could not be satisfactorily refined due to disorder. The Au–P distances determined for **6b** and **6d** are very close to those determined for **5b** and **5d**, while the CN bond lengths of the coordinated nitrile unit show virtually no difference from those in the respective free phosphines **1**.

Complexes **6** were examined as (pre)catalysts in the Au-catalysed cyclisation of propargyl amides **8** to 5-methylene-4,5-dihydrooxazoles (oxazolines) **9** (Scheme 2).[9] Gratifyingly, the cyclisation of the prototypical substrate **8a** proceeded selectively with all catalysts **6** to give **9a** as the sole product, thus enabling us to monitor the reaction conveniently by ^{1}H NMR spectroscopy (Fig. S7, ESI†). The resulting oxazolines were isolated, but they slowly decomposed when exposed to air.[15]

All pre-catalysts **6** gave full conversions within 3 h when used at 1 mol% Au loading (25 °C, [**8a**]$_0$ = 0.25 M, CD_2Cl_2). Nonetheless, the catalysts showed different kinetic profiles. In particular, cyclisation reactions with catalysts bearing aromatic phosphine substituents proceeded faster than those with catalysts bearing dialkylphosphine moieties (Fig. 2). Although relatively minor, the difference in performance between the catalysts can be easily demonstrated by comparing the corresponding yields of **9a** after 1 h, which were approximately 90% for **6c** and **6d**, and 70% for **6a** and **6b**. When using the common pre-catalyst [Au(PPh$_3$)(MeCN)][SbF$_6$], the cyclisation reaction also reached full conversion within 3 h, though at an intermediate rate between **6c**/**6d** and **6a**/**6b**. The reaction rates (k) determined by fitting the ln([**8**]/[**8**]$_0$) *vs.* time plots (see ESI†) corroborate this semi-quantitative assessment (Table 1).

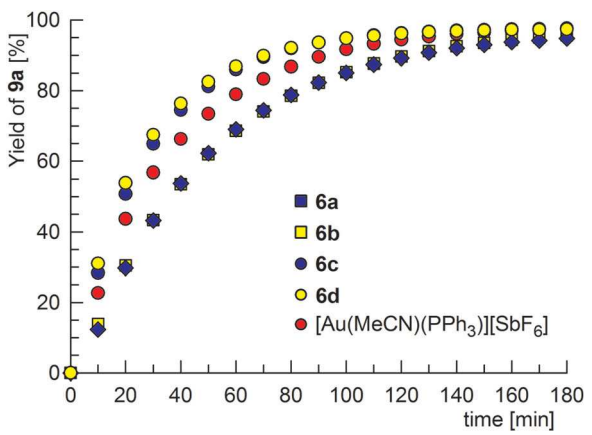

Fig. 2 Kinetic profiles of the cyclisation of **8a** to **9a** catalysed by different Au(I) catalysts ([**8a**]$_0$ = 0.25 M in CD_2Cl_2, 25 °C, [Au] = 1 mol%).

Table 1 Reaction rates of the model cyclisation of substrate **8a** and additional parameters illustrating the properties of ligands **1** and their Au(I) complexes

	Ligand				
Parameter	**1a**	**1b**	**1c**	**1d**	PPh_3
k^a [10^{-3} min^{-1}]	20.8(2)	20.2(2)	32.5(7)	32.9(10)	25.7(7)
ν_{CN} for **1**^{b} [cm^{-1}]	2224	2225	2225[e]	2228	n.a.
ν_{CN} for **6**^{b} [cm^{-1}]	2263	2256	2273[f]	2274	n.a.
Au–P for **6**^{c} [Å]	n.a.	2.242 (av.)	2.225(2)[f]	2.2139(7)	2.228(1)[g]
Au–N for **6**^{c} [Å]	n.a.	2.050 (av.)	2.035(4)[f]	2.032(2)	2.038(5)[g]
E_{dis} for **6**^{d} [kcal mol^{-1}]	27.4	26.8	29.4	32.9	n.a.
$^1J_{SeP}$ for **7** ($CDCl_3$) [Hz]	715	708	741	777	735[h]

[a] Rate constants of the cyclisation of **8a**. Conditions: $[\mathbf{8}]_0$ = 0.25 M in CD_2Cl_2, 1 mol% Au, and 25 °C. Determined from fitting the kinetic profile in the range of 10–60 min. [b] IR spectra recorded in Nujol mulls. [c] Au–P and Au–N distances from X-ray diffraction analysis at 120 or 150 K. [d] Dissociation energies of isolated dimeric cations calculated by DFT. [e] Ref. 3. [f] Ref. 6. [g] Data on $[(Ph_3P)Au(MeCN)][SbF_6]$ from ref. 16. [h] Ref. 17.

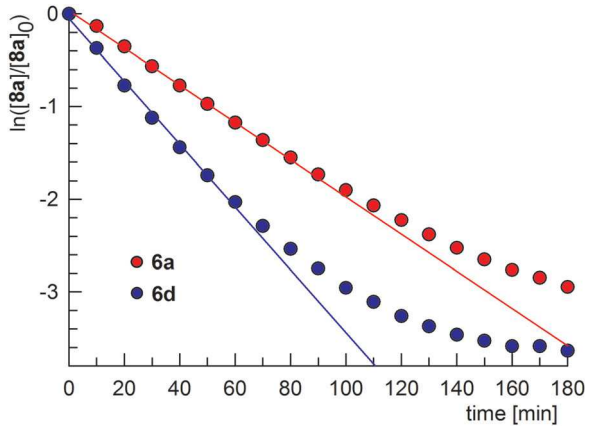

Fig. 3 Kinetic ($\ln([\mathbf{8a}]/[\mathbf{8a}]_0)$ *vs.* time) plots of representative catalysts **6a** and **6d** illustrating the departure from first-order behaviour.

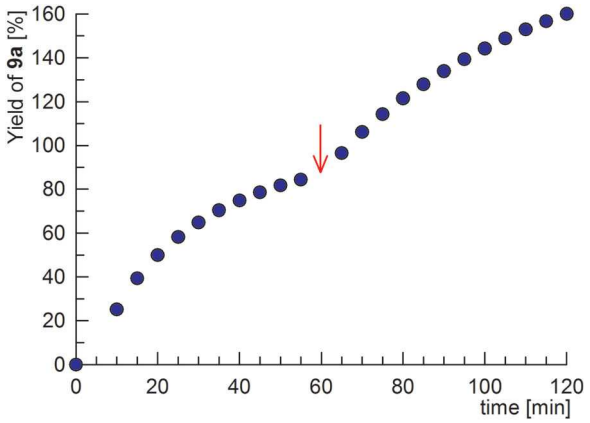

Fig. 4 Kinetic profile of the cyclisation of **8a** to **9a** mediated by **6d** in which additional **8a** was added after 1 h of reaction (indicated by a red arrow).

Further measurements indicated that the cyclisation is a first-order reaction with respect to the amide substrate (Fig. 3 and Fig. S8, ESI†). Our findings thus contrast with previous measurements using $[Au(PR_3)(OTf)]$ catalysts, which showed a linear decrease in substrate concentration over time (0th order reaction).[2b] Such divergence, which was confirmed by independent experiments using the $[Au(PPh_3)(OTf)]$ catalyst, may be attributed to the anion effect ($[SbF_6]^-$ *vs.* OTf^-)[18] and, mainly, to the stabilising role of the nitrile moiety in **6**, whose coordination can prevent decomposition and the formation of gold(I) bis(phosphine) cations or similar species.[19]

The $\ln([\mathbf{8}]/[\mathbf{8}]_0)$ *vs.* time plots for catalysts **6** were linear until approximately 90% conversion, subsequently departing from a linear relationship, which was more pronounced for the faster reacting catalysts (see Fig. 3 and Fig. S8, ESI†). This observation can be explained by catalyst decomposition, which is faster for the more reactive catalysts. Indeed, when an additional equivalent of substrate **8a** was added to the reaction mixture at nearly full conversion (90%), using 1 mol% Au in the form of **6d**, the reaction continued but at a slower rate (approximately half of the original reaction rate, see Fig. 4).

Additional reaction tests performed with the most efficient catalyst **6d** showed that the cyclisation is a first-order reaction in the catalyst (Fig. S9 and S10, ESI†). Using 2 mol% of Au, the reaction with catalyst **6d** reached full conversion within 1 h but proceeded reasonably well also under much lower catalyst loadings (*cf.* 65% conversion after 3 h with 0.25 mol% Au). Remarkably, upon further decreasing the catalyst amount, the reaction slowed down but did not stop. Even with as little as 0.03 mol% Au, the NMR yield of **9a** was 4% after 90 min, and the reaction followed pseudo first-order kinetics. In other words, we have not observed any threshold value below which the reaction did not proceed.[20] Instead, the reaction rate tended towards zero at very low catalyst loadings (Fig. 5). This observation again reflects the unique self-stabilising ability of the $Au(\mathbf{1})^+$ species resulting from reversible dimerisation by nitrile coordination. Unsurprisingly, strongly binding ligands affected this process. For instance, addition of a stoichiometric amount of chloride ions, which coordinate Au(I) stronger than alkynes,[19] stopped the reaction, even at a relatively high catalyst concentration (1 mol% Au, $[\mathbf{8a}]_0$ = 0.25 M).

On the whole, our results confirm that weaker donating auxiliary ligands give rise to more active gold catalysts.[21] The reduced donor ability (basicity) of **1c** and **1d** is clearly expressed by the relatively large $^1J_{PSe}$ coupling constants (see Table 1), which also suggest that the cyano substituent further reduces the donor properties of the entire ferrocene ligand (compare the $^1J_{PSe}$ value of **1d** in Table 1 with the value for $FcP(Se)Ph_2$ of

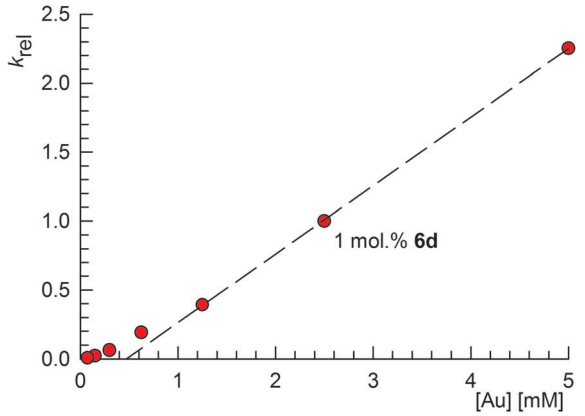

Fig. 5 Variation of the relative reaction rate ($k_{rel} = k/k_{1mol\%}$) as a function of the concentration of gold in the reaction system ([**8a**]$_0$ = 0.25 M, catalyst **6d**).

733 Hz,[22] Fc = ferrocenyl). As stronger π-accepting ligands, **1c** and **1d** form relatively shorter (stronger) Au–P bonds in dimers **6** while the $\nu_{C\equiv N}$ bands of **6c** and **6d** are shifted to higher energies due to stronger σ-donation from a weakly antibonding molecular orbital corresponding to the lone pair at nitrogen.[23] This blue shift in $\nu_{C\equiv N}$ frequencies is in line with the strengthening of the CN → Au interactions suggested by DFT calculations, which show that the energy cost associated with the dissociation of dimers **6** ($[Au_2(\mu\text{-}\mathbf{1})_2]^{2+} \rightarrow 2[Au(\mathbf{1}\text{-}\kappa P)]^+$) is larger in complexes with weaker donating phosphine ligands (**1b** < **1a** < **1c** < **1d**).

Another set of experiments aimed at elucidating the influence of the acyl groups in the substrate on the course of the cyclisation has been performed with amides bearing different substituents in position 4 of their benzene rings, compounds **8a–e**, and with their aliphatic analogue **8f** (Scheme 2). All aromatic amides were efficiently converted into the corresponding oxazolines when using **6d** as the pre-catalyst (1 mol% Au) under standard conditions (Fig. 6). Even though compounds with electron-withdrawing substituents reacted faster, the reaction rates (Table 2) did not correlate with Hammett's constants or with analogous substituent parameters.

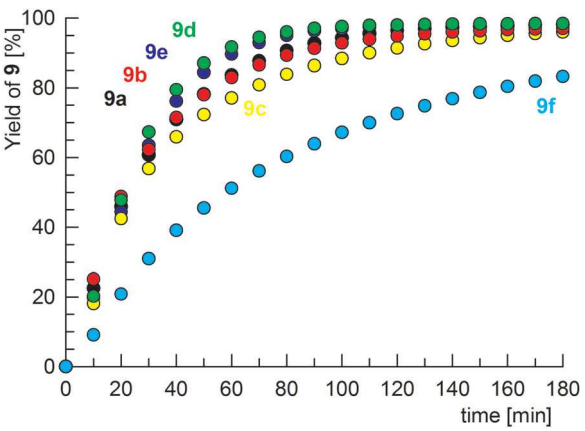

Fig. 6 Kinetic profiles of the cyclisation reactions of different substrates: black – **8a**, red – **8b**, yellow – **8c**, **8d** – green, **8e** – blue, and **8f** – cyan. Conditions: [**8**]$_0$ = 0.125 M in CD_2Cl_2, catalyst **6d** (1 mol% Au), and 25 °C.

Table 2 Reactions rates (k) for the cyclisation of different substrates **8**[a]

Substrate	k [10^{-3} min^{-1}]	Substrate	k [10^{-3} min^{-1}]
8a (Ph)	30.9(7)	**8d** (4-ClC_6H_4)	45.5(3)
8b (4-MeC_6H_4)	29.2(11)	**8e** (4-$CF_3C_6H_4$)	41.3(5)
8c (4-$MeOC_6H_4$)	25.1(15)	**8f** (cyclohexyl)	12.4(3)

[a] Conditions: [**8**]$_0$ = 0.125 M, catalyst **6d** (1 mol% Au), and reaction in CD_2Cl_2 at 25 °C. The rate constants were determined by fitting the kinetic profile over the range 10–60 min.

Indeed, such behaviour matches the proposed reaction mechanism,[9a] which suggests that the coordination of the substrate's triple bond is the initial step. Although the acyl groups in **8** are located far from the alkyne moiety (and are separated by the non-conjugated methylene spacer), they can nevertheless affect other reaction steps (for instance, the nucleophilic attack of the oxygen atom on the coordinated triple bond or the final protodeauration by changing the partial charge at the oxygen atom and the acidity of the NH hydrogen). Conversely, the reaction with amide **8f** was considerably slower (≈80% conversion in 3 h), presumably due to the lack of stabilisation of the reaction intermediates by π-conjugation.

Conclusions

The presence of a nitrile group as a secondary donor moiety in the molecules of supporting phosphine ligands **1** markedly influences the catalytic behaviour of cations $[Au_2(\mu\text{-}\mathbf{1})_2]^{2+}$. These cations, which become active catalysts by simple dissociation, can form again and thus stabilise the active species. Such self-stabilisation markedly differentiates $[Au_2(\mu\text{-}\mathbf{1})_2]^{2+}$ cations from their conventional counterparts $[(R_3P)Au(R'CN)]^+$, primarily by their high catalytic activity, which is preserved even at very low catalyst concentrations, and by the minimised influence of the counter ion (anion coordination is suppressed by the competing nitrile donor). The catalytic activity of $[Au_2(\mu\text{-}\mathbf{1})_2]^{2+}$ can be further increased by introducing less basic phosphine moieties into the structure of the supporting phosphinonitrile ligands. However, such a change decreases the overall chemical stability of the $[Au_2(\mu\text{-}\mathbf{1})_2]^{2+}$ species. Therefore, a judicious choice of the phosphine substituents is essential for achieving optimal catalytic results with these catalysts.

Conflicts of interest

There are no conflicts to declare.

Acknowledgements

This research was supported by the Czech Science Foundation (project no. 17-02495S), by the Grant Agency of Charles University (project no. 130317), and by the Charles University Research Centre program (project no. UNCE/SCI/014).

Notes and references

1 Selected reviews: (*a*) G. Dyker, *Angew. Chem., Int. Ed.*, 2000, **39**, 4237–4239; (*b*) A. S. K. Hashmi, *Chem. Rev.*, 2007, **107**, 3180–3211; (*c*) A. Fürstner and P. W. Davies, *Angew. Chem., Int. Ed.*, 2007, **46**, 3410–3449; (*d*) Z. Li, C. Brouwer and C. He, *Chem. Rev.*, 2008, **108**, 3239–3265; (*e*) N. D. Shapiro and F. D. Toste, *Synlett*, 2010, 675–691; (*f*) R. Dorel and A. M. Echavarren, *Chem. Rev.*, 2015, **115**, 9028–9072; (*g*) D. Pflästerer and A. S. K. Hashmi, *Chem. Soc. Rev.*, 2016, **45**, 1331–1367; (*h*) W. Zi and F. D. Toste, *Chem. Soc. Rev.*, 2016, **45**, 4567–4589; (*i*) A. S. K. Hashmi and F. D. Toste, *Modern Gold Catalyzed Synthesis*, Wiley-VCH, Weinheim, 2012; (*j*) F. D. Toste and V. Michelet, *Gold Catalysis: An Homogeneous Approach*, Imperial College Press, London, 2014.

2 (*a*) D. J. Gorin, B. D. Sherry and F. D. Toste, *Chem. Rev.*, 2008, **108**, 3351–3378; (*b*) W. Wang, G. B. Hammond and B. Xu, *J. Am. Chem. Soc.*, 2012, **134**, 5697–5705; (*c*) D. Malhotra, G. B. Hammond and B. Xu, *Top. Curr. Chem.*, 2015, **357**, 1–23; (*d*) B. Ranieri, I. Escofet and A. M. Echavarren, *Org. Biomol. Chem.*, 2015, **13**, 7103–7118; (*e*) C. A. Gaggioli, G. Ciancaleoni, D. Zuccaccia, G. Bistoni, L. Belpassi, F. Tarantelli and P. Belanzoni, *Organometallics*, 2016, **35**, 2275–2285; (*f*) A. H. Christian, Z. L. Niemeyer, M. S. Sigman and F. D. Toste, *ACS Catal.*, 2017, **7**, 3973–3978.

3 K. Škoch, I. Císařová and P. Štěpnička, *Inorg. Chem.*, 2014, **53**, 568–577.

4 H. Schmidbaur and A. Schier, *Z. Naturforsch.*, 2011, **66b**, 329–350.

5 Additional references: (*a*) D. Wang, R. Cai, S. Sharma, J. Jirak, S. K. Thummanapelli, N. G. Akhmedov, H. Zhang, X. Liu, J. L. Petersen and X. Shi, *J. Am. Chem. Soc.*, 2012, **134**, 9012–9019; (*b*) A. Homs, I. Escofet and A. M. Echavarren, *Org. Lett.*, 2013, **15**, 5782–5785; (*c*) Z. Lu, J. Han, G. B. Hammond and B. Xu, *Org. Lett.*, 2015, **17**, 4534–4537.

6 K. Škoch, I. Císařová and P. Štěpnička, *Chem. – Eur. J.*, 2015, **21**, 15998–16004.

7 B. Michelet, D. Lebœuf, C. Bour, K. Škoch, F. Horký, P. Štěpnička and V. Gandon, *ChemPlusChem*, 2017, **82**, 442–448.

8 K. Škoch, I. Císařová, J. Schulz, U. Siemeling and P. Štěpnička, *Dalton Trans.*, 2017, **46**, 10339–10354.

9 (*a*) A. S. K. Hashmi, J. P. Weyrauch, W. Frey and J. W. Bats, *Org. Lett.*, 2004, **6**, 4391–4394; (*b*) A. S. K. Hashmi, M. Rudolph, S. Schymura, J. Visus and W. Frey, *Eur. J. Org. Chem.*, 2006, 4905–4909; (*c*) A. S. K. Hashmi, A. M. Schuster and F. Rominger, *Angew. Chem., Int. Ed.*, 2009, **48**, 8247–8249; (*d*) J. P. Weyrauch, A. S. K. Hashmi, A. Schuster, T. Hengst, S. Schetter, A. Littmann, M. Rudolph, M. Hamzic, J. Visus, F. Rominger, W. Frey and J. W. Bats, *Chem. – Eur. J.*, 2010, **16**, 956–963.

10 (*a*) C. A. Tolman, *Chem. Rev.*, 1977, **77**, 313–348; (*b*) D. W. Allen and B. F. Taylor, *J. Chem. Soc., Dalton Trans.*, 1982, 51–54; (*c*) A. Muller, S. Otto and A. Roodt, *Dalton Trans.*, 2008, 650–657; (*d*) U. Beckmann, D. Süslüyan and P. C. Kunz, *Phosphorus, Sulfur Silicon Relat. Elem.*, 2011, **186**, 2061–2070.

11 (*a*) I. R. Butler and R. L. Davies, *Synthesis*, 1996, 1350–1354; (*b*) P. Štěpnička in *Ferrocenes: Ligands, Materials and Biomolecules*, ed. P. Štěpnička, Wiley, Chichester, 2008, ch. 5, pp. 177–204.

12 K. Škoch, I. Císařová, F. Uhlík and P. Štěpnička, *Dalton Trans.*, 2018, **47**, 16082–16101.

13 P. Nicpon and D. W. Meek, *Inorg. Chem.*, 1966, **5**, 1297–1298.

14 Coordination of a nitrile moiety is typically associated with a shift of the $\nu_{C\equiv N}$ band towards higher energies as the result of electron density removal from a weakly antibonding molecular orbital (lone pair at N). π-Back donation, which increases the population of antibonding orbitals, is rather weak. For references, see: K. Nakamoto, *Infrared and Raman Spectra of Inorganic and Coordination Compounds, Part B: Applications in Coordination, Organometallic, and Bioinorganic Chemistry*, Wiley, New York, 5th edn, 1997, sect. III-15, pp. 105–115.

15 A. S. K. Hashmi, M. C. B. Jaimes, A. M. Schuster and F. Rominger, *J. Org. Chem.*, 2012, **77**, 6394–6408.

16 E. Herrero-Gómez, C. Nieto-Oberhuber, S. López, J. Benet-Buchholz and A. M. Echavarren, *Angew. Chem., Int. Ed.*, 2006, **45**, 5455–5459.

17 R. P. Pinnell, C. A. Megerle, S. L. Manatt and P. A. Kroon, *J. Am. Chem. Soc.*, 1973, **95**, 977–978.

18 (*a*) D. Zuccaccia, L. Belpassi, A. Macchioni and F. Taranteli, *Eur. J. Inorg. Chem.*, 2013, 4121–4135; (*b*) M. Jia and M. Bandini, *ACS Catal.*, 2015, **5**, 1638–1652; (*c*) J. Schiessl, J. Schulmeister, A. Doppiu, E. Wörner, M. Rudolph, R. Karch and A. S. K. Hashmi, *Adv. Synth. Catal.*, 2018, **360**, 2493–2502.

19 A. Zhdanko, M. Ströbele and M. E. Maier, *Chem. – Eur. J.*, 2012, **18**, 14732–14744.

20 M. Kumar, G. B. Hammond and B. Xu, *Org. Lett.*, 2014, **16**, 3452–3455.

21 Teles *et al.* concluded similarly in their seminal paper from 1998: J. H. Teles, S. Brode and M. Chabanas, *Angew. Chem., Int. Ed.*, 1998, **37**, 1415–1418.

22 B. Milde, M. Lohan, C. Schreiner, T. Rüffer and H. Lang, *Eur. J. Inorg. Chem.*, 2011, 5437–5449.

23 M. L. Kuznetsov, *Russ. Chem. Rev.*, 2002, **71**, 265–282.

Assessing the influence of phosphine substituents on the catalytic properties of self-stabilised digold(I) complexes with supporting ferrocene phosphinonitrile ligands

Ondřej Bárta, Ivana Císařová, Jiří Schulz, and Petr Štěpnička*

Department of Inorganic Chemistry, Faculty of Science, Charles University,

Hlavova 2030, 128 40 Prague, Czech Republic

Supporting Information

Contents

Materials and methods

All syntheses were performed under an argon atmosphere using standard Schlenk techniques. Compounds **1c**,[1] **6c**,[2] [AuCl(tht)],[3] [Au(PPh_3)(MeCN)][SbF_6],[4] and [Au(PPh_3)(OTf)][5] were prepared as previously described. Other chemicals were purchased from commercial suppliers (Sigma-Aldrich and Alfa-Aesar) and were used as received. Dichloromethane, THF and methanol were dried using a PureSolv MD5 solvent purification system (Innovative Technology, USA). Acetone was dried over potassium carbonate and distilled under an argon atmosphere. Other solvents (Lach-Ner, Czech Republic) were of reagent grade and were used without further purification.

NMR spectra were recorded at 25°C on a Varian INOVA 400 (^{1}H, 399.95; ^{13}C, 100.58; and ^{31}P, 161.90 MHz; and ^{19}F, 376.29 MHz) or on a Bruker Avance III HD 400 (^{1}H, 400.13; and ^{13}C, 100.62 MHz) spectrometer at 25°C. ^{1}H NMR spectra measured as a part of the kinetic measurement were recorded on a Varian INOVA 300 spectrometer operating at 299.94 MHz. Chemical shifts (δ in ppm) are given relative to internal tetramethylsilane (^{1}H and ^{13}C) or, alternatively, to neat $CFCl_3$ (^{19}F) and to 85% aqueous H_3PO_4 (^{31}P) as external references. In addition to the usual representation of signal multiplicity (s = single, d = doublet, t = triplet, q = quartet and br = broad, among others),[6] vt and vq are used to denote virtual multiplets due to magnetically non-equivalent protons at cyclopentadienyl rings (spin systems AA′BB′ and AA′BB′X for the cyano- and phosphine-substituted rings, respectively, where A, B = ^{1}H, and X = ^{31}P); fc = ferrocene-1,1′-diyl, Cy = cyclohexyl, Fur = 2-furyl. IR spectra were recorded in Nujol mulls, in the range of 400-4000 cm^{-1} using a Nicolet 6700 FTIR spectrometer. ESI mass spectra were recorded on a Compact QTOF-MS spectrometer (Bruker Daltonics) using samples dissolved in HPLC-grade methanol. Elemental analyses were performed using a Perkin–Elmer 2400 Series II CHNS/O analyser. The presence of clathrated solvent (if any) was confirmed by NMR analysis.

Syntheses and catalytic tests

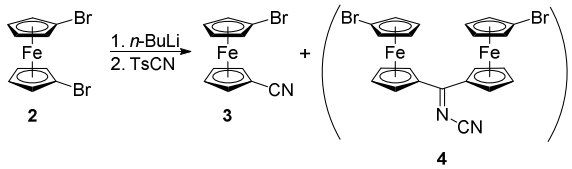

Preparation of 1-bromo-1′-cyanoferrocene (3) and isolation of N-(bis(1′-bromoferrocenyl)-methylene)cyanamide (4). In an oven-dried flask, 1,1′-dibromoferrocene (**2**; 7.91 g, 23.0 mmol) was dissolved in dry THF (100 mL) under an argon atmosphere, and the red solution was cooled to –78°C using a dry ice-ethanol bath. *n*-Butyllithium (9.2 mL of 2.5 M in hexanes, 23.0 mmol) was slowly added, and the resulting orange suspension was stirred at –78°C for 1 h, subsequently adding dropwise a solution of tosyl cyanide (5.0 g, 27.6 mmol) in dry THF (40 mL), pre-cooled to –78°C. The orange colour of the reaction mixture slowly changed to dark red, and the solids dissolved. The reaction mixture was stirred for another 2 hours at –78°C and then at room temperature overnight before quenching by saturated aqueous $NaHCO_3$ (50 mL). The organic phase was separated, and the aqueous layer was back-extracted with diethyl ether (2× 30 mL). The combined organic layers were washed with brine and dried over $MgSO_4$. The crude product was pre-absorbed onto silica gel by evaporation and purified by chromatography over a silica gel column, eluting with hexane/ethyl acetate (3:1). The chromatography resulted in three main bands. The first orange band, which contained ferrocene and bromoferrocene, resulting from unwanted protonolysis, was discarded. Evaporation of the major second orange band provided the target product, which was further crystallised from hot hexane/ethyl acetate. The crystals were filtered off, washed with cold pentane and dried under vacuum. Yield of **3**: 4.98 g (75%), red prisms. Lastly, the third, minor band of intense purple colour was evaporated to give a dark purple oily residue, which was identified as cyanamide **4** (0.53 g). The compound was further purified by dissolution in chloroform and precipitation with hexane. Crystals suitable for structure determination were obtained by liquid-phase diffusion of hexane into a chloroform solution of this compound.

*Analytical data for 1-bromo-1′-cyanoferrocene (**3**).* ^{1}H NMR (299.94 MHz, $CDCl_3$): δ = 4.30 (vt, J' = 1.9 Hz, 2 H, CH of fc), 4.44 (vt, J' = 1.9 Hz, 2 H, CH of fc), 4.57 (vt, J' = 1.9 Hz, 2 H, CH of fc), 4.68 (vt, J' = 1.9 Hz, 2 H, CH of fc) ppm. The data are in accordance with previously published values.[7]

*Analytical data for N-(bis(1′-bromoferrocenyl)methylene)cyanamide (**4**).* ^{1}H NMR (399.95 MHz, $CDCl_3$, 25°C): δ = 4.19 (br s, 2 H, CH of fc), 4.33 (br s, 2 H, CH of fc), 4.46 (br s, 2 H, CH of fc), 4.56 (br s, 2 H, CH of fc), 4.69 (vt, J' = 2.0 Hz, 4 H, CH of fc), 5.07 (br s, 2 H, CH of fc), 5.35 (br s, 2 H, CH of fc) ppm. ^{1}H NMR (399.95 MHz, $CDCl_3$, 50°C): δ = 4.25 (br s, 4 H, CH of fc), 4.50 (br s, 4 H,

CH of fc), 4.67 (vt, J' = 2.0 Hz, 4 H, CH of fc), 5.20 (br s, 4 H, CH of fc) ppm. $^{13}C\{^1H\}$ NMR (100.58 MHz, $CDCl_3$, 25°C): δ = 70.03 (br s, fc), 70.58 (br s, fc), 72.60 (s, fc), 72.98 (br s, fc), 73.66 (br s, fc), 75.70 (br s, fc), 116.13 (s, C≡N), 191.20 (s, C=N) ppm. ESI– MS: *m/z* = 379 ($[Cp(CNCN)fcBr]^-$). IR (Nujol): ν_{max} = 2161 s, 1537 s, 1409 m, 1400 w, 1350 m, 1323 w, 1302 s, 1230 w, 1216 w, 1152 m, 1067 m, 1049 m, 1038 m, 1023 m, 1003 w, 962 w, 897 w, 877 w, 868 m, 843 w, 822 s, 738 w, 663 w, 540 m, 518 m, 495 s, 482 s, 459 m, 423 w cm^{-1}. Anal. Calc. for $C_{22}H_{16}Br_2Fe_2N_2$ (579.9): C 45.57, H 2.78, N 4.83%. Found: C 45.24, H 2.70, N 4.76%.

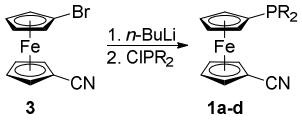

3 **1a-d**

General procedure for the preparation of phosphinonitriles R₂PfcC≡N (1). Under an argon atmosphere, compound **3** (1.45 g, 5.0 mmol) was dissolved in dry THF (40 mL), and the resulting red solution was cooled to –78°C in a dry ice-ethanol bath. An *n*-butyllithium solution (2.0 mL of 2.5 M in hexanes, 5.0 mmol) was added in small portions. The mixture was stirred at –78°C for 1 hour, subsequently adding dropwise the respective chlorophosphine (6.0 mmol). After stirring for an additional hour, the cooling bath was removed, and the reaction mixture was stirred at room temperature for 2 hours (overnight for chloro-di(2-furyl)phosphine). Then, the reaction was quenched by adding saturated aqueous $NaHCO_3$ (10 mL), the organic phase was separated, and the aqueous layer was extracted with diethyl ether (2× 10 mL). The combined organic layers were washed with brine, dried over $MgSO_4$ and evaporated with chromatographic silica gel. The pre-adsorbed crude product was purified by column chromatography on silica gel using a hexane/ethyl acetate (3:1) mixture as the eluent. The first yellow (minor) band, predominantly containing cyanoferrocene, was discarded. The second orange band was collected and evaporated to afford the product, which was further crystallised.

*Preparation of iPr₂PfcC≡N (**1a**)*. The general procedure was used, and the product was crystallised by dissolving in hot heptane and cooling the saturated solution slowly to –18°C. Yield: 1.47 g (90%), red needles. ^1H NMR (399.95 MHz, $CDCl_3$): δ = 1.07 (dd, $^3J_{HH}$ = 7.0 Hz, $^3J_{HP}$ = 7.0 Hz, 6 H, CHMe_2), 1.10 (dd, $^3J_{HH}$ = 7.1 Hz, $^3J_{HP}$ = 9.0 Hz, 6 H, CHMe_2), 1.93 (sept of d, $^3J_{HH}$ = 7.0 Hz, $^2J_{HH}$ = 2.0 Hz, 2 H, C*H*Me_2), 4.34 (vq, J' = 1.6 Hz, 2 H, CH of fc), 4.37 (vt, J' = 1.9 Hz, 2 H, CH of fc), 4.50 (vt, J' = 1.8 Hz, 2 H, CH of fc), 4.63 (vt, J' = 1.9 Hz, 2 H, CH of fc) ppm. $^{13}C\{^1H\}$ NMR (100.58 MHz, $CDCl_3$): δ = 19.82 (d, $^2J_{CP}$ = 10 Hz, CH*C*H_3), 20.03 (d, $^2J_{CP}$ = 15 Hz, CH*C*H_3), 23.38 (d, $^1J_{CP}$ = 11 Hz, *C*HCH$_3$), 52.45 (s, *C*–CN of fc), 72.46 (d, J_{CP} = 2 Hz, CH of fc), 72.52 (s, CH of fc), 72.68 (s, CH of fc), 73.25 (d, J_{CP} = 10 Hz, CH of fc), 79.36 (d, $^1J_{CP}$ = 21 Hz, *C*–P(*i*Pr)$_2$ of fc), 120.00 (s, C≡N) ppm. $^{31}P\{^1H\}$ NMR (161.90 MHz, $CDCl_3$): δ = 0.1 (s, P(*i*Pr)$_2$) ppm. ESI+ MS: *m/z* = 328 ($[M + H]^+$), 350 ($[M + Na]^+$), 366 ($[M + K]^+$). IR (Nujol): ν_{max} = 2224 s, 1364 m. 1307 w, 1233 s, 1197 w, 1156

m, 1055 m, 1040 m, 1030 s, 913 w, 881 w, 859 w, 845 m, 821 s, 655 w, 637 w, 607 w, 558 m, 508 m, 492 s, 476 m, 466 s cm^{-1}. Anal. Calc. for $C_{17}H_{22}FeNP$ (327.2): C 62.41, H 6.78, N 4.28%. Found: C 62.00, H 6.48, N 4.16%.

*Preparation of Cy₂PfcC≡N (**1b**).* This compound was prepared according to the general procedure. The product was crystallised from hot ethyl acetate/heptane. Yield: 1.44 g (71%), orange-red needles. ^{1}H NMR (399.95 MHz, $CDCl_3$): δ = 1.00-1.38 (m, 10 H, Cy), 1.64-1.94 (m, 12 H, Cy), 4.31 (vq, J' = 1.6 Hz, 2 H, CH of fc), 4.36 (vt, J' = 1.9 Hz, 2 H, CH of fc), 4.48 (vt, J' = 1.8 Hz, 2 H, CH of fc), 4.61 (vt, J' = 1.9 Hz, 2 H, CH of fc) ppm. $^{13}C\{^{1}H\}$ NMR (100.58 MHz, $CDCl_3$): δ = 26.78 (s, CH_2 of Cy), 27.62 (d, J_{CP} = 8 Hz, CH_2 of Cy), 27.72 (d, J_{CP} = 11 Hz, CH_2 of Cy), 30.57 (d, J_{CP} = 13 Hz, CH_2 of Cy), 30.67 (d, J_{CP} = 10 Hz, CH_2 of Cy), 33.76 (d, J_{CP} = 11 Hz, CH of Cy), 52.92 (s, *C*–CN of fc), 72.77 (d, J_{CP} = 2 Hz, CH of fc), 72.85 (s, CH of fc), 73.16 (s, CH of fc), 73.96 (d, J_{CP} = 10 Hz, CH of fc), 80.10 (d, $^{1}J_{CP}$ = 20 Hz, *C*–PCy_2 of fc), 120.47 (s, C≡N) ppm. $^{31}P\{^{1}H\}$ NMR (161.90 MHz, $CDCl_3$): δ = –8.0 (s, PCy_2) ppm. ESI+ MS: *m/z* = 408 ($[M + H]^+$), 430 ($[M + Na]^+$), 446 ($[M + K]^+$). IR (Nujol): ν_{max} = 2225 s, 1343 m, 1263 w, 1232 m, 1192 m, 1176 w, 1154 m, 1030 s, 1000 m, 914 m, 884 w, 845 s, 821 s, 556 m, 507 m, 488 s, 462 s, 441 m cm^{-1}. Anal. Calc. for $C_{23}H_{30}FeNP$ (407.3): C 67.82, H 7.42, N 3.44%. Found: C 67.77, H 7.42, N 3.36%.

*Preparation of Fur₂PfcC≡N (**1d**)*. The general procedure described was followed, and the compound was purified by crystallization from hot hexane. Yield: 1.61g (86%), orange needles. ^{1}H NMR (399.95 MHz, $CDCl_3$): δ = 4.24 (vt, J' = 2.0 Hz, 2 H, CH of fc), 4.51 (vt, J' = 2.0 Hz, 2 H, CH of fc), 4.53 (vt of d, J' = 1.8 Hz, J = 0.6 Hz, 2 H, CH of fc), 4.56 (vq, J' = 1.9 Hz, 2 H, CH of fc), 6.41 (dt, J = 3.3 Hz, J = 1.7 Hz, 2 H, CH of Fur), 6.72 (ddd, J = 3.3 Hz, J = 2.0 Hz, J = 0.7 Hz, 2 H, CH of Fur), 7.67 (m, 2 H, CH of Fur) ppm. $^{13}C\{^{1}H\}$ NMR (100.58 MHz, $CDCl_3$): δ = 52.80 (s, *C*–CN of fc), 71.89 (d, J = 1 Hz, CH of fc), 72.60 (s, CH of fc), 73.59 (d, J_{CP} = 5 Hz, CH of fc), 75.68 (d, J_{CP} = 17 Hz, CH of fc), 110.67 (d, J_{CP} = 6 Hz, CH of Fur), 119.58 (s, C≡N), 120.40 (d, J_{CP} = 25 Hz, CH of Fur), 147.06 (d, J_{CP} = 2 Hz, CH of Fur), 151.21 (d, J_{CP} = 8 Hz, C^{ipso} of Fur) ppm. Note: The ^{13}C NMR signal due to *C*–P of fc overlaps with one of the CH resonances. $^{31}P\{^{1}H\}$ NMR (161.90 MHz, $CDCl_3$): δ = –66.1 (s, $PFur_2$) ppm. ESI+ MS: *m/z* = 398 ($[M + Na]^+$). IR (Nujol): ν_{max} = 2228 s, 1552 m, 1312 w, 1231 m, 1220 m, 1210 m, 1163 m, 1155 m, 1123 m, 1108 w, 1059 w, 1028 s, 1015 sh, 1005 s, 912 sh, 903 s, 883 m, 848 m, 834 s, 746 s, 656 m, 646 w, 635 w, 627 w, 596 m, 555 m, 516 w, 502 m, 491 m, 479 s, 471 s, 450 s cm^{-1}. Anal. Calc. for $C_{19}H_{14}FeNO_2P$ (375.1): C 60.83, H 3.76, N 3.73%. Found: C 60.57, H 3.70, N 3.52%.

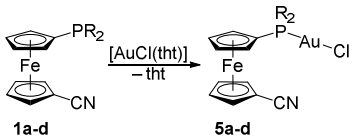

1a-d 5a-d

General procedure for the preparation of complexes [AuCl(R$_2$PfcC≡N-κP)] (5). Solid [AuCl(tht)] (160 mg, 0.50 mmol) and the respective phosphinonitrile (0.50 mmol) were dissolved in dry dichloromethane (5 mL) under an argon atmosphere, and the orange solution was stirred at room temperature for 60 minutes. The product was obtained after evaporating the solvent under reduced pressure.

*Preparation of [AuCl(iPr$_2$PfcC≡N-κP)] (**5a**).* The product was prepared according to the general procedure. The crude product was dissolved in dichloromethane (1 mL), and the solution was poured into an excess of cold pentane. The precipitated solid was filtered off, washed with pentane (to remove residual tetrahydrothiophene) and dried under vacuum. Yield: 267 mg (95%), orange powder. The crystals suitable for structure determination were grown by liquid-phase diffusion of hexane into an acetone solution of the complex.

^{1}H NMR (399.95 MHz, $CDCl_3$): δ = 1.24 (dd, $^3J_{HH}$ = 7.0 Hz, $^3J_{HP}$ = 10.8 Hz, 6 H, CH*Me*$_2$), 1.29 (dd, $^3J_{HH}$ = 7.0 Hz, $^3J_{HP}$ = 9.8 Hz, 6 H, CH*Me*$_2$), 2.32 (d of sept, $^2J_{HP}$ = 8.7 Hz, $^3J_{HH}$ = 7.0 Hz, 2 H, C*H*Me$_2$), 4.55 (vq, J' = 2.0 Hz, 2 H, CH of fc), 4.64 (vt, J' = 2.0 Hz, 2 H, CH of fc), 4.72 (vtd, J' = 1.9 Hz, J' = 1.0 Hz, 2 H, CH of fc), 4.80 (vt, J' = 2.0 Hz, 2 H, CH of fc) ppm. ^{13}C{^{1}H} NMR (100.58 MHz, $CDCl_3$): δ = 19.36 (d, $^2J_{CP}$ = 9 Hz, CH*C*H$_3$), 19.38 (d, $^2J_{CP}$ = 12 Hz, CH*C*H$_3$), 25.34 (d, $^1J_{CP}$ = 36 Hz, *C*HCH$_3$), 53.64 (s, *C*–CN of fc), 70.17 (d, $^1J_{CP}$ = 57 Hz, *C*–P*i*Pr$_2$ of fc), 73.61 (s, CH of fc), 73.98 (s, CH of fc), 73.99 (d, J_{CP} = 10 Hz, CH of fc), 74.30 (d, J_{CP} = 7 Hz, CH of fc), 118.98 (s, C≡N) ppm. ^{31}P{^{1}H} NMR (161.90 MHz, $CDCl_3$): δ = 49.8 (s, P*i*Pr$_2$) ppm. ESI+ MS: *m/z* = 662 ([M + Na]$^+$). IR (Nujol): ν_{max} = 2228 s, 1252 m, 1231 m, 1201 w, 1169 m, 1036 s, 915 w, 889 w, 838 s, 828 s, 679 m, 652 m, 631 w, 547 m, 509 w, 499 m, 486 m, 468 m, 415 m cm^{-1}. Anal. Calc. for $C_{17}H_{23}AuClFeNP$ (559.6): C 36.49, H 3.96, N 2.50%. Found: C 36.84, H 3.89, N 2.53%.

*Preparation of [AuCl(Cy$_2$PfcC≡N-κP)] (**5b**).* The compound was prepared and isolated similarly to the isopropyl analogue. Yield: 316 mg (98%), orange powder. Crystals used for structure determination were grown by liquid-phase diffusion of hexane into an acetone solution of the complex.

^{1}H NMR (399.95 MHz, $CDCl_3$): δ = 1.13-1.52 (m, 10 H, Cy), 1.67-1.78 (m, 2 H, Cy), 1.80-1.94 (m, 4 H, Cy), 1.96-2.15 (m, 6 H, Cy), 4.51 (vq, J' = 2.0 Hz, 2 H, CH of fc), 4.62 (vt, J' = 2.0 Hz, 2 H, CH of fc), 4.70 (vtd, J' = 2.0 Hz, J' = 1.0 Hz, 2 H, CH of fc), 4.77 (vt, J' = 2.0 Hz, 2 H, CH of fc) ppm. ^{13}C{^{1}H} NMR (100.58 MHz, $CDCl_3$): δ = 25.61 (d, J_{CP} = 2 Hz, CH_2 of Cy), 26.45 (d, J_{CP} = 2 Hz, CH_2 of Cy), 26.58 (s, CH_2 of Cy), 29.72 (d, J_{CP} = 2 Hz, CH_2 of Cy), 29.98 (s, CH_2 of Cy), 34.69 (d, J_{CP} = 35 Hz, CH of Cy), 53.70 (s, *C*–CN of fc), 70.84 (d, J_{CP} = 57 Hz, *C*–PCy$_2$ of fc), 73.70 (s, CH of fc), 73.77 (s, CH of fc), 73.98 (d, J_{CP} = 7 Hz, CH of fc), 74.41 (d, J_{CP} = 10 Hz, CH of fc), 119.04 (s, C≡N) ppm. ^{31}P{^{1}H}

NMR (161.90 MHz, $CDCl_3$): δ = 41.4 (s, PCy_2) ppm. ESI+ MS: *m/z* = 662 ($[M + Na]^+$), 678 ($[M + K]^+$). IR (Nujol): ν_{max} = 2224 s, 1347 w, 1310 w, 1267 w, 1231 m, 1201 m, 1181 m, 1170 m, 1111 w, 1038 m, 1005 w, 911 w, 894 w, 848 m, 828 s, 755 w, 736 m, 630 m, 555 m, 542 m, 525 m, 511 w, 493 s, 470 s, 446 m, 433 m cm^{-1}. Anal. Calc. for $C_{23}H_{30}AuClFeNP$ (639.7): C 43.18, H 4.73, N 2.19%. Found: C 43.21, H 4.57, N 2.09%.

*Preparation of [AuCl(Fur₂PfcC≡N-κP)] (**5d**).* The orange oily crude product obtained using the general procedure was dissolved in acetone, and the solution was layered with hexane. Crystallisation over several days afforded orange crystals (used also for structure determination), which were filtered off, washed with pentane and dried under vacuum. Yield: 240 mg (79%), orange needles.

^1H NMR (399.95 MHz, $CDCl_3$): δ = 4.50 (vt, J' = 2.0 Hz, 2 H, CH of fc), 4.62 (vt, J' = 2.0 Hz, 2 H, CH of fc), 4.75 (vq, J' = 1.7 Hz, 2 H, CH of fc), 4.79 (apparent p, J' = 1.8 Hz, 2 H, CH of fc), 6.56 (dt, J = 3.5 Hz, J = 1.7 Hz, 2 H, CH of Fur), 7.11 (ddd, J = 3.5 Hz, J = 3.0 Hz, J = 0.7 Hz, 2 H, CH of Fur), 7.81 (td, J = 1.8 Hz, J = 0.7 Hz, 2 H, CH of Fur) ppm. $^{13}C\{^1H\}$ NMR (100.58 MHz, $CDCl_3$): δ = 53.96 (s, *C*–CN of fc), 69.86 (d, J_{CP} = 83 Hz, *C*–$PFur_2$ of fc), 72.95 (s, CH of fc), 73.49 (s, CH of fc), 75.14 (d, J_{CP} = 10 Hz, CH of fc), 75.93 (d, J_{CP} = 16 Hz, CH of fc), 111.45 (d, J_{CP} = 9 Hz, CH of Fur), 118.54 (s, C≡N), 124.25 (d, J_{CP} = 26 Hz, CH of Fur), 143.22 (d, J_{CP} = 94 Hz, C^{ipso} of Fur), 149.65 (d, J_{CP} = 6 Hz, CH of Fur) ppm. $^{31}P\{^1H\}$ NMR (161.90 MHz, $CDCl_3$): δ = –14.4 (s, $PFur_2$) ppm. ESI+ MS: *m/z* = 630 ($[M + Na]^+$). IR (Nujol): ν_{max} = 2230 s, 1721 w, 1551 m, 1410 w, 1387 m, 1311 w, 1234 w, 1218 m, 1196 m, 1186 m, 1177 m, 1126 s, 1060 w, 1031 m, 1019 s, 1012 sh, 911 m, 892 w, 882 m, 849 m, 836 m, 826 m, 775 s, 763 s, 647 m, 638 m, 626 m, 593 m, 552 s, 540 s, 524 m, 512 m, 476 s, 466 sh cm^{-1}. Anal. Calc. for $C_{19}H_{14}AuClFeNO_2P$ (607.7): C 37.56, H 2.32, N 2.31%. Found: C 37.50, H 2.23, N 2.15%.

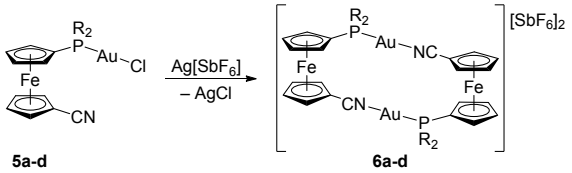

5a-d 6a-d

General procedure for the preparation of dimers [Au₂(μ(P,N)-R₂PfcC≡N)₂][SbF₆]₂ (6). Under an argon atmosphere, $Ag[SbF_6]$ (34.5 mg, 0.10 mmol) and the respective complex **5** (0.10 mmol) were dissolved in dry acetone (3 mL). The orange solution containing a white precipitate (AgCl) was stirred at room temperature, in the dark, for 60 minutes, and subsequently filtered through a PTFE syringe filter (0.45 μm pore size) directly into an excess of cold pentane. Sonication of the resulting orange cloudy mixture induced precipitation of the product, which was completed by allowing the suspension to stand at 5°C for 2 hours. The precipitate was collected, washed with pentane and dried under vacuum.

*Preparation of [Au₂(μ(P,N)-iPr₂PfcC≡N)₂][SbF₆]₂ (**6a**).* The compound was prepared according to the general method. Yield: 62 mg (82%), yellow powder.

^{1}H NMR (399.95 MHz, acetone-d$_6$): δ = 1.35 (dd, $^{3}J_{HH}$ = 7.0 Hz, $^{3}J_{HP}$ = 4.5 Hz, 6 H, CH*Me*$_2$), 1.39 (dd, $^{3}J_{HH}$ = 7.0 Hz, $^{3}J_{HP}$ = 5.7 Hz, 6 H, CH*Me*$_2$), 2.72 (d of sept, $^{2}J_{HP}$ = 8.5 Hz, $^{3}J_{HH}$ = 7.0 Hz, 2 H, C*H*Me$_2$), 4.89 (vq, J' = 2.0 Hz, 2 H, CH of fc), 5.06 (br s, 4 H, CH of fc), 5.35 (br s, 2 H, CH of fc) ppm. ^{31}P{^{1}H} NMR (161.90 MHz, acetone-d$_6$): δ = 49.0 (s, P*i*Pr$_2$) ppm. ESI+ MS: *m/z* = 583 ([Au(*i*Pr$_2$PfcCN)(MeOH)HCN]$^+$). IR (Nujol): ν_{max} = 2263 s, 1312 w, 1247 m, 1206 w, 1184 m, 1173 m, 1087 w, 1040 m, 917 m, 881 w, 850 m, 830 m, 686 w, 657 vs, 554 w, 514 m, 490 m, 471 m cm^{-1}. Anal. Calc. for $C_{34}H_{44}Au_2F_{12}Fe_2N_2P_2Sb_2$ (1519.8): C 26.87, H 2.92, N 1.84%. Found: C 26.66, H 2.75, N 1.69%.

*Preparation of [Au₂(μ(P,N)-Cy₂PfcC≡N)₂][SbF₆]₂ (**6b**)*. The general procedure was used. Yield: 74 mg (88%), orange powder. Crystals suitable for structure determination were obtained by liquid-phase diffusion of hexane into an acetone solution of the complex.

^{1}H NMR (399.95 MHz, acetone-d$_6$): δ = 1.16-1.62 (m, 10 H, Cy), 1.66-1.76 (m, 2 H, Cy), 1.82-1.96 (m, 4 H, Cy), 2.12-2.32 (m, 4 H, Cy), 2.46-2.60 (m, 2 H, Cy), 4.87 (vq, J' = 2.0 Hz, 2 H, CH of fc), 5.06 (br s, 4 H, CH of fc), 5.35 (br s, 2 H, CH of fc) ppm. ^{31}P{^{1}H} NMR (161.90 MHz, acetone-d$_6$): δ = 40.2 (s, PCy$_2$) ppm. ESI+ MS: *m/z* = 631 ([Au(Cy$_2$PfcCN)HCN]$^+$), 689 ([Au(Cy$_2$PfcCN)-(Me$_2$CO)HCN]$^+$). IR (Nujol): ν_{max} = 2256 s, 1711 m, 1294 w, 1272 w, 1243 w, 1243 w, 1220 m, 1202 m, 1174 m, 1113 w, 1058 w, 1041 m, 1004 w, 918 m, 897 w, 851 m, 838 m, 750 w, 657 vs, 609 w, 553 w, 515 m, 497 m, 472 m, 445 w cm^{-1}. Anal. Calc. for $C_{46}H_{60}Au_2F_{12}Fe_2N_2P_2Sb_2$ (1680.1): C 32.89, H 3.60, N 1.67%. Found: C 33.08, H 3.21, N 1.25%.

*Preparation of [Au₂(μ(P,N)-Fur₂PfcC≡N)₂][SbF₆]₂ (**6d**)*. The general procedure was followed. Yield: 71 mg (88%), orange powder. Crystals suitable for structure determination were obtained by liquid phase diffusion of hexane into an acetone solution of the complex.

^{1}H NMR (399.95 MHz, acetone-d$_6$): δ = 4.78 (vt, J' = 2.0 Hz, 2 H, CH of fc), 5.04 (m, 2 H, CH of fc), 5.08 (vq, J' = 1.8 Hz, 2 H, CH of fc), 5.17 (vt, J' = 1.9 Hz, 2 H, CH of fc), 6.80 (dt, J = 3.5 Hz, J = 1.7 Hz, 2 H, CH of Fur), 7.43 (ddd, J = 3.5 Hz, J = 2.8 Hz, J = 0.7 Hz, 2 H, CH of Fur), 8.18 (td, J = 1.9 Hz, J = 0.7 Hz, 2 H, CH of Fur) ppm. ^{31}P{^{1}H} NMR (161.90 MHz, acetone-d$_6$): δ = –16.7 (s, PFur$_2$) ppm. ESI+ MS: *m/z* = 599 ([Au(Fur$_2$PfcCN)HCN]$^+$), 802 ([Au(Fur$_2$PfcCN)(Fur$_2$PC$_5$H$_6$)]$^+$). IR (Nujol): ν_{max} = 2288 sh, 2274 s, 1553 w, 1395 w, 1309 w, 1246 w, 1221 w, 1202 w, 1188 m, 1178 w, 1132 m, 1065 w, 1038 m, 1012 s, 917 sh, 910 m, 885 w, 855 w, 833 m, 772 s, 755 s, 661 vs, 620 w, 609 w, 589 w, 575 m, 561 w, 538 w, 527 m, 514 m, 478 s, 466 s cm^{-1}. Anal. Calc. for $C_{38}H_{28}Au_2F_{12}Fe_2N_2O_4P_2Sb_2$ (1615.7): C 28.25, H 1.75, N 1.73%. Found: C 28.37, H 1.69, N 1.33%.

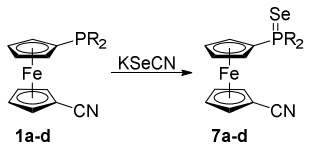

General procedure for the preparation of selenides R_2(Se)PfcC≡N (7).[8] Potassium selenocyanate (39.6 mg, 0.275 mmol) and the respective phosphinonitrile (0.250 mmol) were dissolved in a mixture of dry methanol (4 mL) and dry dichloromethane (1 mL), and the resulting mixture was stirred at room temperature overnight. Following evaporation with chromatography-grade silica gel, the pre-absorbed crude product was purified by column chromatography over silica gel, as specified in detail below.

*Preparation of iPr_2(Se)PfcC≡N (**7a**).* The crude product, prepared according to the general procedure, was purified by column chromatography on silica gel using hexane/ethyl acetate (3:1) as the eluent. Evaporation of the major orange band provided analytically pure product. Yield: 65 mg (64%), orange microcrystalline solid. ^{1}H NMR (399.95 MHz, $CDCl_3$): δ = 1.19 (dd, $^3J_{HH}$ = 7.0 Hz, $^3J_{HP}$ = 3.3 Hz, 6 H, CH*Me*$_2$), 1.23 (dd, $^3J_{HH}$ = 7.0 Hz, $^3J_{HP}$ = 3.6 Hz, 6 H, CH*Me*$_2$), 2.30 (d of sept, $^2J_{HP}$ = 8.4 Hz, $^3J_{HH}$ = 7.0 Hz, 2 H, C*H*Me$_2$), 4.60 (vq, J' = 1.8 Hz, 2 H, CH of fc), 4.64 (vq, J' = 1.7 Hz, 2 H, CH of fc), 4.68 (vt, J' = 2.0 Hz, 2 H, CH of fc), 4.80 (vt, J' = 2.0 Hz, 2 H, CH of fc) ppm. ^{13}C{^{1}H} NMR (100.58 MHz, $CDCl_3$): δ = 16.72 (d, $^2J_{CP}$ = 1 Hz, CH*C*H$_3$), 17.49 (d, $^2J_{CP}$ = 2 Hz, CH*C*H$_3$), 27.64 (d, $^1J_{CP}$ = 45 Hz, *C*HCH$_3$), 53.41 (s, *C*–CN of fc), 73.48 (d, J_{CP} = 8 Hz, CH of fc), 73.66 (s, CH of fc), 73.88 (d, J_{CP} = 9 Hz, CH of fc), 74.05 (s, CH of fc), 75.09 (d, $^1J_{CP}$ = 67 Hz, *C*–P*i*Pr$_2$ of fc), 119.35 (s, C≡N) ppm. ^{31}P{^{1}H} NMR (161.90 MHz, $CDCl_3$): δ = 57.8 (s with ^{77}Se satellites, $^1J_{PSe}$ = 715 Hz, P*i*Pr$_2$) ppm. ESI+ MS: *m/z* = 408 ([M + H]$^+$). IR (Nujol): ν_{max} = 2225 s, 1417 w, 1364 m, 1310 w, 1253 w, 1243 m, 1233 m, 1202 m, 1169 s, 1100 w, 1081 w, 1062 w, 1052 w, 1043 m, 1034 s, 935 w, 911 w, 891 m, 882 m, 859 w, 844 m, 828 s, 818 m, 676 s, 652 s, 629 m, 562 s, 554 s, 510 m, 498 s, 481 m, 470 s, 435 m cm^{-1}. Anal. Calc. for $C_{17}H_{22}FeNPSe$ (406.2): C 50.27, H 5.46, N 3.45%. Found: C 50.26, H 5.10, N 3.44%.

*Preparation of Cy_2(Se)PfcC≡N (**7b**).* The crude product was purified by chromatography on silica gel using hexane/ethyl acetate (1:1). The major orange band was collected and evaporated to afford analytically pure product. Yield: 85 mg (70%), yellow-orange solid. ^{1}H NMR (399.95 MHz, $CDCl_3$): δ = 1.10-1.46 (m, 10 H, Cy), 1.66-1.75 (m, 2 H, Cy), 1.78-1.92 (m, 4 H, Cy), 1.94-2.10 (m, 6 H, Cy), 4.57 (vq, J' = 1.8 Hz, 2 H, CH of fc), 4.63 (vq, J' = 1.7 Hz, 2 H, CH of fc), 4.65 (vt, J' = 2.0 Hz, 2 H, CH of fc), 4.79 (vt, J' = 2.0 Hz, 2 H, CH of fc) ppm. ^{13}C{^{1}H} NMR (100.58 MHz, $CDCl_3$): δ = 25.72 (d, J_{CP} = 2 Hz, CH_2 of Cy), 26.28 (d, J_{CP} = 2 Hz, CH_2 of Cy), 26.34 (d, J_{CP} = 4 Hz, CH_2 of Cy), 26.47 (d, J_{CP} = 3 Hz, CH_2 of Cy), 27.31 (d, J_{CP} = 4 Hz, CH_2 of Cy), 37.05 (d, J_{CP} = 45 Hz, CH of Cy), 53.48 (s, *C*–CN of fc), 73.22 (d, J_{CP} = 8 Hz, CH of fc), 73.81 (s, CH of fc), 73.89 (s, CH of fc), 74.08 (d, J_{CP} = 9 Hz, CH of fc), 75.72 (d, J_{CP} = 67 Hz, *C*–PCy_2 of fc), 119.42 (s, C≡N) ppm. ^{31}P{^{1}H} NMR (161.90 MHz, $CDCl_3$): δ = 49.5 (s with ^{77}Se satellites, $^1J_{PSe}$ = 708 Hz, PCy_2) ppm. ESI+ MS:

m/z = 488 ([M + H]$^+$). IR (Nujol): ν_{max} = 2229 s, 1346 m, 1311 w, 1297 m, 1273 w, 1231 m, 1215 w, 1200 m, 1181 m, 1169 s, 1115 w, 1084 w, 1063 w, 1038 s, 1027 m, 1002 m, 919 m, 896 m, 877 w, 851 m, 841 s, 825 m, 816 s, 748 m, 738 m, 633 m, 553 s, 547 s, 528 m, 512 m, 497 s, 486 m, 462 s, 444 m, 432 m cm^{-1}. Anal. Calc. for $C_{23}H_{30}FeNPSe$ (486.3): C 56.81, H 6.22, N 2.88%. Found: C 56.53, H 6.00, N 2.90%.

*Preparation of Ph$_2$(Se)PfcC≡N (**7c**).* The crude product was prepared as described above and further purified by column chromatography on silica gel with hexane/ethyl acetate (3:1). Only the major orange band was collected. Analytically pure product was obtained after evaporation. Yield: 104 mg (88%), orange solid. ^{1}H NMR (399.95 MHz, $CDCl_3$): δ = 4.52 (vt, *J*′ = 2.0 Hz, 2 H, CH of fc), 4.60 (vt, *J*′ = 2.0 Hz, 2 H, CH of fc), 4.62 (vq, *J*′ = 2.1 Hz, 2 H, CH of fc), 4.71 (vq, *J*′ = 1.8 Hz, 2 H, CH of fc), 7.41-7.52 (m, 6 H, Ph), 7.67-7.74 (m, 4 H, Ph) ppm. ^{13}C{^{1}H} NMR (100.58 MHz, $CDCl_3$): δ = 53.32 (s, *C*–CN of fc), 73.37 (s, CH of fc), 73.61 (s, CH of fc), 74.79 (d, J_{CP} = 9 Hz, CH of fc), 75.28 (d, J_{CP} = 12 Hz, CH of fc), 77.21 (d, J_{CP} = 86 Hz, *C*–PPh$_2$ of fc), 118.88 (s, C≡N), 128.46 (d, J_{CP} = 13 Hz, CH of Ph), 131.65 (d, J_{CP} = 3 Hz, CH of Ph), 131.95 (d, J_{CP} = 11 Hz, CH of Ph), 132.59 (d, J_{CP} = 79 Hz, C^{ipso} of Ph) ppm. ^{31}P{^{1}H} NMR (161.90 MHz, $CDCl_3$): *δ* 31.1 (s with ^{77}Se satellites, $^1J_{PSe}$ = 741 Hz, PPh$_2$) ppm. ESI+ MS: *m/z* 476 ([M + H]$^+$). IR (Nujol): ν_{max} = 2224 s, 1308 m, 1230 m, 1199 w, 1191 w, 1171 s, 1155 m, 1098 s, 1069 w, 1032 s, 997 w, 912 m, 840 s, 827 m, 755 s, 712 m, 702 m, 694 s, 638 m, 575 s, 554 m, 531 s, 490 m, 483 s, 469 m, 452 m, 437 w cm^{-1}. Anal. Calc. for $C_{23}H_{18}FeNPSe$ (474.2): C 58.26, H 3.83, N 2.95%. Found: C 58.00, H 3.65, N 2.90%.

*Preparation of Fur$_2$P(Se)PfcC≡N (**7d**).* The general procedure was followed to synthesize the crude product, which was purified by chromatography on silica gel in hexane/ethyl acetate (1:1). The orange viscous oil, obtained after evaporation of the major orange band, was crystallised from hot hexane. Cooling the solution to –18°C resulted in the formation of orange crystals, which were collected, washed with pentane and dried under vacuum. Yield: 79 mg (70%), orange needles. ^{1}H NMR (399.95 MHz, $CDCl_3$): δ = 4.49 (vt, *J*′ = 2.0 Hz, 2 H, CH of fc), 4.65 (vt, *J*′ = 2.0 Hz, 2 H, CH of fc), 4.70 (vq, *J*′ = 1.8 Hz, 2 H, CH of fc), 4.87 (d of vt, *J* = 2.9 Hz, *J*′ = 1.9 Hz, 2 H, CH of fc), 6.52 (dt, *J* = 3.5 Hz, *J* = 1.7 Hz, 2 H, CH of Fur), 7.13 (ddd, *J* = 3.4 Hz, *J* = 2.5 Hz, *J* = 0.8 Hz, 2 H, CH of Fur), 7.75 (ddd, *J* = 2.2 Hz, *J* = 1.7 Hz, *J* = 0.8 Hz, 2 H, CH of Fur) ppm. ^{13}C{^{1}H} NMR (100.58 MHz, $CDCl_3$): δ = 53.66 (s, *C*–CN of fc), 73.31 (s, CH of fc), 73.57 (s, CH of fc), 74.52 (d, J_{CP} = 11 Hz, CH of fc), 74.59 (d, J_{CP} = 98 Hz, *C*–PFur$_2$) of fc), 75.09 (d, J_{CP} = 14 Hz, CH of fc), 111.21 (d, J_{CP} = 9 Hz, CH of Fur), 119.01 (s, C≡N), 122.68 (d, J_{CP} = 22 Hz, CH of Fur), 146.27 (d, J_{CP} = 116 Hz, C^{ipso} of Fur), 148.78 (d, J_{CP} = 7 Hz, CH of Fur) ppm. ^{31}P{^{1}H} NMR (161.90 MHz, $CDCl_3$): δ = –6.4 (s with ^{77}Se satellites, $^1J_{PSe}$ = 777 Hz, PFur$_2$) ppm. ESI+ MS: *m/z* 456 ([M + H]$^+$). IR (Nujol): ν_{max} = 2226 s, 1548 m, 1388 m, 1361 m, 1311 w, 1232 w, 1208 m, 1200 m, 1175 m, 1126 s, 1061 w, 1054 w, 1035 m, 1004 s, 909 m, 883 w, 840 m, 827 m, 783 m, 774 sh, 768 s, 649 m, 630 m, 593

m, 578 s, 557 m, 536 s, 524 m, 512 m, 483 s, 464 s cm^{-1}. Anal. Calc. for $C_{19}H_{14}FeNO_2PSe$ (454.1): C 50.25, H 3.11, N 3.08%. Found: C 50.20, H 3.05, N 2.92%.

General procedure for the synthesis of propargyl amides 8. Under an argon atmosphere, 4-(dimethylamino)pyridine (61 mg, 0.5 mmol) was dissolved in dry dichloromethane (15 mL), and propargylamine (0.35 mL, 5.5 mmol) and dry triethylamine (0.77 mL, 5.5 mmol) were successively added. The resulting pale yellow solution was cooled in an ice bath, and the appropriate acyl chloride (5.0 mmol) was added dropwise. The reaction mixture was stirred at 0°C for 15 minutes and then at room temperature overnight. After quenching with water (10 mL), the organic layer was separated, and the aqueous layer was extracted with dichloromethane (2× 5 mL). The combined organic layers were washed with brine, dried over anhydrous $MgSO_4$ and evaporated. The crude product was dissolved in hot ethyl acetate/heptane mixture in the presence of charcoal and a small amount of silica gel, which were filtered off, and the colourless filtrate was allowed to cool slowly to 5°C to provide the target amide as a crystalline product.

*N-(Prop-2-yn-1-yl)benzamide (**8a**).*[9] The general procedure was used to prepare **8a**, yielding 0.49 g (62%) of a colourless crystalline solid. ^{1}H NMR (400.13 MHz, $CDCl_3$): δ = 2.28 (t, $^4J_{HH}$ = 2.6 Hz, 1H, C≡CH), 4.25 (dd, J_{HH} = 5.2 Hz, $^4J_{HH}$ = 2.6 Hz, 2 H, CH_2), 6.48 (br s, 1 H, NH), 7.40-7.46 (m, 2 H, Ph), 7.48-7.54 (m, 1 H, Ph), 7.76-7.82 (m, 2 H, Ph) ppm. ^{13}C{^{1}H} NMR (100.62 MHz, $CDCl_3$): δ = 29.78 (s, CH_2), 71.85 (s, C≡*C*H), 79.50 (s, *C*≡CH), 127.04 (s, CH of Ph), 128.61 (s, CH of Ph), 131.78 (s, CH of Ph), 133.73 (s, C^{ipso} of Ph), 167.13 (s, C=O) ppm.

*4-Methyl-N-(prop-2-yn-1-yl)benzamide (**8b**).*[10] The general procedure was used to prepare **8b**, yielding 0.60 g (69%) of a colourless crystalline solid. ^{1}H NMR (400.1g MHz, $CDCl_3$): δ = 2.27 (t, $^4J_{HH}$ = 2.6 Hz, 1 H, C≡CH), 2.39 (s, 3 H, CH_3), 4.24 (dd, J_{HH} = 5.2 Hz, $^4J_{HH}$ = 2.6 Hz, 2 H, CH_2), 6.42 (br s, 1 H, NH), 7.23 (apparent d, J_{HH} = 7.9 Hz, 2 H, CH of C_6H_4), 7.69 (apparent d, J_{HH} = 8.2 Hz, 2 H, CH of C_6H_4) ppm. ^{13}C{^{1}H} NMR (100.62 MHz, $CDCl_3$): δ = 21.47 (s, CH_3), 29.72 (s, CH_2), 71.76 (s, C≡*C*H), 79.64 (s, *C*≡CH), 127.04 (s, CH of C_6H_4), 129.25 (s, CH of C_6H_4), 130.88 (s, C^{ipso} of C_6H_4), 142.24 (s, C^{ipso} of C_6H_4), 167.06 (s, C=O) ppm.

*4-Methoxy-N-(prop-2-yn-1-yl)benzamide (**8c**).*[9] The general procedure was used to prepare **8c**, yielding 0.73 g (77%) of a colourless crystalline solid. ^{1}H NMR (400.13 MHz, $CDCl_3$): δ = 2.27 (t, $^4J_{HH}$ = 2.6 Hz, 1 H, C≡CH), 3.84 (s, 3 H, OCH_3), 4.24 (dd, J_{HH} = 5.2 Hz, $^4J_{HH}$ = 2.6 Hz, 2 H, CH_2), 6.39 (br s, 1 H, NH), 6.92 (apparent d, J_{HH} = 8.9 Hz, 2 H, CH of C_6H_4), 7.76 (apparent d, J_{HH} = 8.9 Hz, 2 H, CH of C_6H_4) ppm. ^{13}C{^{1}H} NMR (100.62 MHz, $CDCl_3$): δ = 29.71 (s, CH_2), 55.41 (s, OCH_3), 71.70 (s, C≡*C*H), 79.74 (s, *C*≡CH), 113.79 (s, CH of C_6H_4), 126.01 (s, C^{ipso} of C_6H_4), 128.89 (s, CH of C_6H_4), 162.39 (s, C^{ipso} of C_6H_4), 166.65 (s, C=O) ppm.

*4-Chloro-N-(prop-2-yn-1-yl)benzamide (**8d**).*[11] The general procedure was used to prepare **8d**, yielding 0.71 g (73%) of a colourless crystalline solid. ^{1}H NMR (400.13 MHz, $CDCl_3$): δ = 2.29 (t, $^{4}J_{HH}$ = 2.6 Hz, 1 H, C≡CH), 4.24 (dd, J_{HH} = 5.2 Hz, $^{4}J_{HH}$ = 2.6 Hz, 2 H, CH_2), 6.45 (br s, 1 H, NH), 7.41 (apparent d, J_{HH} = 8.7 Hz, 2 H, CH of C_6H_4), 7.73 (apparent d, J_{HH} = 8.7 Hz, 2 H, CH of C_6H_4) ppm. ^{13}C{^{1}H} NMR (100.62 MHz, $CDCl_3$): δ = 29.87 (s, CH_2), 72.04 (s, C≡*C*H), 79.26 (s, *C*≡CH), 128.49 (s, CH of C_6H_4), 128.89 (s, CH of C_6H_4), 132.08 (s, C^{ipso} of C_6H_4), 138.10 (s, C^{ipso} of C_6H_4), 166.09 (s, C=O) ppm.

*4-(Trifluoromethyl)-N-(prop-2-yn-1-yl)benzamide (**8e**).*[12] The general procedure was used to prepare **8e**, yielding 0.86 g (76%) of a colourless crystalline solid. ^{1}H NMR (399.95 MHz, $CDCl_3$): δ = 2.30 (t, $^{4}J_{HH}$ = 2.6 Hz, 1 H, C≡CH), 4.27 (dd, J_{HH} = 5.3 Hz, $^{4}J_{HH}$ = 2.6 Hz, 2 H, CH_2), 6.53 (br s, 1 H, NH), 7.68-7.73 (m, 2 H, CH of C_6H_4), 7.88-7.93 (m, 2 H, CH of C_6H_4) ppm. ^{13}C{^{1}H} NMR (100.58 MHz, $CDCl_3$): δ = 29.97 (s, CH_2), 72.23 (s, C≡*C*H), 79.05 (s, *C*≡CH), 123.59 (q, $^{1}J_{CF}$ = 273 Hz, CF_3), 125.70 (q, $^{3}J_{CF}$ = 4 Hz, CH of C_6H_4), 127.55 (s, CH of C_6H_4), 133.55 (q, $^{2}J_{CF}$ = 33 Hz, C^{ipso} of C_6H_4), 136.99 (s, C^{ipso} of C_6H_4), 165.91 (s, C=O) ppm. ^{19}F NMR (376.29 MHz, $CDCl_3$): δ = –63.3 (s, CF_3) ppm.

*N-(Prop-2-yn-1-yl)cyclohexanecarboxamide (**8f**).*[13] The general procedure was used to prepare **8f**, yielding 0.73 g (88%) of a colourless crystalline solid. ^{1}H NMR (400.13 MHz, $CDCl_3$): δ = 1.15-1.33 (m, 3 H, CH_2 of Cy), 1.37-1.51 (m, 2 H, CH_2 of Cy), 1.63-1.71 (m, 1 H, CH_2 of Cy), 1.74-1.92 (m, 4 H, CH_2 of Cy), 2.11 (tt, J_{HH} = 11.7 Hz, J_{HH} = 3.5 Hz, 1 H, CH of Cy), 2.22 (t, $^{4}J_{HH}$ = 2.6 Hz, 1 H, C≡CH), 4.05 (dd, J_{HH} = 5.2 Hz, $^{4}J_{HH}$ = 2.6 Hz, 2 H, CH_2), 5.77 (br s, 1 H, NH) ppm. ^{13}C{^{1}H} NMR (100.62 MHz, $CDCl_3$): δ = 25.68 (s, CH_2 of Cy), 25.70 (s, CH_2 of Cy), 29.09 (s, CH_2), 29.52 (s, CH_2 of Cy), 45.22 (s, CH of Cy), 71.49 (s, C≡*C*H), 79.81 (s, *C*≡CH), 175.65 (s, C=O) ppm.

Kinetic study of gold(I)-catalysed cyclization of propargyl amides 8. *Method A*. The respective amide **8** (typically 0.2 mmol or 0.1 mmol) was dissolved in 0.8 mL of CD_2Cl_2, and the solution was added to a solid catalyst (**6** or [Au(MeCN)(PPh_3)][SbF_6], typically 1 mol.% of Au), which immediately dissolved, forming a yellow solution (colourless when using [Au(MeCN)(PPh_3)]-[SbF_6] as the catalyst), and the reaction mixture was transferred to the NMR tube. NMR spectra were recorded every 10 minutes for 3 hours. Conversion was determined by comparing the integral intensities of the signals due to the methylene group of the starting amide and to product **9**.

Method B (for low catalyst loadings). A stock solution (containing 0.6 mM "Au") was freshly prepared by dissolving **6d** (2.42 mg, 1.5 μmol) in CD_2Cl_2 in a 5-mL volumetric flask. An appropriate amount of stock solution was mixed with a solution of the appropriate *N*-propargylamide **8** (0.2 mmol) in CD_2Cl_2, in a total volume of 0.8 mL. The yellow reaction mixture

was transferred to the NMR tube. NMR spectra were recorded every 10 minutes for 90 min. Conversion was determined as specified above.

Catalyst poisoning experiment. The solution of amide **8a** (31.8 mg, 0.2 mmol) and ($PhCH_2NEt_3$)Cl (0.6 mg, 2.6 μmol) in CD_2Cl_2 (0.8 mL) was added onto the solid **6d** (1.61 mg, 1.0 μmol), which immediately dissolved. The resulting yellow solution was transferred to an NMR tube. ^{1}H NMR spectra were collected every 10 minutes for the period of 30 minutes.

Catalytic experiments with isolation of the product. A solution of the appropriate amide **8** (0.2 mmol) in dry dichloromethane (0.8 mL) was added to a vial loaded with catalyst **6d** (1.61 mg, 1.0 μmol), and the mixture was stirred at room temperature for 3 hours. The product was then isolated by chromatography on a silica gel column using hexane/ethyl acetate (5:1) as the eluent. The evaporation of the eluate provided the product in sufficient purity. Note: Prolonged storage of the product in the presence of oxygen leads to its degradation to peroxo-compounds, as previously described.[12]

*5-Methylene-2-phenyl-4,5-dihydrooxazole (**9a**)*.[9] Colourless liquid. ^{1}H NMR (400.13 MHz, $CDCl_3$): δ = 4.36 (q, $^2J_{HH} \approx {}^4J_{HH} \approx 2.7$ Hz, 1 H, C=C*H*H), 4.65 (t, $^4J_{HH} \approx 2.9$ Hz, 2 H, NCH_2), 4.81 (q, $^2J_{HH} \approx {}^4J_{HH} \approx 3.0$ Hz, 1 H, C=CH*H*), 7.40-7.47 (m, 2 H, CH of C_6H_5), 7.47-7.54 (m, 1 H, CH of C_6H_5), 7.94-8.01 (m, 2 H, CH of C_6H_5) ppm. ^{13}C{^{1}H} NMR (100.62 MHz, $CDCl_3$): δ = 57.77 (s, NCH_2), 83.74 (s, C=*C*H_2), 126.77 (s, C^{ipso} of C_6H_5), 127.99 (s, CH of C_6H_5), 128.48 (s, CH of C_6H_5), 131.79 (s, CH of C_6H_5), 158.85 (s, *C*=CH_2), 163.70 (s, C=N) ppm.

*5-Methylene-2-(4-methylphenyl)-4,5-dihydrooxazole (**9b**)*.[14] Colourless liquid. ^{1}H NMR (400.13 MHz, $CDCl_3$): δ = 2.40 (s, 3 H, CH_3), 4.34 (q, $^2J_{HH} \approx {}^4J_{HH} \approx 2.7$ Hz, 1 H, C=C*H*H), 4.63 (t, $^4J_{HH} \approx 2.9$ Hz, 2 H, NCH_2), 4.80 (q, $^2J_{HH} \approx {}^4J_{HH} \approx 3.0$ Hz, 1 H, C=CH*H*), 7.24 (apparent d, $J_{HH} = 7.6$ Hz, 2 H, CH of C_6H_4), 7.86 (apparent d, $J_{HH} = 8.2$ Hz, 2 H, CH of C_6H_4) ppm. ^{13}C{^{1}H} NMR (100.62 MHz, $CDCl_3$): δ = 21.61 (s, CH_3), 57.72 (s, NCH_2), 83.52 (s, C=*C*H_2), 123.98 (s, C^{ipso} of C_6H_4), 127.95 (s, CH of C_6H_4), 129.21 (s, CH of C_6H_4), 142.26 (s, C^{ipso} of C_6H_4), 158.94 (s, *C*=CH_2), 163.78 (s, C=N) ppm.

*2-(4-Methoxyphenyl)-5-methylene-4,5-dihydrooxazole (**9c**)*.[9] Colourless solid. ^{1}H NMR (400.13 MHz, $CDCl_3$): δ = 3.85 (s, 3 H, CH_3), 4.34 (q, $^2J_{HH} \approx {}^4J_{HH} \approx 2.7$ Hz, 1 H, C=C*H*H), 4.62 (t, $^4J_{HH} \approx 2.8$ Hz, 2 H, NCH_2), 4.78 (q, $^2J_{HH} \approx {}^4J_{HH} \approx 2.9$ Hz, 1 H, C=CH*H*), 6.94 (apparent d, $J_{HH} = 8.9$ Hz, 2 H, CH of C_6H_4), 7.92 (apparent d, $J_{HH} = 8.9$ Hz, 2 H, CH of C_6H_4) ppm. ^{13}C{^{1}H} NMR (100.62 MHz, $CDCl_3$): δ = 55.38 (s, CH_3), 57.70 (s, NCH_2), 83.37 (s, C=*C*H_2), 113.87 (s, CH of C_6H_4), 119.24 (s, C^{ipso} of C_6H_4), 129.75 (s, CH of C_6H_4), 159.01 (s, *C*=CH_2), 162.41 (s, C^{ipso} of C_6H_4), 163.45 (s, C=N) ppm.

*2-(4-Chlorophenyl)-5-methylene-4,5-dihydrooxazole (**9d**)*. Colourless solid. ^{1}H NMR (400.13 MHz, $CDCl_3$): δ = 4.37 (q, $^{2}J_{HH} \approx {}^{4}J_{HH} \approx 2.7$ Hz, 1 H, C=C*H*H), 4.64 (t, $^{4}J_{HH} \approx 2.9$ Hz, 2 H, NCH_2), 4.81 (q, $^{2}J_{HH} \approx {}^{4}J_{HH} \approx 3.0$ Hz, 1 H, C=CH*H*), 7.42 (apparent d, $J_{HH} = 8.7$ Hz, 2 H, CH of C_6H_4), 7.91 (apparent d, $J_{HH} = 8.6$ Hz, 2 H, CH of C_6H_4) ppm. ^{13}C{^{1}H} NMR (100.62 MHz, $CDCl_3$): δ = 57.80 (s, NCH_2), 84.07 (s, C=*C*H_2), 125.26 (s, C^{ipso} of C_6H_4), 128.85 (s, CH of C_6H_4), 129.32 (s, CH of C_6H_4), 138.06 (s, C^{ipso} of C_6H_4), 158.67 (s, *C*=CH_2), 162.85 (s, C=N) ppm. Anal. Calc. for $C_{10}H_8ClNO$ (193.6): C 32.03, H 4.16, N 7.23%. Found: C 62.35, H 4.32, N 6.96%.

*5-Methylene-2-(4-(trifluoromethyl)phenyl)-4,5-dihydrooxazole (**9e**)*.[14] White solid. ^{1}H NMR (399.95 MHz, $CDCl_3$): δ = 4.41 (q, $^{2}J_{HH} \approx {}^{4}J_{HH} \approx 2.8$ Hz, 1 H, C=C*H*H), 4.68 (t, $^{4}J_{HH} \approx 2.9$ Hz, 2 H, NCH_2), 4.85 (q, $^{2}J_{HH} \approx {}^{4}J_{HH} \approx 3.1$ Hz, 1 H, C=CH*H*), 7.71 (apparent d, $J_{HH} = 8.1$ Hz, 2 H, CH of C_6H_4), 8.10 (apparent d, $J_{HH} = 8.0$ Hz, 2 H, CH of C_6H_4) ppm. ^{13}C{^{1}H} NMR (100.58 MHz, $CDCl_3$): δ = 57.89 (s, NCH_2), 84.45 (s, C=*C*H_2), 123.70 (q, $^{1}J_{CF} = 273$ Hz, CF_3), 125.51 (q, $^{3}J_{CF} = 4$ Hz, CH of C_6H_4), 128.39 (s, CH of C_6H_4), 130.12 (s, C^{ipso} of C_6H_4), 133.42 (q, $^{2}J_{CF} = 33$ Hz, C^{ipso} of C_6H_4), 158.54 (s, *C*=CH_2), 162.60 (s, C=N) ppm. ^{19}F NMR (376.29 MHz, $CDCl_3$): δ = –63.3 (s, CF_3) ppm.

*2-Cyclohexyl-5-methylene-4,5-dihydrooxazole (**9f**)*.[15] Colourless liquid. ^{1}H NMR (400.13 MHz, $CDCl_3$): δ = 1.17-1.37 (m, 3 H, CH_2 of Cy), 1.39-1.52 (m, 2 H, CH_2 of Cy), 1.63-1.72 (m, 1 H, CH_2 of Cy), 1.74-1.84 (m, 2 H, CH_2 of Cy), 1.92-2.01 (m, 2 H, CH_2 of Cy), 2.36 (tm, $J_{HH} = 11.3$ Hz, 1 H, CH of Cy), 4.23 (q, $^{2}J_{HH} \approx {}^{4}J_{HH} \approx 2.6$ Hz, 1 H, C=C*H*H), 4.40 (td, $^{4}J_{HH} = 2.9$ Hz, $^{5}J_{HH} = 1.4$ Hz, 2 H, NCH_2), 4.63 (q, $^{2}J_{HH} \approx {}^{4}J_{HH} \approx 2.9$ Hz, 1 H, C=CH*H*) ppm. ^{13}C{^{1}H} NMR (100.62 MHz, $CDCl_3$): δ = 25.53 (s, CH_2 of Cy), 25.80 (s, CH_2 of Cy), 29.38 (s, CH_2 of Cy), 37.38 (s, CH of Cy), 57.13 (s, NCH_2), 82.73 (s, C=*C*H_2), 159.15 (s, *C*=CH_2), 170.67 (s, C=N) ppm.

X-Ray crystallography

Full-set diffraction data ($\pm h \pm k \pm l$, θ_{max} = 26.0 or 27.5°) were collected using a Bruker D8 VENTURE Kappa Duo instrument equipped with a PHOTON100 detector, a IμS micro-focus X-ray tube (Mo Kα radiation, λ = 0.71073 Å) and a Cryostream cooler (Oxford Cryosystems). The structures were solved using direct methods (SHELXT-2014)[16] and subsequently refined by full-matrix least-squares based on F^2 using SHELXL-2014 or SHELXL-2017.[17] All non-hydrogen atoms were refined with anisotropic displacement parameters. The hydrogen atoms were included in their theoretical positions and refined as riding atoms with U_{iso}(H) set to a 1.2U_{eq} of their bonding carbon atom. The cyano group in the structure of **5a** was disordered over two positions. The refined occupancies were 47:53. A recent version of the PLATON program[18] was used to perform geometric calculations and to prepare all structural diagrams. Selected crystallographic data, data collection and structure refinement parameters are outlined in Table S1. The individual structures are discussed below.

CCDC 1909789 (**1d**), 1909790 (**4**), 1909791 (**5a**), 1909792 (**5b**), 1909793 (**5d**), 1909794 (**6b**·Me_2CO), and 1909795 (**6d**), contain the supplementary crystallographic data for this paper. These data are available free of charge from The Cambridge Crystallographic Data Centre.

Table S1. Selected crystallographic data and structure refinement parameters

Compound	**1d**	**4**
Formula	$C_{19}H_{14}FeNO_2P$	$C_{22}H_{16}Br_2Fe_2N_2$
M/g mol^{-1}	375.13	579.89
Crystal system	monoclinic	monoclinic
Space group	$P2_1/c$ (No. 14)	$P2_1/n$ (No. 14)
T/K	150(2)	120(2)
a/Å	10.7290(4)	13.7570(4)
b/Å	19.7011(8)	10.0313(3)
c/Å	7.6835(3)	14.6288(4)
α/deg	90	90
β/deg	93.613(1)	110.809(1)
γ/deg	90	90
V/Å^3	1620.9(1)	1887.10(9)
Z	4	4
μ(Mo Kα)/mm^{-1}	1.039	5.783
F(000)	768	1136
Diffrns collected	16586	27109
Independent diffrns	3704	4317
Observed diffrns[a]	3430	4005
R_{int}[b]/%	2.17	3.48
No. of parameters	217	253
R[c] obsd diffrns/%	2.37	1.93
R, wR[c] all data /%	2.67, 5.97	2.20, 4.57
Δρ/e Å^{-3}	0.33, −0.34	0.39, −0.64

[a] Diffractions with $I > 2\sigma(I)$. [b] Definitions: $R_{int} = \Sigma|F_o^2 - F_o^2(\text{mean})|/\Sigma F_o^2$, where F_o^2(mean) denotes the average intensity of symmetry-equivalent diffractions. [c] $R = \Sigma||F_o| - |F_c||/\Sigma|F_o|$, w$R = [\Sigma\{w(F_o^2 - F_c^2)^2\}/\Sigma w(F_o^2)^2]^{½}$.

Table S1 continued

Compound	**5a**	**5b**	**5d**
Formula	$C_{17}H_{22}AuClFeNP$	$C_{23}H_{30}AuClFeNP$	$C_{19}H_{14}AuClFeNO_2P$
M/g mol^{-1}	559.59	639.71	607.55
Crystal system	monoclinic	monoclinic	monoclinic
Space group	$P2_1/n$ (No. 14)	$P2_1/c$ (No. 14)	$P2_1/c$ (No. 14)
T/K	120(2)	120(2)	150(2)
a/Å	10.3726(5)	9.0034(5)	10.8892(4)
b/Å	9.1257(5)	14.2805(8)	8.6369(3)
c/Å	19.301(1)	17.7023(11)	20.4246(7)
α/deg	90	90	90
β/deg	94.845(2)	99.915(2)	97.231(1)
γ/deg	90	90	90
V/Å^3	1820.5(2)	2242.0(2)	1905.6(1)
Z	4	4	4
μ(Mo Kα)/mm^{-1}	9.076	7.383	8.688
F(000)	1072	1248	1152
Diffrns collected	22513	15883	23652
Independent diffrns	4180	5157	4365
Observed diffrns[a]	3945	4604	4125
R_{int}[b]/%	2.15	2.18	2.29
No. of parameters	211	253	236
R[c] obsd diffrns/%	1.30	1.82	1.43
R, wR[c] all data /%	1.47, 2.66	2.29, 3.59	1.63, 3.10
Δρ/e Å^{-3}	0.49, –0.51	0.48, –0.61	0.41, –0.68

Table S1 continued

Compound	**6b**·Me_2CO	**6d**
Formula	$C_{49}H_{66}Au_2F_{12}Fe_2N_2OP_2Sb_2$	$C_{38}H_{28}Au_2F_{12}Fe_2N_2O_4P_2Sb_2$
M/g mol^{-1}	1738.11	1615.70
Crystal system	triclinic	monoclinic
Space group	$P\bar{1}$ (No. 2)	$P2_1/n$ (No. 14)
T/K	120(2)	120(2)
a/Å	11.534(1)	9.1821(3)
b/Å	12.008(1)	20.4012(6)
c/Å	39.793(5)	12.1762(4)
α/deg	87.710(4)	90
β/deg	85.000(4)	105.018(1)
γ/deg	86.529(4)	90
V/Å^3	54777(1)	2203.0(1)
Z	4	2
μ(Mo Kα)/mm^{-1}	6.963	8.650
F(000)	3328	1504
Diffrns collected	108326	39498
Independent diffrns	23907	5069
Observed diffrns[a]	21388	4704
R_{int}[b]/%	3.65	3.07
No. of parameters	1301	290
R[c] obsd diffrns/%	4.15	1.74
R, wR[c] all data /%	4.86, 8.03	2.07, 3.54
Δρ/e Å^{-3}	2.08, −2.23	1.46, −1.39

Solid-state structure of ***4***

Compound **4** crystallises with the symmetry of the monoclinic space group $P2_1/n$ and with one molecule in the asymmetric unit. The molecular structure of **4** (Figure S1) consists of the central C=N−C≡N moiety doubly substituted by two mutually rotated, chemically equivalent 1′-bromoferrocen-1-yl units. The angle subtended by the cyclopentadienyl planes C(1-5) and C(21-25) is 42.9(1)°. The cyclopentadienyls in both substituents are slightly tilted (the dihedral angles of the cyclopentadienyl planes are 5.4(1)° and 2.0(1)° for the ferrocene units comprising Fe1 and Fe2, respectively). Although the cyclopentadienyl rings at both ferrocene units are eclipsed, their substituents assume different positions. While they are located above each other (τ = 0.6(1)°; τ is the torsion angle C1-Cg1-Cg2-C6, where Cg1 and Cg2 are the centroids of the cyclopentadienyl rings C(1-5) and C(6-10), respectively) in the Fe1 ferrocene unit, they occupy more distant, anticlinal positions (τ = −146.5(1)°) in the Fe2 ferrocene moiety.[19] The ranges of the individual Fe-C bonds were 2.039(2)-2.060(2) Å and 2.022(2)-2.067(2) Å for Fe1 and Fe2, respectively.

The geometric parameters of the cyanoimine moiety of **4** are similar to those in other structurally characterised 1,4-quinonediimines.[20] The three chemically different C-N bonds of **4** are clearly distinguishable by their lengths (C11-N1 = 1.311(2) Å, C12-N1 = 1.336(2) Å, C12-N2 = 1.157(2) Å) and the cyanomine fragment is bent at C11 (C1-C11-C21 = 119.2(1)°). A slight bending is also observed at the terminal C−CN fragment (N1-C12-N2 = 170.7(2)°).

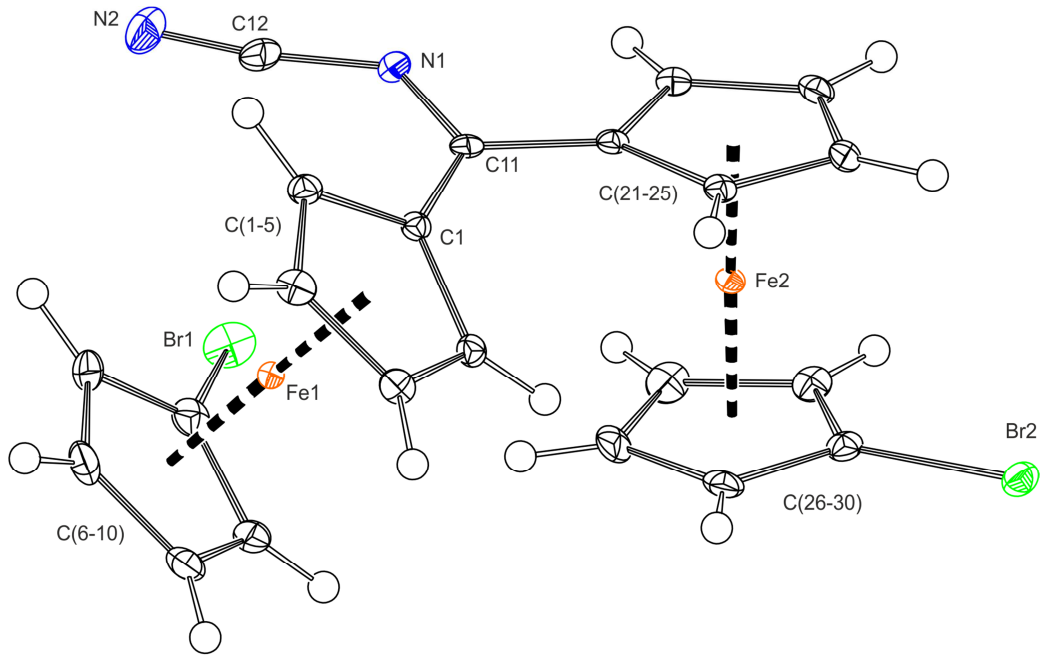

Figure S1. PLATON plot of the molecular structure of cyanoimine **4** showing atom labelling and displacement ellipsoids at the 50% probability level

*Crystal structure of **1d***

Compound **1d** (Figure S2) crystallises with the symmetry of the monoclinic space group $P2_1/c$ and with one molecule in the asymmetric unit. The molecule of **1d** contains an undistorted ferrocene moiety with Fe-C distances in the range of 2.029(1)-2.066(1) Å and with parallel cyclopentadienyl rings (tilt angle 1.82(8)°). The substituents of the central ferrocene unit in positions 1 and 1′ adopt a conformation near anticlinal eclipsed, as evidenced by the τ angle of −148.1(1)° (τ is the torsion angle C1-Cg1-Cg2-C6, where Cg1 and Cg2 are the centroids of the cyclopentadienyl rings C(1-5) and C(6-10), respectively). The nitrile moiety is linear (C11-N = 1.144(2) Å, C1-C11-N = 178.3(2)°) and lies in the plane of its parent cyclopentadienyl ring (the angle subtended by the C11-N bond and by the least-squares cyclopentadienyl plane C(6-10) is 2.5(1)°). Similarly, the vector of the pivotal P-C6 bond departs from the plane of its parent cyclopentadienyl ring C(1-5) by only 3.21(7)°, and the furyl substituents are oriented above the ferrocene unit and to its side; the dihedral angles between the furane rings and the C(1-5) planes are 75.70(9)° and 81.67(9)° for the rings comprising O1 and O2, respectively. The dihedral angle between the planes of the furane rings is 55.83(9)°. The P-C bonds are 1.814(1) Å (C6), 1.803(1) Å (C12), and 1.810(1) Å (C16), and the furane rings show partly localised character (cf. the individual C-C bond lengths C12-C13 1.360(2), C13-C14 1.425(2), C14-C15 1.341(2) Å; C16-C17 1.349(2), C17-C18 1.424(2), C18-C19 1.328(3) Å; the C-O distances in the furane rings are ≈1.37 Å).

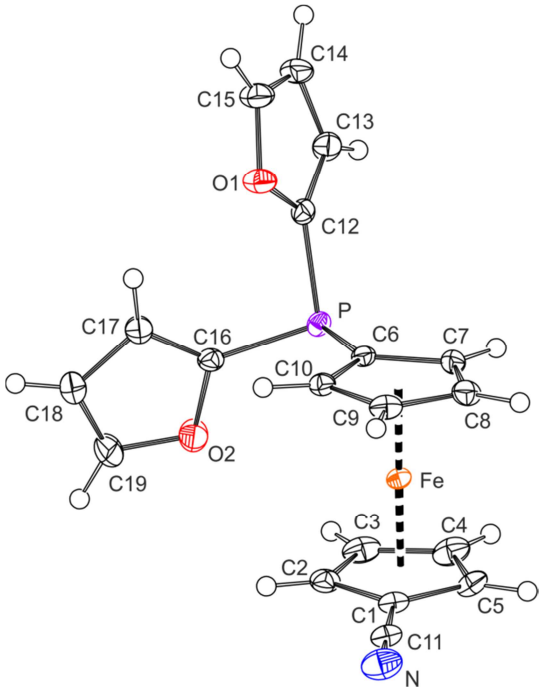

Figure S2. PLATON plot of the molecular structure of phosphine **1d** with atom labelling and displacement ellipsoids at the 50% probability level

*Crystal structures of the chloridogold(I) complexes **5***

Molecular structures of **5a**, **5b** and **5d** are presented in Figure S3, and the selected structural parameters are outlined in Table S2. The coordination environments of the gold(I) ions in these complexes are linear dicoordinate, with Au-donor distances similar to those reported for [AuCl(PPh_3)][21] and [AuCl(**1c**-κ*P*)].[2] The P–Au–Cl arms in **5a**, **5b** and **5d**, extending from the tetrahedral phosphorus atoms, are inclined towards the ferrocene unit. The ferrocene moieties are marginally tilted (up to 5° in **5b**) and assume different conformations in different compounds. In **5a**, the CN-substituted cyclopentadienyl ring is disordered over two positions, corresponding to eclipsed anticlinal and eclipsed synclinal conformations at the ferrocene unit (refined occupancies 53:47). In **5b** and **5d**, the respective conformations are eclipsed synclinal (or 1,2′) and an intermediate conformation near anticlinal eclipsed. When compared to the structure of free ligand **1d**, the structure of **5d** reveals shortened P-C bonds (by 0.01-0.03 Å) due to electron density shift from the substituents to the phosphorus atom and less acute C6-P-C16 and C12-P-C16 angles (the C6-P-C12 angle remains virtually unchanged).

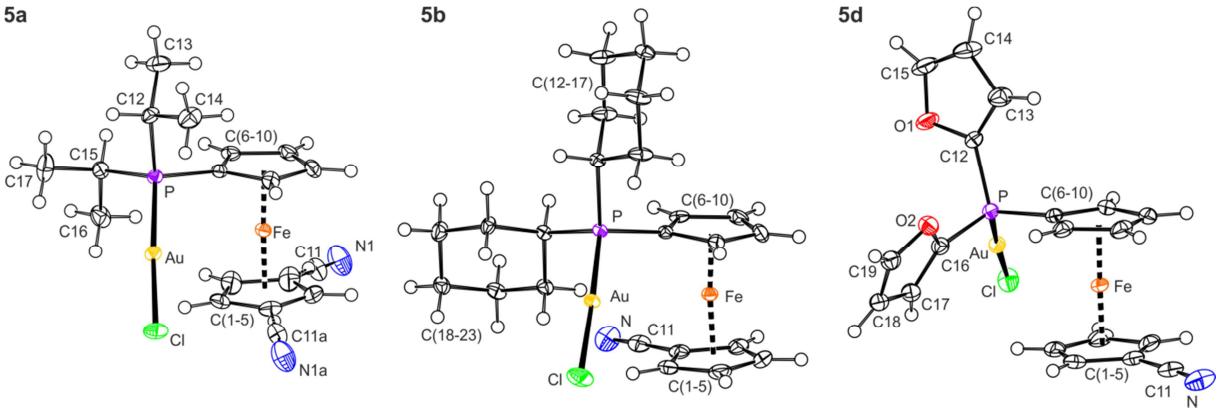

Figure S3. PLATON plots of the molecular structures of **5a**, **5b** and **5d** showing atom labelling and displacement ellipsoids at the 50% probability level. Both orientations of the disordered CN group are shown for **5a**.

Table S2. Selected distances and angles for the chloridogold(I) complexes **5** (in Å and deg)[a]

Parameter	**5a** (*n* = 15)	**5b** (*n* = 1)	**5d** (*n* = 16)
Au-P	2.2361(5)	2.2319(7)	2.2191(6)
Au-Cl	2.2890(5)	2.2850(7)	2.2817(7)
P-Au-Cl	177.17(2)	175.06(3)	176.97(2)
Fe-C (range)	2.030(2)-2.060(2)	2.034(3)-2.054(3)	2.027(2)-2.059(2)
∠Cp1,Cp2	3.2(1)	5.1(2)	1.4(1)
τ	−145.1(2)/71.4(2)[b]	69.5(2)	−155.4(2)
C11-N	1.135(6)	1.143(4)	1.139(4)
P-C6	1.797(2)	1.798(2)	1.788(2)
P-C12	1.844(2)	1.843(2)	1.789(2)
P-C*n*	1.832(2)	1.831(3)	1.779(2)

[a] Parameters Cp1, Cp2 and τ are defined as for the free ligand **1d** (see the previous page). [b] Values pertaining to the two orientations of the disordered nitrile group

*Crystal structures of **6b**·Me$_2$CO and **6d***

Compounds **6b**·Me$_2$CO and **6d** were structurally authenticated by single-crystal X-ray diffraction analysis as cationic digold(I) complexes containing a pair of P,N-bridging phosphinonitrile ligands, whose charge was compensated for by two hexafluoridoantimonate(V) anions. Structure determination of compound **6a** also confirmed the dimeric nature of the complex. However, the structure could not be satisfactorily refined due to extensive disorder. Compound **6d** crystallises with the symmetry of the monoclinic space group $P2_1/n$ with the dimeric unit $[Au_2(\mu(P,N)\text{-}\mathbf{1d})_2]^{2+}$ located around the crystallographic inversion centre which, in turn, renders only half of the complex cation and one $[SbF_6]^-$ anion symmetrically independent. In the case of **6b**·Me$_2$CO, the asymmetric part of the triclinic unit cell (space group *P*–1) contains one complete cationic dimer (Au1 and Au2) and two halves from two additional dimers located at the crystallographic inversion centres (Au3 and Au4), four anions and one acetone molecule. Structural diagrams for **6b**·Me$_2$CO and **6d** are shown in Figures S4-S6, and the relevant structural parameters are outlined in Table S3.

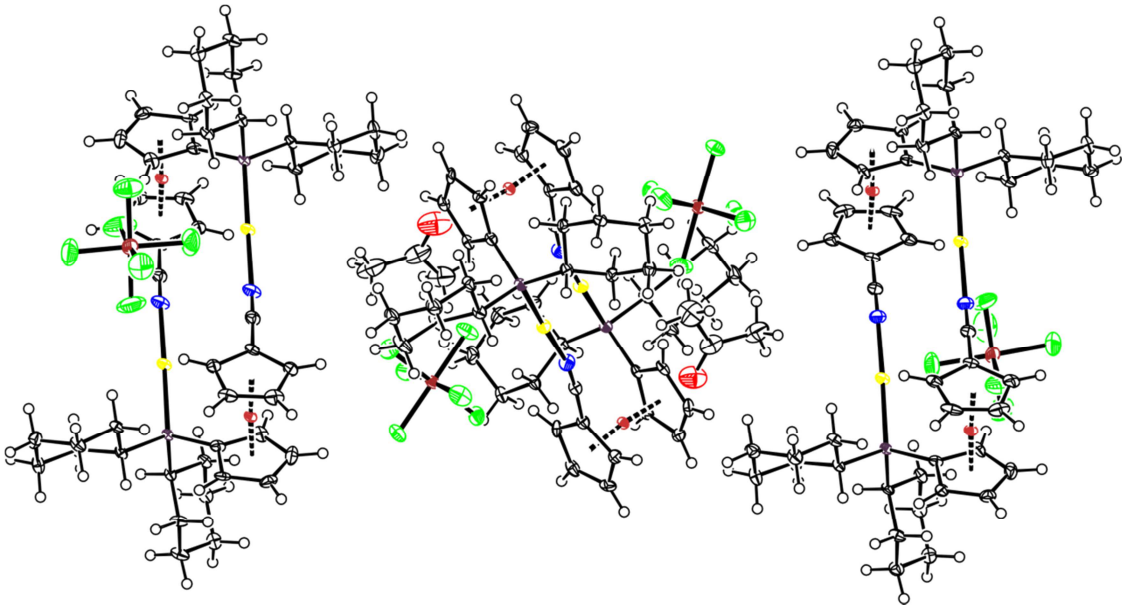

Figure S4. Full PLATON plot of the structure of **6b**·Me_2CO with 50% probability ellipsoids

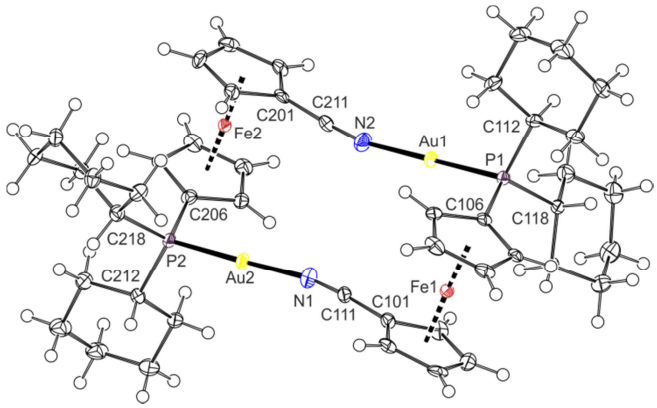

Figure S5. PLATON plot of the complex cation comprising atoms Au1 and Au2 in the structure of **6b**·Me_2CO; displacement ellipsoids are scaled to the 50% probability level.

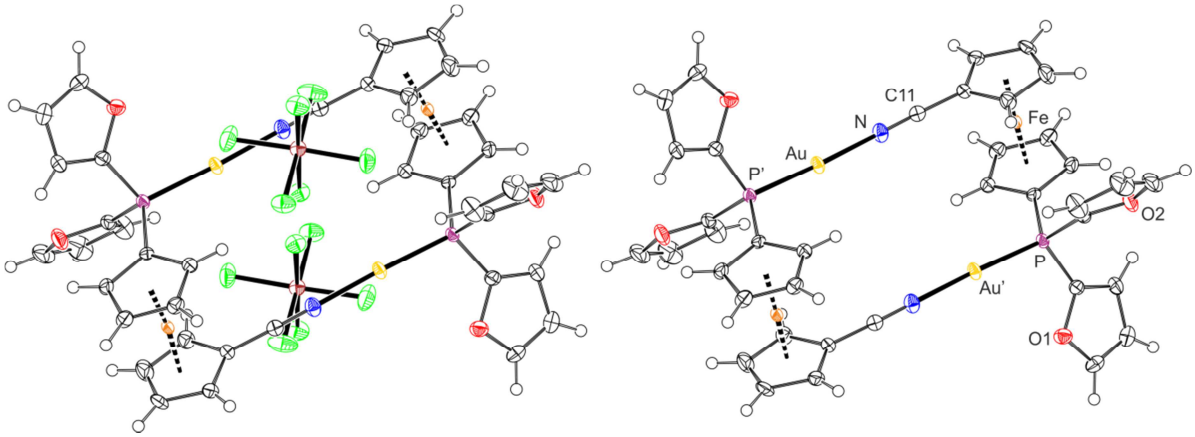

Figure S6. PLATON plot of the molecular structure of **6d** (left); PLATON plot of the complex cation in the structure of **6d** showing atom labelling (right). Displacement ellipsoids enclose 50% probability level. Note: the labelling is strictly analogous to that used for the free ligand **1d**.

The overall geometry of the digold(I) cations in the structures of **6b**·Me_2CO and **6d** is similar to that of the analogous cation resulting from ligand **1d**.[2] Notably, the Au-P and Au-N distances in **6d** are significantly shorter than in **6b**, presumably reflecting the strengthening of these bonds by π-back donation in the complex with the weaker-donating ligand **1d**. Similarly to **5d**, the P-C bonds in **6d** are approximately 0.2 Å shorter than those in the uncoordinated ligand **1d**. By contrast, the C≡N bond lengths remain virtually unaffected by coordination in all cases. The ferrocene moieties assume conformations near synclinal eclipsed (ideal value: τ = 72°), which brings the phosphine moiety to the side of the ferrocene scaffold and thus gives rise to an arrangement in which the P-Au-N moieties are mutually offset. Yet, the variation in the τ parameter among structurally independent but chemically identical fragments in the structure of **6b**·Me_2CO suggests that the coordination of the phosphinonitrile ligands is rather flexible, thus allowing conformational changes within dimeric cations.

Table S3. Selected distances and angles for **6b**·MeCO and **6d** (in Å and deg).[a]

Parameter	**6b**·Me_2CO (Fe1/Au1)	**6b**·Me_2CO (Fe2/Au2)	**6b**·Me_2CO (Fe3/Au3)	**6b**·Me_2CO (Fe4/Au4)	**6d**
Au-P	2.241(2)	2.250(2)	2.237(2)	2.239(2)	2.2139(7)
Au-N	2.048(6)	2.047(6)	2.054(6)	2.050(6)	2.032(2)
P-Au-N	177.7(2)	178.0(2)	174.4(2)	174.4(2)	176.21(7)
Fe-C (range)	2.034(6)-2.064(6)	2.013(6)-2.062(7)	2.021(6)-2.051(7)	2.033(6)-2.058(7)	2.023(3)-2.063(3)
∠Cp1,Cp2	7.5(4)	6.8(4)	3.3(4)	3.3(4)	3.1(2)
τ	–68.2(5)	74.6(4)	–60.5(5)	57.1(5)	–78.4(2)
C11-N	1.137(8)	1.139(9)	1.132(9)	1.140(8)	1.140(3)
P-C6	1.792(6)	1.795(6)	1.797(6)	1.789(6)	1.783(3)
P-C12	1.846(6)	1.841(6)	1.838(6)	1.845(6)	1.792(3)
P-C*n*	1.830(6)	1.846(6)	1.829(6)	1.828(6)	1.785(3)

[a] Parameters Cp1, Cp2 and τ are defined as for the free ligand **1d**; *n* = 18 (**6b**·Me_2CO) or 16 (**6d**).

Additional kinetic plots

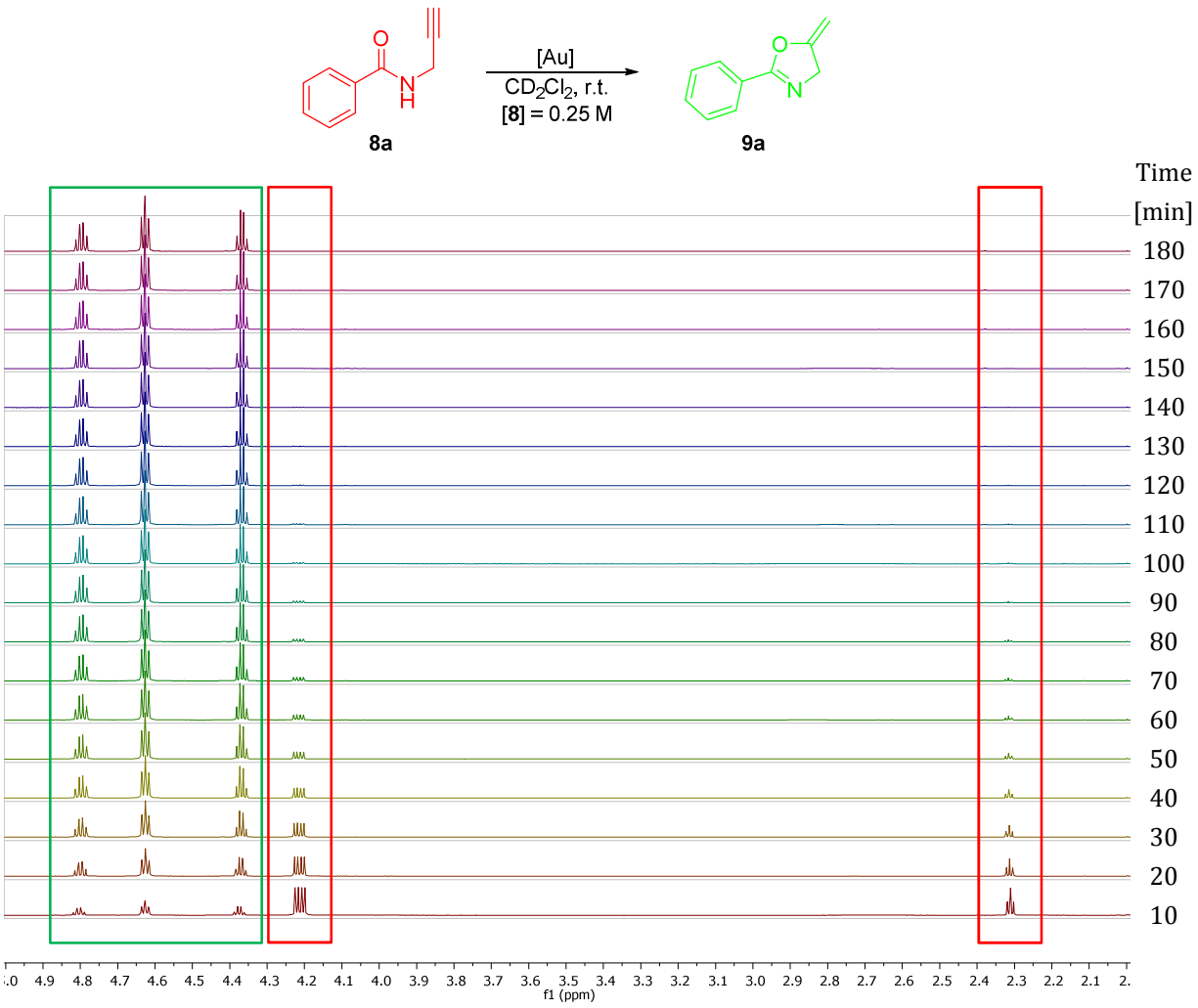

Figure S7. Representative ^{1}H NMR spectra illustrating the conversion of **8a** into **9a** catalysed by complex **6d** (1 mol.% Au, $[\mathbf{8a}]_0$ = 0.25 M) in CD_2Cl_2 at 25°C

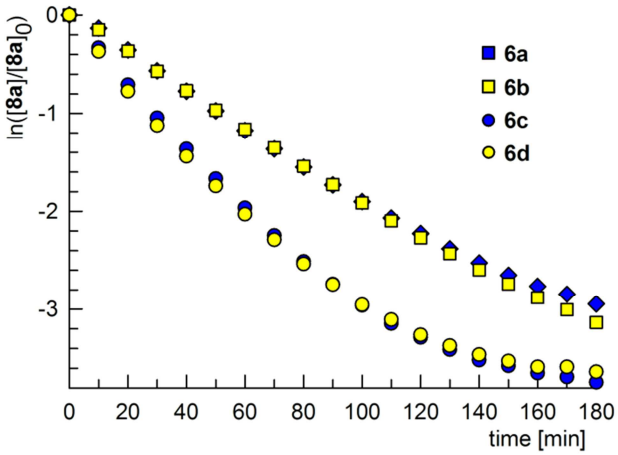

Figure S8. ln([**8a**]/[**8a**]$_0$) vs. time plots of different catalysts illustrating the departure from first-order behaviour at higher conversions (in CD_2Cl_2, [**8a**]$_0$ = 0.25 M, 25°C); the rate constants quoted in the main text were obtained by fitting these curves in the linear range of 10-60 min

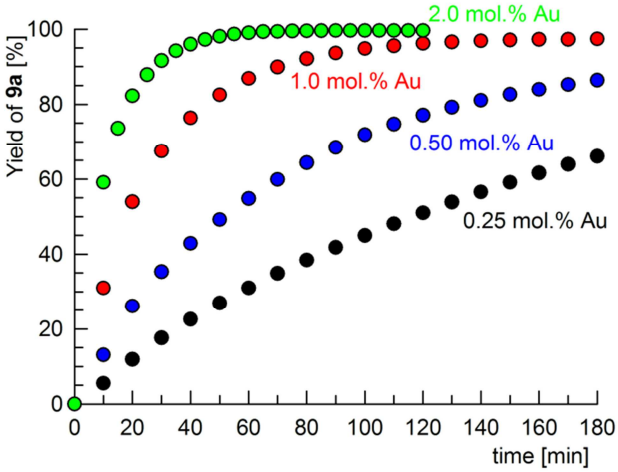

Figure S9. Kinetic profiles for the cyclisation of substrate **8a** catalysed by varying amounts of complex **6d** (in CD_2Cl_2, [**8a**]$_0$ = 0.25 M, 25°C)

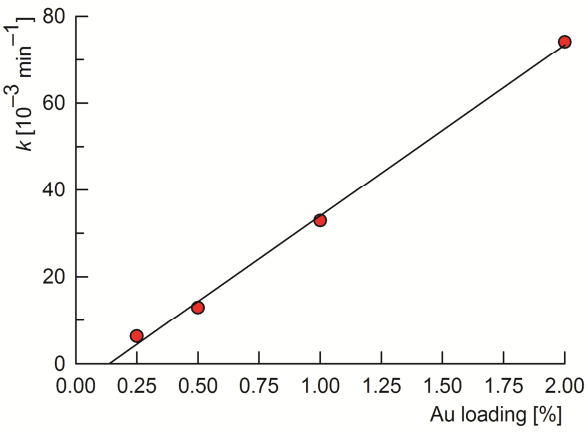

Figure S10. Linear relationship between catalyst concentration and observed reaction rate of the cyclisation of substrate **8a** catalysed by complex **6d** (in CD_2Cl_2, $[\mathbf{8a}]_0$ = 0.25 M, 25°C). Parameters of the linear fit are as follows: k (10^{-3} min^{-1}) = −5(2) + 39(1) c_{Au} (%); R^2 = 0.9975.

DFT computations

DFT calculations have been performed using the PBE0 density functional[22] in conjunction with the SDD (Fe, Au)[23] and cc-pVDZ (C, H, N, O, and P)[24] basis sets, as implemented in the Gaussian 09 program package, revision D.[25] Solvent effects (dichloromethane) have been approximated using the polarised continuum model (PCM).[26] Geometry optimisations were started from geometries determined by crystallographic analysis where possible. Reported energies refer to Gibbs free energies at 298 K. The optimised molecular structures are available in Supporting Information.

References

1 K. Škoch, I. Císařová and P. Štěpnička, *Inorg. Chem.,* 2014, **53**, 568-577.

2 K. Škoch, I. Císařová and P. Štěpnička, *Chem. Eur. J.,* 2015, **21**, 15998-16004.

3 R. Usón, A. Laguna and M. Laguna, *Inorg. Synth.,* 1989, **26**, 85-91.

4 C. Nieto-Oberhuber, M. P. Muñoz, S. López, E. Jiménez-Núñez, C. Nevado, E. Herrero-Gómez, M. Raducan and A. M. Echavarren, *Chem. Eur. J.,* 2006, **12**, 1677-1693.

5 M. Preisenberger, A. Schier and H. Schmidbaur, *J. Chem. Soc., Dalton Trans.,* 1999, 1645-1650.

6 R. M. Silverstein, F. X. Webster and D. J. Kiemle, *Spectrometric Identification of Organic Compounds*, 7th ed., Wiley, Hoboken, 2005.

7 A. Chesney, M. R. Bryce, R. W. J. Chubb, A. S. Batsanov and J. A. K. Howard, *Synthesis,* 1998, 413-416.

8 P. Nicpon and D. W. Meek, *Inorg. Chem.,* 1966, **5**, 1297-1298.

9 X. Meng and S. Kim, *Org. Biomol. Chem.,* 2011, **9**, 4429-4431.

10 R. L. Melen, M. M. Hansmann, A. J. Lough, A. S. K. Hashmi and D. W. Stephan, *Chem. Eur. J.,* 2013, **19**, 11928-11938.

11 N. Willand, M. Desroses, P. Toto, B. Dirié, Z. Lens, V. Villeret, P. Rucktooa, C. Locht, A. Baulard and B. Deprez, *ACS Chem. Biol.,* 2010, ***5***, 1007-1013.

12 A. S. K. Hashmi, M. C. B. Jaimes, A. M. Schuster and F. Rominger, *J. Org. Chem.,* 2012, **77**, 6394-6408.

13 A. Lukin, T. Vedekhina, D. Tovpeko, N. Zhuriloa and M. Krasavin, *RSC Adv.,* 2016, **6**, 57956- 57959.

14 G. C. Senadi, W.-P. Hu, J.-S. Hsiao, J. K. Vandavasi, C.-Y. Chen and J.-J. Wang, *Org. Lett.,* 2012, **14**, 4478-4481.

15 S. Doherty, J. G. Knight, A. S. K. Hashmi, C. H. Smyth, N. A. B. Ward, K. J. Robson, S. Tweedley, R. W. Harrington and W. Clegg, *Organometallics,* 2010, **29**, 4139-4147.

16 G. M. Sheldrick, *Acta Crystallogr., Sect. A: Found. Adv*., 2015, ***71***, 3-8.

17 G. M. Sheldrick, *Acta Crystallogr., Sect. C, Struct. Chem*., 2015, 71, 3-8.

18 A. L. Spek, *J. Appl. Crystallogr*., 2003, 36, 7-13.

19 K.-S. Gan, T. S. A. Hor in *Ferrocenes: Homogeneous Catalysis, Organic Synthesis, Materials Science* (Eds. A. Togni, T. Hayashi), Wiley-VCH, Weinheim, 1995; ch. 1, pp. 3-104

20 Selected examples: a) *N*,*N*′-dicyano-1,4-benzoquinonediimine: G. D. Andreetti, S. Bradamante, P. C. Bizzarri and G. A. Pagani, *Mol. Cryst. Liq. Cryst.,* 1985, **120**, 309-314; b) 2,5-dimethyl-*N*,*N*′-dicyano-1,4-benzoquinonediimine: A. Aumüllerz, P. Erk, S. Hünig, E. Hadicke, K. Peters and H. G. von Schnering, *Chem. Ber.,* 1991, **124**, 2001-2004; c) *N*,*N*′-

dicyano-1,4-indaquinonediimine: E. Tillmanns and F. Schvabenlander, *Acta Crystallogr., Sect. C: Cryst. Struct. Commun*., 1994, **50**, 715-717.

21] S. P. C. Dunstan, P. C. Healy, A. N. Sobolev, E. R. T. Tiekink, A. H. White and M. L. Williams, *J. Mol. Struct.,* 2014, **1072**, 253-259.

22 a) C. Adamo and V. Barone, *J. Chem. Phys.,* 1999, **110**, 6158-6170; b) M. Ernzerhof and G. E. Scuseria, *J. Chem. Phys.,* 1999, **110**, 5029-5036.

23 a) M. Dolg, U. Wedig, H. Stoll and H. J. Preuss, *J. Chem. Phys.,* 1987, **86**, 866-872; b) D. Andrae, U. Haussermann, M. Dolg, H. Stoll and H. Preuss, *Theor. Chim. Acta,* 1990, **77**, 123-141.

24 a) T. H. Dunning, Jr., *J. Chem. Phys.,* 1989, **90**, 1007-1023; b) D. E. Woon and T. H. Dunning, Jr., *J. Chem. Phys.,* 1993, **98**, 1358-1371.

25 Gaussian 09, Revision D.01, M. J. Frisch, G. W. Trucks, H. B. Schlegel, G. E. Scuseria, M. A. Robb, J. R. Cheeseman, G. Scalmani, V. Barone, B. Mennucci, G. A. Petersson, H. Nakatsuji, M. Caricato, X. Li, H. P. Hratchian, A. F. Izmaylov, J. Bloino, G. Zheng, J. L. Sonnenberg, M. Hada, M. Ehara, K. Toyota, R. Fukuda, J. Hasegawa, M. Ishida, T. Nakajima, Y. Honda, O. Kitao, H. Nakai, T. Vreven, J. A. Montgomery, Jr., J. E. Peralta, F. Ogliaro, M. Bearpark, J. J. Heyd, E. Brothers, K. N. Kudin, V. N. Staroverov, R. Kobayashi, J. Normand, K. Raghavachari, A. Rendell, J. C. Burant, S. S. Iyengar, J. Tomasi, M. Cossi, N. Rega, J. M. Millam, M. Klene, J. E. Knox, J. B. Cross, V. Bakken, C. Adamo, J. Jaramillo, R. Gomperts, R. E. Stratmann, O. Yazyev, A. J. Austin, R. Cammi, C. Pomelli, J. W. Ochterski, R. L. Martin, K. Morokuma, V. G. Zakrzewski, G. A. Voth, P. Salvador, J. J. Dannenberg, S. Dapprich, A. D. Daniels, Ö. Farkas, J. B. Foresman, J. V. Ortiz, J. Cioslowski and D. J. Fox, Gaussian, Inc., Wallingford CT, 2009.

26 a) J. Tomasi, B. Mennucci and R. Cammi, *Chem. Rev.,* 2005, **105**, 2999-3093; b) G. Scalmani and M. J. Frisch, *J. Chem. Phys.,* 2010, **132**, 114110-114115.

Copies of the NMR spectra

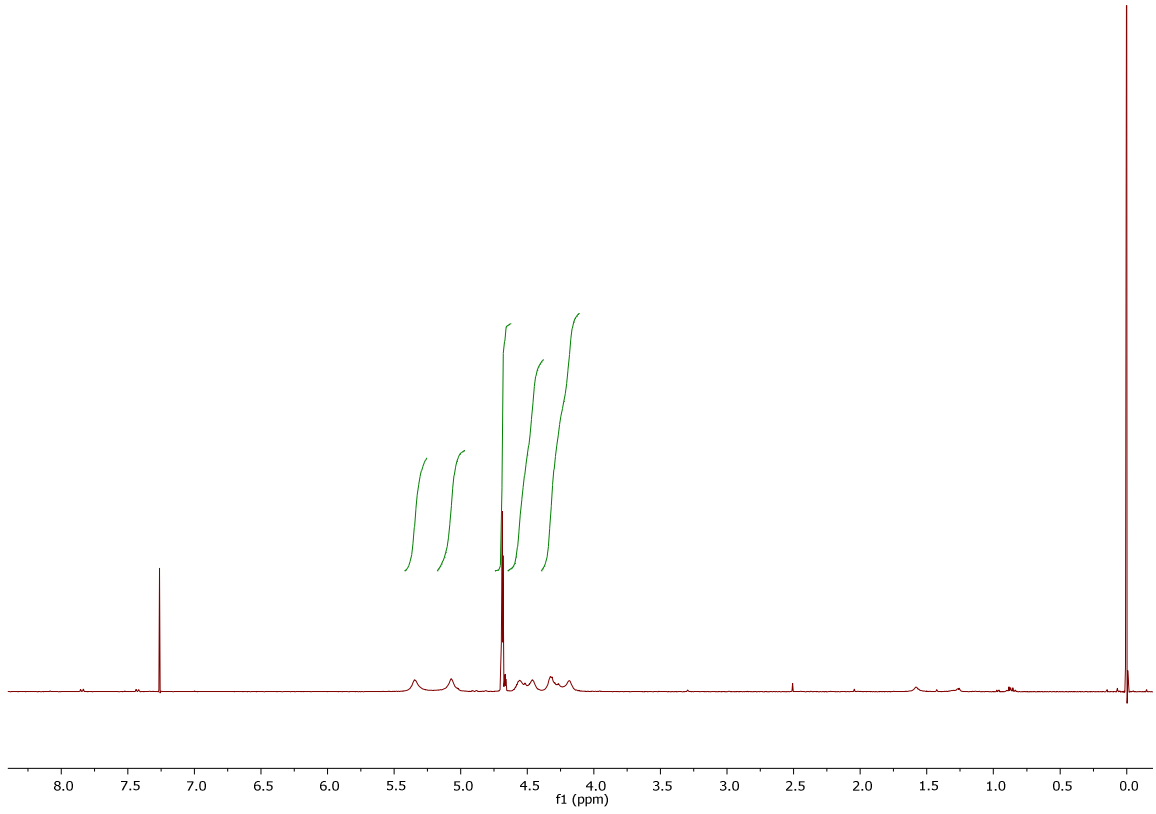

Figure S11. ^{1}H NMR spectrum (400 MHz, $CDCl_3$) of **4**

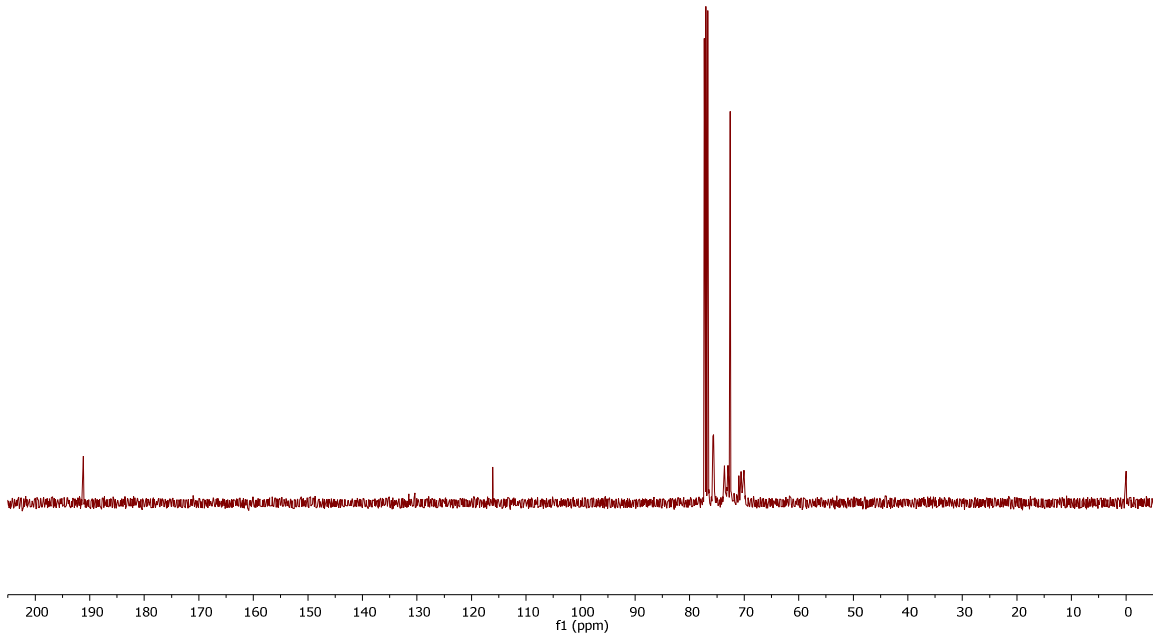

Figure S12. $^{13}C\{^{1}H\}$ NMR spectrum (101 MHz, $CDCl_3$) of **4**

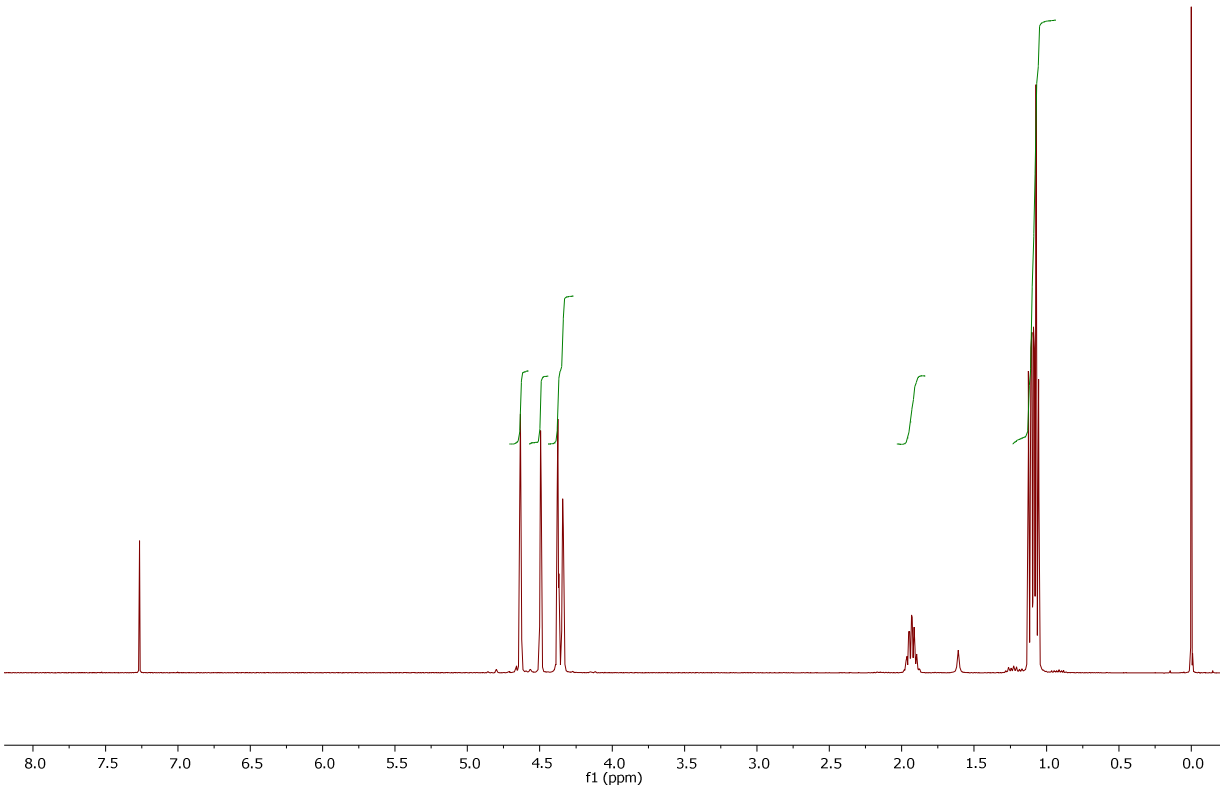

Figure S13. ^{1}H NMR spectrum (400 MHz, $CDCl_3$) of **1a**

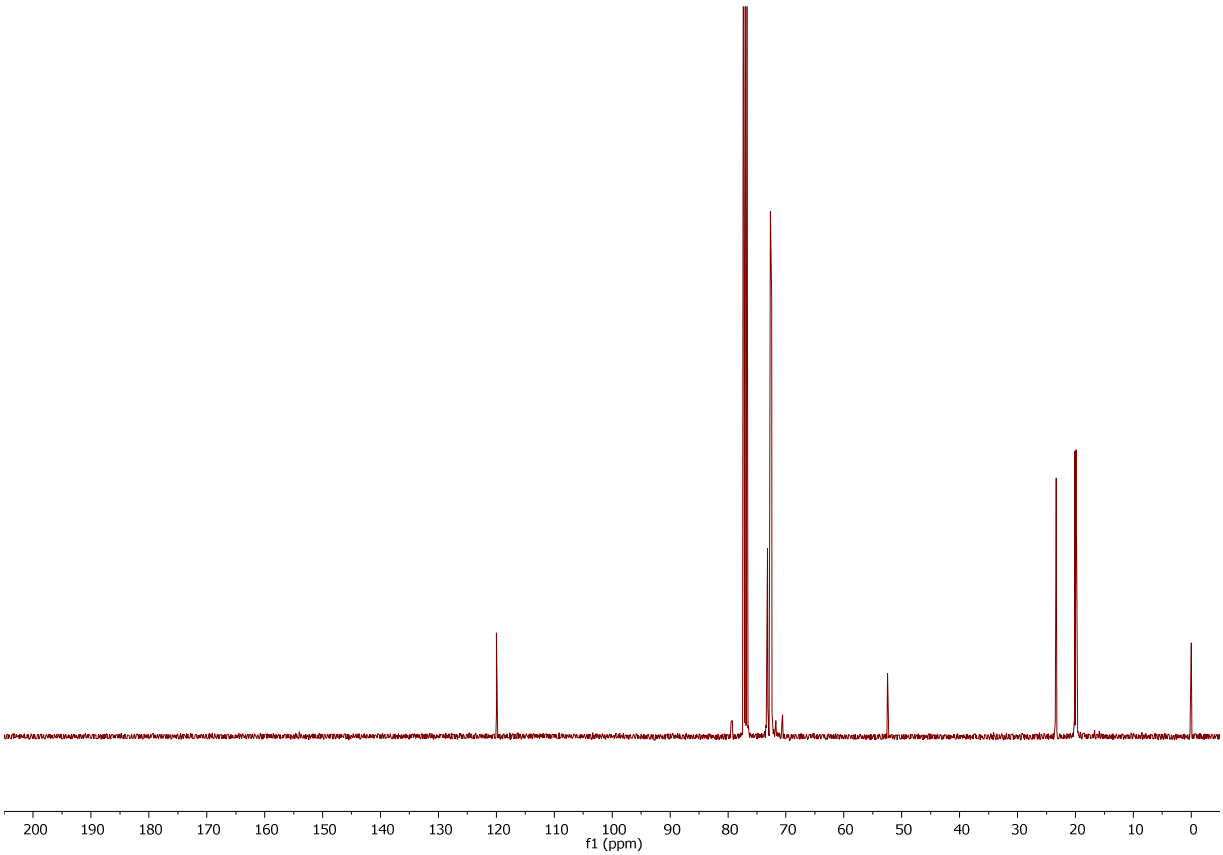

Figure S14. $^{13}C\{^{1}H\}$ NMR spectrum (101 MHz, $CDCl_3$) of **1a**

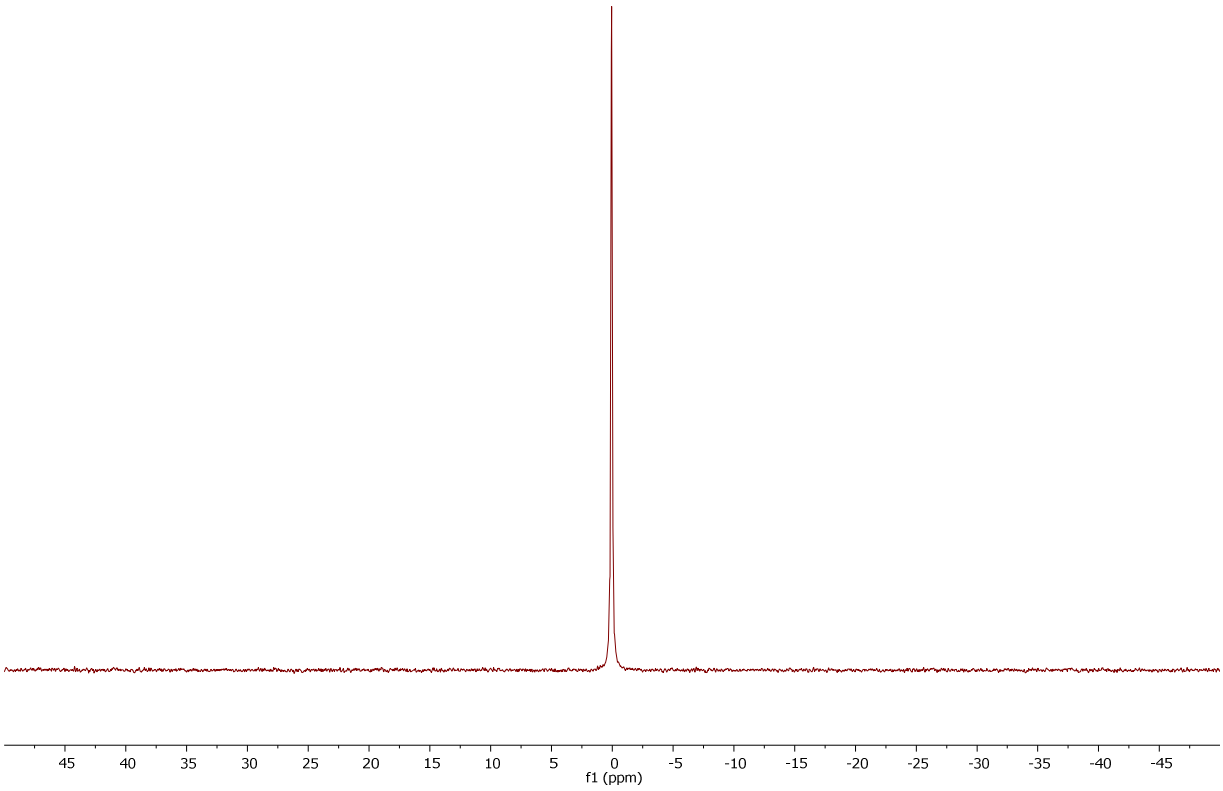

Figure S15. $^{31}P\{^{1}H\}$ NMR spectrum (162 MHz, $CDCl_3$) of **1a**

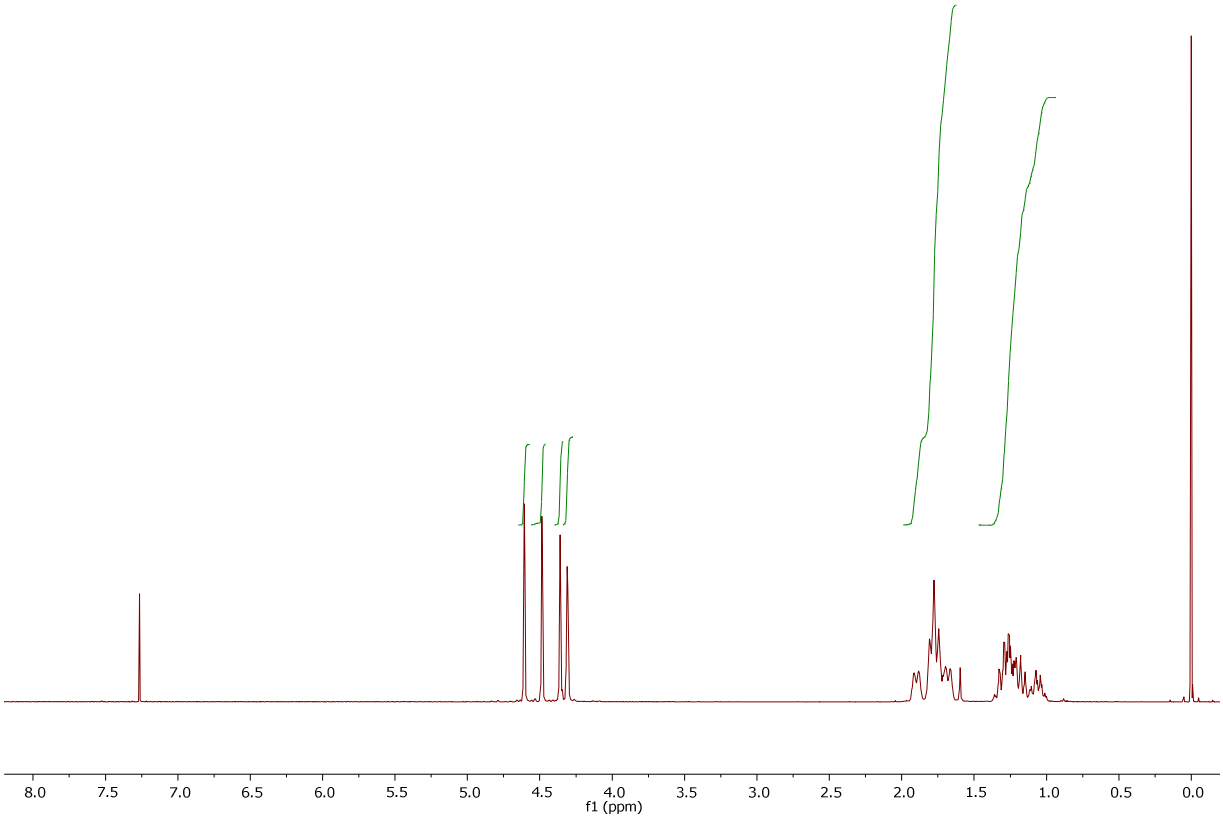

Figure S16. ^{1}H NMR spectrum (400 MHz, $CDCl_3$) of **1b**

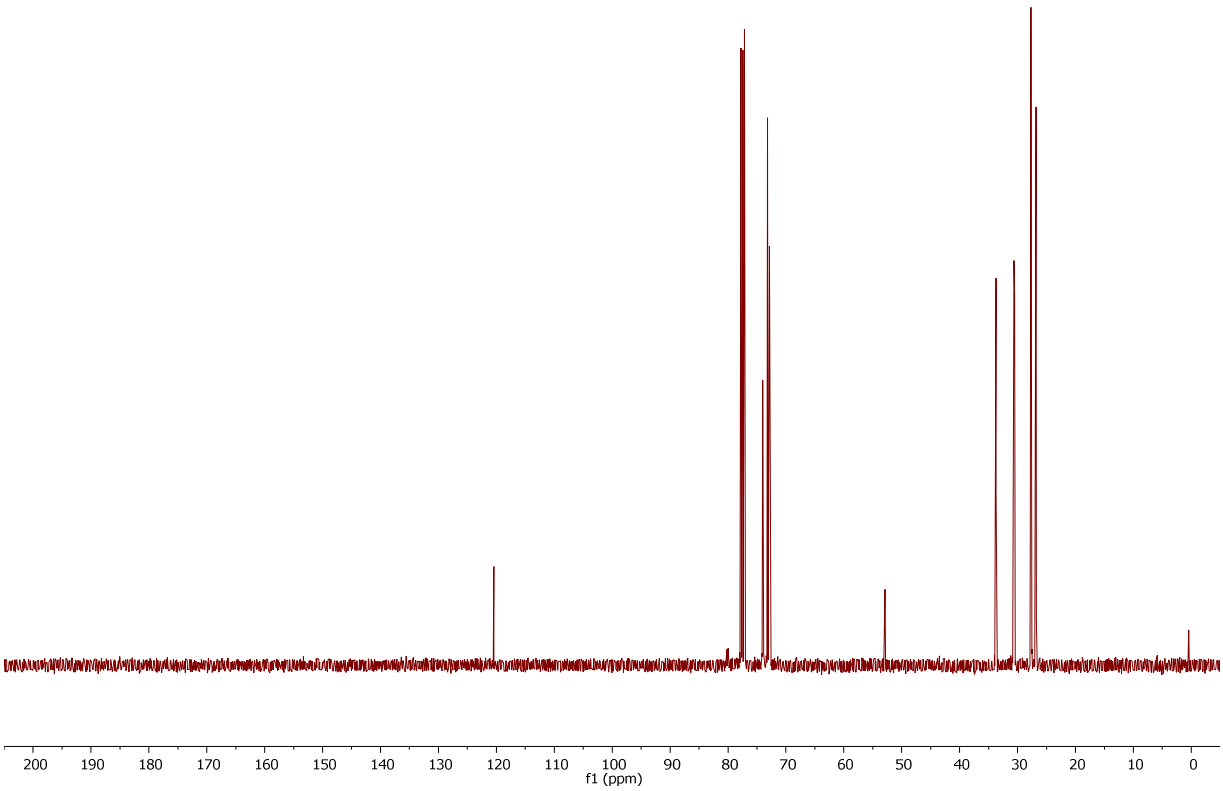

Figure S17. $^{13}C\{^{1}H\}$ NMR spectrum (101 MHz, $CDCl_3$) of **1b**

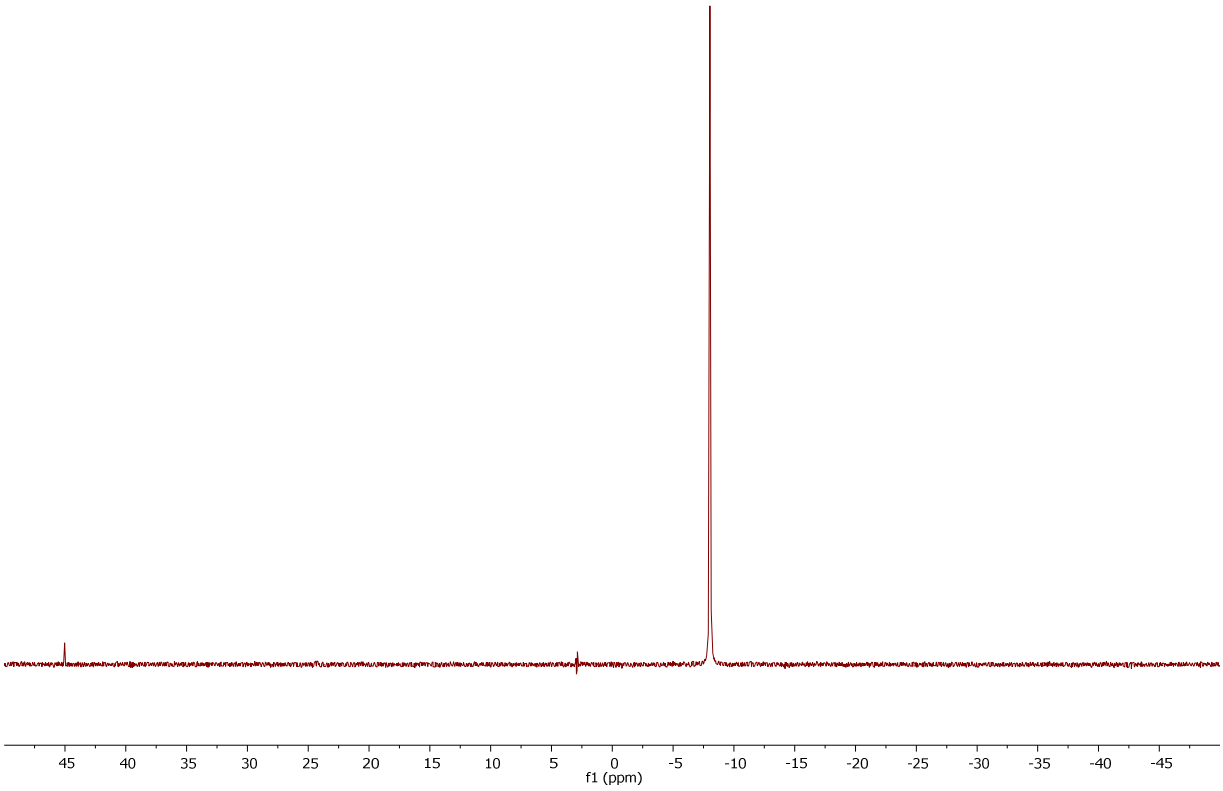

Figure S18. $^{31}P\{^{1}H\}$ NMR spectrum (162 MHz, $CDCl_3$) of **1b**

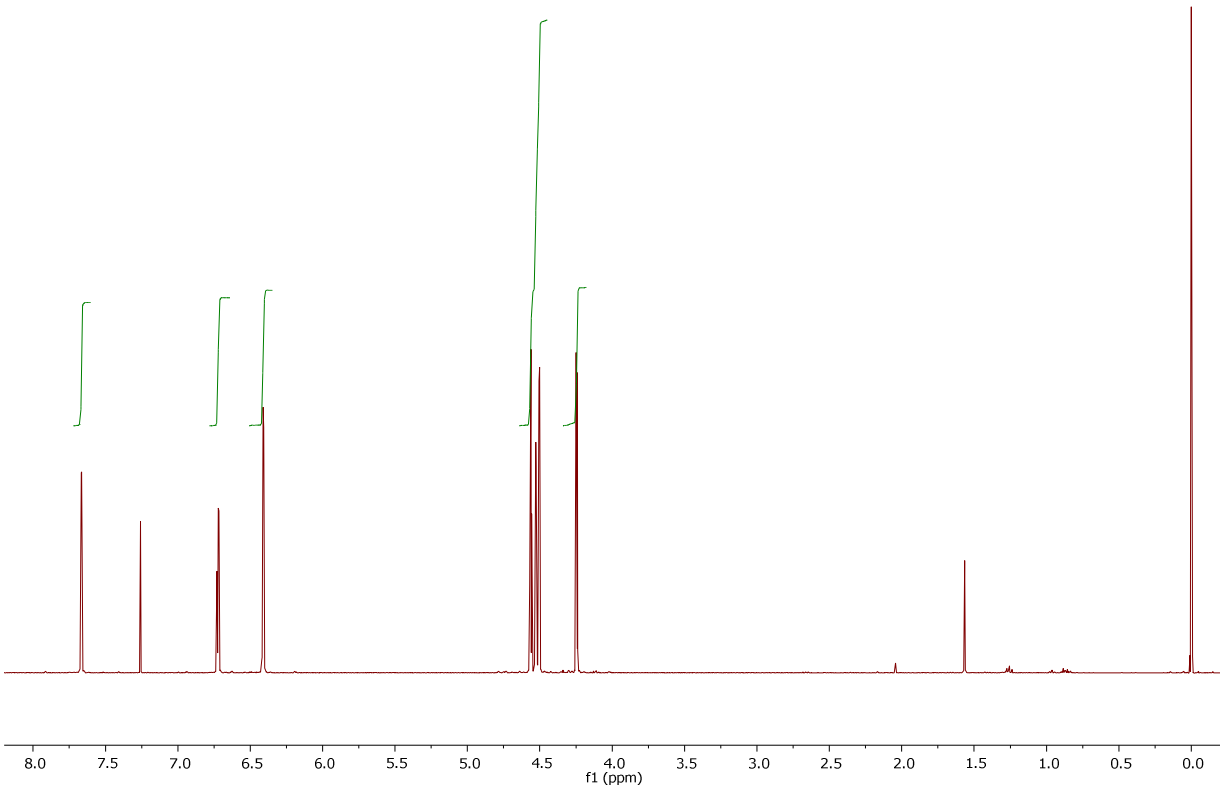

Figure S19. ^{1}H NMR spectrum (400 MHz, $CDCl_3$) of **1d**

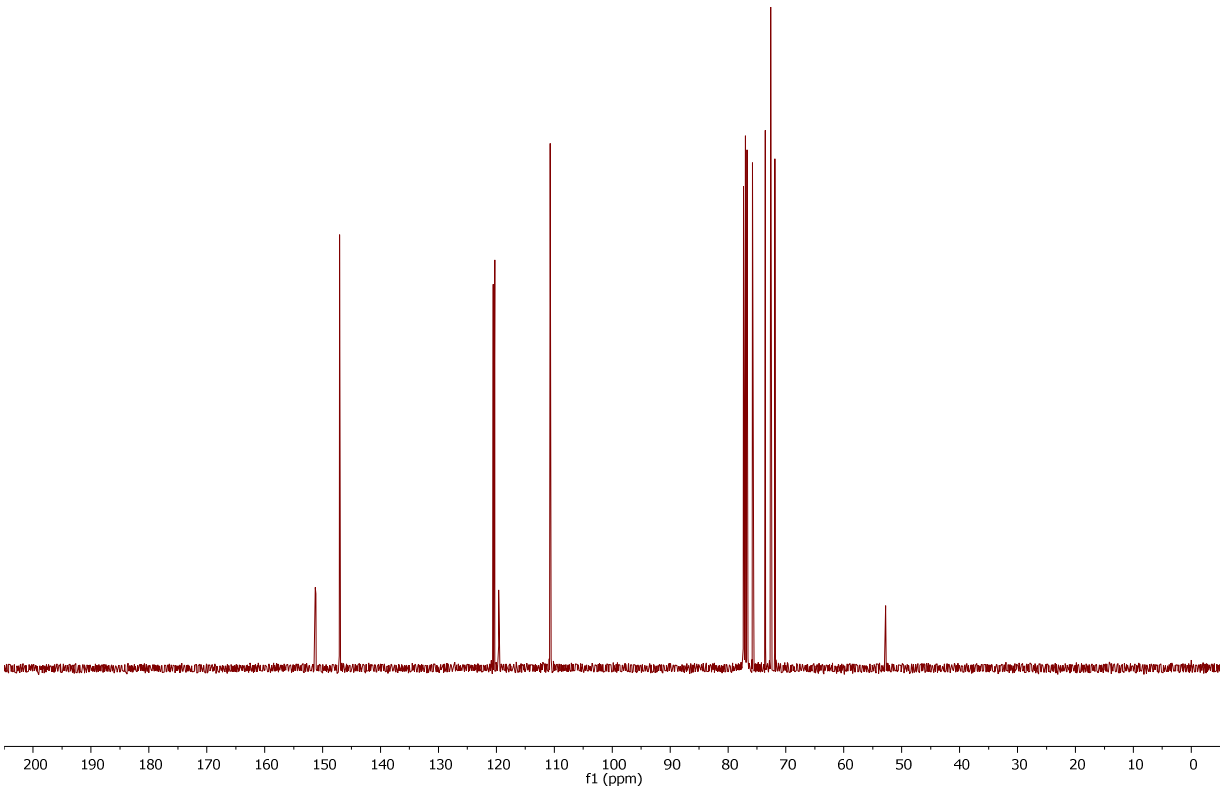

Figure S20. $^{13}C\{^{1}H\}$ NMR spectrum (101 MHz, $CDCl_3$) of **1d**

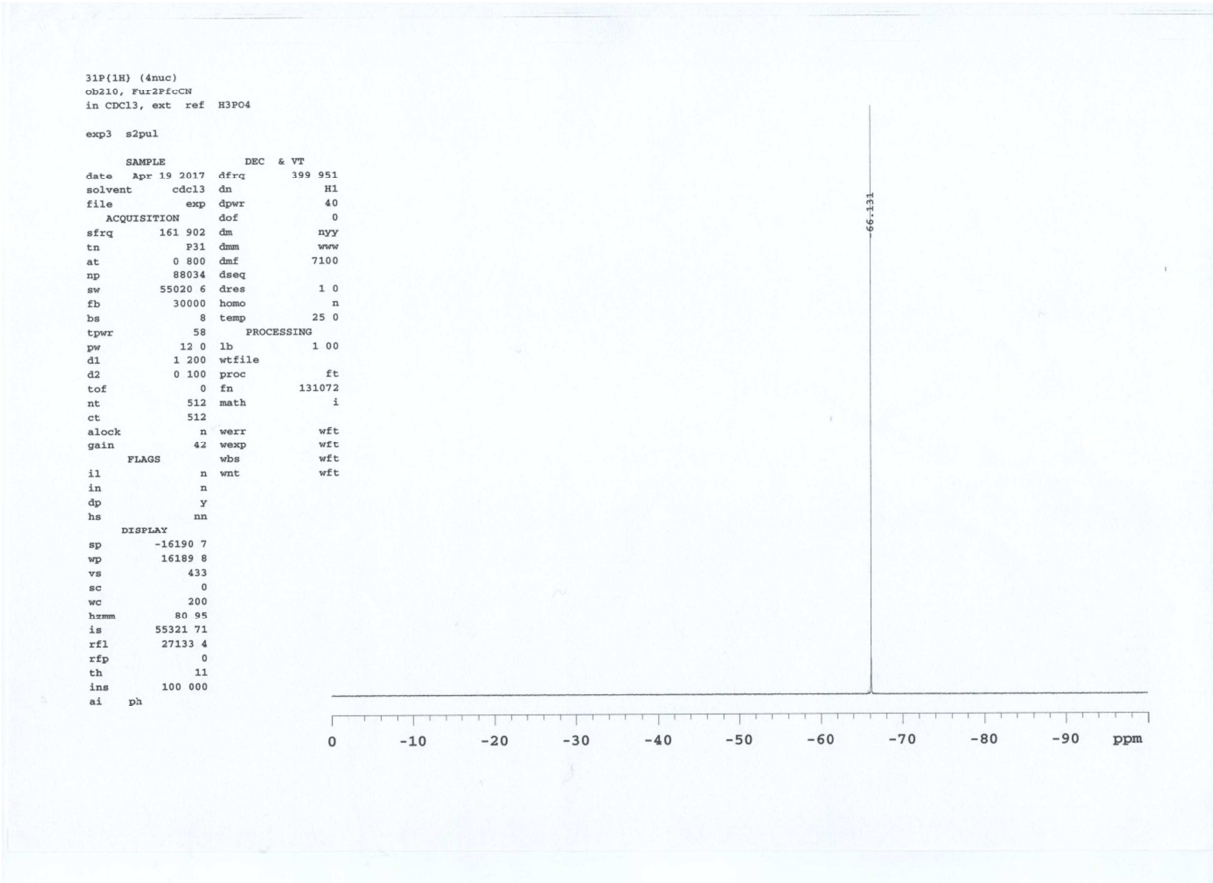

Figure S21. $^{31}P\{^{1}H\}$ NMR spectrum (162 MHz, $CDCl_3$) of **1d**

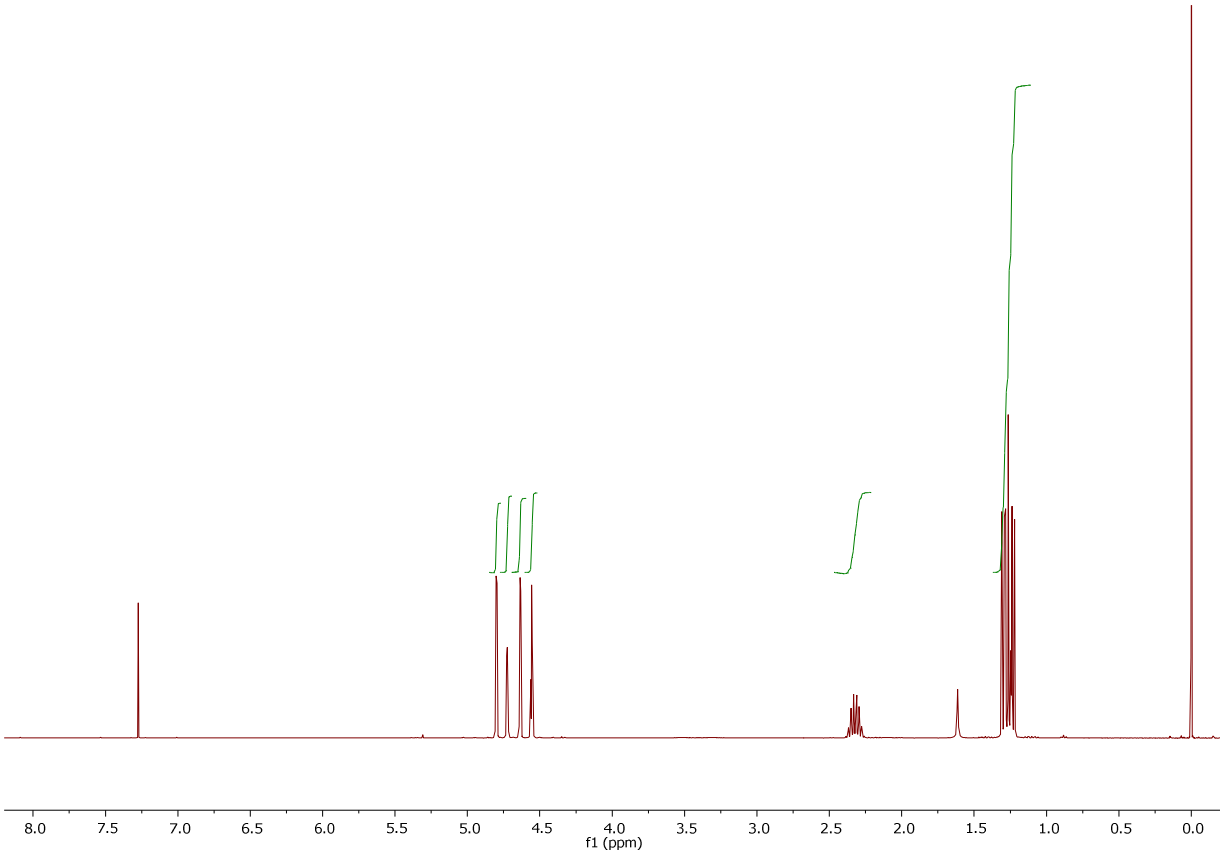

Figure S22. ^{1}H NMR spectrum (400 MHz, $CDCl_3$) of **5a**

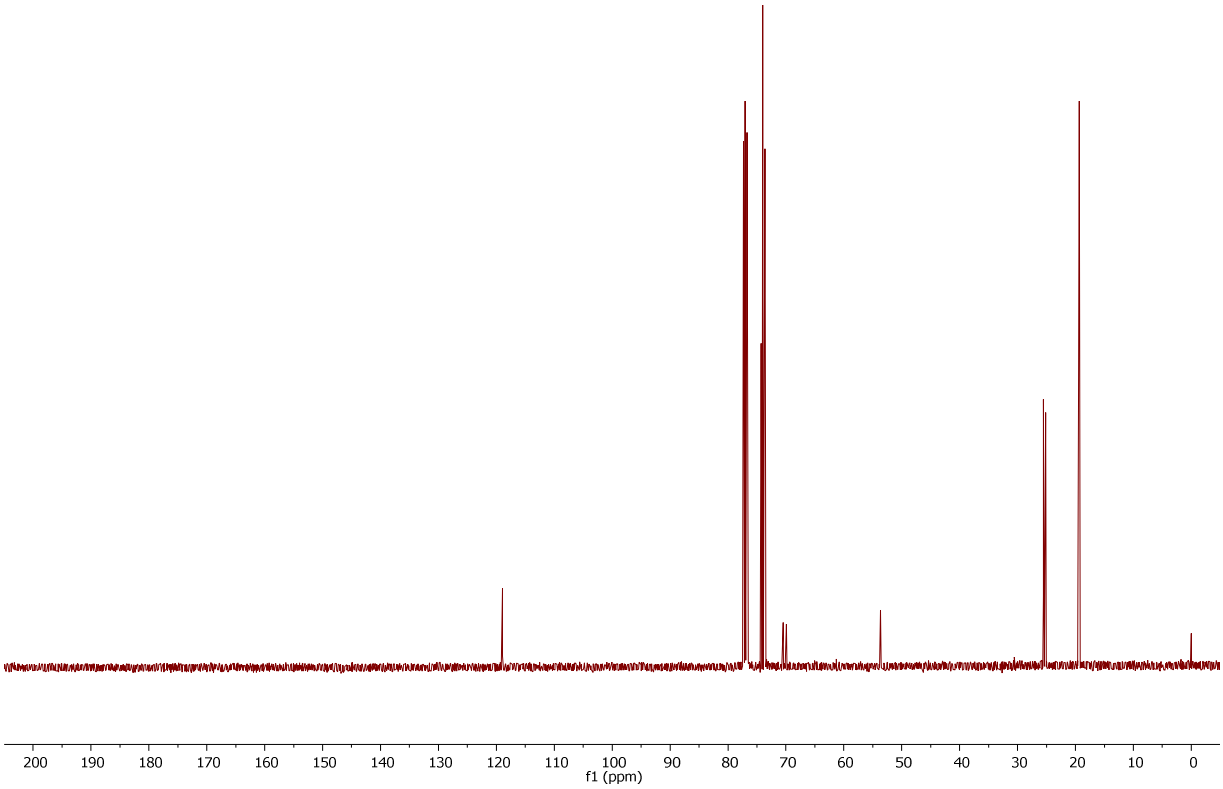

Figure S23. $^{13}C\{^{1}H\}$ NMR spectrum (101 MHz, $CDCl_3$) of **5a**

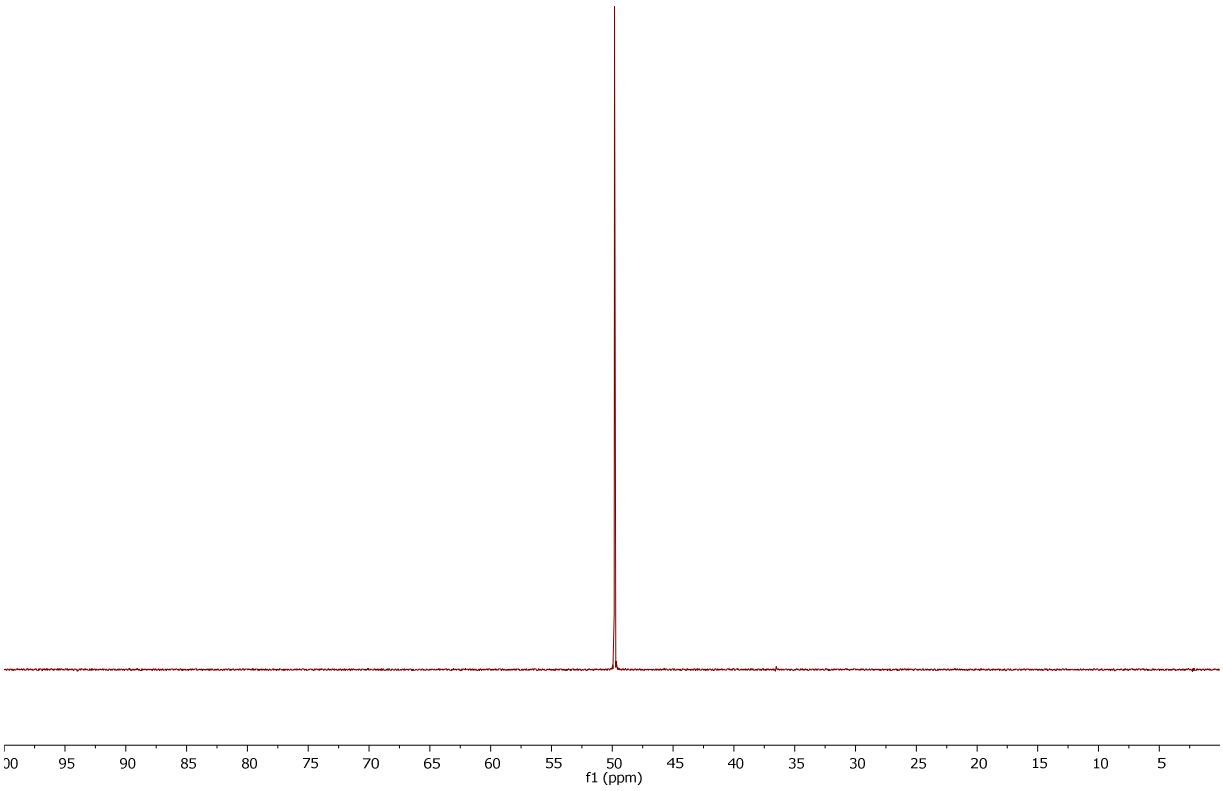

Figure S24. $^{31}P\{^{1}H\}$ NMR spectrum (162 MHz, $CDCl_3$) of **5a**

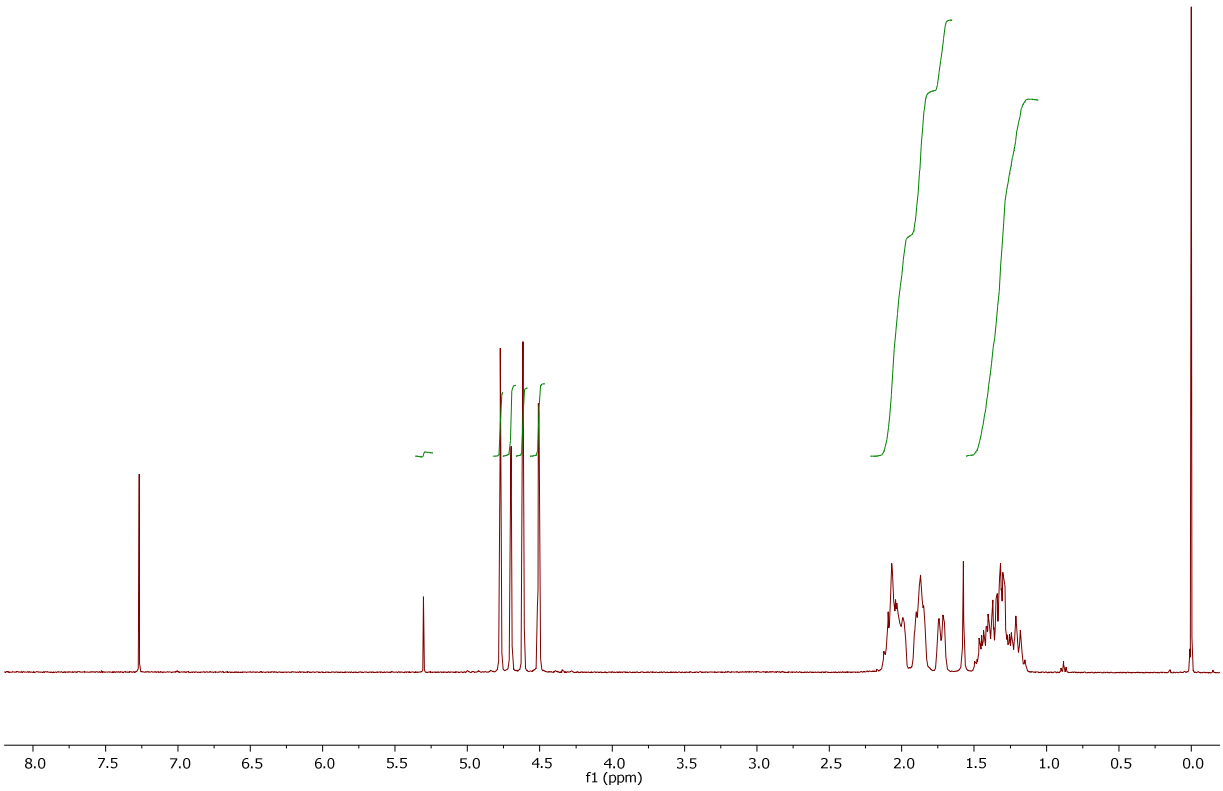

Figure S25. ^{1}H NMR spectrum (400 MHz, $CDCl_3$) of **5b**

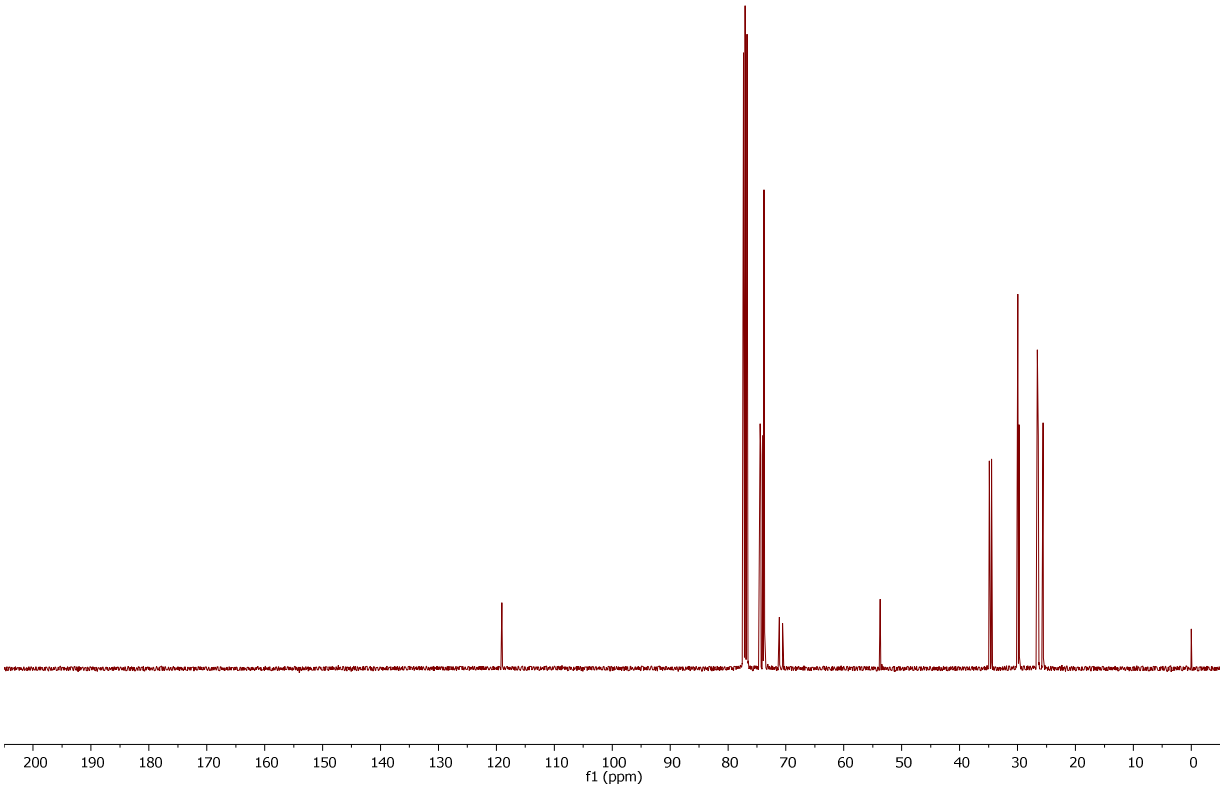

Figure S26. $^{13}C\{^{1}H\}$ NMR spectrum (101 MHz, $CDCl_3$) of **5b**

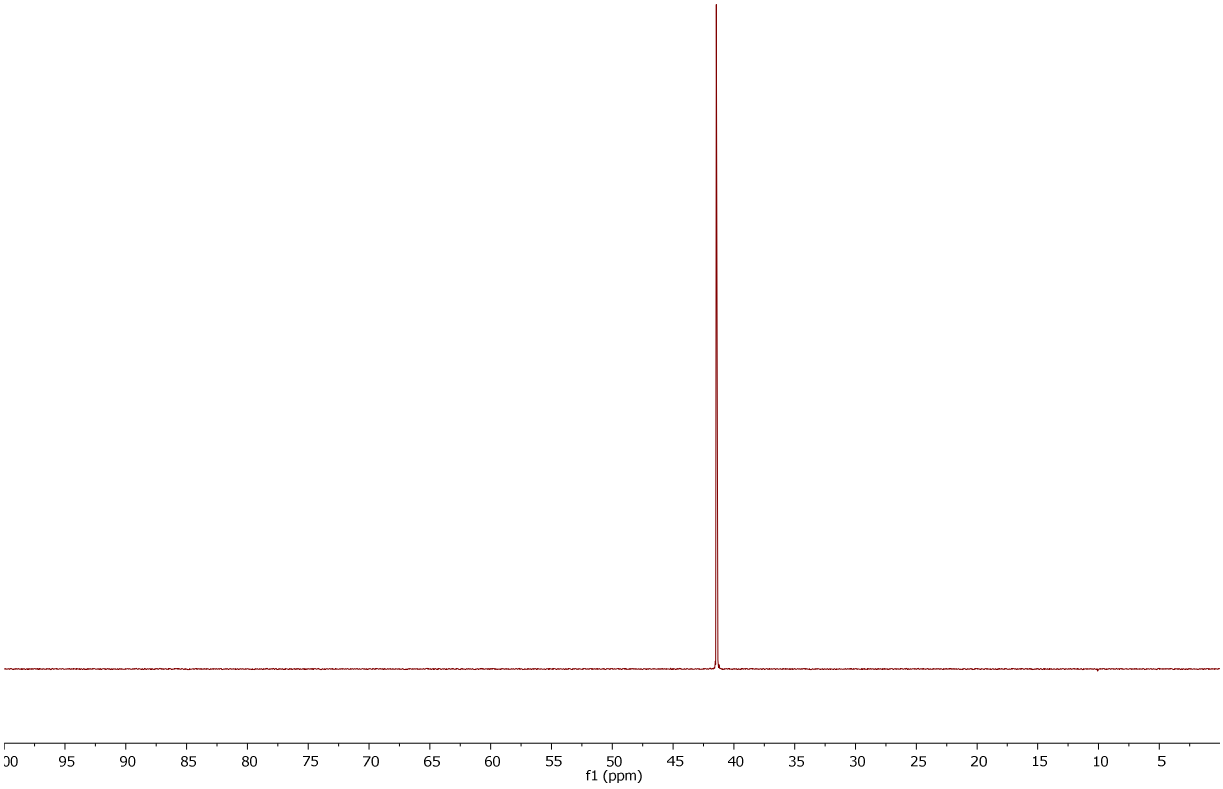

Figure S27. $^{31}P\{^{1}H\}$ NMR spectrum (162 MHz, $CDCl_3$) of **5b**

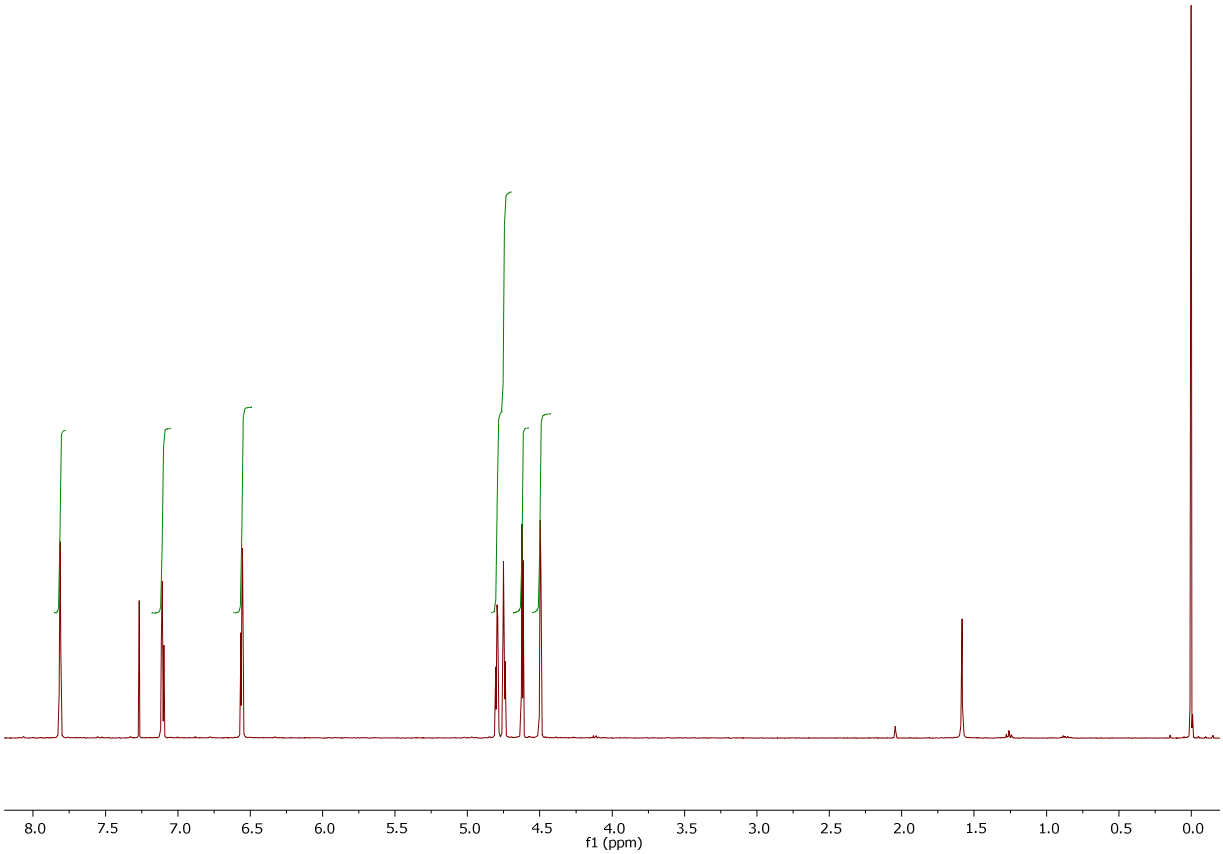

Figure S28. ^{1}H NMR spectrum (400 MHz, $CDCl_3$) of **5d**

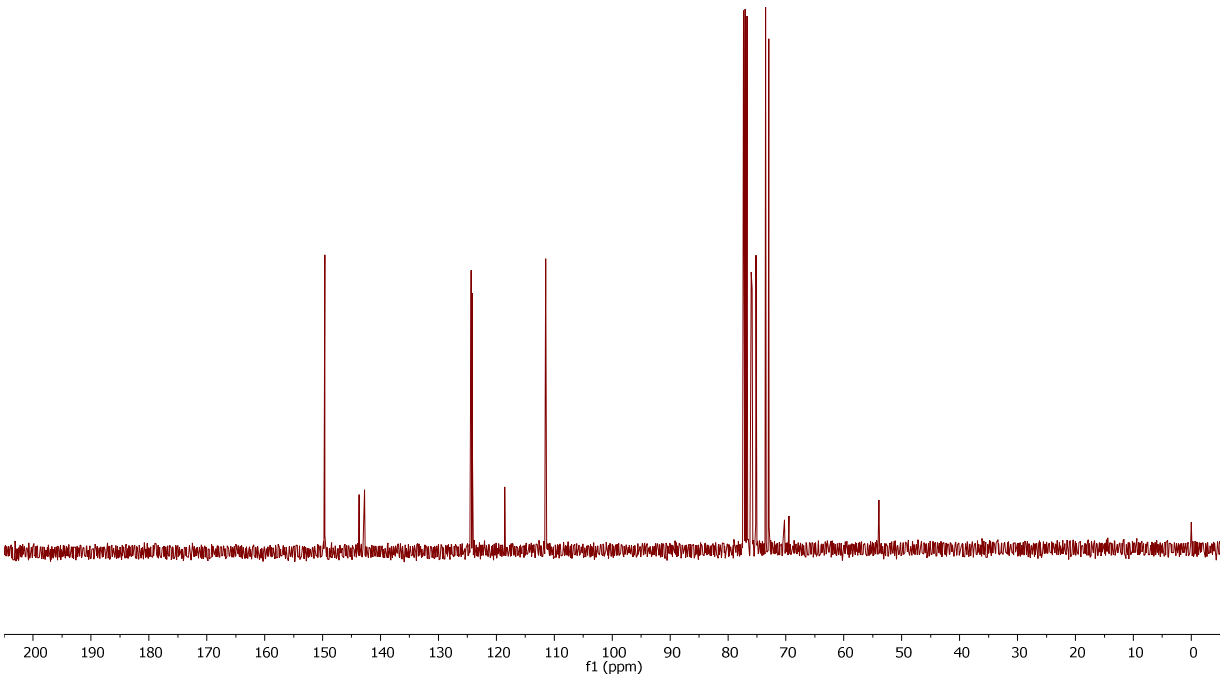

Figure S29. $^{13}C\{^{1}H\}$ NMR spectrum (101 MHz, $CDCl_3$) of **5d**

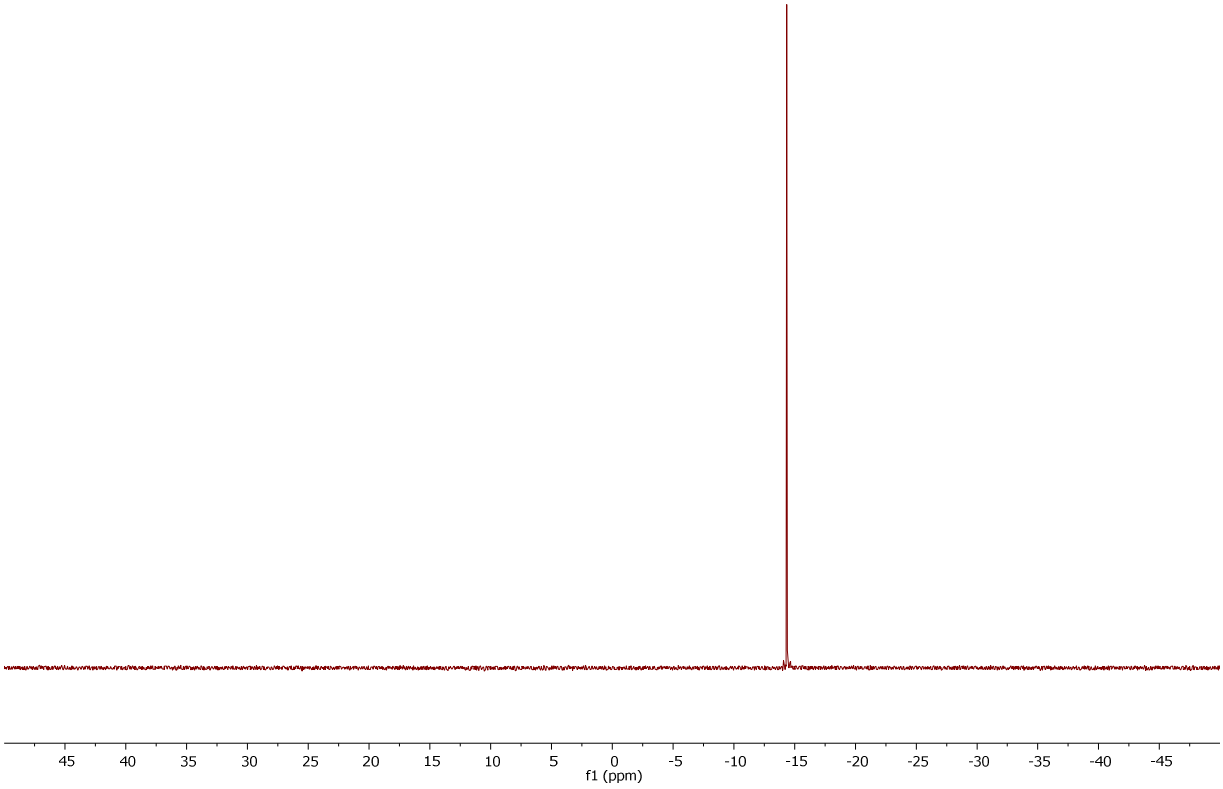

Figure S30. $^{31}P\{^{1}H\}$ NMR spectrum (162 MHz, $CDCl_3$) of **5d**

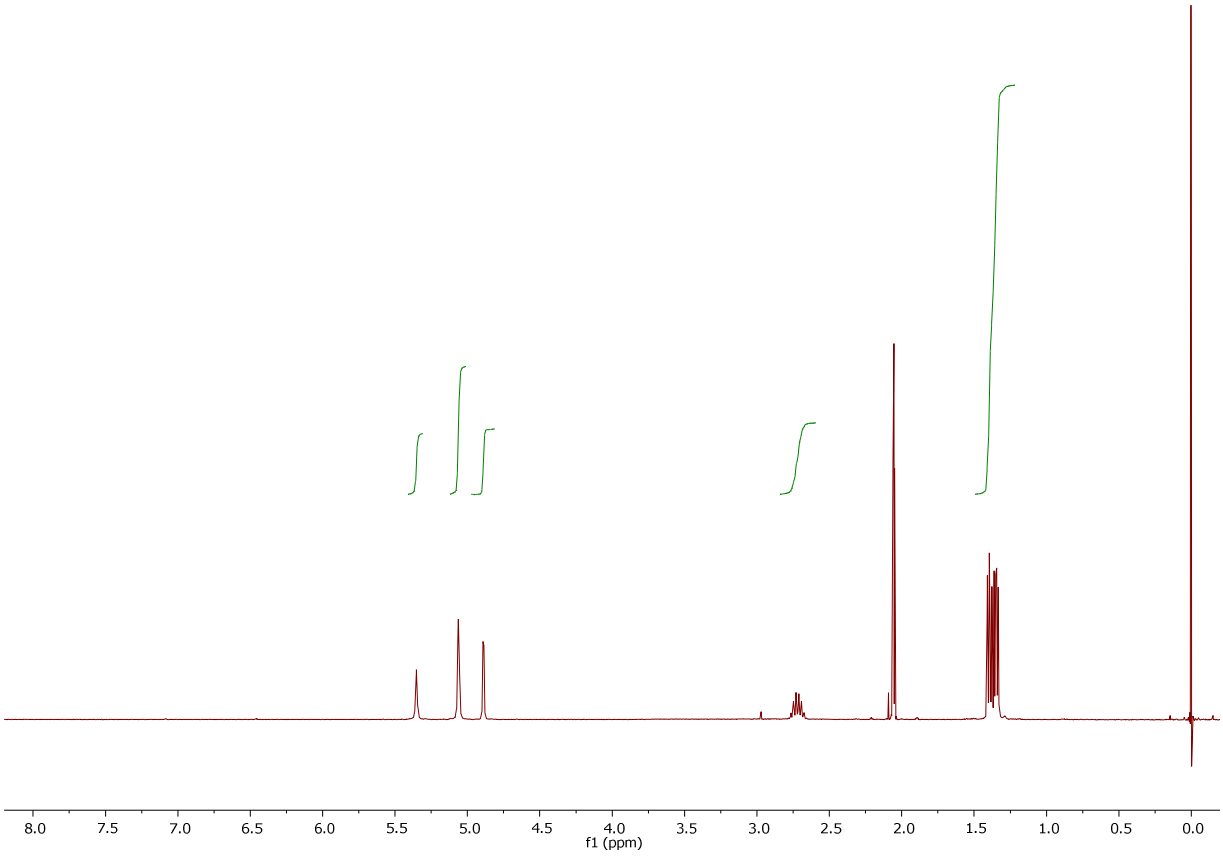

Figure S31. ^{1}H NMR spectrum (400 MHz, acetone-d_6) of **6a**

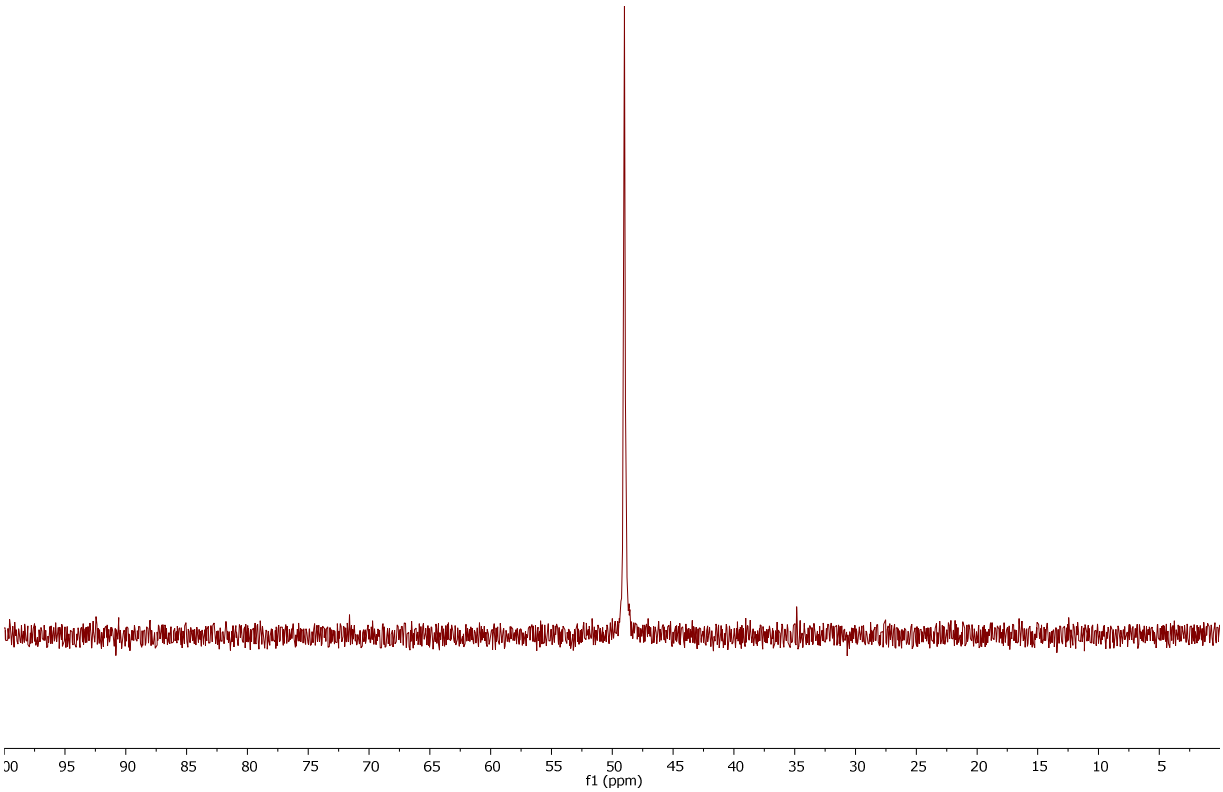

Figure S32. $^{31}P\{^{1}H\}$ NMR spectrum (162 MHz, acetone-d_6) of **6a**

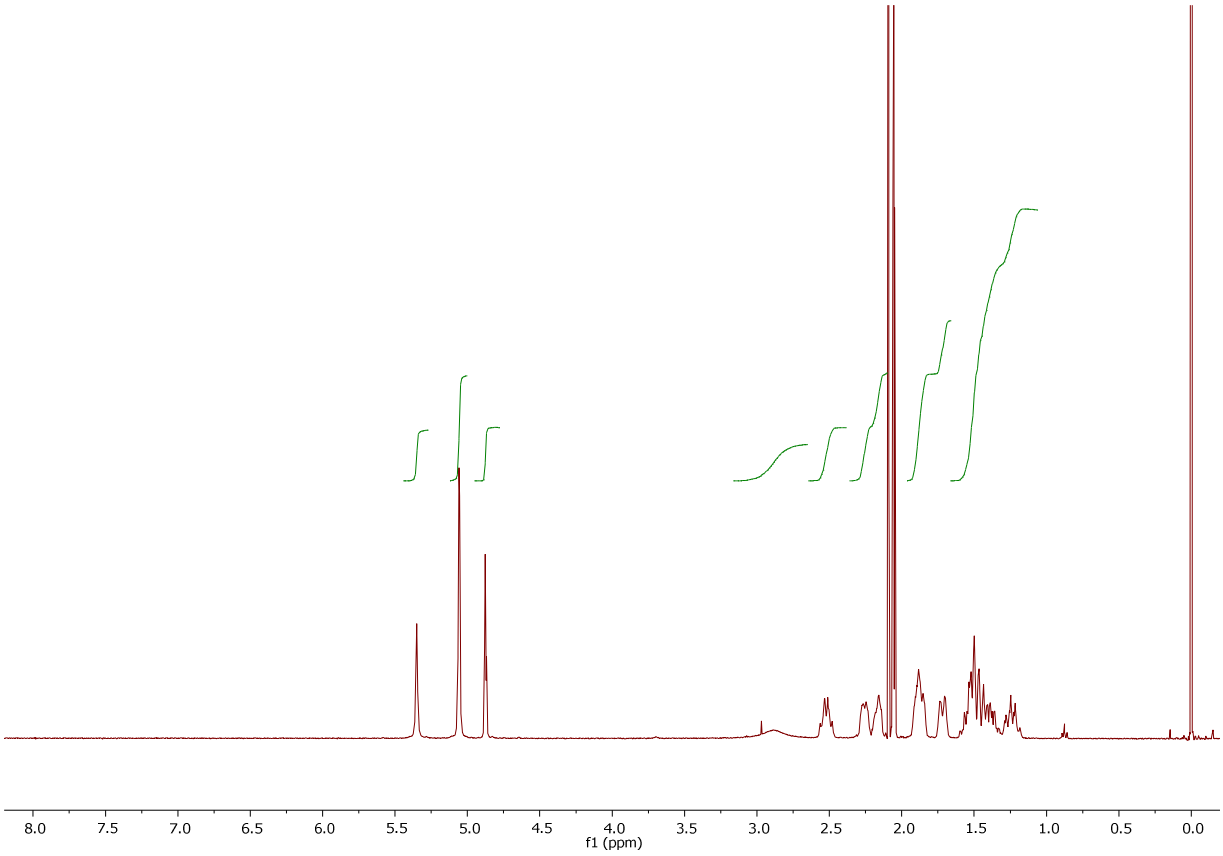

Figure S33. ^{1}H NMR spectrum (400 MHz, acetone-d_6) of **6b**

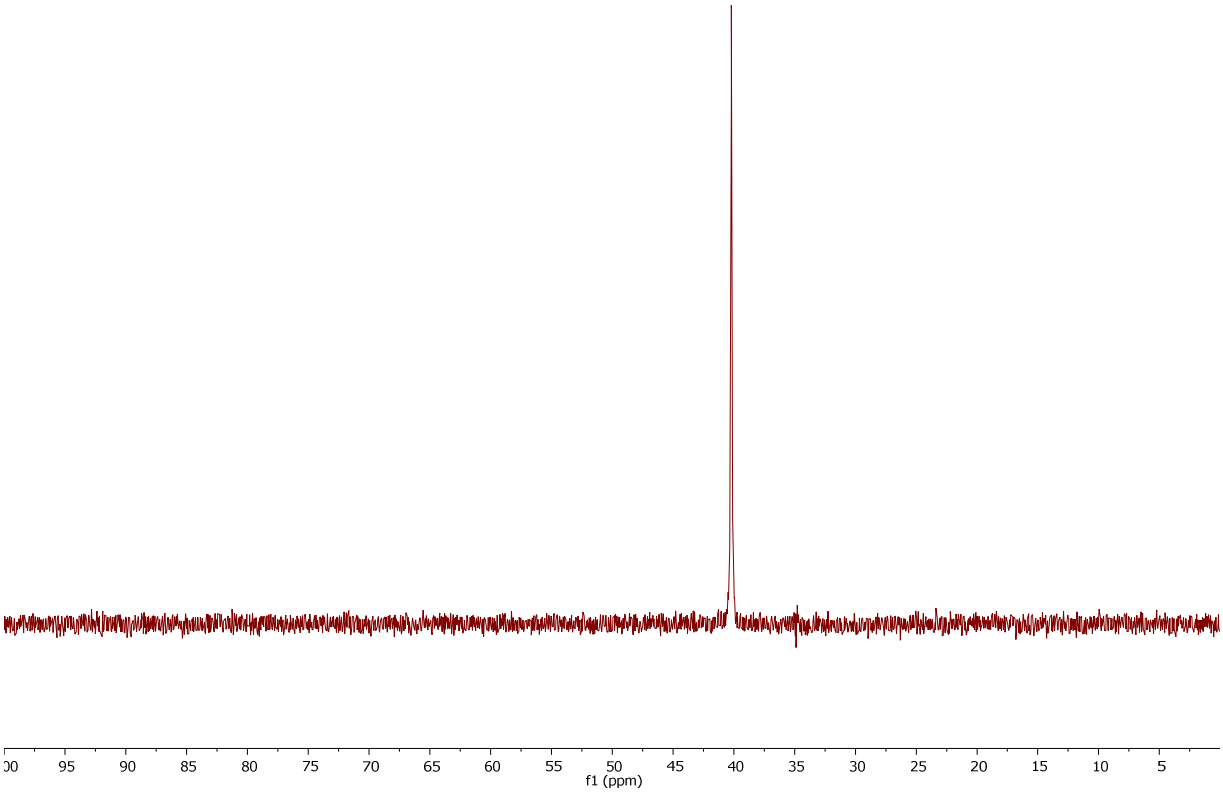

Figure S34. $^{31}P\{^{1}H\}$ NMR spectrum (162 MHz, acetone-d_6) of **6b**

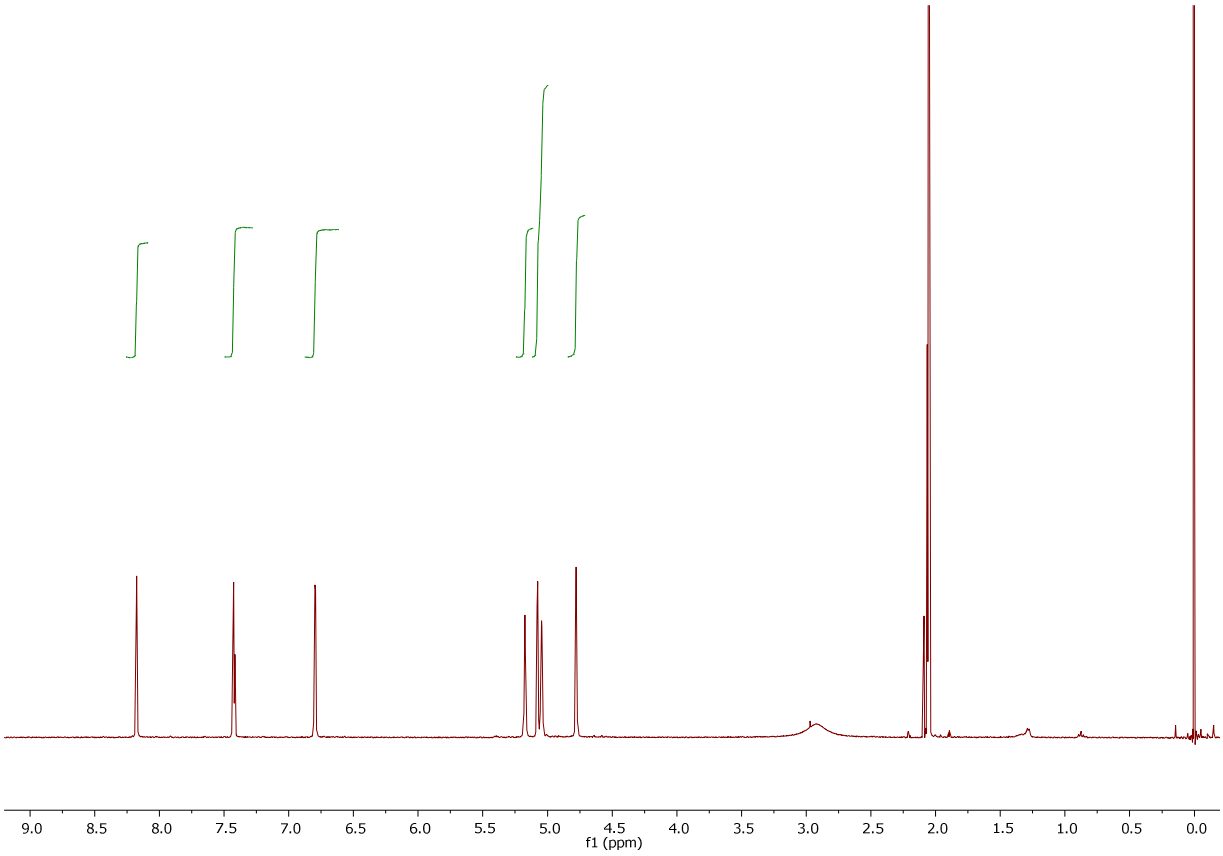

Figure S35. ^{1}H NMR spectrum (400 MHz, acetone-d_6) of **6d**

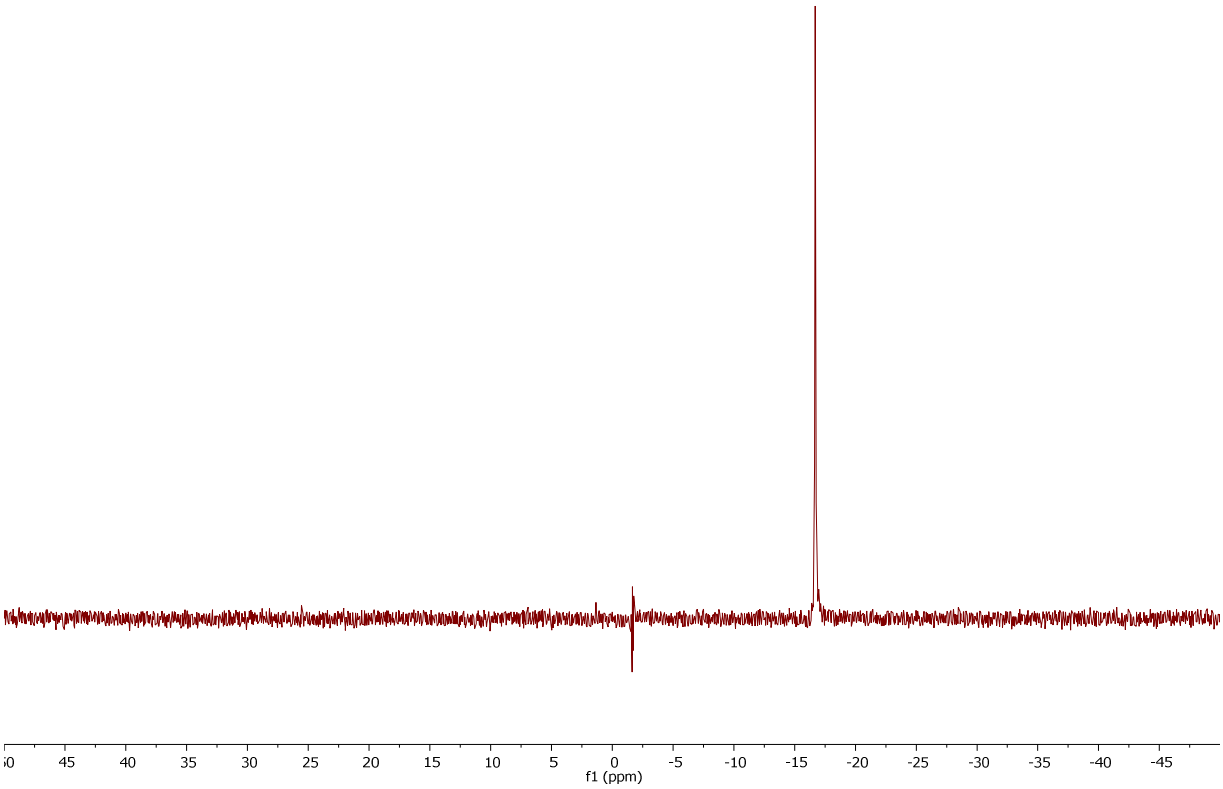

Figure S36. $^{31}P\{^{1}H\}$ NMR spectrum (162 MHz, acetone-d_6) of **6d**

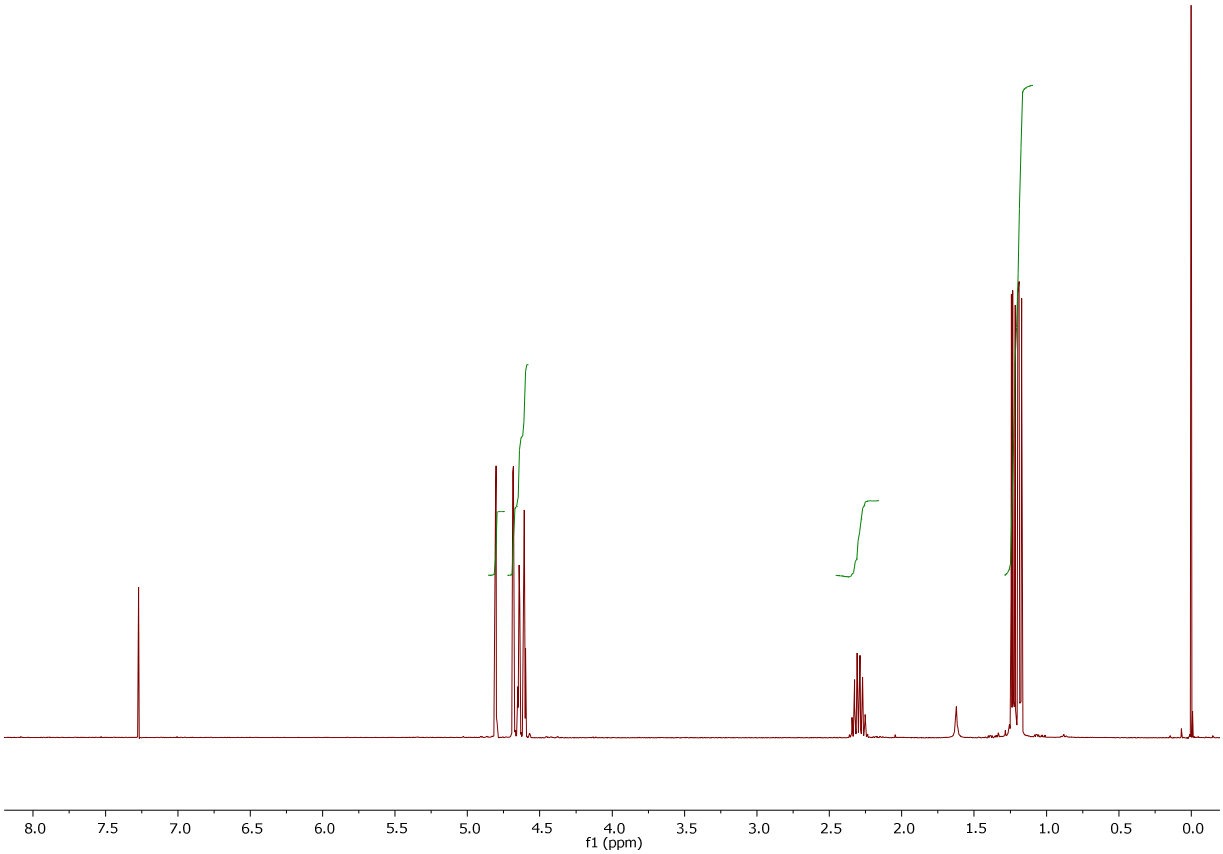

Figure S37. ^{1}H NMR spectrum (400 MHz, $CDCl_3$) of **7a**

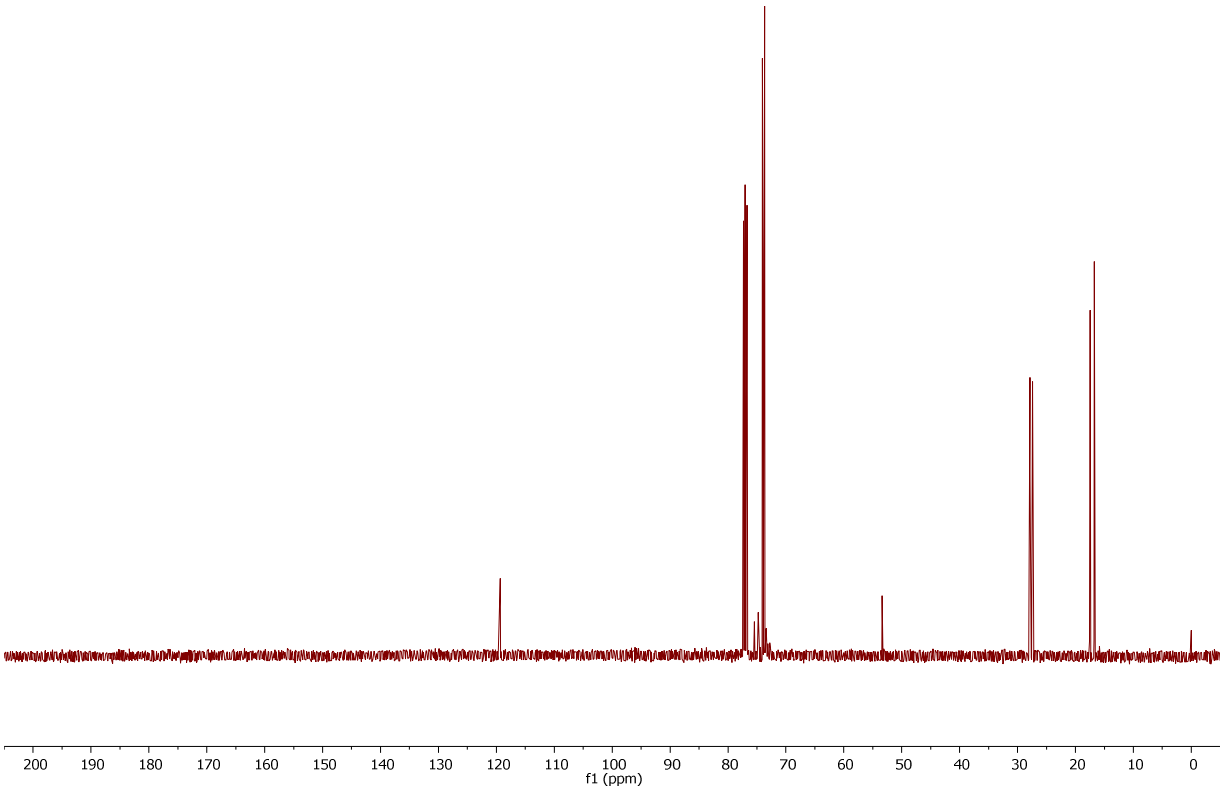

Figure S38. $^{13}C\{^{1}H\}$ NMR spectrum (101 MHz, $CDCl_3$) of **7a**

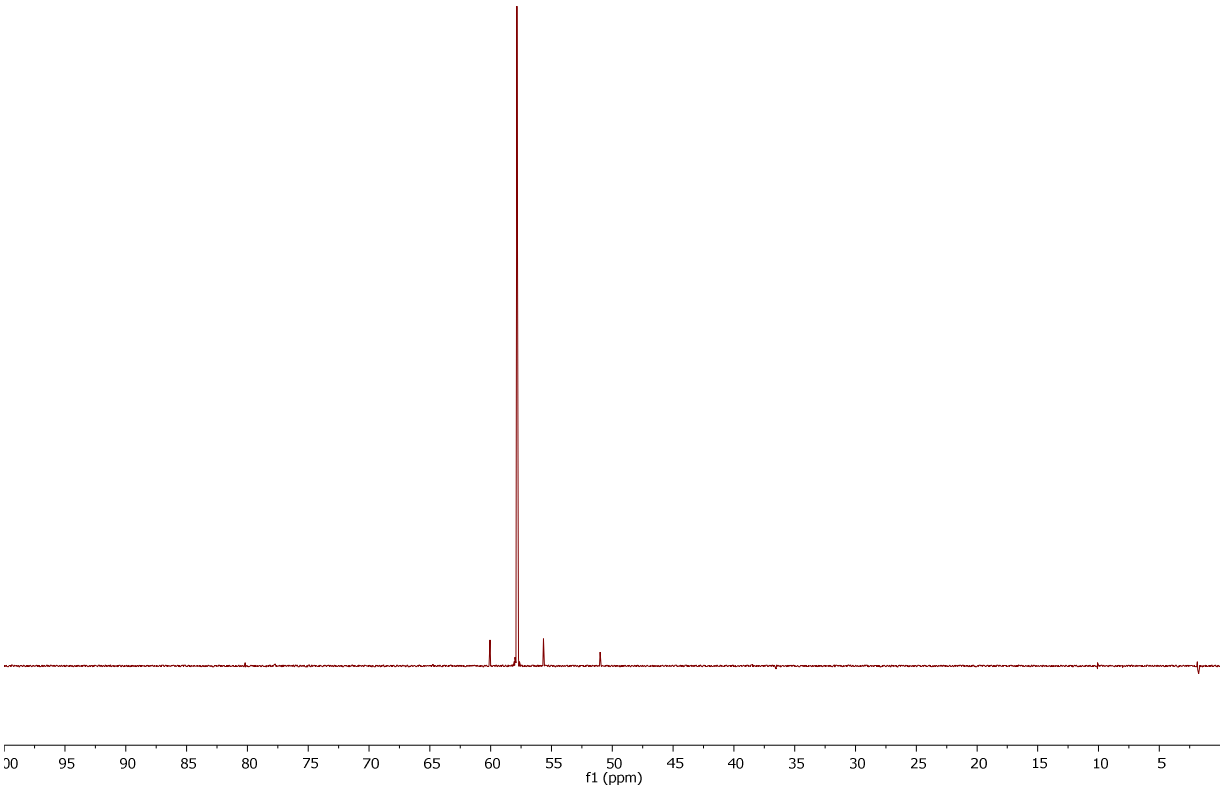

Figure S39. $^{31}P\{^{1}H\}$ NMR spectrum (162 MHz, $CDCl_3$) of **7a**

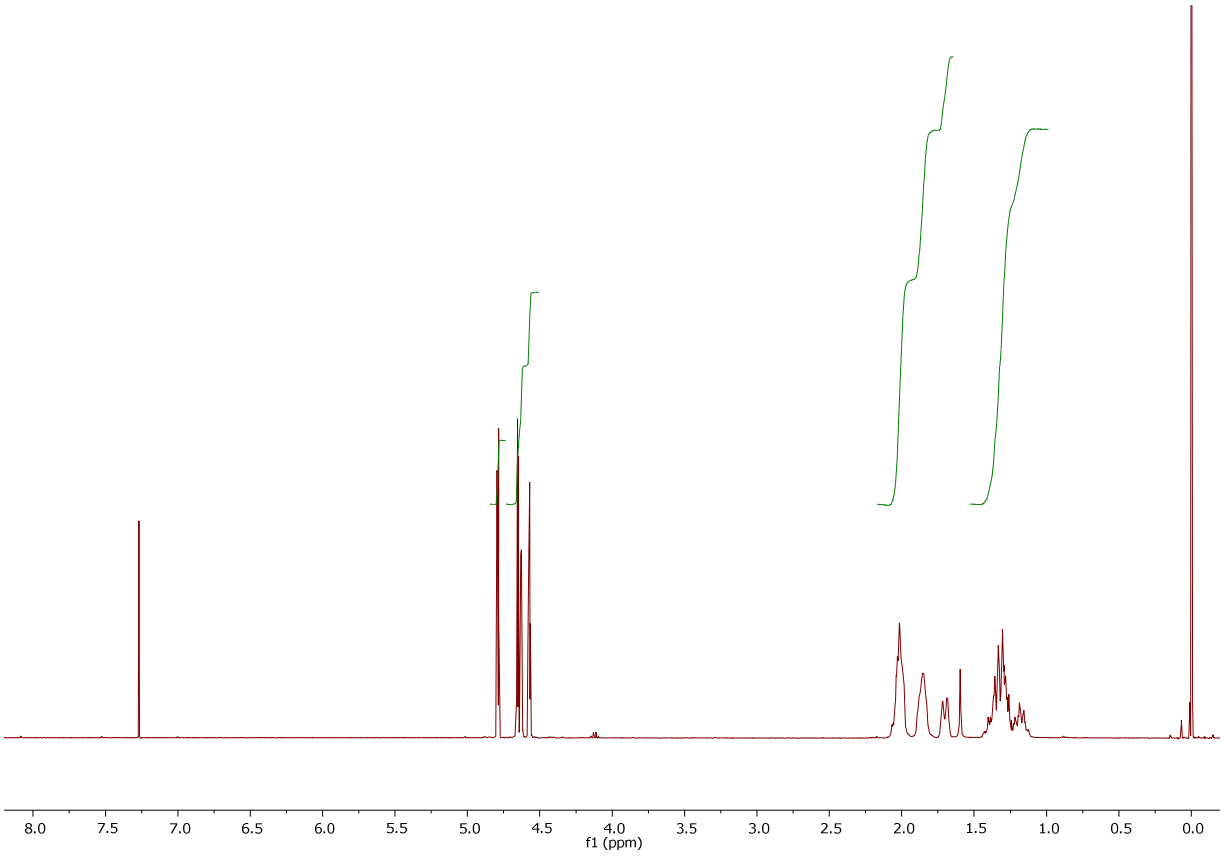

Figure S40. ^{1}H NMR spectrum (400 MHz, $CDCl_3$) of **7b**

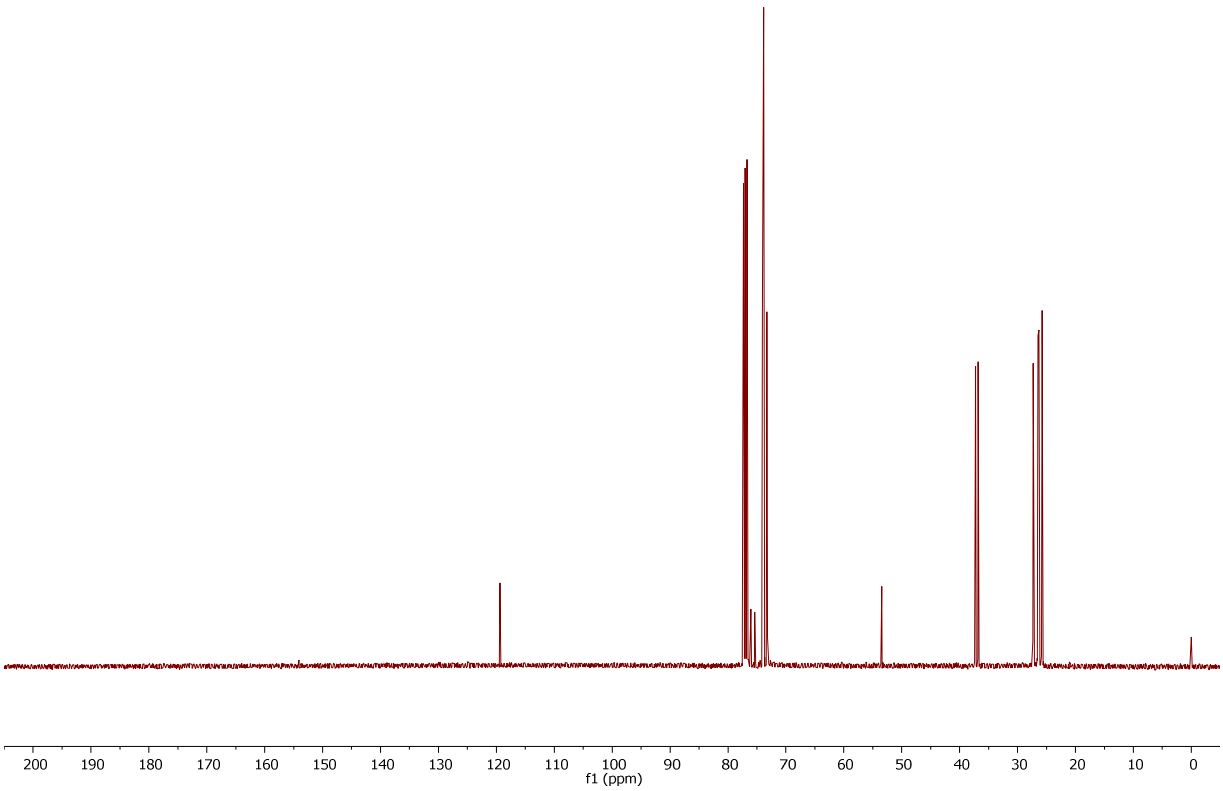

Figure S41. $^{13}C\{^{1}H\}$ NMR spectrum (101 MHz, $CDCl_3$) of **7b**

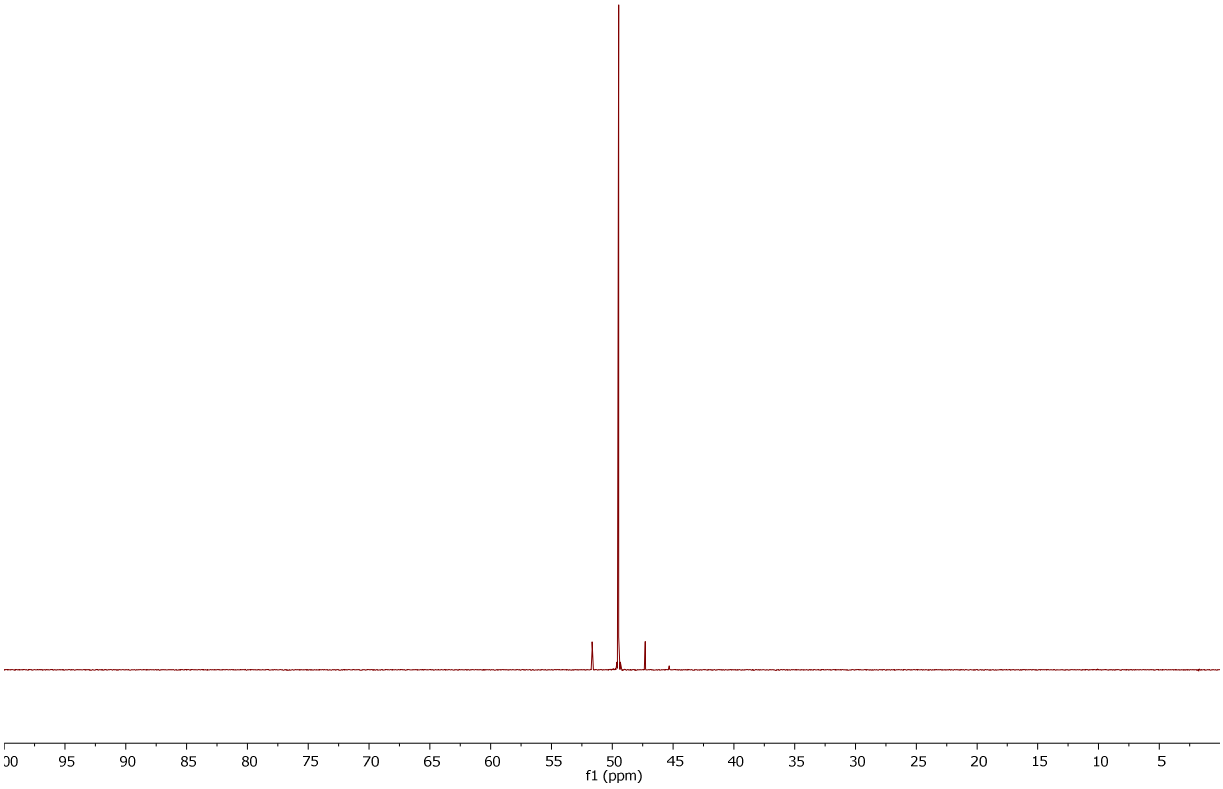

Figure S42. $^{31}P\{^{1}H\}$ NMR spectrum (162 MHz, $CDCl_3$) of **7b**

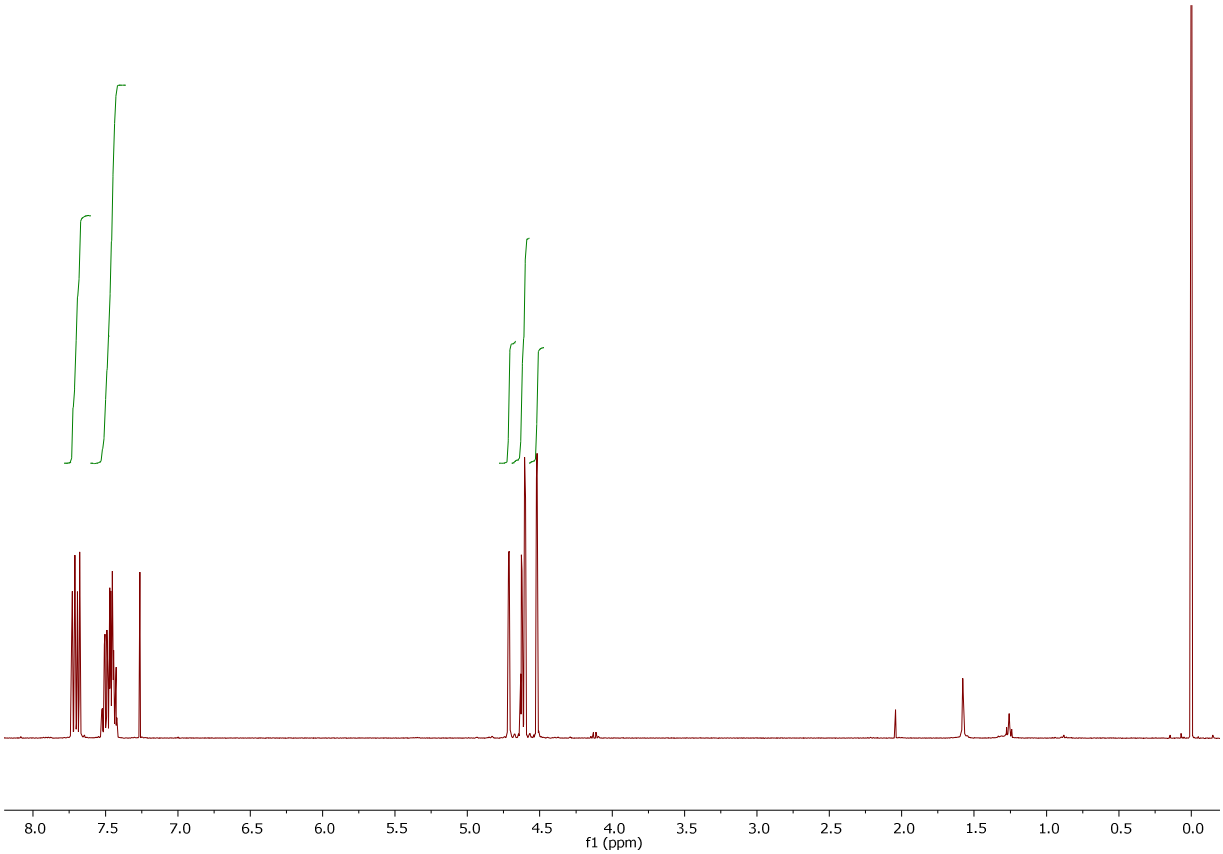

Figure S43. ^{1}H NMR spectrum (400 MHz, $CDCl_3$) of **7c**

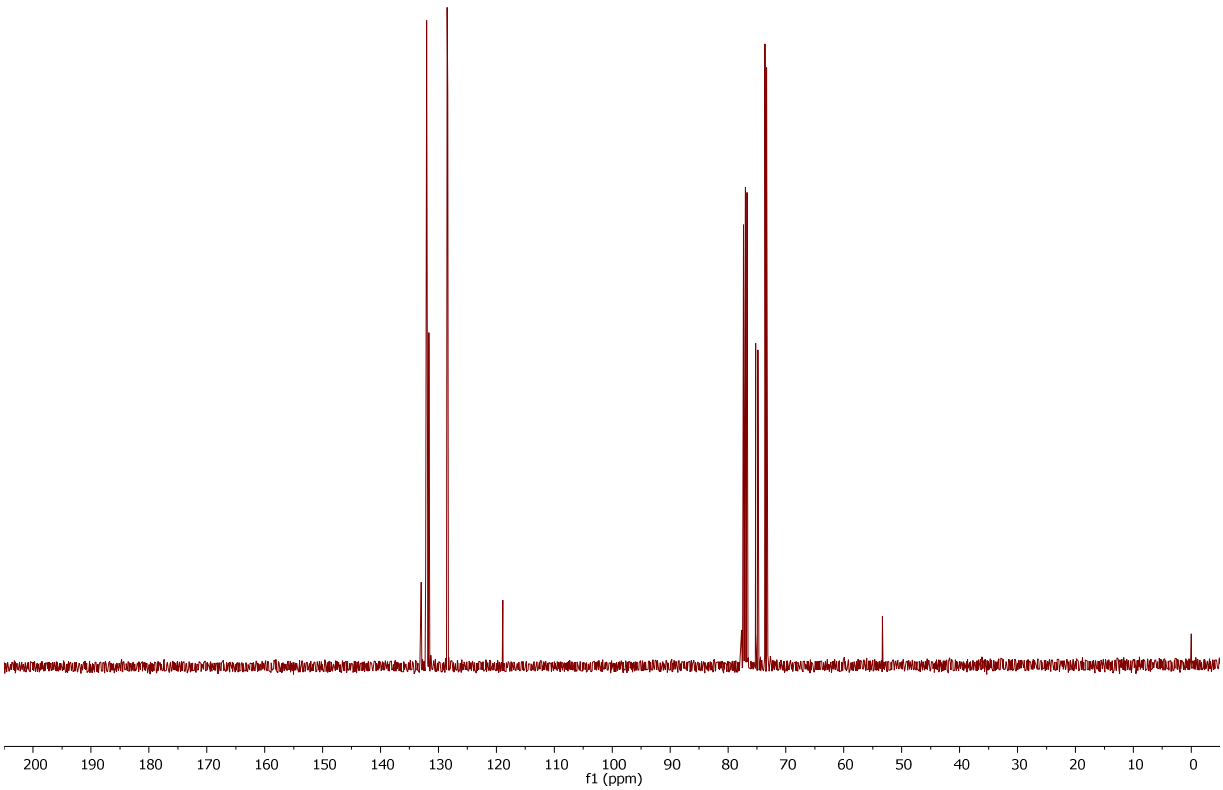

Figure S44. $^{13}C\{^{1}H\}$ NMR spectrum (101 MHz, $CDCl_3$) of **7c**

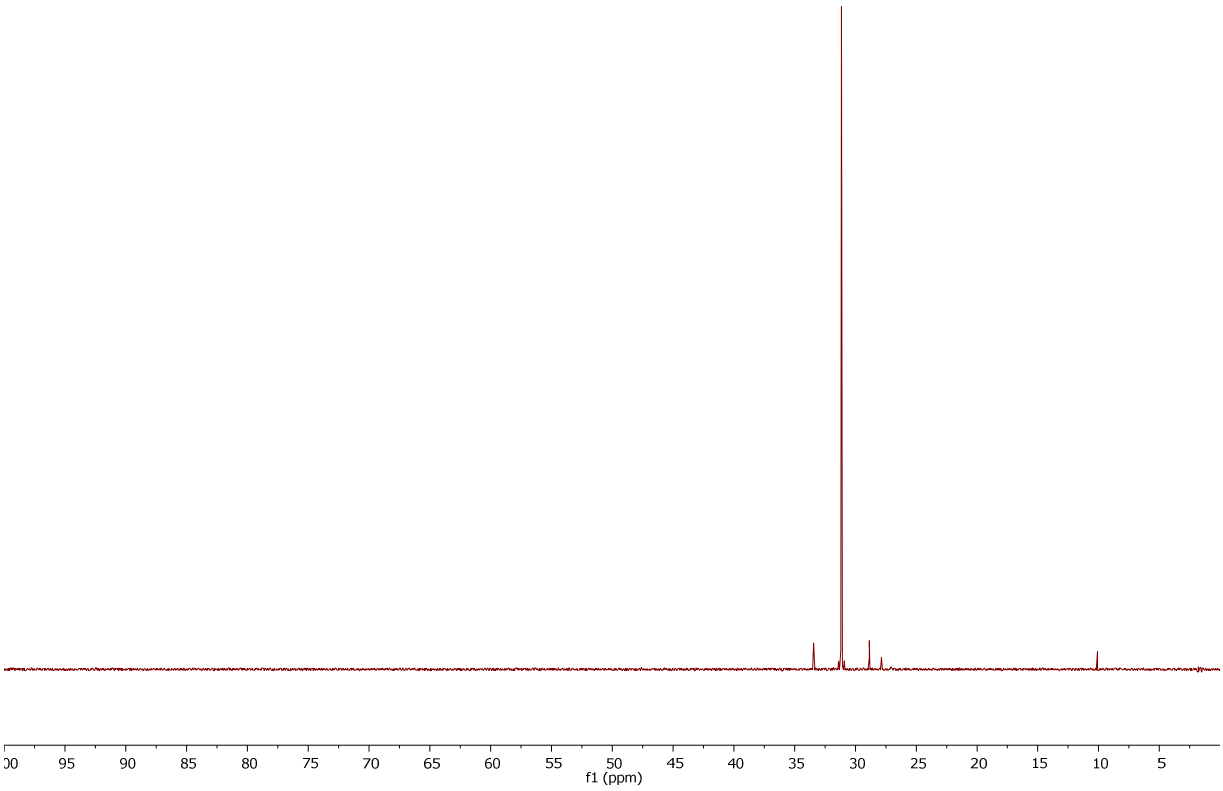

Figure S45. $^{31}P\{^{1}H\}$ NMR spectrum (162 MHz, $CDCl_3$) of **7c**

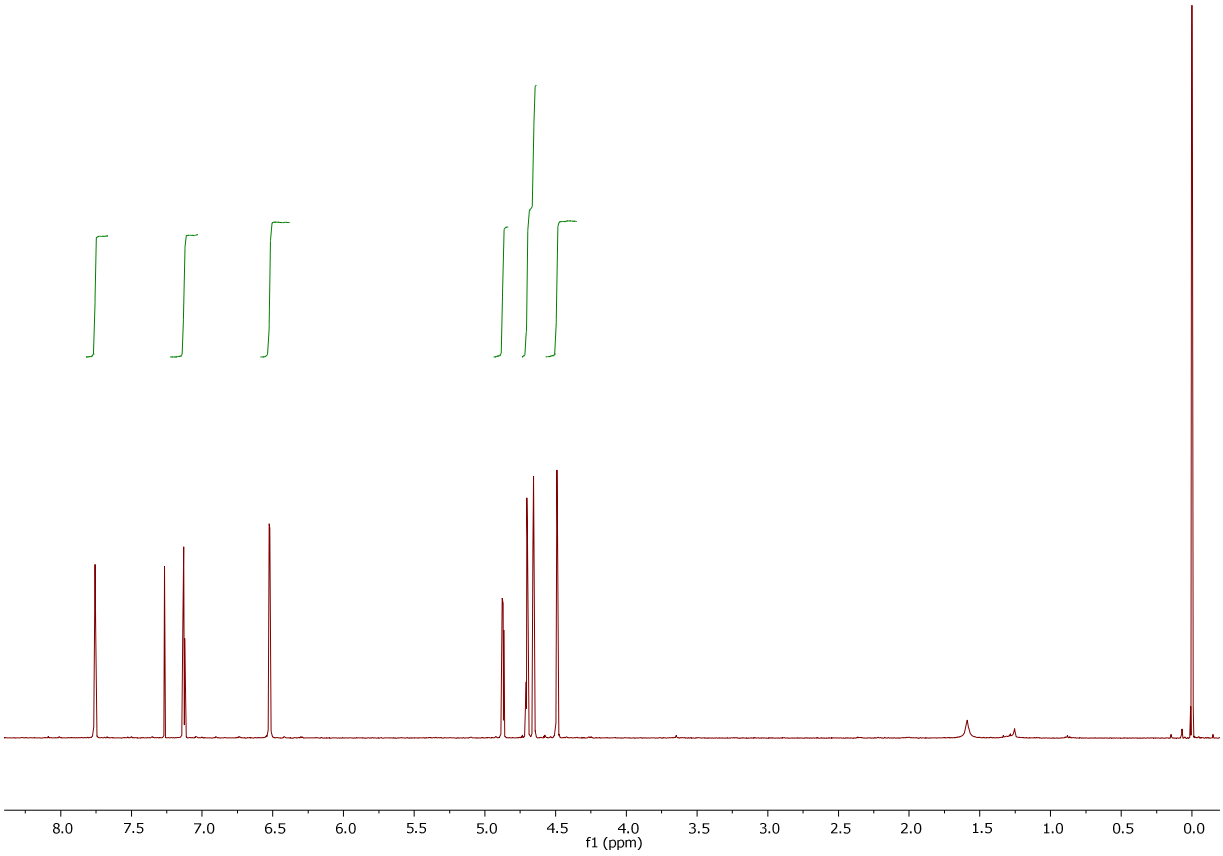

Figure S46. ^{1}H NMR spectrum (400 MHz, $CDCl_3$) of **7d**

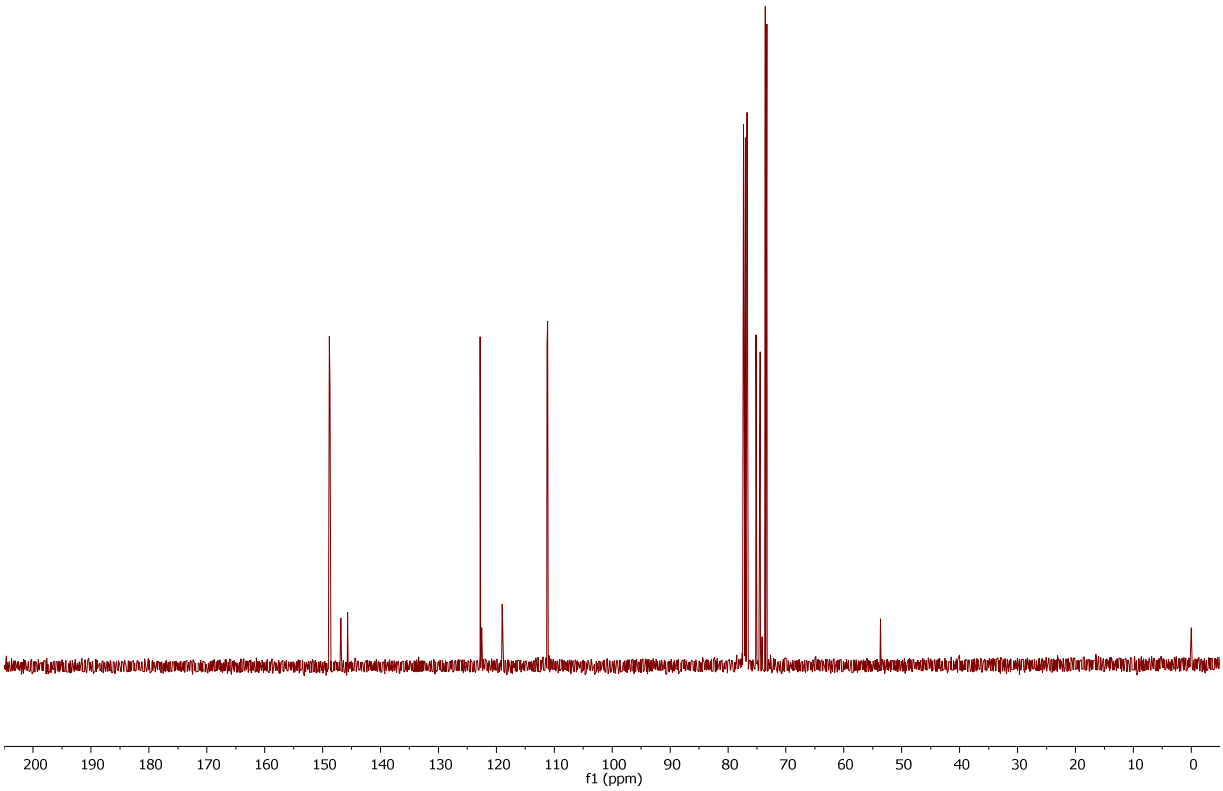

Figure S47. $^{13}C\{^{1}H\}$ NMR spectrum (101 MHz, $CDCl_3$) of **7d**

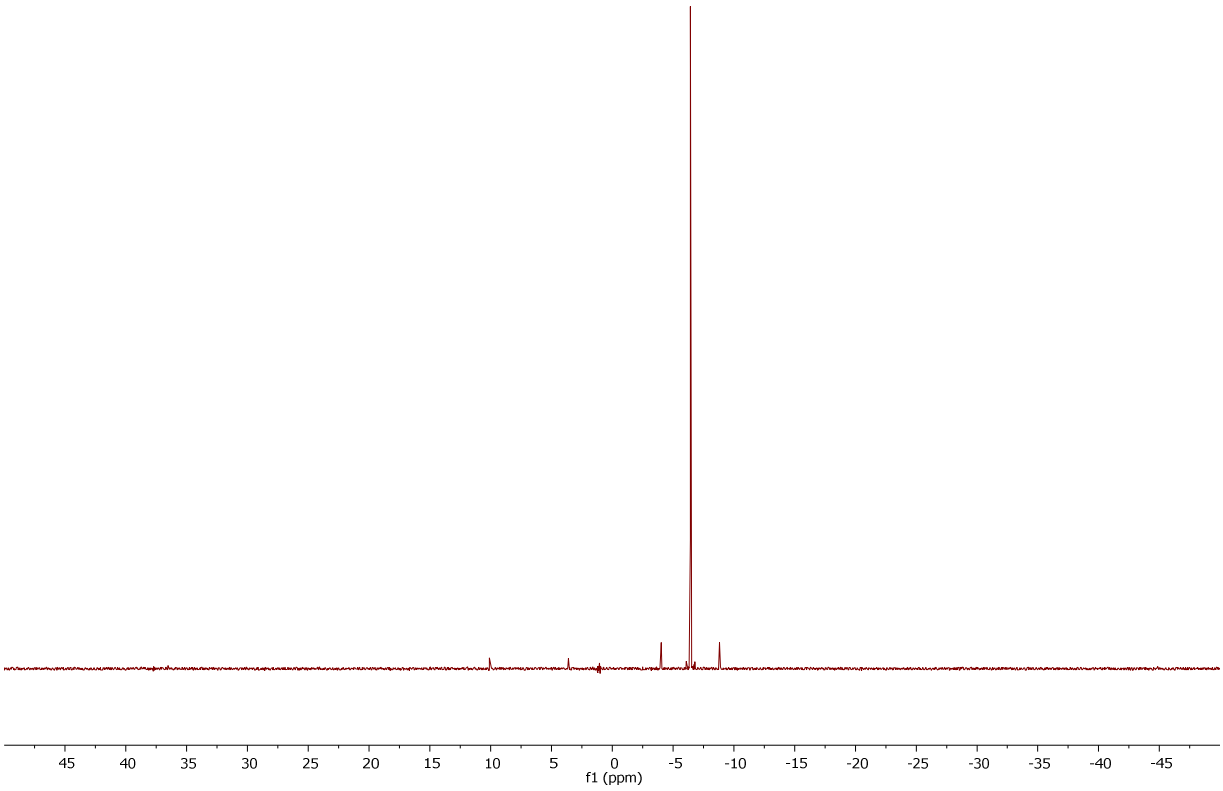

Figure S48. $^{31}P\{^{1}H\}$ NMR spectrum (162 MHz, $CDCl_3$) of **7d**

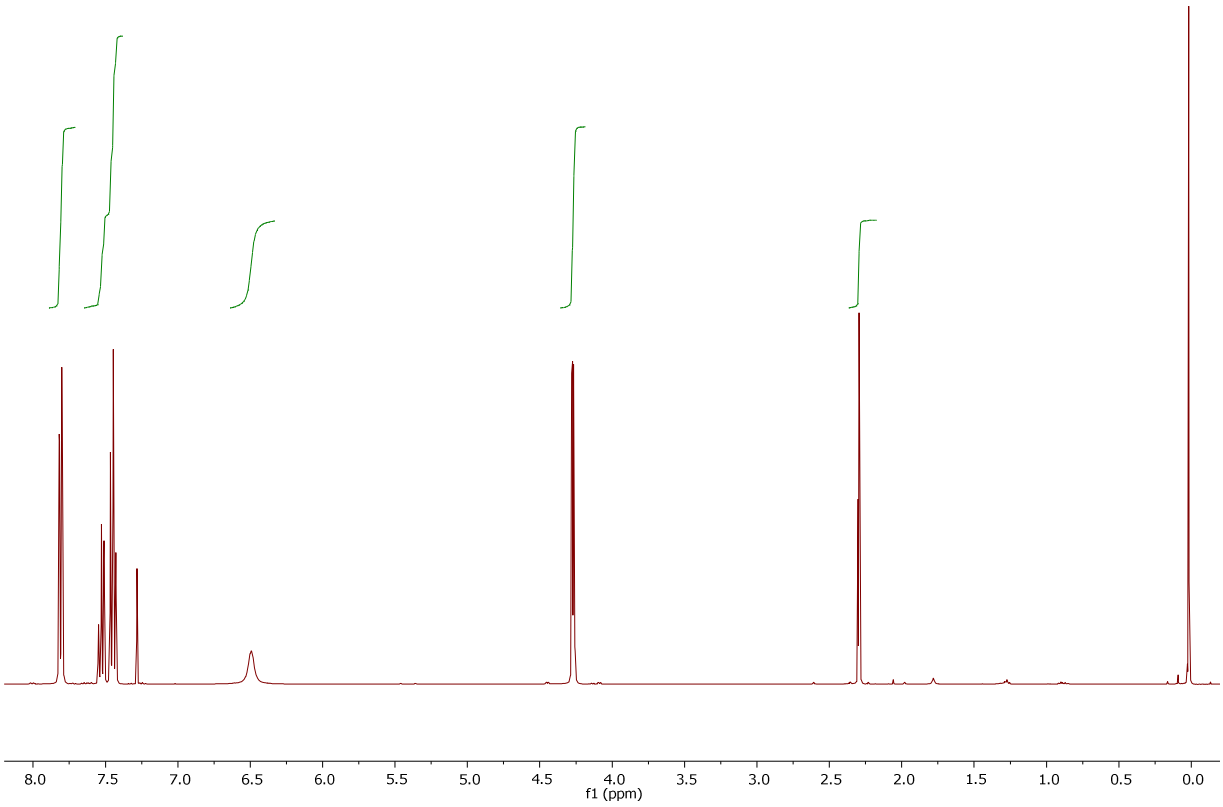

Figure S49. ^{1}H NMR spectrum (400 MHz, $CDCl_3$) of **8a**

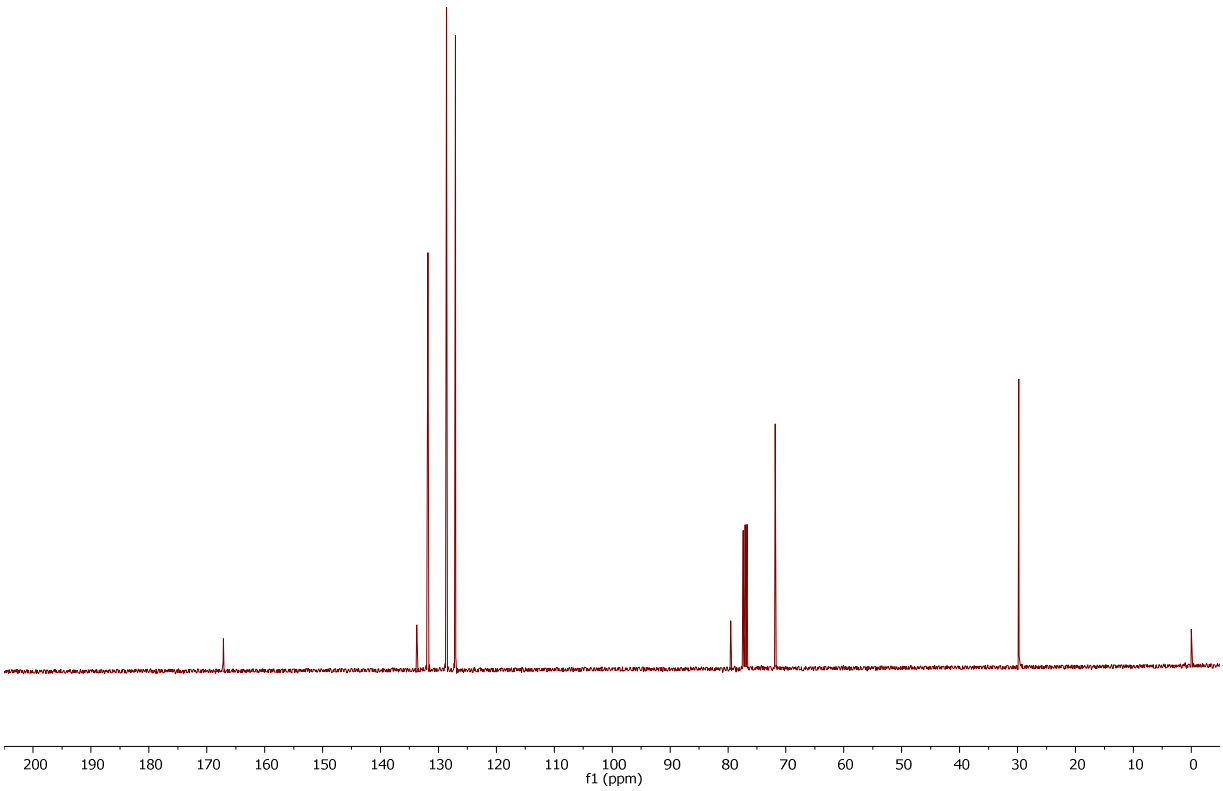

Figure S50. $^{13}C\{^{1}H\}$ NMR spectrum (101 MHz, $CDCl_3$) of **8a**

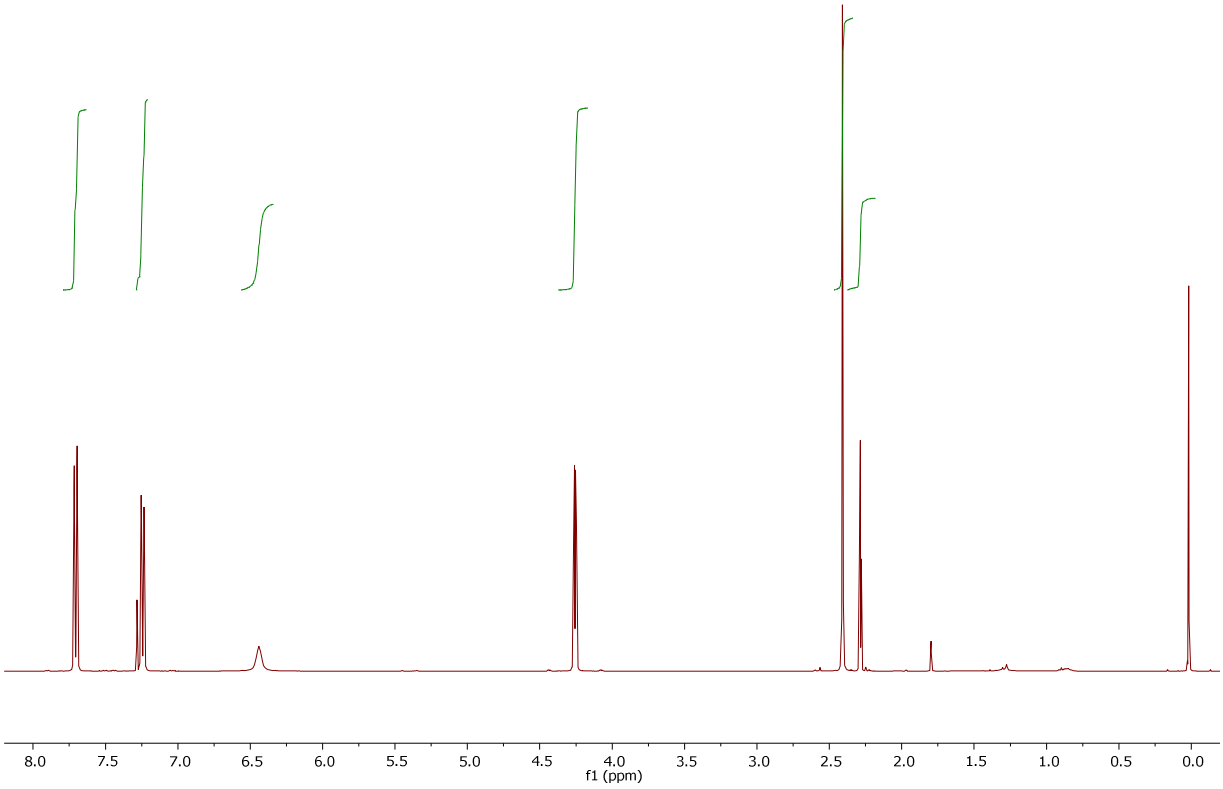

Figure S51. ^{1}H NMR spectrum (400 MHz, $CDCl_3$) of **8b**

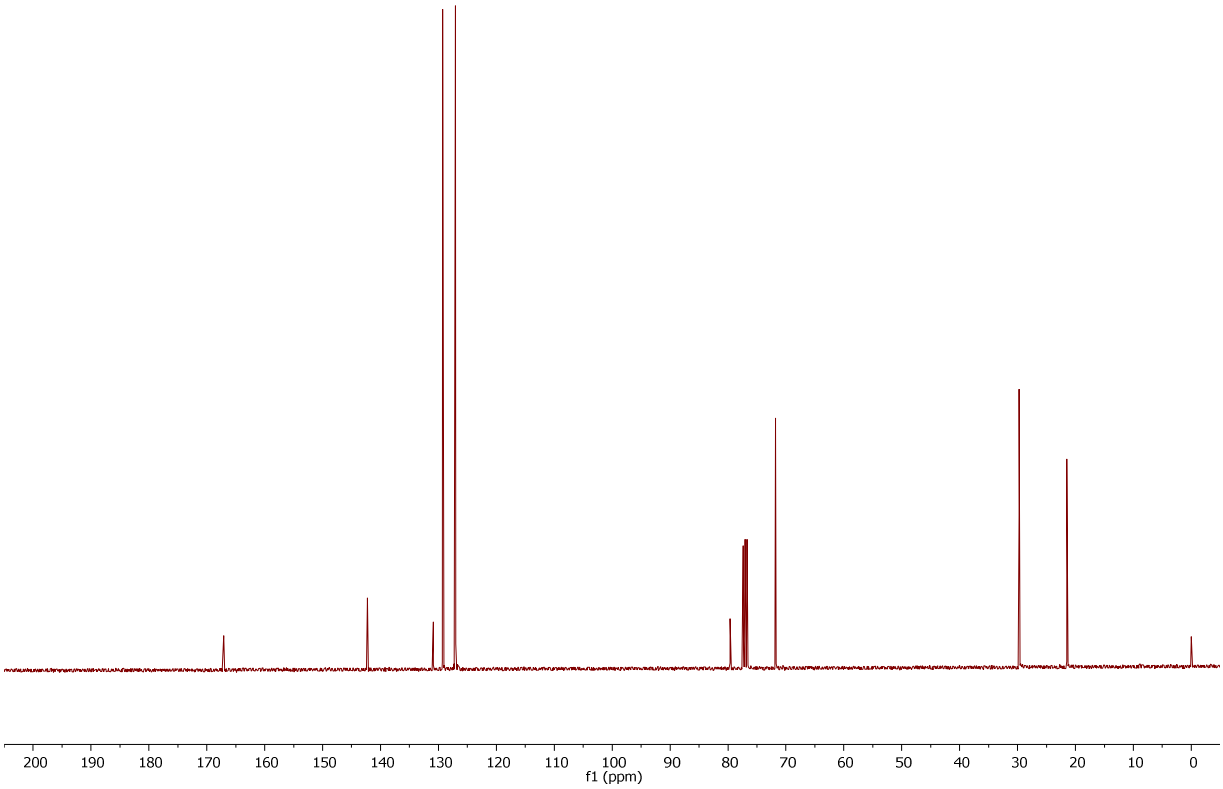

Figure S52. $^{13}C\{^{1}H\}$ NMR spectrum (101 MHz, $CDCl_3$) of **8b**

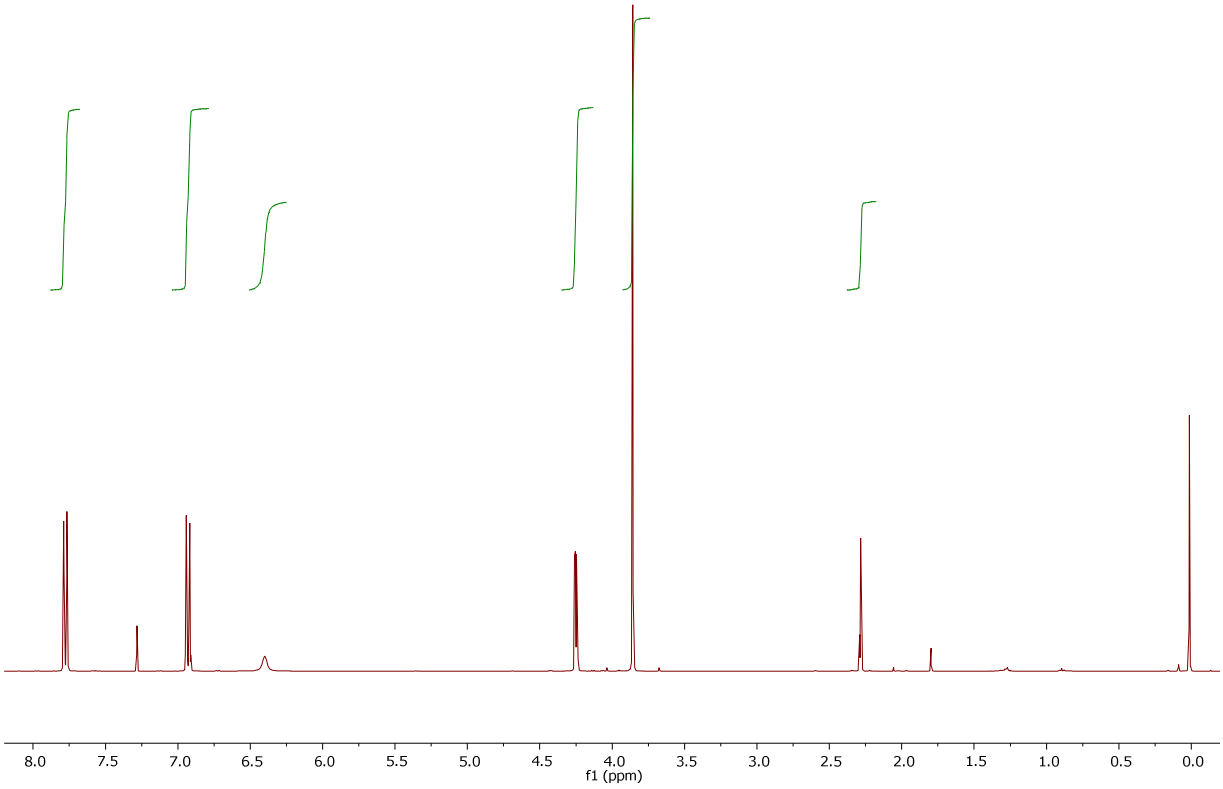

Figure S53. ^{1}H NMR spectrum (400 MHz, $CDCl_3$) of **8c**

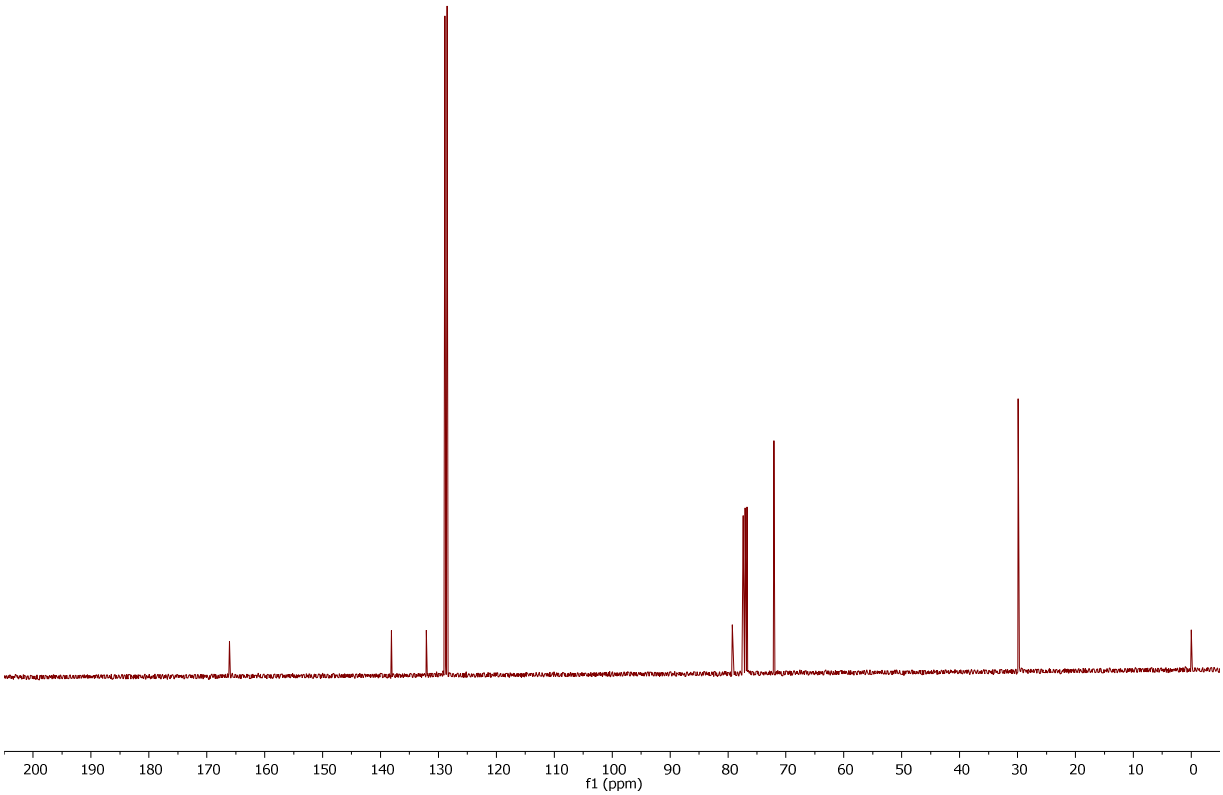

Figure S54. $^{13}C\{^{1}H\}$ NMR spectrum (101 MHz, $CDCl_3$) of **8c**

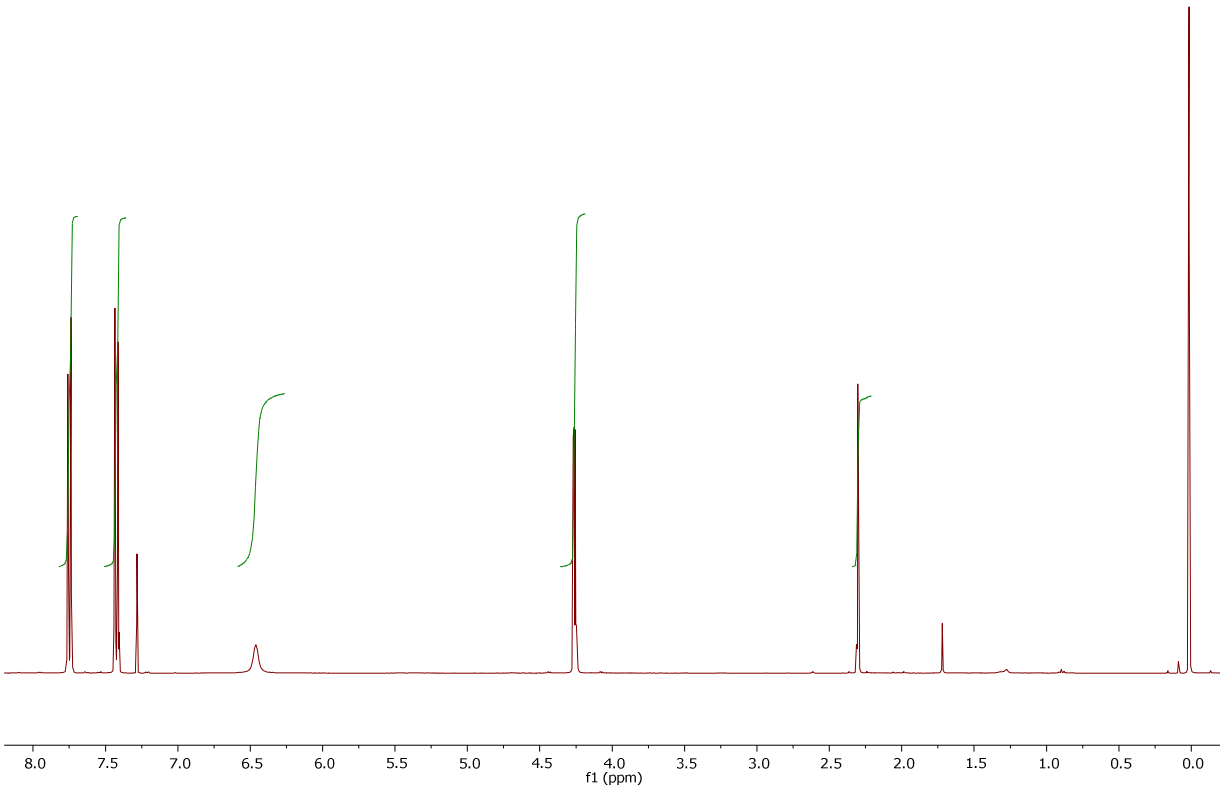

Figure S55. ^{1}H NMR spectrum (400 MHz, $CDCl_3$) of **8d**

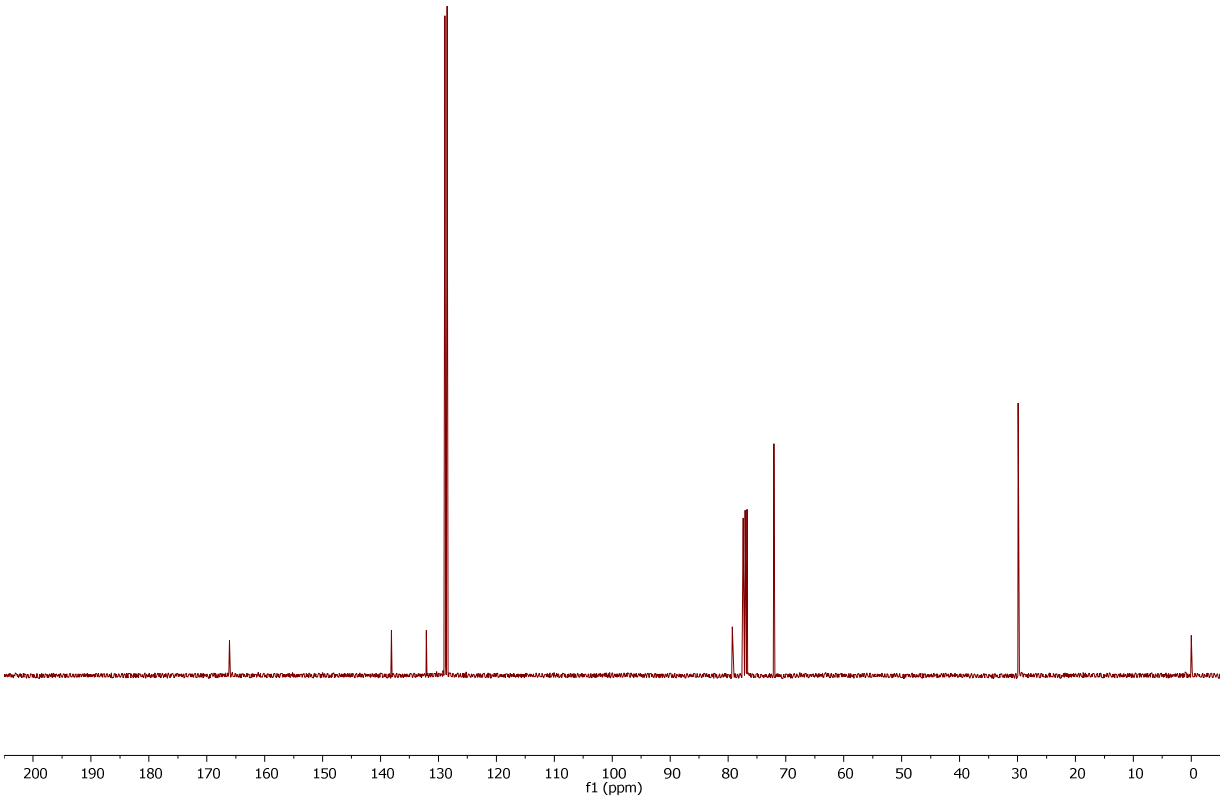

Figure S56. $^{13}C\{^{1}H\}$ NMR spectrum (101 MHz, $CDCl_3$) of **8d**

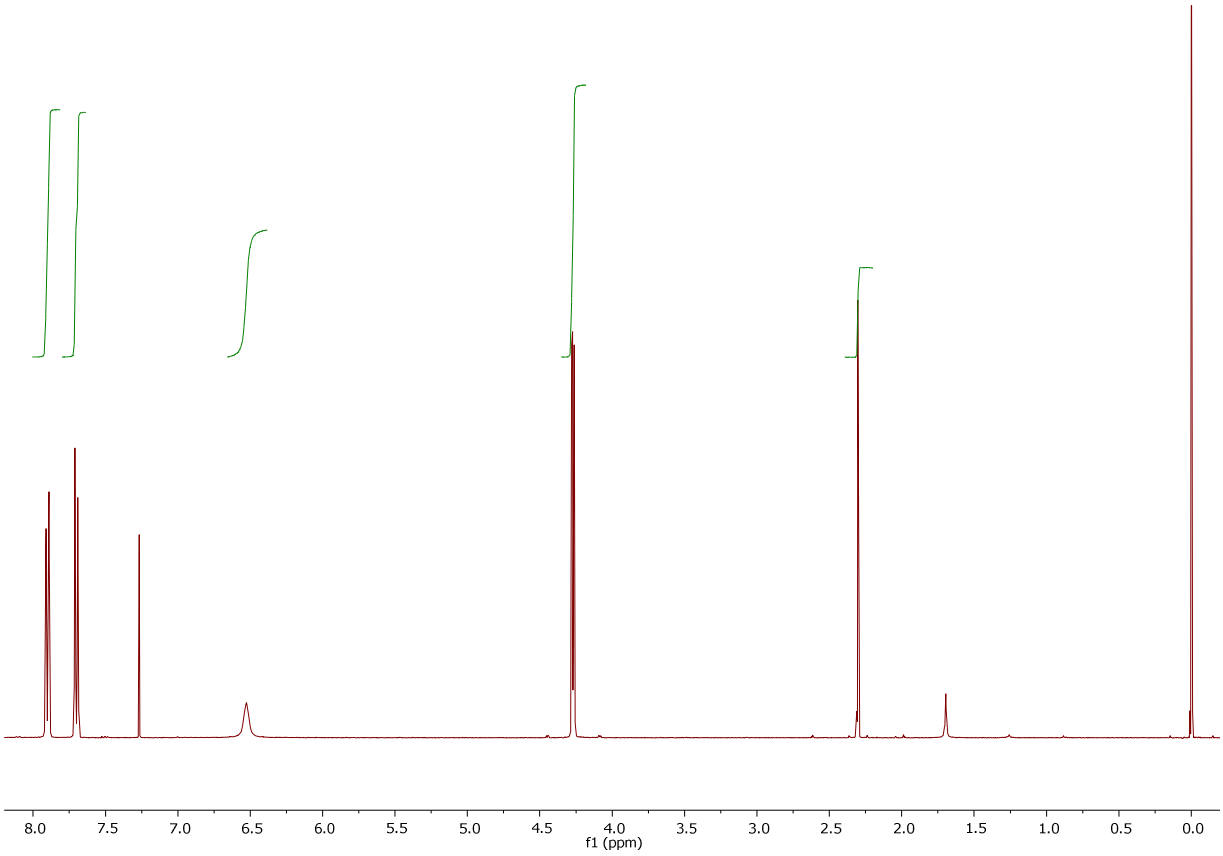

Figure S57. ^{1}H NMR spectrum (400 MHz, $CDCl_3$) of **8e**

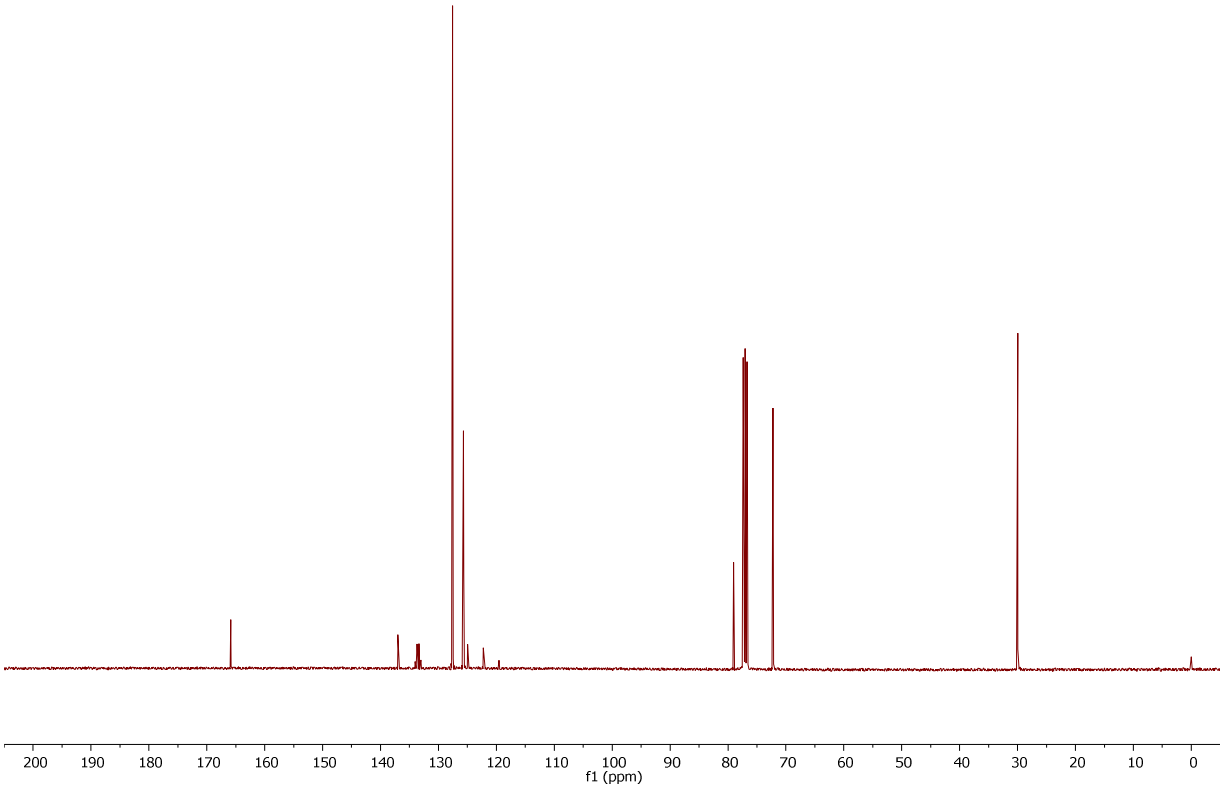

Figure S58. $^{13}C\{^{1}H\}$ NMR spectrum (101 MHz, $CDCl_3$) of **8e**

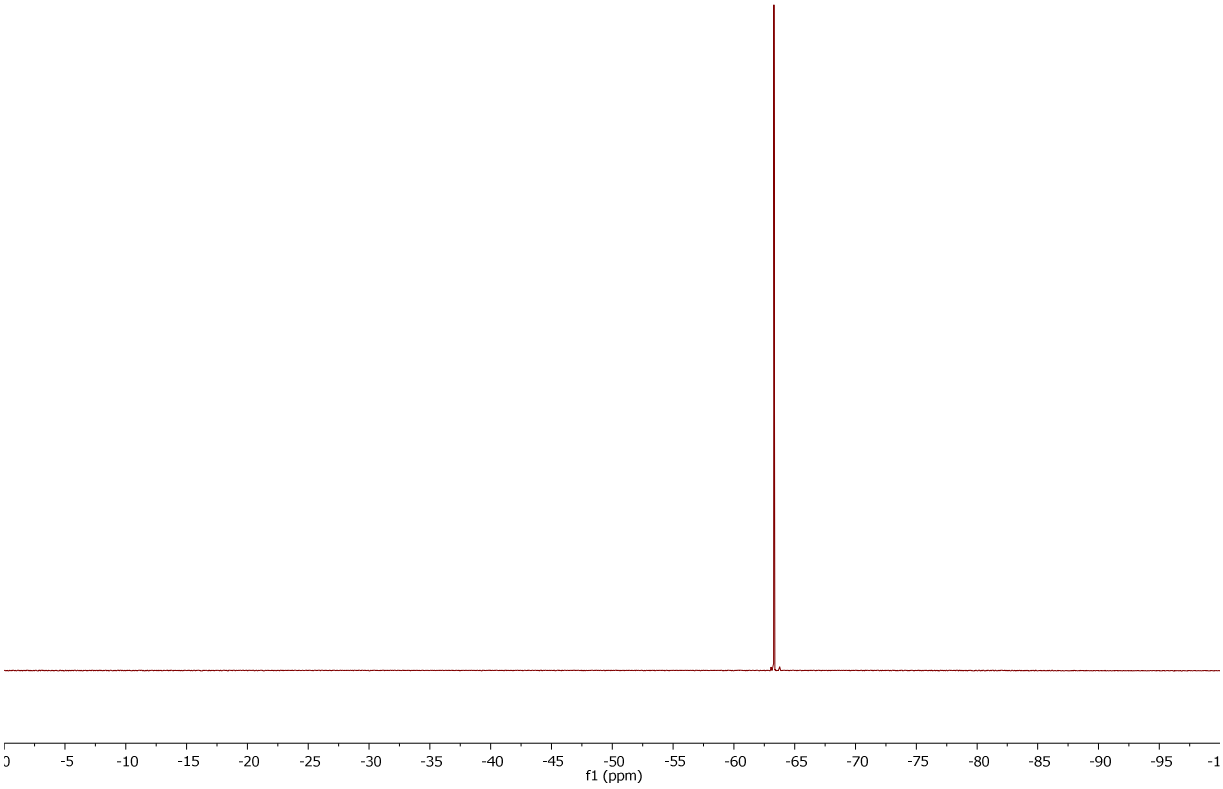

Figure S59. ^{19}F NMR spectrum (376 MHz, $CDCl_3$) of **8e**

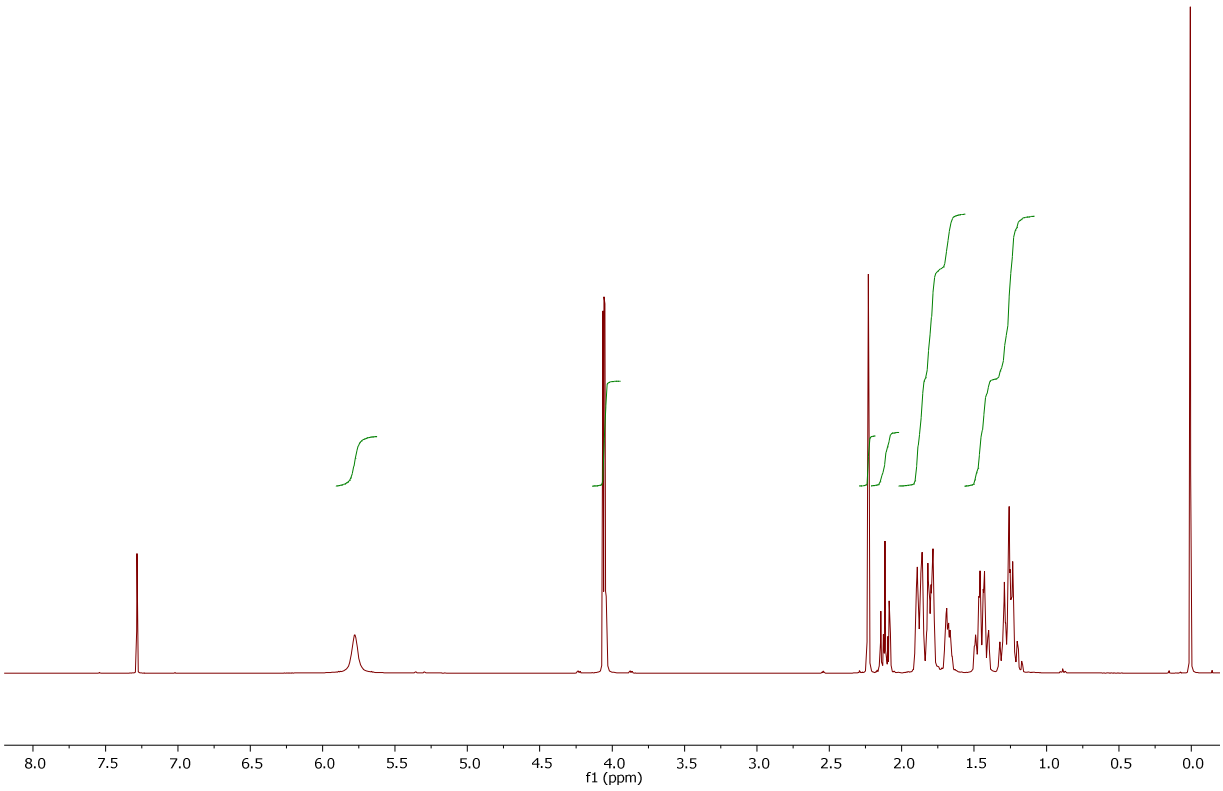

Figure 60. ^{1}H NMR spectrum (400 MHz, $CDCl_3$) of **8f**

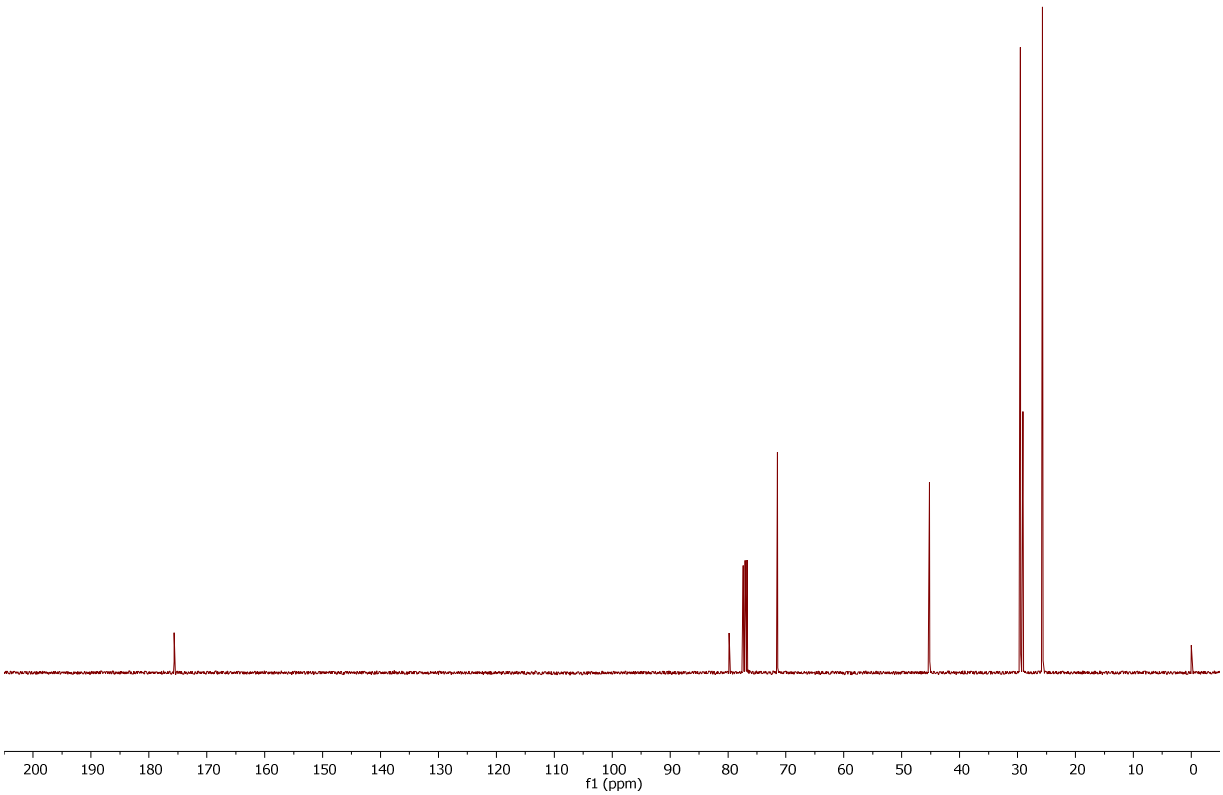

Figure S61. $^{13}C\{^{1}H\}$ NMR spectrum (101 MHz, $CDCl_3$) of **8f**

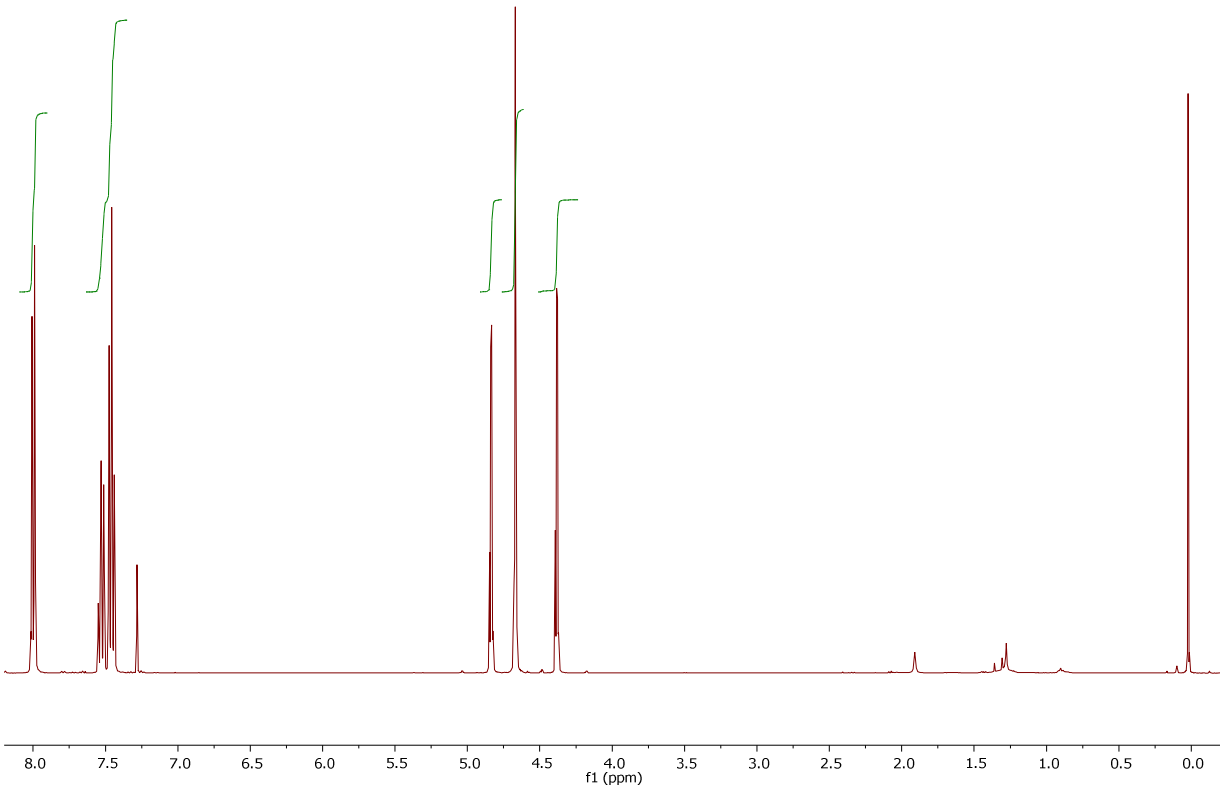

Figure S62. ^{1}H NMR spectrum (400 MHz, $CDCl_3$) of **9a**

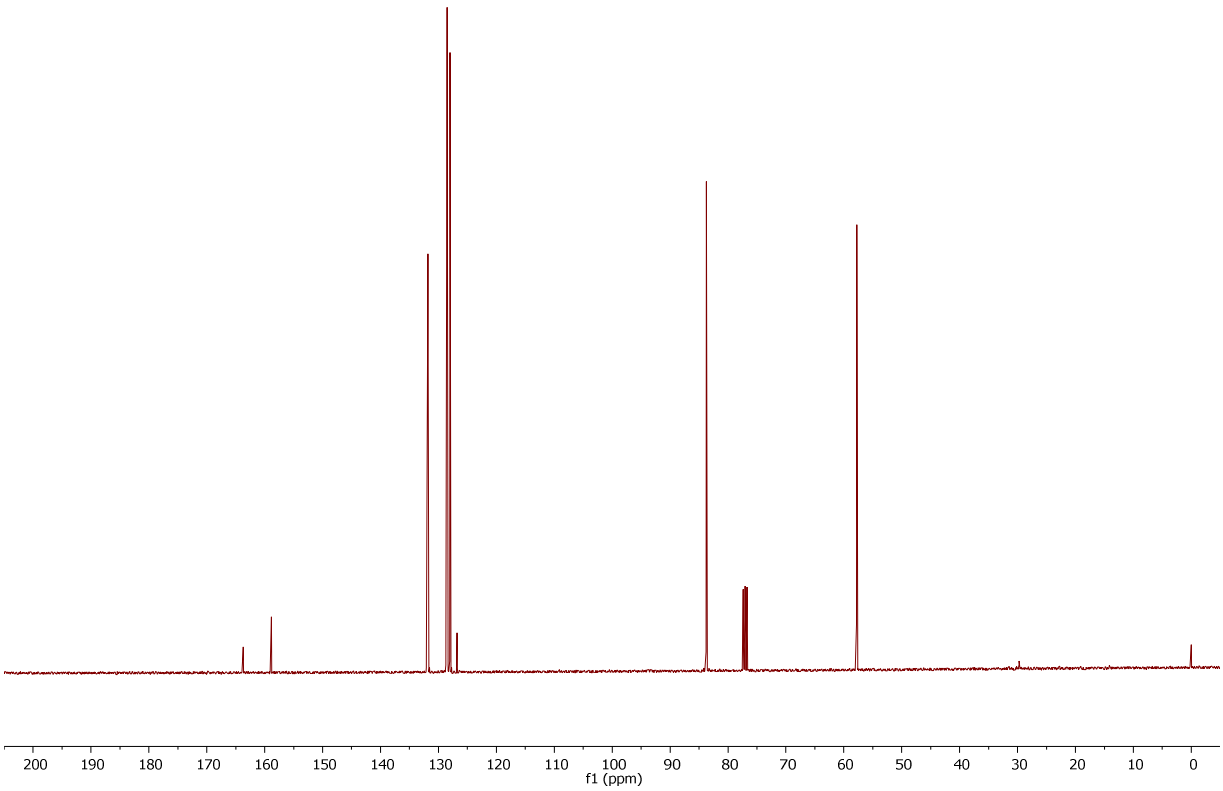

Figure S63. $^{13}C\{^{1}H\}$ NMR spectrum (101 MHz, $CDCl_3$) of **9a**

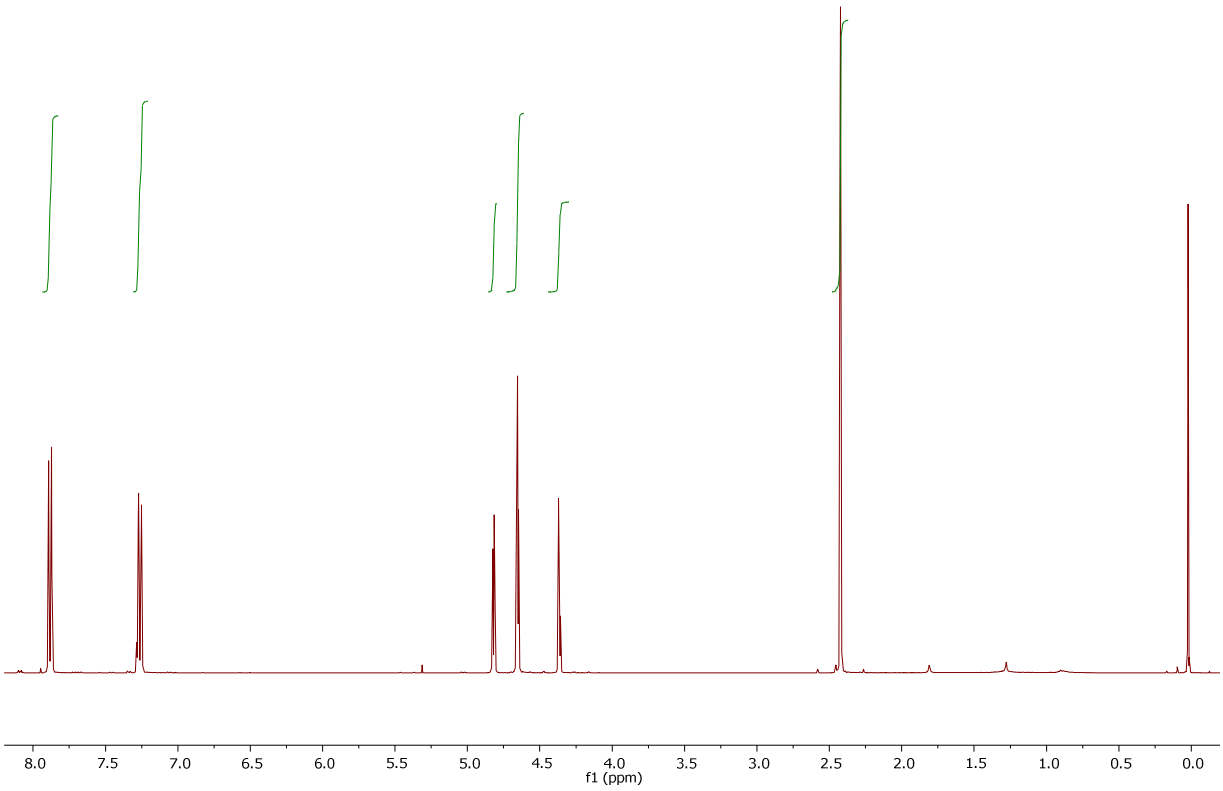

Figure S64. ^{1}H NMR spectrum (400 MHz, $CDCl_3$) of **9b**

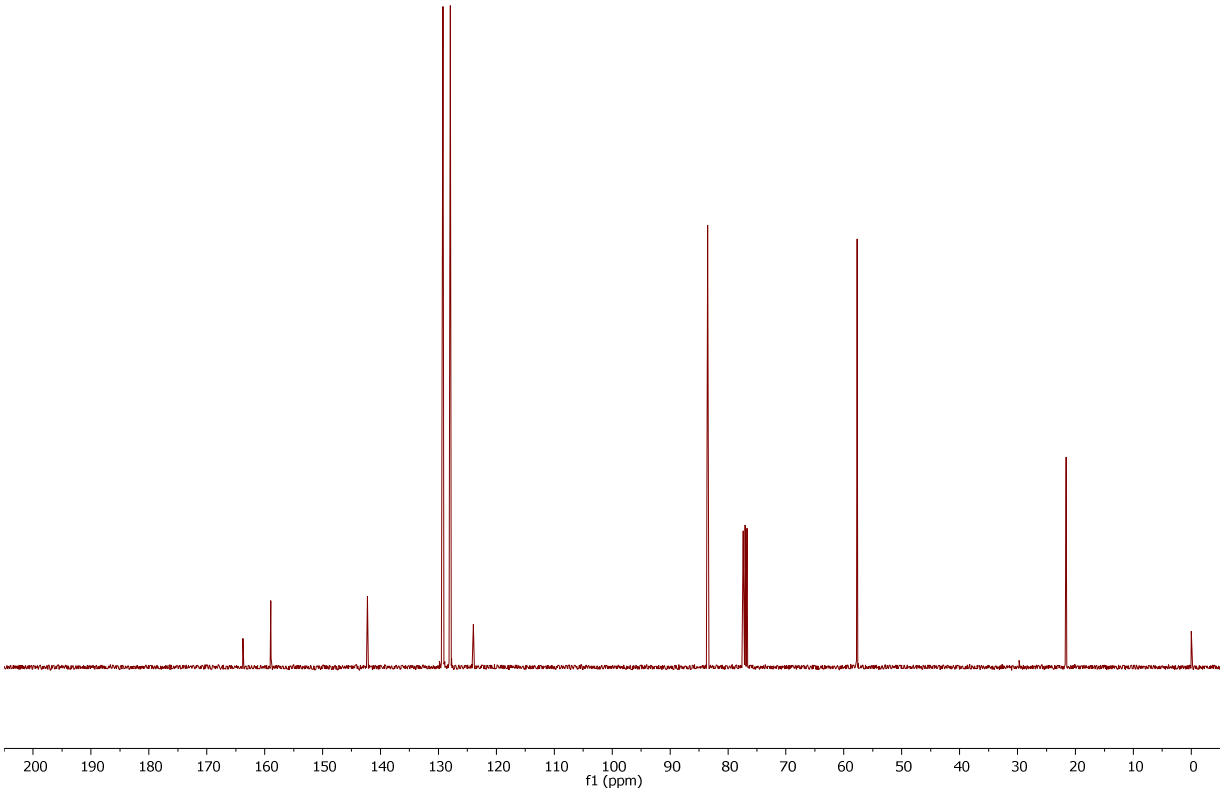

Figure 65. $^{13}C\{^{1}H\}$ NMR spectrum (101 MHz, $CDCl_3$) of **9b**

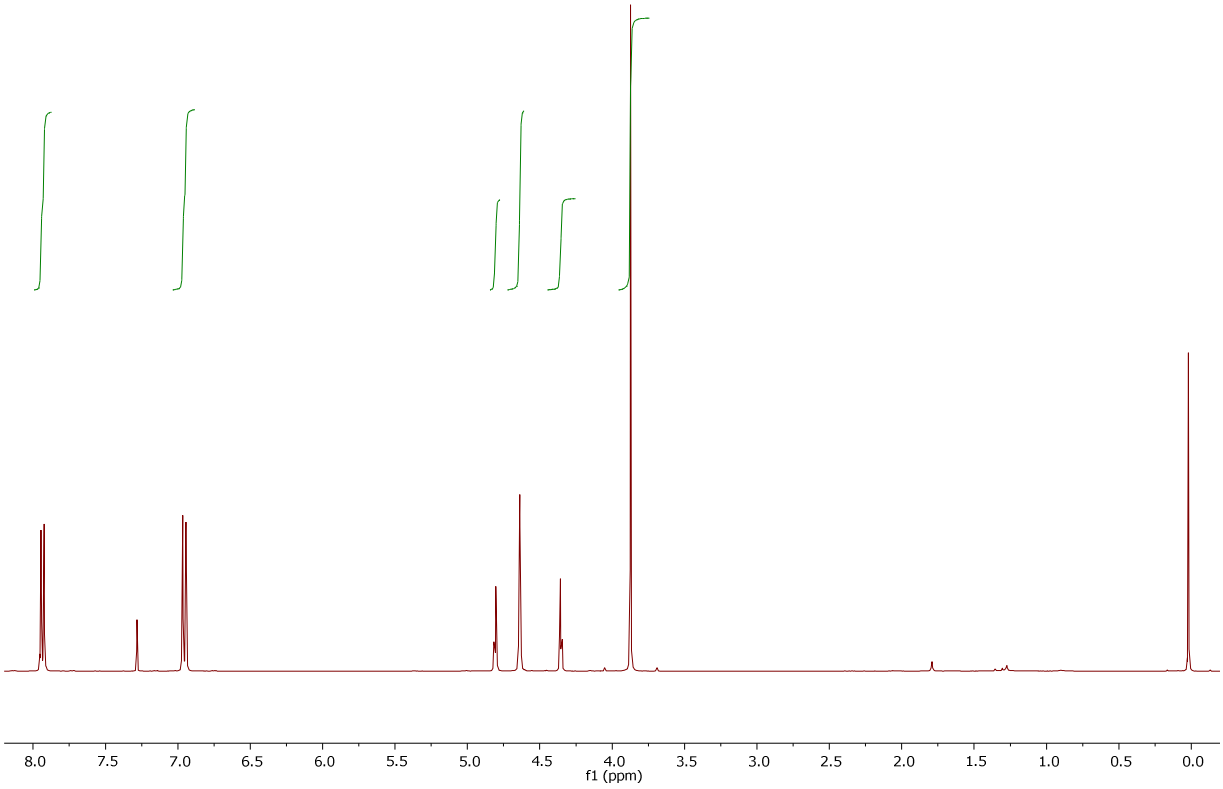

Figure S66. ^{1}H NMR spectrum (400 MHz, $CDCl_3$) of **9c**

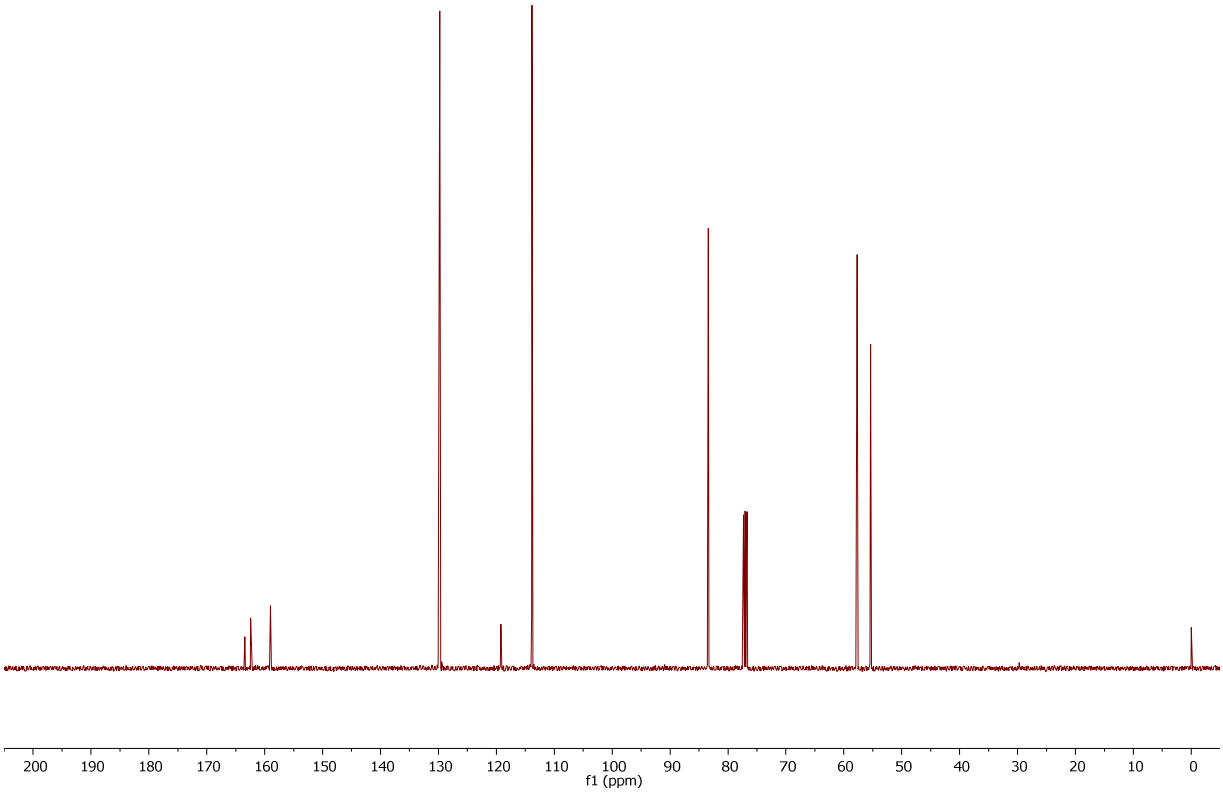

Figure S67. $^{13}C\{^{1}H\}$ NMR spectrum (101 MHz, $CDCl_3$) of **9c**

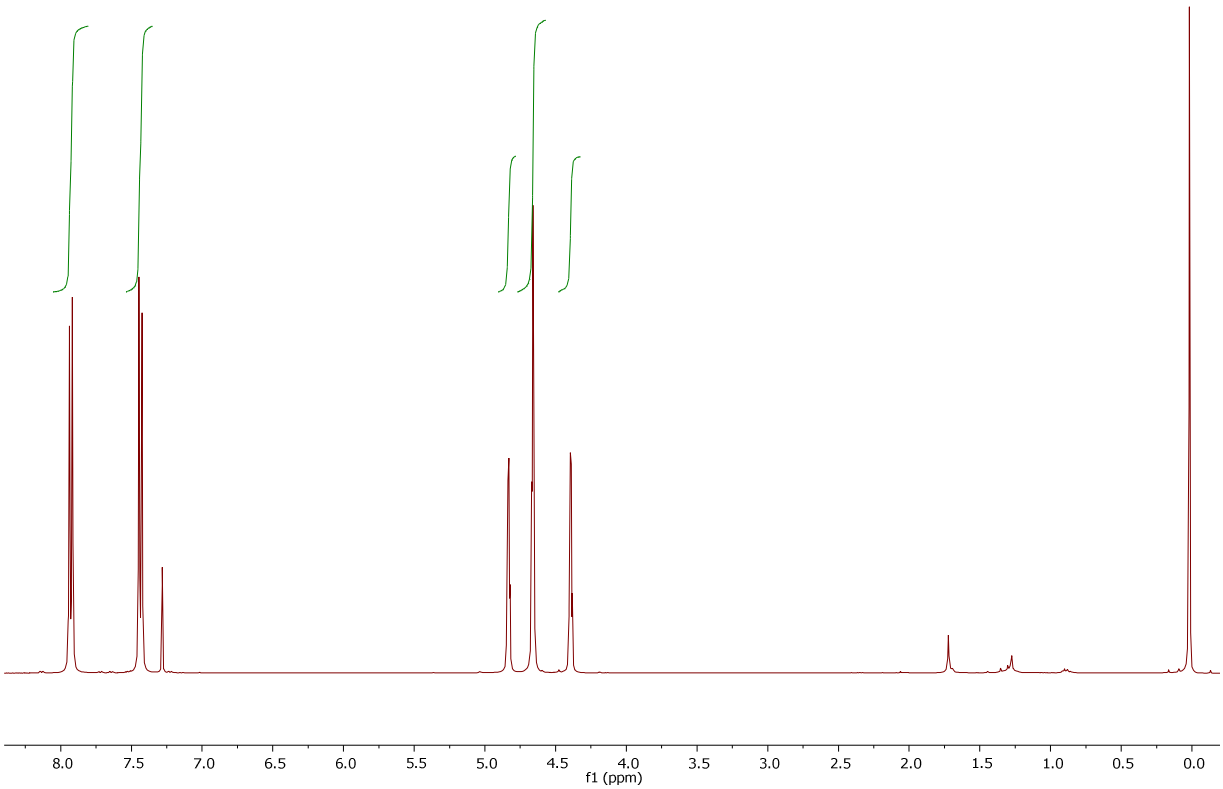

Figure S68. ^{1}H NMR spectrum (400 MHz, $CDCl_3$) of **9d**

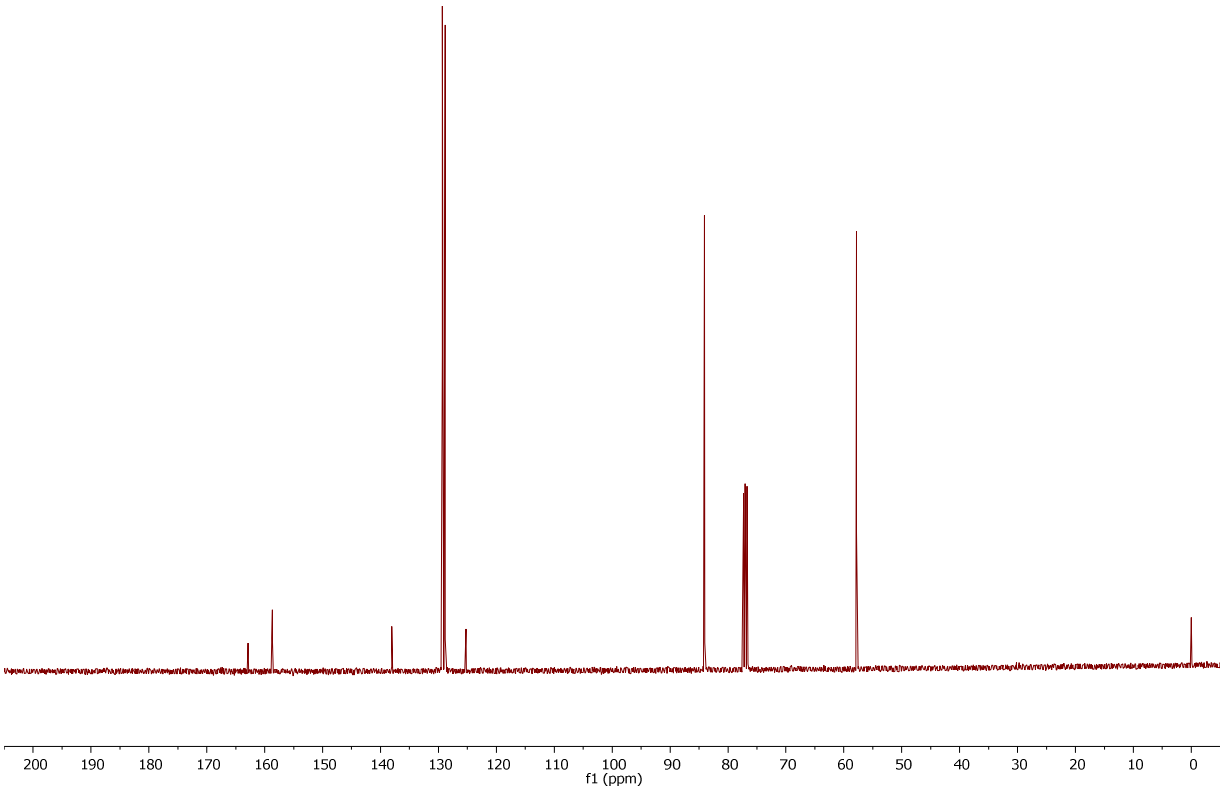

Figure S69. $^{13}C\{^{1}H\}$ NMR spectrum (101 MHz, $CDCl_3$) of **9d**

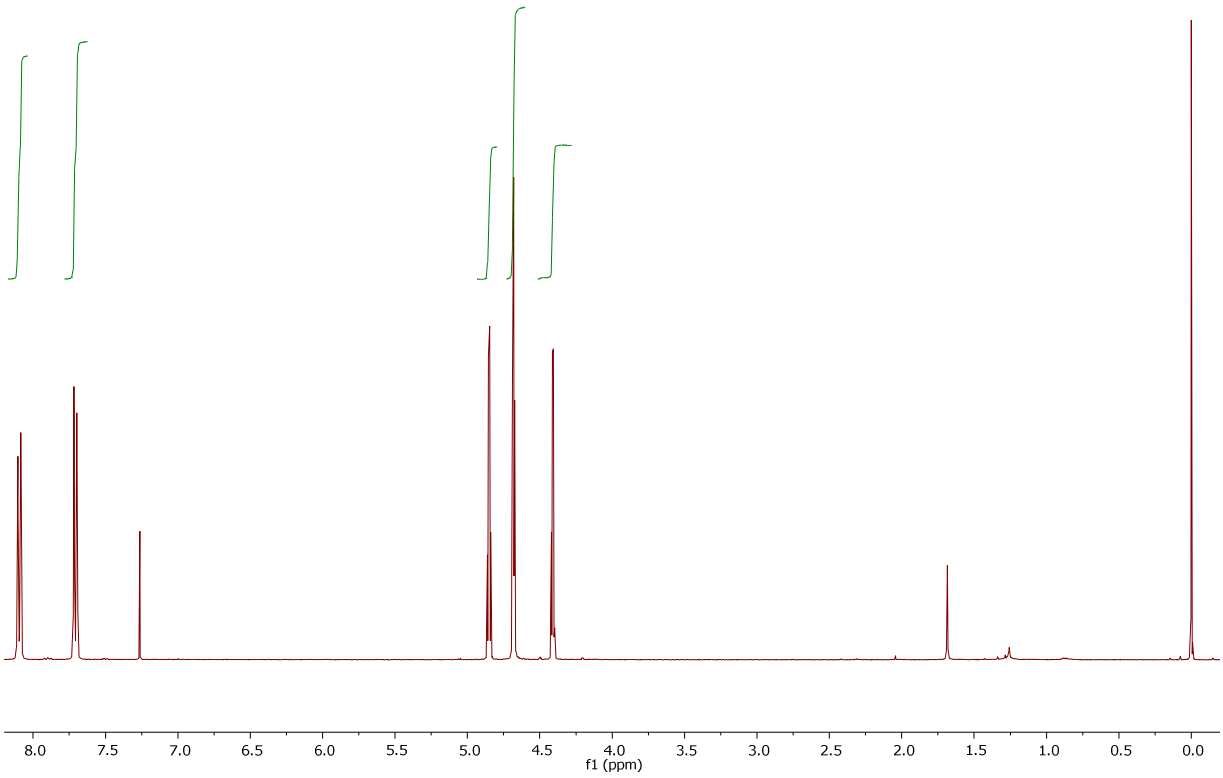

Figure S70. ^{1}H NMR spectrum (400 MHz, $CDCl_3$) of **9e**

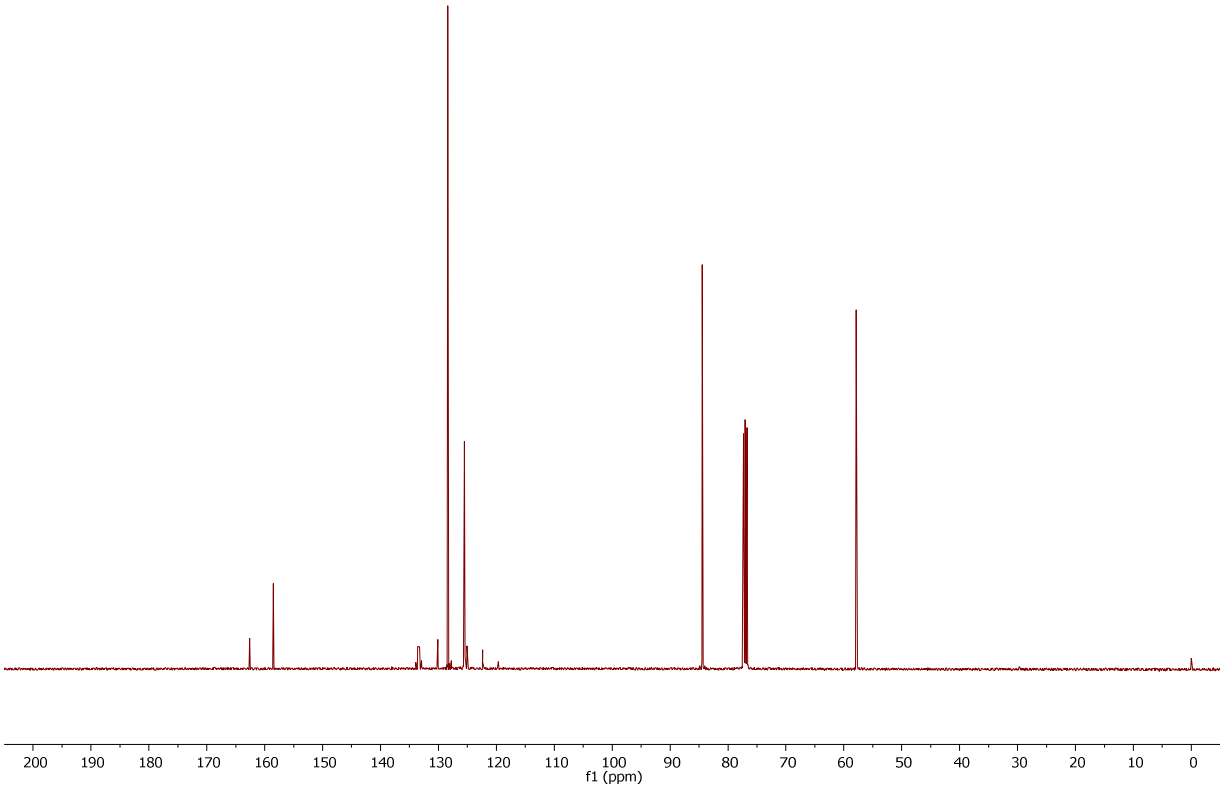

Figure S71. $^{13}C\{^{1}H\}$ NMR spectrum (101 MHz, $CDCl_3$) of **9e**

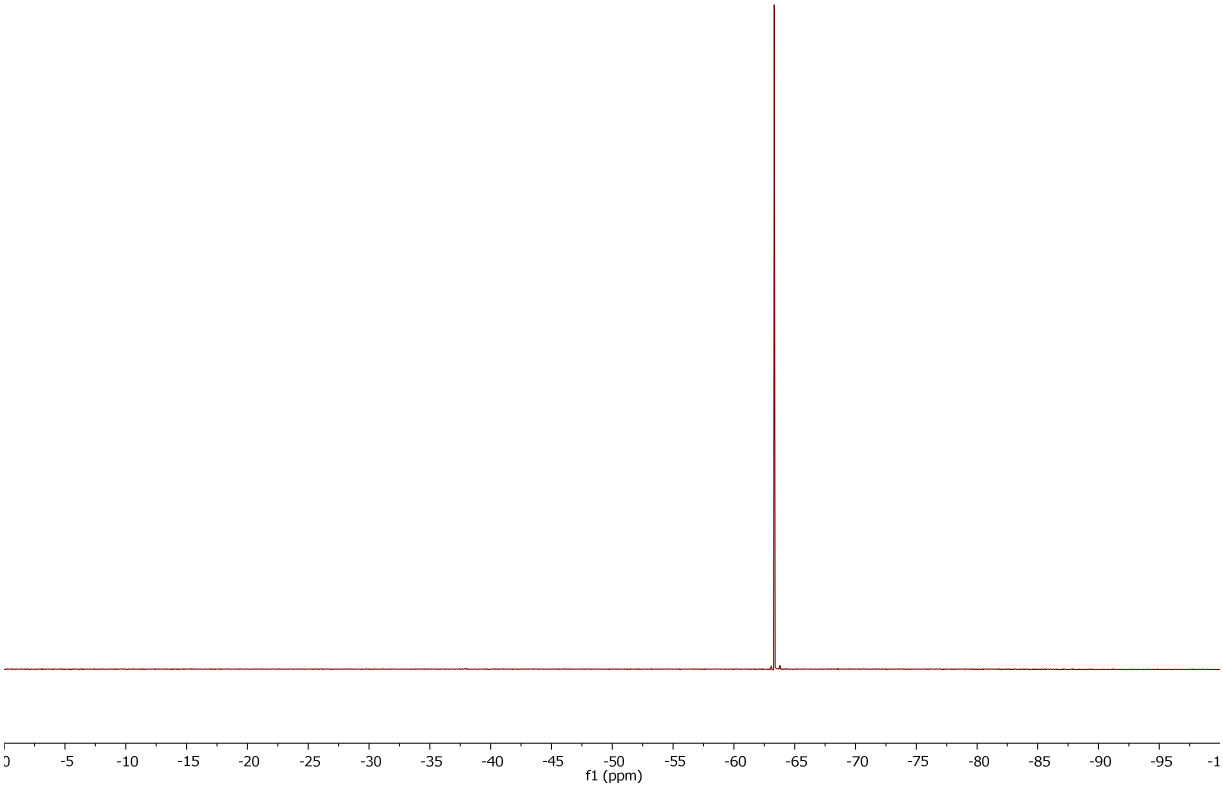

Figure S72. ^{19}F NMR spectrum (376 MHz, $CDCl_3$) of **9e**

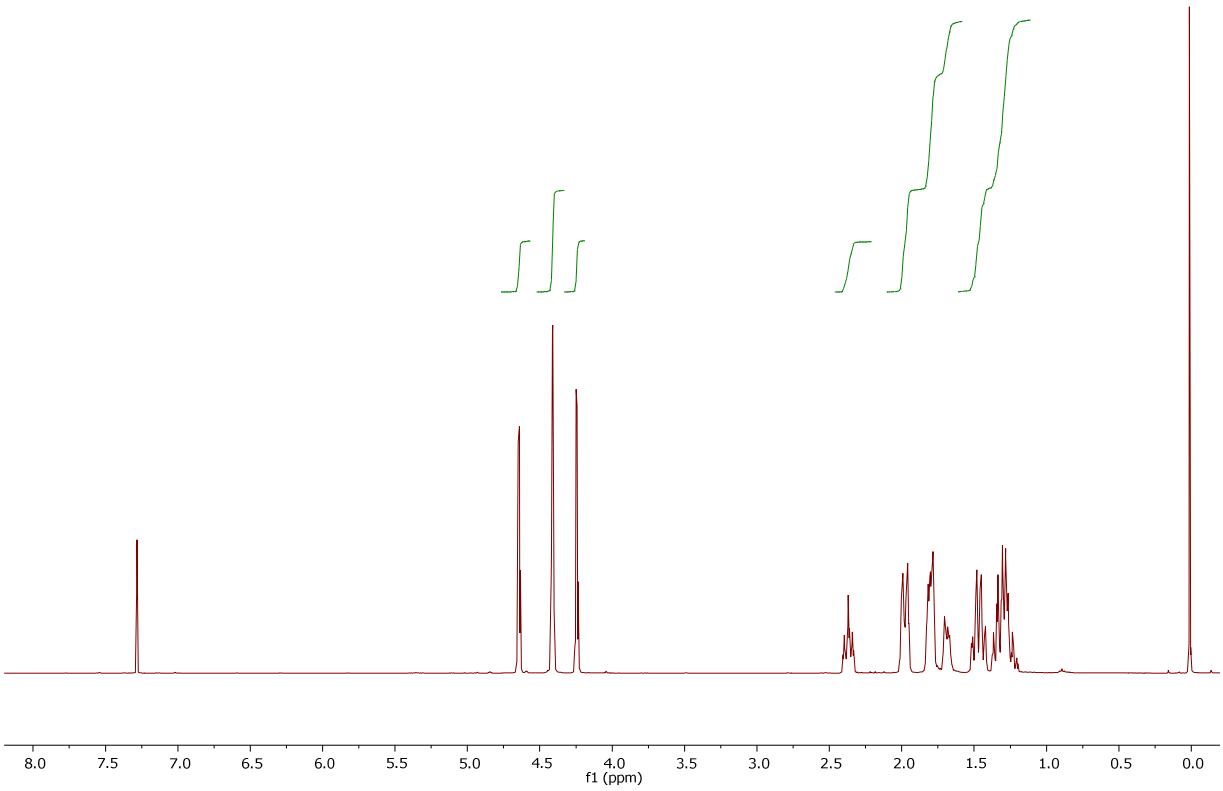

Figure S73. ^{1}H NMR spectrum (400 MHz, $CDCl_3$) of **9f**

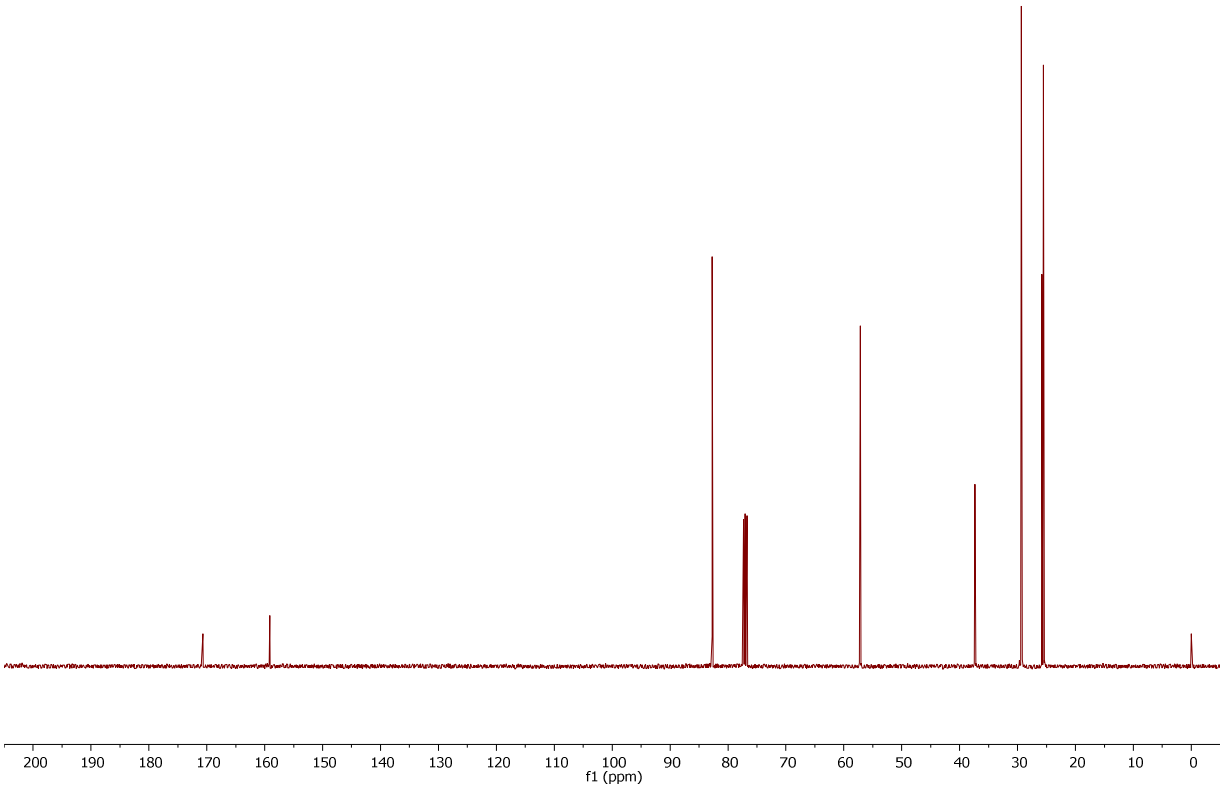

Figure S74. $^{13}C\{^{1}H\}$ NMR spectrum (101 MHz, $CDCl_3$) of **9f**

Appendix B

O. Bárta, I. Císařová, E. Mieczyńska, A. M. Trzeciak, P. Štěpnička, Synthesis and Catalytic Evaluation of Phosphanylferrocene Ligands with Cationic Guanidinium Pendants and Varied Phosphane Substituents. *Eur. J. Inorg. Chem.* **2019**, 4846-4854.

ChemPubSoc Europe

DOI: 10.1002/ejic.201901057

EurJIC European Journal of Inorganic Chemistry

Full Paper

Ferrocene Ligands

Synthesis and Catalytic Evaluation of Phosphanylferrocene Ligands with Cationic Guanidinium Pendants and Varied Phosphane Substituents

Ondřej Bárta,[a] Ivana Císařová,[a] Ewa Mieczyńska,[b] Anna M. Trzeciak,[b] and Petr Štěpnička*[a]

Abstract: This contribution expands the still narrow class of functional ferrocene phosphanes with polar cationic groups, focusing on the synthesis and catalytic use of a series of phosphanylferrocene ligands bearing positively charged guanidinium tags, $[R_2PfcCH_2NHC(NH_2)_2]Cl$ (**3a–d**), where fc = ferrocene-1,1′-diyl, R = isopropyl (**a**), cyclohexyl (**b**), phenyl (**c**), and 2-furyl (**d**). To probe the influence of phosphane substituents, these compounds were studied as supporting ligands in Pd-catalyzed Suzuki–Miyaura cross-coupling of acyl chlorides with arylboronic acids, in analogous coupling of aryl bromides with arylboronic acids, and in Rh-catalyzed hydroformylation of 1-hexene using *trans*-$[RhCl(CO)\{R_2PfcCH_2NHC(NH_2)_2\text{-}\kappa P\}_2]Cl_2$ complexes (**4a–d**) as pre-catalysts. The outcome of the cross-coupling reactions strongly depended on the starting materials, and no ligand generated a universally applicable catalyst when combined with $Pd(OAc)_2$. In the hydroformylation reactions, the catalyst based on **4d** led to lower conversions than all others, which performed rather similarly. Overall, the phenyl-substituted phosphane **3c** emerged as a good compromise, giving rise to reasonably efficient and stable catalysts in most cases (except for Suzuki–Miyaura biaryl cross-couplings, wherein electron-rich alkylphosphanes performed better than **3c**).

Introduction

The highly polar and positively charged guanidinium moiety has been used to modify inherently hydrophobic phosphane molecules, in particular, to increase their affinity towards polar solvents and water.[1,2] In catalysis, the guanidinium unit can further act as a structure-controlling moiety, which exploits its hydrogen-bonding ability to stabilize a specific structure (e.g., the structure of a reaction intermediate) and to direct molecular parts or reaction partners to specific positions.[3] In the chemistry of ferrocene phosphanes,[4] however, the guanidine modifying group has been utilized only scarcely (see compounds **A** and **B** in Scheme 1).[5]

Recently,[6] we have reported the facile synthesis of *N*-{[1′-(diphenylphosphanyl)ferrocene-1-yl]methyl}guanidinium chloride (compound **3c** in Scheme 1) by guanylation[7] of [1′-(diphenylphosphanyl)ferrocene-1-yl]methylamine[8] and preliminary results from catalytic tests of this compound as an auxiliary ligand for Pd-catalyzed cross-coupling reactions. To further develop the chemistry of phosphanylferrocene-guanidine ligands, we aimed to extend the series of such compounds by synthesizing analogues bearing *different* phosphane substituents, compounds **3** (Scheme 1). This contribution therefore describes the preparation of these functional phosphanes[9] and the results from a comparative catalytic study exploiting Pd-catalyzed Suzuki–Miyaura cross-coupling[10] and Rh-catalyzed hydroformylation[11] as benchmark reactions.

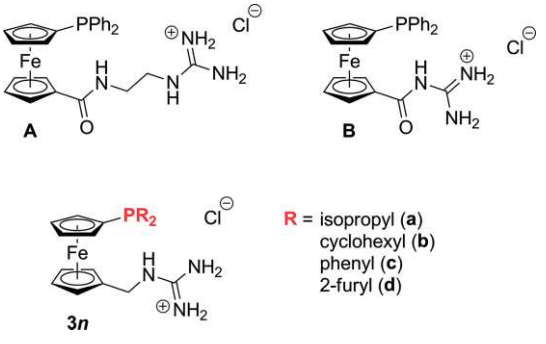

Scheme 1. Phosphinoferrocene ligands bearing guanidinium pendants. Note: among compounds **3**, only **3c** has been reported before.

Results and Discussion

Ligand Synthesis

The series of cationic phosphanylferrocene guanidine ligands **3** was expanded to include a pair of ligands with electronically and sterically similar electron-donating alkyl groups (R = *i*Pr and

[a] *Department of Inorganic Chemistry, Faculty of Science, Charles University, Hlavova 2030, 128 40 Prague, Czech Republic*
E-mail: petr.stepnicka@natur.cuni.cz
http://www.natur.cuni.cz
[b] *Department of Inorganic Chemistry, Faculty of Chemistry, University of Wrocław, ul. F. Joliot-Curie 14, 50-383 Wrocław, Poland*
https://chem.uni.wroc.pl/pl/jednostka-organizacyjna/12

Supporting information and ORCID(s) from the author(s) for this article are available on the WWW under https://doi.org/10.1002/ejic.201901057.

Cy) and another pair of compounds with flat, conjugated, electron-withdrawing aryl groups at the phosphorus atom. Specifically, new guanidinium phosphanes **3a**, **3b** and **3d** were synthesized using a modified approach developed to prepare ligand **3c**.[6] In the first step, the starting phosphanylnitriles **1**[12] were reduced by $Li[AlH_4]$ in THF to give the corresponding phosphanylamines **2** in practically quantitative yields (Scheme 2). Subsequent reactions of the amines **2** with 1*H*-pyrazole-1-carboximidamide hydrochloride in the presence of triethylamine[13] produced phosphanyl-guanidinium salts **3**, which were isolated in moderate to good yields by column chromatography, and subsequently crystallized. As solids, compounds **3** are air-stable and can be stored for months without any precautions. In a solution, however, they are prone to gradual oxidation (particularly when exposed to air).

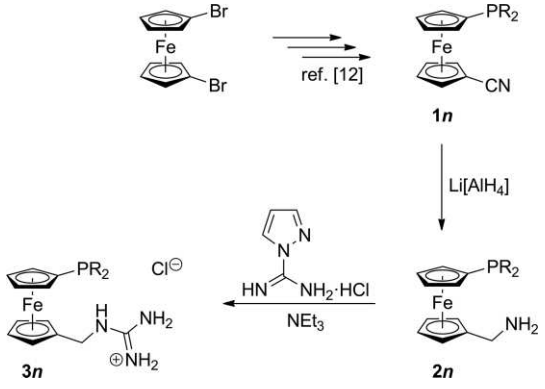

Scheme 2. Synthesis of the ligands **3a**, **3b** and **3d** [R = *i*Pr (**a**), Cy (**b**), and Fur (**d**)].

In their ^1H NMR spectra, compounds **3** displayed four multiplets of the non-equivalent ferrocene protons, a NH-coupled doublet due to the methylene linker ($\delta_H \approx 4$), and the signals of the phosphane substituents. The ^{13}C NMR spectra were also fully consistent with the formulation, showing the expected sets of signals due to the unsymmetrically disubstituted ferrocene moiety (with the resonance due to *C*-CH_2 typically shifted to a lower field, $\delta_C \approx 84$), and the signals due to the methylene linker ($\delta_C \approx 40$) and to the guanidinium carbon atom ($\delta_C \approx 156$). The ^{31}P NMR signals were observed at positions typical for the respective ferrocene phosphanes.[12,14]

The IR spectra of **3** showed broad bands attributable to the N–H stretching modes above 3000 cm^{-1} and several sharp intense bands due to the combined C–N stretching and N–H deformation vibration modes of the guanidinium unit in the 1600–1660 cm^{-1} range.[15] The formulation of **3** was further corroborated by positive-ion ESI MS spectra, which displayed peaks of the respective guanidinium cations, $[R_2PfcCH_2NHC(NH_2)_2]^+$, and their ferrocenylmethylium fragments,[16] $[R_2PfcCH_2]^+$.

In addition to spectroscopic characterization, the crystal structures of **3a** and **3d** were determined by single-crystal X-ray diffraction analysis. The molecular structures are shown in Figure 1, and the pertinent structural data are outlined in Table 1.

For both compounds, structure determination revealed regular ferrocene moieties with similar Fe–C distances and tilt angles below 5°. The ferrocene cyclopentadienyls were eclipsed in both cases; however, while the substituents in **3a** adopted an approximate 1,3′-conformation, those in **3d** were rotated closer to a 1,2′-conformation. The guanidinium fragments were planar and delocalized, showing similar N–C distances (≈ 1.33 Å) and N–C–N angles near 120°. The orientation of the guanidinium planes with respect to the plane of the Cp1 ring differed [the dihedral angles between the guanidine plane and the Cp1 rings were 77.8(1)° in **3a** and 27.1(1)° in **3d**], reflecting intermolecular interactions operating in the crystals. Specifically, the supramolecular structures of both compounds were supported by charge-supported N–H···Cl hydrogen bonds in which the chloride counteranions act as multiple acceptors.[17] When combined, these interactions resulted in the formation of a three-dimensional array in **3a** and in linear H-bonded chains in **3d** (see the Supporting Information).

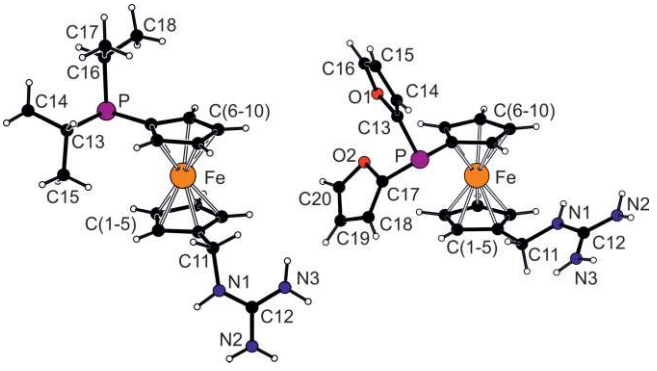

Figure 1. Views of *cations* in the molecular structure of **3a** (left) and **3d** (right). For complete drawings and packing diagrams, see Supporting Information.

Table 1. Selected distances and angles (in Å and deg) for **3a** and **3d**.

Parameter[a]	3a	3d
Fe–C[b]	2.031(2)-2.066(2)	2.041(2)-2.061(2)
∠Cp1,Cp2	4.8(1)	1.3(1)
τ	–138.7(1)	–80.0(1)
C11–N1	1.472(2)	1.463(2)
C1–C11–N1	111.7(1)	111.8(3)
C12–N1	1.327(2)	1.335(3)
C12–N2	1.343(2)	1.330(3)
C12–N3	1.324(2)	1.326(3)
N–C12–N[c]	118.3(2)-122.8(2)	119.7(2)-120.7(2)
P–C6	1.823(2)	1.810(2)
P–C[R][d]	1.861(2)/1.877(2)	1.815(2)/1.805(2)

[a] Definitions: Cp1 and Cp2 are the planes of the cyclopentadienyl rings C(1–5) and C(6–10), respectively. τ is the torsion angle C1–Cg1–Cg2–C6, wherein Cg1 and Cg2 denote the centroids of the cyclopentadienyl rings Cp1/Cp2. [b] Range of Fe–C(1–10) distances. [c] Range of N1–C12–N2/3 and N2–C12–N3 angles. [d] P–C13/C16 and P–C13/C17 distances for **3a** and **3d**, respectively.

As functional phosphanes, compounds **3** were used to prepare cationic Rh^I carbonyl complexes **4** (Scheme 3), which were further catalytically tested (vide infra). All complexes were isolated in analytically pure, albeit often solvated, form as air-stable solids. In ^{31}P NMR spectra, they showed one resonance due to the equivalent phosphane moieties, shifted to a lower field with respect to the corresponding free ligand and split into a doublet by interaction with the monoisotopic Rh ($^1J_{RhP}$ = 122–132 Hz).[18] In addition, the ^{31}P-coupled $^{13}C\{^1H\}$ NMR reso-

nances of these phosphane complexes were observed as characteristic apparent triplets arising from virtual coupling within the ^{12}C-^{31}P-^{103}Rh-^{31}P-^{13}C spin systems.[19] The Rh-bound carbonyl ligands were observed as double triplets at low fields (δ_P = 184–189) in ^{13}C NMR spectra, while they gave rise to strong characteristic C≡O stretching bands in IR spectra. The energy of these bands symptomatically increased with the decrease in donor ability of the phosphane moiety:[20] ν_{max} 1946 (**4b**) ≈ 1947 (**4a**) < 1970 (**4c**) < 1982 (**4d**) (cm^{-1}).

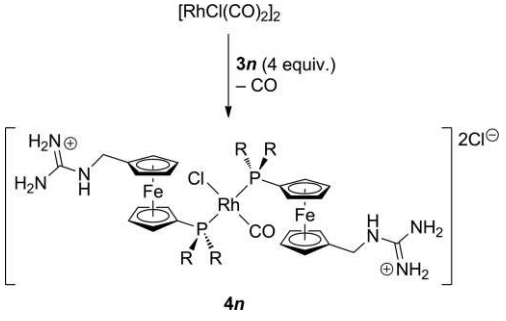

Scheme 3. Synthesis of the Rh^{I} complexes **4a–d** [R = *i*Pr (**a**), Cy (**b**), Ph (**c**), and Fur (**d**)].

Catalytic Evaluation

Pd-Catalyzed Cross-Coupling Reactions

The catalytic properties of the phosphanyl-guanidinium ligands **3** were initially evaluated in Pd-catalyzed Suzuki–Miyaura-type C-C cross-coupling between aromatic acyl chlorides and boronic acids producing substituted benzophenones,[21] under reaction conditions adopted from our previous study.[22] In a model reaction (Scheme 4, results in Table 2), *p*-toluoyl chloride reacted with 4-(trifluoromethyl)phenyl boronic acid in the presence of sodium carbonate as a base and 0.1 mol-% of an in situ-generated Pd catalyst in a vigorously stirred C_6D_6/water (2 mL each) mixture at 50 °C for 1 h to give 4-methyl-4′-

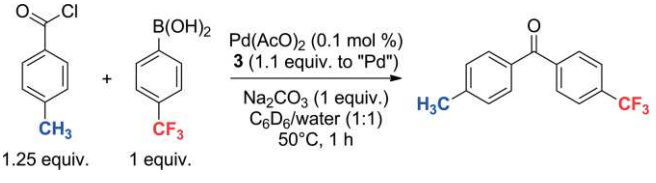

Scheme 4. Pd-catalyzed Suzuki–Miyaura cross-coupling of 4-toluoyl chloride with 4-(trifluoromethyl)phenylboronic acid used for screening experiments.

Table 2. Yields of the coupling product achieved in the model reaction with different in situ formed catalysts.[a]

Catalytic system	NMR Yield	Catalytic system	NMR Yield
$Pd(AcO)_2$	30 %	$Pd(AcO)_2$/**3a**	80 %
$Pd(AcO)_2/PPh_3$	83 %	$Pd(AcO)_2$/**3b**	84 %
$Pd(AcO)_2/PCy_3$	85 %	$Pd(AcO)_2$/**3c**	93 %
$Pd(AcO)_2/FcPPh_2$	86 %	$Pd(AcO)_2$/**3d**	95 %

[a] For conditions, see the text and Experimental section. The yields were determined by ^{19}F NMR spectroscopy and are an average of two independent runs.

(trifluoromethyl)benzophenone. The use of the fluorinated substrate and the deuterated solvent allowed facile reaction monitoring by ^{19}F NMR spectroscopy after adding (trifluoromethyl)benzene as an internal standard.

When unsupported $Pd(AcO)_2$ was utilized as the pre-catalyst, palladium black formed almost immediately in the reaction mixture, and conversion reached only ≈ 30 % after 1 hour. In the presence of an auxiliary phosphane ligand [1.1 equiv. with respect to $Pd(OAc)_2$], the formation of palladium black was visibly slower, and conversion increased to ≈ 85 % (Table 2). Although no marked differences between ligands **3** were noted, ligands bearing electron-poor phosphane substituents (**3c** and **3d**) performed better with some test reaction substrates, affording the coupling product in yields higher than their electron-rich counterparts and non-functional phosphanes (including $FcPPh_2$ as an analogue of **3c**).

Subsequently, substrates incorporating methyl or trifluoromethyl groups in *para* positions or their unsubstituted (phenyl) analogues were used to compare the influence of the substrate on the yield of the coupling product (Scheme 5). This set of experiments was designed so that the trifluoromethyl group was always present in at least one substrate in order to use the same method of yield determination.

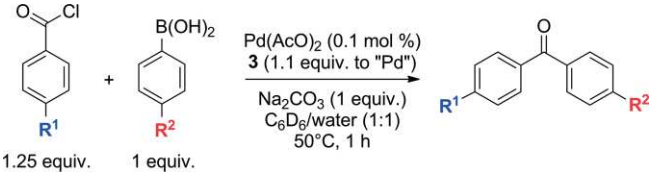

Scheme 5. General depiction of Pd-catalyzed Suzuki–Miyaura cross-couplings of aromatic acyl chlorides with arylboronic acids.

While the model reaction used for initial screening was better mediated by Pd catalysts with the weakest donating phosphane ligands of the series (Table 3, entry 1), no such clear trends or significant differences were found in reactions with other substrates. Generally, yields of 65 % or higher were achieved with all ligand-substrate combinations. However, in the reaction of substrates with exchanged substituents (entry 2), the best results were found when using electronically dissimilar phosphane ligands **3a** and **3c**. Similar results (albeit with uniformly higher yields) were noted in the coupling of benzoyl chloride with 4-(trifluoromethyl)phenylboronic acid (entry 3). The yields of the complementary reaction between phenylboronic acid and 4-$CF_3C_6H_4C(O)Cl$ (entry 4) were generally lower,

Table 3. Influence of substrate substituents in reactions employing different $Pd(OAc)_2$/**3** catalysts.[a]

			Ligand/NMR yield			
Entry	R^1	R^2	**3a**	**3b**	**3c**	**3d**
1	Me	CF_3	80 %	84 %	93 %	95 %
2	CF_3	Me	82 %	71 %	81 %	70 %
3	H	CF_3	89 %	82 %	88 %	81 %
4	CF_3	H	69 %	72 %	74 %	66 %
5	CF_3	CF_3	89 %	85 %	87 %	91 %

[a] For conditions, see the text and Experimental section. The yields were determined by ^{19}F NMR spectroscopy and represent an average of two independent runs.

with **3b** and **3c** giving the best results. Lastly, when the CF_3 group was present in both substrates, $Pd(OAc)_2$/**3d** catalyst provided the best yield of the coupling product despite rather minor variations between individual Pd-**3** catalysts (6 % in absolute figures).

Generally, ligands **3a** and **3d** gave rise to catalysts with the most varying yields, while the Ph_2P-substituted phosphane **3c** proved to be a rather universal ligand for these transformations. As for the substrates, the coupling reaction proceeded better with electron-poor boronic acids. Conversely, relatively worse results were achieved when using electron-poor acyl chlorides, except for coupling reactions in which both reaction components bore electron-withdrawing substituents.

The second Pd-mediated transformation investigated was the archetypal Suzuki–Miyaura biaryl coupling of aryl bromides and boronic acids. This reaction was performed under identical reaction conditions, which were quite challenging considering previous reports on similar ligands.[23] Similarly to other experiments, the screening experiments employed a pair of complementary reaction producing 4-methyl-4′-(trifluoromethyl)biphenyl (Scheme 6, R^1/R^2 = Me/CF_3 and CF_3/Me).

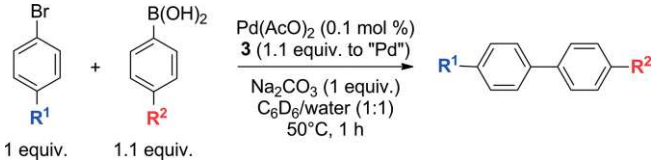

Scheme 6. Pd-catalyzed Suzuki–Miyaura cross-coupling of aryl bromides with arylboronic acids.

In the coupling of 4-bromotoluene with 4-(trifluoromethyl)phenylboronic acid (Table 4), unsupported $Pd(AcO)_2$ ensued in a negligible yields, and poor results were also found when using catalysts containing PPh_3 and $FcPPh_2$ as supporting ligands. Of the tested simple phosphanes, the electron-donating alkyl phosphane PCy_3 performed best. Indeed, the catalysts supported by ligands **3** showed similar trends, albeit with considerably increased yields; the most active catalyst resulted from the isopropyl phosphane **3a**.

Table 4. Results from catalytic tests in Suzuki–Miyaura biaryl coupling.[a]

Catalyst	Substrates/NMR Yield	
	R^1 = Me, R^2 = CF_3	R^1 = CF_3, R^2 = Me
$Pd(AcO)_2$	< 1 %	5 %
$Pd(AcO)_2/PPh_3$	6 %	25 %
$Pd(AcO)_2/PCy_3$	38 %	29 %
$Pd(AcO)_2/FcPPh_2$	8 %	56 %
$Pd(AcO)_2$/**3a**	52 %	75 %
$Pd(AcO)_2$/**3b**	47 %	91 %
$Pd(AcO)_2$/**3c**	14 %	34 %
$Pd(AcO)_2$/**3d**	9 %	7 %

[a] For conditions, see the Experimental section. The yields were determined by ^{19}F NMR spectroscopy and are an average of two independent runs.

Notably, the yields of the coupling product increased upon switching substrate substituents [i.e., in the reaction of 4-(trifluoromethyl)bromobenzene with 4-tolylboronic acid], except for the poorly active Pd/**3d** catalyst, whose performance remained nearly the same and was thus surpassed even by a catalyst based on $FcPPh_2$. The best results in this reaction were achieved when using the bulky and electron-rich cyclohexyl-substituted ligand **3b**, which resulted in nearly quantitative conversion under the specified conditions.

Rh-Catalyzed Hydroformylation

The second type of catalytic reaction was Rh-catalyzed hydroformylation of 1-hexene (Scheme 7). The cationic Rh^I-diphosphane complexes **4a–d** were employed as defined pre-catalysts at a 1-hexene-to-Rh ratio of 400 *without* adding any co-catalyst (free ligands **3** included), and the catalytic reaction was performed under 10 bar of synthesis gas ($CO:H_2$ = 1:1) at 80 °C for 5 h. When performing the reaction in neat 1-hexene and in pure toluene or water as solvents (1.5–3.0 mL of solvent per 1.5 mL of 1-hexene), the yields of the aldehydes were disappointingly low (below 10 %). Substantially better results were found when using DMSO, mostly likely because the catalysts were more soluble in DMSO (Table 5).

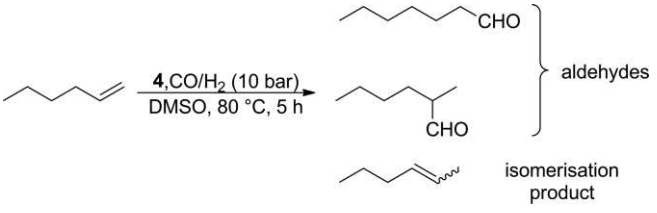

Scheme 7. Rh-catalyzed hydroformylation of 1-hexene and the competing isomerization reaction giving 2-hexene.

Table 5. Summary of the hydroformylation results.[a]

Catal.	S/Rh[b]	Conv. [%]	2-hexene [%]	Aldehydes [%]	*n/iso*
4a	400	95	1	94	1.1
4a	800	92	2	92	1.1
4a	1600	8.4	0.1	8.3	1.4
4b	400	99	1	98	1.1
4b	800	85	1	84	1.1
4b	1600	51	1	50	1.2
4c	400	99	4	95	2.2
4c	800	93	4	89	2.3
4c	1600	47	1	46	2.6
4d	400	59	2	57	2.6
4d	800	53	1.3	52	2.7
4d	1600	43	1	42	2.8

[a] Conditions: 0.75 mL 1-hexene (6 mmol), dimethyl sulfoxide (0.75 mL), 10 bar of syngas (H_2/CO = 1:1), 80 °C, reaction time: 5 h. [b] 1-hexene/Rh ratio.

All catalysts produced heptanals with high selectivity; the fraction of 2-hexene (isomerization product) was lower than 4 % of the amount of aldehydes formed. Complex **4d** bearing the furyl-substituted phosphane ligand led to consistently lowest conversions. This can be explained by the easier dissociation of these weaker-donating phosphane ligands and subsequent catalyst deactivation. However, the selectivity for linear aldehyde (*n/iso* ratio) achieved with this catalyst was the highest among all compounds tested, followed by compound **4c**.

Decreasing the amount of the catalyst (Rh/1-hexene = 800 and 1600; see Table 5) expectedly lowered the conversion but had only a minor effect on the selectivity, especially on the *n/iso* ratio. The catalytic results remained reproducible even at

the lowest catalyst loading. Surprisingly, adding free ligand to the reaction mixture (1 or 2 molar equiv. of **3b** to catalyst **4b**, or 1 molar equiv. of **3c** to catalyst **4c**) adversely affected the catalytic reaction. No pressure drop or products were detected (neither 2-hexene, nor aldehydes), presumably because phosphine ligands compete with olefin and block access to rhodium, thereby inhibiting the reaction.

Conclusions

In summary, we have demonstrated that our synthetic procedure for the preparation of **3c** can be adapted for the synthesis of analogous ligands (from free amines **2**) bearing different phosphane substituents, which – as the only donor groups available in the ligands in their native state – control the catalytic properties of these compounds. The results from the catalytic tests showed that catalytic activity is determined by a delicate interplay between steric and electronic properties of phosphane substituents, which also influence the overall chemical stability of the catalyst (activation/deactivation and possible formation of metal particles), on the one hand, and the properties of the reaction substrates, on the other. For instance, the reaction outcome of Pd-catalyzed cross-coupling reactions mediated by the $Pd(OAc)_2$/**3** system depended not only on the type of reaction (biaryl coupling vs. acylative coupling) but also on the substrates (presumably on the electronic influence of the substituents, whose steric influence can be expected to be minimal). In the case of Rh-catalyst hydroformylation using complexes **4** as precatalysts, the phosphane substituents played a minor role (except for the furyl group).

Unsurprisingly, therefore, no universal ligand was identified in the series. While the results showed that the diphenylphosphanyl-substituted compound **3c** was the most practical in "carbonylative" cross-coupling and hydroformylation, giving rise to reasonably active and stable catalysts, biaryl Suzuki–Miyaura cross-coupling was best mediated by catalysts containing electron-rich alkylphosphane ligands. Conversely, the beneficial effect of the guanidinium pendant was demonstrated for both types of reaction, most likely resulting from enhanced solubility of the catalyst in the polar reaction media.

Experimental Section

Materials and Methods

All syntheses were performed under an argon atmosphere using standard Schlenk techniques. Triethylamine was dried with sodium metal and distilled under an argon atmosphere. Other chemicals were purchased from Sigma-Aldrich or Alfa-Aesar (reagent grade) and used without additional purification. Compounds **1a**, **1b**, and **1d**,[12] and **3c**[6] were prepared as described previously. Anhydrous THF and methanol, used during syntheses, were obtained from a Pure Solv MD5 solvent purification system (Innovative Technology, USA). Acetone was dried with potassium carbonate and distilled under an argon atmosphere. Solvents used for workup and for crystallizations were purchased from LachNer (Czech Republic) and used as received. Deuterated solvents were the products of Armar Chemicals and used as obtained. ^1H, $^{13}C\{^1H\}$, and $^{31}P\{^1H\}$ NMR spectra were recorded at 25 °C on a Varian INOVA 400 spectrometer operating at 399.95, 100.58, and 161.90 MHz, respectively. Chemical shifts (δ in ppm) are given relative to internal tetramethylsilane (^1H and ^{13}C) and to external 85 % aqueous H_3PO_4 (^{31}P) as an external reference. In addition, ^{19}F NMR spectra used to monitor the catalytic reactions, as well as ^1H, ^{13}C and ^{19}F NMR spectra of the catalytic products, were recorded on a Bruker Avance III 400 spectrometer with operating frequencies 400.13, 100.61 and 376.46 MHz using tetramethylsilane (^1H and ^{13}C) as an internal reference, and neat trichlorofluoromethane (^{19}F) as an external reference. In addition to the standard description of signal multiplicity,[24] vt and vq were used to distinguish virtual triplets and quartets due to the magnetically non-equivalent protons at the cyclopentadienyl rings (spin systems AA′BB′ and AA′BB′X for the methylene- and phosphanyl-substituted rings, respectively, where A, B = ^1H, and X = ^{31}P). FTIR spectra were recorded in Nujol mulls on a Nicolet 6700 FTIR spectrometer over the 400–4000 cm^{-1} range. ESI mass spectra were recorded on a Compact QTOF-MS spectrometer (Bruker Daltonics) for samples dissolved in HPLC-grade methanol. Elemental analyses were performed using a Perkin–Elmer 2400 Series II CHNS/O analyzer. The presence of residual solvent(s) was confirmed by NMR analysis.

Syntheses

[1′-(Diisopropylphosphanyl)ferrocene-1-yl]methylamine (2a): 1-Cyano-1′-(diisopropylphosphanyl)ferrocene (**1a**; 1.31 g, 4.0 mmol) was dissolved in dry THF (40 mL), and the resulting red solution was transferred dropwise via a cannula into a separate flask containing $Li[AlH_4]$ (0.46 g, 12.0 mmol), which was cooled to 0 °C in an ice bath. The bubbling turbid mixture was stirred at 0 °C for 15 min and then at room temperature for 4 h. Then, the reaction mixture was cooled on ice and quenched by successively adding water (1 mL), 1 M aqueous NaOH (1.5 mL) and additional water (2 mL). The resulting mixture was stirred while cooling for 15 min and then filtered through a short Celite column. The Celite was washed with diethyl ether (3 × 10 mL), and the combined organic phases were washed with brine (20 mL) and dried with anhydrous $MgSO_4$. The solvents were evaporated under reduced pressure to give 1.28 g (96 %) of **2a** as a viscous orange oil, which was sufficiently pure for further reactions (> 90–95 %; the remaining fraction was the residual solvent). An analytical sample was prepared by flash column chromatography (silica gel, dichloromethane/methanol, 10:1). ^1H NMR (399.95 MHz, $CDCl_3$): δ = 1.07 (dd, $^3J_{HH}$ = 6.9 Hz, $^3J_{HP}$ = 6.9 Hz, 6 H, CHMe_2), 1.10 (dd, $^3J_{HH}$ = 7.0 Hz, $^3J_{HP}$ = 8.7 Hz, 6 H, CHMe_2), 1.92 (sept of d, $^3J_{HH}$ = 7.0 Hz, $^2J_{HP}$ = 2.6 Hz, 2 H, CHMe$_2$), 3.58 (s, 2 H, CH_2NH$_2$), 4.10 (vt, J' = 1.8 Hz, 2 H, fc), 4.15 (m, 4 H, fc), 4.26 (vt, J' = 1.8 Hz, 2 H, fc) ppm. $^{13}C\{^1H\}$ NMR (100.58 MHz, $CDCl_3$): δ = 19.90 (d, $^2J_{CP}$ = 10 Hz, CHMe_2), 20.13 (d, $^2J_{CP}$ = 15 Hz, CHMe_2), 23.43 (d, $^1J_{CP}$ = 11 Hz, CHMe$_2$), 41.16 (s, CH_2NH_2), 68.17 (s, CH of fc), 69.22 (s, CH of fc), 69.81 (d, J_{CP} = 2 Hz, CH of fc), 71.64 (d, J_{CP} = 10 Hz, CH of fc), 76.22 (d, $^1J_{CP}$ = 17 Hz, C^{ipso}-P of fc), 91.26 (s, C^{ipso}-CH_2 of fc) ppm. $^{31}P\{^1H\}$ NMR (161.90 MHz, $CDCl_3$): δ = 1.0 (s, P(iPr)$_2$) ppm. FTIR (Nujol): $\tilde{\nu}_{max}$ 3366 w, 3091 m, 1571 m, 1401 w, 1363 m, 1302 m, 1243 m, 1232 m, 1194 w, 1156 m, 1027 s, 961 w, 917 w, 882 m, 826 s, 656 m, 634 m, 607 m, 496 s, 479 m [cm^{-1}]. HRMS (ESI+): m/z calcd. for $C_{17}H_{27}FeNOP$ ([M + O + H]$^+$) 348.1174, found 348.1174. The compound is rather unstable towards oxidation and, hence, no reliable microanalytical data could be collected.

[1′-(Dicyclohexylphosphanyl)ferrocene-1-yl]methylamine (2b): Starting with 1-cyano-1′-(dicyclohexylphosphanyl)ferrocene (**1b**; 1.43 g, 3.5 mmol) in 50 mL of THF and with $Li[AlH_4]$ (0.40 g, 10.5 mmol), the above procedure afforded **2b** (1.38 g, 96 %) as an orange solid, which was sufficiently pure for further reactions. An analytical sample was prepared by flash column chromatography

over silica gel using a dichloromethane/methanol mixture (20:1 v/v) as the eluent. ^{1}H NMR (399.95 MHz, $CDCl_3$): δ = 1.00–1.36 (m, 10 H, Cy), 1.62–1.84 (m, 10 H, Cy), 1.86–1.96 (m, 4 H, Cy + NH_2), 3.58 (s, 2 H, CH_2NH_2), 4.08 (vt, J' = 1.8 Hz, 2 H, fc), 4.12 (vq, J' = 1.6 Hz, 2 H, fc), 4.13 (vt, J' = 1.7 Hz, 2 H, fc), 4.25 (vt, J' = 1.8 Hz, 2 H, fc) ppm. ^{13}C{^{1}H} NMR (100.58 MHz, $CDCl_3$): δ = 26.43 (d, J_{CP} = 1 Hz, Cy), 27.33 (d, J_{CP} = 8 Hz, Cy), 27.41 (d, J_{CP} = 11 Hz, Cy), 30.25 (d, J_{CP} = 13 Hz, Cy), 30.30 (d, J_{CP} = 10 Hz, Cy), 33.51 (d, J_{CP} = 11 Hz, Cy), 41.10 (s, CH_2NH_2), 68.21 (s, CH of fc), 69.22 (s, CH of fc), 69.79 (d, J_{CP} = 3 Hz, CH of fc), 71.87 (d, J_{CP} = 11 Hz, CH of fc), 76.57 (d, $^1J_{CP}$ = 16 Hz, C^{ipso}-P of fc), 90.92 (s, C^{ipso}-CH_2 of fc) ppm. ^{31}P{^{1}H} NMR (161.90 MHz, $CDCl_3$): δ = –7.2 (s, PCy_2) ppm. FTIR (Nujol): $\tilde{\nu}_{max}$ 3369 w, 3282 w, 3096 m, 3087 m, 2726 w, 2665 w, 1634 w, 1606 m, 1552 m, 1401 w, 1344 m, 1328 m, 1306 m, 1272 w, 1262 m, 1231 m, 1191 m, 1174 w, 1166 w, 1154 m, 1110 w, 1053 w, 1034 s, 1028 sh, 1001 m, 938 w, 913 w, 884 m, 866 s, 858 sh, 848s, 826 s, 745 w, 716 m, 629 w, 602 w, 515 s, 496 s, 474 s, 442 m, 423 w [cm^{-1}]. HRMS (ESI+): *m/z* calcd. for $C_{23}H_{35}FeNP$ ([M + H]$^+$) 412.1857, found 412.1851. Anal. Calc. for $C_{23}H_{34}FeNP$ (411.4): C 67.16, H 8.33, N 3.41 %; found C 66.34, H 8.35, N 3.24 %. The compound is hygroscopic and tenaciously retains residual water.

{1′-[Di(2-furyl)phosphanyl]ferrocene-1-yl}methylamine (2d): Starting with 1-cyano-1′-[di(2-furyl)phosphanyl]ferrocene (**1d**; 1.51 g, 4.0 mmol), the same procedure furnished analytically pure **2d** (1.27 g, 84 %) as an orange solid, which was sufficiently pure for further reactions. ^{1}H NMR (399.95 MHz, [D$_6$]DMSO): δ = 3.24 (s, 2 H, CH_2NH_2), 3.85 (vt, J' = 1.8 Hz, 2 H, fc), 4.03 (vt, J' = 1.8 Hz, 2 H, fc), 4.35 (vq, J' = 1.9 Hz, 2 H, fc), 4.38 (vt of d, J' = 1.9 Hz, J' = 0.7 Hz, 2 H, fc), 6.51 (dt, J = 3.2 Hz, J = 1.7 Hz, 2 H, Fur), 6.76 (ddd, J = 3.3 Hz, J = 2.0 Hz, J = 0.7 Hz, 2 H, Fur), 7.90 (m, 2 H, Fur) ppm. ^{13}C{^{1}H} NMR (100.58 MHz, [D$_6$]DMSO): δ = 40.20 (s, CH_2NH_2), 67.99 (s, 2 × CH of fc), 71.25 (d, J_{CP} = 5 Hz, CH of fc), 71.89 (d, $^1J_{CP}$ = 6 Hz, C^{ipso}-P of fc), 73.62 (d, J_{CP} = 18 Hz, CH of fc), 92.58 (s, C^{ipso}-CH_2 of fc), 110.75 (d, J_{CP} = 6 Hz, CH of Fur), 119.88 (d, J_{CP} = 25 Hz, CH of Fur), 147.31 (d, J_{CP} = 2 Hz, CH of Fur), 151.66 (d, $^1J_{CP}$ = 10 Hz, C^{ipso} of Fur) ppm. ^{31}P{^{1}H} NMR (161.90 MHz, [D$_6$]DMSO): δ = –65.4 (s, $PFur_2$) ppm. FTIR (Nujol): $\tilde{\nu}_{max}$ 3377 m, 3108 m, 3067 m, 2607 w, 1737 w, 1580 m, 1549 m, 1403 m, 1309 w, 1215 w, 1204 w, 1195 m, 1160 m, 1148 s, 1116 s, 1062 m, 1025 s, 1015 s, 1003 s, 978 m, 919 w, 903 m, 883 m, 873 m, 860 s, 836 s, 819 s, 747 vs, 668 sh, 659 m, 646 m, 623 w, 595 m, 523 w, 474 vs, 431 w [cm^{-1}]. HRMS (ESI+): *m/z* calcd. for $C_{19}H_{19}FeNO_2P$ ([M + H]$^+$) 380.0503, found 380.0490. Anal. Calc. for $C_{19}H_{18}FeNO_2P$ (379.2): C 60.19, H 4.79, N 3.69 %; found C 60.09, H 4.81, N 3.50 %.

***N*-{[1′-(Diisopropylphosphanyl)ferrocene-1-yl]methyl}guanidine Hydrochloride (3a):** A solution of amine **1a** (1.26 g, 3.8 mmol) in dry THF (100 mL) was transferred via a cannula onto solid 1*H*-pyrazole-1-carboxamidine hydrochloride (0.61 g, 4.2 mmol), forming an orange suspension. Dry triethylamine (0.62 mL, 4.4 mmol) was added, and the reaction mixture was stirred in the dark overnight. Then, the orange suspension was diluted with methanol (10 mL), which dissolved all solids, and the reaction mixture turned red. The solution was evaporated, and the red oily crude product was purified by chromatography over a silica gel column with dichloromethane/methanol (10:1). The first two minor bands containing impurities were discarded, and the following major orange band was collected and the solvents evaporated. The resulting red viscous product was further crystallized from a hot chloroform/hexane mixture yielding 1.01 g (65 %) of **3a** as a dark orange crystalline solid. Crystals suitable for structure determination were obtained by liquid phase diffusion of hexane into a saturated chloroform solution of the compound. ^{1}H NMR (399.95 MHz, [D$_6$]DMSO): δ = 1.00 (dd, $^3J_{HH}$ = 6.8 Hz, $^3J_{HP}$ = 5.0 Hz, 6 H, CH*Me*$_2$), 1.03 (dd, $^3J_{HH}$ = 6.8 Hz, $^3J_{HP}$ = 7.0 Hz, 6 H, CH*Me*$_2$), 1.87 (sept of d, $^3J_{HH}$ = 7.0 Hz, $^2J_{HP}$ = 2.0 Hz, 2 H, C*H*Me$_2$), 4.09 (vt, J' = 1.8 Hz, 2 H, fc), 4.09 (d, $^3J_{HH}$ = 5.3 Hz, 2 H, CH_2NH), 4.20 (vq, J' = 1.6 Hz, 2 H, fc), 4.25 (vt, J' = 1.8 Hz, 2 H, fc), 4.39 (vt, J' = 1.8 Hz, 2 H, fc), 7.32 (very broad s, 4 H, NH_2 of guanidinium), 7.85 (t, $^3J_{HH}$ = 5.3 Hz, 1 H, CH_2NH) ppm. ^{13}C{^{1}H} NMR (100.58 MHz, [D$_6$]DMSO): δ = 19.69 (d, $^2J_{CP}$ = 11 Hz, CH*Me*$_2$), 19.99 (d, $^2J_{CP}$ = 16 Hz, CH*Me*$_2$), 22.83 (d, $^1J_{CP}$ = 13 Hz, *C*HMe$_2$), 40.02 (s, CH_2NH), 68.89 (s, CH of fc), 69.57 (s, CH of fc), 70.40 (d, J_{CP} = 2 Hz, CH of fc), 71.56 (d, J_{CP} = 10 Hz, CH of fc), 76.24 (d, $^1J_{CP}$ = 20 Hz, C^{ipso}–P of fc), 83.71 (s, C^{ipso}–CH_2 of fc), 156.65 (s, C^{ipso} of guanidinium) ppm. ^{31}P{^{1}H} NMR (161.90 MHz, [D$_6$]DMSO): δ = –0.6 (s, P(*i*Pr)$_2$) ppm. FTIR (Nujol): $\tilde{\nu}_{max}$ 3454 m, 3284 m, 3215 m, 3090 s, 1663 s, 1640 s, 1611 s, 1359 m, 1340 m, 1299 w, 1234 m, 1195 w, 1155 m, 1100 w, 1039 m, 1017 w, 925 w, 884 w, 841 w, 830 m, 816 w, 753 m, 724 w, 655 w, 636 m, 607 m, 585 w, 533 m, 518 w, 501 m, 478 m [cm^{-1}]. MS (ESI+): *m/z* 315 ([*i*Pr$_2$PfcCH$_2$]$^+$), 374 ([*i*Pr$_2$PfcCH$_2$NHC(NH$_2$)$_2$]$^+$). Anal. Calc. for $C_{18}H_{29}ClFeN_3P$ (409.7): C 52.77, H 7.13, N 10.26 %; found C 52.45, H 7.18, N 10.04 %.

***N*-{[1′-(Dicyclohexylphosphanyl)ferrocene-1-yl]methyl}guanidine Hydrochloride (3b):** A solution of amine **2b** (1.65 g, 4.0 mmol) in dry THF (100 mL) was transferred via a cannula onto solid 1*H*-pyrazole-1-carboxamidine hydrochloride (0.65 g, 4.4 mmol), producing a yellow suspension. Dry triethylamine (0.62 mL, 4.4 mmol) was introduced, and the resulting mixture was stirred in the dark overnight. On the following day, the turbid orange mixture was concentrated under vacuum, forming an orange oil as the crude product, which was purified by chromatography over a silica gel column using dichloromethane/methanol (5:1) as the eluent. The first minor bands containing impurities and/or side products were discarded, and the following major orange band was collected. Evaporation led to an orange oil, which was further crystallized from a hot chloroform/hexane mixture to give 1.53 g (78 %) of **3b** as a yellow microcrystalline powder. ^{1}H NMR (399.95 MHz, [D$_6$]DMSO): δ = 0.90–1.34 (m, 10 H, Cy), 1.57–1.78 (m, 10 H, Cy), 1.82–1.92 (m, 2 H, Cy), 4.07 (vt, J' = 1.8 Hz, 2 H, fc), 4.08 (d, $^3J_{HH}$ = 4.2 Hz, 2 H, CH_2NH), 4.16 (vq, J' = 1.6 Hz, 2 H, fc), 4.23 (vt, J' = 1.8 Hz, 2 H, fc), 4.38 (vt, J' = 1.8 Hz, 2 H, fc), 7.31 (very broad s, 4 H, NH_2 of guanidinium), 7.81 (s, 1 H, CH_2NH) ppm. ^{13}C{^{1}H} NMR (100.58 MHz, [D$_6$]DMSO): δ = 26.04 (s, Cy), 26.62 (d, J_{CP} = 9 Hz, Cy), 26.77 (d, J_{CP} = 11 Hz, Cy), 29.74 (d, J_{CP} = 10 Hz, Cy), 29.76 (d, J_{CP} = 13 Hz, Cy), 32.89 (d, J_{CP} = 13 Hz, Cy), 40.03 (s, CH_2NH), 68.90 (s, CH of fc), 69.54 (s, CH of fc), 70.38 (d, J_{CP} = 2 Hz, CH of fc), 71.77 (d, J_{CP} = 11 Hz, CH of fc), 76.59 (d, $^1J_{CP}$ = 19 Hz, C^{ipso}–P of fc), 83.66 (s, C^{ipso}–CH_2 of fc), 156.60 (s, C^{ipso} of guanidinium) ppm. ^{31}P{^{1}H} NMR (161.90 MHz, [D$_6$]DMSO): δ = –9.3 (s, PCy_2) ppm. FTIR (Nujol): $\tilde{\nu}_{max}$ 3331 s, 3253 s, 3136 s, 2667 w, 1660 s, 1644 s, 1608 s, 1558 w, 1411 m, 1341 m, 1262 w, 1239 w, 1199 m, 1176 w, 1156 m, 1109 w, 1083 w, 1039 m, 1029 m, 1000 w, 845 m, 838 m, 819 w, 722 w, 663 m, 630 w, 581 m, 530 w, 505 m, 493 m, 473 m [cm^{-1}]. Anal. Calc. for $C_{24}H_{37}ClFeN_3P$ (489.8): C 58.85, H 7.61, N 8.58 %; found C 58.73, H 7.50, N 8.51 %. MS (ESI+): *m/z* 395 ([Cy$_2$PfcCH$_2$]$^+$), 454 ([Cy$_2$PfcCH$_2$NHC(NH$_2$)$_2$]$^+$).

***N*-({1′-[Di(2-furyl)phosphanyl]ferrocene-1-yl}methyl)guanidine Hydrochloride (3d):** A solution of amine **2d** (1.27 g, 3.4 mmol) in dry THF (80 mL) was transferred via a cannula onto 1*H*-pyrazole-1-carboxamidine hydrochloride (0.54 g, 3.7 mmol), giving rise to an orange suspension. After adding dry triethylamine (0.50 mL, 3.7 mmol), the reaction mixture was stirred in the dark overnight. On the following day, the orange solution was evaporated, and the resulting dark orange oil was subjected to chromatography over a silica gel column using dichloromethane/methanol (10:1) as the eluent. After removing the first yellow band, due to side products, the polarity of the eluent was replaced with dichloromethane/methanol

(5:1) to elute the major orange band due to the product. Subsequent evaporation produced **3d** as a sticky orange foam, which was further crystallized from a hot ethanol/diethyl ether mixture to give 1.18 g (76 %) of analytically pure **3d** as orange crystals (plates). Crystals used for structure determination were grown by liquid-phase diffusion of methyl *tert*-butyl ether into a methanol solution. ^{1}H NMR (399.95 MHz, [D$_6$]DMSO): δ = 3.92 (vt, J' = 1.9 Hz, 2 H, fc), 3.96 (d, $^3J_{HH}$ = 5.7 Hz, 2 H, C*H*$_2$NH), 4.11 (vt, J' = 1.9 Hz, 2 H, fc), 4.44 (vq, J' = 1.9 Hz, 2 H, fc), 4.47 (vt of d, J' = 1.8 Hz, J' = 0.7 Hz, 2 H, fc), 6.52 (dt, J = 3.3 Hz, J = 1.7 Hz, 2 H, Fur), 6.79 (ddd, J = 3.3 Hz, J = 2.0 Hz, J = 0.8 Hz, 2 H, Fur), 7.28 (very broad s, 4 H, NH$_2$ of guanidinium), 7.80 (t, $^3J_{HH}$ = 5.7 Hz, 1 H, CH$_2$N*H*), 7.92 (m, 2 H, Fur) ppm. ^{13}C{^{1}H} NMR (100.58 MHz, [D$_6$]DMSO): δ = 39.67 (s, CH$_2$NH), 68.89 (s, CH of fc), 68.98 (s, CH of fc), 71.84 (d, J_{CP} = 5 Hz, CH of fc), 72.59 (d, $^1J_{CP}$ = 5 Hz, C^{ipso}–P of fc), 74.10 (d, J_{CP} = 18 Hz, CH of fc), 84.48 (s, C^{ipso}–CH$_2$ of fc), 110.81 (d, J_{CP} = 6 Hz, CH of Fur), 120.02 (d, J_{CP} = 25 Hz, CH of Fur), 147.44 (d, J_{CP} = 2 Hz, CH of Fur), 151.47 (d, J_{CP} = 10 Hz, C^{ipso} of Fur), 156.60 (s, C^{ipso} of guanidinium) ppm. ^{31}P{^{1}H} NMR (161.90 MHz, [D$_6$]DMSO): δ = –65.9 (s, PFur$_2$) ppm. FTIR (Nujol): $\tilde{\nu}_{max}$ 3454 s, 3239 s, 3124 s, 3077 sh, 2725 w, 1664 s, 1640 s, 1603 s, 1552 w, 1424 w, 1332 w, 1309 w, 1260 w, 1203 w, 1196 w, 1164 m, 1148 m, 1115 m, 1063 w, 1038 m, 1029 m, 1005 s, 986 w, 933 w, 900 m, 880 w, 838 m, 832 sh, 822 m, 759 w, 747 s, 721 w, 661 w, 650 m, 594 m, 568 m, 536 w, 509 w, 487 m, 474 s, 459 m [cm^{-1}]. MS (ESI+): *m/z* 363 ([Fur$_2$PfcCH$_2$]$^+$), 422 ([Fur$_2$PfcCH$_2$NHC(NH$_2$)$_2$]$^+$). Anal. Calc. for $C_{20}H_{21}ClFeN_3O_2P$ (457.7): C 52.49, H 4.63, N 9.18 %; found C 52.35, H 4.70, N 9.02 %.

General Procedure for the Preparation of Complexes [RhCl(CO){R$_2$PfcCH$_2$NHC(NH$_2$)$_2$-κ*P*}$_2$]Cl$_2$ (4): Dry methanol (5 mL) was added atmosphere to the mixture of [Rh(μ-Cl)(CO)$_2$]$_2$ (29.2 mg, 0.075 mmol) and respective ligand (0.300 mmol). The starting materials dissolved with gas evolution, producing an orange solution, which was stirred at room temperature for 60 minutes. The solvent was evaporated under reduced pressure, leaving amorphous orange solid, which was triturated with acetone. The precipitated product was filtered off, washed with pentane and dried with sodium hydroxide under vacuum. The yield of the product typically exceeds 90 %.

Analytical data for 4a. Yellow solid. ^{1}H NMR (399.95 MHz, [D$_6$]DMSO): δ = 1.22 (d of vt, $J_1 \approx J_2 \approx$ 7.3 Hz, 12 H, CH*Me*$_2$), 1.35 (d of vt, $J_1 \approx J_2 \approx$ 7.5 Hz, 12 H, CH*Me*$_2$), 2.74 (m, 4 H, *CH*Me$_2$), 4.14 (d, $^3J_{HH}$ = 5.2 Hz, 4 H, C*H*$_2$NH), 4.35 (vt, J' = 1.8 Hz, 4 H, fc), 4.37 (vt, J' = 1.8 Hz, 4 H, fc), 4.56 (vt, J' = 1.8 Hz, 4 H, fc), 4.67 (vt, J' = 1.7 Hz, 4 H, fc), 7.32 (br s, 8 H, NH$_2$ of guanidinium), 7.88 (s, 2 H, CH$_2$N*H*) ppm. ^{13}C{^{1}H} NMR (100.58 MHz, [D$_6$]DMSO): δ = 18.65 (s, CH*Me*), 20.02 (s, CH*Me*), 25.47 (vt, J' = 13 Hz, *CH*Me), 39.87 (s, CH$_2$NH), 69.30 (s, CH of fc), 70.70 (s, CH of fc), 71.30 (vt, J' = 3 Hz, s, CH of fc), 73.73 (vt, J' = 5 Hz, s, CH of fc), 74.64 (vt, J' = 19 Hz, s, C^{ipso}–P of fc), 84.44 (s, C^{ipso}–CH$_2$ of fc), 156.67 (s, C^{ipso} of guanidinium), 188.37 (dt, $^1J_{RhC}$ = 74 Hz, $^2J_{PC}$ = 16 Hz, C≡O) ppm. ^{31}P{^{1}H} NMR (161.90 MHz, [D$_6$]DMSO): δ = 38.2 (d, $^1J_{RhP}$ = 122 Hz, P(*i*Pr)$_2$) ppm. FTIR (Nujol): $\tilde{\nu}_{max}$ 3319 m, 3245 m, 3134 s, 1947 s, 1935 sh, 1707 w, 1663 s, 1653 s, 1341 w, 1305 w, 1252 w, 1226 w, 1195 w, 1161 m, 1092 w, 1041 sh, 1030 m, 928 w, 885 w, 834 m, 820 w, 665 m, 629 m, 616 w, 603 w, 580 m, 545 w, 535 w, 485 m [cm^{-1}]. MS (ESI+): *m/z* 293 ([M – 3Cl]$^{3+}$), 439 ([M – 2Cl – HCl]$^{2+}$), 877 ([M – Cl – 2HCl]$^+$), 913 ([M – Cl – HCl]$^+$). Anal. calcd. for $C_{37}H_{58}Cl_3Fe_2N_6OP_2Rh$·0.5Me$_2$CO·0.5H$_2$O (1023.9): C 45.17, H 6.10, N 8.21 %; found C 44.93, H 5.77, N 8.00 %.

Analytical data for 4b. Yellow solid. ^{1}H NMR (399.95 MHz, [D$_6$]DMSO): δ = 1.06–1.34 (m, 12 H, Cy), 1.40–1.55 (m, 8 H, Cy), 1.60–1.69 (m, 4 H, Cy), 1.70–1.82 (m, 8 H, Cy), 1.93–2.03 (m, 4 H, Cy), 2.16–2.27 (m, 4 H, Cy), 2.41–2.52 (m, 4 H, Cy), 4.13 (d, $^3J_{HH}$ = 5.6 Hz, 4 H, C*H*$_2$NH), 4.30 (vt, J' = 1.8 Hz, 4 H, fc), 4.35 (vt, J' = 1.8 Hz, 4 H, fc), 4.55 (vt, J' = 1.7 Hz, 4 H, fc), 4.62 (m, 4 H, fc), 7.10 (br s, 4 H, NH$_2$ of guanidinium), 7.52 (br s, 4 H, NH$_2$ of guanidinium), 7.84 (t, $^3J_{HH}$ = 5.4 Hz, 2 H, CH$_2$N*H*) ppm. ^{13}C{^{1}H} NMR (100.58 MHz, [D$_6$]DMSO): δ = 25.90 (s, Cy), 26.80 (two vt, 2 × Cy), 28.44 (s, Cy), 29.55 (s, Cy), 35.86 (vt, J' = 12 Hz, Cy), 69.38 (s, CH of fc), 70.62 (s, CH of fc), 71.26 (s, CH of fc), 74.15 (vt, J' = 5 Hz, CH of fc), 74.29 (vt, J' = 19 Hz, C^{ipso}–P of fc), 84.46 (s, C^{ipso}–CH$_2$ of fc), 156.63 (s, C^{ipso} of guanidinium), 188.78 (dt, $^1J_{RhC}$ = 74 Hz, $^2J_{PC}$ = 16 Hz, C≡O) ppm. The signal due to the methylene spacer overlaps with the solvent resonance. ^{31}P{^{1}H} NMR (161.90 MHz, [D$_6$]DMSO): δ = 29.8 (d, $^1J_{RhP}$ = 122 Hz, PCy$_2$) ppm. FTIR (Nujol): $\tilde{\nu}_{max}$ 3326 m, 3158 m, 1946 s, 1939 sh, 1665 s, 1645 s, 1342 w, 1328 w, 1306 w, 1291 w, 1266 w, 1195 w, 1172 w, 1162 m, 1034 m, 1007 w, 854 w, 848 w, 825 m, 747 m, 625 w, 578 m, 481 m, 467 m [cm^{-1}]. MS (ESI+): *m/z* 346 ([M – 3Cl]$^{3+}$), 519 ([M – 2Cl – HCl]$^{2+}$), 1037 ([M – Cl –2HCl]$^+$), 1073 ([M – Cl – HCl]$^+$). Anal. Calc. for $C_{49}H_{74}Cl_3Fe_2N_6OP_2Rh$·H$_2$O (1164.1): C 50.56, H 6.58, N 7.22 %; found C 50.31, H 6.42, N 6.99 %.

Analytical data for 4c. Yellow solid. ^{1}H NMR (399.95 MHz, [D$_6$]DMSO): δ = 4.05 (d, $^3J_{HH}$ = 5.7 Hz, 4 H, C*H*$_2$NH), 4.38 (vt, J' = 1.7 Hz, 4 H, fc), 4.40 (vt, J' = 1.7 Hz, 4 H, fc), 4.44 (s, 4 H, fc), 4.62 (vt, J' = 1.7 Hz, 4 H, fc), 7.44–7.52 (m, 12 H, Ph), 7.56–7.64 (m, 8 H, Ph), 7.87 (s, 2 H, CH$_2$N*H*). ^{13}C{^{1}H} NMR (100.58 MHz, [D$_6$]DMSO): δ = 69.48 (s, CH of fc), 70.92 (s, CH of fc), 72.60 (vt, J' = 2 Hz, CH of fc), 74.33 (vt, J' = 26 Hz, C^{ipso}–P of fc), 74.64 (vt, J' = 6 Hz, CH of fc), 84.96 (s, C^{ipso}–CH$_2$ of fc), 128.08 (vt, J' = 5 Hz, CH of Ph), 130.17 (s, CH of Ph), 133.37 (vt, J' = 13 Hz, CH of Ph), 134.34 (vt, J' = 23 Hz, C^{ipso} of Ph), 156.66 (s, C^{ipso} of guanidinium), 187.18 (dt, $^1J_{RhC}$ = 74 Hz, $^2J_{PC}$ = 16 Hz, C≡O) ppm. The signal due to the methylene linker overlaps with the solvent resonance. ^{31}P{^{1}H} NMR (161.90 MHz, [D$_6$]DMSO): δ = 22.6 (d, $^1J_{RhP}$ = 126 Hz, PPh$_2$) ppm. FTIR (Nujol): $\tilde{\nu}_{max}$ 3316 m, 3141 s, 1970 s, 1647 s, 1435 s, 1339 w, 1306 w, 1164 m, 1097 m, 1071 w, 1028 m, 833 m, 746 m, 695 s, 627 w, 572 m, 535 m, 515 m, 496 s, 471 m [cm^{-1}]. MS (ESI+): *m/z* 507 ([M – 2Cl – HCl]$^{2+}$), 525 ([M – 2Cl]$^{2+}$). Anal. calcd. for $C_{49}H_{50}Cl_3Fe_2N_6OP_2Rh$·0.25 Me$_2$CO·H$_2$O (1154.4): C 51.76, H 4.67, N 7.28 %; found C 51.63, H 4.64, N 6.73 %.

Analytical data for 4d. Yellow solid. ^{1}H NMR (399.95 MHz, [D$_6$]DMSO): δ = 4.10 (d, $^3J_{HH}$ = 5.3 Hz, 4 H, C*H*$_2$NH), 4.33 (s, 4 H, fc), 4.38 (s, 4 H, fc), 4.65 (s, 4 H, fc), 4.69 (s, 4 H, fc), 6.63 (s, 4 H, Fur), 6.90 (d, J = 3 Hz, 4 H, Fur), 7.30 (br s, 8 H, NH$_2$ of guanidinium), 7.85 (t, $^3J_{HH}$ = 5.3 Hz, 2 H, CH$_2$N*H*), 8.07 (s, 4 H, Fur) ppm. ^{13}C{^{1}H} NMR (100.58 MHz, [D$_6$]DMSO): δ = 69.59 (s, CH of fc), 70.27 (vt, J' = 30 Hz, C^{ipso}–P of fc), 70.45 (s, CH of fc), 72.61 (s, CH of fc), 74.58 (vt, J' = 6 Hz, CH of fc), 85.14 (s, C^{ipso}–CH$_2$ of fc), 111.04 (s, CH of Fur), 122.10 (vt, J' = 16 Hz, CH of Fur), 146.61 (vt, J' = 36 Hz, C^{ipso} of Fur), 148.37 (s, CH of Fur), 156.64 (s, C$_{ipso}$ of guanidinium), 184.92 (d, $^1J_{RhC} \approx$ 62 Hz, C≡O) ppm. The signal due to the methylene spacer is probably obscured by the solvent resonance. ^{31}P{^{1}H} NMR (161.90 MHz, [D$_6$]DMSO): δ = –10.9 (d, $^1J_{RhP}$ = 132 Hz, PFur$_2$) ppm. FTIR (Nujol): $\tilde{\nu}_{max}$ 3110 s, 1982 s, 1663 s, 1647 s, 1550 w, 1366 m, 1341 w, 1308 w, 1236 w, 1213 w, 1196 w, 1168 m, 1121 m, 1062 w, 1028 w, 1009 s, 907 w, 883 w, 833 w, 750 m, 650 w, 621 w, 593 w, 573 m, 534 m, 489 s, 475 sh [cm^{-1}]. MS (ESI+): *m/z* 422 ([Fur$_2$PfcCH$_2$NHC(NH$_2$)$_2$]$^+$), 438 ([Fur$_2$POfcCH$_2$NHC(NH$_2$)$_2$]$^+$), 487 ([M – 2Cl – HCl]$^{2+}$), 505 ([M – 2Cl]$^{2+}$), 973 ([M – Cl – 2HCl]$^+$). Anal. calcd. for $C_{41}H_{42}Cl_3Fe_2N_6O_5P_2Rh$·0.5Me$_2$CO·0.5H$_2$O (1119.8): C 45.59, H 4.14, N 7.51 %; found C 45.51, H 4.21, N 7.00 %.

Pd-Catalyzed Cross-coupling of Acyl Chlorides with Boronic Acids: In a typical reaction, a dry Schlenk flask was charged successively with the respective aroyl chloride (1.25 mmol), boronic acid (1.0 mmol), sodium carbonate (1.0 mmol) and ligand (1.1 μmol). An

argon atmosphere was established, and the flask was stoppered with a septum. Deuterated benzene (1.8 mL), deaerated water (2.0 mL) and, finally, a 5 mM solution of palladium(II) acetate in deuterated benzene (0.2 mL, 1.0 μmol) were introduced. The resulting mixture was vigorously stirred at 50 °C for 60 minutes. After cooling to room temperature, the mixture was diluted with water (5 mL) to dissolve the crystallizing ionic components and (trifluoromethyl)benzene (146.1 mg, 1.0 mmol) was added as an internal standard. Conversions were determined by integration of ^{19}F NMR spectra recorded in filtered benzene phase (PTFE syringe filter, 0.45 μm pore size). Characterization data of the coupling products are given in Supporting Information.

Pd-Catalyzed Cross-coupling of Aryl Bromides with Boronic Acids: In a typical run, a dry Schlenk flask was charged with the appropriate aryl bromide (1.0 mmol), boronic acid (1.1 mmol), sodium carbonate (1.0 mmol) and a ligand (1.1 μmol). An argon atmosphere was established and the flask was sealed with a septum. Deuterated benzene (1.8 mL), deaerated water (2.0 mL) and, finally, 5 mM solution of palladium(II) acetate in deuterated benzene (0.2 mL, 1.0 μmol) were added. The resulting mixture was vigorously stirred at 50 °C for 60 minutes. After cooling to room temperature, the mixture was diluted with water (5 mL) to dissolve the crystallizing ionic components and (trifluoromethyl)benzene (146.1 mg, 1.0 mmol) was added as an internal standard. The benzene phase was filtered as described above and analyzed by ^{19}F NMR spectroscopy to determine the conversion. Characterization data of the coupling products are available in Supporting Information.

Hydroformylation Experiments: These experiments were performed in in a 50 mL stainless steel autoclave equipped with a manometer, a thermostat, a magnetic stirrer and a gas inlet/outlet system. The catalyst was placed in the autoclave and, subsequently, 1-hexene and dimethyl sulfoxide (0.75 mL each) were added under nitrogen atmosphere. The autoclave was closed, flushed three times with hydrogen (5 bar) and, finally, pressurized with syngas (H_2/CO = 1:1) to 10 bar and heated to 80 °C for 5 h. When the reaction was finished, the autoclave was cooled to ambient temperature and depressurized. The organic phase was separated from the solid residue by vacuum transfer and analyzed by GC (Hewlett-Packard 5890 II) and GC–MS (Hewlett-Packard 5971A).

X-ray Crystallography

Full-sphere diffraction data (θ_{max} = 26° for **3a**, and 27.5° for **3d**; completeness > 99 %) were recorded using a Nonius Kappa CCD diffractometer equipped with a Bruker Apex II detector (**3d**), or a Bruker D8 VENTURE Kappa Duo diffractometer with a PHOTON100 detector (**3a**) at 150(2) K. The data were corrected for absorption using multi-scan methods included in the diffractometer software.

Both structures were solved by direct methods (SHEXLT-2014) and subsequently refined by full-matrix least-squares based on F^2 using SHELXL-2014.[25] Compound **3d** was treated as a two-component, non-merohedral twin (twinning matrix: {–1 0 –0.350; 0 –1 0; 0 0 1}, the refined contributions of the two domains: 79:21). All non-hydrogen atoms were refined with anisotropic displacement parameters. The hydrogen atoms residing on the nitrogen atoms (NH) were located on difference density maps and refined as riding atoms with U_{iso}(H) assigned to 1.2U_{eq} of their pivotal atom. Hydrogen atoms bonded to carbon atoms were placed in their theoretical positions and refined similarly. A recent version of the PLATON program[26] was used to prepare all structural diagrams and to calculate all geometric parameters. The numeric values are rounded to their estimated deviations (ESDs) given to one decimal place. Parameters pertaining to atoms in constrained positions are given without ESDs. Selected crystallographic data and refinement parameters are given in Supporting Information (Table S1).

CCDC 1955576 (for **3a**), and 1955577 (for **3d**) contain the supplementary crystallographic data for this paper. These data can be obtained free of charge from The Cambridge Crystallographic Data Centre.

Acknowledgments

This work has been supported by the Grant Agency of Charles University (project no. 130317) and by Charles University Research Centre program (project UNCE/SCI/014).

Keywords: Phosphane ligands · Ferrocene ligands · Hydroformylation · Cross-coupling · Palladium · Rhodium

[1] a) F. Joó, *Aqueous Organometallic Catalysis*, Kluwer, Dordrecht, **2001**; b) *Aqueous-Phase Organometallic Catalysis, 2nd ed* (Eds.: B. Cornils, W. Herrmann), Wiley-VCH, Weinheim, **2004**; c) C.-J. Li, *Chem. Rev.* **2005**, *105*, 3095–3165; d) R. N. Butler, A. G. Coyne, *Chem. Rev.* **2010**, *110*, 6302–6337; e) K. H. Shaughnessy, *Chem. Rev.* **2009**, *109*, 643–710.

[2] For examples of phosphane ligands with guanidinium tags, see: a) A. Hessler, O. Stelzer, H. Dibowski, K. Worm, F. P. Schmidtchen, *J. Org. Chem.* **1997**, *62*, 2362–2369; b) O. Herd, A. Hessler, M. Hingst, P. Machnitzki, M. Tepper, O. Stelzer, *Catal. Today* **1998**, *42*, 413–420; c) P. Machnitzki, M. Tepper, K. Wenz, O. Stelzer, E. Herdtweck, *J. Organomet. Chem.* **2000**, *602*, 158–169; d) P. Wasserscheid, H. Waffenschmidt, P. Machnitzki, K. W. Kottsieper, O. Stelzer, *Chem. Commun.* **2001**, 451–452; e) H. Dibowski, F. P. Schmidtchen, *Tetrahedron* **1995**, *51*, 2325–2330; f) P. Guerreiro, V. Ratovelomanana-Vidal, J.-P. Genêt, P. Dellis, *Tetrahedron Lett.* **2001**, *42*, 3423–3426.

[3] a) T. Šmejkal, B. Breit, *Angew. Chem. Int. Ed.* **2008**, *47*, 311–315; *Angew. Chem.* **2008**, *120*, 317; b) T. Šmejkal, B. Breit, *Angew. Chem. Int. Ed.* **2008**, *47*, 3946–3949; *Angew. Chem.* **2008**, *120*, 4010; c) L. Diab, T. Šmejkal, J. Geier, B. Breit, *Angew. Chem. Int. Ed.* **2009**, *48*, 8022–8026; *Angew. Chem.* **2009**, *121*, 8166; d) T. Šmejkal, D. Gribkov, J. Geier, M. Keller, B. Breit, *Chem. Eur. J.* **2010**, *16*, 2470–2478; e) D. Fuchs, G. Rousseau, L. Diab, U. Gellrich, B. Breit, *Angew. Chem. Int. Ed.* **2012**, *51*, 2178–2182; *Angew. Chem.* **2012**, *124*, 2220.

[4] a) *Ferrocenes: Ligands, Materials and Biomolecules* (Ed.: P. Štěpnička), Wiley, Chichester, **2008**; b) *Ferrocenes: Homogeneous Catalysis, Organic Synthesis, Materials Science* (Eds.: A. Togni, T. Hayashi), VCH, Weinheim, **1995**; c) R. C. J. Atkinson, V. C. Gibson, N. J. Long, *Chem. Soc. Rev.* **2004**, *33*, 313–328; d) R. Gómez Arrayás, J. Adrio, J. C. Carretero, *Angew. Chem. Int. Ed.* **2006**, *45*, 7674–7715; *Angew. Chem.* **2006**, *118*, 7836.

[5] H. Charvátová, I. Císařová, P. Štěpnička, *Eur. J. Inorg. Chem.* **2017**, 288–296.

[6] O. Bárta, I. Císařová, P. Štěpnička, *Eur. J. Inorg. Chem.* **2017**, 489–495.

[7] A. R. Katritzky, B. V. Rogovoy, *ARKIVOC* **2005**, 49–87.

[8] K. Škoch, I. Císařová, P. Štěpnička, *Organometallics* **2015**, *34*, 1942–1956.

[9] a) A. Bader, E. Lindner, *Coord. Chem. Rev.* **1991**, *108*, 27–110; b) C. S. Slone, D. A. Weinberger, C. A. Mirkin, *Prog. Inorg. Chem.* **1999**, *48*, 233–350; c) P. Braunstein, F. Naud, *Angew. Chem. Int. Ed.* **2001**, *40*, 680–699; *Angew. Chem.* **2001**, *113*, 702.

[10] a) N. Miyaura, A. Suzuki, *Chem. Rev.* **1995**, *95*, 2457–2483; b) N. Miyaura, *Top. Curr. Chem.* **2002**, *219*, 11–59; c) N. Miyaura in *Metal-Catalyzed Cross-Coupling Reactions* (Eds.: A. de Meijere, F. Diederich), 2nd ed., Wiley-VCH, Weinheim, **2004**; Vol. 1, chapter 2, pp. 41–123; d) *Palladium-Catalyzed Coupling Reactions* (Ed.: Á. Molnár), Wiley-VCH, Weinheim, **2013**; e) I. Maluenda, O. Navarro, *Molecules* **2015**, *20*, 7528–7557.

[11] a) *Hydroformylation: Fundamentals, Processes, and Applications in Organic Synthesis* (Eds.: A. Börner, R. Franke), Wiley-VCH: Weinheim, **2016**, vols. 1 and: 2; b) *Rhodium Catalyzed Hydroformylation* (Eds.: P. W. N. M. van Leeuwen, C. Claver), Kluwer: New York, **2002**; c) B. Breit, W. Seiche, *Synthesis* **2001**, 1–36.

[12] O. Bárta, I. Císařová, J. Schulz, P. Štěpnička, *New J. Chem.* **2019**, *43*, 11258–11262.

[13] M. S. Bernatowicz, Y. Wu, G. R. Matsueda, *J. Org. Chem.* **1992**, *57*, 2497–2502.

[14] J. Schulz, P. Vosáhlo, F. Uhlík, I. Císařová, P. Štěpnička, *Organometallics* **2017**, *36*, 1828–1841.

[15] a) M. Drozd, *Mater. Sci. Eng. B* **2007**, *136*, 20–28; b) M. Drozd, D. Dudzic, *Spectrochim. Acta Part A* **2013**, *115*, 345–356.

[16] a) W. Henderson, A. G. Oliver, A. J. Downard, *Polyhedron* **1996**, *15*, 1165–1173; b) Yu. S. Nekrasov, R. S. Skazov, A. A. Simenel, L. V. Snegur, I. V. Kachala, *Russ. Chem. Bull.* **2006**, *55*, 1368–1371.

[17] a) J. H. Bryden, *Acta Crystallogr.* **1957**, *10*, 677–680; b) D. J. Haas, D. R. Harris, H. H. Mills, *Acta Crystallogr.* **1965**, *19*, 676–679; c) I. Matulková, H. Solařová, P. Štěpnička, I. Císařová, T. Janda, P. Němec, I. Němec, *Opt. Mater.* **2015**, *42*, 39–46.

[18] For similar complexes, see: a) P. Štěpnička, I. Císařová, *J. Chem. Soc., Dalton Trans.* **1998**, 2807–2811; b) M. Zábranský, I. Císařová, A. M. Trzeciak, W. Alsalahi, P. Štěpnička, *Organometallics* **2019**, *38*, 479–488 and ref. 14.

[19] W. H. Hersh, *J. Chem. Educ.* **1997**, *74*, 1485–1488 and references cited therein.

[20] a) S. Vastag, B. Heil, L. Markó, *J. Mol. Catal.* **1979**, *5*, 189–195; b) A. Roodt, S. Otto, G. Steyl, *Coord. Chem. Rev.* **2003**, *245*, 121–137.

[21] M. Blangetti, H. Rosso, C. Prandi, A. Deagostino, P. Venturello, *Molecules* **2013**, *18*, 1188–1213.

[22] H. Solařová, I. Císařová, P. Štěpnička, *Organometallics* **2014**, *33*, 4131–4147.

[23] a) J. Kühnert, M. Dušek, J. Demel, H. Lang, P. Štěpnička, *Dalton Trans.* **2007**, 2802–2811; b) P. Štěpnička, M. Lamač, I. Císařová, *Polyhedron* **2004**, *23*, 921–928; c) J. Tauchman, I. Císařová, P. Štěpnička, *Organometallics* **2009**, *28*, 3288–3302; d) P. Štěpnička, J. Schulz, T. Klemann, U. Siemeling, I. Císařová, *Organometallics* **2010**, *29*, 3187–3200; e) P. Štěpnička, B. Schneiderová, J. Schulz, I. Císařová, *Organometallics* **2013**, *32*, 5754–5765.

[24] R. M. Silverstein, F. X. Webster, D. J. Kiemle, *Spectrometric Identification of Organic Compounds*, 7th ed., Wiley, Hoboken, **2005**.

[25] G. M. Sheldrick, *Acta Crystallogr., Sect. C Struct. Chem.* **2015**, *71*, 3–8.

[26] A. L. Spek, *J. Appl. Crystallogr.* **2003**, *36*, 7–13.

Received: September 30, 2019

Appendix C

O. Bárta, R. Gyepes, I. Císařová, A. Alemayehu, P. Štěpnička, Synthesis and study of Fe→Pd interactions in unsymmetric Pd(II) complexes with phosphinoferrocene guanidine ligands. *Dalton Trans.* **2020**, *49*, 4225-4229.

Dalton Transactions

ROYAL SOCIETY OF CHEMISTRY

COMMUNICATION

Cite this: *Dalton Trans.*, 2020, **49**, 4225

Received 4th March 2020,
Accepted 16th March 2020

DOI: 10.1039/d0dt00812e

rsc.li/dalton

Synthesis and study of Fe → Pd interactions in unsymmetric Pd(II) complexes with phosphinoferrocene guanidine ligands†

Ondřej Bárta, Róbert Gyepes, Ivana Císařová, Adam Alemayehu and Petr Štěpnička *

Readily available phosphinoferrocene guanidines coordinate Pd(II) as P,N-chelating or κ³P,N,Fe-bound ligands. As the latter, they give rise to the first donor-asymmetric complexes featuring Fe–Pd dative bonds, which were studied using direct (spectroscopic and electrochemical) methods and theoretical (DFT) approaches.

The discovery that ferrocene ligands can bind transition metals in κ³-fashion when using a pair of donor groups in positions 1 and 1′ of the ferrocene scaffold and the electron-rich iron atom in coordination (Scheme 1)[1,2] has expanded the already wide coordination chemistry of ferrocene ligands.[3] As yet, however, this specific bonding mode has only been achieved with symmetrical ligands such as 1,1′-ferrocene dithiolates and bis(thioethers),[1,4] diphosphines,[5] bis(imines) and bis(guanidines).[6] Considering our interest[7] in donor-unsymmetric ligands structurally related to the iconic 1,1′-bis(diphenylphosphino)ferrocene (dppf),[8] we hypothesized that ferrocene phosphino-guanidines could behave similarly, albeit as previously unknown donor-asymmetric P,N,Fe-ligands. While phosphines modified with guanidinium moieties have been extensively studied as hydrophilic ligands,[9] the chemistry of phosphines bearing non-protonated guanidine moieties, which can serve as additional donor sites, remains practically unexplored.[10] Accordingly, we aimed to synthesize phosphinoferrocene guanidines **1** and to study their coordination behaviour towards Pd(II) as a model metal ion (Scheme 1).

Initially, the target ligands **1a–c** were prepared by $ZnEt_2$-mediated addition[11] of **2**[12] across the respective carbodiimides RN═C═NR in toluene at 60 °C (Scheme 2). In contrast to similar reactions employing aminoferrocene,[13] these reactions required a higher amount of the additive (10 mol%) and longer reaction times, especially when using bulkier diimides. Nevertheless, we found subsequently that compounds **1a–c** can be advantageously obtained by addition of *in situ* deprotonated **2** to carbodiimides in THF (Scheme 2). These reactions proceeded cleanly and rapidly regardless of the diimide used.

In addition to characteristic signals due to the phosphinoferrocenyl moiety and to the guanidine substituents, NMR spectra of **1** displayed the resonance of the guanidine carbon at $\delta_C \approx 151$. While the solution NMR spectra of alkyl-substituted guanidines **1a** and **1b** suggested the presence of single isomers with the NH protons located at the alkyl-substituted nitrogen atoms (this arrangement was also encountered in the solid state for **1a**; see Scheme 2 and the ESI†), compound **1c** was a mixture of two amine-imine tautomers (Scheme 3). VT NMR measurements revealed that the "other" isomer **1c′** is exclusively present in toluene solution at low temperatures (0 °C and below; the same isomer was observed in the solid state) while, at higher temperatures, tautomers **1c** and **1c′** co-exist in dynamic equilibrium, which results in averaging when further raising the temperature (see the ESI†).

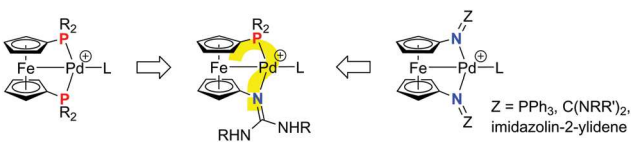

Scheme 1

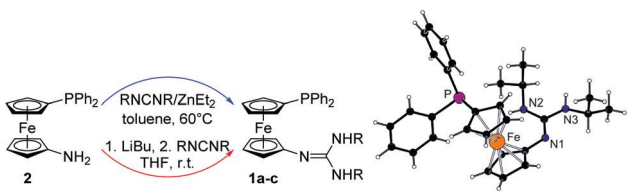

2 1a-c

Scheme 2 (left) Synthesis of phosphinoferrocene guanidines **1** (R = isopropyl (**a**), cyclohexyl (**b**), and 2,6-xylyl (**c**)). (right) View of the molecular structure of **1a**.

Department of Inorganic Chemistry, Faculty of Science, Charles University, Hlavova 2030, 128 40 Prague, Czech Republic. E-mail: petr.stepnicka@natur.cuni.cz

†Electronic supplementary information (ESI) available: Complete experimental details, crystallographic data and additional structural diagrams, copies of the NMR spectra, and coordinates of the DFT optimized structures (as XYZ files). CCDC 1985908–1985914. For ESI and crystallographic data in CIF or other electronic format see DOI: 10.1039/d0dt00812e

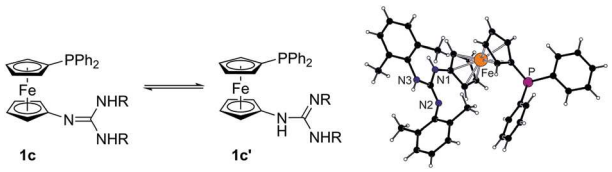

Scheme 3 (left) Amine-imine tautomers of **1c** (R = 2,6-xylyl). (right) View of the molecular structure of **1c**.

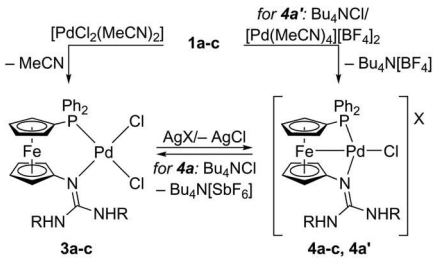

Scheme 4 (left) Coordination of phosphinoferrocene guanidines **1** (R = isopropyl (**a**), cyclohexyl (**b**), and 2,6-xylyl (**c**); X = SbF_6 (**4a–c**) and BF_4 (**4a′**)).

When reacted with $[PdCl_2(MeCN)_2]$ in dichloromethane (Pd : **1** = 1 : 1), ligands **1a** and **1b** produced deep red, chelate complexes **3a** and **3b** (Scheme 4), which were fully characterised, including structure determination. Conversely, when using the bulkier ligand **1c**, the same reaction afforded a mixture of the analogous chelate complex **3c** (δ_P 25.1), two other species tentatively formulated as [PdCl(**1c**-κ^3P,N,Fe)]Cl (δ_P −4.0) and [PdCl(μ-Cl)(**1c**-κP)]$_2$ (δ_P 35.7),[14] and several minor components. The loss of selectivity in the complexation of **1c** apparently results from the increased steric demands of the bulky ligand **1c**, which promote the formation of the aforementioned, sterically less encumbered products (Note: traces of the respective species comprising κ^3P,N,Fe-bound ligands were also detected in the reactions with **1a** and **1b**).

Subsequent chloride removal with $Ag[SbF_6]$ converted **3a** and **3b** into the cationic complexes **4a** and **4b** containing the ferrocene ligand as a triple P,N,Fe-donor (Scheme 4). A similar complex containing ligand **1c** was obtained by adding a silver (I) salt to a $[PdCl_2(MeCN)_2]$/**1c** mixture. Alternatively, complex **4a′** was prepared in the reaction of $[Pd(MeCN)_4][BF_4]_2$ with **1a**, using Bu_4NCl (both 1 equiv.) as a chloride source. All these reactions proceed selectively to produce complexes **4** as deep red, air-stable solids in 70–80% isolated yields, and were reversible. The reaction of **4a**/**4b** with BuN_4Cl (1 equiv.) cleanly transformed these compounds back to their precursors **3a**/**3b**. In contrast, the same reaction with **4c** gave the same complicated product mixture.

The chelate coordination of **1a**/**1b** in **3a**/**3b** was manifested by shifts of the ^{31}P NMR and guanidine ^{13}C NMR signals to lower fields ($\Delta\delta_P \approx 42$ ppm, $\Delta\delta_C(CN_3) \approx 10$ ppm). Furthermore, complexes **3** displayed eight resonances due to ferrocene CH groups, indicating fixed conformations, which render ferrocene protons diasterotopic. No such features were observed in the spectra of **4**. In this case, however, the ^{1}H NMR signals due to ferrocene protons were markedly anisochronic (*cf.* $\Delta\delta_H$ = 0.42 for **1a**, 1.64 for **3a**, and 2.47 for **4a**), as typically found in compounds featuring ferrocene units perturbed by Fe–Pd interactions.[4–6] Compounds **4** showed ^{31}P NMR signals at $\delta_P \approx -5$, and the guanidine resonances in between those of **1** and **3**.

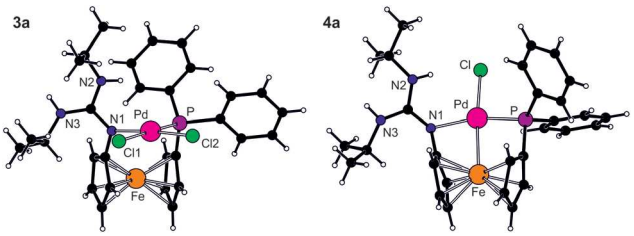

Fig. 1 Views of the molecular structure of **3a** (left) and of the cation of **4a** (right). Selected interatomic distances (in Å) for **3a**: Pd–P 2.2711(6), Pd–N1 2.043(2), Pd–Cl1 2.3688(6), Pd–Cl2 2.2863(6); for **4a**: Pd–Fe 2.7590(5), Pd–P 1.947(7), Pd–N1 2.084(2), Pd–Cl 2.3755(6).

The structures of **3a**, **3b** and **4a–c** were authenticated by X-ray diffraction analysis (see Fig. 1 and ESI†). While the coordination sphere of Pd in **3a** was rather regular (albeit with unlike Pd-donor distance and the Pd–Cl bond lengths affected by *trans* influence), that of Pd in **4a** was markedly distorted as a result of compromise between the steric demands of the ferrocene moiety and the Fe → Pd interaction. The approach of the palladium atom to the iron results in an opening of the ferrocene scaffold, which formally converts the ferrocene ligand from a *cis*- into a *trans*-chelating donor (*cf.* P–Pd–N1 91.43(5)° in **3a**, and 163.01(6)° in **4a**), and also brings the pivotal carbons from the ferrocene moiety (*C*–N and *C*–P) closer to the Pd atom. The Pd–Fe distances (**4a**: 2.7590(5) Å, **4b**: 2.7956(5) Å, and **4c**: 2.7821(5) Å) are only slightly longer than the sum of the covalent radii (2.71 Å)[15] and almost halfway between the values reported for complexes containing the corresponding symmetrical ligands, [Pd(dppf-κ^3P,P′,Fe)(PPh$_3$)][BF$_4$]$_2$ [5a] and [PdCl({Fe(η^5-C$_5$H$_4$N=C(NR$_2$)$_2$}$_2$-κ^3N,N′,Fe)]$_2$[PdCl$_4$] (NR$_2$ = NMe$_2$, N(CH$_2$)$_4$).[6a]

To follow changes at the iron atom, representative compounds **1a**, **3a** and **4a′** were studied by UV-Vis spectroscopy, by cyclic voltammetry and by Mössbauer spectroscopy. Thus, when converting **1a** into **3a**, the weak broad band due to ferrocene d–d transitions[16] that was observed in the UV-Vis spectrum of the free ligand (448 nm; Fig. 2) was replaced by a tailing band extending from the UV region. In contrast, the spectrum of **4a′** showed two relatively stronger maxima at approximately 335 and 418 nm, resulting from convolution of multiple bands attributed to d–d and CT transitions based on the results from DFT computations (see the ESI†).

In cyclic voltammogram (Fig. 2), the free ligand **1a** exhibited a reversible oxidation at −0.29 V *vs.* the ferrocene/ferrocenium reference.[6a] Such a low oxidation potential can be explained by the strong electron-donating character of the guanidine moiety, which prevails over the influence of the weakly

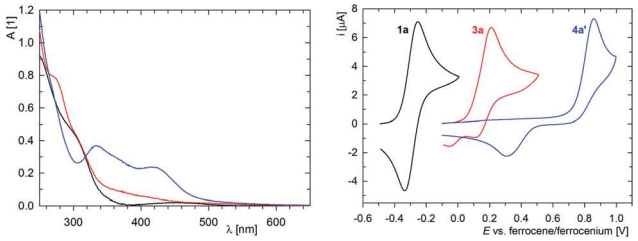

Fig. 2 (left) UV-Vis spectra of **1a**, **3a** and **4a′** (1×10^{-5} M solutions in CH_2Cl_2, optical path 1 cm) and (right) cyclic voltammograms of the same compounds (at glassy carbon electrode in CH_2Cl_2/0.1 M $Bu_4N[PF_6]$, scan rate 0.1 V s^{-1}).

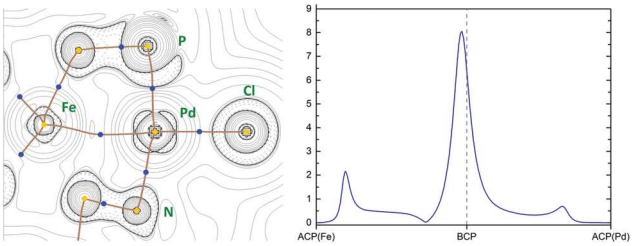

Fig. 3 (left) Laplacian contours (positive – full back lines, negative – dashed black lines), bond paths (brown lines), atomic critical points (ACP; yellow circles) and bond critical points (BCP; blue circles) in the plane intersecting atoms Pd, Fe and P of **4a***. Other types of critical points are omitted from the graph for clarity (right) Bond ellipticity along the bond path connecting the ACP of Fe and Pd in **4a***.

electron-withdrawing phosphine moiety, thereby facilitating ferrocene oxidation. In this context, it is worth mentioning that the $^1J_{PSe}$ coupling constant[17] 729 Hz, determined for phosphine selenide resulting from **1a**, compound **5a**, is lower than that of $FcP(Se)Ph_2$ (733 Hz; Fc = ferrocenyl),[18] suggesting only a minor increase in the basicity of the phosphine group in **1a** with respect to the parent phosphinoferrocene lacking the guanidine substituent. This in turn suggests that the electron-donating ability of the guanidine unit mainly affects the directly bonded ferrocene unit, while it is not efficiently transmitted further to the phosphine substituent.

Conversely, complex **3a** showed an irreversible oxidation at +0.22 V, *i.e.*, more positively shifted by nearly 0.5 V due to electron density transfer from the ligand to Pd.[19] Complex **4a** also gave rise to an irreversible oxidation, albeit shifted to an even higher potential (0.86 V).[20] Overall, the observed trend in the redox potentials matched the gradual increase in the donation from the ferrocene ligand to Pd upon coordination, converting the neutral P,N-complex into the cationic, P,N,Fe-ligated species.[21]

The Mössbauer spectra of **1a**, **3a**, and **4a′** recorded at ambient temperature (see ESI†) displayed symmetrical doublets with isomer shifts (IS) similar to those of the ferrocene itself (0.44 mm s^{-1}; see the ESI†).[19] The quadrupole splitting (QS) increased from **1a** (2.28 mm s^{-1}) to **3a** (2.30 mm s^{-1}) and, further, to **4a′** (2.48 mm s^{-1}), which also showed the largest IS (0.47 mm s^{-1}).

Complementarily, the bonding in Pd-**1** complexes was studied by DFT computations on **3a** and on the cation of **4a** (denoted henceforth as **4a***). A clear distinction between these species was suggested by the Pd–Fe Mayer Bond Orders (MBO's), which were 0.206 and 0.007 for **4a*** and **3a**, respectively. Additional evidence of a metal–metal interaction in **4a*** was provided by electron density topology analysis based on Atoms in Molecules (AIM),[22] which suggested a bond critical point (BCP) located approximately halfway on the bond path interconnecting the Fe and Pd atoms in **4a*** (Fig. 3), while no analogous BCP was found for **3a** (see ESI†).

The orbital character of the Fe–Pd interaction in **4a*** was analysed using the Lewis model derived from Natural Bond Orbital (NBO) theory.[23] Because of the weak nature of this interaction, NBO provided no evidence of a regular Pd–Fe bond but reported two significant Fe → Pd lone-pair delocalisations. The donor set on the iron for both these delocalisations arose from mixing its $3d_{x^2-y^2}$ and $3d_{z^2}$ orbitals in a nearly equal ratio. The first delocalisation from Fe to the Pd 5s valence acceptor had energy 24.77 kJ mol^{-1}, and the other involving Pd $5p_y$ Rydberg acceptor had energy 23.05 kJ mol^{-1}. The partitioning of the Pd–Fe overlap into two acceptor orbitals, together with the weak character of this interaction, increased the electron-density ellipticity at the corresponding BCP to ε = 6.40. This large ellipticity, suggesting an unstable BCP, is the result of confining the electron density mostly to one plane, while a slight displacement of its maximum with respect to the BCP along the bond path suggests a polarization of this metal–metal interaction (Fig. 3).

The metal–metal bonding in **4a*** was facilitated by the decrease in the population of the Pd 5s orbital, used otherwise for coordinating chloride ligands in **3a** (the 5s orbital occupancy 0.318 in **3a** decreased to 0.236 in **4a***). Unsurprisingly, the Pd atom attempts to compensate for its ligand loss by generating secondary interactions with the ferrocene moiety, which are absent in **3a** (MBO's below 0.01). In addition to the Fe–Pd interaction, notable overlaps were discernible with the ferrocene *ipso* carbons carrying the P and N atoms in **4a*** (MBO's 0.113 and 0.147). In conclusion, the Fe–Pd interaction in **4a*** occurs because the palladium alleviates its coordination unsaturation by overlapping with possible donors at the ferrocene moiety, including the electron-rich iron atom. Notably, significant asymmetry in the interactions between the Pd and the conventional donors (N, P, Cl) was evident from the topology results (Fig. 3, parameters in the ESI†). The BCP's located in the positive region of Laplacian for the harder donors (Cl, N) suggest considerable bond ionicity, while a mostly covalent interaction was found with the phosphine moiety. These findings were corroborated by NBO, which reported a single bond to P bond from Pd, with all remaining overlaps treated as delocalisations with this metal.

In summary, we reported here a facile and modular synthesis of phosphinoferrocene guanidines as new, donor-asymmetric ferrocene ligands and their coordination behaviour

towards Pd(II). Two series of mutually interconvertible Pd(II) complexes were synthesised and characterised in which the ligands behave as conventional P,N-chelating and as the rather exotic P,N,Fe-bound ligands forming weak Fe → Pd dative bonds. The guanidine moiety, which serves as a source of additional donor atoms in the ligands, allows the formation of rigid chelate complexes and, as a strongly electron-donating moiety, also renders the ferrocene moiety exceedingly electron rich, thereby facilitating the Pd–Fe interactions. The different ligating properties of the P and N donor atoms are reflected in the geometric and electronic asymmetry of the coordination sphere, which in turn correspond with the hybrid nature of the reported ligands.

Conflicts of interest

There are no conflicts to declare.

Acknowledgements

We acknowledge the support from the Czech Science Foundation (project no. 19-09334S).

Notes and references

1 D. Seyferth, B. W. Hames, T. G. Rucker, M. Cowie and R. S. Dickson, *Organometallics*, 1983, **2**, 472.
2 M. R. Ringenberg, *Chem. – Eur. J.*, 2019, **25**, 2396.
3 (*a*) *Ferrocenes: Ligands, Materials and Biomolecules*, ed. P. Štěpnička, Wiley, Chichester, 2008; (*b*) R. C. J. Atkinson, V. C. Gibson and N. J. Long, *Chem. Soc. Rev.*, 2004, **33**, 313; (*c*) R. Goméz Arrayás, J. Adrio and J. C. Carretero, *Angew. Chem., Int. Ed.*, 2006, **45**, 7674.
4 (*a*) S. Akabori, T. Kumagai, T. Shirahige, S. Sato, K. Kawazoe, C. Tamura and M. Sato, *Organometallics*, 1987, **6**, 526; (*b*) M. Sato, M. Sekino, M. Katada and S. Akabori, *J. Organomet. Chem.*, 1989, **377**, 327; (*c*) S. Takemoto, S. Kuwata, Y. Nishibayashi and M. Hidai, *Inorg. Chem.*, 1998, **37**, 6428.
5 (*a*) M. Sato, H. Shigeta, M. Sekino and S. Akabori, *J. Organomet. Chem.*, 1993, **458**, 199; (*b*) O. V. Gusev, A. M. Kalsin, M. G. Peterleitner, P. V. Petrovskii, K. A. Lyssenko, N. G. Akhmedov, C. Bianchini, A. Meli and W. Oberhauser, *Organometallics*, 2002, **21**, 3637; (*c*) M. A. Zuideveld, B. H. G. Swennenhuis, P. C. J. Kamer and P. W. N. M. van Leeuwen, *J. Organomet. Chem.*, 2001, **637–639**, 805; (*d*) P. W. N. M. van Leeuwen, M. A. Zuideveld, B. H. G. Swennenhuis, Z. Freixa, P. C. J. Kamer, K. Goubitz, J. Fraanje, M. Lutz and A. L. Spek, *J. Am. Chem. Soc.*, 2003, **125**, 5523; (*e*) K. M. Gramigna, J. V. Oria, C. L. Mandell, M. A. Tiedemann, W. G. Dougherty, N. A. Piro, W. S. Kassel, B. C. Chan, P. L. Diaconescu and C. Nataro, *Organometallics*, 2013, **32**, 5966; (*f*) B. L. Blass, R. Hernández Sánchez, V. A. Decker, M. J. Robinson, N. A. Piro, W. S. Kassel, P. L. Diaconescu and C. Nataro, *Organometallics*, 2016, **35**, 462; (*g*) K. D. Cabrera, A. T. Rowland, J. M. Szarko, P. L. Diaconescu, M. W. Bezpalko, W. S. Kassel and C. Nataro, *Dalton Trans.*, 2017, **46**, 5702.
6 (*a*) L. R. R. Klapp, C. Bruhn, M. Leibold and U. Siemeling, *Organometallics*, 2013, **32**, 5862. For structurally related compounds with ferrocene N,N-donors, see: (*b*) C. Metallinos, D. Tremblay, F. B. Barrett and N. J. Taylor, *J. Organomet. Chem.*, 2006, **691**, 2044; (*c*) M. Abubekerov, S. I. Khan and P. L. Diaconescu, *Organometallics*, 2017, **36**, 4394; (*d*) K. Jess, D. Baabe, T. Bannenberg, K. Brandhorst, M. Freytag, P. G. Jones and M. Tamm, *Inorg. Chem.*, 2015, **54**, 12032.
7 For recent examples, see: (*a*) K. Škoch, I. Císařová, F. Uhlík and P. Štěpnička, *Dalton Trans.*, 2018, **47**, 16082; (*b*) M. Zábranský, I. Císařová and P. Štěpnička, *Organometallics*, 2018, **37**, 1615; (*c*) M. Zábranský, I. Císařová, A. M. Trzeciak, W. Alsalahi and P. Štěpnička, *Organometallics*, 2019, **38**, 479; (*d*) F. Horký, I. Císařová, J. Schulz and P. Štěpnička, *J. Organomet. Chem.*, 2019, **891**, 44; (*e*) P. Vosáhlo, J. Schulz, K. Škoch, I. Císařová and P. Štěpnička, *New J. Chem.*, 2019, **43**, 4463; (*f*) K. Škoch, J. Schulz, I. Císařová and P. Štěpnička, *Organometallics*, 2019, **38**, 3060; (*g*) O. Bárta, I. Císařová, J. Schulz and P. Štěpnička, *New J. Chem.*, 2019, **43**, 11258; (*h*) K. Škoch, P. Vosáhlo, I. Císařová and P. Štěpnička, *Dalton Trans.*, 2020, **49**, 1011; (*i*) P. Štěpnička, *Coord. Chem. Rev.*, 2017, **353**, 223 and ref. 12.
8 (*a*) K.-S. Gan and T. S. A. Hor, *1,1'-Bis(diphenylphosphino) ferrocene. Coordination Chemistry, Organic Syntheses, and Catalysis in Ferrocenes: Homogeneous Catalysis, Organic Synthesis Materials Science*, ed. A. Togni and T. Hayashi, Wiley-VCH, Weinheim, 1995, ch. 1, pp. 3–104; (*b*) S. W. Chien and T. S. A. Hor, *The Coordination and Homogeneous Catalytic Chemistry of 1,1'-Bis(diphenylphosphino)ferrocene and its Chalcogenide Derivatives in Ferrocenes: Ligands, Materials and Biomolecules*, ed. P. Štěpnička, Wiley, Chichester, 2008, ch. 2, pp. 33–116.
9 Reviews: (*a*) K. H. Shaughnessy, *Chem. Rev.*, 2009, **109**, 643; (*b*) *Aqueous-Phase Organometallic Catalysis*, ed. B. Cornils and W. Herrmann, Wiley-VCH, Weinheim, 2nd edn, 2004. For phosphinoferrocene guanidinium salts, see: (*c*) H. Charvátová, I. Císařová and P. Štěpnička, *Eur. J. Inorg. Chem.*, 2017, 288; (*d*) O. Bárta, I. Císařová and P. Štěpnička, *Eur. J. Inorg. Chem.*, 2017, 489; (*e*) O. Bárta, I. Císařová, E. Mieczyńska, A. M. Trzeciak and P. Štěpnička, *Eur. J. Inorg. Chem.*, 2019, 4846.
10 (*a*) P. Machnitzki, M. Tepper, K. Wenz, O. Stelzer and E. Herdtweck, *J. Organomet. Chem.*, 2000, **602**, 158; (*b*) T. S. Teets, J. A. Labinger and J. E. Bercaw, *Organometallics*, 2013, **32**, 5530; (*c*) M. Carmona, J. Ferrer, R. Rodríguez, V. Passarelli, F. J. Lahoz, P. García-Orduña, L. Cañadillas-Delgado and D. Carmona, *Chem. – Eur. J.*, 2019, **25**, 13665.

11 (*a*) C. Alonso-Moreno, F. Carrillo-Hermosilla, A. Garcés, A. Otero, I. López-Solera, A. M. Rodríguez and A. Antiñolo, *Organometallics*, 2010, **29**, 2789.

12 K. Škoch, I. Císařová, J. Schulz, U. Siemeling and P. Štěpnička, *Dalton Trans.*, 2017, **46**, 10339.

13 D. Nieto, S. Bruña, A. González-Vadillo, J. Perles, F. Carrillo-Hermosilla, A. Antiñolo, J. M. Padrón, G. B. Plata and I. Cuadrado, *Organometallics*, 2015, **34**, 5407.

14 P. Štěpnička, I. Císařová and R. Gyepes, *Eur. J. Inorg. Chem.*, 2006, 926 and ref. 7*e*.

15 B. Cordero, V. Gómez, A. E. Platero-Prats, M. Revés, J. Echeverría, E. Cremades, F. Barragán and S. Alvarez, *Dalton Trans.*, 2008, 2832.

16 U. Salzner, *J. Chem. Theory Comput.*, 2013, **9**, 4064 and references cited therein.

17 (*a*) C. A. Tolman, *Chem. Rev.*, 1977, **77**, 313; (*b*) D. W. Allen and B. F. Taylor, *J. Chem. Soc., Dalton Trans.*, 1982, 51; (*c*) A. Muller, S. Otto and A. Roodt, *Dalton Trans.*, 2008, 650; (*d*) U. Beckmann, D. Süslüyan and P. C. Kunz, *Phosphorus, Sulfur Silicon Relat. Elem.*, 2011, **186**, 2061.

18 B. Milde, M. Lohan, C. Schreiner, T. Rüffer and H. Lang, *Eur. J. Inorg. Chem.*, 2011, 5437.

19 The difference in the first oxidation potentials of dppf and [$PdCl_2$(dppf-κ_2P,P')] is approximately 0.4 V: B. Corain, B. Longato, G. Favero, D. Ajò, G. Pilloni, U. Russo and F. R. Kreissl, *Inorg. Chim. Acta*, 1989, **157**, 259.

20 The primary oxidation of **4a′** is followed by further processes generating an electrochemically active species showing a pair of counter-waves at 0.31 and 0.42 V.

21 DFT computations showed significant contribution of iron-based orbitals to HOMO in all cases, see the ESI.†

22 R. F. W. Bader, *Chem. Rev.*, 1991, **91**, 893.

23 A. E. Reed, L. A. Curtiss and F. Weinhold, *Chem. Rev.*, 1988, **88**, 899.

Supporting Information

for

Synthesis and study of Fe → Pd interactions in unsymmetric Pd(II) complexes with phosphinoferrocene guanidine ligands

*Ondřej Bárta, Róbert Gyepes, Ivana Císařová, Adam Alemayehu and Petr Štěpnička**

Contents

EXPERIMENTAL

Materials and methods

All syntheses were performed under an argon atmosphere using standard Schlenk techniques. Solvents were purchased from Lach-Ner (Czech Republic, analytical grade) and used without further purification (typically during chromatography or for crystallisation). Tetrahydrofuran, methanol and dichloromethane (HPLC quality) utilised for syntheses were dried using a Pure Solv MD-5 solvent purification system (Innovative Technology, USA). Toluene was dried over sodium and distilled under an argon atmosphere. 1-(Diphenylphosphino)-1′-aminoferrocene was prepared by following the literature procedure.[1] Other starting materials were products of Merck, Alfa-Aesar and TCI and were used as received.

^{1}H, ^{13}C and ^{31}P NMR spectra were recorded at 25°C (unless otherwise stated) on a Varian INOVA 400 spectrometer operating at 399.95, 100.58, and 161.90 MHz, respectively. The chemical shifts (δ in ppm) are given relative to tetramethylsilane (^{1}H and ^{13}C) as internal reference, and to 85% aqueous H_3PO_4 (^{31}P) as external reference. FTIR spectra were recorded on a Nicolet 6700 FTIR spectrometer over the range of 400-4000 cm^{-1}. The spectra were collected in diffuse reflectance (DRIFTS) mode using samples diluted with KBr. ESI mass spectra were recorded with a Compact QTOF-MS spectrometer (Bruker Daltonics) from samples dissolved in HPLC-grade methanol. The UV-Vis absorption spectra were measured on a UNICAM UV 300 (Thermo Spectronic) spectrometer from dichloromethane solutions (c = $5 \cdot 10^{-5}$ M) in the range of 200-800 nm. Elemental analyses were determined with a Perkin–Elmer 2400 Series II CHNS/O analyser. The presence of residual solvent (if any) was confirmed by NMR analysis. Details of electrochemical and Mössbauer spectroscopy measurements as well as of theoretical computations are provided below.

The following abbreviations are used in the text below: fc = ferrocene-1,1′-diyl, *i*Pr = *iso*-propyl, Cy = cyclohexyl, Xyl = 2,6-dimethylphenyl (xylyl); vt and vq denote virtual triplets and quartets arising from the PPh_2- and N-substituted cyclopentadienyl rings in the ^{1}H NMR spectra.

Syntheses

General procedures for the synthesis of guanidines $Ph_2PfcN=C(NHR)_2$ (1)

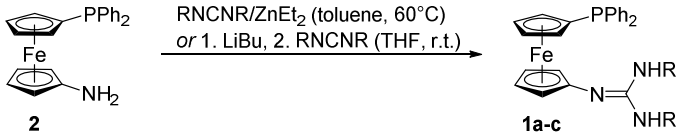

Method A (adopted from ref. [2]). 1-(Diphenylphosphino)-1′-aminoferrocene (**2**; 0.77 g, 2.0 mmol) was introduced into a flask equipped with a stirring bar and a condenser, and argon atmosphere was established. Dry toluene (40 mL) was introduced via syringe followed by a solution of the respective carbodiimide (2.2 mmol) in toluene (10 mL). Finally, diethylzinc (0.2 mL of 1M solution in hexanes, 0.2 mmol) was added and the resulting orange solution was heated at 60 °C for the indicated time (3 hours for R = *i*Pr, 5 hours for R = Cy, and overnight for R = Xyl) during which time the solution turned red. After cooling to room temperature, the reaction was terminated by adding dry methanol (1 mL), and the turbid, dark orange solution was filtered through a Celite pad. A crude product obtained by evaporation of the filtrate (typically as an orange viscous oil) was further purified depending on the guanidine substitution as described below.

Method B. 1-(Diphenylphosphino)-1′-aminoferrocene (**2**; 0.77 g, 2.0 mmol) was dissolved in dry tetrahydrofuran (15 mL) under argon atmosphere. The orange solution was cooled on ice and *n*-butyllithium (1.25 mL of 1.6 M solution in hexanes, 2.0 mmol) was added dropwise, whereupon the mixture turned red. The solution was stirred for 15 minutes while cooling and then a solution of the appropriate carbodiimide (2.0 mmol) in dry tetrahydrofuran (10 mL) was added (the colour of the reaction mixture turned orange again). The resulting solution was stirred at room temperature for 2 hours and then the reaction was terminated by water addition (5 mL). The organic phase was separated and the aqueous phase was extracted with diethyl ether (5 mL). Combined organic fractions were washed with brine (5 mL) and dried over magnesium sulfate. Subsequent filtration and evaporation under reduced pressure afforded a crude product, which was further purified depending on the substitution pattern.

Note: Both methods are optimised to provide almost quantitative conversion of the starting materials. Thus, the purification procedures described below are applicable for both methods.

***N*-[1′-(diphenylphosphino)ferrocene-1-yl]-*N*′,*N*′′-bis(1-methylethyl)guanidine (1a).** The crude product was crystallised from hot hexane (ca. 50 mL). Tiny orange needles, that developed while the solution was gradually cooled to 4 °C, were isolated, washed with pentane and dried

under vacuum. Yield of **1a** for *method A*: 0.87 g (85%), for *method B*: 0.76 g (74%); orange crystalline solid. Crystals suitable for structure determination were obtained analogously.

^{1}H NMR ($CDCl_3$): δ 1.18 (d, $^{3}J_{HH}$ = 6.4 Hz, 12 H, CHMe_2), 3.77 (broad s, 2 H, C*H*Me_2), 3.96 (m, 4 H, CH of fc), 4.08 (vq, J' = 1.9 Hz, 2 H, CH of fc), 4.38 (vt, J' = 1.7 Hz, 2 H, CH of fc), 7.27-7.32 (m, 6 H, CH of PPh_2), 7.33-7.39 (m, 4 H, CH of PPh_2). Signals due to guanidine NH were not observed. ^{13}C{^{1}H} NMR ($CDCl_3$): δ 23.49 (s, CHMe_2), 42.87 (broad s, *C*HMe_2), 62.19 (s, CH of fc), 66.16 (d, J_{CP} = 2 Hz, CH of fc), 71.58 (d, J_{CP} = 4 Hz, CH of fc), 72.76 (d, J_{CP} = 14 Hz, CH of fc), 75.04 (d, $^{1}J_{CP}$ = 5 Hz, C^{ipso}–P of fc), 106.89 (s, C^{ipso}–N of fc), 128.06 (d, J_{CP} = 7 Hz, CH of PPh_2), 128.29 (s, CH of PPh_2), 133.42 (d, J_{CP} = 19 Hz, CH of PPh_2), 139.16 (d, $^{1}J_{CP}$ = 10 Hz, C^{ipso} of PPh_2), 150.72 (s, C^{ipso} of guanidine). ^{31}P{^{1}H} NMR ($CDCl_3$): δ –16.5 (s). ESI+ MS: *m*/*z* 512 ([M + H]$^{+}$); ESI– MS: *m*/*z* 510 ([M – H]$^{-}$). FTIR (DRIFTS): ν_{max} 3401 m, 3353 m, 3092 w, 3068 w, 3052 w, 2977 m, 2930 w, 2871 w, 1594 s, 1530 s, 1479 s, 1463 m, 1433 m, 1380 m, 1363 m, 1343 w, 1302 w, 1292 w, 1256 w, 1191 w, 1178 m, 1158 m, 1133 w, 1086 w, 1024 m, 892 w, 856 w, 844 w, 820 m, 812 w, 802 w, 743 s, 720 w, 698 s, 654 w, 542 w, 521 w, 508 w, 492 m, 483 m, 459 w, 442 w cm^{-1}. Anal. Calc. for $C_{29}H_{34}FeN_3P$ (511.4): C 68.11, H 6.70, N 8.22%. Found: C 68.11, H 6.90, N 8.12%.

***N*-[1′-(diphenylphosphino)ferrocene-1-yl]-*N*′,*N*′′-dicyclohexylguanidine (1b).** The crude product was purified by column chromatography on silica gel. Firstly, non-polar impurities and traces of the starting materials were removed using hexane/ethyl acetate 3:1 (v/v) and then the mobile phase was changed to hexane/ethyl acetate/triethylamine 25:25:1 mixture and the major orange band due to the product was collected and evaporated. The orange waxy residue was lyophilised and residual solvents were removed under high vacuum. Yield of **1b** for *method A*: 1.06 g (90%), for *method B*: 1.02 g (86%); light orange powder. The compound is hygroscopic.

^{1}H NMR ($CDCl_3$): δ 1.04-1.42 (m, 10 H, Cy), 1.56-1.78 (m, 6 H, Cy), 1.92-2.04 (m, 4 H, Cy), 3.37 (broad s, 2 H, Cy), 3.96 (vt, J' = 1.8 Hz, 2 H, CH of fc), 3.97 (vt, J' = 1.7 Hz, 2 H, CH of fc), 4.07 (vq, J' = 1.8 Hz, 2 H, CH of fc), 4.38 (vt, J' = 1.7 Hz, 2 H, CH of fc), 7.27-7.32 (m, 6 H, CH of PPh_2), 7.32-7.39 (m, 4 H, CH of PPh_2). Signals due to guanidine NH were not observed. ^{13}C{^{1}H} NMR ($CDCl_3$): δ 25.10 (s, Cy), 25.65 (s, Cy), 33.99 (s, Cy), 50.10 (broad s, Cy), 62.17 (s, CH of fc), 66.25 (s, CH of fc), 71.67 (d, J_{CP} = 4 Hz, CH of fc), 72.75 (d, J_{CP} = 14 Hz, CH of fc), 74.94 (d, $^{1}J_{CP}$ = 5 Hz, C^{ipso}–P of fc), 106.94 (s, C^{ipso}–N of fc), 128.06 (d, J_{CP} = 7 Hz, CH of PPh_2), 128.30 (s, CH of PPh_2), 133.44 (d, J_{CP} = 19 Hz, CH of PPh_2), 139.13 (d, $^{1}J_{CP}$ = 10 Hz, C^{ipso} of PPh_2), 150.72 (s, C^{ipso} of guanidine). ^{31}P{^{1}H} NMR ($CDCl_3$): δ –16.5 (s). ESI+ MS: *m*/*z* 592 ([M + H]$^{+}$); ESI– MS: *m*/*z* 590 ([M – H]$^{-}$). FTIR (DRIFTS): ν_{max} 3343 m, 3068 w, 3050 w, 2928 s, 2852 s, 1608 s, 1521 s, 1477 s, 1450 m, 1433 m, 1382 m, 1365 w, 1343 m, 1255 w, 1235 w, 1191 w, 1158 m, 1135 m, 1113 w, 1091 w, 1026 m, 889 w, 822 m, 743 s, 697 s, 631 w, 519 w, 489 m, 456 w cm^{-1}. Anal. Calc. for $C_{35}H_{42}FeN_3P{\cdot}½H_2O$ (600.6): C 70.00, H 7.22, N 7.00%. Found: C 70.08, H 7.05, N 7.05%.

***N*-[1′-(diphenylphosphino)ferrocene-1-yl]-*N*′,*N*′′-bis(2,6-dimethylphenyl)guanidine (1c).** The crude product was purified by column chromatography on silica gel using hexane/ethyl acetate 3:1 (v/v) mixture as an eluent. After a pale yellow band of unreacted phosphinoamine **2** was removed, the mobile phase was changed to hexane/ethyl acetate/triethylamine 25:25:1 mixture and the major orange band containing the product was collected and evaporated. The resulting orange viscous oil was crystallised from hot heptane (ca. 30 mL). Orange prisms (also used for structure determination) obtained by cooling the solution gradually to room temperature were isolated by suction, washed with pentane and dried under vacuum. Yield of **1c** for *method A*: 1.05 g (82%), for *method B*: 0.97 g (76%); orange crystalline solid.

^{1}H NMR (toluene-d$_8$, –25°C): δ 1.96 (s, 6 H, CH$_3$), 2.42 (s, 6 H, CH$_3$), 3.63 (vt, *J*′ = 1.9 Hz, 2 H, CH of fc), 4.08 (vq, *J*′ = 1.8 Hz, 2 H, CH of fc), 4.29 (s, 1 H, NH), 4.32 (vt, *J*′ = 1.7 Hz, 2 H, CH of fc), 4.46 (vt, *J*′ = 1.9 Hz, 2 H, CH of fc), 4.85 (s, 1 H, NH), 6.71 (d, J_{HH} = 7.6 Hz, 2 H, aromatics), 6.82 (t, J_{HH} = 7.5 Hz, 1 H, aromatics), 6.94-7.06 (m, 7 H, aromatics), 7.19 (d, J_{HH} = 7.5 Hz, 2 H, aromatics), 7.30-7.42 (m, 4 H, aromatics). ^{1}H NMR (toluene-d$_8$, 100°C): δ 2.27 (s, 12 H, CH$_3$), 3.76 (vt, *J*′ = 2.0 Hz, 2 H, CH of fc), 4.07 (vq, *J*′ = 1.9 Hz, 2 H, CH of fc), 4.24 (vt, *J*′ = 1.7 Hz, 2 H, CH of fc), 4.36 (s, 2 H, CH of fc), 4.94 (broad s, 2 H, NH), 6.87-6.93 (m, 2 H, aromatics), 6.95-7.11 (m, 10 H, aromatics), 7.36-7.43 (m, 4 H, aromatics). ^{31}P{^{1}H} NMR (CDCl$_3$, 25°C): δ –17.1 (s, major tautomer), –19.3 (s, minor tautomer). ESI+ MS: *m*/*z* 636 ([M + H]$^+$), 668 ([M + MeOH + H]$^+$); ESI– MS: *m*/*z* 634 ([M – H]$^-$), 666 ([M + MeOH – H]$^-$). FTIR (DRIFTS): ν_{max} 3423 m, 3365 m, 3086 w, 3066 w, 3051 w, 3012 w, 2974 w, 2959 w, 2917 w, 2852 w, 1659 s, 1589 m, 1568 w, 1538 s, 1476 s, 1432 m, 1390 m, 1365 m, 1354 m, 1295 m, 1249 w, 1235 w, 1213 m, 1193 m, 1179 w, 1159 m, 1094 m, 1068 w, 1061 w, 1044 w, 1028 m, 1022 m, 994 w, 979 w, 943 w, 914 w, 885 w, 867 w, 848 w, 826 m, 796 w, 776 m, 762 m, 746 s, 700 s, 632 w, 621 w, 521 w, 493 m, 453 m, 441 w cm^{-1}. Anal. Calc. for $C_{39}H_{38}FeN_3P$ (635.6): C 73.70, H 6.03, N 6.61%. Found: C 73.52, H 6.01, N 6.54%.

Preparation of complexes cis-[PdCl$_2${Ph$_2$PfcN=C(NHR)$_2$-κ^{2}P,N}] (3) for R = iPr, Cy.

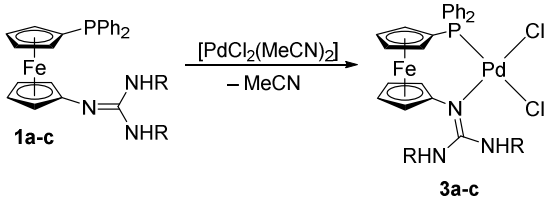

This method is applicable only for the *iso*-propyl and cyclohexyl substituted guanidines, where *cis*-[PdCl$_2${Ph$_2$PfcN=C(NHR)$_2$-κ^2*P*,*N*}] is the dominant product (traces of the corresponding **4**-type complexes are also detected). For the xylyl-substituted ligand, this protocol leads to a mixture of three major coordination species (see the main text).

Bis(acetonitrile)dichloropalladium(II) (130 mg, 0.5 mmol) and the respective ligand **1** (0.5 mmol) were dissolved in dry dichloromethane (15 mL) under argon atmosphere. The dark red solution was stirred at room temperature for 2 hours and then was filtered through a PTFE syringe filter (0.45 μm pore size) and evaporated under vacuum. Sonication of the dark red crude product in a minimum amount of acetone (ca. 5 mL) resulted in the formation of precipitate, which was collected, washed with pentane and dried under vacuum.

***cis*-[PdCl$_2${Ph$_2$PfcN=C(NHiPr)$_2$-κ^2*P*,*N*}] (3a).** Following the general procedure, 317 mg of rusty brown powder was isolated. Recrystallization by liquid phase diffusion of methyl *tert*-butyl ether into a dichloromethane solution of the product over several days afforded 286 mg (83%) of **3a** as red crystals. Crystals suitable for structure determination were obtained by diffusion of diethyl ether vapours into a chloroform solution of the compound.

^{1}H NMR (CD_2Cl_2): δ 1.22 (broad s, 12 H, CH*Me*$_2$), 3.34-4.16 (very broad s, 2 H, C*H*Me$_2$), 3.96 (m, 1 H, CH of fc), 4.24 (m, 1 H, CH of fc), 4.29 (m, 1 H, CH of fc), 4.39 (m, 1 H, CH of fc), 4.49 (m, 1 H, CH of fc), 4.72 (m, 1 H, CH of fc), 5.37 (m, 1 H, CH of fc), 5.60 (m, 1 H, CH of fc), 7.28-7.34 (m, 2 H, CH of PPh$_2$), 7.35-7.43 (m, 3 H, CH of PPh$_2$), 7.45-7.52 (m, 2 H, CH of PPh$_2$), 7.55-7.62 (m, 1 H, CH of PPh$_2$), 7.91-8.00 (m, 2 H, CH of PPh$_2$). Signals due to guanidine NH were not observed. ^{13}C{^{1}H} NMR (CD_2Cl_2): δ 23.76 (s, CH*Me*$_2$), 47.18 (s, *C*HMe$_2$), 65.81 (s, CH of fc), 68.82 (s, CH of fc), 68.99 (s, CH of fc), 69.67 (s, CH of fc), 71.66 (d, $^1J_{CP}$ = 60 Hz, C^{ipso}–P of fc), 71.82 (d, J_{CP} = 6 Hz, CH of fc), 74.43 (d, J_{CP} = 10 Hz, CH of fc), 76.10 (d, J_{CP} = 4 Hz, CH of fc), 78.56 (d, J_{CP} = 20 Hz, CH of fc), 111.62 (d, J_{CP} = 2 Hz, C^{ipso}–N of fc), 127.94 (d, J_{CP} = 12 Hz, CH of PPh$_2$), 128.93 (d, J_{CP} = 11 Hz, CH of PPh$_2$), 129.69 (d, $^1J_{CP}$ = 51 Hz, C^{ipso} of PPh$_2$), 130.48 (d, J_{CP} = 3 Hz, CH of PPh$_2$), 131.94 (d, J_{CP} = 3 Hz, CH of PPh$_2$), 132.89 (d, J_{CP} = 10 Hz, CH of PPh$_2$), 133.12 (d, $^1J_{CP}$ = 57 Hz, C^{ipso} of PPh$_2$), 134.53 (d, J_{CP} = 11 Hz, CH of PPh$_2$), 160.87 (s, C^{ipso} of guanidine). ^{31}P{^{1}H} NMR (CD_2Cl_2): δ 26.3 (s). ESI+ MS: *m*/*z* 616 ([M – HCl – Cl]$^+$), 654 ([M – Cl]$^+$). FTIR (DRIFTS): ν_{max} 3288 s, 2974 m, 2959 w, 2928 w, 2867 w, 1578 s, 1560 s, 1482 m, 1463 m, 1435 m, 1405 w, 1387 m, 1365 w, 1322 m, 1308 w, 1256 w, 1196 w, 1171 m, 1130 w, 1099 m, 1090 w, 1030 w, 1020 m, 818 m, 751 m, 746 m, 708 w, 696 s, 632 w, 526 s, 506 m, 477 s cm^{-1}. Anal. Calc. for $C_{29}H_{34}Cl_2FeN_3PPd$ (688.8): C 50.57, H 4.98, N 6.10%. Found: C 50.05, H 4.79, N 5.81%. The samples isolated from chlorinated solvents are typically contaminated with another species (ca. 3%), presumably [PdCl$_3$(**1aH**-κ*P*)].[3]

***cis*-[PdCl$_2${Ph$_2$PfcN=C(NHCy)$_2$-κ^2*P*,*N*}] (3b).** General procedure provided 321 mg (83%) of **3b** as a rusty powder. Crystals used for structure determination were obtained by liquid-phase diffusion of hexane into a 1,2-dichloroethane solution of the product. The precipitated product is sufficiently pure for further synthesis. An analytical sample was obtained by recrystallization as

described. However, partial decomposition of the product during the recrystallization was observed. Consequently, the yield decreased to only 196 mg (51%) of red crystals of **3b**.

^{1}H NMR (CD_2Cl_2): δ 0.90-2.10 (m, 20 H, Cy), 2.90-3.70 (very broad s, 2 H, Cy), 3.97 (m, 1 H, CH of fc), 4.24 (m, 1 H, CH of fc), 4.28 (m, 1 H, CH of fc), 4.38 (m, 1 H, CH of fc), 4.47 (m, 1 H, CH of fc), 4.74 (m, 1 H, CH of fc), 5.35 (m, 1 H, CH of fc), 5.69 (m, 1 H, CH of fc), 7.27-7.43 (m, 5 H, CH of PPh_2), 7.43-7.52 (m, 2 H, CH of PPh_2), 7.55-7.63 (m, 1 H, CH of PPh_2), 7.88-7.97 (m, 2 H, CH of PPh_2). Signals due to guanidine NH were not observed. ^{13}C{^{1}H} NMR (CD_2Cl_2): δ 25.27 (broad s, Cy), 25.63 (s, Cy), 34.32 (broad s, Cy), 65.78 (s, CH of fc), 68.82 (s, CH of fc), 68.91 (s, CH of fc), 69.56 (s, CH of fc), 71.65 (d, J_{CP} = 6 Hz, CH of fc), 71.84 (d, J_{CP} = 60 Hz, C^{ipso}–P of fc), 74.55 (d, J_{CP} = 10 Hz, CH of fc), 76.07 (d, J_{CP} = 4 Hz, CH of fc), 78.57 (d, J_{CP} = 20 Hz, CH of fc), 111.68 (d, J_{CP} = 2 Hz, C^{ipso}–N of fc), 127.91 (d, J_{CP} = 11 Hz, CH of PPh_2), 128.90 (d, J_{CP} = 11 Hz, CH of PPh_2), 129.72 (d, $^1J_{CP}$ = 51 Hz, C^{ipso} of PPh_2), 130.45 (d, J_{CP} = 3 Hz, CH of PPh_2), 131.89 (d, J_{CP} = 2 Hz, CH of PPh_2), 132.91 (d, J_{CP} = 10 Hz, CH of PPh_2), 133.03 (d, $^1J_{CP}$ = 56 Hz, C^{ipso} of PPh_2), 134.50 (d, J_{CP} = 10 Hz, CH of PPh_2), 160.64 (s, C^{ipso} of guanidine). ^{31}P{^{1}H} NMR (CD_2Cl_2): δ 25.7 (s). ESI+ MS: 728 ([M – Cl – HCl + MeOH]$^+$). FTIR (DRIFTS): ν_{max} 3402 w, 3277 m, 3120 w, 3059 w, 3002 w, 2931 s, 2852 m, 1574 s, 1568 sh, 1482 m, 1449 s, 1436 s, 1405 w, 1389 w, 1355 m, 1331 w, 1304 m, 1275 w, 1259 w, 1236 m, 1208 w, 1195 w, 1169 m, 1149 w, 1102 m, 1090 w, 1051 w, 1028 m, 1000 w, 979 w, 944 w, 889 w, 873 w, 857 w, 842 w, 818 m, 748 s, 709 m, 691 s, 669 w, 648 m, 632 m, 564 w, 535 m, 520 s, 500 m, 477 s, 441 w, 429 w cm^{-1}. Anal. Calc. for $C_{35}H_{42}Cl_2FeN_3PPd{\cdot}CHCl_3$ (888.3): C 48.68, H 4.88, N 4.73%. Found: C 48.77, H 4.81, N 4.60%. Analytical sample was obtained from chloroform. Similarly to the previous case, samples isolated from chlorinated solvents typically contain trace amounts of other species (ca. 3%), most likely [$PdCl_3$(**1bH**-κ*P*)].[3]

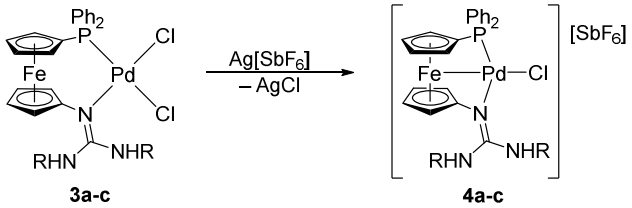

3a-c **4a-c**

Preparation of [PdCl{Ph$_2$PfcN=C(NHiPr)$_2$-κ^{3}P,N,Fe}][SbF$_6$] (4a). A mixture of **3a** (138 mg, 0.2 mmol) and silver(I) hexafluoroantimonate (69 mg, 0.2 mmol) in dry dichloromethane (10 mL) was stirred at room temperature for 2 hours with a protection from direct day light. The resulting dark red suspension was filtered through a PTFE syringe filter (pore size 0.45 μm). The filtrate was concentrated to ca. 3 mL and layered with methyl *tert*-butyl ether. Crystallisation over several days afforded dark red crystals (also used for structure determination), which were isolated by suction, washed with diethyl ether and dried under vacuum. Yield of **4a**: 125 mg (70%), dark red crystals.

^{1}H NMR (CD_2Cl_2): δ 1.28 (d, $^{3}J_{HH}$ = 6.4 Hz, 12 H, CH*Me*$_2$), 3.31 (vt, J' = 2.1 Hz, 2 H, CH of fc), 3.35 (m, 2 H, CH of fc), 3.65 (d of sept, $^{3}J_{HH}$ = 8.4 Hz, $^{3}J_{HH}$ = 6.4 Hz, 2 H, C*H*Me$_2$), 5.70 (vt, J' = 2.2 Hz, 2 H, CH of fc), 5.78 (m, 2 H, CH of fc), 6.59 (very broad s, 2 H, NH), 7.50-7.55 (m, 4 H, CH of PPh_2), 7.59-7.66 (m, 2 H, CH of PPh_2), 8.13-8.21 (m, 4 H, CH of PPh_2). ^{13}C{^{1}H} NMR (CD_2Cl_2): δ 22.91 (s, CH*Me*$_2$), 46.38 (s, *C*HMe$_2$), 61.15 (d, $^{1}J_{CP}$ = 50 Hz, C^{ipso}–P of fc), 66.26 (s, CH of fc), 73.92 (d, J_{CP} = 11 Hz, CH of fc), 80.82 (s, CH of fc), 86.79 (d, J_{CP} = 8 Hz, CH of fc), 98.05 (d, J_{CP} = 4 Hz, C^{ipso}–N of fc), 124.48 (d, $^{1}J_{CP}$ = 60 Hz, C^{ipso} of PPh_2), 129.77 (d, J_{CP} = 12 Hz, CH of PPh_2), 133.34 (d, J_{CP} = 3 Hz, CH of PPh_2), 135.59 (d, J_{CP} = 13 Hz, CH of PPh_2), 158.71 (s, C^{ipso} of guanidine). ^{31}P{^{1}H} NMR (CD_2Cl_2): δ –5.1 (s). ESI+ MS: *m*/*z* 616 ([M – SbF_6 – HCl]$^+$), 654 ([M – SbF_6]$^+$). FTIR (DRIFTS): ν_{max} 3303 m, 3251 m, 3129 w, 2980 w, 2966 w, 1593 s, 1565 s, 1485 s, 1465 m, 1439 m, 1404 m, 1390 m, 1371 w, 1344 w, 1317 w, 1286 w, 1186 w, 1170 w, 1152 w, 1129 w, 1108 m, 1093 w, 1045 w, 843 m, 756 m, 743 w, 720 w, 703 m, 688 w, 661 s, 656 sh, 644 m, 627 w, 535 m, 517 m, 493 w, 481 w, 462 w cm^{-1}. Anal. Calc. for $C_{29}H_{34}ClF_6FeN_3PPdSb$ (889.1): C 39.18, H 3.85, N 4.73%. Found: C 39.13, H 3.76, N 4.62%.

Preparation of [PdCl{Ph$_2$PfcN=C(NHiPr)$_2$-κ^{3}P,N,Fe}][BF$_4$] (4a′). *Method A*. A mixture of **3a** (138 mg, 0.2 mmol) and silver(I) tetrafluoroborate (39 mg, 0.2 mmol) in dry dichloromethane (10 mL) was stirred at room temperature for 2 hours. The resulting dark red suspension was filtered through a PTFE syringe filter (pore size 0.45 μm). The filtrate was concentrated to the volume of ca. 3 mL and layered with methyl *tert*-butyl ether. Crystallisation over several days afforded dark red crystals, which were isolated, washed with diethyl ether and dried under vacuum. Yield of **4a′**: 108 mg (73%), dark red crystals.

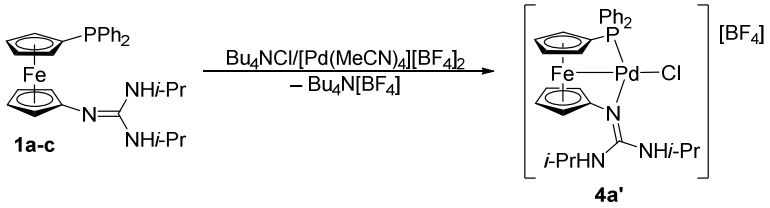

Method B. A mixture of **1a** (102 mg, 0.2 mmol), tetrakis(acetonitrile)palladium(II) tetrafluoroborate (89 mg, 0.2 mmol) and tetrabutylammonium chloride (56 mg, 0.2 mmol) in dry dichloromethane (10 mL) was stirred at room temperature for 2 hours. The resulting dark red solution was filtered through a PTFE syringe filter (pore size 0.45 μm). The filtrate was concentrated to ca. 3 mL and layered with methyl *tert*-butyl ether. Crystallisation over several days afforded dark red crystals, which were isolated, washed with diethyl ether and dried under vacuum. Yield of **4a′**: 97 mg (66%), dark red crystals.

^{1}H NMR (CD_2Cl_2): δ 1.28 (d, $^{3}J_{HH}$ = 6.4 Hz, 12 H, CH*Me*$_2$), 3.29 (vt, J' = 2.1 Hz, 2 H, CH of fc), 3.34 (m, 2 H, CH of fc), 3.68 (d of sept, $^{3}J_{HH}$ = 8.4 Hz, $^{3}J_{HH}$ = 6.4 Hz, 2 H, C*H*Me$_2$), 5.78 (vt, J' = 2.2 Hz,

2 H, CH of fc), 5.85 (m, 2 H, CH of fc), 6.73 (very broad s, 2 H, NH), 7.49-7.56 (m, 4 H, CH of PPh_2), 7.58-7.65 (m, 2 H, CH of PPh_2), 8.13-8.22 (m, 4 H, CH of PPh_2). $^{13}C\{^1H\}$ NMR (CD_2Cl_2): δ 20.94 (s, CH*Me*$_2$), 44.40 (s, *C*HMe$_2$), 59.37 (d, $^1J_{CP}$ = 50 Hz, C^{ipso}–P of fc), 64.27 (s, CH of fc), 72.02 (d, J_{CP} = 11 Hz, CH of fc), 79.21 (s, CH of fc), 85.21 (d, J_{CP} = 8 Hz, CH of fc), 96.49 (d, J_{CP} = 4 Hz, C^{ipso}–N of fc), 122.80 (d, $^1J_{CP}$ = 60 Hz, C^{ipso} of PPh_2), 127.81 (d, J_{CP} = 12 Hz, CH of PPh_2), 131.34 (d, J_{CP} = 3 Hz, CH of PPh_2), 133.66 (d, J_{CP} = 13 Hz, CH of PPh_2), 156.90 (s, C^{ipso} of guanidine). $^{31}P\{^1H\}$ NMR (CD_2Cl_2): δ –4.6 (s). ESI+ MS: *m*/*z* 616 ([M – BF_4 – HCl]$^+$), 652 ([M – BF_4]$^+$). FTIR (DRIFTS): 3297 m, 3256 m, 3118 m, 3065 w, 2977 m, 2933 w, 2875 w, 1593 s, 1564 s, 1485 s, 1460 m, 1440 m, 1405 m, 1390 m, 1371 m, 1345 m, 1316 m, 1283 m, 1188 w, 1167 m, 1152 m, 1129 m, 1104 s, 1066 s, 1035 s, 999 m, 927 w, 913 w, 848 m, 780 w, 760 m, 743 m, 721 w, 704 m, 691 m, 655 w, 627 m, 535 m, 519 m, 502 m, 490 m, 484 m, 462 m, 431 w cm^{-1}. Anal. Calc. for $C_{29}H_{34}BClF_4FeN_3PPd$ (740.1): C 47.06, H 4.63, N 5.68%. Found: C 46.92, H 4.47, N 5.39%.

Preparation of [PdCl{Ph$_2$PfcN=C(NHCy)$_2$-κ^{3}P,N,Fe}][SbF$_6$] (4b). A mixture of **3b** (154 mg, 0.2 mmol) and silver(I) hexafluoroantimonate (69 mg, 0.2 mmol) in dry dichloromethane (10 mL) was stirred at room temperature for 2 hours. The resulting dark red suspension was filtered through a PTFE syringe filter (pore size 0.45 μm) and evaporated. Diffusion of pentane vapours into a fluorobenzene solution of the crude product resulted in the formation of dark crystalline solid, which was collected, washed with pentane and dried under vacuum. Yield of **4b**: 138 mg (71%), dark brown-red microcrystalline solid. Thus obtained material tends to retain traces of fluorobenzene as indicated by NMR analysis (see the spectra below). Crystals used for structure determination were obtained by liquid-phase diffusion of hexane into a fluorobenzene solution.

^1H NMR (CD_2Cl_2): δ 1.16-1.46 (m, 10 H, Cy), 1.56-1.68 (m, 2 H, Cy), 1.74-1.86 (m, 4 H, Cy), 1.92-2.02 (m, 4 H, Cy), 3.20-3.30 (m, 2 H, Cy), 3.30 (vt, *J*′ = 2.1 Hz, 2 H, CH of fc), 3.35 (vq, *J*′ = 2.3 Hz, 2 H, CH of fc), 5.71 (vt, *J*′ = 2.1 Hz, 2 H, CH of fc), 5.79 (vq, *J*′ = 1.9 Hz, 2 H, CH of fc), 7.49-7.56 (m, 4 H, CH of PPh_2), 7.59-7.65 (m, 2 H, CH of PPh_2), 8.12-8.22 (m, 4 H, CH of PPh_2). Signal(s) due guanidine NH were not observed due to broadening. $^{13}C\{^1H\}$ NMR (CD_2Cl_2): δ 25.09 (s, Cy), 25.48 (s, Cy), 33.40 (s, Cy), 61.10 (d, J_{CP} = 50 Hz, C^{ipso}–P of fc), 66.40 (s, CH of fc), 73.93 (d, J_{CP} = 11 Hz, CH of fc), 80.74 (s, CH of fc), 86.78 (d, J_{CP} = 8 Hz, CH of fc), 97.79 (s, C^{ipso}–N of fc), 124.47 (d, J_{CP} = 60 Hz, C^{ipso} of PPh_2), 129.77 (d, J_{CP} = 12 Hz, CH of PPh_2), 133.35 (d, J_{CP} = 3 Hz, CH of PPh_2), 135.59 (d, J_{CP} = 13 Hz, CH of PPh_2), 158.37 (s, C^{ipso} of guanidine). $^{31}P\{^1H\}$ NMR (CD_2Cl_2): δ –5.2 (s, PPh_2). ESI+ MS: 728 ([M – SbF_6 – HCl + MeOH]$^+$). FTIR (DRIFTS): ν_{max} 3380 w, 3245 w, 3120 w, 2933 s, 2856 m, 1595 s, 1556 s, 1482 s, 1450 m, 1438 s, 1404 m, 1369 m, 1351 m, 1312 w, 1288 w, 1263 w, 1243 w, 1189 w, 1151 w, 1103 m, 1042 w, 1029 w, 891 w, 845 m, 750 m, 716 w, 702 m, 693 m, 660 s, 564 w, 534 m, 517 m, 484 m, 468 m cm^{-1}. Anal. Calcd for $C_{35}H_{42}ClF_6FeN_3PPdSb{\cdot}CHCl_3$

(1088.5): C 39.72, H 3.98, N 3.86%. Found: C 39.99, H 3.92, N 3.89% (analytical sample free of fluorobenzene residua was obtained from chloroform).

Preparation of [PdCl{Ph$_2$PfcN=C(NHXyl)$_2$-κ^{3}P,N,Fe}][SbF$_6$] (4c). A mixture of **1c** (127 mg, 0.2 mmol) and bis(acetonitrile)dichloropalladium(II) (52 mg, 0.2 mmol) in dry dichloromethane (5 mL) was stirred at room temperature for 2 hours. The resulting dark red solution was transferred via cannula into a solution of silver(I) hexafluoroantimonate (69 mg, 0.2 mmol) in dry dichloromethane (5 mL). The resulting dark red suspension was stirred at room temperature for an additional 1 hour and then filtered through a PTFE syringe filter (pore size 0.45 μm). The filtrate was concentrated to approximately 3 mL and layered with methyl *tert*-butyl ether. Crystallisation over several days afforded dark red crystals (also used for structure determination), which were isolated, washed with diethyl ether and dried under vacuum. Yield of **4c**: 142 mg (70%), dark red crystalline solid.

^{1}H NMR (CD_2Cl_2): δ 2.18 (s, 6 H, CH_3), 2.55 (s, 6 H, CH_3), 2.99 (vt, J' = 2.0 Hz, 2 H, CH of fc), 3.28 (vq, J' = 2.3 Hz, 2 H, CH of fc), 5.13 (vt, J' = 2.0 Hz, 2 H, CH of fc), 5.68 (vq, J' = 1.8 Hz, 2 H, CH of fc), 5.97 (s, 1 H, NH), 6.98 (d, J_{HH} = 7.6 Hz, 2 H, CH of Xyl), 7.15 (t, J_{HH} = 7.6 Hz, 1 H, CH of Xyl), 7.26-7.33 (m, 3 H, CH of Xyl), 7.50-7.56 (m, 4 H, CH of PPh_2), 7.59-7.65 (m, 2 H, CH of PPh_2), 8.13-8.21 (m, 4 H, CH of PPh_2), 10.16 (s, 1 H, NH). ^{13}C{^{1}H} NMR (CD_2Cl_2): δ 18.68 (s, CH_3), 19.00 (s, CH_3), 60.65 (d, $^1J_{CP}$ = 50 Hz, C^{ipso}–P of fc), 66.69 (s, CH of fc), 73.67 (d, J_{CP} = 11 Hz, CH of fc), 79.90 (s, CH of fc), 86.87 (d, J_{CP} = 8 Hz, CH of fc), 94.33 (d, J_{CP} = 4 Hz, C^{ipso}–N of fc), 124.26 (d, $^1J_{CP}$ = 61 Hz, C^{ipso} of PPh_2), 129.46 (s, CH of Xyl), 129.78 (s, CH of Xyl), 129.80 (d, J_{CP} = 12 Hz, CH of PPh_2), 129.84 (s, 2× CH of Xyl), 132.36 (s, C^{ipso}–N of Xyl), 132.57 (s, C^{ipso}–N of Xyl), 133.39 (d, J_{CP} = 3 Hz, CH of PPh_2), 135.54 (d, J_{CP} = 13 Hz, CH of PPh_2), 137.34 (s, C^{ipso}–CH_3 of Xyl), 138.12 (s, C^{ipso}–CH_3 of Xyl), 155.01 (d, J_{CP} = 4 Hz, C^{ipso} of guanidine). ^{31}P{^{1}H} NMR (CD_2Cl_2): δ –5.6 (s). ESI+ MS: 776 ([M – SbF_6]$^+$). FTIR (DRIFTS): ν_{max} 3336 m, 3219 w, 3119 w, 3068 w, 2977 w, 1604 s, 1584 s, 1534 s, 1483 m, 1471 m, 1438 m, 1404 w, 1380 w, 1361 w, 1328 w, 1312 w, 1293 w, 1207 w, 1188 w, 1168 w, 1106 m, 1071 w, 1035 w, 999 w, 847 m, 781 m, 749 m, 719 w, 704 m, 691 m, 660 s, 630 w, 538 w, 528 m, 519 m, 505 w, 476 m, 464 m, 445 w cm^{-1}. Anal. Calc. for $C_{39}H_{38}ClF_6FeN_3PPdSb$ (1013.2): C 46.23, H 3.78, N 4.15%. Found: C 46.00, H 3.64, N 3.94%.

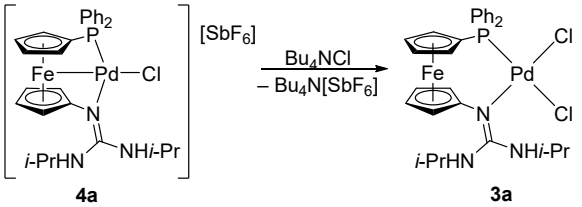

4a **3a**

Reaction of [PdCl{Ph$_2$PfcN=C(NHiPr)$_2$-κ^{3}P,Fe,N}][SbF$_6$] (4a) with tetrabutylammonium chloride. A mixture of **4a** (44 mg, 0.05 mmol) and tetrabutylammonium chloride (14 mg, 0.05

mmol) in dry dichloromethane (2 mL) was stirred at room temperature for 1 hour after which time the volatiles were evaporated under vacuum. The red residue was triturated with acetone. Brick red precipitate was isolated and washed repeatedly with acetone and diethyl ether. The crude product was further crystallised by diffusion of diethyl ether into a dichloromethane solution. After several days, 28 mg (81%) of red crystals was isolated and identified as *cis*-[$PdCl_2${$Ph_2PfcN=C(NHiPr)_2$-κ^2*P*,*N*}] (**3a**) by NMR spectroscopy.

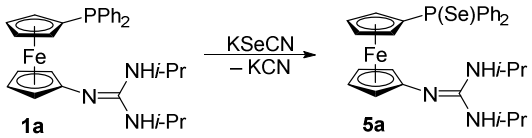

Preparation of a phosphino selenide $Ph_2P(Se)fcN=C(NHiPr)_2$ (5a). Following a literature method,[4] mixture of **1a** (128 mg, 0.250 mmol) and potassium selenocyanate (40 mg, 0.275 mmol) in dry methanol (5 mL) was stirred with exclusion of direct day light at room temperature overnight. Next day, the resulting orange solution was evaporated under reduced pressure. The orange waxy residue was redissolved in ethyl acetate and filtered through a short pad of Celite to remove inorganic salts. The clear orange filtrate was evaporated and the residue was recrystallized from hot heptane. Cooling the solution gradually to 4 °C resulted in a formation of orange crystals, which were isolated by suction, washed with pentane and dried under vacuum. Yield of **5a**: 101 mg (68%), orange crystalline solid.

^{1}H NMR ($CDCl_3$): δ 1.18 (d, $^3J_{HH}$ = 6 Hz, 12 H, CH*Me*$_2$), 3.73 (broad s, 2 H, C*H*Me$_2$), 3.99 (vt, J' = 1.9 Hz, 2 H, CH of fc), 4.14 (vt, J' = 1.9 Hz, 2 H, CH of fc), 4.44 (vq, J' = 2.0 Hz, 2 H, CH of fc), 4.53 (vq, J' = 1.7 Hz, 2 H, CH of fc), 7.36-7.47 (m, 6 H, CH of P(Se)Ph$_2$), 7.68-7.76 (m, 4 H, CH of P(Se)Ph$_2$). Signals due to NH of guanidine were not observed. ^{13}C{^{1}H} NMR ($CDCl_3$): δ 23.44 (s, CH*Me*$_2$), 42.92 (s, C*H*Me$_2$), 62.89 (s, CH of fc), 67.61 (s, CH of fc), 72.83 (d, $^1J_{CP}$ = 90 Hz, C_{ipso}–P of fc), 73.22 (d, J_{CP} = 12 Hz, CH of fc), 73.33 (d, J_{CP} = 10 Hz, CH of fc), 108.29 (s, C^{ipso}–N of fc), 128.11 (d, J_{CP} = 13 Hz, CH of P(Se)Ph$_2$), 131.06 (d, J_{CP} = 3 Hz, CH of P(Se)Ph$_2$), 132.06 (d, J_{CP} = 11 Hz, CH of P(Se)Ph$_2$), 133.78 (d, $^1J_{CP}$ = 78 Hz, C^{ipso} of P(Se)Ph$_2$), 150.99 (s, C^{ipso} of guanidine). ^{31}P{^{1}H} NMR ($CDCl_3$): δ 32.4 (s with ^{77}Se satellites, $^1J_{PSe}$ = 729 Hz, P(Se)Ph$_2$). ESI+ MS: *m*/*z* 592 ([M + H]$^+$). FTIR (DRIFTS): ν_{max} 3386 m, 3328 m, 3087 w, 3072 w, 3046 w, 3031 w, 2974 m, 2951 m, 2931 w, 2867 w, 1592 s, 1540 s, 1475 s, 1434 m, 1386 m, 1366 m, 1343 m, 1311 w, 1304 w, 1291 w, 1257 m, 1206 w, 1175 m, 1165 s, 1099 m, 1082 w, 1074 w, 1056 w, 1034 m, 1018 m, 998 w, 943 w, 893 w, 865 w, 832 m, 820 w, 812 w, 753 m, 745 m, 721 m, 711 m, 704 m, 696 m, 691 m, 653 m, 624 m, 587 m, 572 s, 536 m, 486 s, 478 m, 446 m, 430 w cm^{-1}. Anal. Calc. for $C_{29}H_{34}FeN_3PSe$ (590.4): C 59.00, H 5.80, N 7.12%. Found: C 58.69, H 5.84, N 6.96%.

X-RAY CRYSTALLOGRAPHY

Full-sphere diffraction data ($\pm h \pm k \pm l$, θ_{max} = 27.5°) were collected using a Nonius Kappa CCD diffractometer equipped with an Apex II image plate detector (**1c**) or a Bruker D8 VENTURE Kappa Duo diffractometer with a PHOTON10 detector (all other compounds), both equipped with a Cryostream Cooler (Oxford Cryosystems). Graphite monochromated Mo Kα radiation (λ = 0.71073 Å) was used in all cases.

The structures were solved by direct methods (SHELXT-2014[5]) and then refined by full-matrix least quares based on F^2 (SHELXL-2014 or 2017[6]). All non-hydrogen atoms were refined with anisotropic displacement parameters. The guanidine hydrogen atoms (NH) were located on difference density maps and subsequently refined as riding atoms with U_{iso}(H) set to 1.2U_{eq}(N). Hydrogens residing on the carbon atoms were included in their theoretical positions and were refined analogously. Particular details of structure refinement are as follows. The crystals of **4b** were inversion twins (space group $P2_1$). The refined contributions from the two enantiomeric domains were 88:12. Finally, the solvent molecule in the structure of **4c**·1/4CH_2Cl_2 was partly disordered around the crystallographic inversion centres and was modelled over two positions. Selected crystallographic data and refinement parameters are summarised in Table S1.

All geometric calculations were performed and the structural diagrams were obtained using the recent version of PLATON program.[7] Numerical values were rounded to one decimal place with respect to their estimated deviations (ESDs). Parameters pertaining to atoms in geometrically constrained positions (hydrogens) are given without ESDs.

Table S1. Summary of relevant crystallographic data and refinement parameters

Compound	**1a**	**1c**	**3a**	**3b**
Formula	$C_{29}H_{34}FeN_3P$	$C_{39}H_{38}FeN_3P$	$C_{29}H_{34}Cl_2FeN_3PPd$	$C_{35}H_{42}Cl_2FeN_3PPd$
M	511.41	635.54	688.71	768.83
Crystal system	monoclinic	triclinic	monoclinic	triclinic
Space group	$P2_1/c$ (no. 14)	$P\bar{1}$ (no. 2)	$P2_1/n$ (no. 14)	$P\bar{1}$ (no. 2)
T/K	150(2)	120(2)	150(2)	120(2)
a/Å	9.5758(4)	10.1594(5)	13.2176(5)	11.7326(6)
b/Å	33.194(1)	12.8169(6)	13.0451(4)	11.9790(6)
c/Å	8.9652(3)	14.602(1)	16.9643(7)	12.1754(6)
α/°	90	115.562(2)	90	84.599(1)
β/°	115.621(1)	96.014(2)	98.462(2)	75.101(1)
γ/°	90	106.604(2)	90	81.174(2)
V/Å^3	2569.5(2)	1585.5(2)	2893.2(2)	1631.4(1)
Z	4	2	4	2
F(000)	1080	668	1400	788
μ(Mo Kα)/mm^{-1}	0.672	0.559	1.387	1.239
Diffrns collected	34672	22259	66149	32420
Indep diffrns	5903	7258	6626	7490
Observed[a] diffrns	5135	6455	5709	7086
R_{int}[b]/%	2.43	2.18	4.59	1.94
No. of parameters	311	401	338	389
R[b] obsd diffrns/%	2.80	2.99	2.36	1.95
R, wR[b] all data/%	3.53, 6.95	3.51, 7.43	3.22, 5.55	2.13, 4.77
Δρ/e Å^{-3}	0.28, –0.36	0.46, –0.26	0.86, –0.62	0.46, –0.58

[a] Diffractions with $I > 2\sigma(I)$. [b] Definitions: $R_{int} = \Sigma \left| F_o^2 - F_o^2(\text{mean}) \right| / \Sigma F_o^2$, where F_o^2(mean) is the average intensity of symmetry-equivalent diffractions. $R = \Sigma \left| \left| F_o \right| - \left| F_c \right| \right| / \Sigma \left| F_o \right|$, $wR = [\Sigma\{w(F_o^2 - F_c^2)^2\}/\Sigma w(F_o^2)^2]^{1/2}$.

Table S1 continued

Compound	**4a**	**4b**	**4c**·1/4CH_2Cl_2
Formula	$C_{29}H_{34}ClF_6FeN_3PPdSb$	$C_{35}H_{42}ClF_6FeN_3PPdSb$	$C_{39.25}H_{38.50}Cl_{1.50}F_6FeN_3PPdSb$
M	889.01	969.13	1034.37
Crystal system	monoclinic	monoclinic	triclinic
Space group	$P2_1/c$ (no. 14)	$P2_1$ (no.4)	$P\bar{1}$ (no. 2)
T/K	150(2)	120(2)	120(2)
a/Å	16.6294(3)	10.5019(6)	10.8536(5)
b/Å	10.3070(2)	10.3649(6)	11.6697(5)
c/Å	20.8488(4)	17.1490(9)	17.6614(8)
α/°	90	90	97.120(1)
β/°	105.720(1)	103.169(2)	106.206(1)
γ/°	90	90	108.550(1)
V/Å^3	3439.8(1)	1817.6(2)	1980.1(2)
Z	4	2	2
F(000)	1752	964	1025
μ(Mo Kα)/mm^{-1}	1.893	1.800	1.691
Diffrns collected	31019	31988	40664
Indep diffrns	7899	8246	9024
Observed[a] diffrns	7428	8207	8646
R_{int}[b]/%	1.57	1.45	2.42
No. of parameters	392	443	503
R[b] obsd diffrns/%	2.22	1.24	2.37
R, wR[b] all data/%	2.44, 5.49	1.26, 3.17	2.49, 6.06
Δρ/e Å^{-3}	1.76, –0.66	0.42, –0.45	1.49, –1.46

The structures of **1a** and **1c** (Figures S1 and S2, data in Table S2) comprise regular ferrocene moiety, showing similar Fe-C distances and tilt angles of approximately 65.5° (**1a**) and 1.4° (**1c**). Conformation of the 1,1'-disubstituted ferrocene units differ in both compounds. While the cyclopentadienyl rings in the isopropyl-substituted guanidine **1a** adopt an approximately 1,2' conformation[8] ($\tau \approx 84°$; ideal value: 72°), those of **1c** bearing the sterically more demanding 2,6-xylyl substituents at the guanidine nitrogens assume a more opened conformation with $\tau \approx 129°$. The geometry of the phosphine substituent is unexceptional and compares well with that in (diphenylphosphino)ferrocene.[9] The guanidine fragments bonding to the other cyclopentadienyl ring are planar (within approximately 0.01 Å) and show pronounced variation in the individual C-N bonds according to their type (amine *vs*. imine). The dihedral angles between the least-squares guanidine planes {C23, N1, N2, N3} and the cyclopentadienyl rings C(6-10) are 24.72(8)° in **1a** and 8.09(9)° in the more bulky guanidine **1c**.

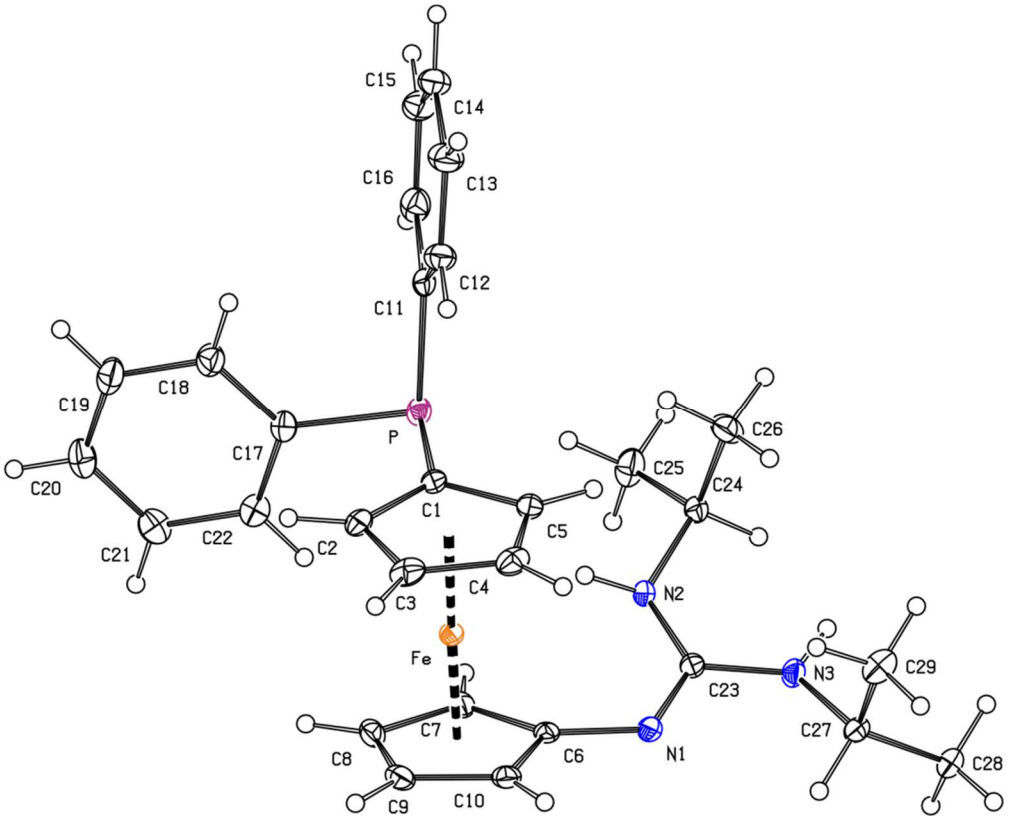

Figure S1. View of the molecular structure of **1a** showing the displacements ellipsoids at the 30% probability level.

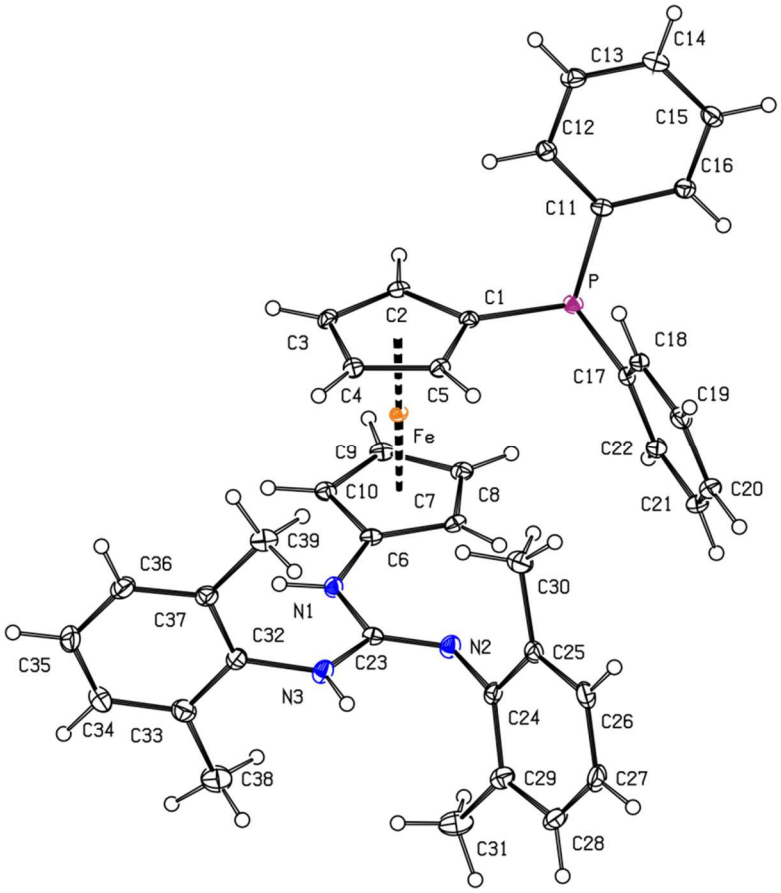

Figure S2. View of the molecular structure of **1c** with 30% probability displacements ellipsoids.

Table S2. Selected distances and angles for **1a** and **1c** (in Å and deg)

Parameter[a]	**1a**	**1c**
Fe-Cg1/Fe-Cg2	1.6421(8)/1.6581(8)	1.6510(7)/1.6649(7)
∠Cp1,Cp2	5.52(8)	1.39(9)
T	84.2(1)	129.4(1)
P-C1	1.809(2)	1.817(2)
P-C11/P-C17	1.837(2)/1.843(2)	1.838(2)/1.838(2)
C6-N1	1.395(2)	1.405(2)
C23-N1	1.308(2)	1.376(2)
C23-N2	1.371(2)	1.282(2)
C23-N3	1.366(2)	1.376(2)
N1-C23-N2/N3	126.0(1)/117.6(1)	120.6(2)/114.5(1)
N2-C23-N3	116.3(1)	124.9(2)
N2-C24/N3-C*n*[b]	1.472(2)/ 1.462(2)	1.413(2)/1.436(2)

[a] Cp1 and Cp2 are the cyclopentadienyl rings C(1-5) and C(6-10), respectively; Cg1/Cg2 denote their corresponding centroids. τ torsion angle C1-Cg1-Cg2-C6. [b] *n* = 27 for **1a**, *n* = 32 for **1c**.

The crystal structures of dichloride complexes **3a** and **3b** (Figure S3 and Table S3) share many common features. The presence of different ligating fragments causes a distortion of the coordination environment around Pd from a regular square in both cases. There have been reported no crystal structure for a similar compound in the Cambridge Structural Database (*viz.*, a $PdCl_2$ complex featuring a P,N-chelating ferrocene ligand whose donor atoms are directly attached to the ferrocene scaffold)[10] and, hence, the structural parameters can only be compared to [$LPdCl_2$] complexes featuring analogous *symmetrical* bidentate ligands. Thus, the Pd-N bond lengths, which are the shortest among Pd-donor distances, are only slightly shorter than those in a complex featuring 1,1'-bis([4,5-dimethyl-1,3-diisopropyl-1,3-dihydro-2*H*-imidazol-2-ylidene]-amino)ferrocene as ligand L (2.088(2) Å),[11] while the Pd-P distances in **3a** and **3b** are similar to those determined for [$PdCl_2$(dppf)] (2.283(1) and 2.301(1) Å for 1/1 chloroform solvate at room temperature; dppf =1,1'-bis(diphenylphosphino)ferrocene).[12] The asymmetry of the chelating ligand reflects further to the $PdCl_2$ fragment, wherein the chemically non-equivalent Pd-Cl bonds are affected by *trans*-influence (Pd-Cl2 > Pd-Cl1).[13] Notably, however, the coordination spheres of the Pd atoms exert only marginal angular distortions. The smallest interligand angle in both structures is the N1-Pd-Cl1 angle (≈86°), while the angle associated with the P,N-chelating ligand departs from the ideal value (90°) only insignificantly. This indeed corresponds with the τ_4 index[14] of 0.06 and 0.09 for **3a** and **3b**, respectively, which are very close to the value expected for ideally planar arrangement (τ_4 = 0).

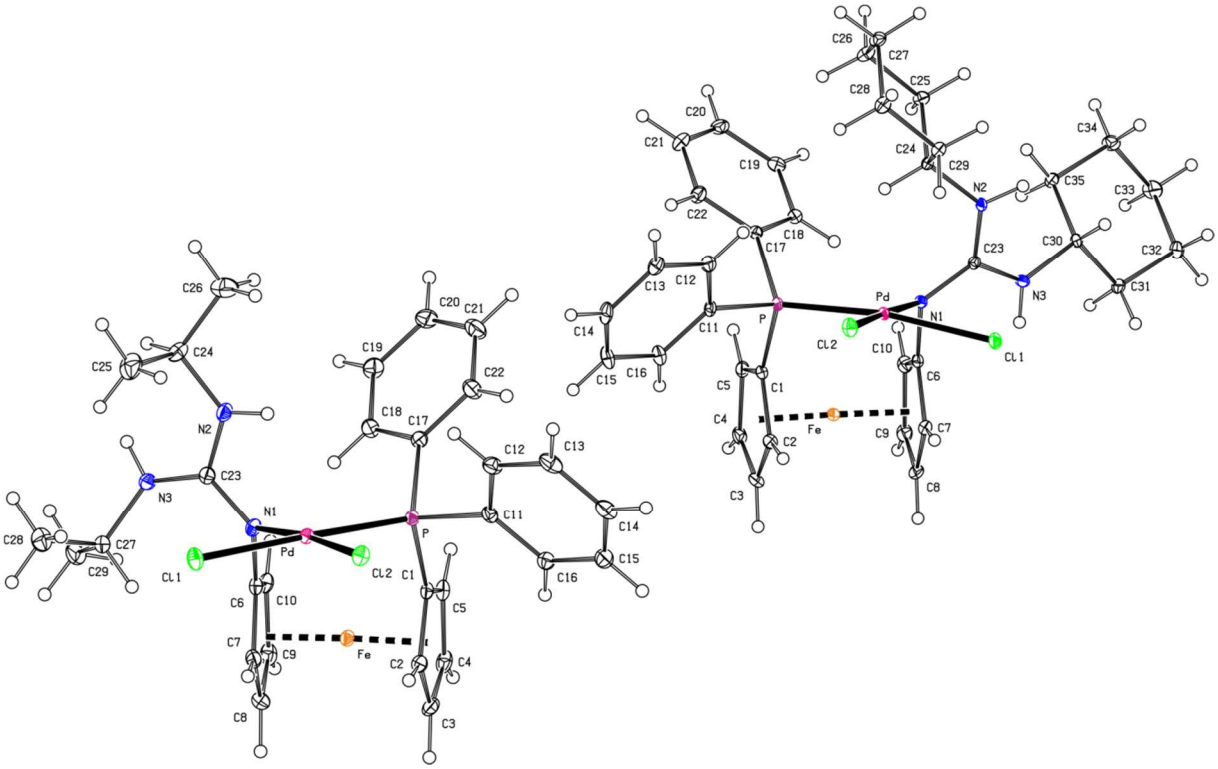

Figure S3. Views of the molecular structure of **3a** (left) and **3b** (right) showing displacement ellipsoids scaled to the 30% probability level.

The ferrocene cyclopentadienyls in **3a** and **3b** are tilted by approximately 5° and assume eclipsed conformations (1,1') that corresponds with chelate coordination of the phosphino-guanidine ligands. The P-C bonds in **3a** are slightly yet statistically significantly shorter than in the free ligand **1a**, presumably as the result of electron density shift from the aromatic rings towards phosphorus caused by donation of the phosphorus lone pair (P → Pd). In addition, the coordination results in an elongation of the N1-C6 and C23-N1 bonds and shortening of the remaining C23-N2 and C23-N3 bonds more distant from the coordination site. The guanidine planes {C23, N1, N2, N2 } are twisted with respect to their bonding cyclopentadienyl rings (*cf*. the dihedral angles 68.0(1)° and 71.24(9)° for **3a** and **3b**, respectively).

Table S3. Selected distances and angles for **3a** and **3b** (in Å and deg)

Parameter[a]	**3a**	**3b**
Pd-P	2.2711(6)	2.2776(4)
Pd-N1	2.043(2)	2.061(1)
Pd-Cl1	2.3688(6)	2.3828(4)
Pd-Cl2	2.2863(6)	2.2906(5)
P-Pd-N1	91.43(5)	90.85(4)
Cl1-Pd-Cl2	89.96(2)	89.88(2)
P-Pd-Cl2	91.89(2)	92.96(2)
N1-Pd-Cl1	86.59(5)	86.36(4)
Fe-Cg1/Fe-Cg2	1.644(1)/ 1.647(1)	1.6417(7)/1.6433(7)
∠Cp1,Cp2	4.9(1)	5.03(9)
τ	–1.4(1)	–5.7(1)
P-C1	1.792(2)	1.800(2)
P-C11/P-C17	1.817(2)/1.829(2)	1.817(2)/1.829(2)
C6-N1	1.414(3)	1.422(2)
C23-N1	1.337(3)	1.343(2)
C23-N2	1.344(3)	1.338(2)
C23-N3	1.340(3)	1.348(2)
N1-C23-N2/N3	116.6(2)/124.0(2)	122.0(1)/120.2(1)
N2-C23-N3	119.4(2)	117.9(1)
N2-C24/N3-C*n*[b]	1.467(3)/1.473(3)	1.468(2)/1.469(2)

[a] The parameters are defined as for free ligands (see footnotes to Table S2). [b] *n* = 27 for **3a**, *n* = 30 for **3b**.

When compared with their parent compounds **3**, the cationic complexes **4** (Figure S4 and Table S4) generally exhibit shorter Pd-P bonds, practically identical Pd-N distances and Pd-Cl bond lengths similar to the Pd-Cl1 bonds in **3**, which are elongated due to *trans* influence of the phosphine donors. The coordination spheres of Pd in **4a-c** show considerable angular distortions: the palladium atom is displaced from the midpoint of the formal coordination plane defined by the Fe, P, N and Cl atoms towards the terminal chloride. This can be illustrated by the P-Pd-N1 angles 163.01(6)° in **4a**, 162.46(5)° in **4b**, and 163.15(5)° in **4c**, and also by the *cis* interligand angles, which increase from P/N1-Pd-Fe (≈80-82°) through P-Pd-Cl (≈95°) to N1-Pd-Cl (≈102°). In contrast, the Fe-Pd-Cl diagonal is practically linear (174.85(2)° for **4a**, 175.52(5) for **4b**, and 176.81(2)° for **4c**) and the distance between palladium atom and the ferrocene iron (2.76-2.80 Å) is in all cases slightly longer than the sum of the respective covalent radii (1.39 Å for Pd and 1.32 Å for low-spin Fe).[15]

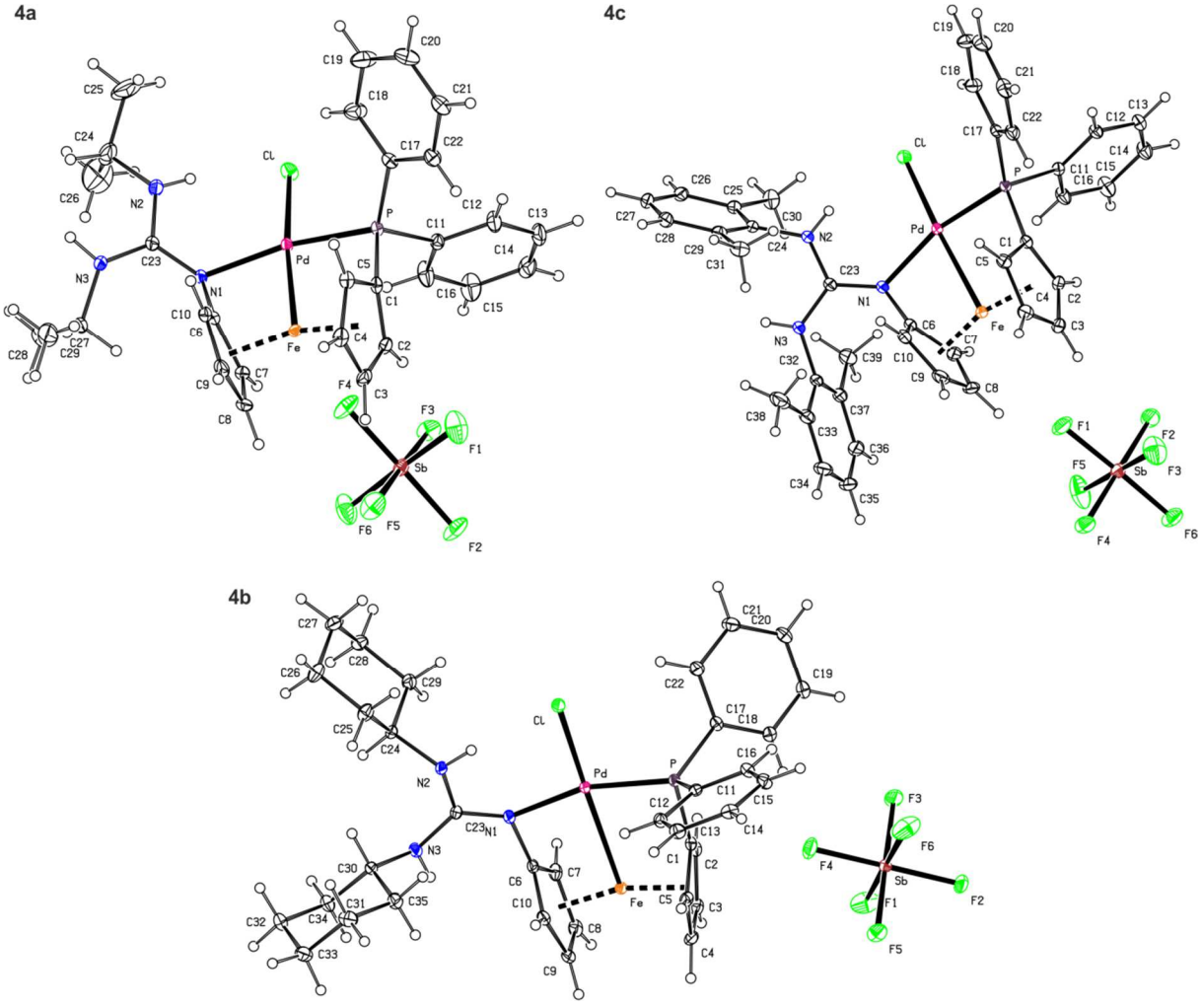

Figure S4. Views of the structures of **4a**, **4b** and **4c**·1/4CH_2Cl_2 (*N.B.* the solvent molecule in the structure of **4c**·1/4CH_2Cl_2 was omitted for clarity). Displacement ellipsoids enclose the 30% probability level.

Because of the palladium ion penetrating towards the iron atom, the ferrocene cyclopentadienyls are tilted by approximately 25° in **4a** and by 23° in the other two complexes, while they assume an eclipsed conformation ($\tau < 6°$), fixed by P,N-chelate coordination. The opening of the ferrocene core results in an elongation of the Fe-C bonds, mainly at the open side bearing the P and N1 donor atoms (*i.e.*, of the Fe-C1 and Fe-C6 bonds). An inspection of the structural data for free ligand **1a** and both its complexes (**3a** and **4a**) revealed that the P-C bond of the coordinated phosphine moiety in **4a** are shorter than in the free ligands and even in the dichloride complexes (**1a** > **3a** > **4a**). While decreasing the differentiation (= increasing the conjugation) of the guanidine C-N bonds, the coordination results in elongation of the C6-N1 bond. Still, however, this bond remains the shortest among the N-C(terminal) bonds (ca. 1.38 Å *vs*. the N-C(iPr/Cy) and N-Xyl bonds of 1.48 and 1.44 Å, respectively). This in turn brings the C6 atom into the proximity of the Pd atom (Pd-C6 = 2.471(2) Å for **4a**, 2.542(2) Å for **4b**, and 2.541(2) Å for **4c**; *N.B*. the distance between Pd and C1 of ca. 2.9 Å is substantially longer due to the longer P-C bond) and allows for additional interactions as suggested by DFT computations (see the main text). The guanidine planes {C23,N1,N2,N3} in **4a-c** are twisted with respect to their bonding cyclopentadienyl rings C(6-10), the interplanar angles being 61.2(1)° in **4a**, 75.9(1)° in **4b**, and 71.1.(1)° in **4c**.

Table S4. Selected distances and angles for **4a**, **4b** and **4c**·1/4CH_2Cl_2 (in Å and deg)

Parameter[a]	**4a**	**4b**	**4c**·1/4CH_2Cl_2
Pd-Fe	2.7590(5)	2.7956(5)	2.7821(5)
Pd-P	2.1947(7)	2.1822(6)	2.1850(6)
Pd-N1	2.084(2)	2.051(2)	2.065(2)
Pd-Cl	2.3755(6)	2.3352(6)	2.3514(6)
P-Pd-Cl	95.24(2)	95.09(2)	94.99(2)
P-Pd-Fe	80.25(2)	82.25(2)	82.63(2)
N1-Pd-Cl	101.62(6)	102.33(5)	101.86(5)
N1-Pd-Fe	82.99(5)	80.23(5)	80.53(5)
Fe-Cg1/Fe-Cg2	1.698(1)/1.709(1)	1.700(1)/1.695(1)	1.696(1)/1.692(1)
∠Cp1,Cp2	24.6(1)	22.8(1)	23.0(1)
τ	–5.9(2)	3.7(2)	–4.5(2)
P-C1	1.775(2)	1.773(2)	1.771(2)
P-C11/P-C17	1.803(2)/1.807(2)	1.804(2)/1.802(2)	1.803(2)/1.802(2)
C6-N1	1.379(3)	1.388(3)	1.384(3)
C23-N1	1.342(3)	1.323(3)	1.329(3)
C23-N2	1.337(3)	1.344(3)	1.339(3)
C23-N3	1.337(3)	1.365(3)	1.352(3)
N1-C23-N2/N3	117.9(2)/123.1(2)	118.7(2)/122.4(2)	117.9(2)/123.1(2)
N2-C23-N3	119.0(2)	118.9(2)	118.9(2)
N2-C24/N3-C*n*[b]	1.490(4)/1.477(4)	1.479(3)/1.478(3)	1.435(3)/1.440(3)

[a] The parameters are defined as for free ligands (see footnotes to Table S2). [b] n = 27 for **4a**, n = 30 for **4b**, and n = 32 for **4c**.

ELECTROCHEMISTRY

Cyclic voltammograms were recorded with a multipurpose potentiostat μAUTOLAB III (Eco Chemie, Netherlands) at room temperature using a standard three-electrode cell with glassy carbon disc electrode (2 mm diameter) as the working electrode, platinum sheet auxiliary electrode, and Ag/AgCl (KCl) reference electrode. The compounds were dissolved in anhydrous dichloromethane to give a solution containing 1 mM of the analysed compound and 0.1 M $Bu_4N[PF_6]$ (Fluka, purissimum for electrochemistry) as the supporting electrolyte. The solutions were deaerated with argon before the measurement and then kept under an argon blanket. Decamethylferrocene (Alfa-Aesar) was added as an internal standard for the final scans, and the redox potentials were converted into the ferrocene/ferrocenium scale by subtracting 0.548 V.[16]

Representative cyclic voltammograms are shown in Figure S5. Compound **1a** displays a reversible oxidation at $E^{\circ\prime}$ = −0.29 V (determined as a mean of the cathodic and anodic peak potentials), which is followed by additional irreversible redox transitions at higher potentials.[17] The fact that **1a** is oxidized more easily than ferrocene itself can be explained by a strong electron donating ability of the guanidine moiety, which prevails over the weakly electron-withdrawing influence of the phosphine moiety (*N.B.* (diphenylphosphino)ferrocene is oxidised at approximately 65 mV *vs*. the ferrocene/ferrocenium reference;[17] this indeed corresponds with the value of the Hammett's σ_p constant for the PPh_2 moiety of 0.19[18]).

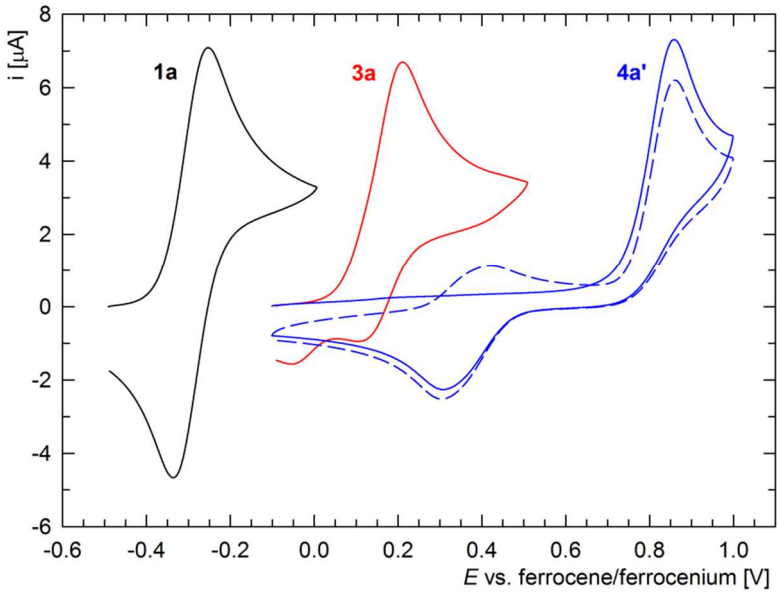

Figure S5. Cyclic voltammograms of **1a**, **3a** and **4a'** (first scan in full line, second scan in dashed line) as recorded at 0.1 V s^{-1} scan rate on glassy carbon electrode on 1 mM solutions containing 0.1 M Bu_4NPF_6 as the base electrolyte.

Complex **3a** exhibits an essentially irreversible wave at 0.22 V, which is approximately shifted by ≈0.5 V with respect to the oxidation of the free ligand. This shift can be attributed to a lower electron density at the ferrocene core resulting from a diminished electron-donating ability of the *coordinated* guanidine moiety. A further anodic shift is noted for complex **4a'** showing an irreversible oxidation wave at 0.86 V. In this case, the first oxidation results in the formation of another redox-active species, giving rise to a pair of waves at approximately 0.31 and 0.42 V during the second scan (Figure S5). Overall, the shift of the redox waves due to **3a** and **4a'** suggests a decrease of the electron density at the ferrocene moiety by coordination and, in the second case, also by the loss of the negatively charged chloride ligand from the Pd centre.

MÖSSBAUER SPECTROSCOPY

The Mössbauer spectra (Figure S6) were recorded at room temperature in transmission mode (sample concentration: 30 mg cm^{-2}) using ^{57}Co deposited in a Rh matrix as the γ-ray source, moving with constant acceleration over the velocity range from −10 to 10 mm s^{-1}, and NaI:Tl scintillation detector. The spectrometer (Wissel, Germany) was calibrated by using α-Fe foil, which was also utilised as the reference for isomer shift (IS) determination. The spectra were fitted using the NORMOS program employing Lorentizan peak profile and least squares optimisation. The determined parameters are summarised in Table S5.

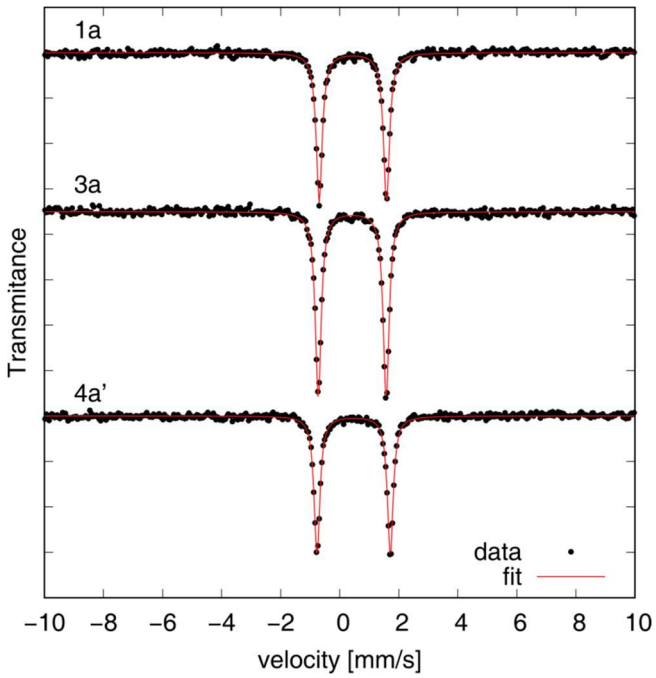

Figure S6. Mössbauer spectra of **1a**, **3a** and **4a'**

Table S5. Summary of Mössbauer parameters

Compound	Signal	IS (mm s^{-1})	QS (mm s^{-1})	FWHM (mm s^{-1})
1a	doublet	0.45	2.28	0.24
3a	doublet	0.42	2.30	0.24
4a'	doublet	0.47	2.48	0.23

VARIABLE TEMPERATURE ^{1}H NMR SPECTRA OF 1c

The variable-temperature (VT) NMR spectra of phosphinoferrocene guanidine **1c** illustrating the structural dynamics of this compound, namely the tautomer equilibria, are shown in Figure S7.

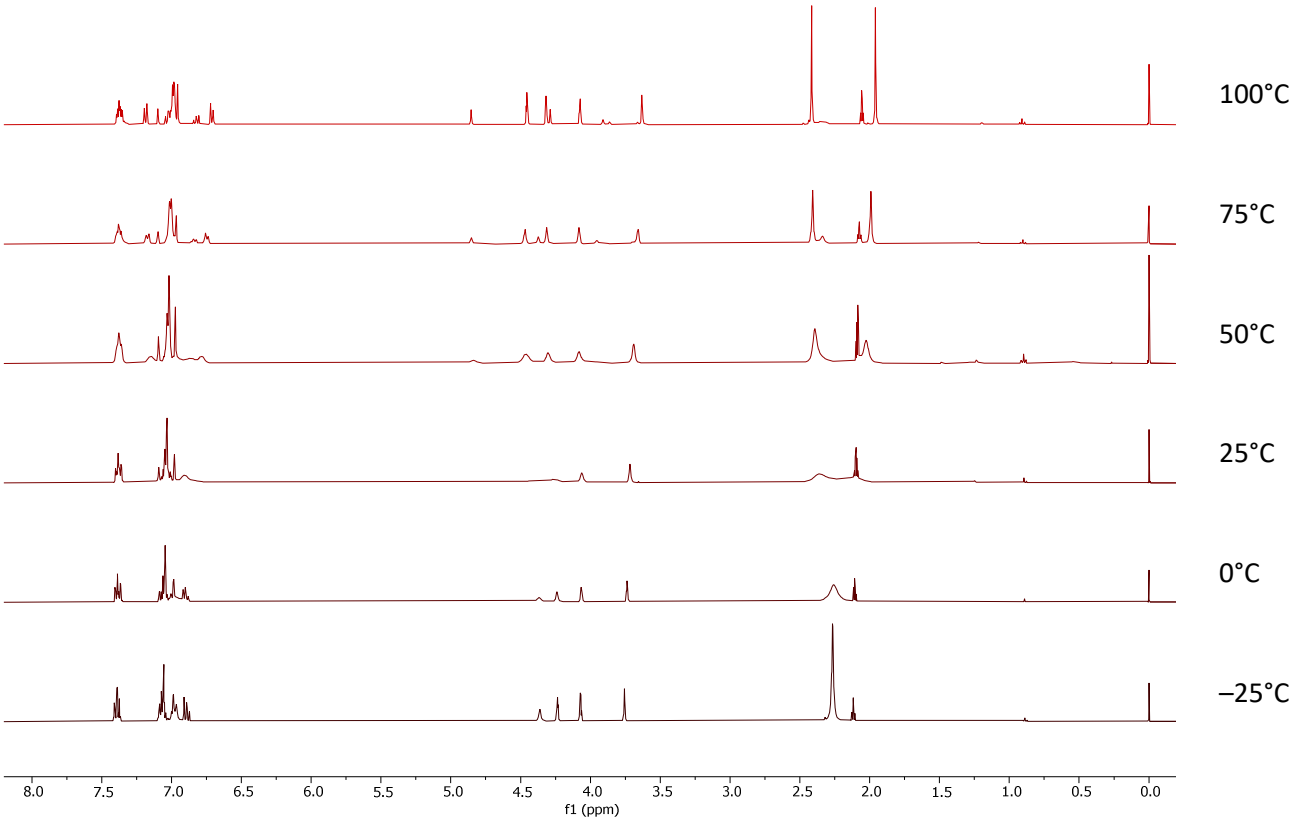

Figure S7. VT ^{1}H NMR spectra (toluene-d_8, 400 MHz) of **1c**.

COPIES OF THE NMR SPECTRA

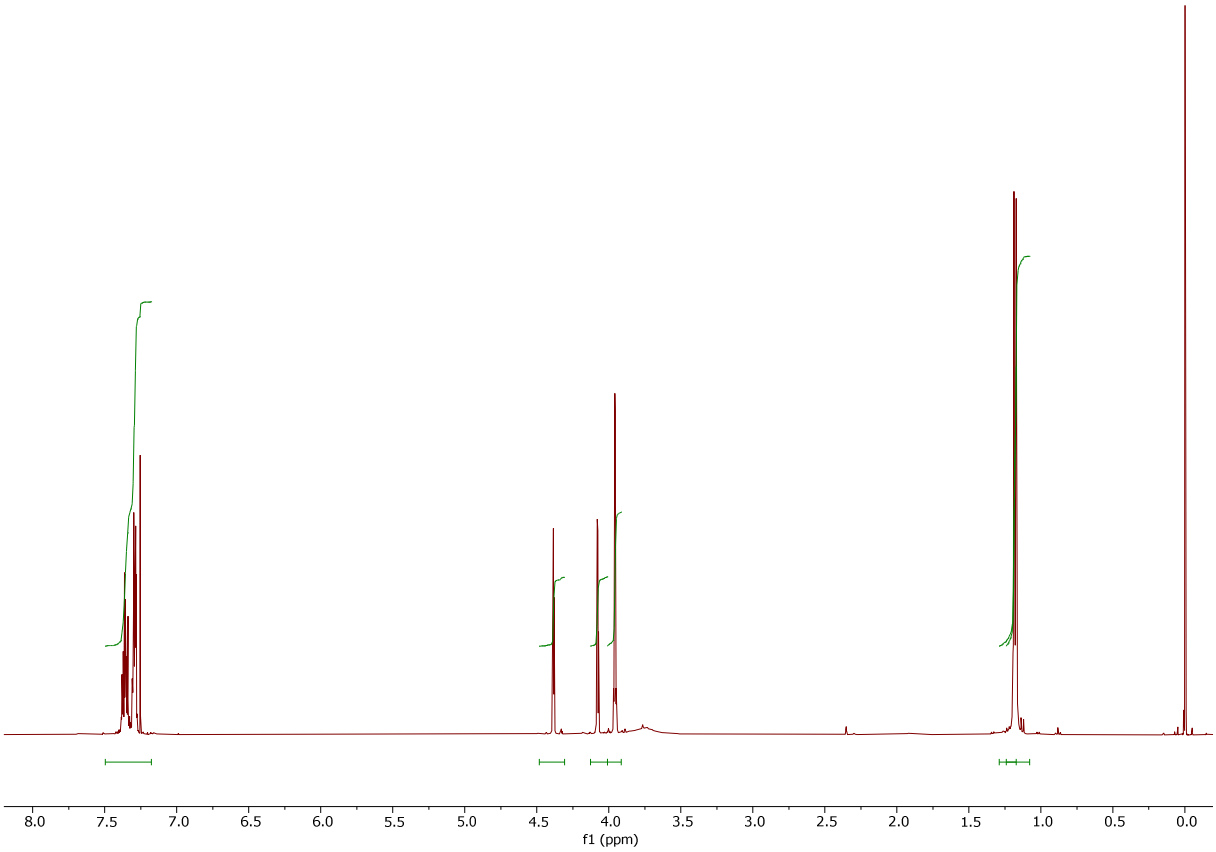

Figure S8. ^{1}H NMR ($CDCl_3$, 400 MHz, 25 °C) spectrum of **1a**.

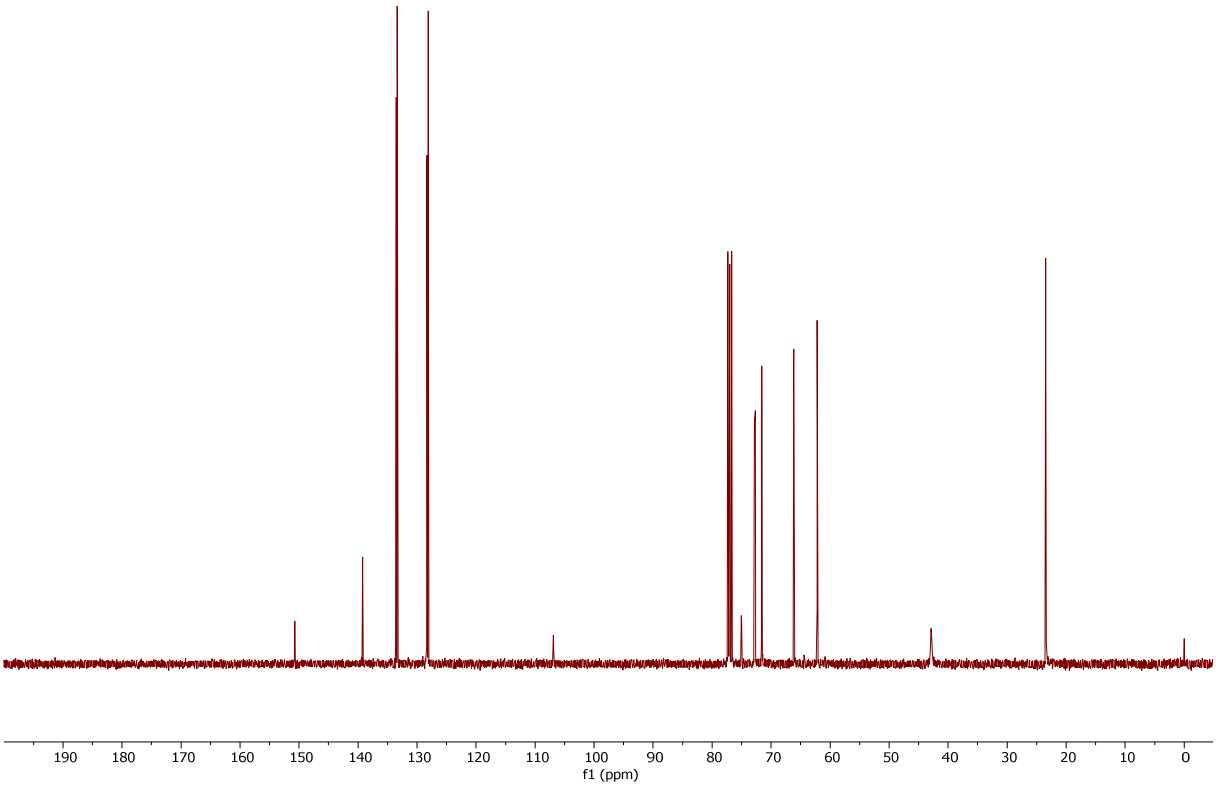

Figure S9. $^{13}C\{^{1}H\}$ NMR ($CDCl_3$, 101 MHz, 25 °C) spectrum of **1a**.

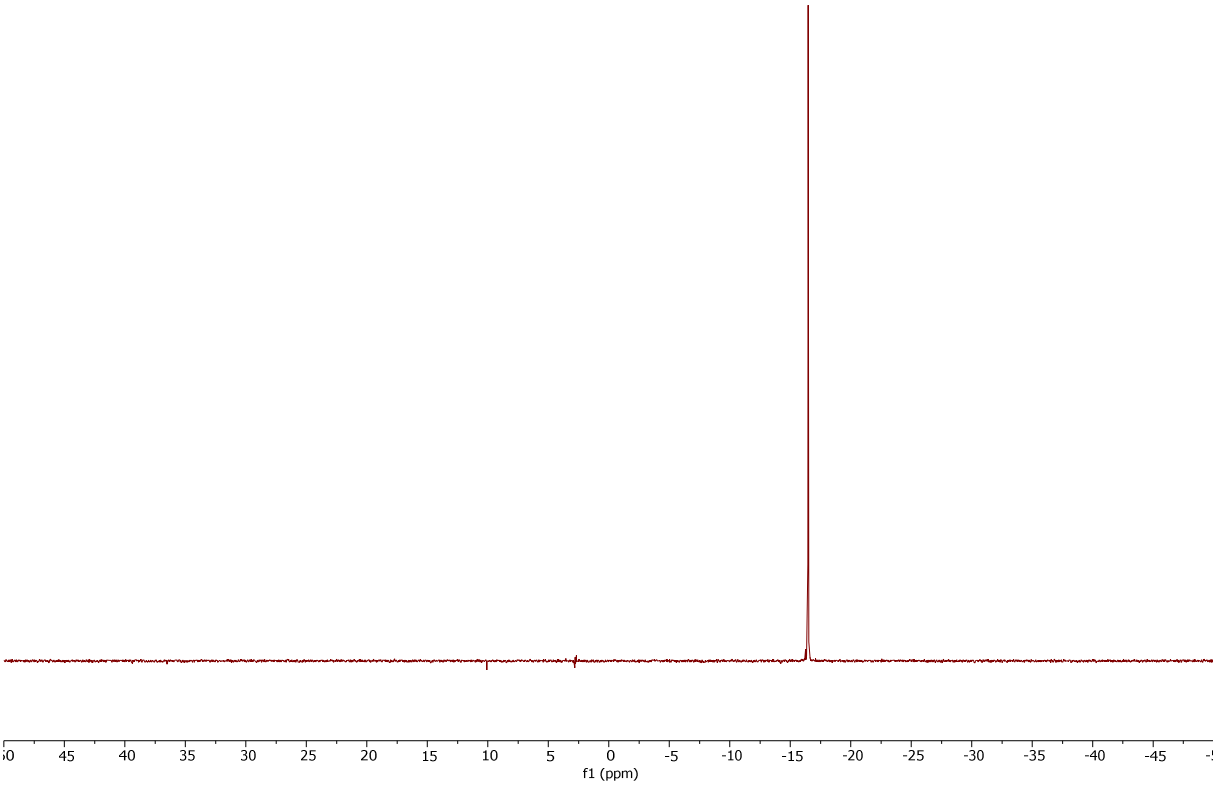

Figure S10. $^{31}P\{^{1}H\}$ NMR ($CDCl_3$, 162 MHz, 25 °C) spectrum of **1a**.

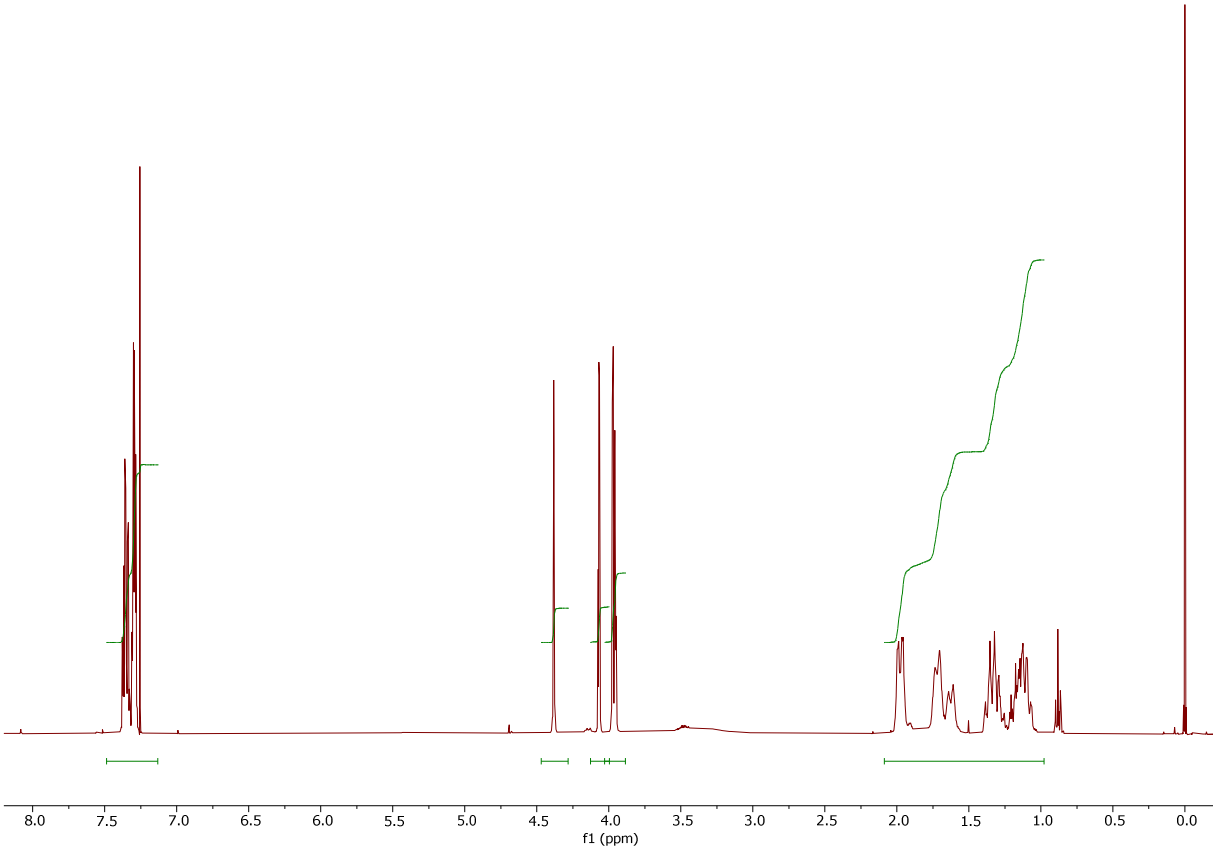

Figure S11. ^{1}H NMR ($CDCl_3$, 400 MHz, 25 °C) spectrum of **1b**.

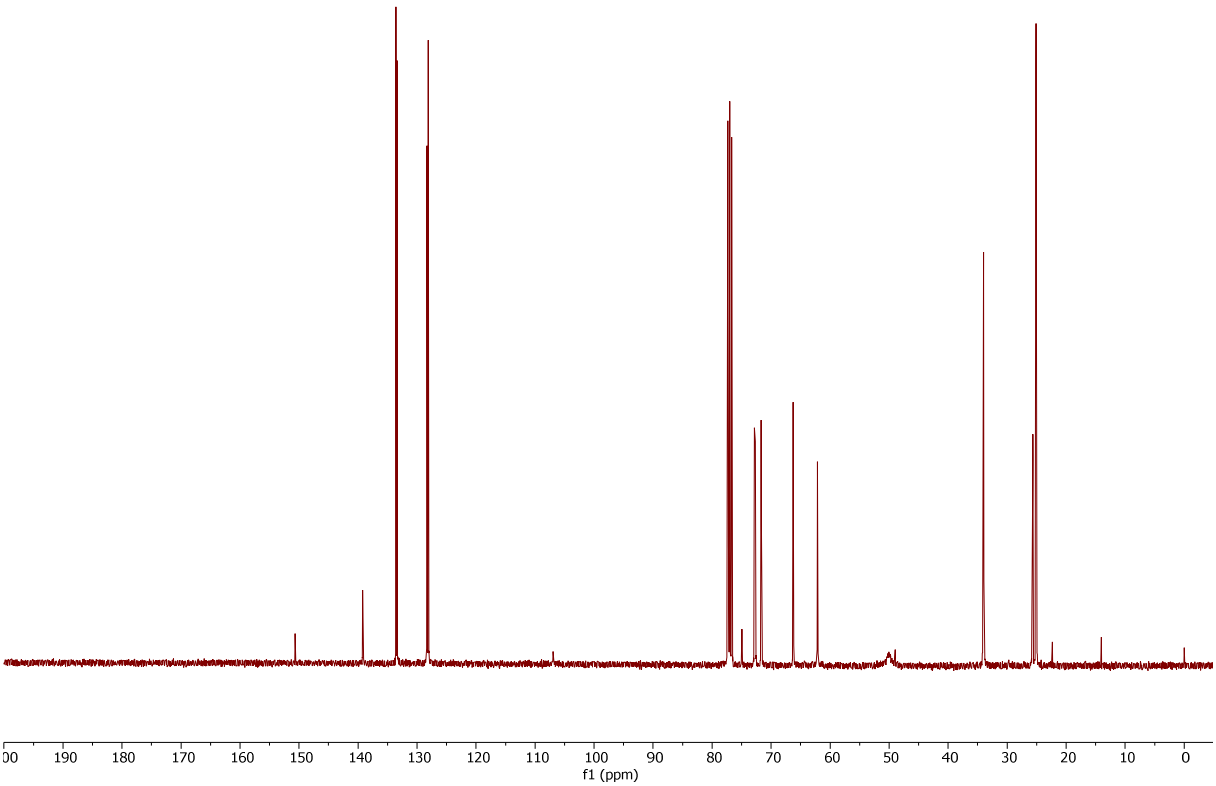

Figure S12. $^{13}C\{^{1}H\}$ NMR ($CDCl_3$, 101 MHz, 25 °C) spectrum of **1b**.

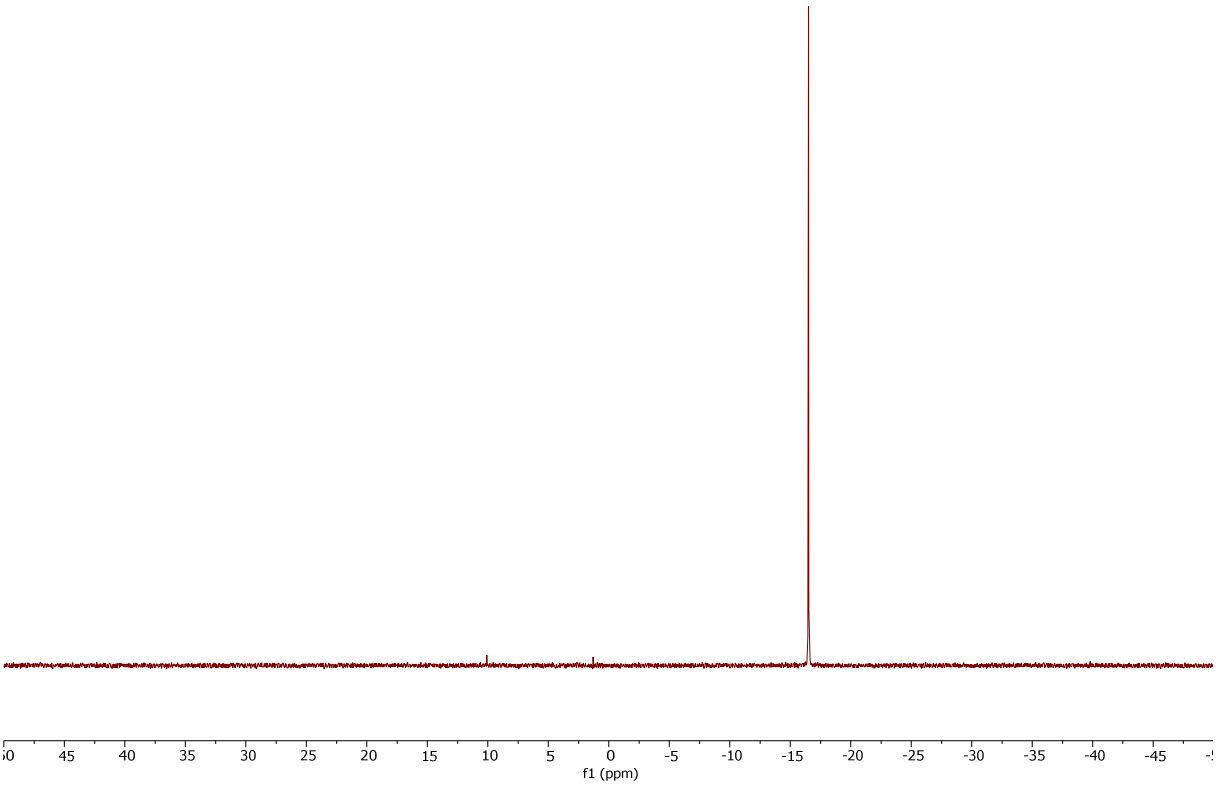

Figure S13. $^{31}P\{^{1}H\}$ NMR ($CDCl_3$, 162 MHz, 25 °C) spectrum of **1b**.

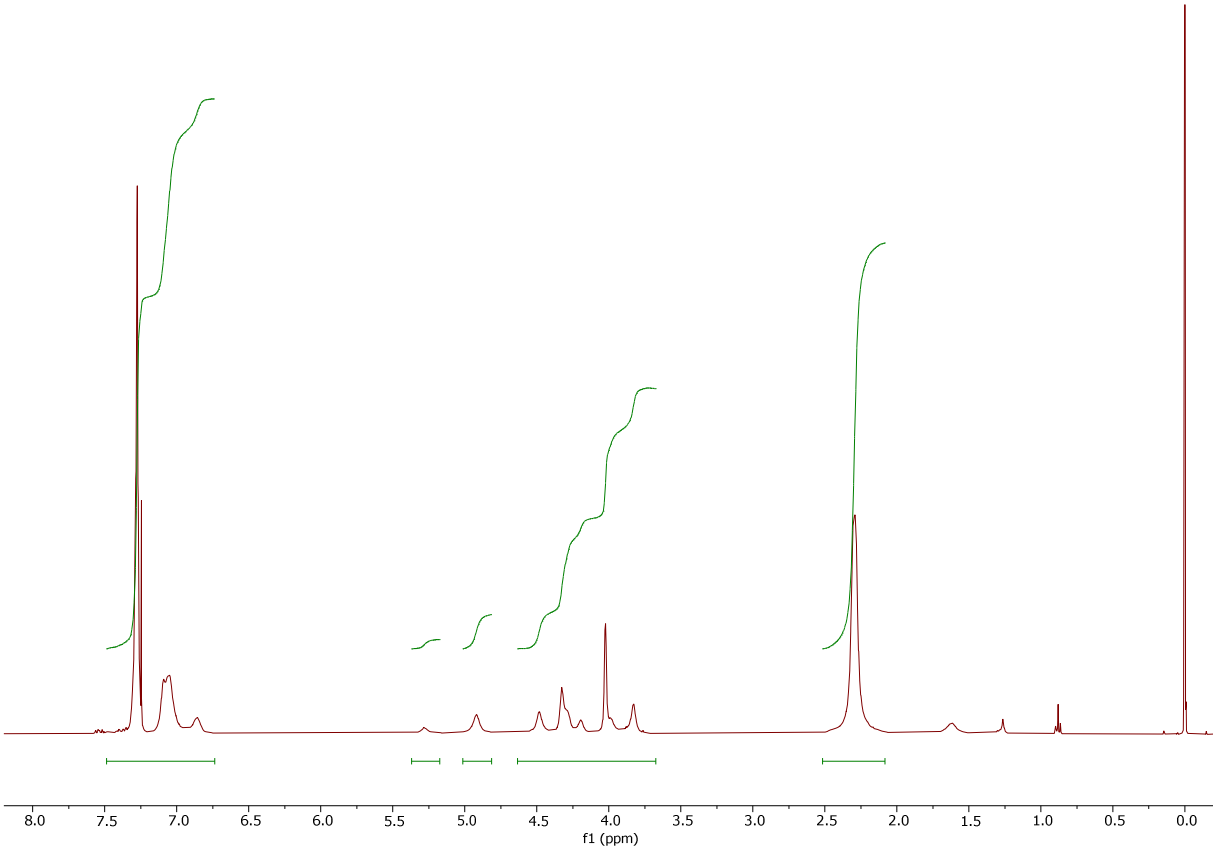

Figure S14. ^{1}H NMR ($CDCl_3$, 400 MHz, 25 °C) spectrum of **1c**.

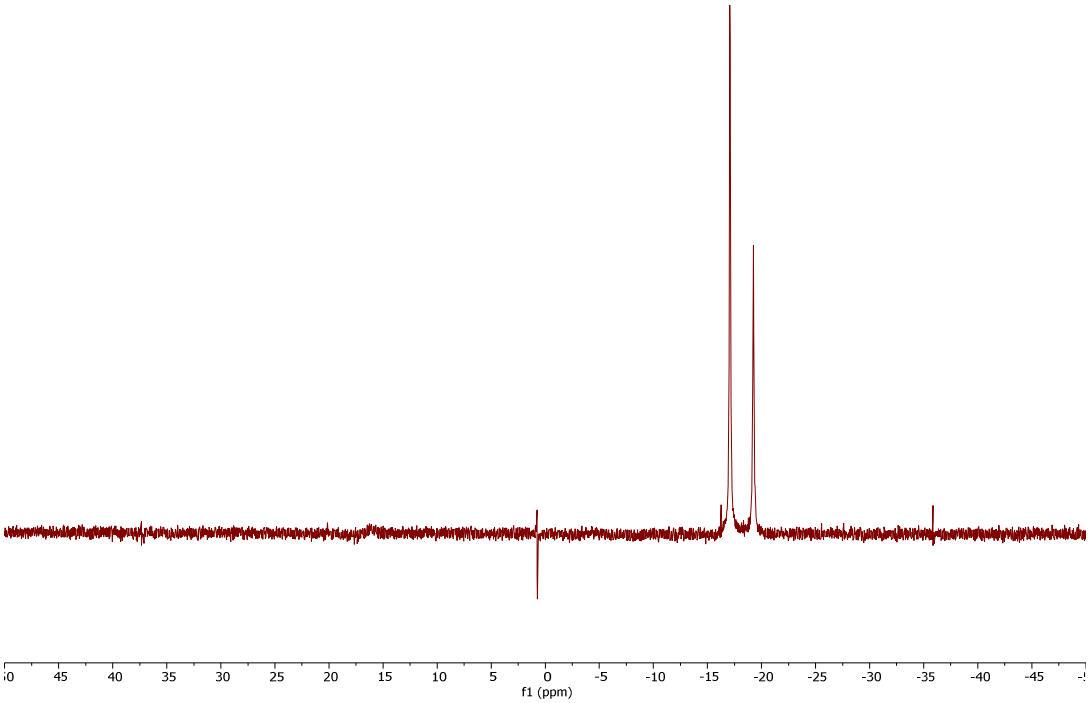

Figure S15. $^{31}P\{^{1}H\}$ NMR ($CDCl_3$, 162 MHz, 25 °C) spectrum of **1b** (the sharp minor peaks are electronic artifacts).

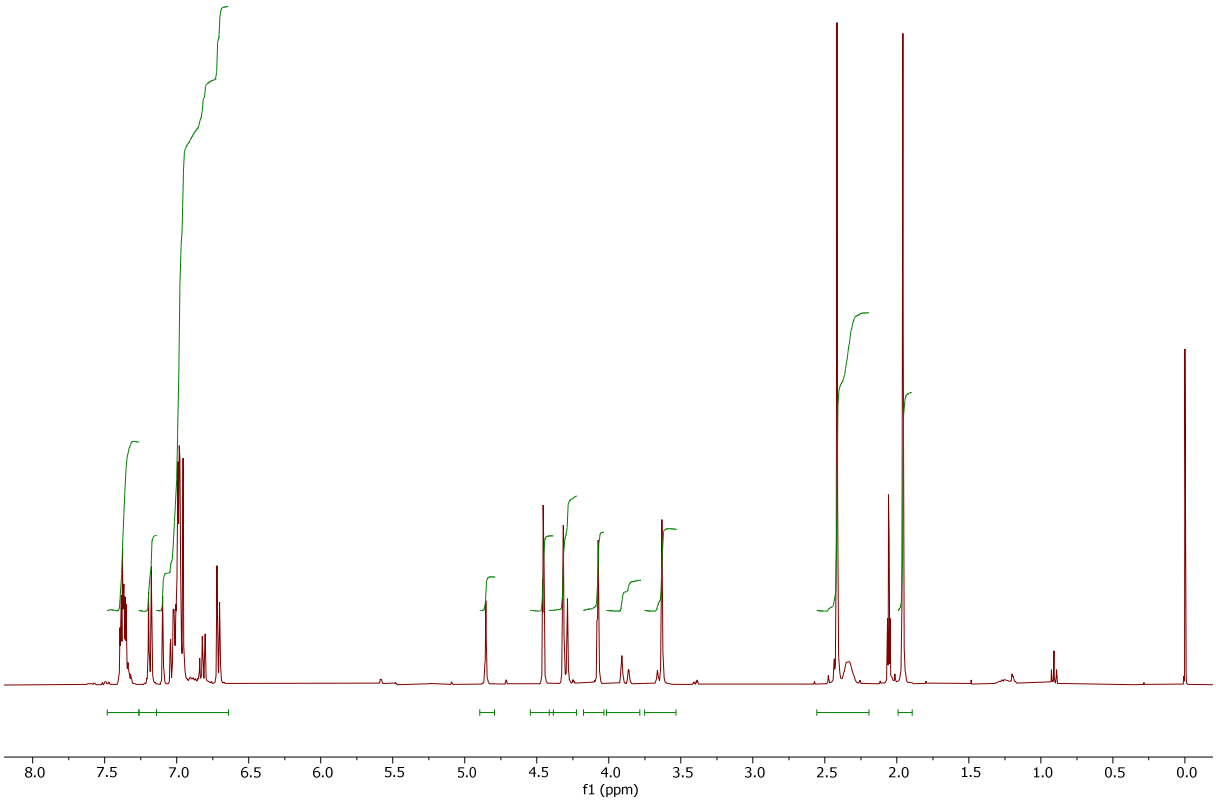

Figure S16. ^{1}H NMR (toluene-d_8, 400 MHz, −25 °C) spectrum of **1c**.

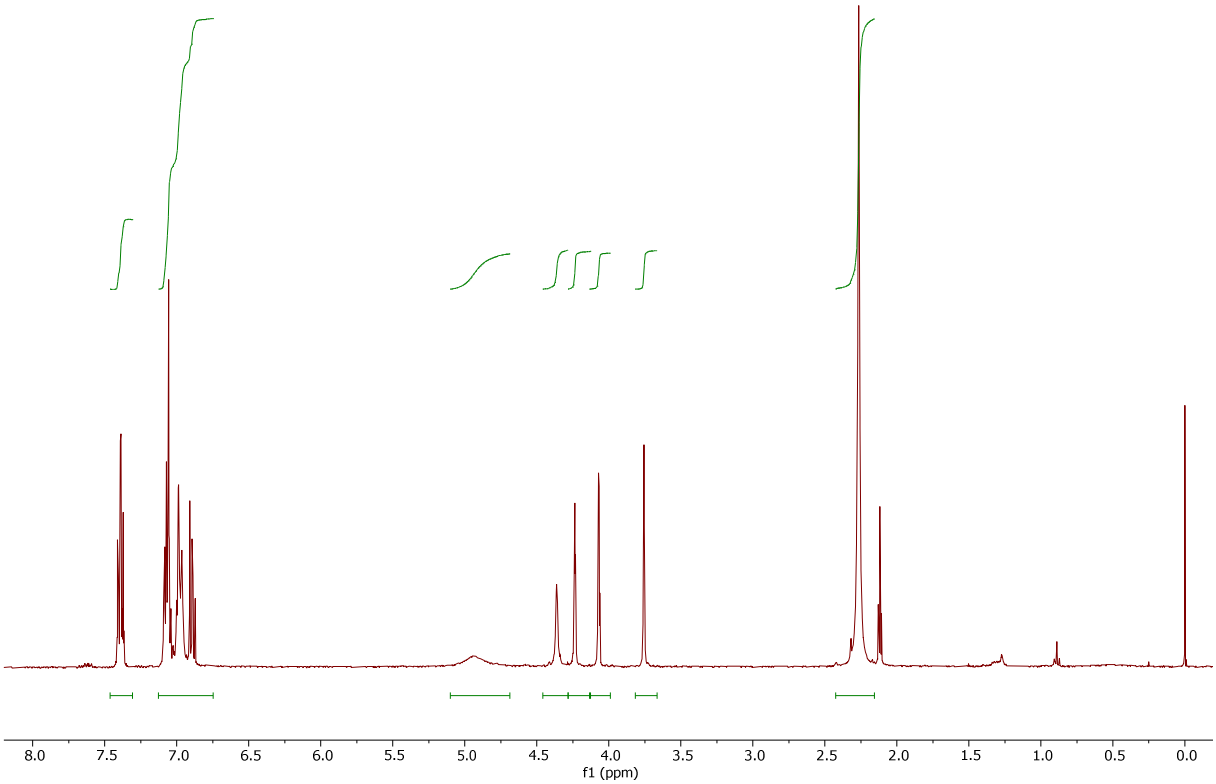

Figure S17. ^{1}H NMR (toluene-d_8, 400 MHz, 100 °C) spectrum of **1c**.

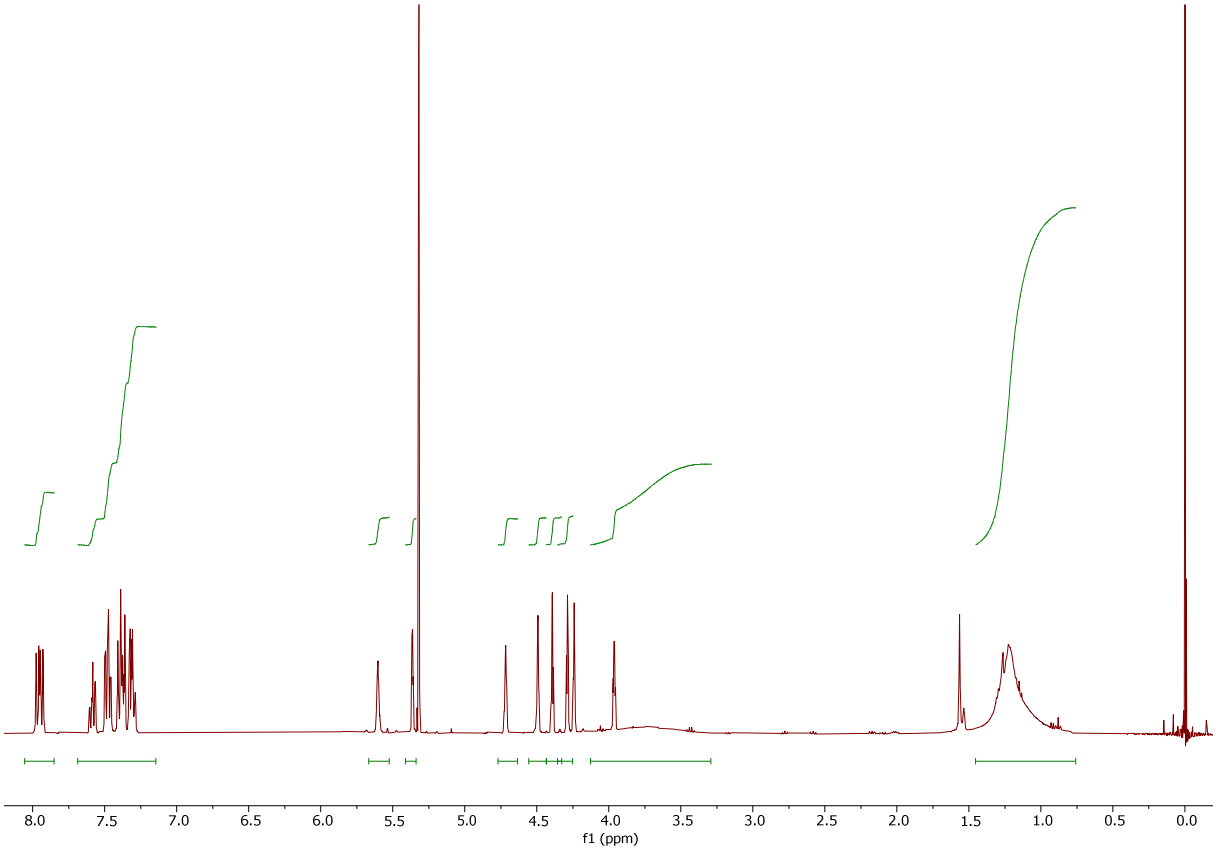

Figure S18. ^{1}H NMR (CD_2Cl_2, 400 MHz, 25 °C) spectrum of **3a**.

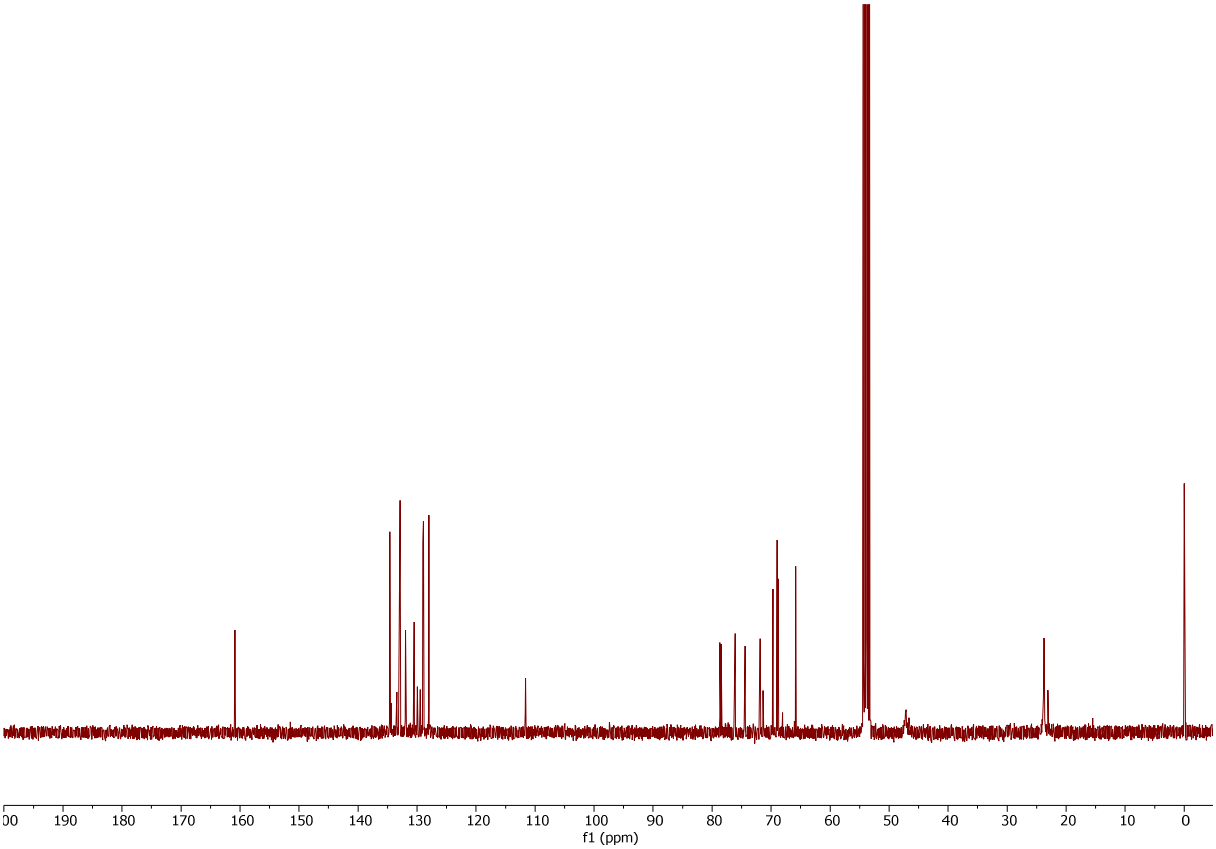

Figure S19. $^{13}C\{^{1}H\}$ NMR (CD_2Cl_2, 101 MHz, 25 °C) spectrum of **3a**.

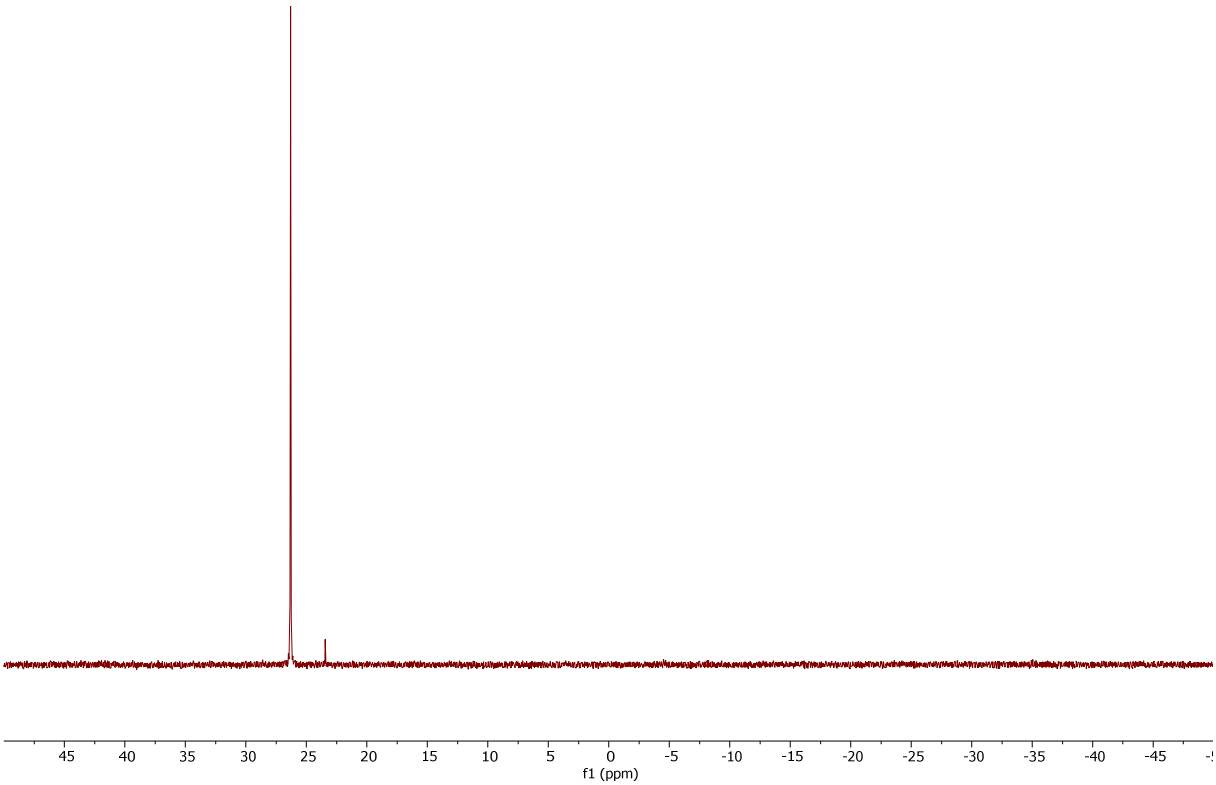

Figure S20. $^{31}P\{^{1}H\}$ NMR (CD_2Cl_2, 162 MHz, 25 °C) spectrum of **3a**.

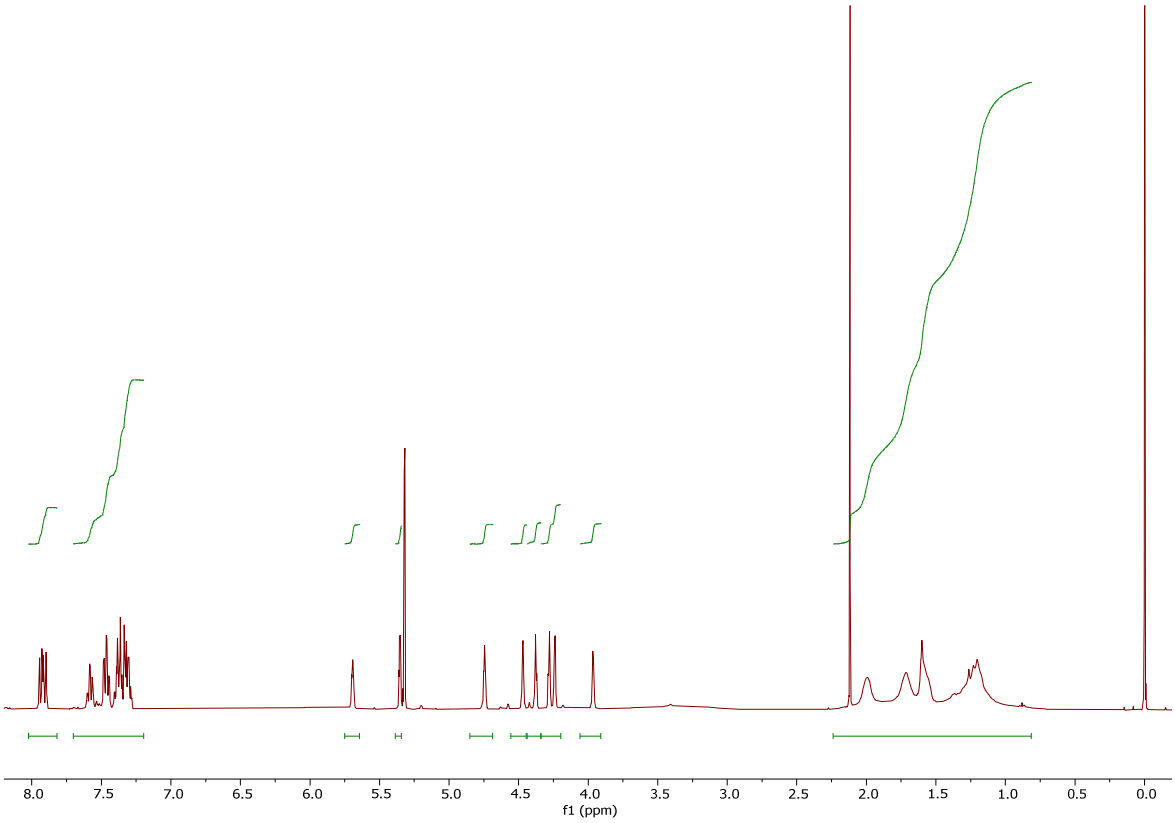

Figure S21. ^{1}H NMR (CD_2Cl_2, 400 MHz, 25 °C) spectrum of **3b**. The signal at δ_H 2.12 is due to residual acetone.

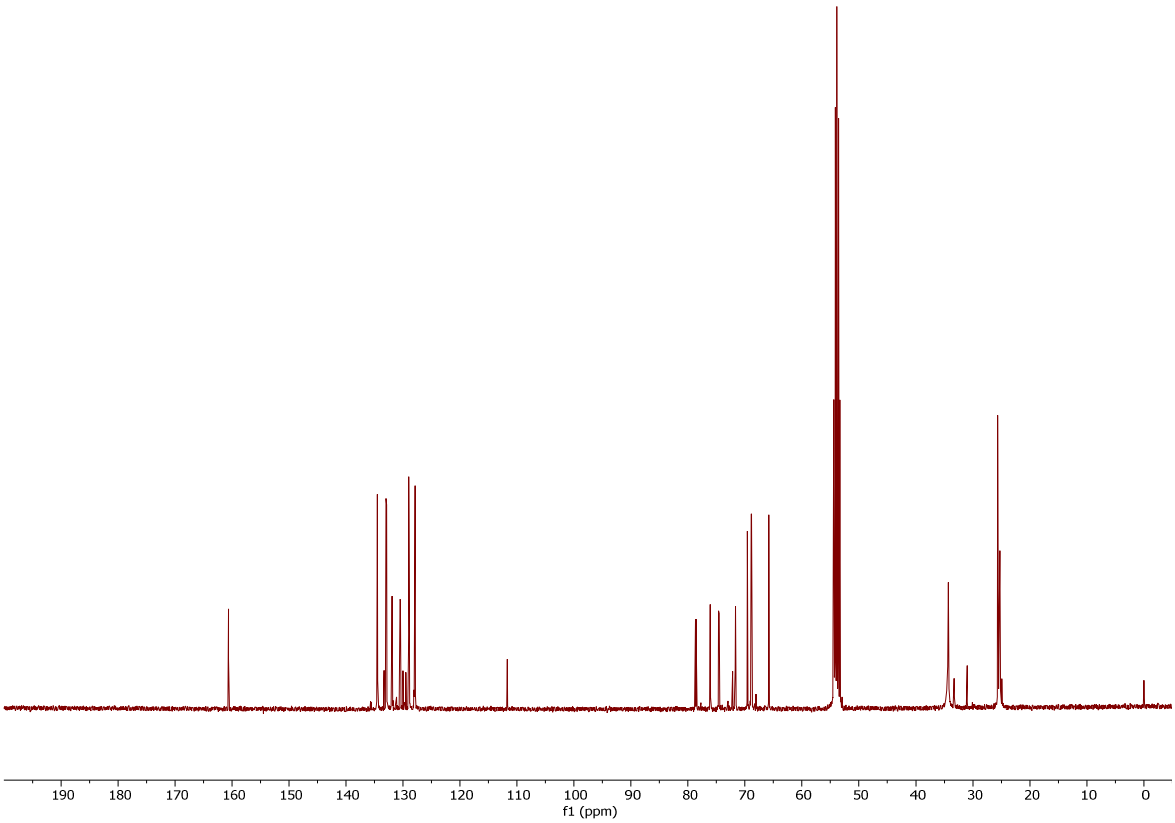

Figure S22. $^{13}C\{^{1}H\}$ NMR (CD_2Cl_2, 101 MHz, 25 °C) spectrum of **3b**.

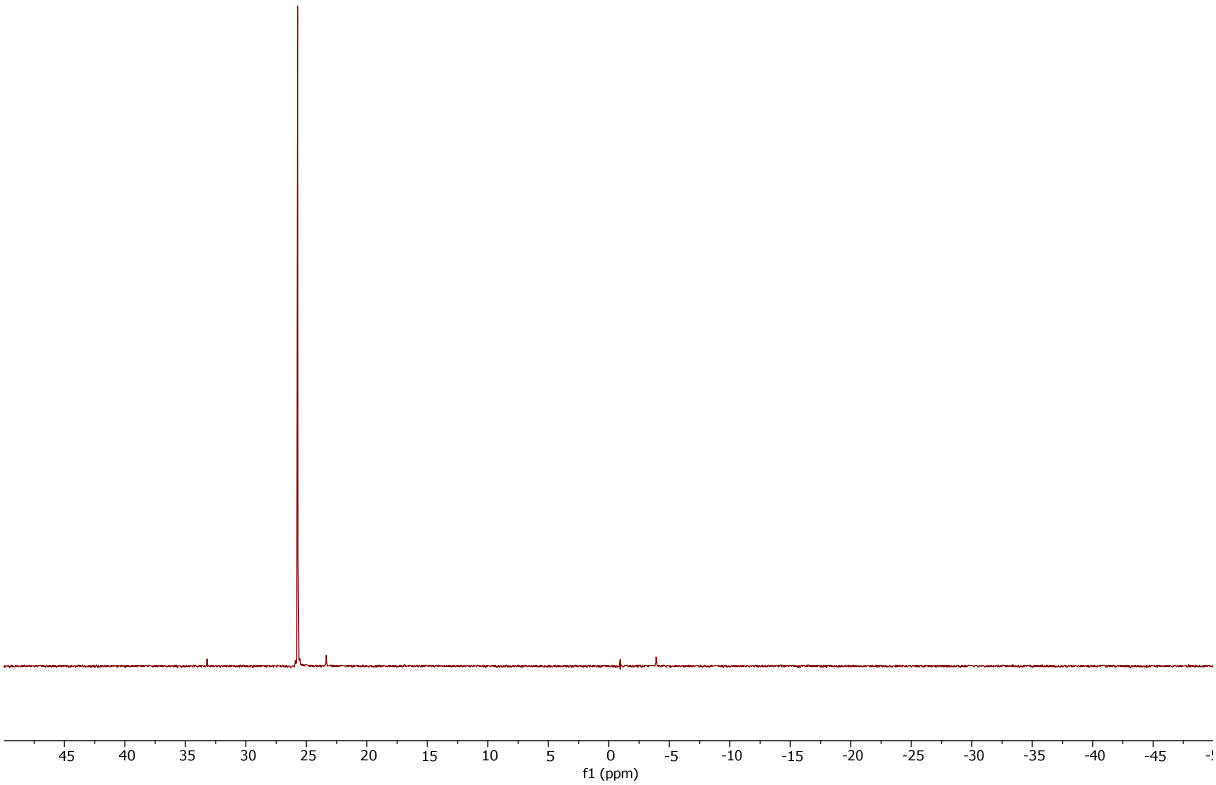

Figure S23. $^{31}P\{^{1}H\}$ NMR (CD_2Cl_2, 162 MHz, 25 °C) spectrum of **3b**.

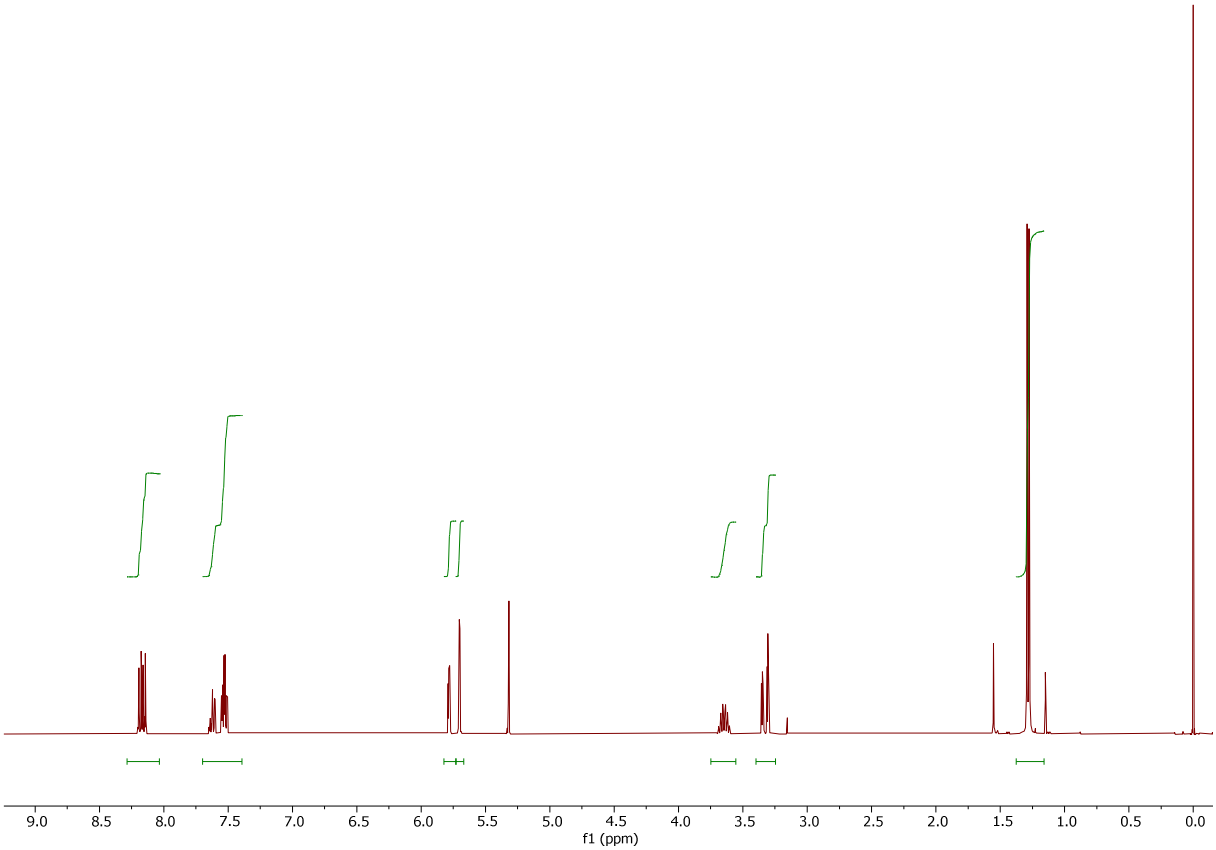

Figure 24. ^{1}H NMR (CD_2Cl_2, 400 MHz, 25 °C) spectrum of **4a**.

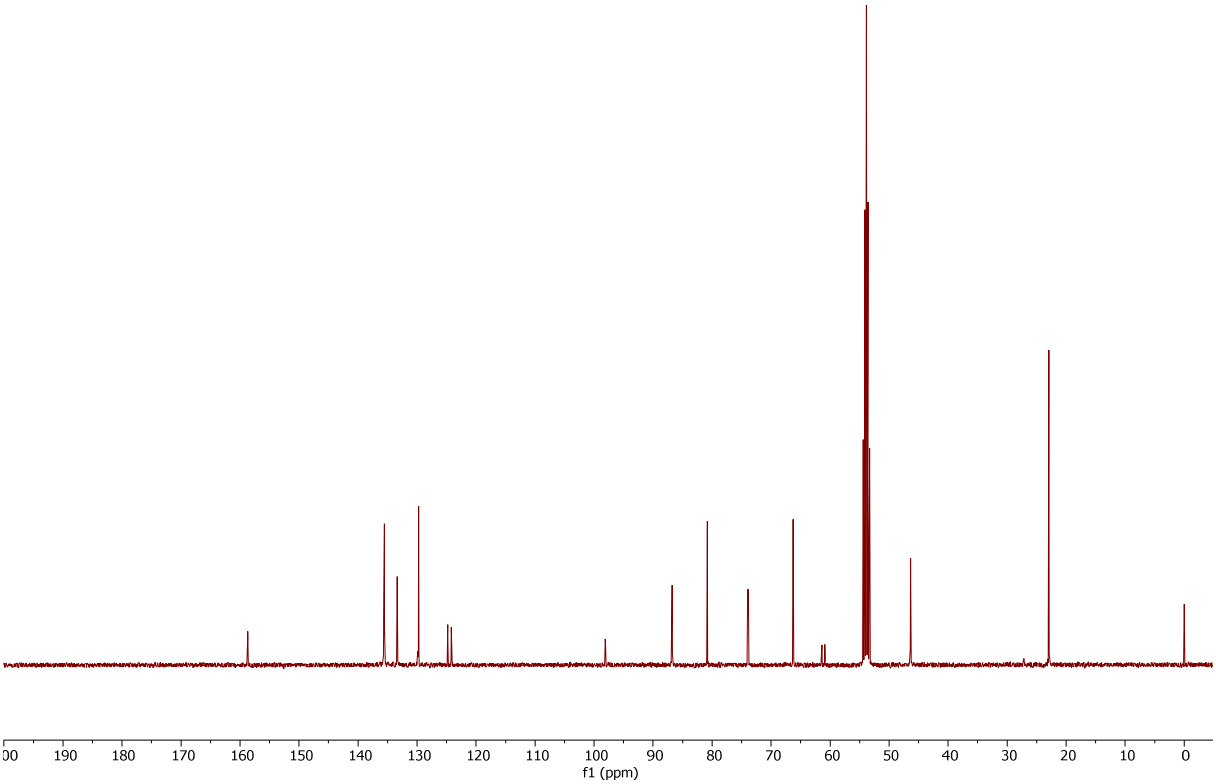

Figure S25. $^{13}C\{^{1}H\}$ NMR (CD_2Cl_2, 101 MHz, 25 °C) spectrum of **4a**.

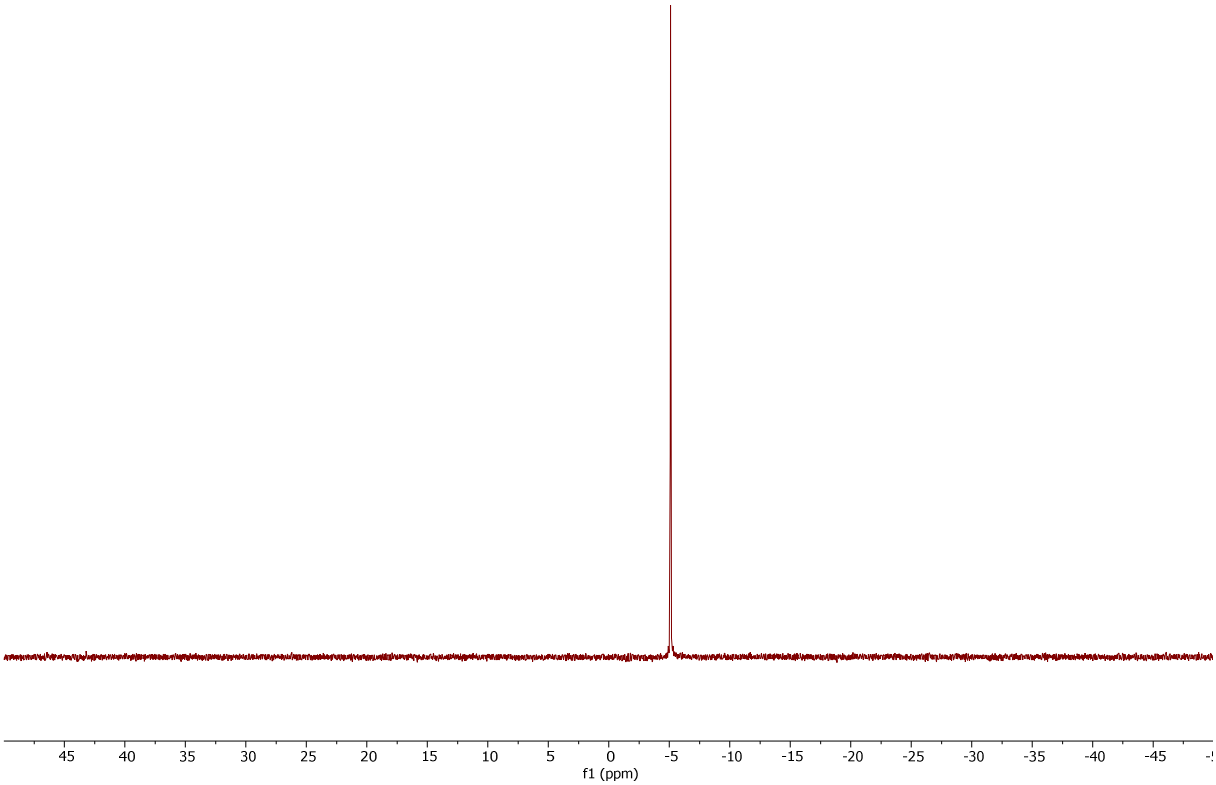

Figure S26. $^{31}P\{^{1}H\}$ NMR (CD_2Cl_2, 162 MHz, 25 °C) spectrum of **4a**.

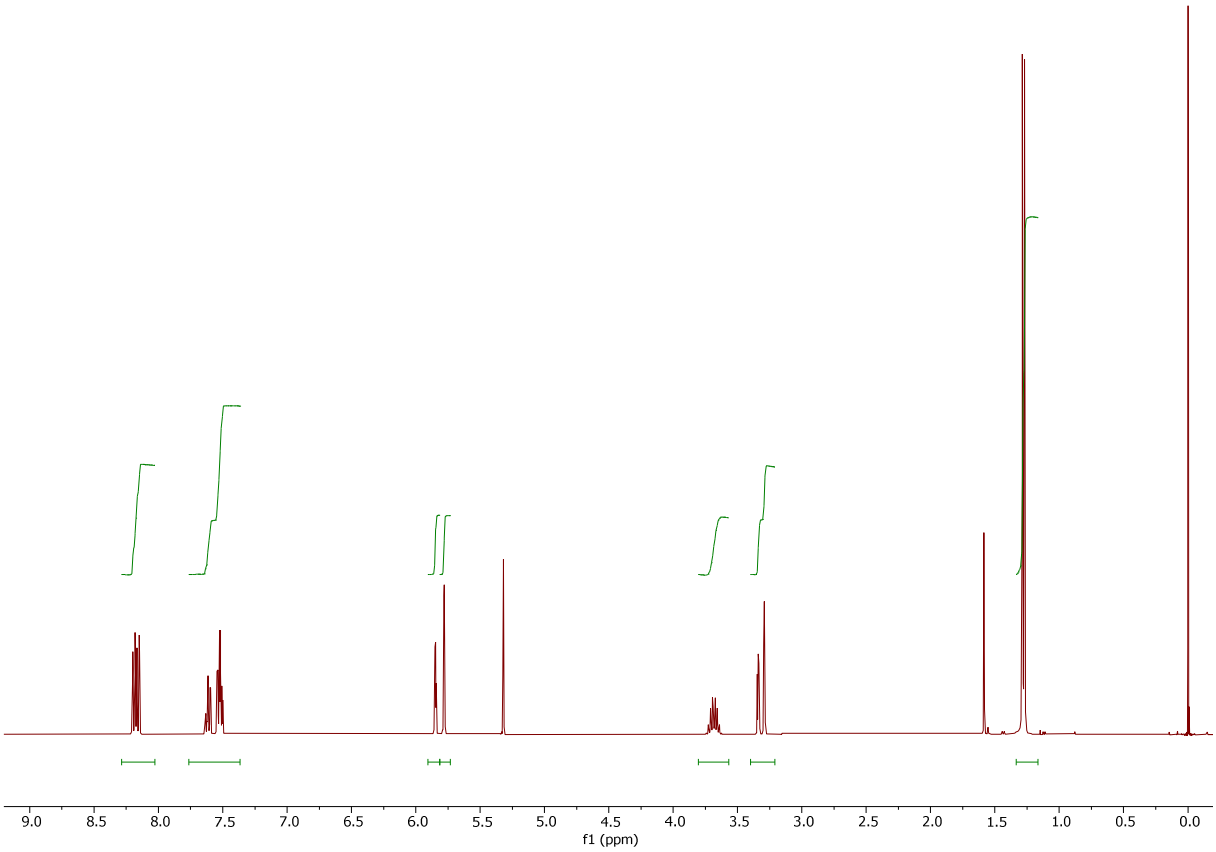

Figure S27. ^{1}H NMR (CD_2Cl_2, 400 MHz, 25 °C) spectrum of **4a'**.

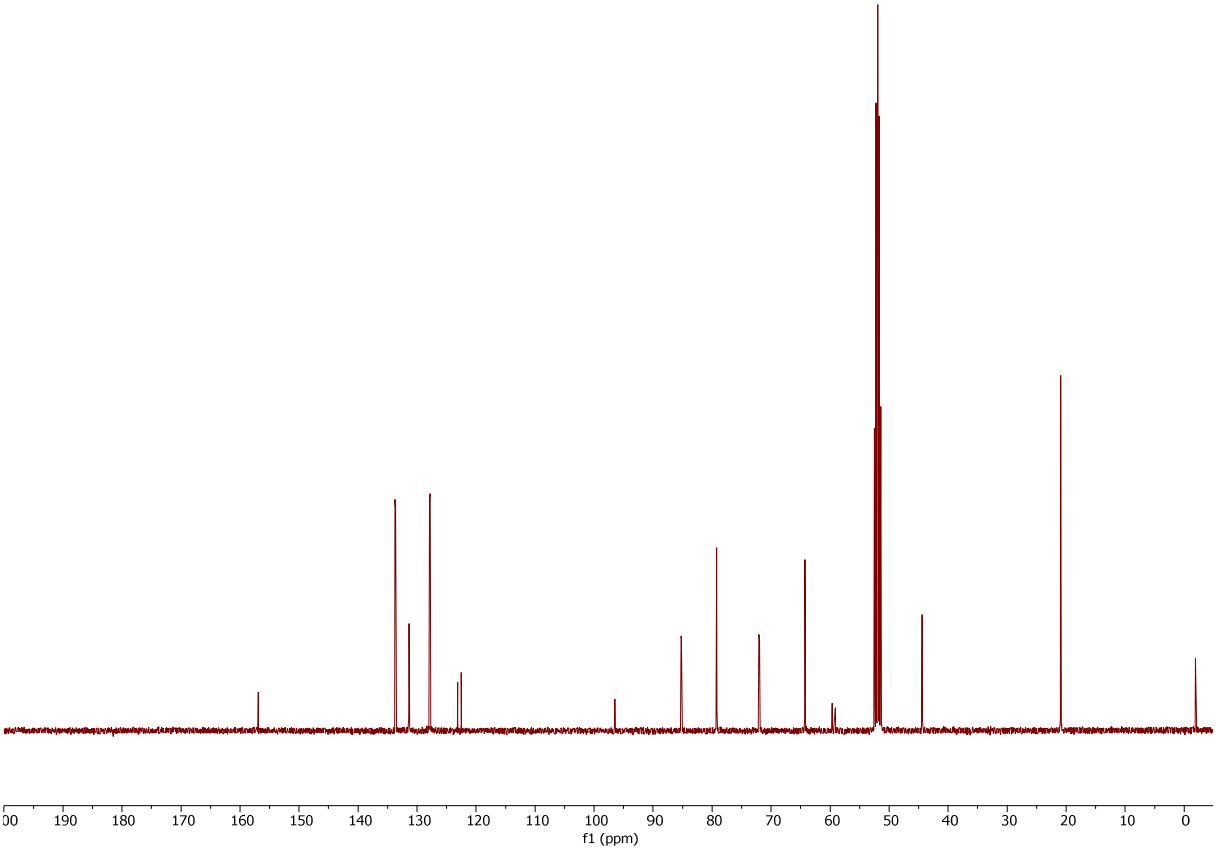

Figure S28. $^{13}C\{^{1}H\}$ NMR (CD_2Cl_2, 101 MHz, 25 °C) spectrum of **4a'**.

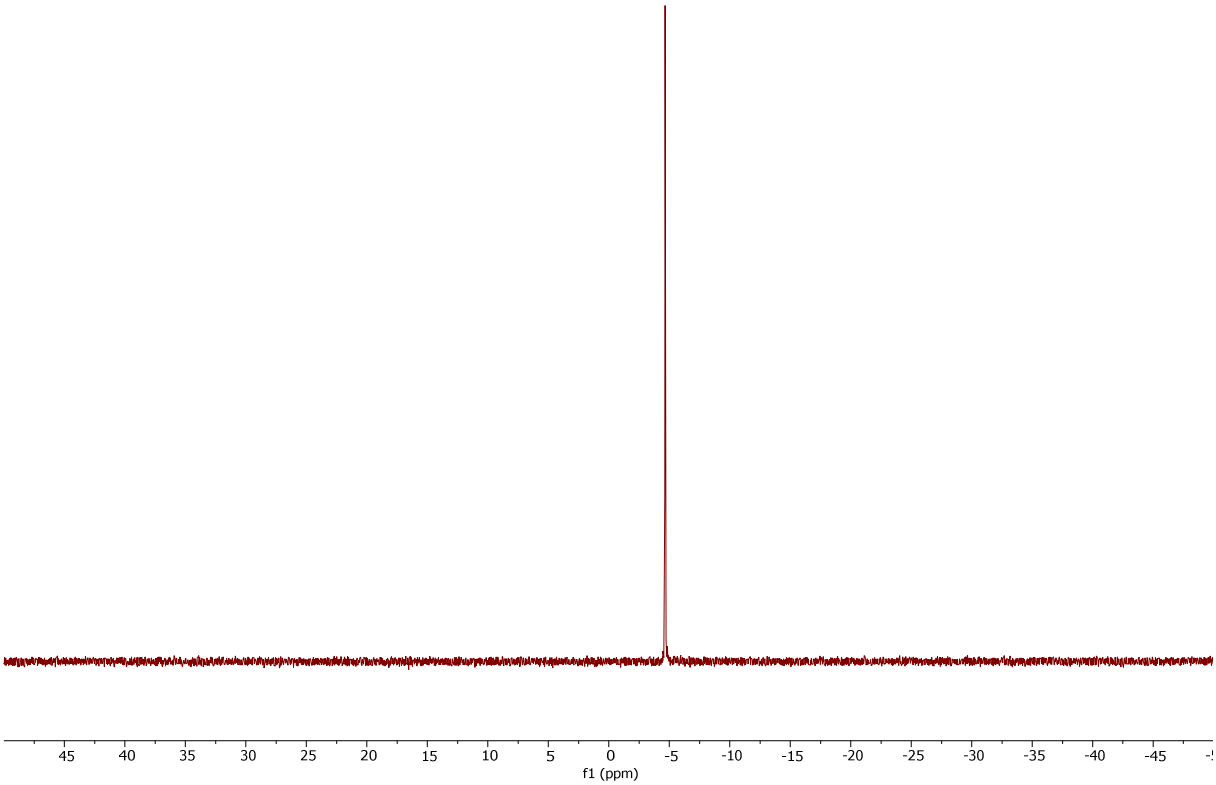

Figure S29. $^{31}P\{^{1}H\}$ NMR (CD_2Cl_2, 162 MHz, 25 °C) spectrum of **4a'**.

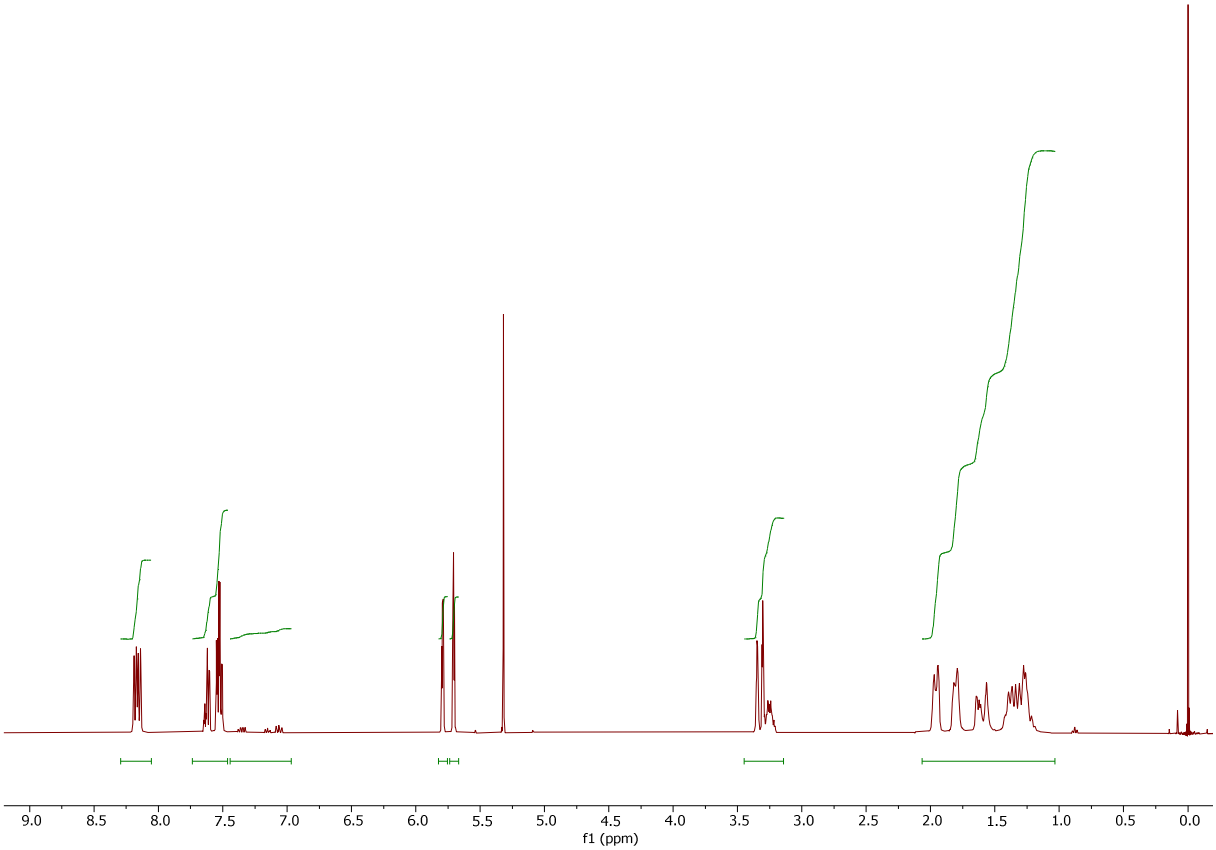

Figure S30. ^{1}H NMR (CD_2Cl_2, 400 MHz, 25 °C) spectrum of **4b**. The signals at δ_H 7.02-7.40 are due to residual fluorobenzene used for crystallisation.

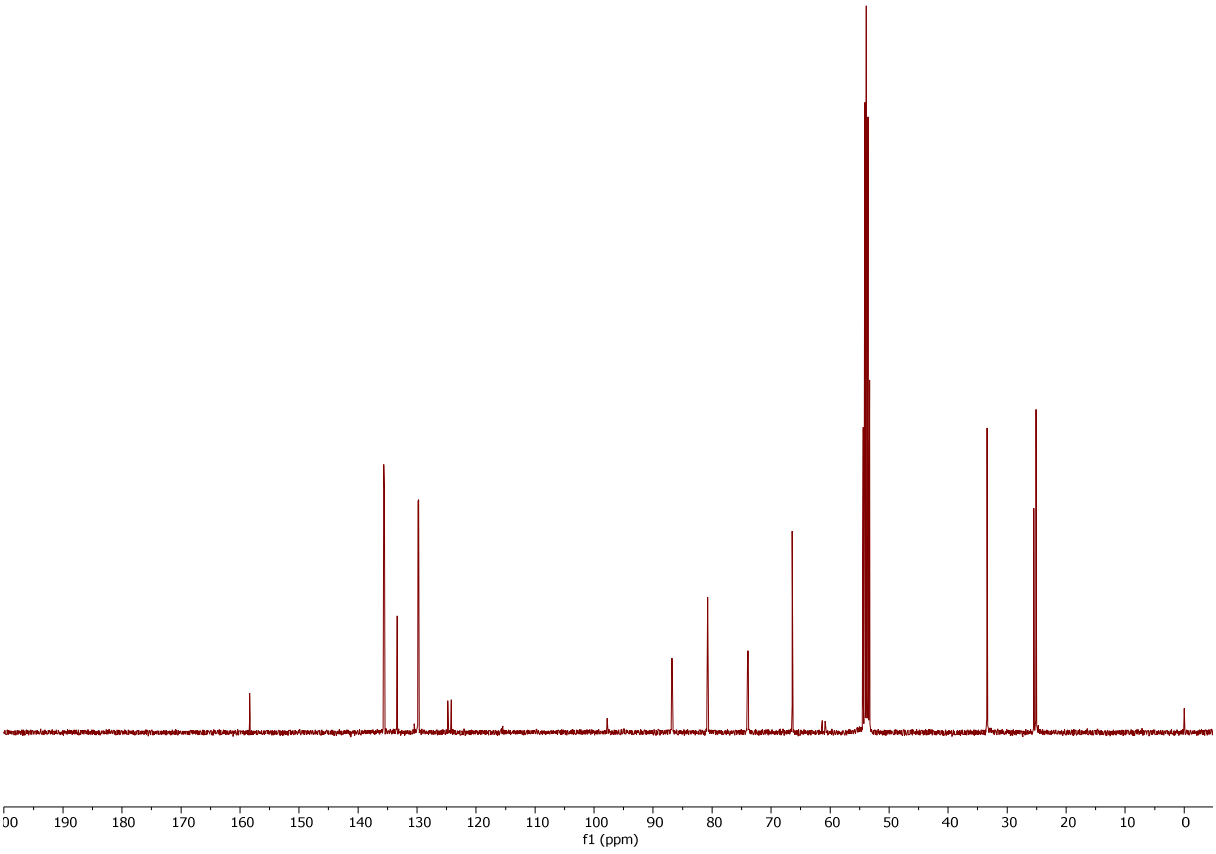

Figure S31. $^{13}C\{^{1}H\}$ NMR (CD_2Cl_2, 101 MHz, 25 °C) spectrum of **4b**.

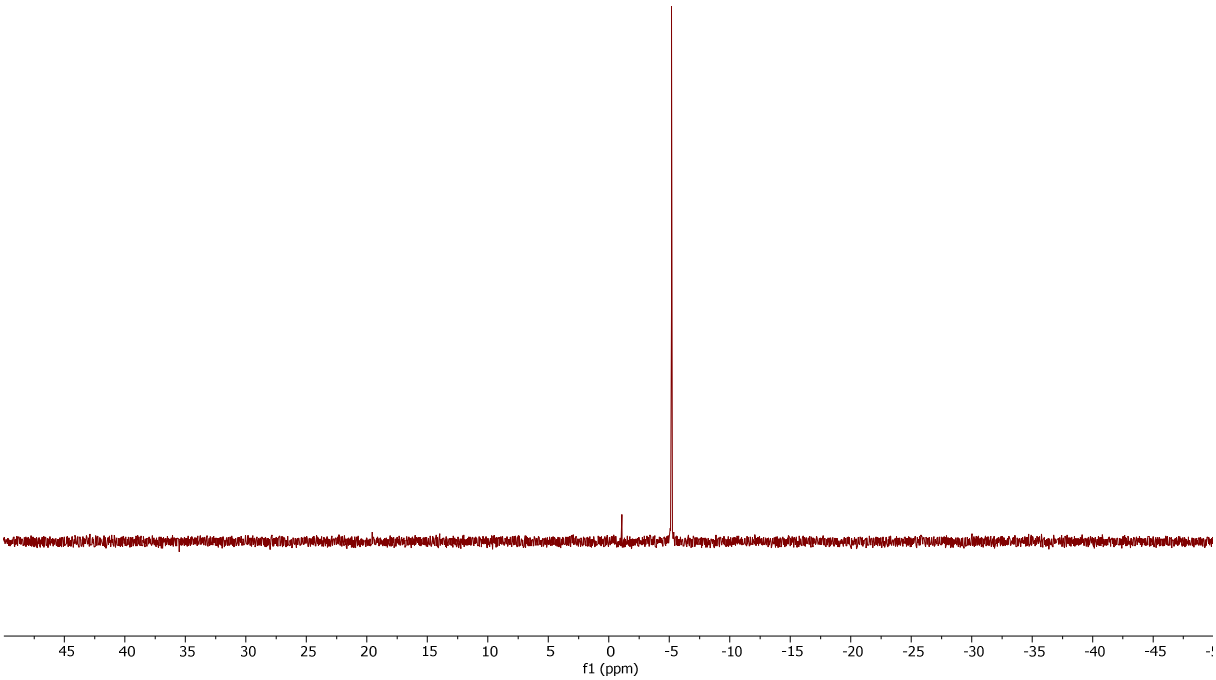

Figure S32. $^{31}P\{^{1}H\}$ NMR (CD_2Cl_2, 162 MHz, 25 °C) spectrum of **4b**.

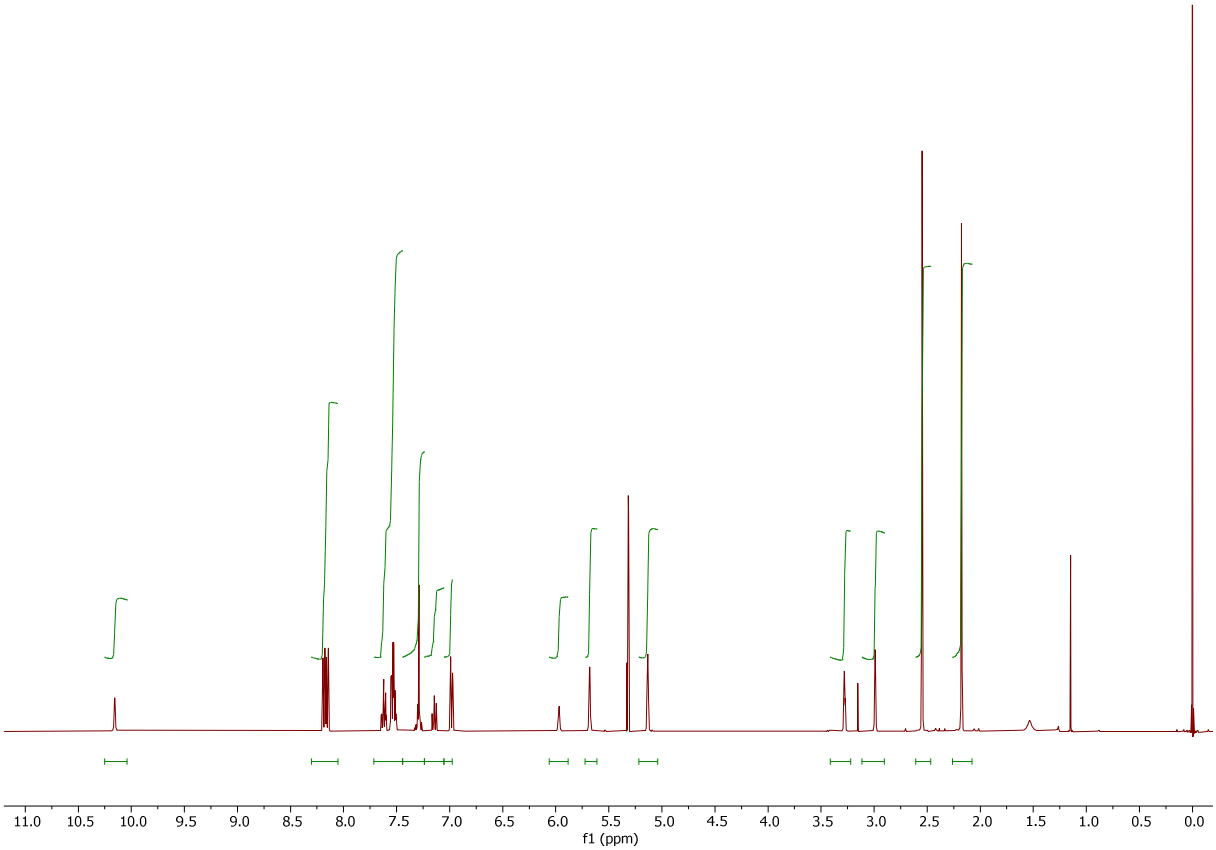

Figure S33. ^{1}H NMR (CD_2Cl_2, 400 MHz, 25 °C) spectrum of **4c**.

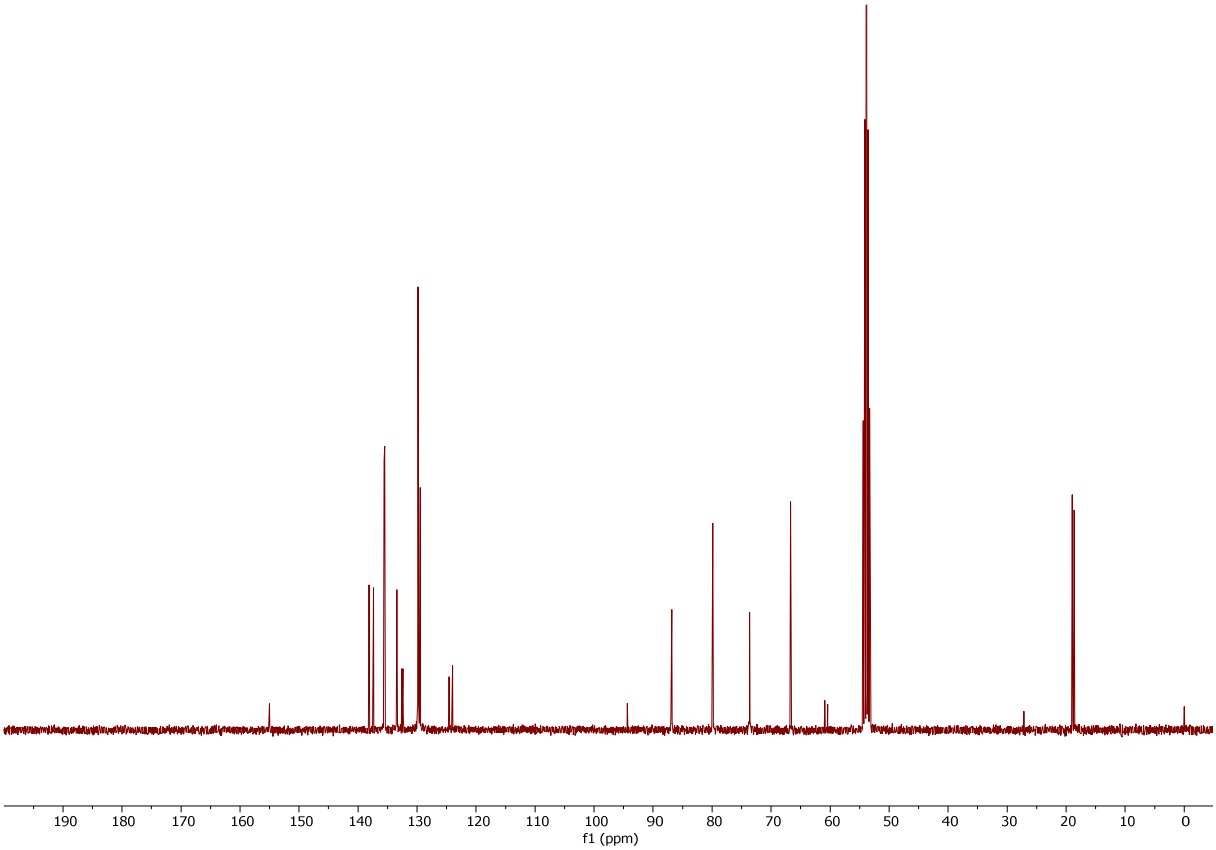

Figure S34. $^{13}C\{^{1}H\}$ NMR (CD_2Cl_2, 101 MHz, 25 °C) spectrum of **4c**.

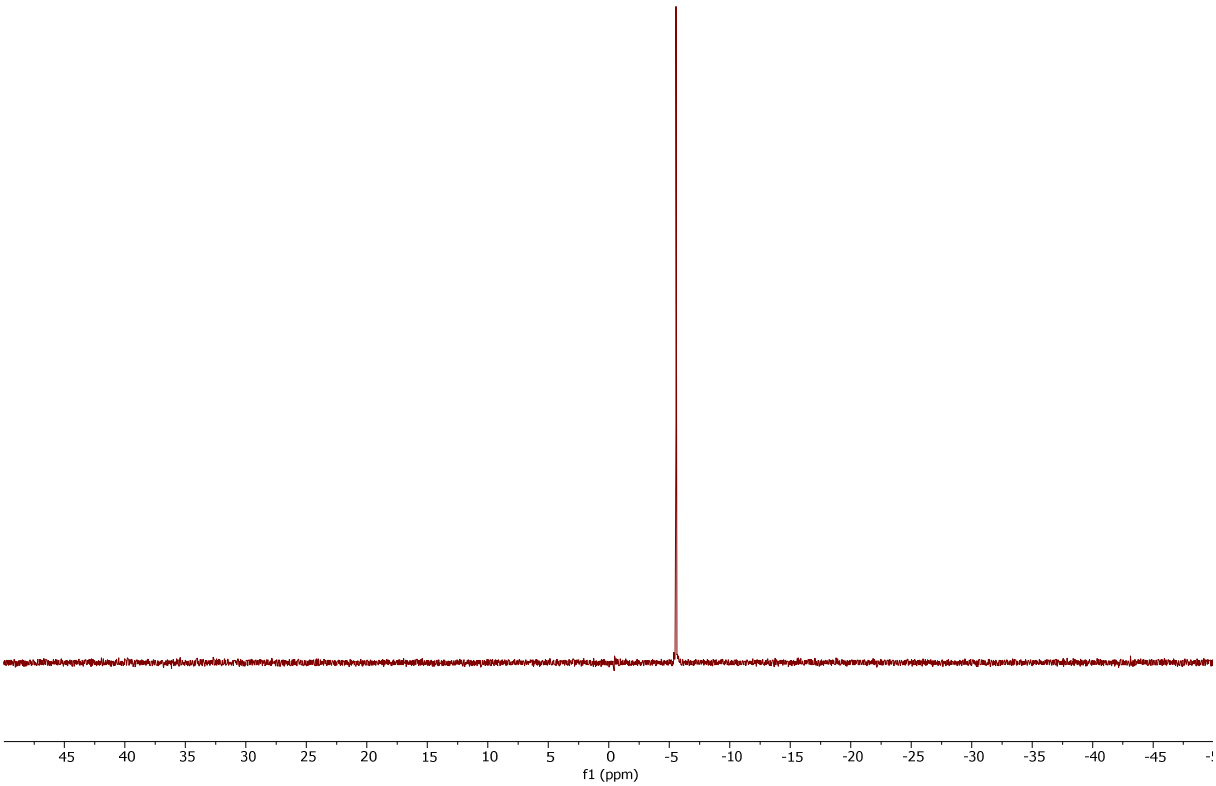

Figure 35. $^{31}P\{^{1}H\}$ NMR (CD_2Cl_2, 162 MHz, 25 °C) spectrum of **4c**.

DFT COMPUTATIONS

Computational Details

Computational studies of **3a** and **4a*** were carried out using Gaussian 16, Revision A.03.[19] Geometry optimizations employed the M11 functional,[20] the LANL2DZ ECP[21] for the Pd atoms and the 6-31+G(d,p) basis set[22] for all other atoms. Dichloromethane as solvent was accounted for during computations by adopting the Polarizable Continuum Model (PCM).[23] Geometry optimizations used estimated Hessians at the beginning of the optimization steps. Electronic excitations were computed by time-dependant DFT using the PBE1PBE functional[24] , the Stuttgart–Dresden pseudopotentials[25] for the Pd atoms and the 6-311++G(3d,p) basis set for all other atoms. Topology analyses were done using Multiwfn[26] and NBO analyses used the NBO program, version 6.0.19.[27]

Results

Compound	**3a**	**4a***
LUMO	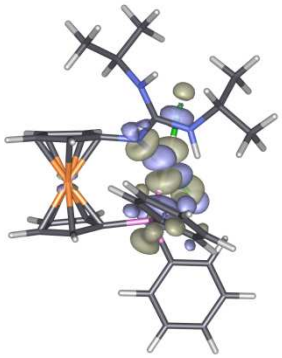	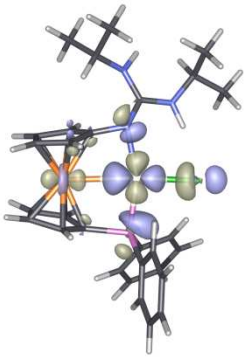
	E = −0.01873 a.u.	*E* = −0.05026 a.u.
HOMO	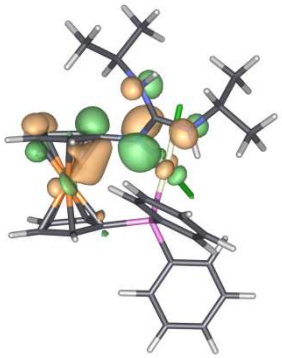	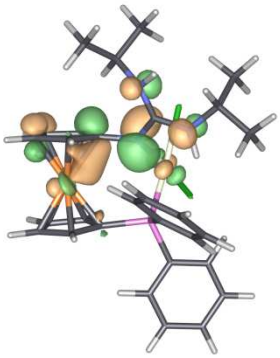
	E = −0.32262 a.u.	*E* = −0.34353 a.u.

Figure S36. Frontier molecular orbitals of **3a** and **4a*** (orbital contours were drawn on 5% probability level)

Frontier orbital contributions of **3a** and **4a*** (*Note: only contributions exceeding 1% are listed. The atoms are labelled in accordance with the xyz files deposited in the ESI)*.

3a – HOMO (orb. 161): N6(p)=28.52%; C14(p)=11.20%; Fe2(d)=7.77%; N7(p)=6.69%; C17(p)=5.93%; C15(p)=5.61%; N8(p)=5.52%; C16(p)=5.14%; Pd1(d)=3.98%; C9(p)=2.63%; Cl4(p)=2.00%; C18(p)=1.61%; C31(p)=1.54%; Cl3(p)=1.36%; C11(p)=1.33%.

3a – LUMO (orb. 162): Pd1(d)=37.04%; P5(p)=10.46%; Cl4(p)=8.28%; Cl3(p)=6.81%; N6(p)=5.05%; C28(p)=4.15%; P5(s)=3.37%; C26(p)=3.16%; C25(p)=2.72%; C30(p)=2.19%; C19(p)=1.63%; N6(s)=1.62%; C20(p)=1.25%; P5(d)=1.15%; Fe2(d)=1.12%; C22(p)=1.07%.

4a* – **HOMO** (orb. 152): N5(p)=25.75%; Fe2(d)=10.22%; C13(p)=7.53%; P4(p)=6.90%; Cl3(p)=5.63%; N6(p)=5.59%; C14(p)=4.40%; N7(p)=3.84%; C16(p)=3.57%; Pd1(p)=3.16%; C15(p)=2.99%; Pd1(d)=2.47%; C18(p)=1.27%; P4(s)=1.20%; Pd1(s)=1.10%; C8(p)=1.10%; C17(p)=1.02%

4a* – LUMO (orb. 153): Pd1(d)=35.90%; P4(p)=10.24%; Cl3(p)=10.13%; Fe2(d)=8.13%; N5(p)=5.26%; P4(s)=4.36%; Pd1(s)=3.76%; C14(p)=1.81%; C17(p)=1.71%; C13(p)=1.53%; C24(p)=1.30%; C18(p)=1.16%; C30(p)=1.14%; C8(p)=1.05%; C16(p)=1.03%; C15(p)=1.02%

Parameters of the bonds within the coordination spheres of **3a** and **4a*** discussed in the main text are summarised in Table S6.

Table S6. MBO's around the Pd atom and electron density Laplacian ($\nabla^2\rho(\mathbf{r})$) values at the BCP's located on the bond paths connecting the Atomic Critical Points corresponding to these bonds

Compound	**3a**		**4a***	
Parameter	MBO	$\nabla^2\rho(\mathbf{r})$	MBO	$\nabla^2\rho(\mathbf{r})$
Pd–Fe	0.206	no BCP	0.007	0.057
Pd–N	0.517	0.406	0.430	0.364
Pd-P	0.950	0.088	0.882	0.070
Pd–Cl	0.602 (*trans*-P) 0.665 (*trans*-N)	0.195(*trans*-P) 0.223 (*trans*-N)	0.660	0.217

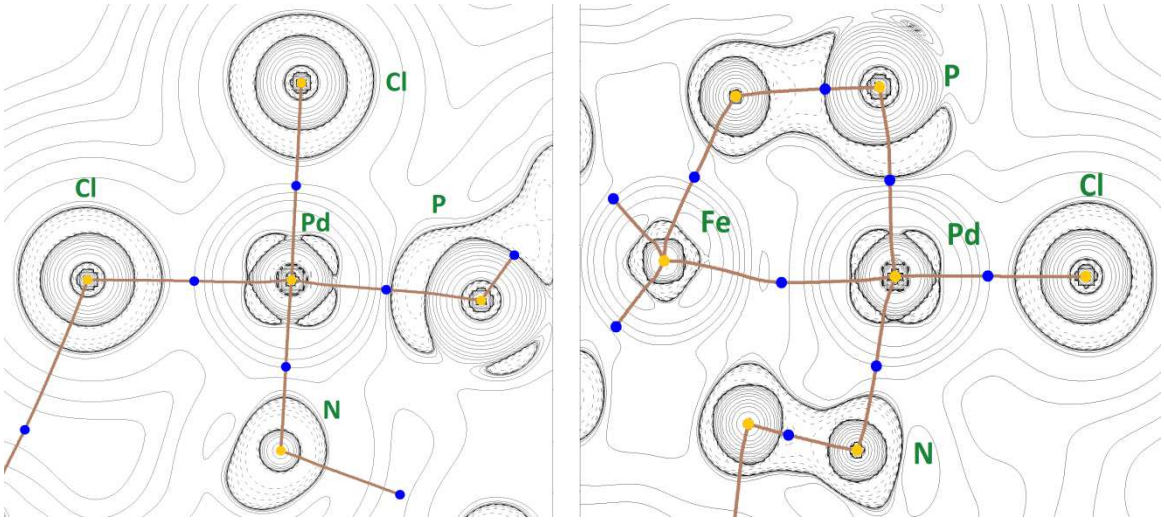

Figure S37. Laplacian contours (positive – full back lines, negative – dashed black lines), Bond Paths (brown lines), Atomic Critical Points (yellow circles) and Bond Critical Points (blue circles) in the plane defined by the Pd, Cl and Cl2 atoms for **3a** (left) and in the plane intersecting atoms Pd, Fe and P of **4a*** (right). Other types of critical points are omitted from the graph for clarity.

The UV-Vis spectrum of **4a'** recorded in dichloromethane is displayed in Fig. S38. This spectrum incorporates several overlapping peaks and their exact maxima have been determined by deconvoluting the experimental spectrum into individual peaks of Gaussian shapes. These experimental maxima have been compared with the 24 lowest excitation energies computed by time-dependant DFT (Tables S7 and S8).

Computational results suggested the presence of several forbidden transitions at lower energies (in the visible light region), which manifested themselves experimentally as a broad and elevated baseline slightly above 500 nm. However, attempts to include this broad peak in the deconvolution resulted in failures, as its inclusion triggered serious numerical instabilities and yielded predicted spectra in serious disagreement with the experimental one. Hence, the final deconvolution was done by omitting this experimental maximum.

Among the computed excitations of **4a***, the first one with the lowest energy occurred at 554.9 nm and was followed by five subsequent excitations, close in energy. All these excitations are allowed only slightly, as they become generated from the combination of transitions taking place between various d orbitals residing on both metals. Each of these d-d transitions include a mixture of over ten contributions that employ the combination of different source and different target d orbitals and their superposition is responsible for the broad shoulder appearing in the range 500–600 nm.

The first allowed and easily discernible maximum appearing at 410.9 nm is a mixed d–d and charge–transfer transition (Fig. S39), which is obtained from electronic excitation to the LUMO. This excitation takes place simultaneously from the HOMO and from the two orbitals located beneath in an approximately equal ratio, whereby each of these orbitals incorporates a significant contribution from both metals and the chloride ligand.

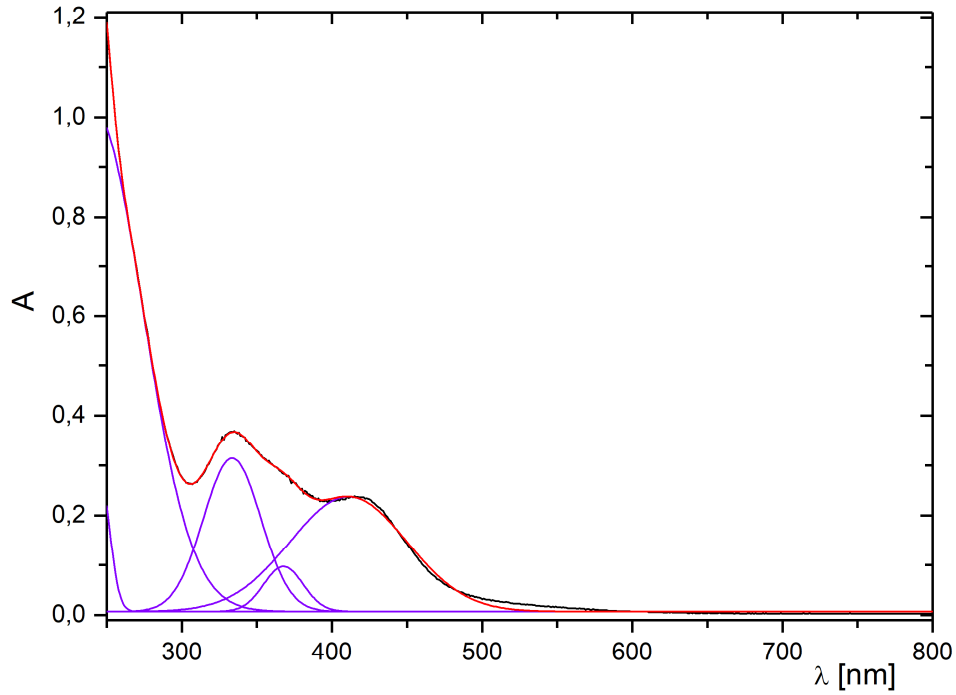

Figure S38. Experimental UV-Vis spectrum of **4a'** recorded in CH_2Cl_2 (black line) and its deconvolution into Gaussian bands (violet lines). The red line represents the sum of the individual Gaussian bands.

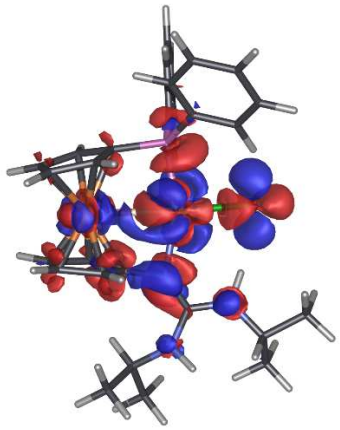

Figure S39. Plot of electron density difference between the ground state and the 7th excited state of **4a*** (probability level 0.1%).

Table S7. Experimental (E_{EXP}), computed excitation energies (E_{TDDFT}), experimental peak areas (A_{EXP}), computed oscillator strengths (f_{TDDFT}). The experimental values reported below are maxima obtained from the experimental spectrum deconvolution of **4a'** in CH_2Cl_2; computed values were obtained for **4a*** in CH_2Cl_2.

E_{EXP} [nm]	A_{EXP}	E_{TDDFT} [nm]	f_{TDDFT}
410.9	22.50	445.4; 415.9	0.0532; 0.0210
367.7	2.96	397.4	0.0299
333.5	14.78	349.2	0.2398
241.7 (incomplete)		not computed	

Table S8. Computed excitation energies for the first 24 excitations of **4a***.

No.	**Energy [eV]**	**Energy [nm]**	**f**	**No.**	**Energy [eV]**	**Energy [nm]**	**f**
1	2.2342	554.93	0.0037	13	3.5398	350.26	0.0910
2	2.2382	553.94	0.0001	14	3.5502	349.24	0.2398
3	2.3612	525.09	0.0018	15	4.0856	303.47	0.0117
4	2.4451	507.07	0.0016	16	4.2352	292.75	0.0044
5	2.5972	477.38	0.0105	17	4.2631	290.83	0.0024
6	2.6690	464.53	0.0009	18	4.2802	289.67	0.0086
7	2.7838	445.38	0.0532	19	4.3429	285.49	0.0093
8	2.9813	415.87	0.0210	20	4.3503	285.00	0.0102
9	3.0283	409.42	0.0112	21	4.4423	279.10	0.0332
10	3.1196	397.43	0.0299	22	4.4574	278.15	0.1405
11	3.2104	386.20	0.0076	23	4.5436	272.88	0.0442
12	3.5162	352.61	0.0151	24	4.5761	270.94	0.0335

REFERENCES

1 K. Škoch, I. Císařová, J. Schulz, U. Siemeling and P. Štěpnička, *Dalton Trans.*, 2017, **46**, 10339.

2 D. Nieto, S. Bruña, A. M. González-Vadillo, J. Perles, F. Carrillo-Hermosilla, A. Antiñolo, J. M. Padron, G. B. Plata and I. Cuadrado, *Organometallics*, 2015, **34**, 5407.

3 O. Bárta, I. Císařová, P. Štěpnička, *Eur. J. Inorg. Chem.,* 2017, 489.

4 P. Nicpon and D. W. Meek, *Inorg. Chem.,* 1966, **5**, 1297.

5 G. M. Sheldrick, *Acta Crystallogr., Sect. A: Found. Adv.,* 2015, **71**, 3.

6 G. M. Sheldrick, *Acta Crystallogr., Sect. C: Struct. Chem.,* 2015, **71**, 3.

7 a) A. L. Spek, *J. Appl. Crystallogr*., 2003, **36**, 7; b) A. L. Spek, *Acta Crystallogr. D, Biol. Crystallogr*., 2009, **65**, 148.

8 S. I. Kirin, H.-B. Kraatz and N. Metzler-Nolte, *Chem. Soc. Rev.,* 2006, **35**, 348.

9 J. A. Adeleke and L.-K. Liu, *Acta Crystallogr., Sect. C: Struct. Chem*., 1993, **49**, 680.

10 Cambridge Structural Database, version 5.40 of November 2018, with updates from February and May 2019.

11 K. Jess, D. Baabe, T. Bannenberg, K. Brandhorst, M. Freytag, P. G. Jones and M. Tamm, *Inorg. Chem.*, 2015, **54**, 12032.

12 T. Hayashi, M. Konishi, Y. Kobori, M. Kumada, T. Higuchi and K. Hirotsu, *J. Am. Chem. Soc*., 1984, **106**, 158.

13 a) T. G. Appleton, H. C. Clark and L. E. Manzer, *Coord. Chem. Rev*., 1973, **10**, 335; b) F. R. Hartley, *Chem. Soc. Rev*., 1973, **2**, 163.

14 L. Yang, D. R. Powell and R. P. Houser, *Dalton Trans*., 2007, 955.

15 B. Cordero, V. Gómez, A. E. Platero-Prats, M. Revés, J. Echeverría, E. Cremades, F. Barragán and S. Alvarez, *Dalton Trans*., 2008, 2832.

16 F. Barrière and W. E. Geiger, *J. Am. Chem. Soc.*, 2006, **128**, 3980.

17 J. Podlaha, P. Štěpnička, J. Ludvík and I. Císařová, *Organometallics,* 1996, **15**, 543.

18 C. Hansch, A. Leo and R. W. Taft, *Chem. Rev*., 1991, **91**, 165.

19. M. J. Frisch, G. W. Trucks, H. B. Schlegel, G. E. Scuseria, M. A. Robb, J. R. Cheeseman, G. Scalmani, V. Barone, G. A. Petersson, H. Nakatsuji, X. Li, M. Caricato, A. V. Marenich, J. Bloino, B. G. Janesko, R. Gomperts, B. Mennucci, H. P. Hratchian, J. V. Ortiz, A. F. Izmaylov, J. L. Sonnenberg, D. Williams-Young, F. Ding, F. Lipparini, F. Egidi, J. Goings, B. Peng, A. Petrone, T. Henderson, D. Ranasinghe, V. G. Zakrzewski, J. Gao, N. Rega, G. Zheng, W. Liang, M. Hada, M. Ehara, K. Toyota, R. Fukuda, J. Hasegawa, M. Ishida, T. Nakajima, Y. Honda, O. Kitao, H. Nakai, T. Vreven, K. Throssell, J. A. Montgomery, Jr., J. E. Peralta, F. Ogliaro, M. J. Bearpark, J. J. Heyd, E. N. Brothers, K. N. Kudin, V. N. Staroverov, T. A. Keith, R. Kobayashi, J.

Normand, K. Raghavachari, A. P. Rendell, J. C. Burant, S. S. Iyengar, J. Tomasi, M. Cossi, J. M. Millam, M. Klene, C. Adamo, R. Cammi, J. W. Ochterski, R. L. Martin, K. Morokuma, O. Farkas, J. B. Foresman and D. J. Fox, Gaussian, Inc., Wallingford CT, 2016.

20. R. Peverati and D. G. Truhlar, *J. Phys. Chem. Lett.,* 2011, **2**, 2810.
21. P. J. Hay and W. R. Wadt, *J. Chem. Phys.*, 1985, **82**, 270.
22. R. Ditchfield, W. J. Hehre, and J. A. Pople, *J. Chem. Phys.*, 1971, **54**, 724.
23. J. Tomasi, B. Mennucci, and R. Cammi, *Chem. Rev.*, 2005, **105**, 2999.
24. C. Adamo and V. Barone, *J. Chem. Phys.*, 1999, **110** 6158.
25. U. Wedig, M. Dolg, H. Stoll and H. Preuss, in *Quantum Chemistry: The Challenge of Transition Metals and Coordination Chemistry;* A. Veillard, Ed.; Reidel and Dordrecht, 1986, 79.
26. T. Lu and F. Chen, *J. Comput. Chem.,* 2012, **33**, 580.
27. E. D. Glendening, J. K. Badenhoop, A. E. Reed, J. E. Carpenter, J. A. Bohmann, C. M. Morales, C. R. Landis and F. Weinhold, Theoretical Chemistry Institute, University of Wisconsin, Madison, WI, 2013.

Appendix D

Synthetic procedures, characterisation data and selected crystallographic parameters for compounds **17**-**26**. *Unpublished results*.

EXPERIMENTAL

Materials and methods

All synthetic procedures were performed under an atmosphere of an inert gas (argon or nitrogen) using standard Schlenk techniques and dried, deoxygenated solvents. Chloroform and acetonitrile (analytical grade) were dried over calcium hydride and distilled under an argon atmosphere. Dichloromethane and tetrahydrofuran (HPLC grade) were purified using a Pure Solv MD-5 (Inovative Technology, USA) solvent purification system. For other purposes, typically for crystallisations, analytical grade solvents (Lach-Ner, Czech Republic) were used without further purification. The commercially available starting materials were the products of Merck, Alfa-Aesar and TCI and were used as received. Compounds $Ph_2PfcN{=}C(NH\textit{i}Pr)_2$ (**13a**) and *cis*-[$PdCl_2${$Ph_2PfcN{=}C(NH\textit{i}Pr)_2$-$\kappa^2$*P,N*}] (**15a**) were prepared as previously described.[1]

The NMR spectra were recorded at 25°C on a Varian INOVA 400 spectrometer operating at 399.95 MHz (^{1}H), 100.58 MHz (^{13}C) and 161.90 MHz (^{31}P). Chemical shifts (δ in ppm) are given relative to tetramethylsilane as an internal reference (^{1}H and ^{13}C), and to 85% aqueous H_3PO_4 as an external reference (^{31}P). FTIR spectra of samples diluted with KBr were recorded in diffuse reflectance mode (DRIFTS) over the range of 400-4000 cm^{-1} on a Nicolet 6700 FTIR spectrometer. ESI mass spectra were recorded with a Compact QTOF-MS spectrometer (Bruker Daltonics) from samples dissolved in HPLC-grade solvents (methanol, acetonitrile or acetone). Elemental analyses were determined with a Perkin–Elmer 2400 Series II CHNS/O analyser. The presence of residual solvent (if any) was confirmed by NMR analysis.

The following abbreviations are used in the text below: fc = ferrocene-1,1′-diyl, *i*Pr = *iso*-propyl, BArF = tetrakis[3,5-bis(trifluoromethyl)phenyl]borate; vt and vq denote virtual triplets and quartets in the NMR spectra.

Synthesis

Preparation of cis-[$PtCl_2${$Ph_2PfcN{=}C(NHiPr)_2$-κ^2P,N}] (17)

A mixture of **13a** (256 mg, 0.5 mmol) and *cis*-dichlorobis(dimethylsulfoxide)platinum(II) (211 mg, 0.50 mmol) in dry chloroform (20 mL) was stirred at room temperature for 2 hours. The resulting orange solution was filtered through a PTFE syringe filter (pore size 0.45 μm) and the filtrate was layered with diethyl ether. After several days, tiny yellow crystals formed, which were isolated by suction. To remove residual clathrated solvents, the crystals were grinded and the obtained yellow powder was dried under vacuum. Yield of **17**: 331 mg (85%), yellow

powder. The crystals suitable for X-ray structure determination were obtained by liquid-phase diffusion of diethyl ether into the chloroform solution of **17**.

^{1}H NMR (CD_2Cl_2): δ 0.90-1.50 (br m, 12 H, CH*Me*$_2$), 3.40-4.00 (br m, 2 H, C*H*Me$_2$), 3.96 (m, 1 H, CH of fc), 4.22 (m, 1 H, CH of fc), 4.29 (m, 2 H, CH of fc), 4.34 (m, 1 H, CH of fc), 4.69 (m, 1 H, CH of fc), 5.12 (m, 1 H, CH of fc), 5.43 (m, 1 H, CH of fc), 6.33 (br s, 1 H NH), 7.28-7.48 (m, 7 H, PPh_2), 7.52-7.58 (m, 1 H, PPh_2), 7.82-7.90 (m, 2 H, PPh_2). ^{13}C{^{1}H} NMR (CD_2Cl_2): δ 23.30 (br s, CH*Me*$_2$), 24.22 (br s, CH*Me*$_2$), 47.30 (br s, *C*HMe$_2$), 65.98 (s, CH of fc), 68.22 (s, CH of fc), 68.49 (s, CH of fc), 69.08 (s, CH of fc), 71.27 (d, J_{CP} = 70 Hz, C^{ipso}–P of fc), 71.73 (d, J_{CP} = 7 Hz, CH of fc), 73.97 (d, J_{CP} = 10 Hz, CH of fc), 75.20 (d, J_{CP} = 6 Hz, CH of fc), 77.92 (d, J_{CP} = 18 Hz, CH of fc), 110.85 (d, J_{CP} = 2 Hz, C^{ipso}–N of fc), 127.76 (d, J_{CP} = 11 Hz, PPh_2), 128.73 (d, J_{CP} = 11 Hz, PPh_2), 129.50 (d, J_{CP} = 62 Hz, C^{ipso}–P of PPh_2), 130.40 (d, J_{CP} = 3 Hz, PPh_2), 131.20 (d, J_{CP} = 66 Hz, C^{ipso}–P of PPh_2), 131.68 (d, J_{CP} = 3 Hz, PPh_2), 133.05 (d, J_{CP} = 10 Hz, PPh_2), 134.42 (d, J_{CP} = 11 Hz, PPh_2), 159.76 (s, C^{ipso} of guanidine). ^{31}P{^{1}H} NMR (CD_2Cl_2): δ 2.2 (s with ^{195}Pt satellites, $^{1}J_{PPt}$ = 4125 Hz). ESI+ MS: *m*/*z* 742 ([M – Cl]$^{+}$). IR (DRIFTS): ν_{max} 3298 s, 3093 w, 3059 w, 3046 w, 2975 m, 2928 w, 2867 w, 1582 s, 1559 s, 1482 w, 1463 m, 1435 s, 1404 w, 1387 m, 1365 w, 1323 m, 1309 m, 1258 w, 1211 w, 1196 m, 1171 m, 1130 w, 1102 m, 1093 m, 1054 w, 1030 w, 1201 m 999 w, 936 w, 868 w, 846 w, 832 w, 817 m, 801 w, 750 m, 709 w, 697 s, 636 w, 623 w, 547 m, 531 s, 516 m, 508 m, 482 s, 452 w, 432 w. Anal. Calc. for $C_{29}H_{34}Cl_2FeN_3PPt$ (777.4): C 44.80, H 4.41, N 5.41%. Found: C 45.06, H 4.38, N 5.51%.

Preparation of [Pt(μ-Cl){Ph$_2$PfcN=C(NHiPr)$_2$-κ^{2}P,N}]$_2$(BArF)$_2$ (18)

A mixture of **17** (155 mg, 0.20 mmol) and sodium tetrakis[3,5-bis(trifluoromethyl)-phenyl]borate (177 mg, 0.20 mmol) in dry chloroform (10 mL) was stirred at room temperature for 2 hours, during which time the suspension slowly turned from orange to orange-red. The separated sodium chloride was filtered off and the clear filtrate was evaporated. The orange-red waxy residue was dissolved in chloroform (approximately 5 mL) to form a saturated solution. Crystallisation at 8 °C for several days produced orange-red crystals (also used for structure determination), which were separated by suction. To remove residual solvents, the crystals were grinded and the obtained orange-red powder was dried under vacuum. Yield of **18**: 273 mg (85%), orange-red powder. *Note: Only one of the four possible stereoisomers was identified by X-ray structure elucidation. However, signals attributable to four distinct species were observed in the NMR spectra (see below). The two major and two minor isomers observed immediately after dissolving the crystalline material equilibrated over time to approximately 1:1:1:1 mixture, suggesting an equilibrium between the stereoisomers in solution.*

^{1}H NMR (CD_2Cl_2): δ 0.50-1.60 (br m, 48 H, CH*Me*$_2$), 2.90-4.10 (br m, 8 H, C*H*Me$_2$), 4.09 (m, 1 H, CH of fc), 4.12 (m, 2 H, CH of fc), 4.20 (m, 1 H, CH of fc), 4.27 (m, 1 H, CH of fc), 4.32 (m, 2 H,

CH of fc), 4.36 (m, 1 H, CH of fc), 4.39 (m, 2 H, CH of fc), 4.41 (m, 2 H, CH of fc), 4.45 (m, 2 H, CH of fc), 4.49 (m, 1 H, CH of fc), 4.53 (m, 2 H, CH of fc), 4.61 (m, 2 H, CH of fc), 4.69 (m, 1 H, CH of fc), 4.86 (m, 2 H, CH of fc), 4.92 (m, 1 H, CH of fc), 4.99 (m, 3 H, CH of fc), 5.12 (m, 1 H, CH of fc), 5.27 (m, 1 H, CH of fc), 5.44 (m, 1 H, CH of fc), 5.51 (m, 1 H, CH of fc), 5.57 (m, 1 H, CH of fc), 5.61 (m, 1 H, CH of fc), 7.14-7.26 (m, 4 H, aromatic CH), 7.30-7.46 (m, 8 H, aromatic CH), 7.48-7.59 (m, 12 H, aromatic CH), 7.60-7.78 (m, 28 H, aromatic CH). Signals due to NH of guanidine were not observed. $^{31}P\{^{1}H\}$ NMR (CD_2Cl_2): δ 2.3, 3.0, 5.0, 5.4 (4× s with ^{195}Pt satellites). The $^{1}J_{PPt}$ interaction constants were not resolved. ESI+ MS: *m*/*z* 705 ($[Pt\{Ph_2PfcN{=}C(NHiPr)(NiPr)\}]^+$), 741 ($[PtCl\{Ph_2PfcN{=}C(NHiPr)_2\}]^+$). IR (DRIFTS): ν_{max} 3402 w, 3339 w, 2976 w, 1609 m, 1586 s, 1511 m, 1488 w, 1466 w, 1440 m, 1393 w, 1375 w, 1356 s, 1304 w, 1282 s, 1161 s, 1128 s, 1101 s, 1053 w, 1043 w, 1030 w, 1001 w, 932 w, 897 m, 887 m, 840 m, 824 w, 774 m, 712 m, 701 w, 692 m, 682 m, 672 m, 637 m, 578 w, 546 w, 527 w, 514 w, 508 m, 500 w, 450 w. Anal. Calc. for $C_{122}H_{92}B_2Cl_2F_{48}Fe_2N_6P_2Pt_2$ (3210.4): C 45.64, H 2.89, N 2.62%. Found: C 45.27, H 2.93, N 2.80%.

Preparation of [Ph₂PfcNHC(NHiPr)₂]Cl (19)

To a solution of **13a** (1.02 g, 2.0 mmol) in dry dichloromethane (15 mL), a solution of hydrogen chloride (1.6 mL, 1.25 M in methanol, 2.0 mmol) was added and the resulting orange solution was stirred at room temperature. After 10 minutes (*Note: longer reaction times led to partial oxidation of the phosphine*), the stirring was discontinued and the volatiles were evaporated. The crude product was further crystallized from ethyl acetate/hexane mixture. Yield of **19**: 0.96 g (88%), orange microcrystalline powder. Crystals suitable for X-ray structure elucidation were obtained by liquid-phase diffusion of hexane into the ethyl acetate solution of **19**.

^{1}H NMR ($CDCl_3$): δ 1.24 (d, $^{3}J_{HH}$ = 6.4 Hz, 12 H, CH*Me*$_2$), 3.89 (sept, $^{3}J_{HH}$ = 6.4 Hz, 2 H, C*H*Me$_2$), 4.05 (vt, *J′* = 1.9 Hz, 2 H, CH of fc), 4.18 (m, 4 H, CH of fc), 4.60 (vt, *J′* = 1.7 Hz, 2 H, CH of fc), 7.30-7.40 (m, 10 H, PPh_2). Signals due to NH of guanidinium were not observed. $^{13}C\{^{1}H\}$ NMR ($CDCl_3$): δ 23.02 (s, CH*Me*$_2$), 45.03 (s, *C*HMe$_2$), 64.82 (broad s, CH of fc), 67.47 (s, CH of fc), 72.72 (d, J_{CP} = 3 Hz, CH of fc), 73.67 (d, J_{CP} = 14 Hz, CH of fc), 76.25 (d, J_{CP} = 4 Hz, C^{ipso}–P of fc), 128.31 (d, J_{CP} = 7 Hz, PPh_2), 128.79 (s, PPh_2), 133.43 (d, J_{CP} = 20 Hz, PPh_2), 138.01 (d, J_{CP} = 9 Hz, C^{ipso} of PPh_2), 153.39 (s, C^{ipso} of guanidinium). Signal due to C^{ipso}–N of fc was not identified. $^{31}P\{^{1}H\}$ NMR ($CDCl_3$): δ –18.2 (s, PPh_2). ESI+ MS: *m*/*z* 512 ($[M - Cl]^+$). IR (DRIFTS): ν_{max} 3289 s, 3240 w, 3173 m, 3119 m, 3095 m, 3056 s, 2979 s, 2874 m, 2800 s, 2737 m, 1636 s, 1605 s, 1569 m, 1529 w, 1478 s, 1459 m, 1444 m, 1432 m, 1406 m, 1386 m, 1370 m, 1358 w, 1339 m, 1313 w, 1260 m, 1215 w, 1201 w, 1158 m, 1127 m, 1091 m, 1068 w, 1057 w, 1043 w, 1027 m, 1020 w, 999 w, 947 m, 928 w, 911 w, 890 w, 868 w, 828 m, 818 w, 811 w, 780 w, 742 s, 717 m, 696 s, 683 m, 639 w, 630 w, 588 w, 566 w, 533 w, 519 w, 502 m, 487 s, 456 w, 437 w. Anal. Calc. for $C_{29}H_{35}ClFeN_3P$ (547.9): C 63.57, H 6.44, N 7.67%. Found: C 63.04, H 6.29, N 7.49%.

Preparation of [Ph_2PfcNHC(NHiPr)$_2$][SbF_6]·CH_2Cl_2 (20·CH_2Cl_2)

A suspension of **19** (274 mg, 0.50 mmol) and potassium hexafluoroantimonate(V) (165 mg, 0.60 mmol) in dry dichloromethane (10 mL) was stirred at room temperature overnight. On the next day, the precipitated potassium chloride was filtered off and the clear orange filtrate was concentrated under reduced pressure to the approximate volume of 5 mL and layered with hexane. Crystallisation by liquid-phase diffusion over several days at 8 °C afforded orange prismatic crystals, which were isolated by suction, washed with pentane and dried under vacuum. Yield of **20**·CH_2Cl_2: 263 mg (63%), orange crystalline solid. Crystals suitable for X-ray structure determination were obtained by the same procedure as the bulk material.

^{1}H NMR ($CDCl_3$): δ 1.32 (d, $^3J_{HH}$ = 6.2 Hz, 12 H, CH*Me*$_2$), 3.96 (d of sept, $J \approx {}^3J_{HH}$ = 6.2 Hz, 2 H, C*H*Me$_2$), 4.16 (vq, J' = 1.8 Hz, 2 H, CH of fc), 4.24 (vt, J' = 2.0 Hz, 2 H, CH of fc), 4.35 (vt, J' = 2.0 Hz, 2 H, CH of fc), 4.52 (vt, J' = 1.8 Hz, 2 H, CH of fc), 5.30 (s, 2 H, CH_2Cl_2), 5.44 (s, 2 H, NH), 7.33-7.41 (m, 10 H, PPh_2), 7.71 (s, 1 H, NH). ^{13}C{^{1}H} NMR ($CDCl_3$): δ 22.40 (s, CH*Me*$_2$), 45.17 (d, J = 2 Hz, *C*HMe$_2$), 53.43 (s, CH_2Cl_2), 67.32 (s, CH of fc), 68.98 (s, CH of fc), 72.63 (d, J_{CP} = 3 Hz, CH of fc), 73.67 (d, J_{CP} = 12 Hz, CH of fc), 76.22 (s, C^{ipso}–P of fc), 87.68 (s, C^{ipso}–N of fc), 128.73 (d, J_{CP} = 8 Hz, PPh_2), 129.54 (s, PPh_2), 133.44 (d, J_{CP} = 19 Hz, PPh_2), 135.80 (d, J_{CP} = 4 Hz, C^{ipso}–P of PPh_2), 152.95 (C^{ipso} of guanidinium). ^{31}P{^{1}H} NMR ($CDCl_3$): δ –21.8 (s). ESI+ MS: *m*/*z* 512 ([M – SbF_6]$^+$). IR (DRIFTS): ν_{max} 3389 m, 3225 m, 3109 w, 3055 w, 2981 m, 2941 w, 2882 w, 1634 s, 1614 s, 1471 m, 1435 s, 1394 m, 1375 m, 1326 m, 1265 w, 1214 w, 1195 w, 1162 m, 1132 w, 1093 w, 1071 w, 1052 w, 1029 m, 999 w, 946 w, 875 w, 842 w, 821 m, 748 s, 698 s, 662 s, 565 w, 518 w, 488 m, 463 w. Anal. Calc. for $C_{29}H_{35}F_6FeN_3PSb$·CH_2Cl_2 (833.1): C 43.25, H 4.48, N 5.04%. Found: C 43.16, H 4.15, N 4.92%.

Preparation of [$PdCl_3${Ph_2PfcNHC(NHiPr)$_2$-κP}] (21)

To a solution of **15a** (138 mg, 0.20 mmol) in dry dichloromethane (10 mL), a solution of hydrogen chloride (0.4 mL, 0.5 M in methanol, 0.2 mmol) was added, and the resulting red solution was stirred at room temperature for 30 minutes, after which time the volatiles were evaporated. The red residue was dissolved in chloroform (2 mL) and the dark red solution was kept at –18°C. After several days, the separated solid was isolated by suction, washed with pentane and dried under vacuum. Yield of **21**·2.5$CHCl_3$: 165 mg (81%), red microcrystalline powder. *Note: The product originally formulated as a chloroform solvate slowly releases the clathrated solvent as indicated by the elemental analysis.* Crystals suitable for structure determination were obtained by gradual cooling of the saturated chloroform solution.

^{1}H NMR (CD_2Cl_2/CD_3OD): δ 1.27 (d, $^3J_{HH}$ = 6.1 Hz, 12 H, CH*Me*$_2$), 4.03 (sept, $^3J_{HH}$ = 6.1 Hz, 2 H, C*H*Me$_2$), 4.44 (m, 2 H, CH of fc), 4.60 (m, 2 H, CH of fc), 4.76 (m, 2 H, CH of fc), 5.19 (m, 2 H, CH

of fc), 6.13 (s, 1 H, NH), 7.36 (s, 2 H, $CHCl_3$), 7.36-7.43 (m, 4 H, PPh_2), 7.47-7.52 (m, 2 H, PPh_2), 7.53-7.60 (m, 4 H, PPh_2). $^{13}C\{^1H\}$ NMR (CD_2Cl_2/CD_3OD): δ 22.88 (s, $CHMe_2$), 45.93 (s, $CHMe_2$), 68.15 (s, CH of fc), 68.92 (s, CH of fc), 73.02 (d, J_{CP} = 7 Hz, CH of fc), 73.37 (d, J_{CP} = 63 Hz, C^{ipso}–P of fc), 77.87 (d, J_{CP} = 9 Hz, CH of fc), 78.05 (s, $CHCl_3$), 93.58 (s, C^{ipso}–N of fc), 128.09 (d, J_{CP} = 11 Hz, PPh_2), 130.74 (d, J_{CP} = 57 Hz, C^{ipso}–P of PPh_2), 131.30 (d, J_{CP} = 3 Hz, PPh_2), 134.34 (d, J_{CP} = 10 Hz, PPh_2), 154.23 (s, C^{ipso} of guanidinium). $^{31}P\{^1H\}$ NMR (CD_2Cl_2/CD_3OD): δ 23.9 (s). ESI+ MS: m/z 652 ($[M - Cl - HCl]^+$). IR (DRIFTS): ν_{max} 3408 w, 3239 m, 3201 m, 3111 m, 3077 m, 2975 m, 2933 w, 1633 s, 1601 s, 1508 w, 1482 m, 1470 m, 1454 m, 1436 s, 1391 m, 1373 m, 1320 m, 1260 w, 1211 w, 1165 s, 1130 m, 1100 m, 1063 w, 1033 m, 998 w, 942 w, 910 w, 840 w, 825 w, 747 s, 711 m, 694 s, 664 w, 625 m, 545 m, 525 s, 505 s, 476 s, 452 w, 428 w, 418 w. Anal. Calc. for $C_{29}H_{35}Cl_3FeN_3PPd \cdot 1.5\ CHCl_3$ (904.3): C 40.51, H 4.07, N 4.65%. Found: C 40.75, H 4.34, N 4.63%.

Preparation of [PdCl(μ-Cl){Ph_2PfcNHC(NHiPr)$_2$-κP}]$_2$[SbF_6]$_2$ (23)

A mixture of **20**·CH_2Cl_2 (75 mg, 0.10 mmol) and bis(acetonitrile)dichloropalladium(II) (26 mg, 0.10 mmol) in dry dichloromethane (5 mL) was stirred at room temperature for 1 hour. Then, the purple-red solution was filtered through a PTFE syringe filter (pore size 0.45 μm), concentrated under reduced pressure to the volume of approximately 2 mL and layered with diethyl ether. Crystallization over several days afforded dark red crystals (also used for structure determination), which were isolated by suction, washed with diethyl ether and dried under vacuum. During the isolation, the crystals disintegrated to dark red powder presumably due to the loss of clathrated solvent. Yield of **23**: 82 mg (89%), dark red powder.

^1H NMR (CD_2Cl_2/CD_3OD): δ 1.24 (d, $^3J_{HH}$ = 6.3 Hz, 12 H, $CHMe_2$), 3.89 (d of sept, $J \approx {}^3J_{HH}$ = 6.3 Hz, 2 H, $CHMe_2$), 4.58 (vt, J' = 1.8 Hz, 2 H, CH of fc), 4.65 (vq, J' = 1.8 Hz, 2 H, CH of fc), 4.74 (vq, J' = 1.7 Hz, 2 H, CH of fc), 4.96 (vt, J' = 1.8 Hz, 2 H, CH of fc), 6.18 (s, 2 H, NH), 7.39-7.48 (m, 4 H, PPh_2), 7.52-7.63 (m, 6 H, PPh_2). $^{13}C\{^1H\}$ NMR (CD_2Cl_2/CD_3OD): δ 22.63 (s, $CHMe_2$), 45.59 (s, $CHMe_2$), 68.72 (s, CH of fc), 69.42 (s, CH of fc), 71.70 (d, J_{CP} = 67 Hz, C^{ipso}–P of fc), 74.39 (d, J_{CP} = 9 Hz, CH of fc), 76.69 (d, J_{CP} = 10 Hz, CH of fc), 92.95 (s, C^{ipso}–N of fc), 128.76 (d, J_{CP} = 12 Hz, PPh_2), 132.46 (s, PPh_2), 134.12 (d, J_{CP} = 10 Hz, PPh_2), 153.40 (s, C^{ipso} of guanidinium). The signal due to C^{ipso}–P of Ph was not observed. $^{31}P\{^1H\}$ NMR (CD_2Cl_2/CD_3OD): δ 31.2 (s). ESI+ MS: m/z 652 ($[PdCl\{Ph_2PfcNC(NHiPr)_2\}]^+$). IR (DRIFTS): ν_{max} 3357 m, 3260 m, 3115 w, 2982 m, 2939 w, 1634 s, 1609 s, 1482 m, 1471 m, 1437 s, 1394 m, 1375 m, 1331 m, 1213 w, 1193 w, 1169 s, 1132 m, 1103 m, 1063 w, 1032 m, 999 w, 945 w, 871 w, 848 w, 836 m, 751 m, 714 m, 692 s, 665 s, 640 s, 623 w, 571 w, 548 m, 526 s, 503 s, 495 s, 482 s, 447 w. Anal. Calc. for $C_{58}H_{70}Cl_4F_{12}Fe_2N_6P_2Pd_2Sb_2$ (1851.0): C 37.64, H 3.81, N 4.54%. Found: C 37.52, H 3.58, N 4.37%.

Preparation of trans-[PdCl$_2${Ph$_2$PfcNHC(NHiPr)$_2$-κP}$_2$][SbF$_6$]$_2$ (24)

A mixture of **20**·CH_2Cl_2 (75 mg, 0.10 mmol), bis(acetonitrile)dichloropalladium(II) (26 mg, 0.05 mmol) and dry dichloromethane (2 mL) was stirred at room temperature for 2 hours, whereupon it deposited an orange-red solid. The precipitate was collected, washed with diethyl ether and dried under vacuum. Yield of **24**: 77 mg (92%), orange-red powder. Crystals suitable for X-ray structure elucidation were obtained by liquid-phase diffusion of diethyl ether into a methanolic solution of **24**.

^{1}H NMR (CD_2Cl_2/CD_3OD): δ 1.13 (d, $^3J_{HH}$ = 6.4 Hz, 12 H, CH*Me*$_2$), 3.60 (sept, $^3J_{HH}$ = 6.4 Hz, 2 H, C*H*Me$_2$), 4.38 (vt, *J′* = 2.0 Hz, 2 H, CH of fc), 4.43 (m, 2 H, CH of fc), 4.60 (m, 2 H, CH of fc), 4.63 (vt, *J′* = 2.0 Hz, 2 H, CH of fc), 7.39-7.46 (m, 4 H, PPh$_2$), 7.47-7.54 (m, 2 H, PPh$_2$), 7.58-7.65 (m, 4 H, PPh$_2$). ^{13}C{^{1}H} NMR (CD_2Cl_2/CD_3OD): δ 22.49 (s, CH*Me*$_2$), 45.49 (s, *C*HMe$_2$), 67.05 (s, CH of fc), 69.10 (s, CH of fc), 73.61 (vt, *J′* = 4 Hz, CH of fc), 74.24 (vt, *J′* = 28 Hz, C^{ipso}–P of fc), 78.34 (vt, *J′* = 5 Hz, CH of fc), 92.91 (s, C^{ipso}–N of fc), 128.77 (vt, *J′* = 5 Hz, PPh$_2$), 130.89 (vt, *J′* = 25 Hz, C^{ipso}–P of PPh$_2$), 131.60 (s, PPh$_2$), 134.48 (vt, *J′* = 6 Hz, PPh$_2$), 153.07 (s, C^{ipso} of guanidinium). ^{31}P{^{1}H} NMR (CD_2Cl_2/CD_3OD): δ 16.9 (s). ESI+ MS: *m*/*z* 616 ([Pd{Ph$_2$PfcNC(NH*i*Pr)(N*i*Pr)}]$^+$), 652 ([PdCl{Ph$_2$PfcNC(NH*i*Pr)$_2$}]$^+$), 1435 ([PdCl$_2${Ph$_2$PfcNHC(NH*i*Pr)$_2$}$_2$][SbF$_6$]$^+$). IR (DRIFTS): ν_{max} 3389 m, 3315 m, 3095 m, 2982 m, 2933 w, 2876 w, 1651 s, 1613 s, 1478 m, 1435 m, 1403 w, 1392 m, 1374 m, 1352 w, 1338 w, 1306 w, 1199 w, 1168 m, 1132 w, 1099 m, 1063 w, 1037 w, 1028 m, 859 w, 848 m, 831 w, 745 m, 711 w, 691 m, 659 s, 642 m, 622 w, 565 w, 540 w, 520 m, 490 s, 476 m, 458 w. Anal. Calc. for $C_{58}H_{70}Cl_2F_{12}Fe_2N_6P_2PdSb_2$ (1673.7): C 41.62, H 4.22, N 5.02%. Found: C 41.40, H 4.11, N 5.25%.

Preparation of [PdCl{Ph$_2$PfcN=C(NHiPr)(NiPr)-κ^{3}P,N,N′}]·Et$_2$O (25·Et$_2$O)

A suspension of **15a** (0.69 g, 1.0 mmol) in dry tetrahydrofuran (20 mL) was cooled to 0 °C in an ice bath and a solution of potassium bis(trimethylsilyl)amide (1.0 mL of 1M solution in THF, 1.0 mmol) was added. The mixture was stirred for 15 minutes while cooling and then for another 45 minutes at room temperature. During this time the solid starting material completely dissolved to give dark red solution, which was subsequently filtered through a PTFE syringe filter (pore size 0.45 μm) and evaporated. The dark red residue was extracted with hot diethyl ether to prepare a saturated solution, which was left to stand at –18 °C. After several days, dark red crystals, which formed, were collected, washed with pentane and dried under vacuum. Yield of **25**·Et_2O: 0.59 g (81%), dark red crystalline solid. The crystals suitable for X-ray structure determination were obtained by the same procedure as the bulk material.

^{1}H NMR (C_6D_6): δ 0.67 (d, $^3J_{HH}$ = 6.3 Hz, 6 H, CH*Me*$_2$), 1.12 (t, $^3J_{HH}$ = 7.0 Hz, 6 H, OCH$_2$C*H*$_3$), 1.57 (d, $^3J_{HH}$ = 6.3 Hz, 6 H, CH*Me*$_2$), 3.10 (d of sept, $^3J_{HH}$ = 9.7 Hz, $^3J_{HH}$ = 6.3 Hz, 1 H, C*H*Me$_2$), 3.20 (d, $^3J_{HH}$ = 9.7 Hz, 1 H, NH), 3.26 (q, $^3J_{HH}$ = 7.0 Hz, 4 H, OC*H*$_2$CH$_3$), 3.31 (d of sept, J_{HP} = 14.9 Hz, $^3J_{HH}$ =

6.3 Hz, 1 H, C*H*Me$_2$), 3.53 (vt, *J′* = 1.8 Hz, 2 H, CH of fc), 3.96 (m, 2 H, CH of fc), 4.49 (vt, *J′* = 1.9 Hz, 2 H, CH of fc), 4.77 (m, 2 H, PPh$_2$), 6.99-7.08 (m, 6 H, PPh$_2$), 7.94-8.05 (m, 4 H, PPh$_2$). ^{13}C{^{1}H} NMR (C$_6$D$_6$): δ 15.57 (s, OCH$_2$*C*H$_3$), 23.21 (s, CH*Me*$_2$), 24.36 (s, CH*Me*$_2$), 43.99 (s, *C*HMe$_2$), 47.52 (d, J_{CP} = 5 Hz, *C*HMe$_2$), 65.41 (s, CH of fc), 65.88 (s, O*C*H$_2$CH$_3$), 67.67 (s, CH of fc), 71.21 (d, J_{CP} = 8 Hz, CH of fc), 77.66 (d, J_{CP} = 12 Hz, CH of fc), 81.66 (d, J_{CP} = 55 Hz, C^{ipso}–P of fc), 116.92 (s, C^{ipso}–N of fc), 127.95 (d, J_{CP} = 12 Hz, PPh$_2$), 130.57 (d, J_{CP} = 2 Hz, PPh$_2$), 131.88 (d, J_{CP} = 50 Hz, C^{ipso}–P of PPh$_2$), 135.18 (d, J_{CP} = 11 Hz, PPh$_2$), 168.73 (d, J_{CP} = 5 Hz, C^{ipso} of guanidinate). ^{31}P{^{1}H} NMR (C$_6$D$_6$): δ 35.3 (s). ESI+ MS: *m*/*z* 616 ([Pd{Ph$_2$PfcNC(NH*i*Pr)(N*i*Pr)}]$^+$), 648 ([Pd(OMe){Ph$_2$PfcNC(NH*i*Pr)$_2$}]$^+$). IR (DRIFTS): ν_{max} 3323 m, 3074 w, 3054 m, 3022 w, 2975 s, 2961 m, 2932 m, 2870 m, 2810 w, 1596 s, 1586 s, 1483 m, 1450 s, 1436 s, 1399 s, 1381 s, 1364 m, 1348 m, 1324 m, 1253 m, 1205 w, 1194 w, 1169 m, 1149 m, 1126 w, 1100 s, 1074 m, 1045 w, 1026 m, 999 w, 986 m 933 m, 896 w, 867 w, 854 w, 841 w, 816 m, 748 m, 708 m, 694 s, 673 w, 635 m, 591 w, 542 m, 522 m, 508 m, 497 m, 483 m, 455 w, 444 w. Anal. Calc. for C$_{29}$H$_{33}$ClFeN$_3$PPd·Et$_2$O (726.4): C 54.56, H 5.97, N 5.78%. Found: C 54.08, H 6.02, N 5.63%.

Preparation of [Pd{Ph$_2$PfcN=C(NHiPr)(NiPr)-κ^{3}P,N,N'}(dmap)][SbF$_6$] (26)

A dark red suspension of **25**·Et$_2$O (145 mg, 0.20 mmol) and silver(I) hexafluoroantimonate (69 mg, 0.20 mmol) in dry acetonitrile (10 mL) was stirred at room temperature with an exclusion of direct daylight for 1 hour. The precipitated silver(I) chloride was filtered off using PTFE syringe filter (pore size 0.45 μm) and the dark red filtrate was treated with a solution of 4-(dimethylamino)pyridine (24 mg, 0.20 mmol) in dry dichloromethane (2 mL). The mixture was stirred at room temperature for additional 30 minutes before the volatiles were evaporated under reduced pressure. The dark red solid residue was redissolved in dichloromethane (3 mL) and the solution was layered with methyl *tert*-butyl ether. Crystallisation over several days afforded dark red crystals, which were isolated by suction, washed with pentane and dried under vacuum. Yield of **26**: 160 mg (82%), dark red crystalline solid. The crystals used for X-ray structure determination were obtained by the same procedure as the bulk material.

^{1}H NMR (CD$_2$Cl$_2$): δ 0.82 (d, $^3J_{HH}$ = 6.3 Hz, 6 H, CH*Me*$_2$), 0.94 (d, $^3J_{HH}$ = 6.4 Hz, 6 H, CH*Me*$_2$), 2.90 (s, 6 H, NMe$_2$), 3.01 (d of sept, $^3J_{HH}$ = 9.4 Hz, $^3J_{HH}$ = 6.4 Hz, 1 H, C*H*Me$_2$), 3.35 (sept, $^3J_{HH}$ = 6.3 Hz, 1 H, C*H*Me$_2$), 3.69 (d, $^3J_{HH}$ = 9.4 Hz, 1 H, NH), 3.90 (vt, *J′* = 2.1 Hz, 2 H, CH of fc), 4.49 (vq, *J′* = 1.6 Hz, 2 H, CH of fc), 4.99 (vq, *J′* = 2.1 Hz, 2 H, CH of fc), 5.32 (vt, *J′* = 1.1 Hz, 2 H, CH of fc), 6.12 (m, 2 H, CH of dmap), 7.31-7.37 (m, 4 H, PPh$_2$), 7.43-7.49 (m, 2 H, PPh$_2$), 7.58-7.66 (m, 4 H, PPh$_2$), 7.71 (m, 2 H, CH of dmap). ^{13}C{^{1}H} NMR (CD$_2$Cl$_2$): δ 23.24 (s, CH*Me*$_2$), 24.17 (s, CH*Me*$_2$), 39.40 (s, NMe$_2$), 44.42 (s, *C*HMe$_2$), 46.36 (d, J_{CP} = 4 Hz, *C*HMe$_2$), 66.33 (s, CH of fc), 67.90 (s, CH of fc), 72.64 (d, J_{CP} = 8 Hz, CH of fc), 77.77 (d, J_{CP} = 59 Hz, C^{ipso}–P of fc), 78.15 (d, J_{CP} = 13 Hz, CH of fc), 108.50 (s, CH of dmap), 115.65 (d, J_{CP} = 1 Hz, C^{ipso}–N of fc), 128.96 (d, J_{CP} = 11 Hz, PPh$_2$), 129.74 (d, J_{CP} =

50 Hz, C^{ipso}–P of PPh_2), 131.55 (d, J_{CP} = 3 Hz, PPh_2), 134.04 (d, J_{CP} = 12 Hz, PPh_2), 150.67 (d, J_{CP} = 1 Hz, CH of dmap), 154.81 (s, C^{ipso}–N of dmap), 170.45 (d, J_{CP} = 4 Hz, C^{ipso} of guanidinate). $^{31}P\{^1H\}$ NMR (CD_2Cl_2): δ 35.9 (s). ESI+ MS: *m*/*z* 616 ([Pd{Ph_2PfcNC(NH*i*Pr)(N*i*Pr)}]$^+$), 738 ([Pd{Ph_2PfcNC(NH*i*Pr)(N*i*Pr)}(dmap)]$^+$). IR (DRIFTS): ν_{max} 3387 m, 3091 w, 3054 w, 2971 m, 2930 m, 2870 w, 1617 s, 1578 s, 1537 s, 1482 m, 1437 m, 1399 s, 1389 s, 1365 m, 1326 m, 1310 w, 1252 m, 1225 s, 1174 m, 1123 w, 1102 m, 1073 m, 1026 m, 999 w, 983 w, 948 w, 931 w, 896 w, 867 w, 856 w, 834 w, 816 m, 750 m, 711 w, 700 m, 657 s, 635 w, 541 m, 522 m, 510 m, 495 m, 484 m, 445 w. Anal. Calc. for $C_{36}H_{43}F_6FeN_5PPdSb$ (974.7): C 44.36, H 4.45, N 7.18%. Found: C 44.36, H 4.12, N 7.11%.

X-RAY CRYSTALLOGRAPHY

Full-sphere diffraction data ($\pm h \pm k \pm l$, θ_{max} = 27.5°) were collected using a Bruker D8 VENTURE Kappa Duo diffractometer equipped with a PHOTON100 detector and a Cryostream Cooler (Oxford Cryosystems). Monochromated Mo Kα radiation (λ = 0.71073 Å) was employed, with the exception of compound **17**, for which Cu Kα radiation (λ = 1.54178 Å) was used.

The structures were solved using direct methods (SHELXT-2014)[2] and subsequently refined by full-matrix least-squares based on F^2 using SHELXL-2014 or SHELXL-2017.[3] All non-hydrogen atoms were refined with anisotropic displacement parameters. The hydrogen atoms were included in their theoretical positions and refined as riding atoms with U_{iso}(H) set to a 1.2U_{eq}(N) and 1.2U_{eq}(C), respectively.

Geometric calculations were performed and the structural diagrams were obtained using the recent version of PLATON program.[4] Numerical values were rounded to one decimal place with respect to their estimated deviations (ESDs). Parameters pertaining to atoms in geometrically constrained positions (hydrogens) are given without ESDs.

Table D.1. Summary of relevant crystallographic data and refinement parameters.

Compound	**17**	**18**·2$CHCl_3$	**19**
Formula	$C_{29}H_{34}Cl_2FeN_3PPt$	$C_{124}H_{94}B_2Cl_8F_{48}Fe_2N_6P_2Pt_2$	$C_{29}H_{35}ClFeN_3P$
M	777.40	3449.09	547.87
Crystal system	monoclinic	triclinic	monoclinic
Space group	$P2_1/n$ (no. 14)	$P\bar{1}$ (no. 2)	$P2_1/c$ (no. 14)
T/K	120(2)	120(2)	125(2)
a/Å	13.1436(4)	14.1749(4)	13.9859(6)
b/Å	13.0775(4)	14.2935(4)	9.5728(4)
c/Å	16.9749(4)	17.5227(4)	20.6633(9)
α/°	90	70.720(1)	90
β/°	98.675(2)	89.867(1)	99.693(2)
γ/°	90	83.515(1)	90
V/Å^3	2884.4(1)	3327.4(2)	2727.0(2)
Z	4	1	4
F(000)	1528	1696	1152
μ(Mo Kα)/mm^{-1}	15.381	2.612	0.732
Diffrns collected	25775	44765	42321
Indep diffrns	4754	13077	6268
Observed[a] diffrns	3749	12097	5720
R_{int}[b]/%	8.20	2.67	2.15
No. of parameters	338	878	323
R[b] obsd diffrns/%	3.54	2.81	2.61
R, wR[b] all data/%	5.73, 7.01	3.18, 6.95	2.98, 6.63
Δρ/e Å^{-3}	0.87, –0.88	3.09, –1.08	0.49, –0.37

[a] Diffractions with $I > 2\sigma(I)$. [b] Definitions: $R_{int} = \Sigma\,|F_o^2 - F_o^2(\text{mean})|\,/\Sigma F_o^2$, where F_o^2(mean) is the average intensity of symmetry-equivalent diffractions. $R = \Sigma\,||F_o| - |F_c||/\Sigma\,|F_o|$, $wR = [\Sigma\{w(F_o^2 - F_c^2)^2\}/\Sigma w(F_o^2)^2]^{1/2}$.

Table D.1 continued

Compound	**20**·CH_2Cl_2	**21**·2.5$CHCl_3$	**23**·2CH_2Cl_2
Formula	$C_{30}H_{37}Cl_2F_6FeN_3PSb$	$C_{31.5}H_{37.5}Cl_{10.5}FeN_3PPd$	$C_{60}H_{74}Cl_8F_{12}Fe_2N_6P_2Pd_2Sb_2$
M	833.09	1023.59	2020.79
Crystal system	triclinic	triclinic	triclinic
Space group	P–1 (no. 2)	P–1 (no. 2)	P–1 (no. 2)
T/K	150(2)	120(2)	150(2)
a/Å	9.5123(5)	12.5962(5)	13.7155(9)
b/Å	9.6515(6)	13.5142(6)	15.400(1)
c/Å	20.813(1)	14.1211(6)	19.757(1)
α/°	95.262(2)	114.103(1)	88.358(2)
β/°	98.024(2)	93.921(1)	85.451(2)
γ/°	114.946(2)	108.668(1)	65.734(2)
V/Å^3	1691.3(2)	2022.9(2)	3792.3(5)
Z	2	2	2
F(000)	836	1026	1992
μ(Mo Kα)/mm^{-1}	1.491	1.564	1.933
Diffrns collected	48922	40304	55268
Indep diffrns	7771	9326	14923
Observed[a] diffrns	7285	8566	11850
R_{int}[b]/%	2.07	1.74	3.19
No. of parameters	426	433	855
R[b] obsd diffrns/%	3.79	2.83	4.93
R, wR[b] all data/%	4.03, 9.83	3.20, 6.73	6.60, 13.77
Δρ/e Å^{-3}	1.85, –1.38	1.62, –1.04	2.53, –1.54

Table D.1 continued

Compound	**24**	**25**·Et_2O	**26**
Formula	$C_{58}H_{70}Cl_2F_{12}Fe_2N_6P_2PdSb_2$	$C_{33}H_{43}ClFeN_3OPPd$	$C_{36}H_{43}F_6FeN_5PPdSb$
M	1673.64	726.37	974.72
Crystal system	triclinic	monoclinic	orthorhombic
Space group	P–1 (no. 2)	$P2_1/n$ (no. 14)	$Pbca$ (no. 61)
T/K	120(2)	120(2)	125(2)
a/Å	9.830(2)	13.2618(6)	17.1620(9)
b/Å	10.785(2)	11.2018(5)	20.788(1)
c/Å	16.810(2)	21.993(1)	21.742(1)
α/°	90.376(8)	90	90
β/°	104.974(6)	101.127(1)	90
γ/°	112.399(5)	90	90
V/Å^3	1580.6(4)	3205.8(3)	7756.9(7)
Z	1	4	8
F(000)	832	1496	3888
μ(Mo Kα)/mm^{-1}	1.784	1.177	1.622
Diffrns collected	32266	48171	93777
Indep diffrns	7260	7383	8927
Observed[a] diffrns	6401	6938	8331
R_{int}[b]/%	3.40	2.02	2.13
No. of parameters	389	376	488
R[b] obsd diffrns/%	3.64	2.00	2.07
R, wR[b] all data/%	4.38, 7.85	2.22, 5.13	2.32, 4.97
Δρ/e Å^{-3}	0.99, –0.96	0.40, –0.77	0.80, –0.67

REFERENCES

1. O. Bárta, R. Gyepes, I. Císařová, A. Alemayehu, P. Štěpnička, *Dalton Trans.* **2020**, *49*, 4225-4229.
2. G. M. Sheldrick, *Acta Crystallogr., Sect. A: Found. Adv.* **2015**, *71*, 3-8.
3. G. M. Sheldrick, *Acta Crystallogr., Sect. C: Struct. Chem.* **2015**, *71*, 3-8.
4. A. L. Spek, *J. Appl. Crystallogr.* **2003**, *36*, 7–13.